NIST GCR 96-701

ENERGY-BASED METHOD FOR LIQUEFACTION POTENTIAL EVALUATION, PHASE I - FEASIBILITY STUDY

Farhang Ostadan
Nan Deng
Ignacio Arango

Bechtel Corporation
San Francisco, CA 94119

A Report to:

U.S. Department of Commerce
Technology Administration
National Institute of Standards and Technology
Building and Fire Research Laboratory
Gaithersburg, MD 20899

August 1996

U.S. Department of Commerce
Michael Kantor, *Secretary*
Technology Administration
Mary L. Good, *Under Secretary for Technology*
National Institute of Standards and Technology
Arati Prabhakar, *Director*

ABSTRACT

This report presents the results of the first phase of a three-phase study on the development and application of the energy-based method for prediction of the liquefaction potential of sandy soils. The formulation of the method is based on the convolution of the basic elements from both the "stress" and "strain" approaches and is very flexible in incorporating the special characteristics of ground motion such as the near-field effects. The feasibility phase consists of the tasks: 1) to collect and synthesize laboratory data; 2) to perform ground response analyses at the Wildlife Site, which suffered a massive ground liquefaction failure during the Superstition Hills Earthquake; and finally 3) to compare and to assess the differences between the field and the laboratory data. Even though the scope of the feasibility study did not permit cyclic testing of the soil samples from the Wildlife Site, the correlation of the field response data and the applicable laboratory data are strong. The results of this phase suggest that development of an energy-based method to evaluate liquefaction potential is feasible.

KEYWORDS: building technology; liquefaction; strain energy; earthquake; ground response; cyclic testing; laboratory measurements; ground motion; pore pressure.

ACKNOWLEDGMENT

The study was sponsored by the National Institute of Standards and Technology (NIST) under the Contract No. 50SBNB5C8640. Drs. R. Andrus and R. Chung of NIST provided support and guidance throughout the course of the study. The authors gratefully acknowledge the support and supply of laboratory data by Dr. J. Koester from the U. S. Army Corps of Engineers. Dr. S. Glaser from the Colorado School of Mines generously provided the data recorded at the Wildlife Site and made many helpful suggestions during the course of the study. The report was reviewed by Mr. M. Lewis, geotechnical manager, in Bechtel National.

TABLE OF CONTENTS

	PAGE
ABSTRACT	**i**
ACKNOWLEDGMENT	**ii**
TABLE OF CONTENTS	**iii**
LIST OF TABLES	**vi**
LIST OF FIGURES	**vii**
LIST OF SYMBOLS	**xv**
UNITS CONVERSION FACTORS	**xvi**
CHAPTER 1	**1-1 through 1-3**
INTRODUCTION	**1-1**
1.1 BACKGROUND	1-1
1.2 PURPOSE	1-2
1.3 OVERVIEW OF THE REPORT	1-2
CHAPTER 2	**2-1 through 2-36**
COLLECTION AND SYNTHESIS OF LABORATORY DATA	**2-1**
2.1 STRAIN ENERGY COMPUTATION	2-1
2.2 CYCLIC TRIAXIAL TESTS ON MONTEREY NO. 0 SAND, PERFORMED AT THE UNIVERSITY OF CALIFORNIA, BERKELEY (UCB)	2-2
2.3 CYCLIC TRIAXIAL TESTS ON SOIL SAMPLES FROM THE SAVANNAH RIVER SITE, PERFORMED AT THE UNIVERSITY OF CALIFORNIA, BERKELEY (UCB)	2-3
2.4 CYCLIC TORSIONAL TESTS ON SOIL SAMPLES, PERFORMED AT THE UNIVERSITY OF COLORADO (UOC)	2-4

PAGE

2.5 CYCLIC TRIAXIAL TESTS ON SOIL SAMPLES FROM THE NORTHRIDGE SITE, PERFORMED AT THE UNIVERSITY OF CALIFORNIA, BERKELEY (UCB) 2-4

2.6 CYCLIC TRIAXIAL TESTS ON CLEAN SANDS PERFORMED AT THE WAYNE STATE UNIVERSITY (WSU) 2-5

2.7 SUMMARY DATA BY FIGUEROA et al. 2-5

2.8 SUMMARY OF ALL LABORATORY DATA 2-6

CHAPTER 3 **3-1 through 3-20**

WILDLIFE SITE: SOILS AND EARTHQUAKE DATA **3-1**

3.1 BACKGROUND 3-1

3.2 WILDLIFE SITE 3-1

3.3 STRATIGRAPHY AND SOIL PROPERTIES AT THE WILDLIFE SITE 3-1

3.4 INSTRUMENTATION AT THE WILDLIFE SITE 3-2

3.5 RECORDED EARTHQUAKE DATA 3-3

CHAPTER 4 **4-1 through 4-64**

GROUND RESPONSE ANALYSES AND COMPARISON WITH THE LABORATORY DATA **4-1**

4.1 METHODS OF ANALYSES 4-1

4.2 RESULTS OF THE GROUND RESPONSE ANALYSES USING THE COMPUTER PROGRAM SHAKE 4-2

4.3 RESULTS OF THE GROUND RESPONSE ANALYSES USING THE COMPUTER PROGRAM BDESRA (MODIFIED DESRA) 4-3

	PAGE
4.4 RESULTS OF THE GROUND RESPONSE ANALYSES BASED ON DIRECT INTERPOLATION OF RECORDED MOTIONS	4-4
4.5 RESULTS OF THE GROUND RESPONSE ANALYSES USING THE COMPUTER PROGRAM SHAKE AND EPRI SOIL CURVES	4-5
4.6 COMPARISON OF THE RESULTS OF GROUND RESPONSE ANALYSES	4-5
4.7 COMPARISON OF THE RESULTS OF GROUND RESPONSE ANALYSES WITH THE LABORATORY DATA	4-6
CHAPTER 5	**5-1 through 5-2**
SUMMARY AND RECOMMENDATION	**5-1**
CHAPTER 6	**6-1 through 6-4**
REFERENCES	**6-1**
APPENDIX A	**A-1 through A-42**
LABORATORY TESTS ON MONTEREY NO. 0 SAND, PERFORMED AT THE UNIVERSITY OF CALIFORNIA, BERKELEY	
APPENDIX B	**B-1 through B-46**
LABORATORY TESTS ON SOIL SAMPLES FROM THE SAVANNAH RIVER SITE, PERFORMED AT THE UNIVERSITY OF CALIFORNIA, BERKELEY	
APPENDIX C	**C-1 through C-20**
LABORATORY TESTS ON SOIL SAMPLES, PERFORMED AT THE UNIVERSITY OF COLORADO	
APPENDIX D	**D-1 through D-18**
LABORATORY TESTS ON SOIL SAMPLES FROM THE NORTHRIDGE SITE, PERFORMED AT THE UNIVERSITY OF CALIFORNIA, BERKELEY	

LIST OF TABLES

Table 2.1 Summary of the Cyclic Triaxial Test Data on Monterey No. 0 Sand Performed at University of California, Berkeley

Table 2.2 Average Material Properties at the SRS Site

Table 2.3 Summary of the Cyclic Triaxial Test Data on SRS Soil Samples Performed at University of California, Berkeley

Table 2.4 Summary of the Cyclic Torsional Test Data on Clean and Silty Sands Performed at University of Colorado

Table 2.5 Summary of the Cyclic Triaxial Test Data on Northridge Samples Performed at University of California, Berkeley

Table 2.6 Summary of the Cyclic Triaxial Test Data on Clean Sands Performed at Wayne State University

Table 3.1 Summary of the Wildlife Site Earthquake Data and Recorded Time Histories

Table 4.1 Summary of Strain Energy Computation from Ground Response Analyses (November 24, 1987, 1315 GMT Earthquake)

LIST OF FIGURES

Figure 1.1 Relationships Between Stress Ratio Causing Liquefaction and $(N_1)_{60}$ Values for Silty Sands for M = 7-1/2 Earthquakes (Seed et al., 1985)

Figure 2.1 Typical Time History Records of a Strain-Controlled Cyclic Triaxial Test

Figure 2.2 A Typical Plot of Shear Stress-Strain Hysteresis Loops Developed During Cyclic Triaxial Tests

Figure 2.3 Grain Size Distribution for Monterey No. 0 Sand (Arango, 1994)

Figure 2.4 Strain Energy at Liquefaction Onset as a Function of Relative Density for Monterey No. 0 Sand - UCB Data

Figure 2.5 Strain Energy at Liquefaction Onset as a Function of Frequencies of Loading for Monterey No. 0 Sand - UCB Data

Figure 2.6 Generalized Subsurface Soil Profile at the SRS Site

Figure 2.7 Typical Grain Size Distribution Curve for Tobacco Road Soil Material - SRS (Riemer and Seed, 1994)

Figure 2.8 Strain Energy as a Function of Confining Pressure for SRS Soil Samples - UCB Data

Figure 2.9 Grain Size Distribution of Silty Sands - UOC Samples (Koester, 1992)

Figure 2.10 Strain Energy at Liquefaction Onset as a Function of Relative Density for Clean Sands - UOC Data

Figure 2.11 Strain Energy at Liquefaction Onset as a Function of Confining Pressure for Silty Sands - UOC Data

Figure 2.12 Grain Size Distribution Curves for the Northridge Site Soil Samples (Arango and Migues, 1996)

Figure 2.13 Strain Energy at Liquefaction Onset as a Function of Relative Density for the Northridge Samples - UCB Data

Figure 2.14 Grain Size Distribution Curves for Monterey No. 0 and Kasumigaura Sands (Al-Khatib, 1994)

Figure 2.15 Strain Energy at Liquefaction Onset as a Function of Relative Density for Monterey No. 0 and Kasumigaura Sands - WSU Data

Figure 2.16 Effect of Cyclic Loading Types on Strain Energy at Liquefaction Onset for Monterey No. 0 Sand - WSU Data

Figure 2.17 Effect of Cyclic and Transient Loading on Strain Energy at Liquefaction Onset for Monterey No. 0 Sand - WSU Data

Figure 2.18 Grain Size Distribution Curves for Soil Samples for the Lower San Fernando Dam and the Reid Bedford Sand (Figueroa et al., 1995)

Figure 2.19 Comparison of Strain Energy at Liquefaction Onset for All Test Groups - Clean Sands

Figure 2.20 Comparison of Strain Energy at Liquefaction Onset for All Test Groups - Silty Sands

Figure 3.1 Map of California with Locations of Parkfield and Wildlife Liquefaction Arrays

Figure 3.2 Wildlife Liquefaction Array - Geotechnical Properties (Bennett et al., 1984)

Figure 3.3 Main Geological Units at the Wildlife Site and Their Geotechnical Characteristics (Bennett et al., 1984)

Figure 3.4 Comparison of Shear Wave Velocity Profiles from Crosshole and SASW Tests at Wildlife Site (Bierschwale and Stokoe, 1984)

Figure 3.5 Variation in Normalized Shear Modulus with Shearing Strain for Channel Fill Sand (Ladd, 1982)

Figure 3.6 Variation in Normalized Shear Modulus with Shearing Strain for Imperial Valley Clays (Turner and Stokoe, 1982)

Figure 3.7 Variation in Damping Ratio with Shearing Strain for Imperial Valley Soils (Ladd, 1982; Turner and Stokoe, 1982)

Figure 3.8 Instrumentation of the Wildlife Site (Bennett et al., 1984)

Figure 3.9 Location Map of the Wildlife Site and the Epicenters of the Elmore Ranch ($M_s = 6.2$) and Superstition Hills ($M_s = 6.6$) Earthquakes (Porcella et al., 1987)

Figure 3.10 Earthquake Time Histories at 1315 GMT, November 24, 1987 at Wildlife Array - Horizontal Motions in 360° Direction

Figure 3.11 Earthquake Time Histories at 1315 GMT, November 24, 1987 at Wildlife Array - Horizontal Motions in 90° Direction

Figure 3.12 Earthquake Time Histories at 1315 GMT, November 24, 1987 at Wildlife Array - Vertical Motions

Figure 3.13 Acceleration Response Spectra at 5% Damping - Wildlife Liquefaction Array, November 24, 1987, 1315 GMT Earthquake - Comparison of the Spectral Characteristics of Horizontal Motions

Figure 3.14 Acceleration Response Spectra at 5% Damping - Wildlife Liquefaction Array, November 24, 1987, 1315 GMT Earthquake - Comparison of the Spectral Characteristics of Vertical Motions

Figure 3.15 Normalized Pore Water Pressure Ratios - Wildlife Liquefaction Array, November 24, 1987, 1315 GMT Event (Matasovic et al., 1993)

Figure 4.1 Wildlife Site Soil Profile Used in Response Analysis Based on Average of SASW and Crosshole Shear Wave Velocity Measurements

Figure 4.2 Acceleration Response Spectra at 5% Damping - Wildlife Liquefaction Array, November 24, 1987, 1315 GMT Earthquake - Comparison of Horizontal Motions in 360 Degree Direction - SHAKE Output at Ground Surface Calculated Using Crosshole Shear Wave Velocity Measurements

Figure 4.3 Acceleration Response Spectra at 5% Damping - Wildlife Liquefaction Array, November 24, 1987, 1315 GMT Earthquake - Comparison of Horizontal Motions in 360 Degree Direction - SHAKE Output at Ground Surface Calculated Using SASW Shear Wave Velocity Measurements

Figure 4.4 Acceleration Response Spectra at 5% Damping - Wildlife Liquefaction Array, November 24, 1987, 1315 GMT Earthquake - Comparison of Horizontal Motions in 360 Degree Direction - SHAKE Output at Ground Surface Calculated Using Average of SASW and Crosshole Shear Wave Velocity Measurements

Figure 4.5 Acceleration Response Spectra at 5% Damping - Wildlife Liquefaction Array, November 24, 1987, 1315 GMT Earthquake - Comparison of Horizontal Motions in 360 Degree Direction - SHAKE Output at Depth of 7.5 m with Cutoff Frequency of 25 Hz

Figure 4.6 Acceleration Response Spectra at 5% Damping - Wildlife Liquefaction Array, November 24, 1987, 1315 GMT Earthquake - Comparison of Horizontal Motions in 90 Degree Direction - SHAKE Output at Ground Surface Calculated Using Average of SASW and Crosshole Shear Wave Velocity Measurements

Figure 4.7 Maximum Acceleration Distribution over Depth from SHAKE Results - Wildlife Site, November 24, 1987, 1315 GMT Earthquake in 360° Direction

Figure 4.8 Maximum Acceleration Distribution over Depth from SHAKE Results - Wildlife Site, November 24, 1987, 1315 GMT Earthquake in 90° Direction

Figure 4.9 Maximum Shear Stress Distribution over Depth from SHAKE Results - Wildlife Site, November 24, 1987, 1315 GMT Earthquake in 360° Direction

Figure 4.10 Maximum Shear Stress Distribution over Depth from SHAKE Results - Wildlife Site, November 24, 1987, 1315 GMT Earthquake in 90° Direction

Figure 4.11 Maximum Shear Strain Distribution over Depth from SHAKE Results - Wildlife Site, November 24, 1987, 1315 GMT Earthquake in 360° Direction

Figure 4.12 Maximum Shear Strain Distribution over Depth from SHAKE Results - Wildlife Site, November 24, 1987, 1315 GMT Earthquake in 90° Direction

Figure 4.13 Shear Stress Time History at Depth 4.21 m from SHAKE Output - Wildlife Site, November 24, 1987, 1315 GMT Earthquake in 360° Direction

Figure 4.14 Shear Strain Time History at Depth 4.21 m from SHAKE Output - Wildlife Site, November 24, 1987, 1315 GMT Earthquake in 360° Direction

Figure 4.15 Shear Stress-Shear Strain Hysteresis Loop at Depth 4.21 m. Calculated from SHAKE Output - Wildlife Site, November 24, 1987, 1315 GMT Earthquake in 360° Direction. Soil Properties are Based on the Average of SASW and Crosshole Shear Wave Velocity Measurements

Figure 4.16 Accumulation of Strain Energy in Liquefied Sand Layer - Wildlife Site, November 24, 1987, 1315 GMT Earthquake in 360° Direction - SHAKE Analysis Output

Figure 4.17 Accumulation of Strain Energy in Liquefied Sand Layer - Wildlife Site, November 24, 1987, 1315 GMT Earthquake in 90° Direction - SHAKE Analysis Output

Figure 4.18 Accumulation of Strain Energy in Liquefied Sand Layer - Wildlife Site, November 24, 1987, 1315 GMT Earthquake - Summation of SHAKE Analysis Output in both 360° and 90° Directions

Figure 4.19 Acceleration Response Spectra at 5% Damping - Wildlife Liquefaction Array, November 24, 1987, 1315 GMT Earthquake - Comparison of Horizontal Motions in 360° Direction - BDESRA Output, Total Stress Analysis

Figure 4.20 Acceleration Response Spectra at 5% Damping - Wildlife Liquefaction Array, November 24, 1987, 1315 GMT Earthquake - Comparison of Horizontal Motions in 90° Direction - BDESRA Output, Total Stress Analysis

Figure 4.21 Maximum Shear Stress Distribution over Depth from BDESRA Results of Total Stress Analyses - Wildlife Site, November 24, 1987, 1315 GMT Earthquake

Figure 4.22 Maximum Shear Strain Distribution over Depth from BDESRA Results of Total Stress Analyses - Wildlife Site, November 24, 1987, 1315 GMT Earthquake

Figure 4.23 Accumulation of Strain Energy in Liquefied Sand Layer - Wildlife Site, November 24, 1987, 1315 GMT Earthquake in 360° Direction - BDESRA Output, Total Stress Analysis

Figure 4.24 Accumulation of Strain Energy in Liquefied Sand Layer - Wildlife Site, November 24, 1987, 1315 GMT Earthquake in 90° Direction - BDESRA Output, Total Stress Analysis

Figure 4.25 Accumulation of Strain Energy in Liquefied Sand Layer - Wildlife Site, November 24, 1987, 1315 GMT Earthquake - Summation of BDESRA Total Stress Analysis Output in both 360° and 90° Directions

Figure 4.26 Acceleration Response Spectra at 5% Damping - Wildlife Liquefaction Array, November 24, 1987, 1315 GMT Earthquake - Comparison of Horizontal Motions in 360° Direction - BDESRA Output, Effective Stress Analysis

Figure 4.27 Acceleration Response Spectra at 5% Damping - Wildlife Liquefaction Array, November 24, 1987, 1315 GMT Earthquake - Comparison of Horizontal Motions in 90° Direction - BDESRA Output, Effective Stress Analysis

Figure 4.28 Maximum Shear Stress Distribution over Depth from BDESRA Results of Effective Stress Analyses - Wildlife Site, November 24, 1987, 1315 GMT Earthquake

Figure 4.29 Maximum Shear Strain Distribution over Depth from BDESRA Results of Effective Stress Analyses - Wildlife Site, November 24, 1987, 1315 GMT Earthquake

Figure 4.30 Accumulation of Strain Energy in Liquefied Sand Layer - Wildlife Site, November 24, 1987, 1315 GMT Earthquake in 360° Direction - BDESRA Output, Effective Stress Analysis

Figure 4.31 Accumulation of Strain Energy in Liquefied Sand Layer - Wildlife Site, November 24, 1987, 1315 GMT Earthquake in 90° Direction - BDESRA Output, Effective Stress Analysis

Figure 4.32 Accumulation of Strain Energy in Liquefied Sand Layer - Wildlife Site, November 24, 1987, 1315 GMT Earthquake - Summation of BDESRA Effective Stress Analysis Output in both 360° and 90° Directions

Figure 4.33 Normalized Pore Water Pressure Generation in Liquefied Sand Layer - Wildlife Site, November 24, 1987, 1315 GMT Earthquake in 360° Direction, BDESRA Output, Effective Stress Analysis

Figure 4.34 Normalized Pore Water Pressure Generation in Liquefied Sand Layer - Wildlife Site, November 24, 1987, 1315 GMT Earthquake in 90° Direction, BDESRA Output, Effective Stress Analysis

Figure 4.35 Methodology Adopted in Estimating the Dynamic Stress and Strain Time Histories in a Soil Layer from Field Records (After Zeghal and Elgamal, 1994)

Figure 4.36 Shear Stress Time History at Depth of 5.06 m (16.6 ft) Based on Direct Interpolation of Recorded Motions, Wildlife Site, November 24, 1987, 1315 GMT Earthquake in 360° Direction

Figure 4.37 Shear Strain Time History at Depth of 5.06 m (16.6 ft) Based on Direct Interpolation of Recorded Motions, Wildlife Site, November 24, 1987, 1315 GMT Earthquake in 360° Direction

Figure 4.38 Shear Stress-Strain Hysteresis Loop at Depth of 5.06 m (16.6 ft) Based on Direct Interpolation of Recorded Motions, Wildlife Site, November 24, 1987, 1315 GMT Earthquake in 360° Direction

Figure 4.39 Shear Stress Time History at Depth of 5.06 m (16.6 ft) Based on Direct Interpolation of Recorded Motions, Wildlife Site, November 24, 1987, 1315 GMT Earthquake in 90° Direction

Figure 4.40 Shear Strain Time History at Depth of 5.06 m (16.6 ft) Based on Direct Interpolation of Recorded Motions, Wildlife Site, November 24, 1987, 1315 GMT Earthquake in 90° Direction

Figure 4.41 Shear Stress-Strain Hysteresis Loop at Depth of 5.06 m (16.6 ft) Based on Direct Interpolation of Recorded Motions, Wildlife Site, November 24, 1987, 1315 GMT Earthquake in 90° Direction

Figure 4.42 Accumulation of Strain Energy in Liquefied Sand Layer Based on Direct Interpolation of Recorded Motions, Wildlife Site, November 24, 1987, 1315 GMT Earthquake in 360° Direction

Figure 4.43 Accumulation of Strain Energy in Liquefied Sand Layer Based on Direct Interpolation of Recorded Motions, Wildlife Site, November 24, 1987, 1315 GMT Earthquake in 90° Direction

Figure 4.44 Accumulation of Strain Energy in Liquefied Sand Layer Based on Direct Interpolation of Recorded Motions, Wildlife Site, November 24, 1987, 1315 GMT Earthquake - Summation of Strain Energy in both 360° and 90° Directions

Figure 4.45 Comparison of Shear Modulus Degradation Curves used in SHAKE Analyses

Figure 4.46 Comparison of Damping Curves used in SHAKE Analyses

Figure 4.47 Acceleration Response Spectra at 5% Damping - Wildlife Liquefaction Array, November 24, 1987, 1315 GMT Earthquake - Comparison of Horizontal Motions in 360° Direction - SHAKE Output with EPRI (1993) Soil Curves

Figure 4.48 Acceleration Response Spectra at 5% Damping - Wildlife Liquefaction Array, November 24, 1987, 1315 GMT Earthquake - Comparison of Horizontal Motions in 90° Direction - SHAKE Output with EPRI (1993) Soil Curves

Figure 4.49 Shear Stress Time History at Depth of 4.21 m (13.8 ft) from SHAKE Output with EPRI (1993) Soil Curves - Wildlife Site, November 24, 1987, 1315 GMT Earthquake in 360° Direction

Figure 4.50 Shear Strain Time History at Depth of 4.21 m (13.8 ft) from SHAKE Output with EPRI (1993) Soil Curves - Wildlife Site, November 24, 1987, 1315 GMT Earthquake in 360° Direction

Figure 4.51 Shear Stress-Strain Hysteresis Loop at Depth of 4.21 m (13.8 ft). Calculated from SHAKE Output - Wildlife Site, November 24, 1987, 1315 GMT Earthquake in 360° Direction. Soil Properties are Based on the Average of SASW and Crosshole Shear Wave Velocity Measurements. The EPRI (1993) G/Gmax and Damping Curves are used in the Calculation

Figure 4.52 Accumulation of Strain Energy in Liquefied Sand Layer - Wildlife Site, November 24, 1987, 1315 GMT Earthquake in 360° Direction - SHAKE Output Using EPRI (1993) Soil Curves

Figure 4.53 Accumulation of Strain Energy in Liquefied Sand Layer - Wildlife Site, November 24, 1987, 1315 GMT Earthquake in 90° Direction - SHAKE Output Using EPRI (1993) Soil Curves

Figure 4.54 Accumulation of Strain Energy in Liquefied Sand Layer - Wildlife Site, November 24, 1987, 1315 GMT Earthquake - Summation of Strain Energy in both 360° and 90° Directions - SHAKE Output Using EPRI (1993) Soil Curves

Figure 4.55 Total Strain Energy at Liquefaction Onset. Calculated from Ground Response Analyses

Figure 4.56 Total Strain Energy at Liquefaction Onset. Calculated from Ground Response Analyses (with All Points in Unliquefied Layers Removed)

Figure 4.57 Comparison of Total Strain Energy at Liquefaction Onset. Ground Response Analyses and Laboratory Data - Wildlife Site, November 24, 1987, 1315 GMT Earthquake

LIST OF SYMBOLS

a, $a(t)$	acceleration at time t in cm/sec^2
CPT	cone penetration data
d, $d(t)$	displacement at time t in cm
D_r	relative density - %
FC	fines content
G	soil shear modulus
G_{max}	maximum soil shear modulus
N	SPT, blow-count
N_1	blow-count normalized to 1 ksc
$(N_1)_{60}$	normalized blow-count for a 60 percent energy ratio
v, $v(t)$	velocity at time t in cm/sec
δE, E_{liq}	energy per volume at the onset of liquefaction, $Joules/m^3$
$\Delta\gamma(t)$	shear strain increment from time t to $t + \Delta t$
γ, $\gamma(t)$	shear strain
γ_d	dry unit weight, kN/m^3
r_u	pore pressure ratio
σ'_c	effective confining pressure, kPa
SPT	standard penetration test
Σ	summation
τ, $\tau(t)$	shear stress
$\bar{\tau}(t)$	average shear stress at times t and $t + \Delta t$

UNITS CONVERSION FACTORS

1 Joules	0.0007376 ft-kip
1 kg/cm^2	2.048 kip/ft^2
1 km	0.621 miles
1 kN	0.225 kips
1 kN/m^2	0.02088 kip/ft^2
1 kN/m^3	6.366 lb/ft^3
1 m	3.281 ft
1 m^2	10.76 ft^2
1 m^3	35.31 ft^3

CHAPTER 1

INTRODUCTION

1.1 BACKGROUND

Liquefaction failure has been and continues to be a major cause of damage during earthquakes. The direct and indirect costs associated with ground failure may far exceed the damage caused by other types of failures such as structural collapses. Due to the enormous damage potential, research in the areas of liquefaction prediction and mitigation has continued, and the respective technologies have significantly improved over the years.

Two basic methods are currently used to predict liquefaction potential. The most widely used method, based on laboratory data and field performance data, was developed by Seed et al. (1983, 1985). In this method, the cyclic stress ratio in the field is predicted based on a simple or a more detailed ground response analysis, and the demand resulting from the design earthquake is established. The cyclic shear strength of the material can be obtained from laboratory testing of the soil samples or from the penetration data (Standard Penetration Test [SPT] data or Cone Penetration Test [CPT] data) along with the index and gradation properties of the soil samples. The most widely used curves to predict the capacity of the soil in terms of cyclic shear strength are the set of curves by Seed et al. (1985), shown in Figure 1.1. From knowledge of the penetration resistance and the fines content in the soil materials, the cyclic shear strength can be determined. However, the application of this method involves several empirical factors, including the corrections for sample disturbance, earthquake magnitude, and overburden pressure. Recently, Arango (1994) presented the new developments for this method, including the effects of higher frequency of loading on the cyclic shear strength of the soil and most notably, the recommendations made for revising the correction factors for earthquake magnitudes. Another recent study (Koester, 1992) has shown that the correction for overburden pressure is also a function of the fines content and that a reduction of the cyclic shear strength due to overburden pressure will significantly decrease if the fines content of the materials increases. The recent publication by Ishihara (1993) also provides an adjustment factor to incorporate the plasticity effects of the fines on the cyclic shear strength of the materials. Over the years, the "stress" method has proved to be a conservative and reliable method for the prediction of liquefaction potential, especially for distant earthquake events, which was the basis of the data used for development of this method. However, the method lacks the flexibility to incorporate recently recognized characteristics of the earthquake ground motions such as the near-field effects. For example, the "fling" effect resulting from the source and directivity of the rupture which was recently observed in the Kobe and the Northridge earthquakes, concentrates most of the energy in a short period of time. Such effects, combined with a much higher intensity of the ground motion in excess of 1g peak ground acceleration recorded in urban areas in recent major earthquakes, require a more robust approach to investigate the liquefaction potential in such regions.

The second method for predicting liquefaction potential is based on the "strain" approach. This method was developed among others by Dobry et al. (1982). In this method, the shear strain in the field is compared with the laboratory data relating cyclic shear strain to excess pore pressure to determine the liquefaction potential. Similar to the "stress" method, the "strain" method also requires ground response analyses and laboratory testing of the soil samples. The "strain" method is fundamentally different from the "stress" method and lacks the wide range of the field and the laboratory data bases that exist for the "stress" approach.

The "strain energy" method discussed in this report incorporates the basic elements of both the stress and strain approaches in the formulation. In this method, the amount of total strain energy at the onset of liquefaction is obtained from the stress and strain time histories from laboratory testing and is compared with the same energy in the field due to the design earthquake motion. The basis for this method is the observation made on the laboratory data that the build-up of the excess pore pressure is proportional to the total strain energy in all loading cycles up to the initial liquefaction. This observation has prompted the formulation of the "energy-based" method. This method has been investigated in recent years by several researchers, including Figueroa et al. (1994, 1995) and Kagawa et al. (1990).

1.2 PURPOSE

The purpose of this study is to evaluate the feasibility of the development and application of the strain energy method for general use. The study is expected to continue with two additional phases that will develop generic "strain energy" liquefaction curves as a function of the most relevant soil properties and generic "strain energy" demand as a function of seismicity data and a wide range of site soil data and profiles. The limited scope of the feasibility study did not permit laboratory testing for the purpose of the "strain energy" computation. Available laboratory data were used for this purpose.

1.3 OVERVIEW OF THE REPORT

In this report, Chapter 1 includes the introduction and scope of the study. Chapter 2 presents the collection and synthesis of the laboratory data. Chapter 3 discusses the soil and earthquake data from the Wildlife Site. The ground response analyses and comparison of the results with the laboratory data are presented in Chapter 4. Finally, Chapter 5 presents the summary and the recommendation. The references are listed in Chapter 6. All the laboratory data used in this report are presented in Appendices A through D.

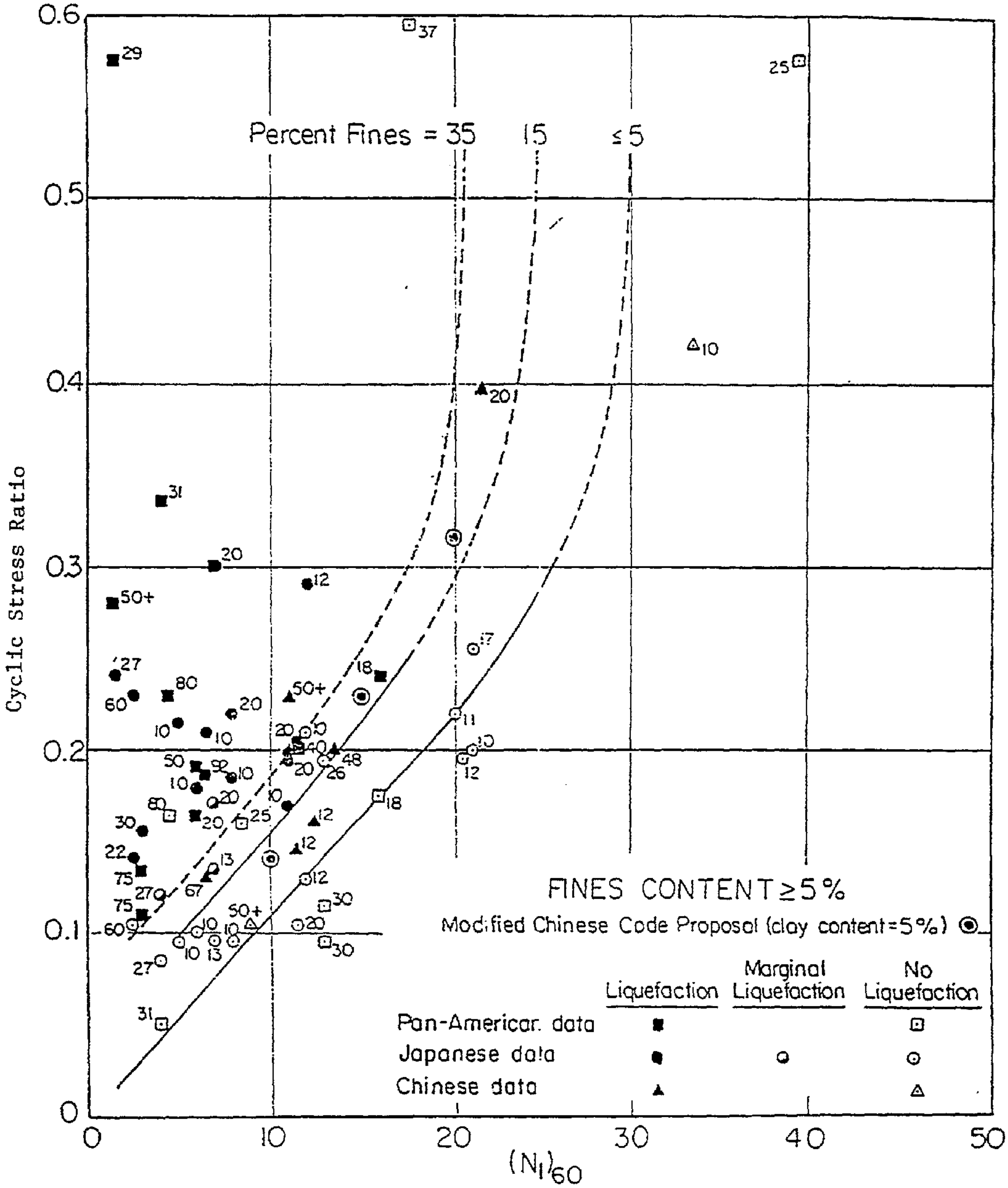

Figure 1.1 - Relationships Between Stress Ratio Causing Liquefaction and $(N_1)_{60}$ Values for Silty Sands for M = 7-1/2 Earthquakes (Seed et al., 1985)

CHAPTER 2

COLLECTION AND SYNTHESIS OF LABORATORY DATA

Computation of the strain energy requires access to the stress and strain time histories from cyclic (triaxial or simple shear) tests in the laboratory. Such data are usually computer storage-intensive and are not maintained for a long period. However, an attempt was made to collect the available and reliable data to characterize the strain energy. Most of the data were obtained in connection with various recent Bechtel projects. The laboratory data used in this study are from:

- The cyclic stress- and strain-controlled tests on Monterey No. 0 sand, performed at the University of California, Berkeley.

- The stress-controlled tests on soil samples from the Savannah River Site (SRS), performed at the University of California, Berkeley.

- The cyclic torsional shear tests on clean and silty sands, performed at the University of Colorado.

- The cyclic triaxial tests on clean sands, performed at Wayne State University.

- The summary of the laboratory data reduced to a set of relationships to compute strain energy, as developed by Figueroa et al.

Altogether, a total of 150 cyclic test data sets have been processed. A limited number of these were excluded in the process due to peculiar stress and strain patterns and incompleteness of the respective time histories. The computation of the strain energy from each data set and a discussion on the validity of each group of tests follow.

2.1 STRAIN ENERGY COMPUTATION

In a typical cyclic laboratory test, the stress, strain and pore pressure time histories are recorded. Typical recorded time histories for a strain-controlled cyclic triaxial test are shown in Figure 2.1. Hysteresis loops can be developed from the shear stress and strain time histories. The hysteresis loops corresponding to the stress and strain time histories shown in Figure 2.1 are shown in Figure 2.2. From the shear stress, $\tau(t)$, and the shear strain, $\gamma(t)$ at time t, the time history of the total strain energy up to time t, E(t), is computed from:

$$E(T) = \sum_{t=0}^{T} \bar{\tau}(t).\Delta\gamma(t) \qquad (2.1)$$

where t is the time, $\sum$ is summation over the time increment Δt up to time t, $\bar{\tau}(t)$ is the average shear stress from time t to $t + \Delta t$, and $\Delta\gamma(t)$ is the shear strain increment from time t to $t + \Delta t$. The strain energy for each cycle of loading amounts to the area inside the hysteresis loop. The computation of the instantaneous energy and its summation over time intervals were performed until the onset of the liquefaction, at which time the pore pressure ratio reached a value of unity. The summation of the energy at this time, E_{Liq}, was used as the measure of the capacity of the soil sample against initial liquefaction occurrence in terms of the strain energy.

2.2 CYCLIC TRIAXIAL TESTS ON MONTEREY NO. 0 SAND, PERFORMED AT THE UNIVERSITY OF CALIFORNIA, BERKELEY (UCB)

The data were prepared as part of the Bechtel in-house technical research led by Arango (1994). The gradation curve for Monterey No. 0 sand is shown in Figure 2.3. The tests were both stress- and strain-controlled. The samples were prepared at relative densities ranging from 40% to 60%, and the loads were applied at frequencies ranging from 0.10 Hz to 20 Hz. All tests were conducted at a confining pressure of 100 kPa. More detailed information about the testing program and the testing apparatus may be obtained from Riemer (Riemer et al., 1994). A total of 20 tests from this group were incorporated in this study. A summary of the test data, including the computed total strain energy to the onset of liquefaction for each test, is presented in Table 2.1. The recorded stress, strain, pore pressure (in terms of the pore pressure ratio r_u), and the computed time history of the strain energy for each test are shown in Appendix A. In addition to the strain energy time history, the energy time history normalized to the total energy at the time of $r_u = 1$, (E_{Liq}), is also plotted and compared with the r_u time history, e. g. see Page A-3. As shown in these plots, the normalized strain energy increase follows the pattern of the pore pressure ratio increase and, on the average, shows a very good agreement for all the tests at a wide range of frequencies and at all the relative densities tested. The agreement holds whether the data are obtained from the stress- or the strain-controlled tests. As stated earlier, this observation was the basis for formulation of the strain energy method.

A summary of the results in terms of the total energy as a function of relative density is shown in Figure 2.4. As expected, the total energy to the onset of liquefaction increases as the relative density of the sample increases. It can also be observed in this figure that the scatter in the strain-controlled test data is less severe than the scatter in the data from the stress-controlled test results.

The strain energy for each test as a function of the frequency of loading is plotted in Figure 2.5, which shows a decreasing total energy as the frequency of loading increases. In this figure, the frequency of loading has a more pronounced effect on the total energy obtained from the stress-controlled tests than the strain-controlled tests. In addition, the strain-controlled tests require lower total energy to develop initial liquefaction as compared to the stress-controlled tests. It should also be noted that for a typical strain-controlled test, the pore pressure build-up takes place at a much faster rate in the first several cycles of loading. On the other hand, in the stress-controlled test, the rate of pore pressure build-up increases towards the end of loading cycles. This observation can also be made from the shape and size of the respective hysteresis loops. In the strain-controlled tests, the largest loops are the earlier loops, and they decrease in size as the sample degrades due to the pore pressure build-up. The opposite trend takes place in a stress-controlled test, as shown in Appendix A, e. g. Pages A-4 and A-16.

2.3 CYCLIC TRIAXIAL TESTS ON SOIL SAMPLES FROM THE SAVANNAH RIVER SITE, PERFORMED AT THE UNIVERSITY OF CALIFORNIA, BERKELEY (UCB)

The laboratory program for this group of tests was developed as part of one of the Bechtel projects for the Department of Energy (DOE) at the Savannah River Site (SRS). Subsurface conditions for the site under consideration are shown in Figure 2.6. The soil layers of primary interest were the Tobacco Road (TR3 and TR4) and the Santee formations.

A comprehensive site investigation program was conducted at the site. Relevant average soil properties of each soil layer at the SRS site, shown in Figure 2.6 are summarized in Table 2.2.

Most of the cyclic load tests were conducted on undisturbed soil samples from the Tobacco Road formation from depths of 16 m to 23 m. As shown in Table 2.2, this material has an average fines content of 23%, including 9% clay content (minus 2 micron particle size) and an average plasticity index of 25%. A typical gradation curve for the Tobacco Road Materials is shown in Figure 2.7. A total of 22 cyclic stress-controlled tests at 1 Hz were performed (Riemer and Seed, 1994). The confining pressure ranged from 200 kPa to 750 kPa. A summary of the test data and of the total strain energy for each test in this group is presented in Table 2.3. Notable characteristic of this group of tests is the large confining pressure used in the tests and the relatively large fines content in the soil samples tested. The plots of shear stress, strain, total energy and normalized energy, pore pressure ratios, and the hysteresis loops for this group are shown in Appendix B. As shown in this appendix, the increase of the normalized energy in general follows the pore pressure ratio increase up to the pore pressure ratio of one. A summary of the total energy as a function of the confining pressure is shown in Figure 2.8. As expected, the total strain energy is greater for the samples tested at higher confining pressures. For the same confining pressure, tests on samples having a higher dry density resulted in the development of a larger total energy. This trend is similar to the trend observed in Figure 2.4 with respect to the relative density of the samples.

2.4 CYCLIC TORSIONAL TESTS ON SOIL SAMPLES, PERFORMED AT THE UNIVERSITY OF COLORADO (UOC)

The time histories for this group of tests were provided by Koester (1992). The test data were developed as part of the research work for a doctoral dissertation at the University of Colorado (UOC). Only the time histories from nine tests were available. The tests were performed using the stress-controlled hollow torsional simple shear test apparatus. The cyclic loading was applied at a frequency of 0.1 Hz. Both clean sands and sands with fines content up to 45% were tested.

The silty sand samples were prepared with a density such that the void ratio of the sample matched that of the parent clean sand at the selected relative densities. The confining pressure in the tests ranged from 200 kPa to 300 kPa. A summary of the soil data and the test results in terms of the total energy is shown in Table 2.4, whereas the gradation curve is shown in Figure 2.9. A more detailed description of the sample preparation and testing program can be obtained from Koester (1992).

The time histories of the stress, strain, pore pressure ratio, total energy, and hysteresis loops for this group are presented in Appendix C. In general, the hysteresis loops in this group of tests start with a few narrow loops followed by one or two large loops before reaching the initial liquefaction stage, suggesting a sudden contraction and collapse of the samples. This behavior may have been the cause of the relatively low densities of the samples. The test results in terms of the total strain energy as a function of relative density for the clean sand are shown in Figure 2.10. The results show a relatively large scatter in the energy at low relative densities. The results of the silty sand samples as a function of the confining pressure are shown in Figure 2.11. These results show relatively less scatter in the data.

2.5 CYCLIC TRIAXIAL TESTS ON SOIL SAMPLES FROM THE NORTHRIDGE SITE, PERFORMED AT THE UNIVERSITY OF CALIFORNIA, BERKELEY (UCB)

The samples for this group of tests were prepared as part of the National Science Foundation (NSF)/Bechtel research work led by Arango (Arango and Migues, 1996). As part of the test program, a total of 8 reconstituted clean sand samples were prepared and tested in a stress-controlled cyclic triaxial test device. The samples were prepared at relative densities ranging from 35% to 90%. The gradation curves for two soil samples are shown in Figure 2.12. A summary of the test data and of the computed total strain energy is presented in Table 2.5. Time history plots are included in Appendix D. Test results in terms of the total strain energy as a function of relative density is presented in

Figure 2.13. As shown previously, the total strain energy increases as the relative density increases.

2.6 CYCLIC TRIAXIAL TESTS ON CLEAN SANDS, PERFORMED AT WAYNE STATE UNIVERSITY (WSU)

The summary results of 91 cyclic triaxial stress-controlled tests on clean sands was presented in the doctoral dissertation by Al-Khatib (1994). The tests were performed at Wayne State University (WSU). All tests were performed on clean sands consisting of Monterey No. 0 and Kasumigaura sand (K-sand). The gradation curves for the two sands are shown in Figure 2.14. The breakdown of the tests is as follows:

- 28 tests on K-sand at low frequency with cyclic reversal loading (two-way cyclic loading)
- 28 tests on Monterey No. 0 sand at low frequency with cyclic reversal loading
- 25 tests on Monterey No. 0, low frequency and one-way loading
- 10 tests on Monterey No. 0 with earthquake simulated loading using the El Centro and Taft records

Time histories of the test data were not available; however, the total energy in terms of axial stress/strain has been reported by Al-Khatib (1994). The total energy was converted to the total energy in terms of the shear strain and shear stress attributes and are summarized in Table 2.6. The results in terms of the total strain energy as a function of relative density for the cyclic reversal loading cases are shown in Figure 2.15 which shows a similar trend to the one observed in the UCB data (see Figure 2.4). As shown in this figure, both the K-sand and the Monterey No. 0 sand have similar capacity in terms of total energy and consistently show an increase of the total energy with an increase in the relative density. The scatter in the data appear to be minimal.

The results in terms of the cyclic one-way and two-way loadings are compared in Figure 2.16. As shown, the two-way loading results in lower total energy capacity as compared to the one-way loading. This trend is consistent with the intuitive indication that soil resistance to liquefaction will be higher due to the less damaging effects of the one-way loading. Finally, the results of the two-way loading are compared with the earthquake loading in Figure 2.17. The earthquake loading results in the lower total energy. Altogether, the results of this group of tests appear to be more uniform with little scatter in terms of the total energy.

2.7 SUMMARY DATA BY FIGUEROA et al.

A series of torsional shear hollow cylinder tests were performed on both clean sand and silty sand by Figueroa et al. (1994, 1995). Samples from the Reid Bedford sand (clean sand) were tested at relative densities ranging from 50% to 70%. The silty sand from the

Lower San Fernando Dam (LSFD) were tested at relative densities of 57% to 92%. The gradation curves for both materials are shown in Figure 2.18. Each sample was successively tested at confining pressures of 41.4 kPa, 82.7 kPa, and 124.1 kPa. Actual data points for this group of tests are not available. However, the authors performed regression analyses of the test results in terms of total strain energy and identified the most relevant parameters affecting the results of clean sand and silty sand. Based on the test results, the authors recommended the following relationships (Figueroa et al., 1995):

Clean sand

$$\text{Log } \delta E = 2.062 + 0.0039\ \sigma_c' + 0.0124\ D_r \tag{2.2}$$

Silty sand

$$\text{Log } \delta E = 2.529 + 0.00474\ \sigma_c' \tag{2.3}$$

where δE is the total strain energy in Joules/m^3, σ_c' is the effective confining pressure in kPa, and D_r is the relative density in percent. The relationship for clean sand shows the confining pressure as one of the variables. However, the importance of this parameter is very small due to the small coefficient associated with this parameter in Equation 2.2.

2.8 SUMMARY OF ALL LABORATORY DATA

Based on the results of the five groups of tests outlined above, summary plots have been prepared to evaluate consistency between the various test groups.

For clean sand, the results of tests on Monterey No. 0 performed at the UCB (20 tests), the data on clean sands from the WSU (81 tests), the data from the Northridge samples (8 tests) also tested at the UCB, and the data from the UOC (4 tests) are compared with the relationship by Figueroa et al. in Figure 2.19. As shown in this figure, except for the data from the UOC, the remaining groups show a quite consistent pattern of the rate of energy dissipation and of the total energy absorbed. The confining pressure used in the tests at the UOC was at least 2 to 3 times larger than the pressure used for the rest of the tests. Also, the differences in the shape and size of the sand particles may have contributed to some of the differences in the results. For relative densities in the range of 40% to 70%, the data from UCB, WSU, and Figueroa et al. are in relatively good agreement.

For silty sands, the results from the Savannah River Site (SRS) are compared with the data from the UOC and the relationship by Figueroa et al. in Figure 2.20. The fines content in each group are: 28% for the samples from the lower San Fernando Dam (Figuero et al., 1995), 20% to 45% for soil samples tested at UOC (Koester, 1992), and the average 23% for samples taken from the SRS site. The Plasticity Index of the materials in the groups also varies from 10 to 25%. Unfortunately, the confining pressures used for each group of tests do not overlap. Nevertheless, each group of results follows the pattern of the previous group and a consistent trend is maintained.

All of the results indicate that for clean sands, the energy to liquefaction can be quantified in terms of the relative density and the confining pressure. However, the limited data available does not permit a study of effects of the grain size and shape on the total energy.

Summary of the results for silty sands also shows that the energy to liquefaction can be quantified in terms of the effective confining pressure. However, the effects of the plasticity index, the amount, and the type of fine need to be studied in the future.

As stated earlier in the report, the scope of this feasibility study did not include laboratory testing. However, comparison of the data available from the various researchers and practitioners at different institutes shows remarkably good agreement. This observation leads to the conclusion that development of generic total strain energy relationship as a measure of soil resistance against liquefaction by means of laboratory testing is feasible. If consistent sampling, sample handling, and testing methods and specifications are followed, the results are expected to be more consistent and vary within narrower limits.

Table 2.1 - Summary of the Cyclic Triaxial Test Data on Monterey No. 0 Sand Performed at University of California, Berkeley

No.	Test ID	Sample	D_r(%)	E_{liq} (J/m^3)	FC (%)	γ_d (kN/m^3)	Control	σ_c' (kPa)	Freq. (Hz)	Load Shape
1	MONT4	Monterey No.0	61.8	2677	2	15.6	Stress	100	1	Sinusoidal 2-way
2	MONT10	Monterey No.0	61.0	1933	2	15.5	Stress	100	1	Sinusoidal 2-way
3	MONT11	Monterey No.0	60.6	988	2	15.5	Stress	100	10	Sinusoidal 2-way
4	MONT12	Monterey No.0	61.0	2481	2	15.5	Stress	100	1	Sinusoidal 2-way
5	MONT14	Monterey No.0	60.2	1583	2	15.5	Stress	100	20	Sinusoidal 2-way
6	MONT15	Monterey No.0	60.5	1245	2	15.5	Stress	100	10	Sinusoidal 2-way
7	MONT17	Monterey No.0	61.0	1878	2	15.5	Strain	100	1	Sinusoidal 2-way
8	MONT18	Monterey No.0	61.0	1187	2	15.5	Strain	100	10	Sinusoidal 2-way
9	MONT19	Monterey No.0	60.6	1483	2	15.5	Strain	100	15	Sinusoidal 2-way
10	MONT20	Monterey No.0	40.9	851	2	15.0	Strain	100	1	Sinusoidal 2-way
11	MONT21	Monterey No.0	41.8	880	2	15.0	Strain	100	1	Sinusoidal 2-way
12	MONT22	Monterey No.0	42.3	1078	2	15.0	Strain	100	1	Sinusoidal 2-way
13	MONT24	Monterey No.0	51.8	2736	2	15.3	Stress	100	1	Sinusoidal 2-way
14	MONT25	Monterey No.0	50.4	2985	2	15.3	Stress	100	1	Sinusoidal 2-way
15	MONT26	Monterey No.0	49.9	2769	2	15.2	Stress	100	1	Sinusoidal 2-way
16	MONT30	Monterey No.0	41.9	708	2	15.0	Strain	100	10	Sinusoidal 2-way
17	MONT33	Monterey No.0	40.5	829	2	15.0	Strain	100	10	Sinusoidal 2-way
18	MONT35	Monterey No.0	61.8	4211	2	15.6	Stress	100	0.1	Sinusoidal 2-way
19	MONT37	Monterey No.0	61.6	1388	2	15.5	Strain	100	1	Sinusoidal 2-way
20	MONT38	Monterey No.0	61.8	704	2	15.6	Strain	100	10	Sinusoidal 2-way

Table 2.2 - Average Material Properties at the SRS Site

PARAMETER/SOIL LAYER	TR3/TR4 AVG	SANTEE AVG
SPT N-VALUE	15	58
SHEAR WAVE VELOCITY, m/sec (ft/s)	364 (1193)	381 (1251)
CONE TIP RESISTANCE, Qc, tsf	52	111
FRICTION RATIO	3	1
Qc/N	3.5	1.9
PERCENT FINES (<.074 mm)	23	25
PERCENT SILT	9	12
PERCENT CLAY (<.002 mm)	14	13
PLASTICITY INDEX, %	25	31
LIQUID LIMIT, %	45	55
PLASTICITY INDEX (-200 MATERIAL), %	101	78
LIQUID LIMIT (-200 MATERIAL), %	144	112
DRY DENSITY, KN/m^3 (pcf)	16 (102)	13.8 (88)
WATER CONTENT, %	22	32
WET DENSITY, KN/m^3 (pcf)	19.6 (125)	6.4 (116)
SPECIFIC GRAVITY	2.68	2.67
VOID RATIO	0.625	0.876
AT-REST LAT. EARTH PRESS. COEFF	0.46	0.44
OVERCONSOLIDATION RATIO	1.89	1.26
TOTAL COHESION, kPa (ksf)	91 (1.9)	-
TOTAL FRICTION ANGLE, degree	13	-
EFFECTIVE COHESION, kPa (ksf)	0	0
EFFECTIVE FRICTION ANGLE, degree	33	34
DILATION ANGLE, degree	1.7	1.3

Table 2.3 - Summary of the Cyclic Triaxial Test Data on SRS Soil Samples Performed at University of California, Berkeley

No.	Test ID	Sample	D_r(%)	E_{liq} (J/m^3)	FC (%)	γ_d (kN/m^3)	Control	σ_c' (kPa)	Freq. (Hz)	Load Shape
1	B23P2BCY	Santee	N/A	14675	33.7	16.0	Stress	400	1	Sinusoidal 2-way
2	B23P2MCY	Santee	N/A	16782	35.6	16.4	Stress	400	1	Sinusoidal 2-way
3	B23P2TCY	Santee	N/A	11402	32.6	16.8	Stress	400	1	Sinusoidal 2-way
4	B23P3BCY	Tobacco Rd.	N/A	4929	16.6	16.4	Stress	200	1	Sinusoidal 2-way
5	B23P3MCY	Tobacco Rd.	N/A	5585	18.5	15.2	Stress	200	1	Sinusoidal 2-way
6	B23P3TCY	Tobacco Rd.	N/A	2924	20.5	16.6	Stress	200	1	Sinusoidal 2-way
7	B12P5BCY	Tobacco Rd.	N/A	14918	27.0	15.8	Stress	300	1	Sinusoidal 2-way
8	B12P5MCY	Tobacco Rd.	N/A	49114	26.8	16.8	Stress	300	1	Sinusoidal 2-way
9	B12P5TCY	Tobacco Rd.	N/A	5450	22.3	18.0	Stress	300	1	Sinusoidal 2-way
10	B12P7BCY	Tobacco Rd.	N/A	7666	15.7	15.9	Stress	375	1	Sinusoidal 2-way
11	B12P7MCY	Tobacco Rd.	N/A	14482	17.0	16.3	Stress	375	1	Sinusoidal 2-way
12	B12P7TCY	Tobacco Rd.	N/A	3852	15.7	16.2	Stress	375	1	Sinusoidal 2-way
13	B2P5BCYC	Tobacco Rd.	N/A	11672	25.4	14.7	Stress	500	1	Sinusoidal 2-way
14	B2P5MCYC	Tobacco Rd.	N/A	23344	29.6	15.4	Stress	500	1	Sinusoidal 2-way
15	B2P5TCYC	Tobacco Rd.	N/A	8819	26.6	16.7	Stress	500	1	Sinusoidal 2-way
16	B23P4BCY	Tobacco Rd.	N/A	21667	11.4	14.6	Stress	750	1	Sinusoidal 2-way
17	B23P4MCY	Tobacco Rd.	N/A	36680	16.5	15.5	Stress	700	1	Sinusoidal 2-way
18	B23P4TCY	Tobacco Rd.	N/A	17968	28.0	N/A	Stress	750	1	Sinusoidal 2-way
19	B29P2TCY	Tobacco Rd.	N/A	23637	23.0	16.7	Stress	750	1	Sinusoidal 2-way
20	B2P6BCY	Tobacco Rd.	N/A	17985	18.9	16.7	Stress	725	1	Sinusoidal 2-way
21	B2P6MCY	Tobacco Rd.	N/A	19831	20.1	16.5	Stress	743	1	Sinusoidal 2-way
22	B2P6TCYC	Tobacco Rd.	N/A	14446	22.4	16.0	Stress	750	1	Sinusoidal 2-way

Table 2.4 - Summary of the Cyclic Torsional Test Data on Clean and Silty Sands Performed at University of Colorado

No.	Test ID	Sample	D_r(%)	E_{liq} (J/m^3)	FC (%)	γ_d (kN/m^3)	P. I.	Control	σ_c' (kPa)	Freq. (Hz)	Load Shape
1	UOFC5	F11	32.6	3728	0	14.5		Stress	199.9	0.1	Sinusoidal 2-way
2	UOFC7	F11	41.0	12495	0	14.7		Stress	204.8	0.1	Sinusoidal 2-way
3	UOFC9	F11	42.0	16997	0	14.8		Stress	304.1	0.1	Sinusoidal 2-way
4	UOFC13	F43	N/A	3450	20	15.3	10.0	Stress	299.9	0.1	Sinusoidal 2-way
5	UOFC14	F46	N/A	4753	20	15.2	25.0	Stress	199.9	0.1	Sinusoidal 2-way
6	UOFC15	F46	N/A	2485	20	15.2	25.0	Stress	201.3	0.1	Sinusoidal 2-way
7	UOFC17	F64	N/A	3427	45	16.2	15.0	Stress	203.4	0.1	Sinusoidal 2-way
8	UOFC18	F64	N/A	3993	45	16.2	15.0	Stress	190.3	0.1	Sinusoidal 2-way
9	UOFC23	F11	45.3	7437	0	14.9		Stress	199.9	0.1	Sinusoidal 2-way

Table 2.5 - Summary of the Cyclic Triaxial Test Data on Northridge Samples Performed at University of California, Berkeley

No.	Test ID	Sample	D_r(%)	E_{liq} (J/m^3)	FC (%)	γ_d (kN/m^3)	Control	σ_c' (kPa)	Freq. (Hz)	Load Shape
1	BTC2CY1	Northridge Sand	58.3	5930	5	14.5	Stress	100	1	Sinusoidal 2-way
2	BTC2CY2	Northridge Sand	78.4	2247	5	15.5	Stress	100	1	Sinusoidal 2-way
3	BTC3CY1	Northridge Sand	82.3	5146	5	15.7	Stress	100	1	Sinusoidal 2-way
4	BTC3CY2	Northridge Sand	89.9	3813	5	16.1	Stress	100	1	Sinusoidal 2-way
5	BTC3CY3	Northridge Sand	97.2	36156	5	16.5	Stress	100	1	Sinusoidal 2-way
6	BTC4CY1	Northridge Sand	93.7	7874	5	16.3	Stress	100	1	Sinusoidal 2-way
7	BTC4CY2	Northridge Sand	100.0	6647	5	16.7	Stress	100	1	Sinusoidal 2-way
8	BTC6CY1	Northridge Sand	35.2	3206	5	13.5	Stress	100	1	Sinusoidal 2-way

Table 2.6 - Summary of the Cyclic Triaxial Test Data on Clean Sands Performed at Wayne State University

No.	Test ID	Sample	D_r(%)	E_{liq} (J/m^3)	FC (%)	γ_d (kN/m^3)	Control	σ_c' (kPa)	Freq. (Hz)	Load Shape
1	WS6-1-1	K-Sand	67.0	2211	2.5	15.8	Stress	44.3	0.1	Sinusoidal 2-way
2	WS6-1-2	K-Sand	65.0	2397	2.5	15.7	Stress	56.5	0.1	Sinusoidal 2-way
3	WS6-1-3	K-Sand	59.0	1893	2.5	15.4	Stress	68.9	0.1	Sinusoidal 2-way
4	WS6-1-4	K-Sand	40.0	397	2.5	14.7	Stress	33.8	0.1	Sinusoidal 2-way
5	WS6-1-5	K-Sand	32.0	293	2.5	14.4	Stress	38.6	0.1	Sinusoidal 2-way
6	WS6-1-6	K-Sand	74.0	2163	2.5	16.1	Stress	26.2	0.1	Sinusoidal 2-way
7	WS6-1-7	K-Sand	52.0	424	2.5	15.2	Stress	22.8	0.1	Sinusoidal 2-way
8	WS6-1-8	K-Sand	66.0	1690	2.5	15.7	Stress	36.5	0.1	Sinusoidal 2-way
9	WS6-1-9	K-Sand	34.0	289	2.5	14.5	Stress	35.2	0.1	Sinusoidal 2-way
10	WS6-1-10	K-Sand	48.0	486	2.5	15.0	Stress	31.8	0.1	Sinusoidal 2-way
11	WS6-1-11	K-Sand	42.0	394	2.5	14.8	Stress	31.9	0.1	Sinusoidal 2-way
12	WS6-1-12	K-Sand	23.0	1857	2.5	14.1	Stress	35.2	0.1	Sinusoidal 2-way
13	WS6-1-13	K-Sand	29.0	223	2.5	14.3	Stress	35.3	0.1	Sinusoidal 2-way
14	WS6-1-14	K-Sand	50.0	463	2.5	15.1	Stress	27.0	0.1	Sinusoidal 2-way
15	WS6-1-15	K-Sand	38.0	320	2.5	14.6	Stress	32.5	0.1	Sinusoidal 2-way
16	WS6-1-16	K-Sand	55.0	642	2.5	15.3	Stress	32.4	0.1	Sinusoidal 2-way
17	WS6-1-17	K-Sand	51.0	615	2.5	15.1	Stress	35.2	0.1	Sinusoidal 2-way
18	WS6-1-18	K-Sand	58.0	899	2.5	15.4	Stress	35.9	0.1	Sinusoidal 2-way
19	WS6-1-19	K-Sand	37.0	309	2.5	14.6	Stress	34.5	0.1	Sinusoidal 2-way
20	WS6-1-20	K-Sand	47.0	467	2.5	15.0	Stress	33.1	0.1	Sinusoidal 2-way
21	WS6-1-21	K-Sand	39.0	379	2.5	14.7	Stress	34.5	0.1	Sinusoidal 2-way
22	WS6-1-22	K-Sand	61.0	1120	2.5	15.5	Stress	35.2	0.1	Sinusoidal 2-way
23	WS6-1-23	K-Sand	56.0	739	2.5	15.3	Stress	34.6	0.1	Sinusoidal 2-way
24	WS6-1-24	K-Sand	30.0	237	2.5	14.3	Stress	36.0	0.1	Sinusoidal 2-way
25	WS6-1-25	K-Sand	57.0	768	2.5	15.4	Stress	33.9	0.1	Sinusoidal 2-way
26	WS6-1-26	K-Sand	38.0	358	2.5	14.6	Stress	35.2	0.1	Sinusoidal 2-way
27	WS6-1-27	K-Sand	44.0	456	2.5	14.9	Stress	34.5	0.1	Sinusoidal 2-way

Table 2.6 - Summary of the Cyclic Triaxial Test Data on Clean Sands Performed at Wayne State University (Continued)

No.	Test ID	Sample	D_r(%)	E_{liq} (J/m^3)	FC (%)	γ_d (kN/m^3)	Control	σ_c' (kPa)	Freq. (Hz)	Load Shape
28	WS6-1-28	K-Sand	31.0	268	2.5	14.4	Stress	37.2	0.1	Sinusoidal 2-way
29	WS6-2-1	Monterey No. 0	62.0	1162	2	15.8	Stress	32.9	0.1	Sinusoidal 2-way
30	WS6-2-2	Monterey No. 0	57.0	802	2	15.6	Stress	33.6	0.1	Sinusoidal 2-way
31	WS6-2-3	Monterey No. 0	36.0	302	2	14.8	Stress	32.5	0.1	Sinusoidal 2-way
32	WS6-2-4	Monterey No. 0	39.0	361	2	14.9	Stress	34.3	0.1	Sinusoidal 2-way
33	WS6-2-5	Monterey No. 0	38.0	424	2	14.8	Stress	43.1	0.1	Sinusoidal 2-way
34	WS6-2-6	Monterey No. 0	52.0	710	2	15.4	Stress	41.4	0.1	Sinusoidal 2-way
35	WS6-2-7	Monterey No. 0	58.0	1083	2	15.6	Stress	42.9	0.1	Sinusoidal 2-way
36	WS6-2-8	Monterey No. 0	60.0	1264	2	15.7	Stress	39.6	0.1	Sinusoidal 2-way
37	WS6-2-9	Monterey No. 0	65.0	1747	2	15.9	Stress	42.7	0.1	Sinusoidal 2-way
38	WS6-2-10	Monterey No. 0	59.0	926	2	15.7	Stress	34.4	0.1	Sinusoidal 2-way
39	WS6-2-11	Monterey No. 0	66.0	1749	2	15.9	Stress	40.8	0.1	Sinusoidal 2-way
40	WS6-2-12	Monterey No. 0	26.0	215	2	14.4	Stress	34.5	0.1	Sinusoidal 2-way
41	WS6-2-13	Monterey No. 0	32.0	252	2	14.6	Stress	31.0	0.1	Sinusoidal 2-way
42	WS6-2-14	Monterey No. 0	30.0	239	2	14.6	Stress	31.8	0.1	Sinusoidal 2-way
43	WS6-2-15	Monterey No. 0	55.0	762	2	15.5	Stress	37.0	0.1	Sinusoidal 2-way
44	WS6-2-16	Monterey No. 0	54.0	615	2	15.5	Stress	32.4	0.1	Sinusoidal 2-way
45	WS6-2-17	Monterey No. 0	47.0	436	2	15.2	Stress	33.5	0.1	Sinusoidal 2-way
46	WS6-2-18	Monterey No. 0	44.0	413	2	15.1	Stress	32.3	0.1	Sinusoidal 2-way
47	WS6-2-19	Monterey No. 0	42.0	320	2	15.0	Stress	27.7	0.1	Sinusoidal 2-way
48	WS6-2-20	Monterey No. 0	72.0	1179	2	16.2	Stress	16.5	0.1	Sinusoidal 2-way
49	WS6-2-21	Monterey No. 0	28.0	194	2	14.5	Stress	28.1	0.1	Sinusoidal 2-way
50	WS6-2-22	Monterey No. 0	41.0	374	2	15.0	Stress	33.4	0.1	Sinusoidal 2-way
51	WS6-2-23	Monterey No. 0	35.0	251	2	14.7	Stress	28.2	0.1	Sinusoidal 2-way
52	WS6-2-24	Monterey No. 0	51.0	533	2	15.3	Stress	33.8	0.1	Sinusoidal 2-way
53	WS6-2-25	Monterey No. 0	53.0	462	2	15.4	Stress	25.9	0.1	Sinusoidal 2-way
54	WS6-2-26	Monterey No. 0	33.0	232	2	14.7	Stress	27.3	0.1	Sinusoidal 2-way

Table 2.6 - Summary of the Cyclic Triaxial Test Data on Clean Sands Performed at Wayne State University (Continued)

No.	Test ID	Sample	D_r(%)	E_{liq} (J/m^3)	FC (%)	γ_d (kN/m^3)	Control	σ_c' (kPa)	Freq. (Hz)	Load Shape
55	WS6-2-27	Monterey No. 0	49.0	532	2	15.3	Stress	35.3	0.1	Sinusoidal 2-way
56	WS6-2-28	Monterey No. 0	56.0	608	2	15.5	Stress	27.3	0.1	Sinusoidal 2-way
57	WS6-3-1	Monterey No. 0	51.0	2423	2	15.3	Stress	61.0	0.1	Sinusoidal 1-way
58	WS6-3-2	Monterey No. 0	33.0	1114	2	14.7	Stress	67.6	0.1	Sinusoidal 1-way
59	WS6-3-3	Monterey No. 0	30.0	755	2	14.6	Stress	60.4	0.1	Sinusoidal 1-way
60	WS6-3-4	Monterey No. 0	54.0	3151	2	15.5	Stress	67.1	0.1	Sinusoidal 1-way
61	WS6-3-5	Monterey No. 0	53.0	2589	2	15.4	Stress	58.8	0.1	Sinusoidal 1-way
62	WS6-3-6	Monterey No. 0	43.0	1306	2	15.0	Stress	45.3	0.1	Sinusoidal 1-way
63	WS6-3-7	Monterey No. 0	28.0	547	2	14.5	Stress	51.8	0.1	Sinusoidal 1-way
64	WS6-3-8	Monterey No. 0	71.0	4468	2	16.1	Stress	45.6	0.1	Sinusoidal 1-way
65	WS6-3-9	Monterey No. 0	46.0	1679	2	15.1	Stress	52.5	0.1	Sinusoidal 1-way
66	WS6-3-10	Monterey No. 0	61.0	1944	2	15.7	Stress	33.1	0.1	Sinusoidal 1-way
67	WS6-3-11	Monterey No. 0	62.0	2047	2	15.8	Stress	32.3	0.1	Sinusoidal 1-way
68	WS6-3-12	Monterey No. 0	38.0	633	2	14.8	Stress	29.6	0.1	Sinusoidal 1-way
69	WS6-3-13	Monterey No. 0	68.0	2952	2	16.0	Stress	34.7	0.1	Sinusoidal 1-way
70	WS6-3-14	Monterey No. 0	66.0	3813	2	15.9	Stress	48.6	0.1	Sinusoidal 1-way
71	WS6-3-15	Monterey No. 0	73.0	5014	2	16.2	Stress	44.5	0.1	Sinusoidal 1-way
72	WS6-3-16	Monterey No. 0	56.0	2148	2	15.5	Stress	43.1	0.1	Sinusoidal 1-way
73	WS6-3-17	Monterey No. 0	55.0	2031	2	15.5	Stress	42.3	0.1	Sinusoidal 1-way
74	WS6-3-18	Monterey No. 0	58.0	2622	2	15.6	Stress	48.6	0.1	Sinusoidal 1-way
75	WS6-3-19	Monterey No. 0	49.0	1184	2	15.3	Stress	31.9	0.1	Sinusoidal 1-way
76	WS6-3-20	Monterey No. 0	32.0	441	2	14.6	Stress	31.7	0.1	Sinusoidal 1-way
77	WS6-3-21	Monterey No. 0	82.0	5103	2	16.6	Stress	40.5	0.1	Sinusoidal 1-way
78	WS6-3-22	Monterey No. 0	50.0	1073	2	15.3	Stress	26.8	0.1	Sinusoidal 1-way
79	WS6-3-23	Monterey No. 0	52.0	1655	2	15.4	Stress	40.3	0.1	Sinusoidal 1-way
80	WS6-3-24	Monterey No. 0	36.0	511	2	14.8	Stress	27.5	0.1	Sinusoidal 1-way
81	WS6-3-25	Monterey No. 0	37.0	666	2	14.8	Stress	34.1	0.1	Sinusoidal 1-way

Table 2.6 - Summary of the Cyclic Triaxial Test Data on Clean Sands Performed at Wayne State University (Continued)

No.	Test ID	Sample	D_r(%)	E_{liq} (J/m^3)	FC (%)	γ_d (kN/m^3)	Control	σ_c' (kPa)	Freq. (Hz)	Load Shape
82	WS6-4-1	Monterey No. 0	49.0	51	2	15.3	Stress	42.0	Earthquake	Earthquake
83	WS6-4-2	Monterey No. 0	61.0	79	2	15.7	Stress	40.7	Earthquake	Earthquake
84	WS6-4-3	Monterey No. 0	53.0	57	2	15.4	Stress	40.1	Earthquake	Earthquake
85	WS6-4-4	Monterey No. 0	40.0	36	2	14.9	Stress	42.6	Earthquake	Earthquake
86	WS6-4-5	Monterey No. 0	89.0	105	2	17.0	Stress	15.2	Earthquake	Earthquake
87	WS6-4-6	Monterey No. 0	44.0	40	2	15.1	Stress	41.3	Earthquake	Earthquake
88	WS6-4-7	Monterey No. 0	35.0	33	2	14.7	Stress	43.2	Earthquake	Earthquake
89	WS6-4-8	Monterey No. 0	31.0	28	2	14.6	Stress	41.6	Earthquake	Earthquake
90	WS6-4-9	Monterey No. 0	71.0	71	2	16.1	Stress	23.4	Earthquake	Earthquake
91	WS6-4-10	Monterey No. 0	80.0	190	2	16.5	Stress	43.9	Earthquake	Earthquake

Test I.D.:	MONT19	**Controlled Parameter:**	Strain
Relative Density (%):	60.6	**Initial Effective Stress (kPa):**	100
Applied Shear Strain (%):	*0.25*	**Frequency (Hz):**	15

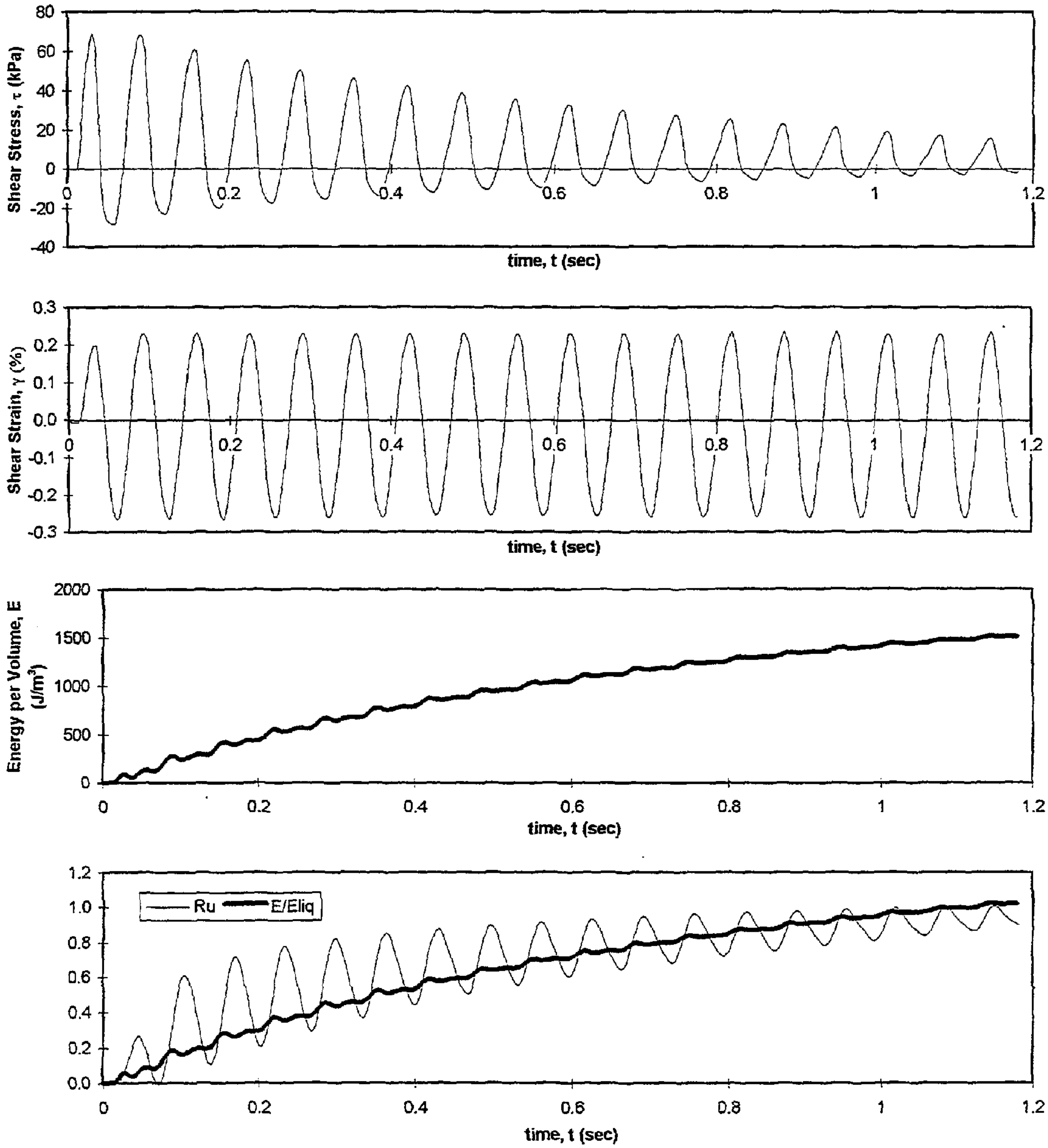

Figure 2.1 - Typical Time History Records of a Strain-Controlled Cyclic Triaxial Test

Test I.D.:	MONT19	**Controlled Parameter:**	Strain
Relative Density (%):	60.6	**Initial Effective Stress (kPa):**	100
Applied Shear Strain (%):	0.25	**Frequency (Hz):**	15

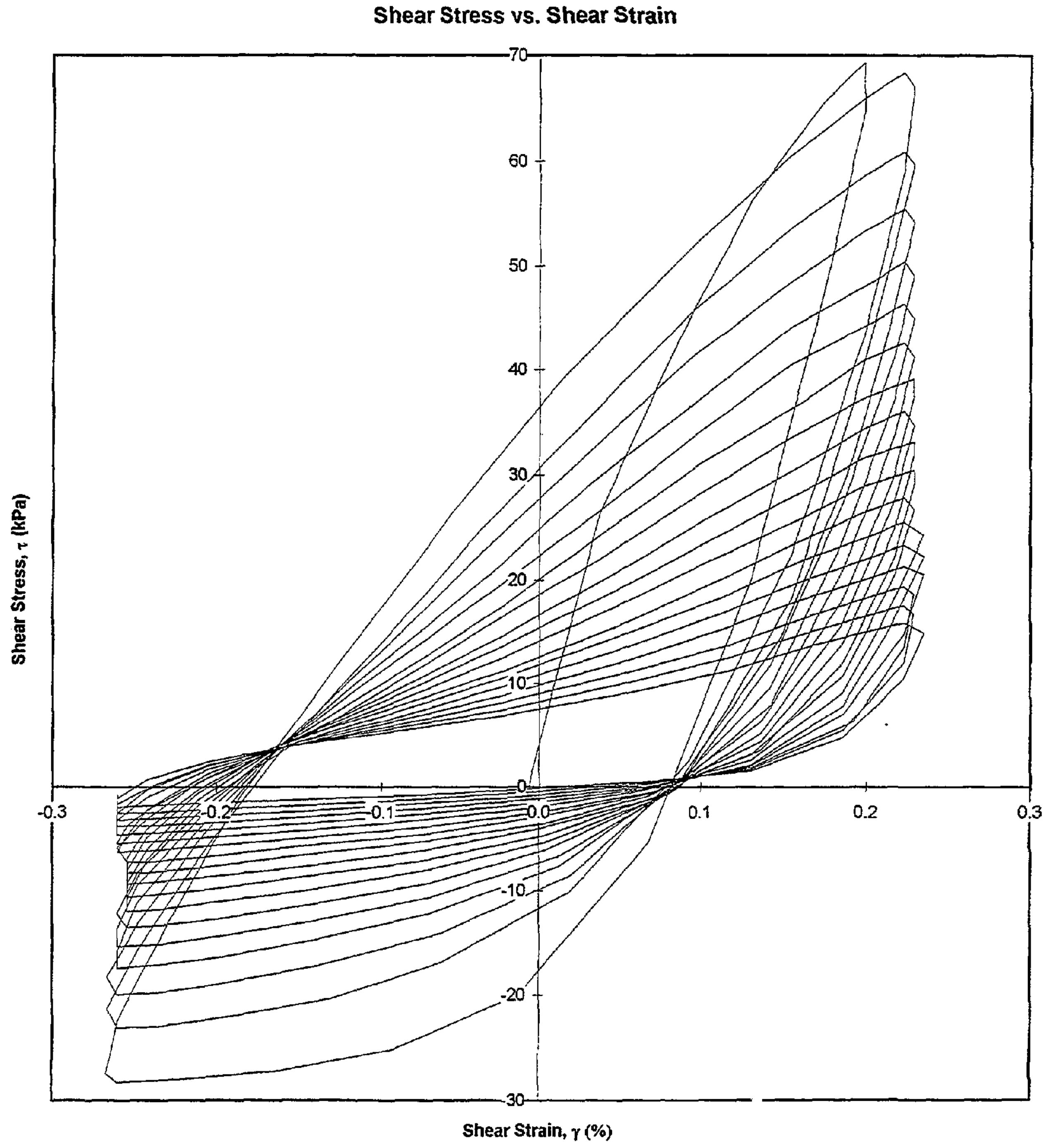

Figure 2.2 - A Typical Plot of Shear Stress - Shear Strain Hysteresis Loops Developed During Cyclic Triaxial Tests

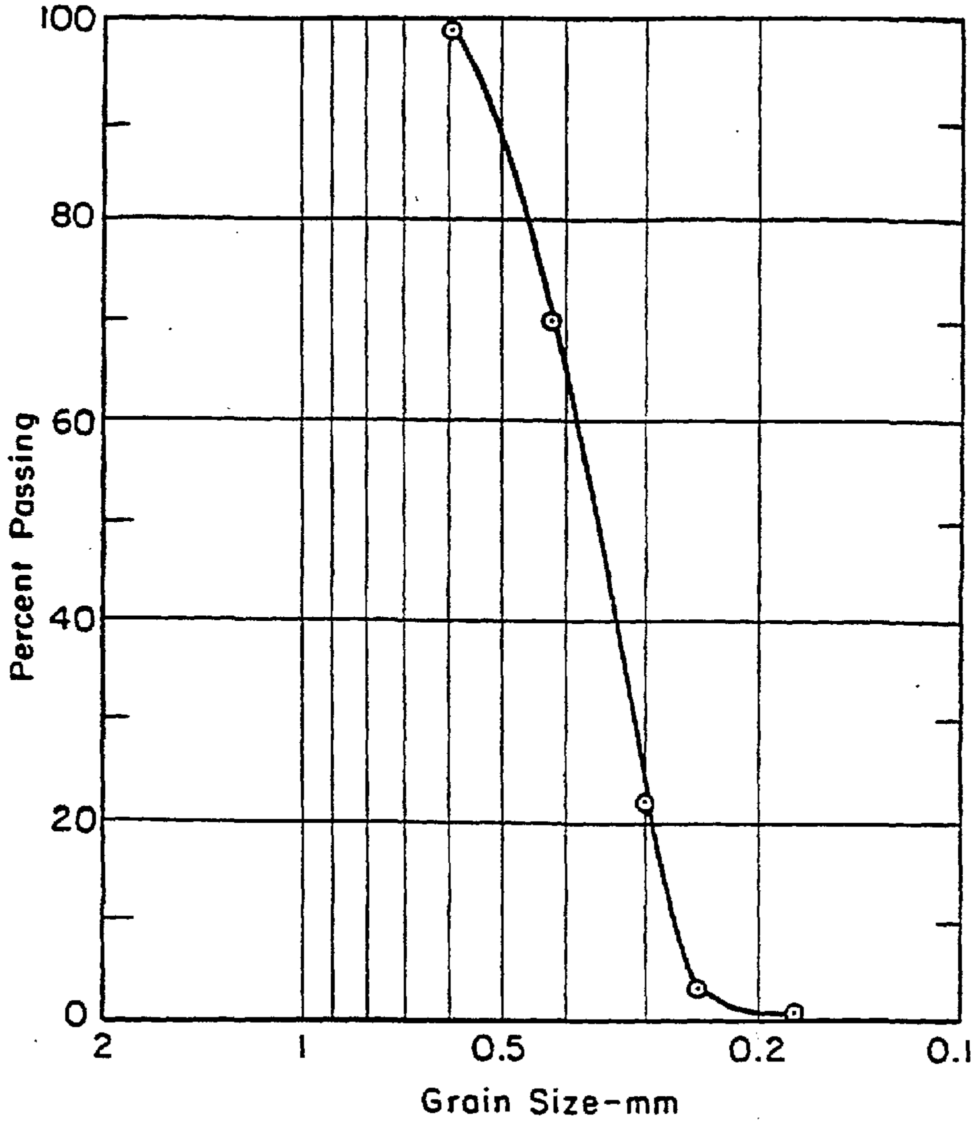

Figure 2.3 - Grain Size Distribution Curve for Monterey No. 0 Sand (Arango, 1994)

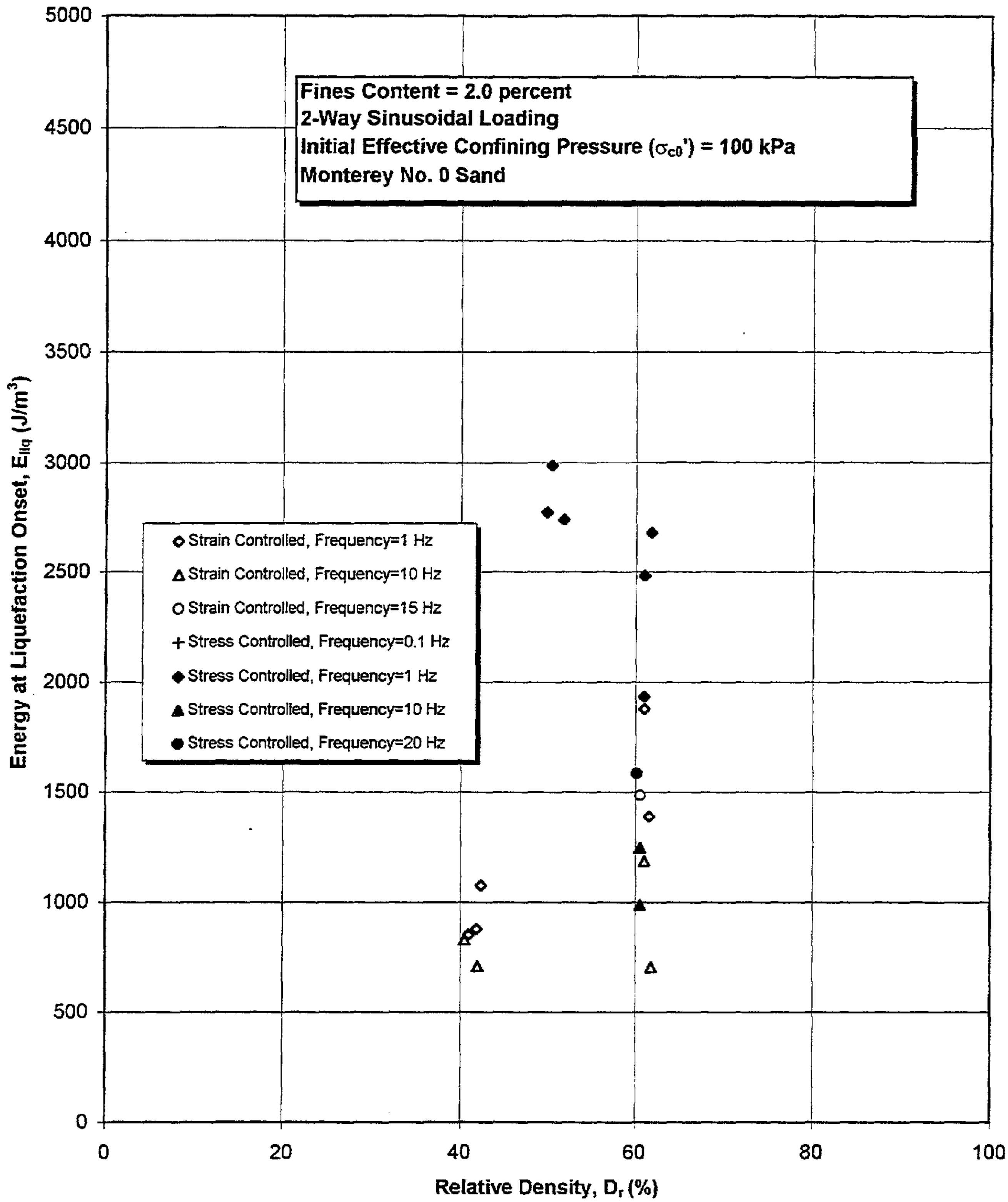

Figure 2.4 - Strain Energy at Liquefaction Onset as a Function of Relative Density for Monterey No. 0 Sand - UCB Data

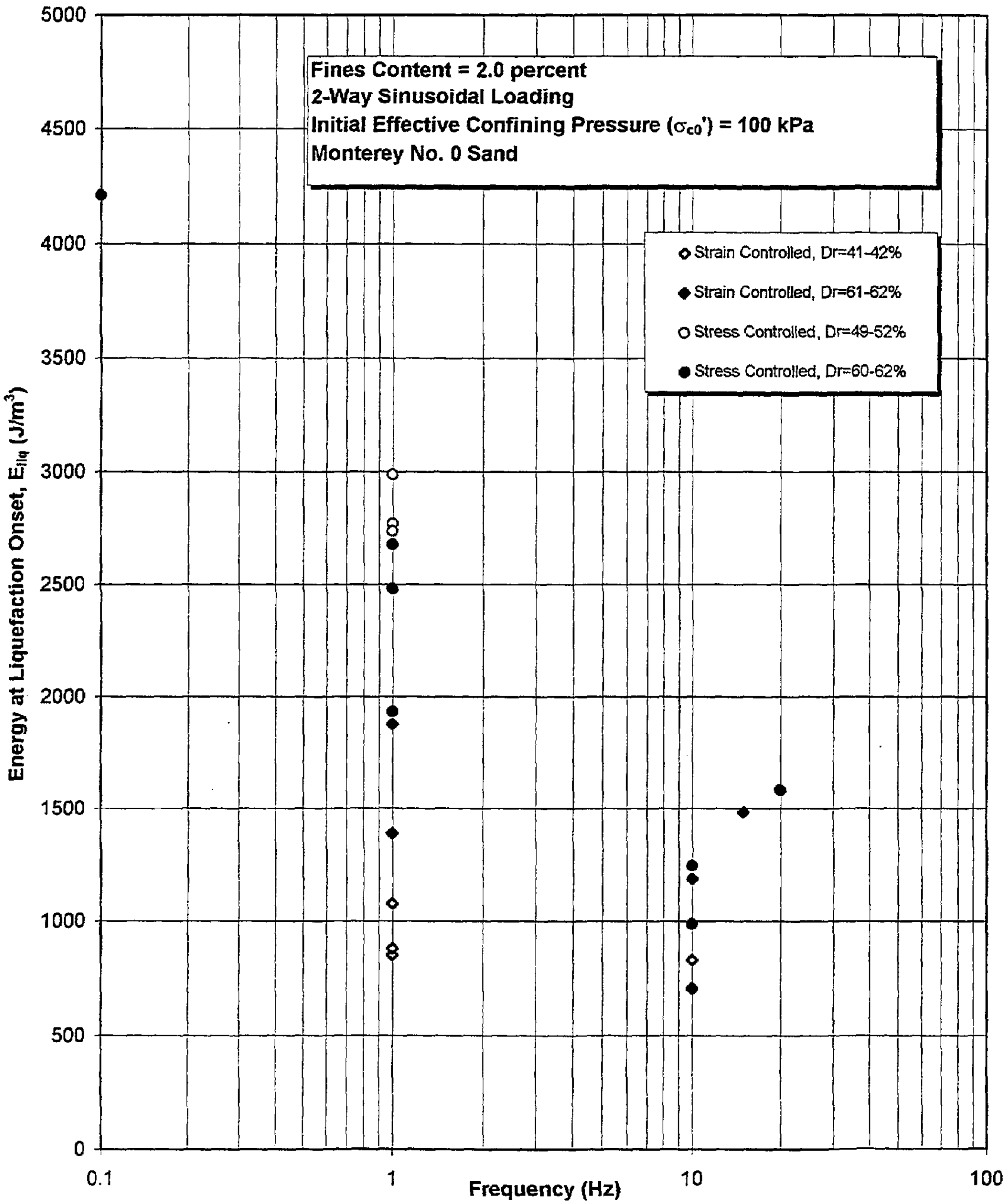

Figure 2.5 - Strain Energy at Liquefaction Onset as a Function of Frequencies of Loading for Monterey No. 0 Sand - UCB Data

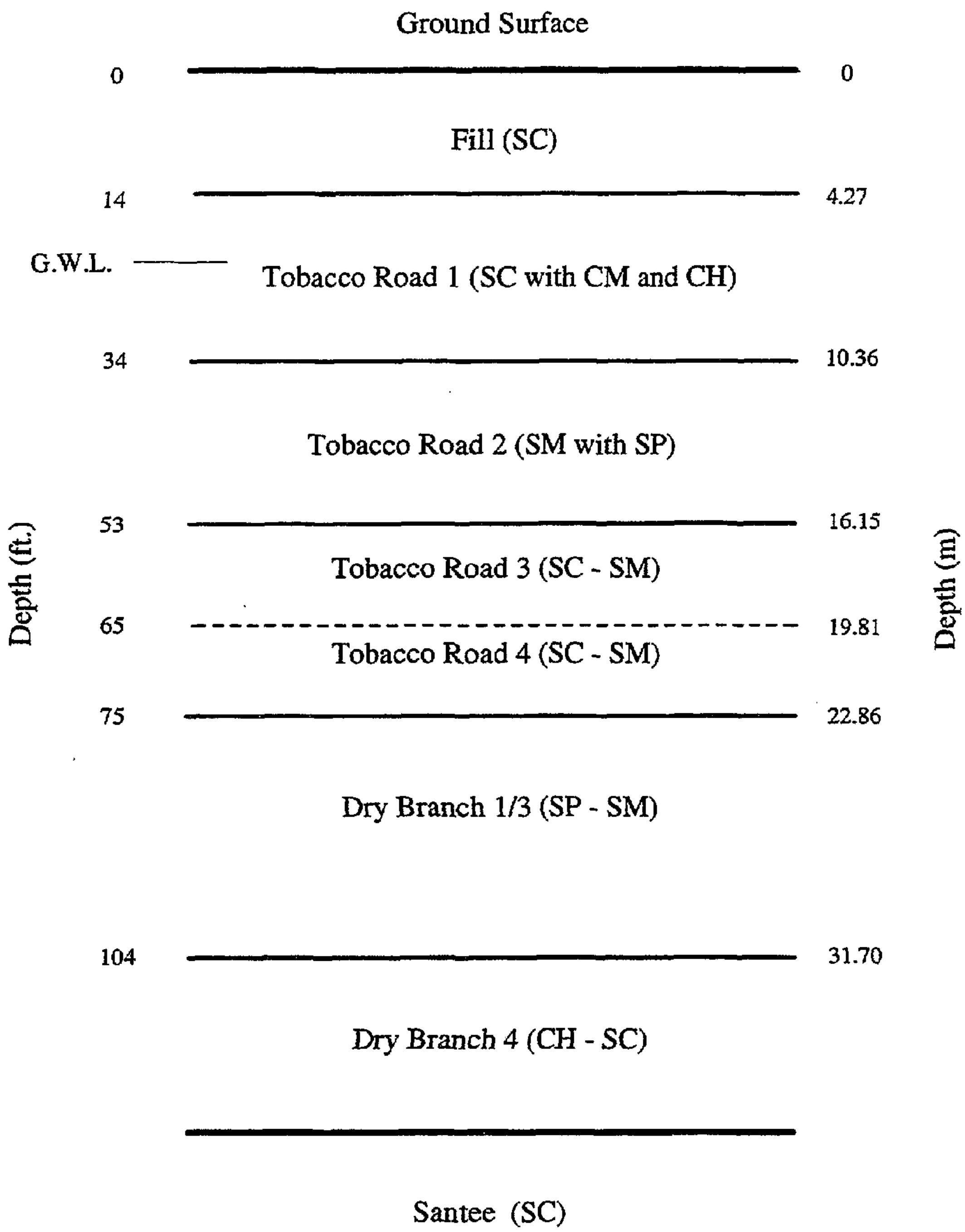

Figure 2.6 - Generalized Subsurface Soil Profile at SRS Site

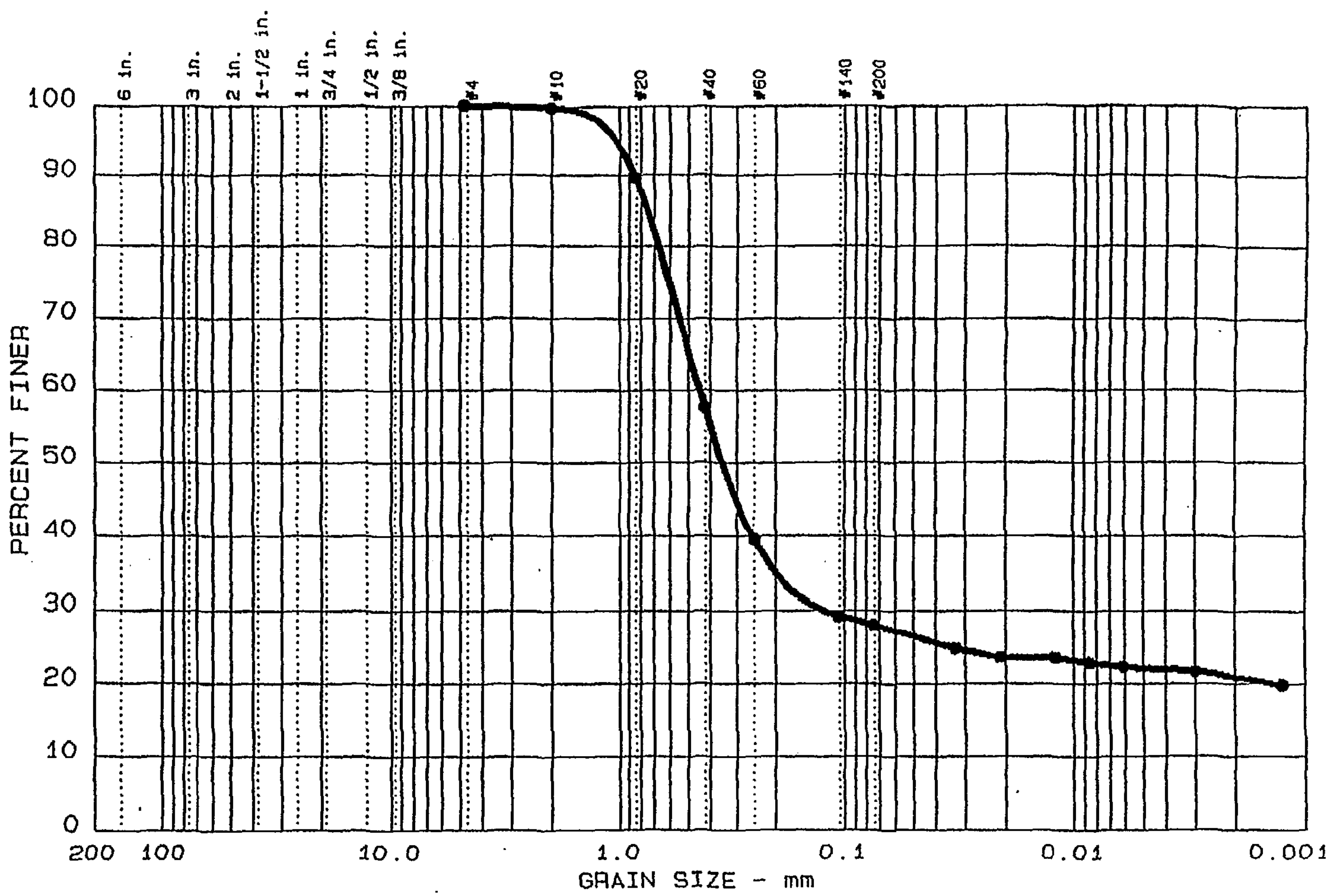

Figure 2.7 - Typical Grain Size Distribution Curve for Tobacco Road Soil Material, SRS (Riemer and Seed, 1994)

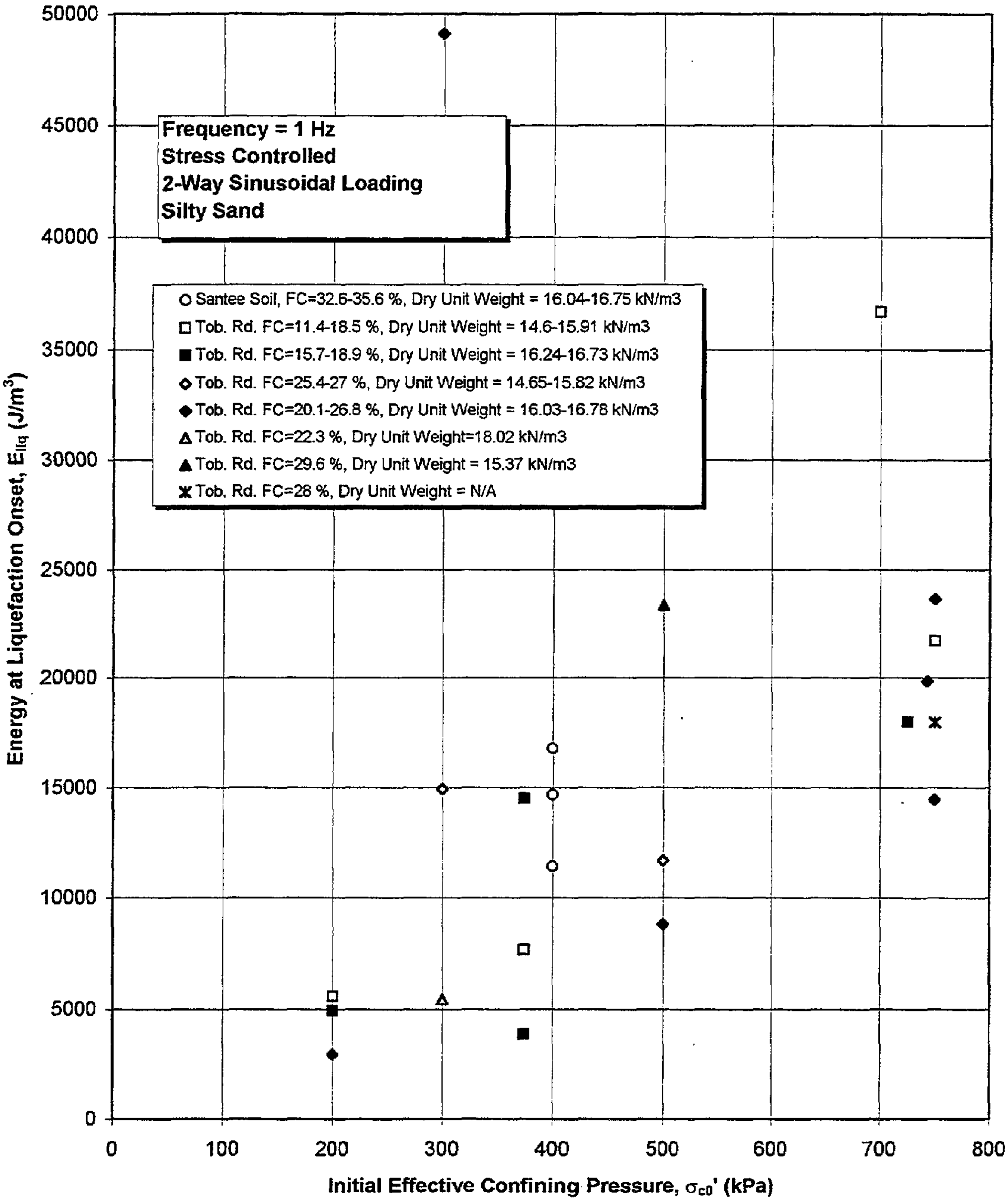

Figure 2.8 - Strain Energy at Liquefaction Onset as a Function of Confining Pressure for SRS Soil Samples - UCB Data

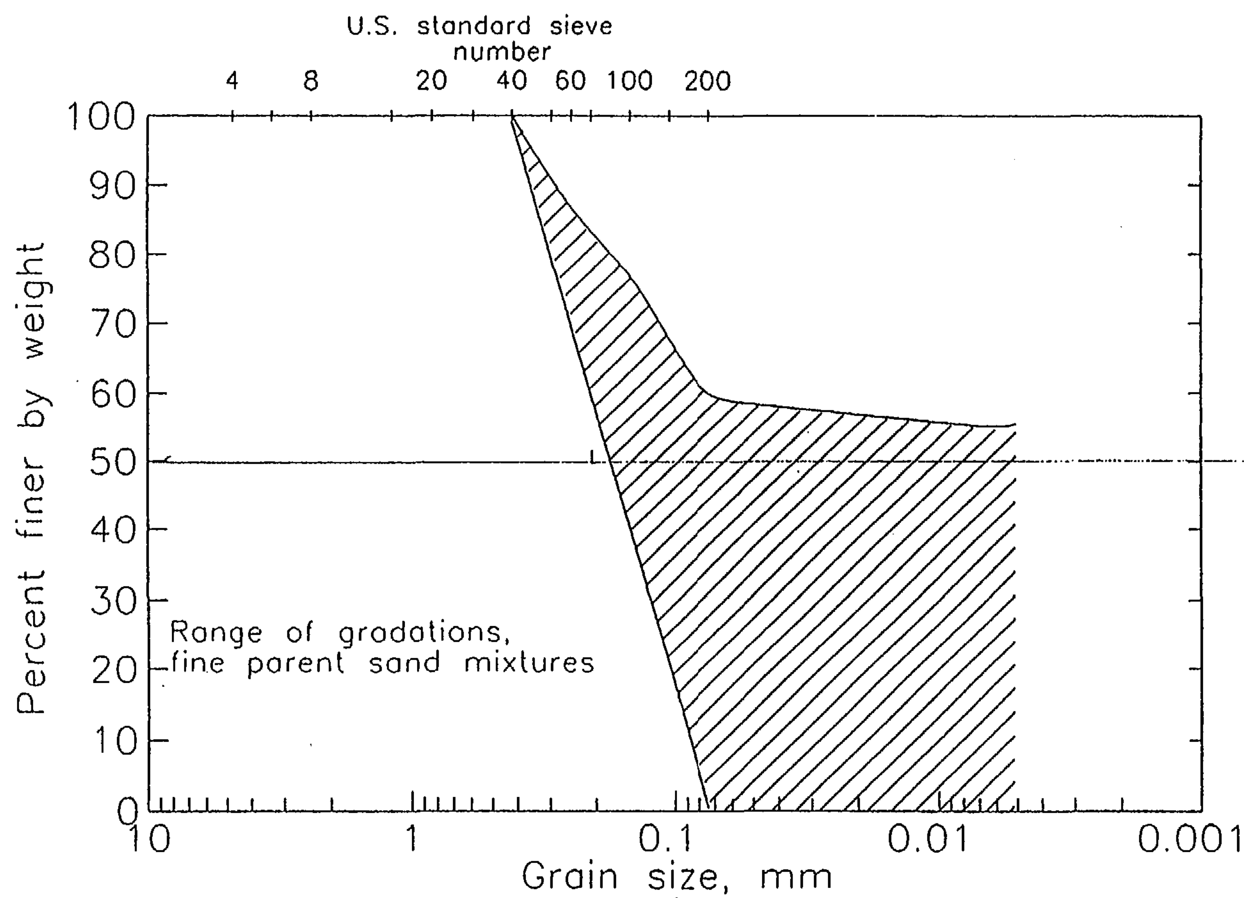

Figure 2.9 - Grain Size Distribution of Silty Sands - University of Colorado Samples (Koester, 1992)

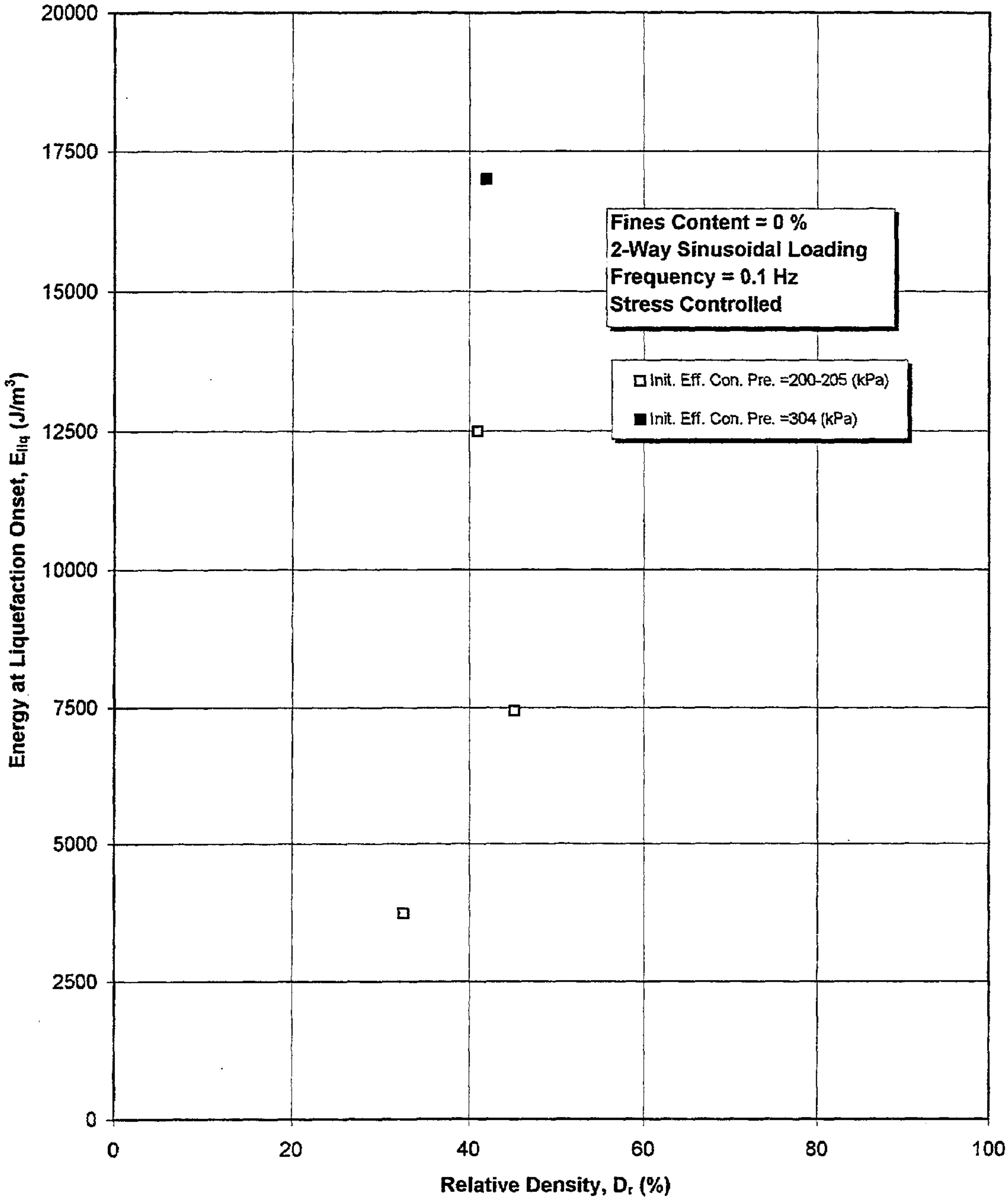

Figure 2.10 - Strain Energy at Liquefaction Onset as a Function of Relative Density for Clean Sands - University of Colorado Data

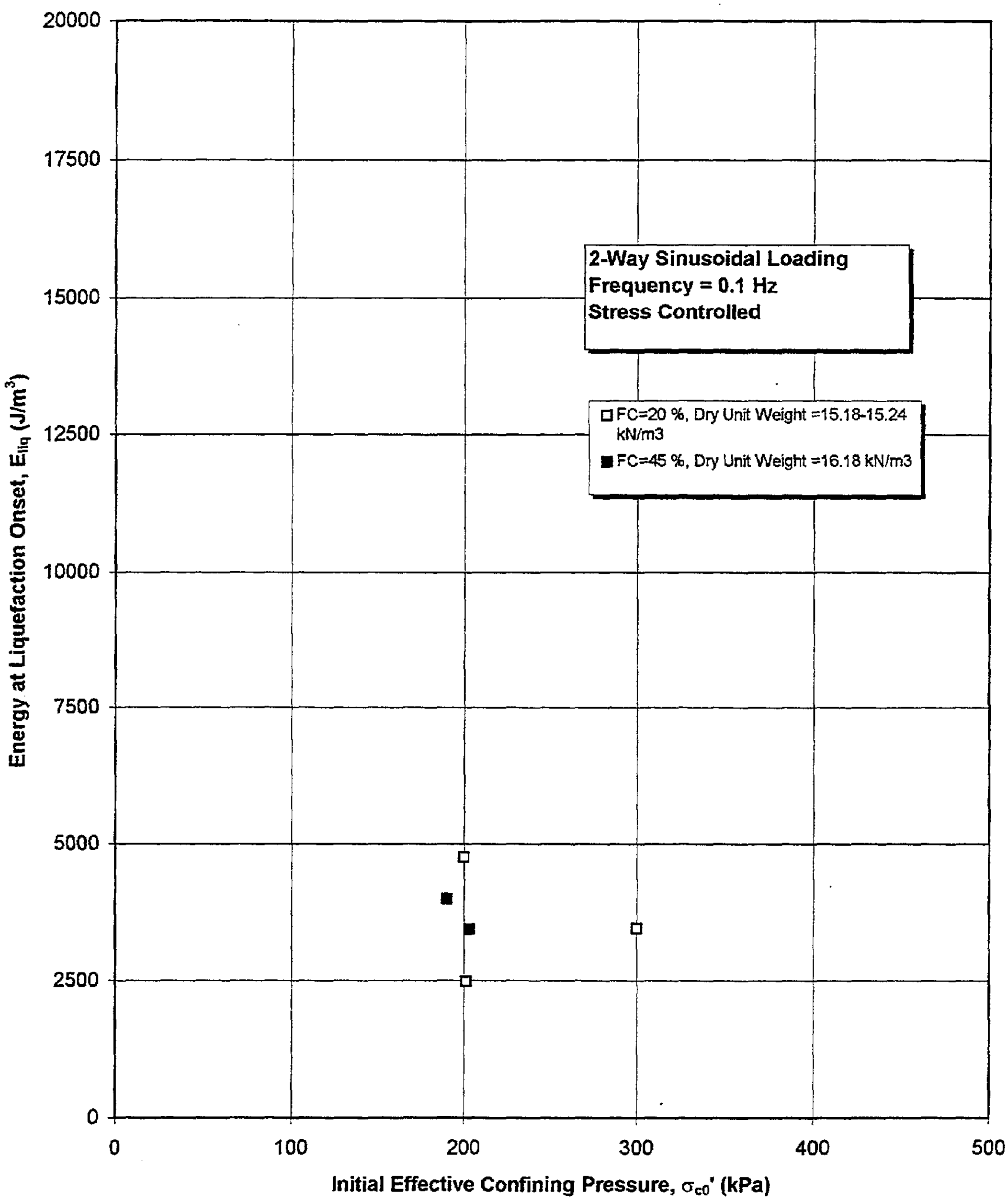

Figure 2.11 - Strain Energy at Liquefaction Onset as a Function of Confining Pressure for Silty Sands - University of Colorado Data

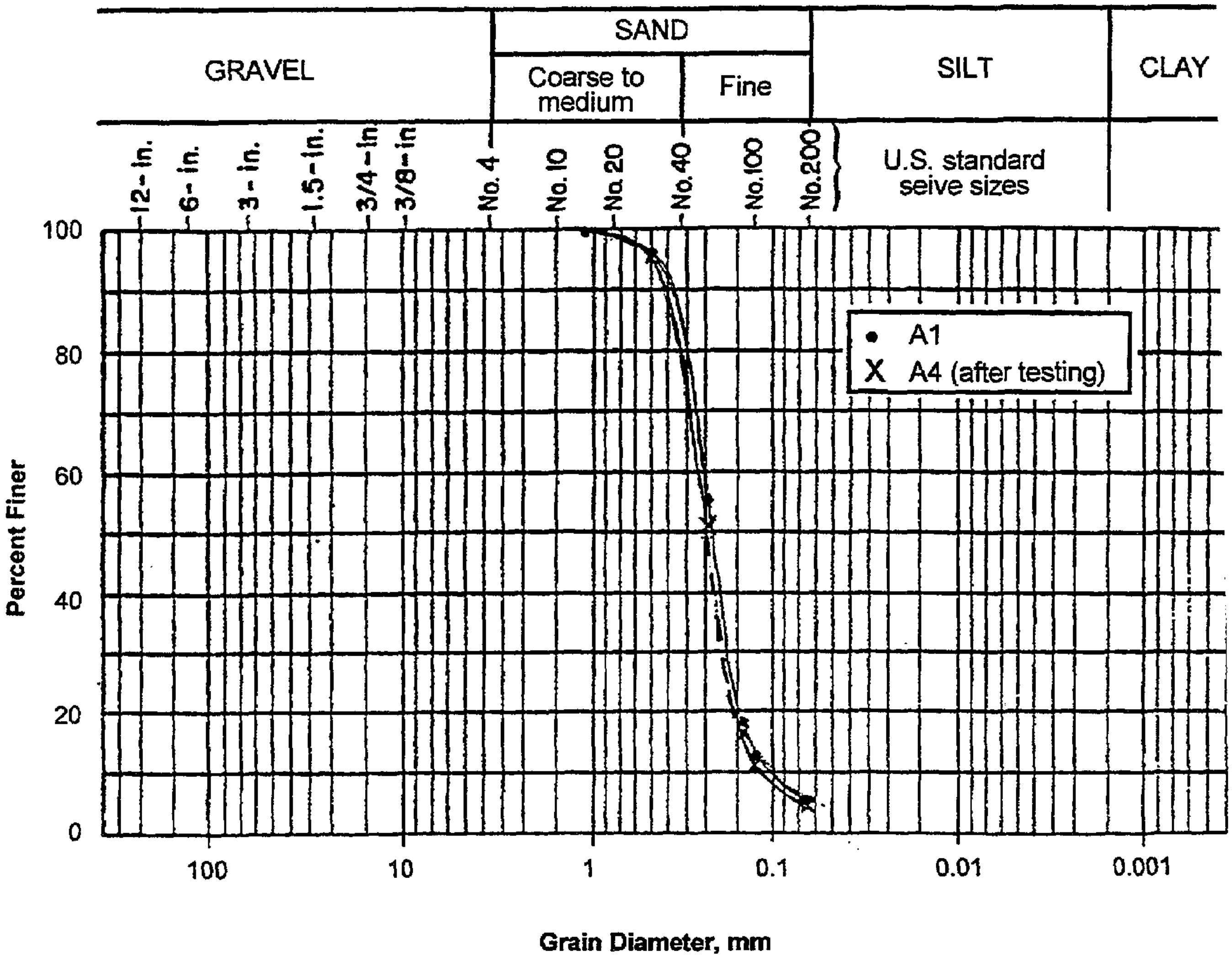

Figure 2.12 - Grain Size Distribution Curves for the Northridge Site Soil Samples (Arango and Migues, 1996)

Test I.D.:	MONT4	**Controlled Parameter:**	Stress
Relative Density (%):	61.8	**Initial Effective Stress (kPa):**	100
Applied Stress Ratio:	0.31	**Frequency (Hz):**	1

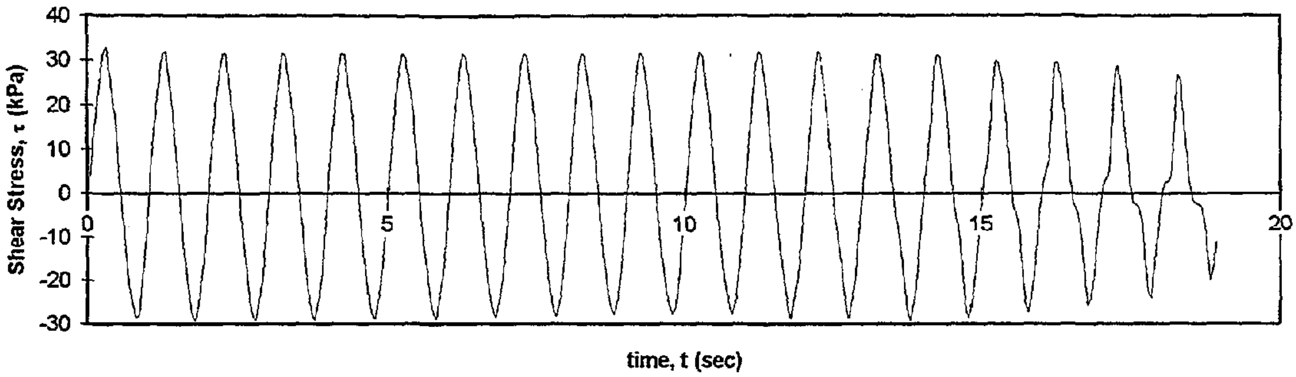

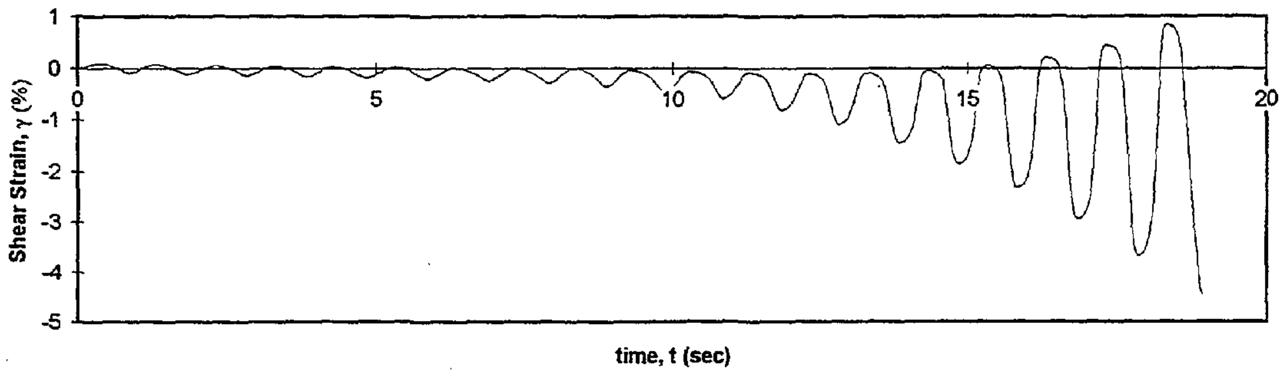

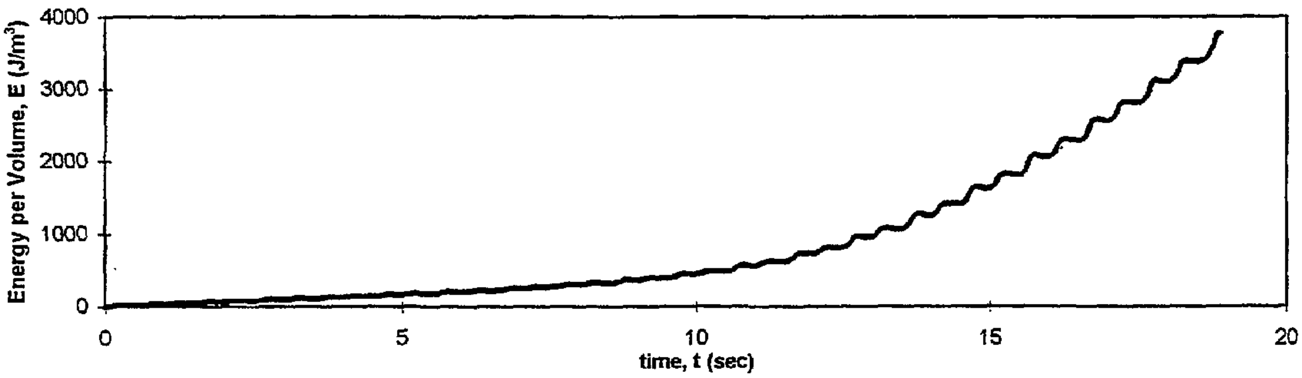

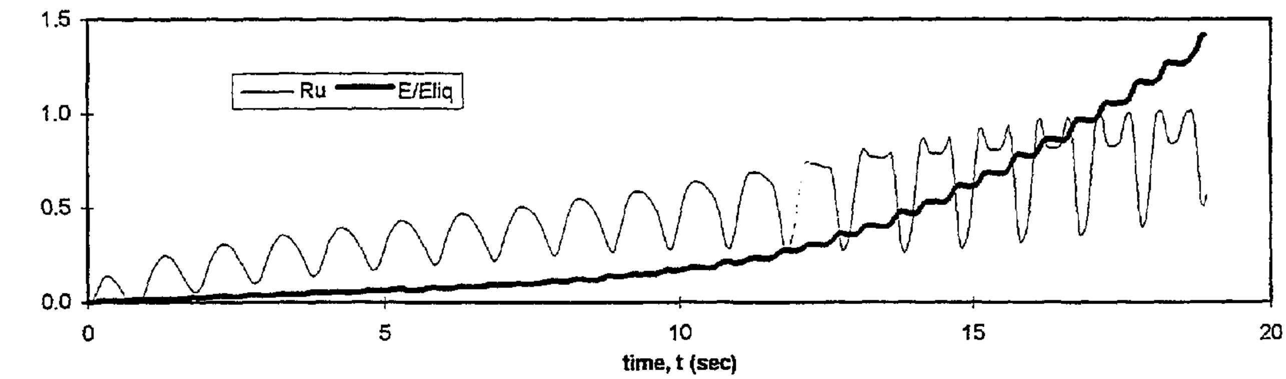

Test I.D.:	MONT4	**Controlled Parameter:**	Stress
Relative Density (%)	61.8	**Initial Effective Stress (kPa):**	100
Applied Stress Ratio:	0.31	**Frequency (Hz):**	1

Shear Stress vs. Shear Strain

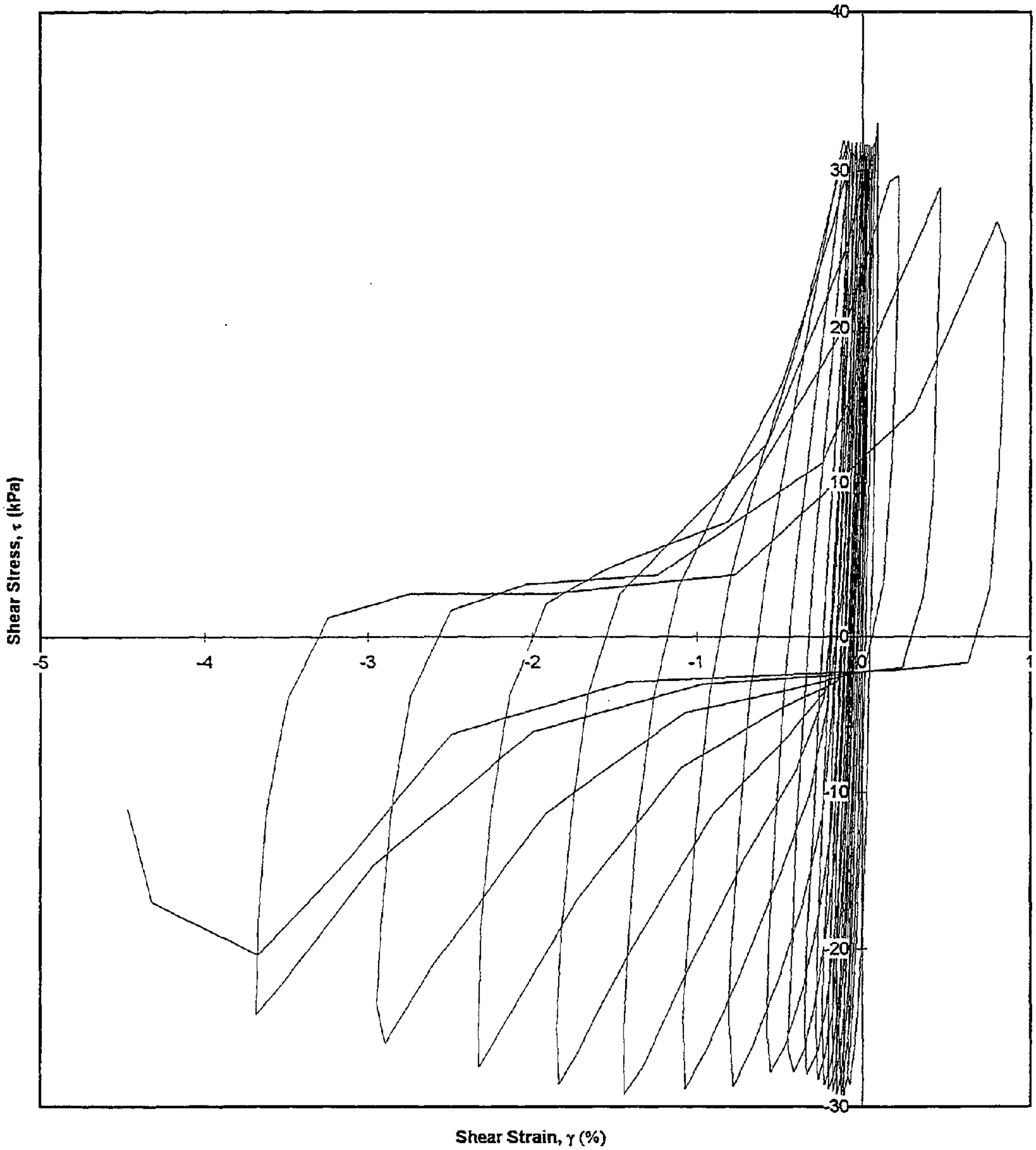

Test I.D.:	MONT10	**Controlled Parameter:**	Stress
Relative Density (%):	61	**Initial Effective Stress (kPa):**	100
Applied Stress Ratio:	0.27	**Frequency (Hz):**	1

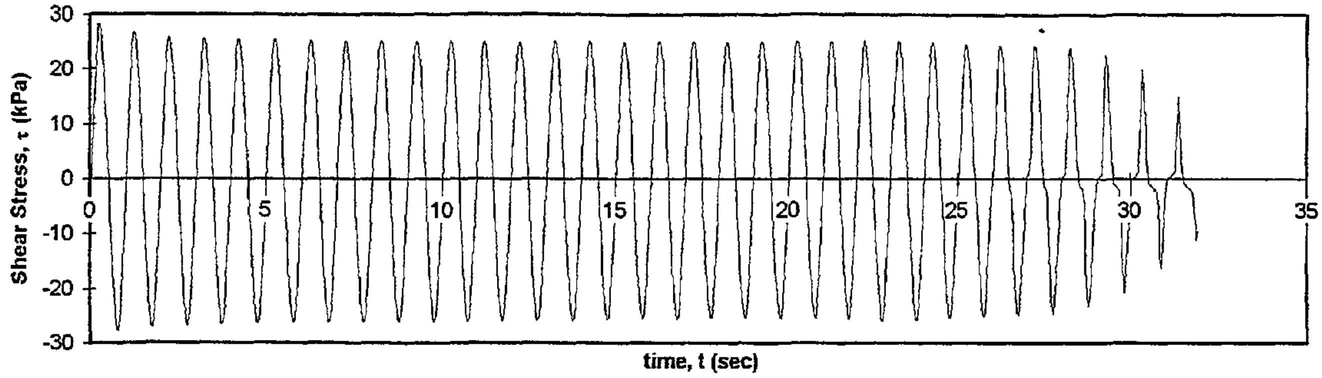

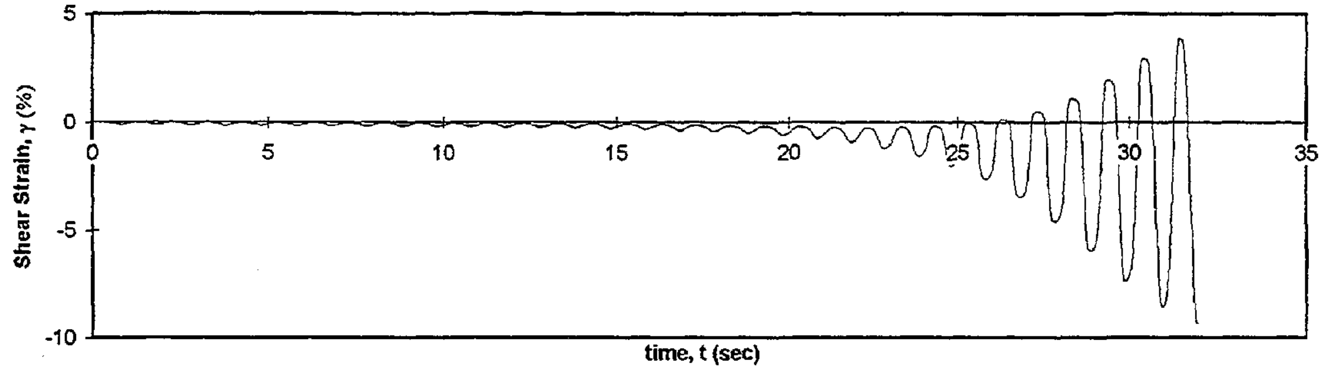

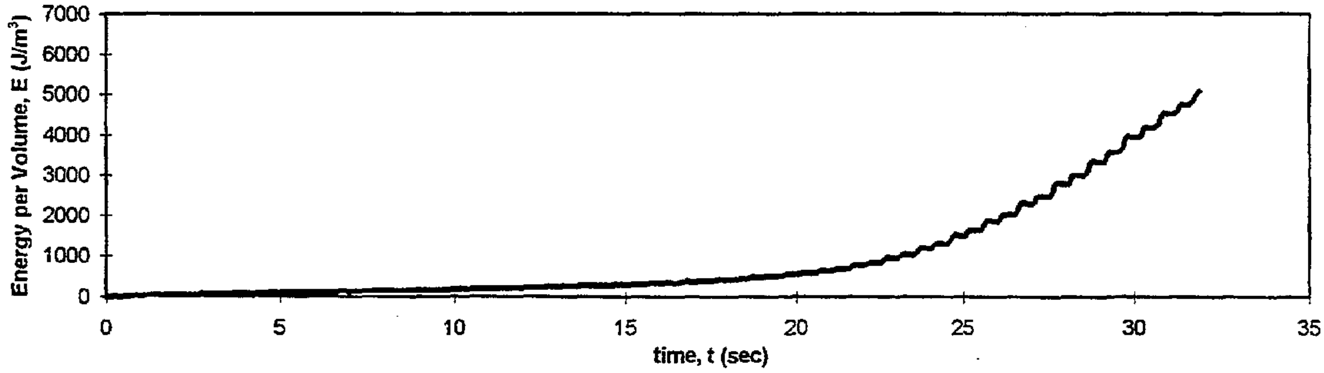

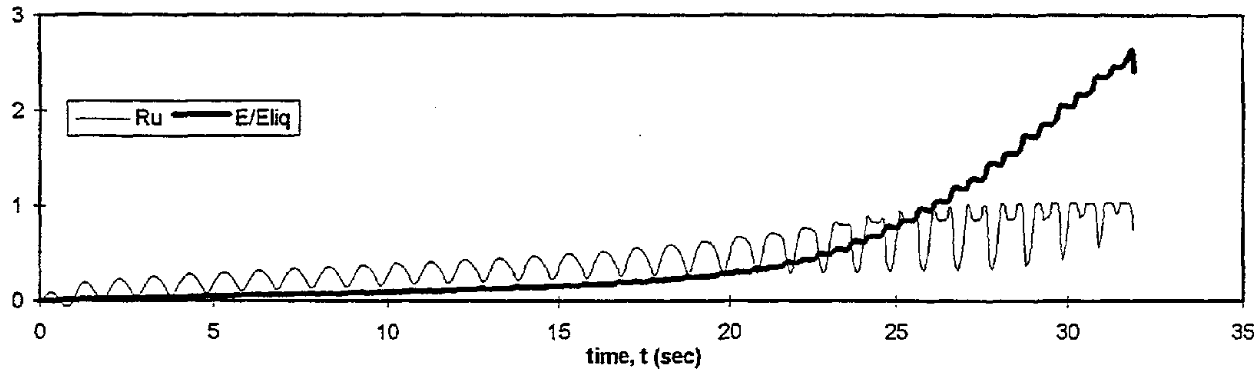

Test I.D.:	MONT10	**Controlled Parameter:**	Stress
Relative Density (%):	61	**Initial Effective Stress (kPa):**	100
Applied Stress Ratio:	0.27	**Frequency (Hz):**	1

Shear Stress vs. Shear Strain

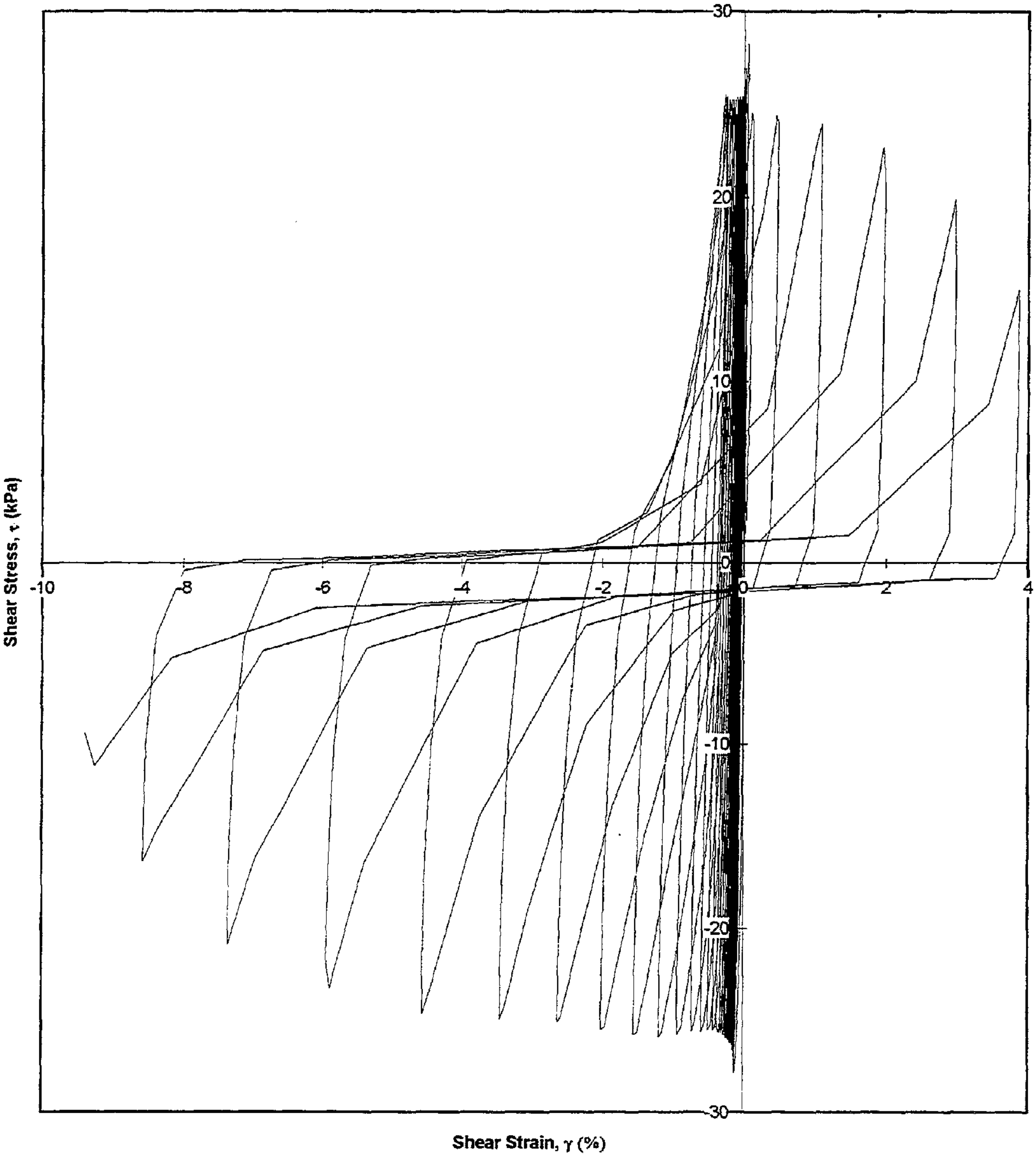

d:\nit\itp\cy_files\MONT10.XLS

8/21/96 9:46 AM

Test I.D.:	MONT11	**Controlled Parameter:**	Stress
Relative Density (%):	60.6	**Initial Effective Stress (kPa):**	100
Applied Stress Ratio:	0.3	**Frequency (Hz):**	10

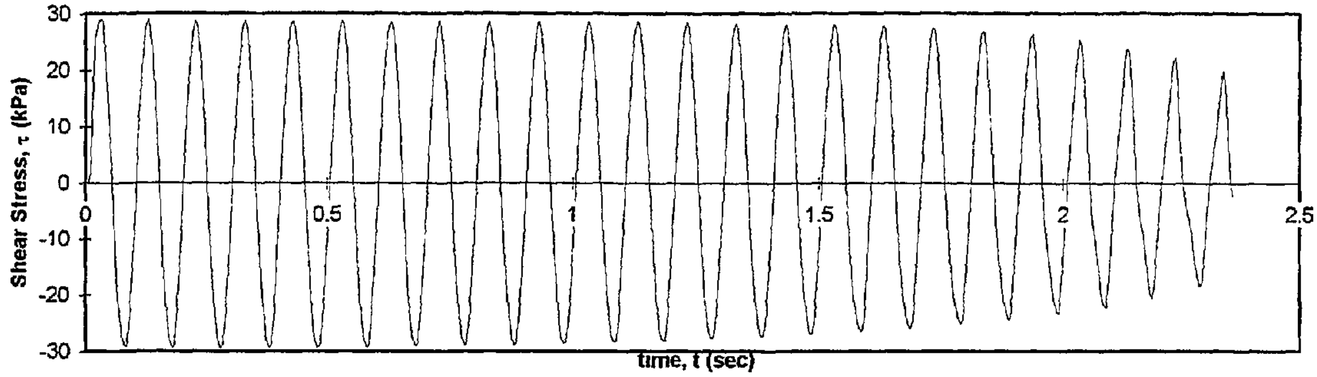

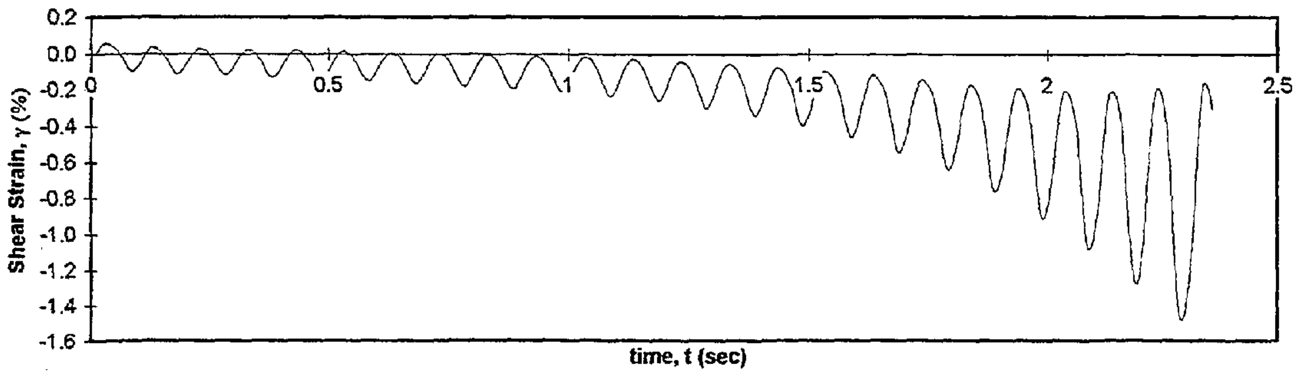

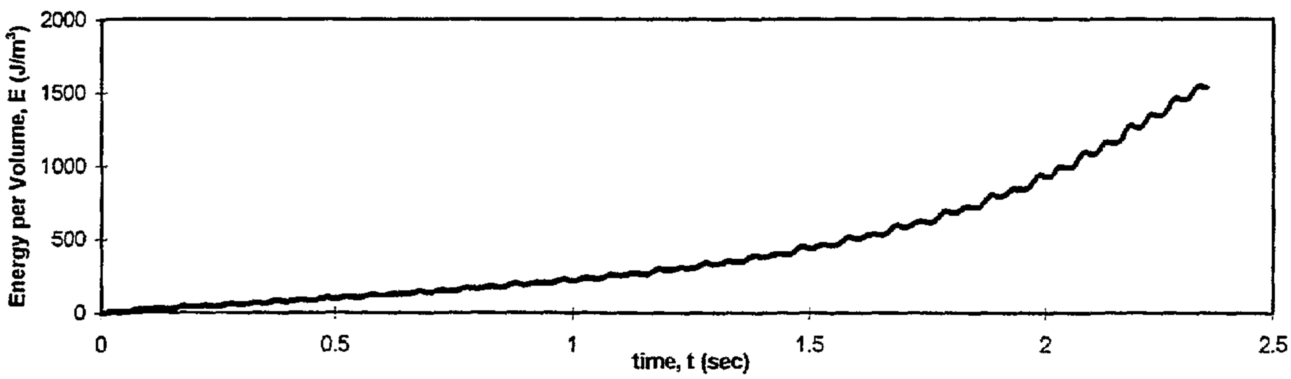

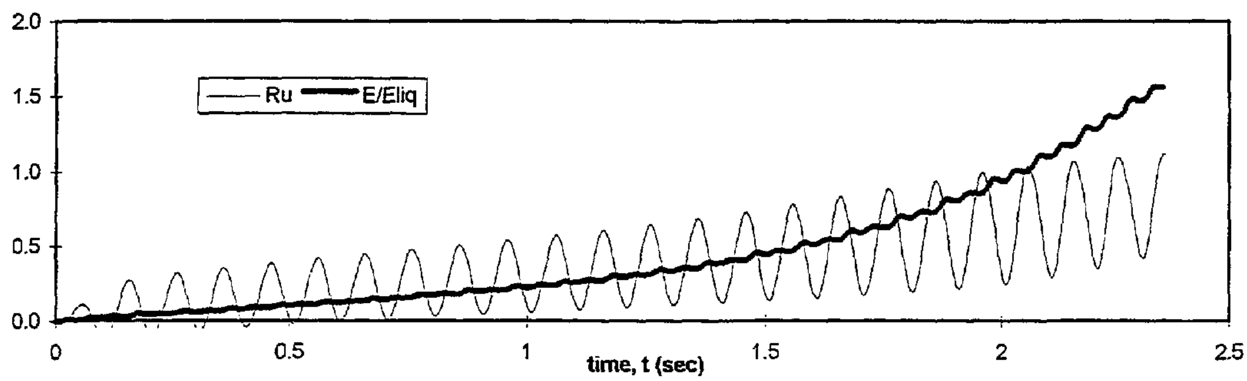

Test I.D.:	MONT11	**Controlled Parameter:**	Stress
Relative Density (%):	60.6	**Initial Effective Stress (kPa):**	100
Applied Stress Ratio:	0.3	**Frequency (Hz):**	10

Shear Stress vs. Shear Strain

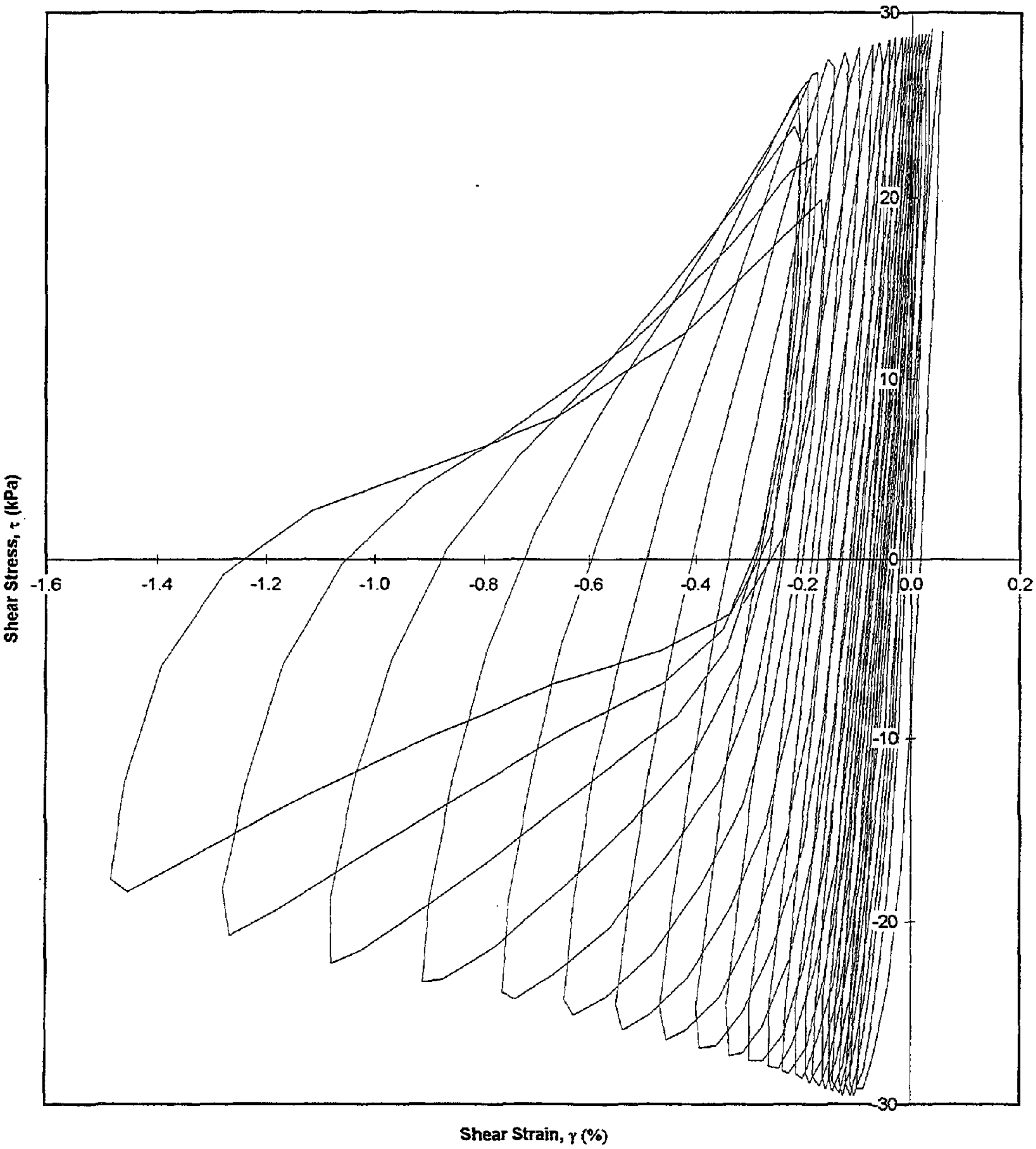

Test I.D.:	MONT12	**Controlled Parameter:**	Stress
Relative Density (%):	61	**Initial Effective Stress (kPa):**	100
Applied Stress Ratio:	0.23	**Frequency (Hz):**	1

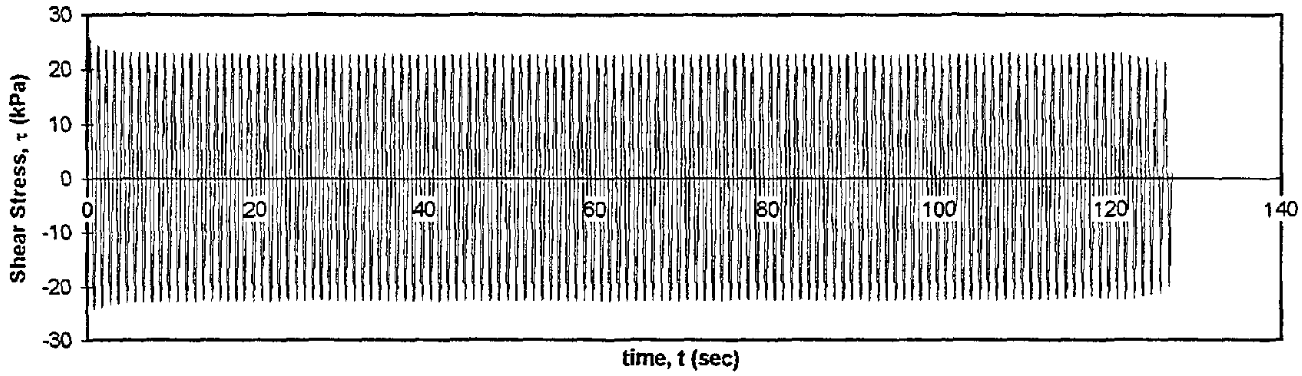

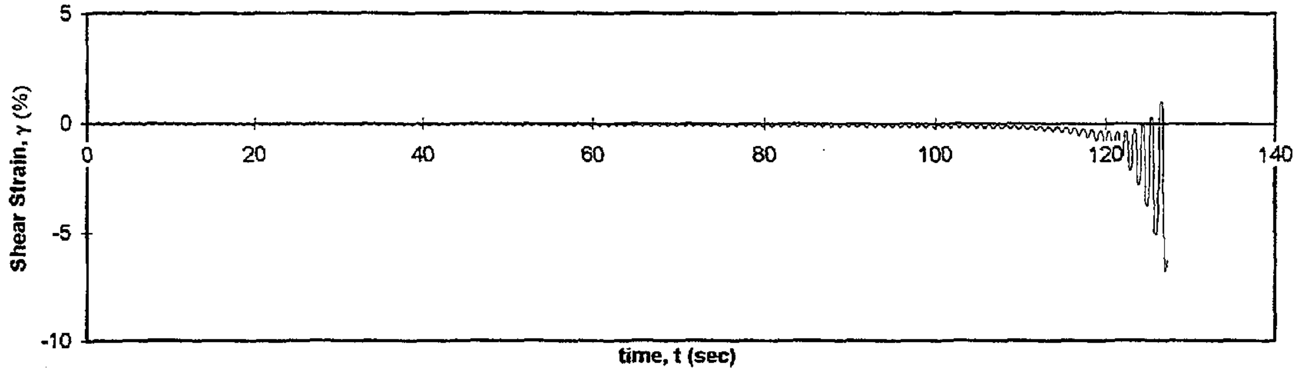

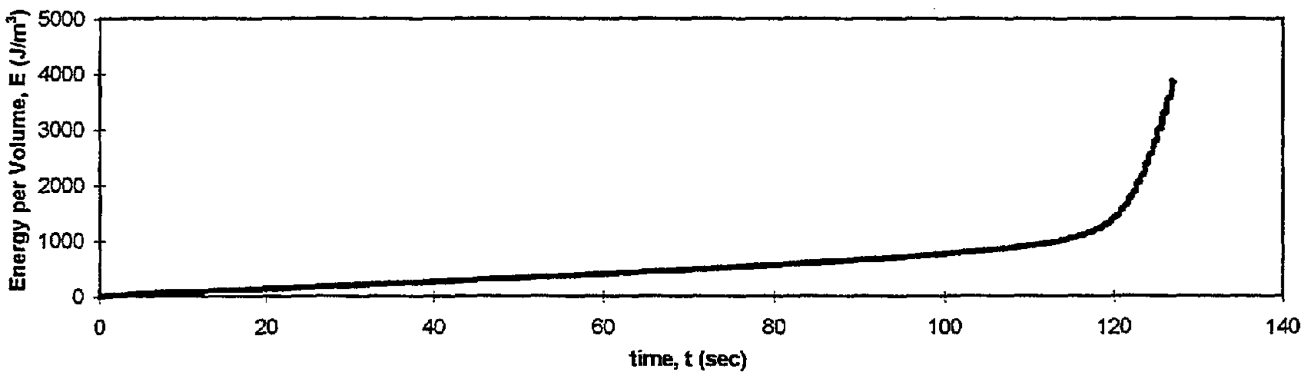

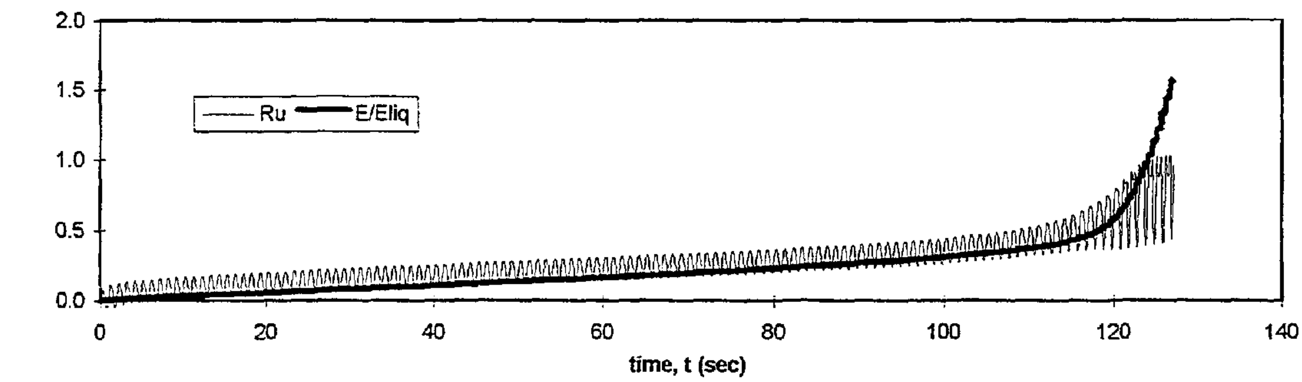

Test I.D.:	MONT12	**Controlled Parameter:**	Stress
Relative Density (%):	61	**Initial Effective Stress (kPa):**	100
Applied Stress Ratio:	0.23	**Frequency (Hz):**	1

Shear Stress vs. Shear Strain

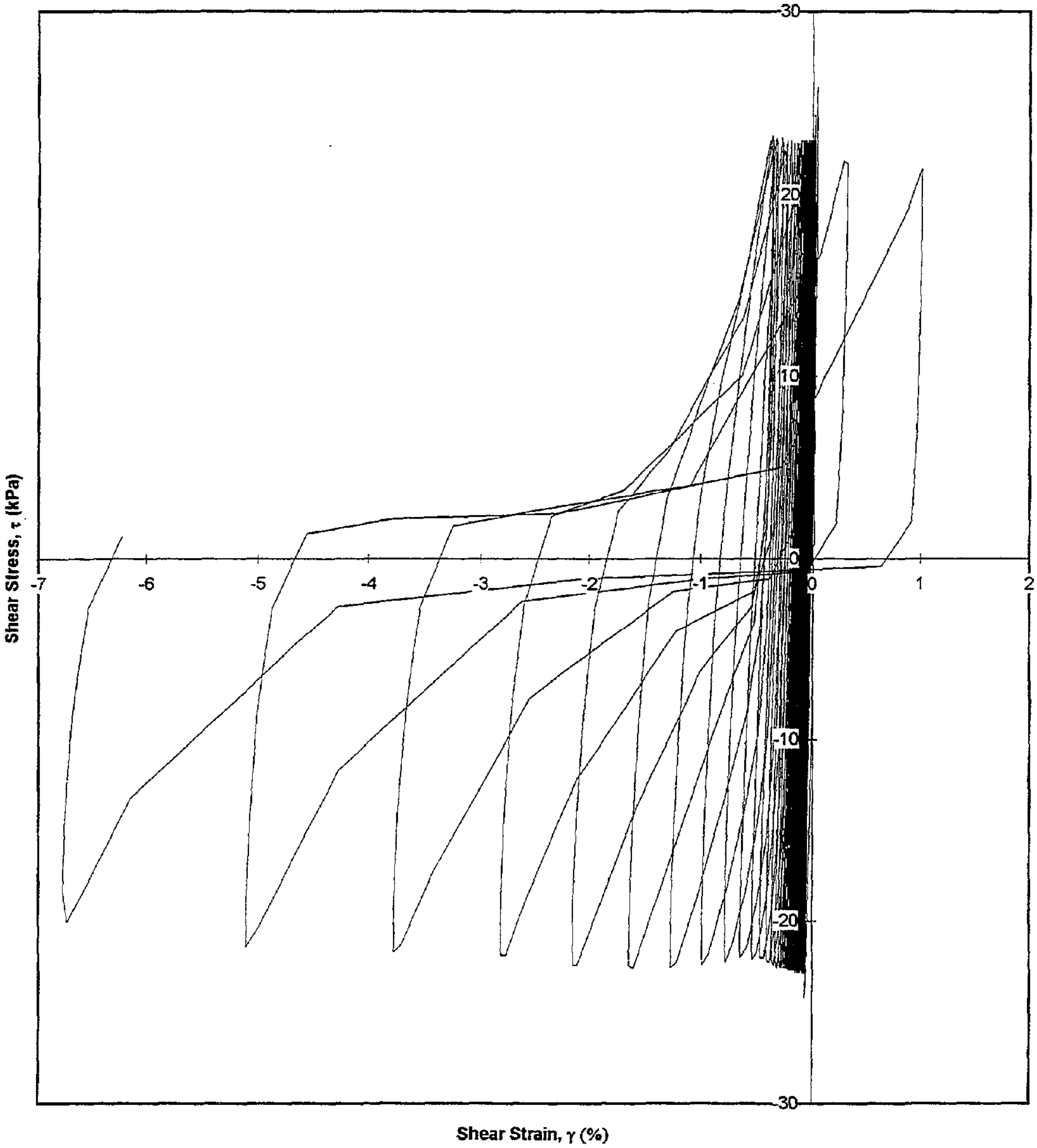

Test I.D.:	MONT14	**Controlled Parameter:**	Stress
Relative Density (%):	60.2	**Initial Effective Stress (kPa):**	100
Applied Stress Ratio:	0.3	**Frequency (Hz):**	20

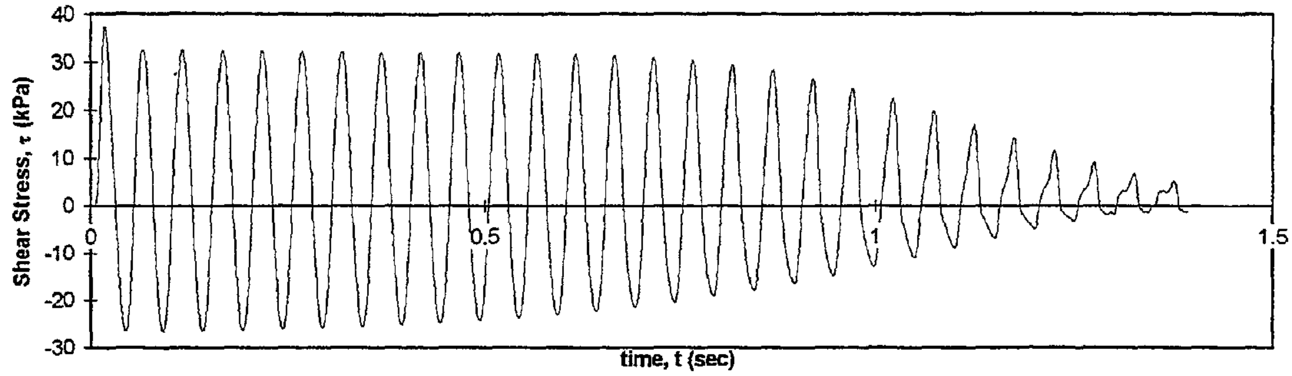

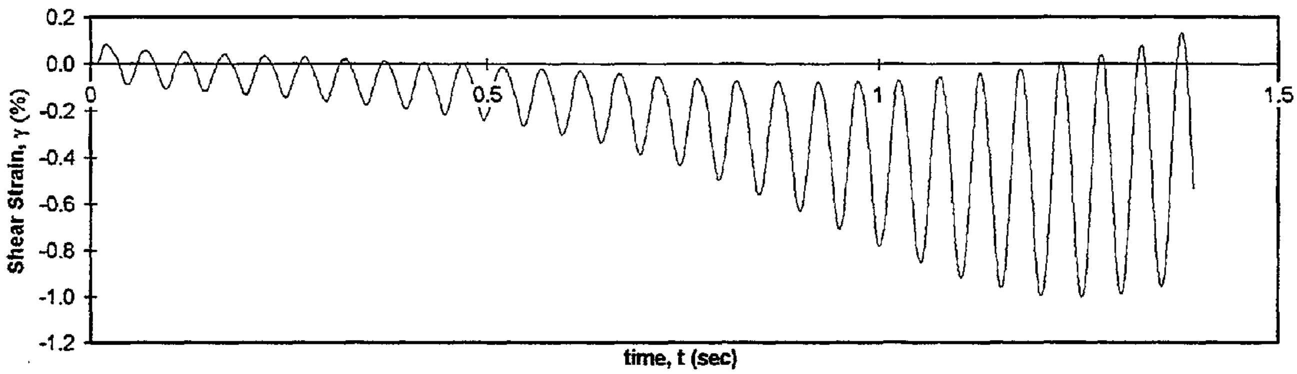

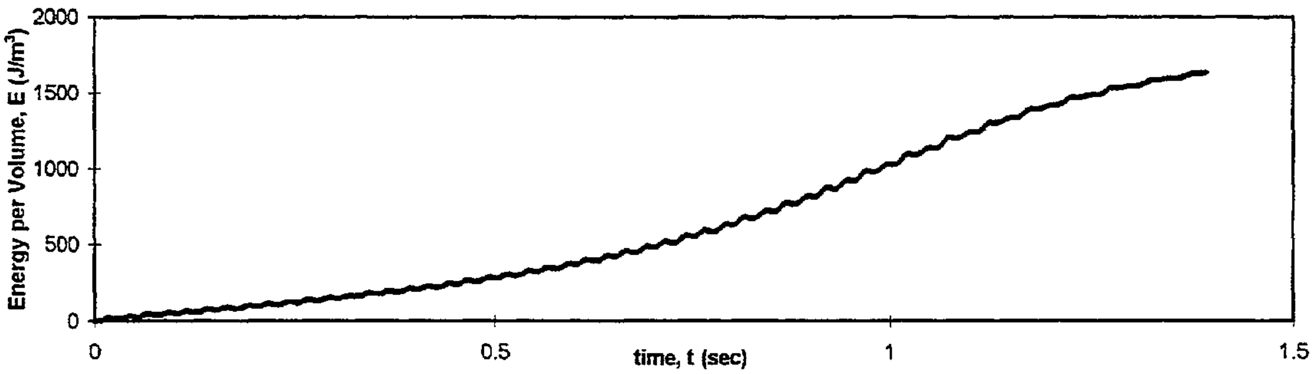

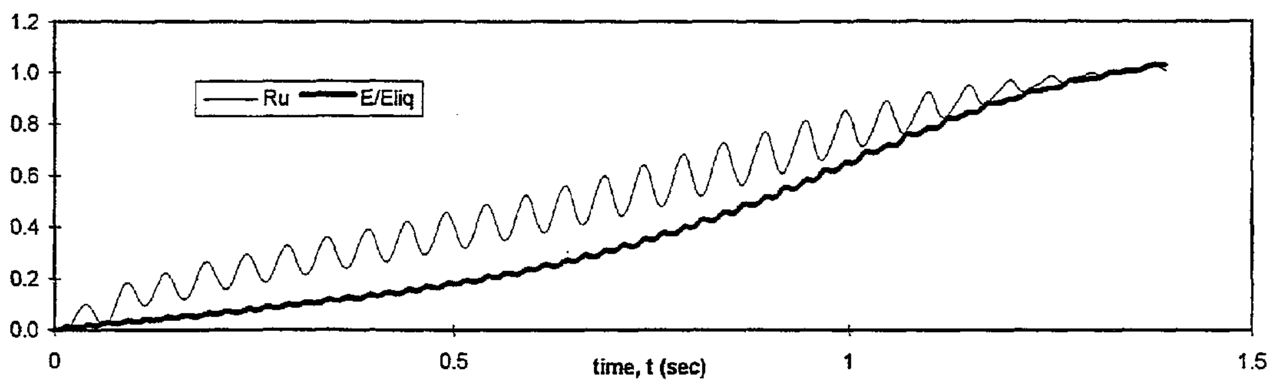

d:\nit\itp\cy_files\MONT14.XLS 8/15/96 11:24 AM

Test I.D.:	MONT14	**Controlled Parameter:**	Stress
Relative Density (%):	60.2	**Initial Effective Stress (kPa):**	100
Applied Stress Ratio:	0.3	**Frequency (Hz):**	20

Shear Stress vs. Shear Strain

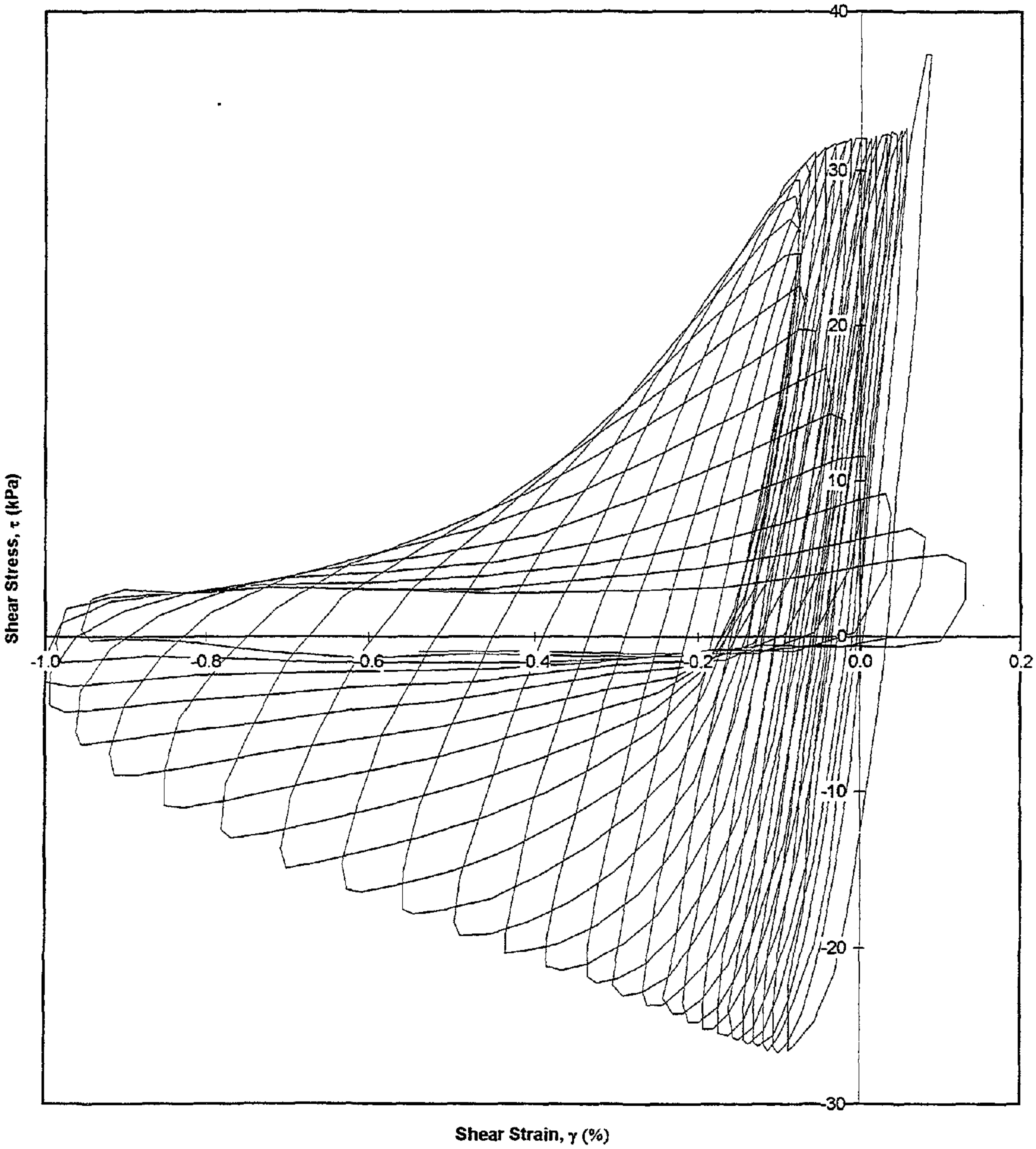

d:\nit\itp\cy_files\MONT14.XLS 8/15/96 11:24 AM

Test I.D.:	MONT15	**Controlled Parameter:**	Stress
Relative Density (%):	60.5	**Initial Effective Stress (kPa):**	100
Applied Stress Ratio:	0.22	**Frequency (Hz):**	10

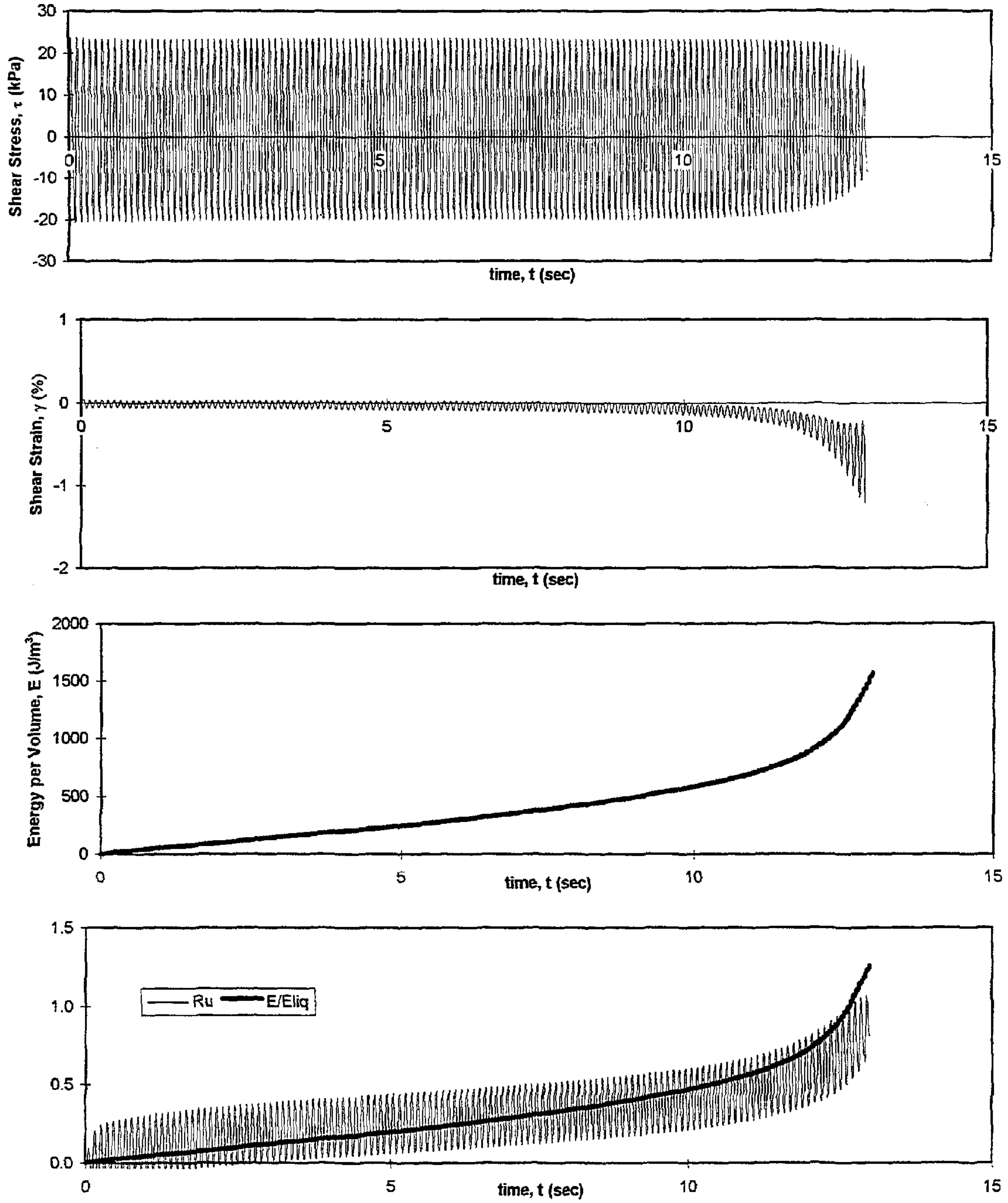

d:\nit\itp\cy_files\MONT15.XLS 8/15/96 11:28 AM

Test I.D.:	MONT15	**Controlled Parameter:**	Stress
Relative Density (%):	60.5	**Initial Effective Stress (kPa):**	100
Applied Stress Ratio:	0.22	**Frequency (Hz):**	10

Shear Stress vs. Shear Strain

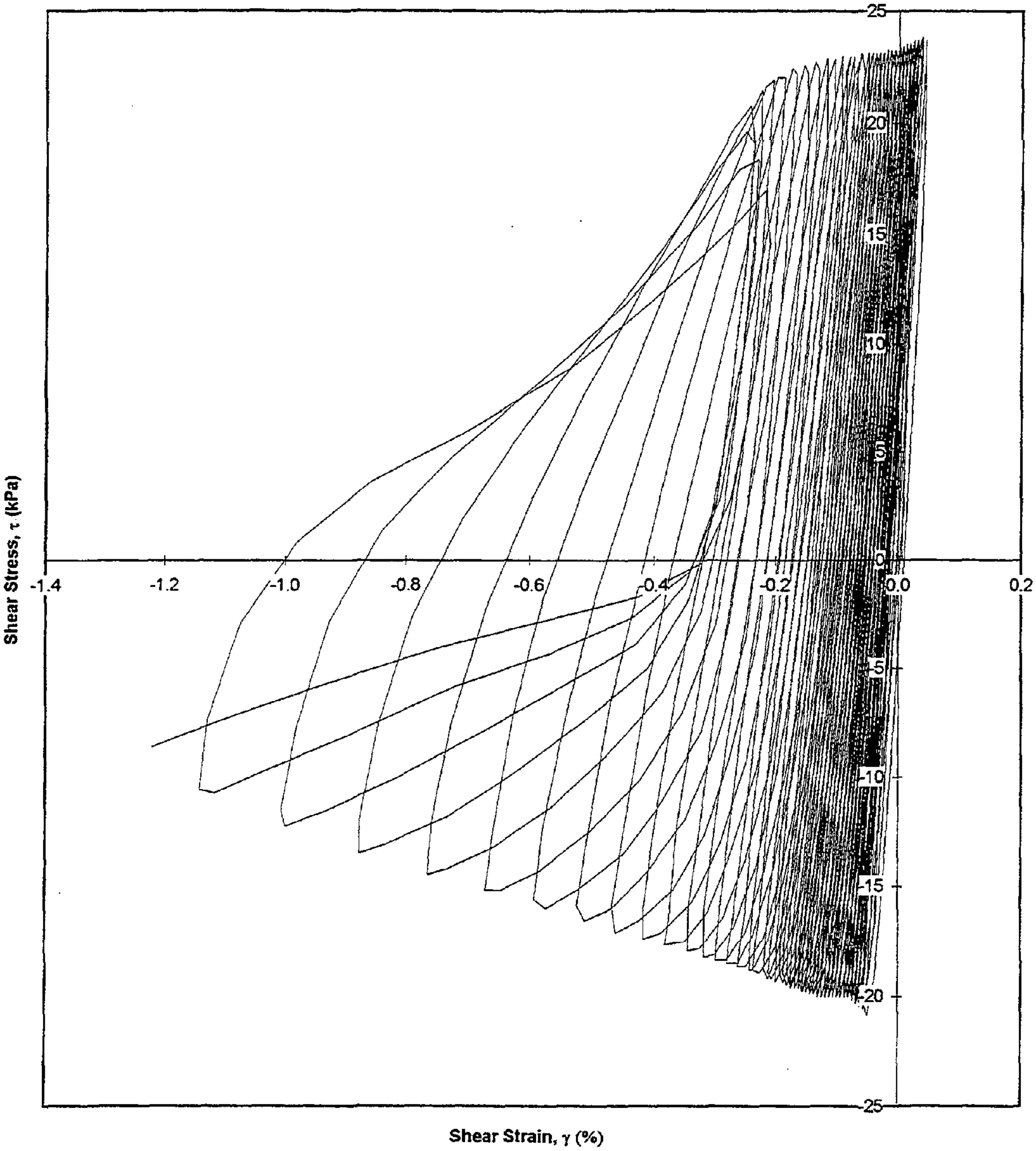

d:\nit\itp\cy_files\MONT15.XLS 8/15/96 11:28 AM

Test I.D.:	MONT17	**Controlled Parameter:**	Strain
Relative Density (%):	61	**Initial Effective Stress (kPa):**	100
Applied Shear Strain (%):	0.25	**Frequency (Hz):**	1

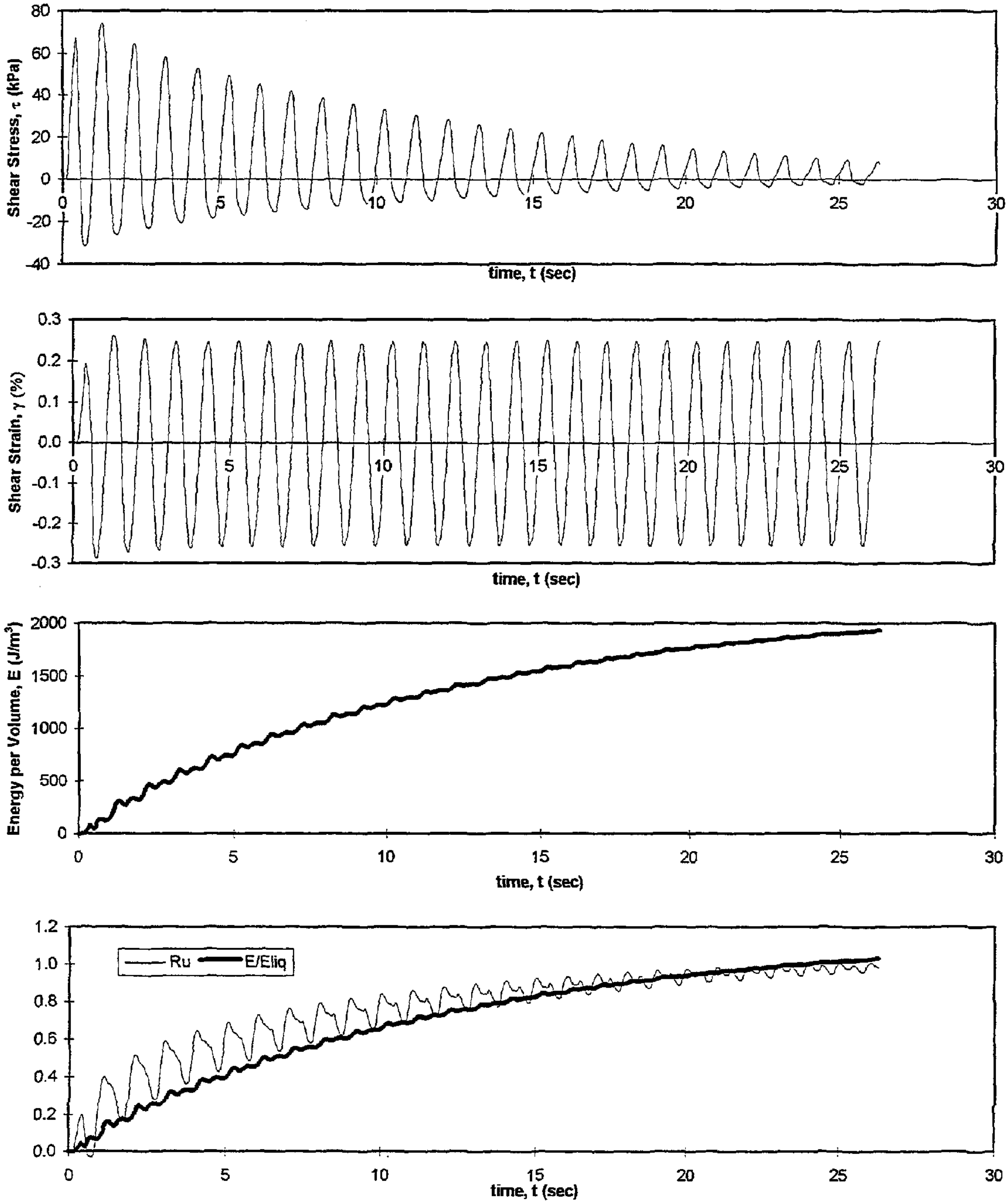

d:\nit\itp\cy_files\MONT17.XLS 8/15/96 11:31 AM

Test I.D.:	MONT17	**Controlled Parameter:**	Strain
Relative Density (%):	61	**Initial Effective Stress (kPa):**	100
Applied Shear Strain (%):	0.25	**Frequency (Hz):**	1

Shear Stress vs. Shear Strain

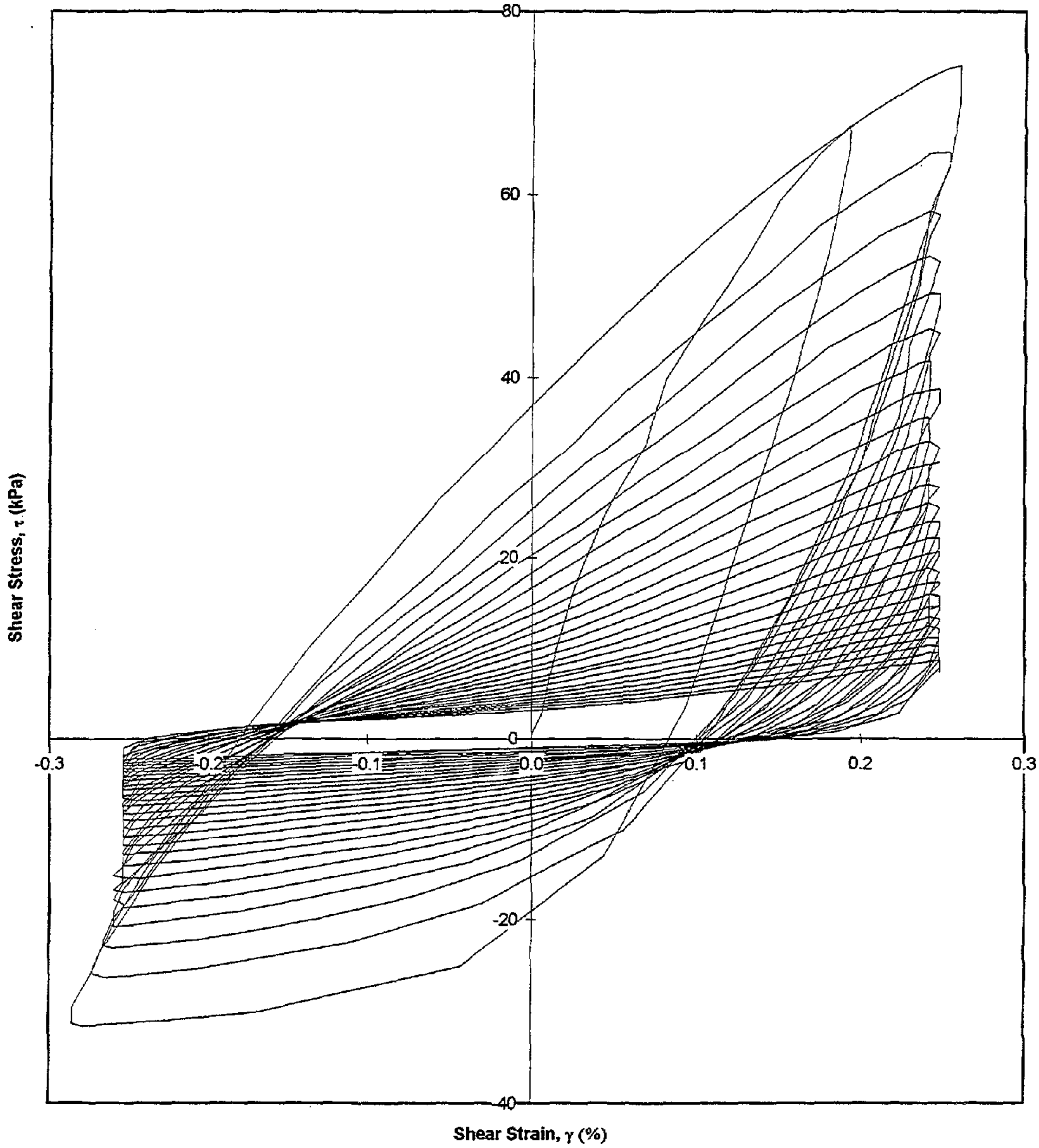

Test I.D.:	MONT18	**Controlled Parameter:**	Strain
Relative Density (%):	61	**Initial Effective Stress (kPa):**	100
Applied Shear Strain (%):	0.25	**Frequency (Hz):**	10

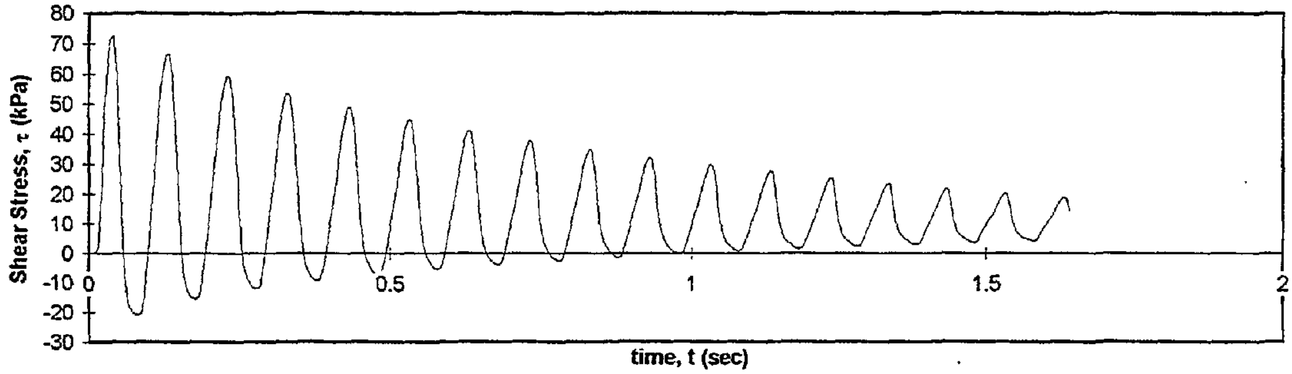

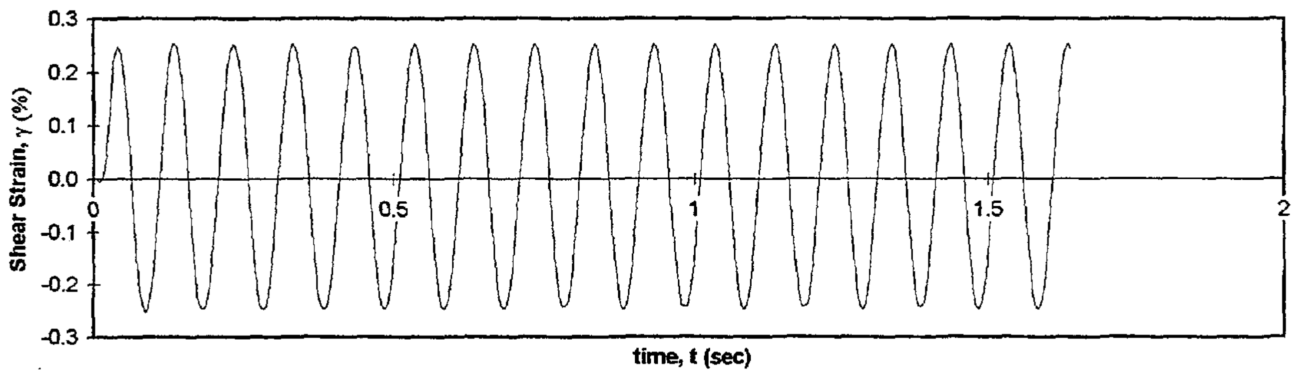

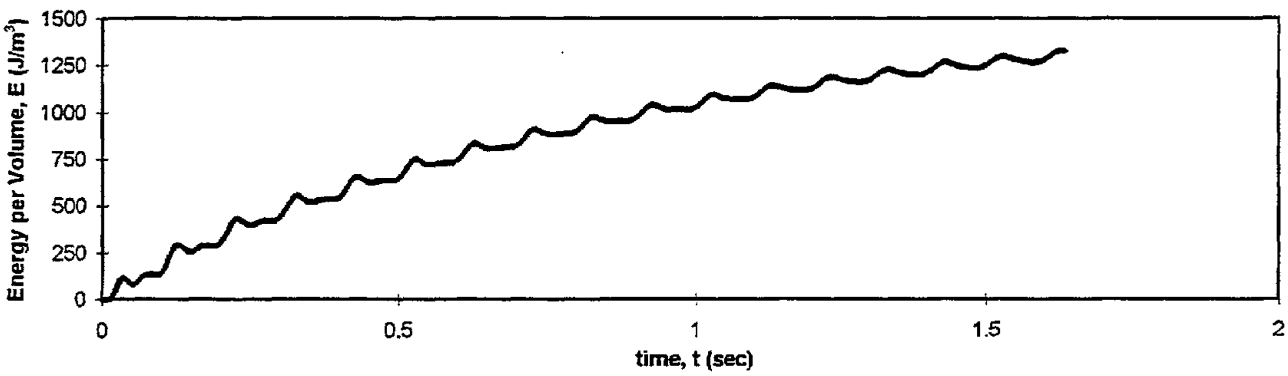

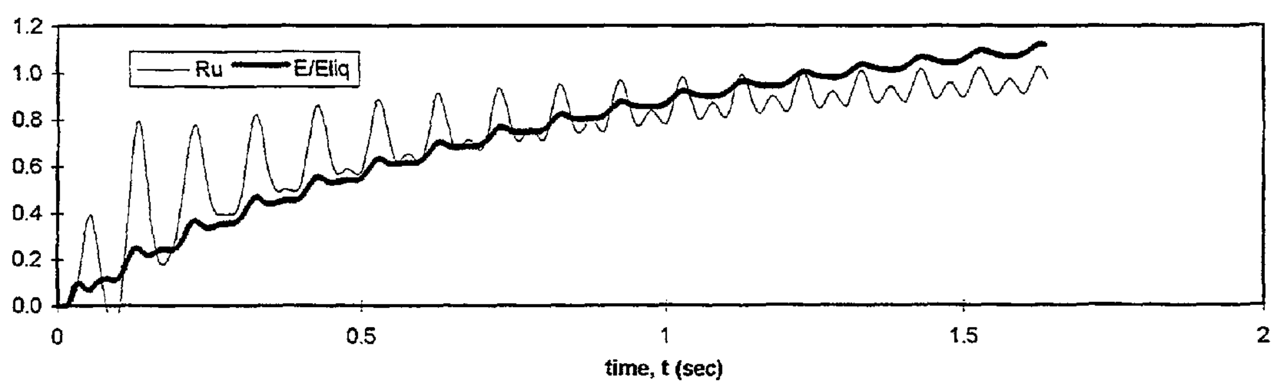

Test I.D.:	MONT18	**Controlled Parameter:**	Strain
Relative Density (%):	61	**Initial Effective Stress (kPa):**	100
Applied Shear Strain (%):	0.25	**Frequency (Hz):**	10

Shear Stress vs. Shear Strain

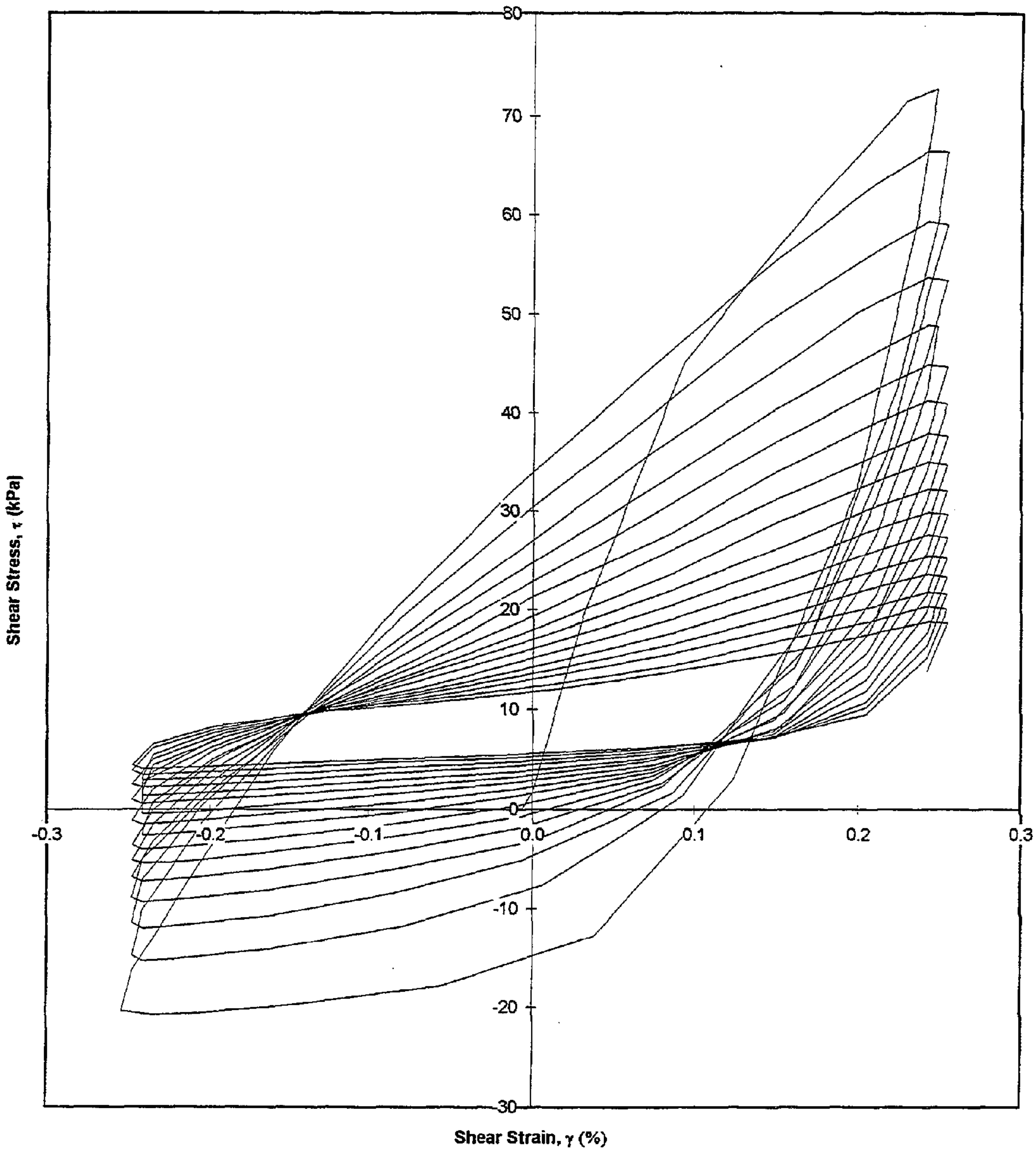

Test I.D.:	MONT19	**Controlled Parameter:**	Strain
Relative Density (%):	60.6	**Initial Effective Stress (kPa):**	100
Applied Shear Strain (%):	0.25	**Frequency (Hz):**	15

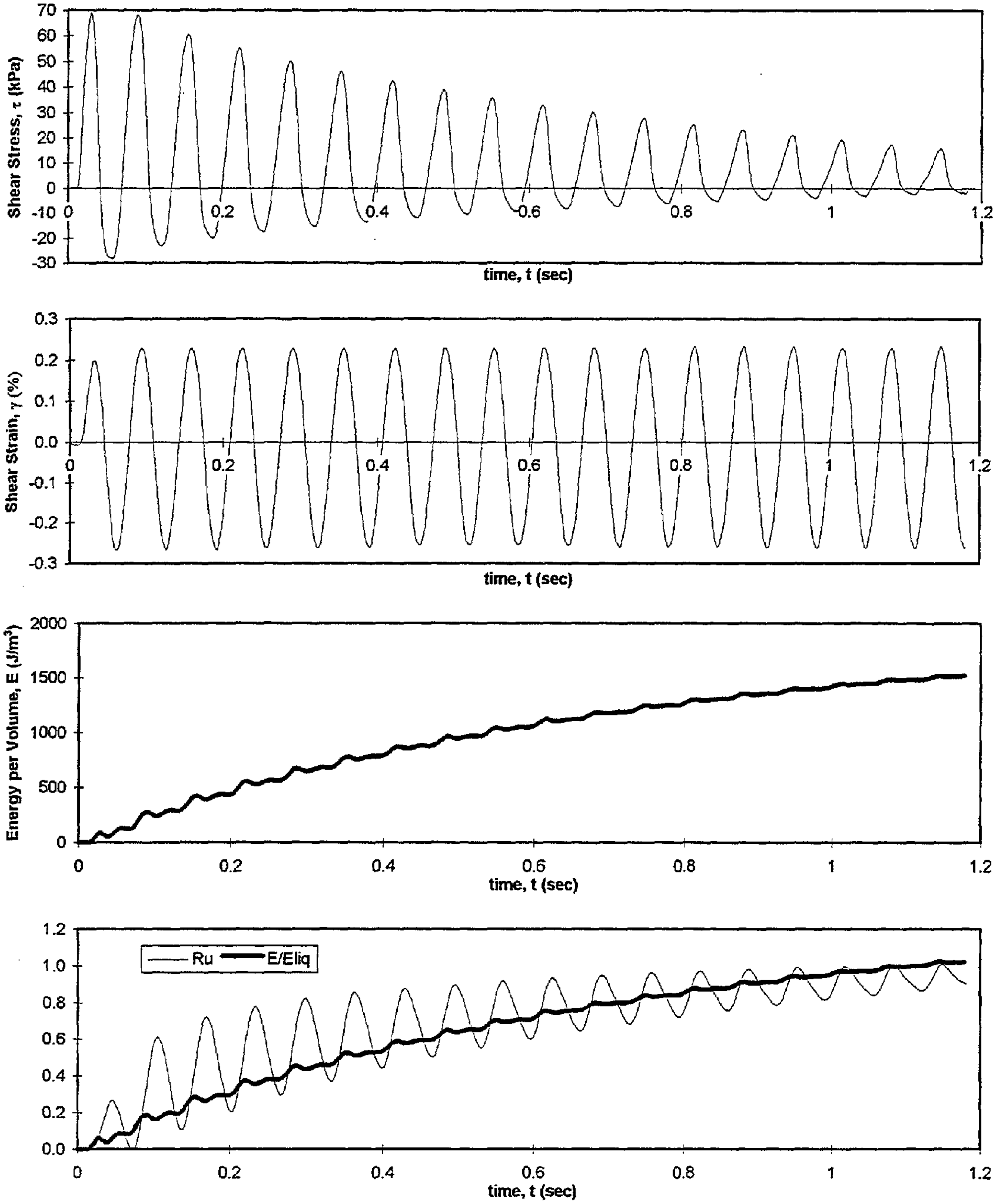

Test I.D.:	MONT19	**Controlled Parameter:**	Strain
Relative Density (%):	60.6	**Initial Effective Stress (kPa):**	100
Applied Shear Strain (%):	0.25	**Frequency (Hz):**	15

Shear Stress vs. Shear Strain

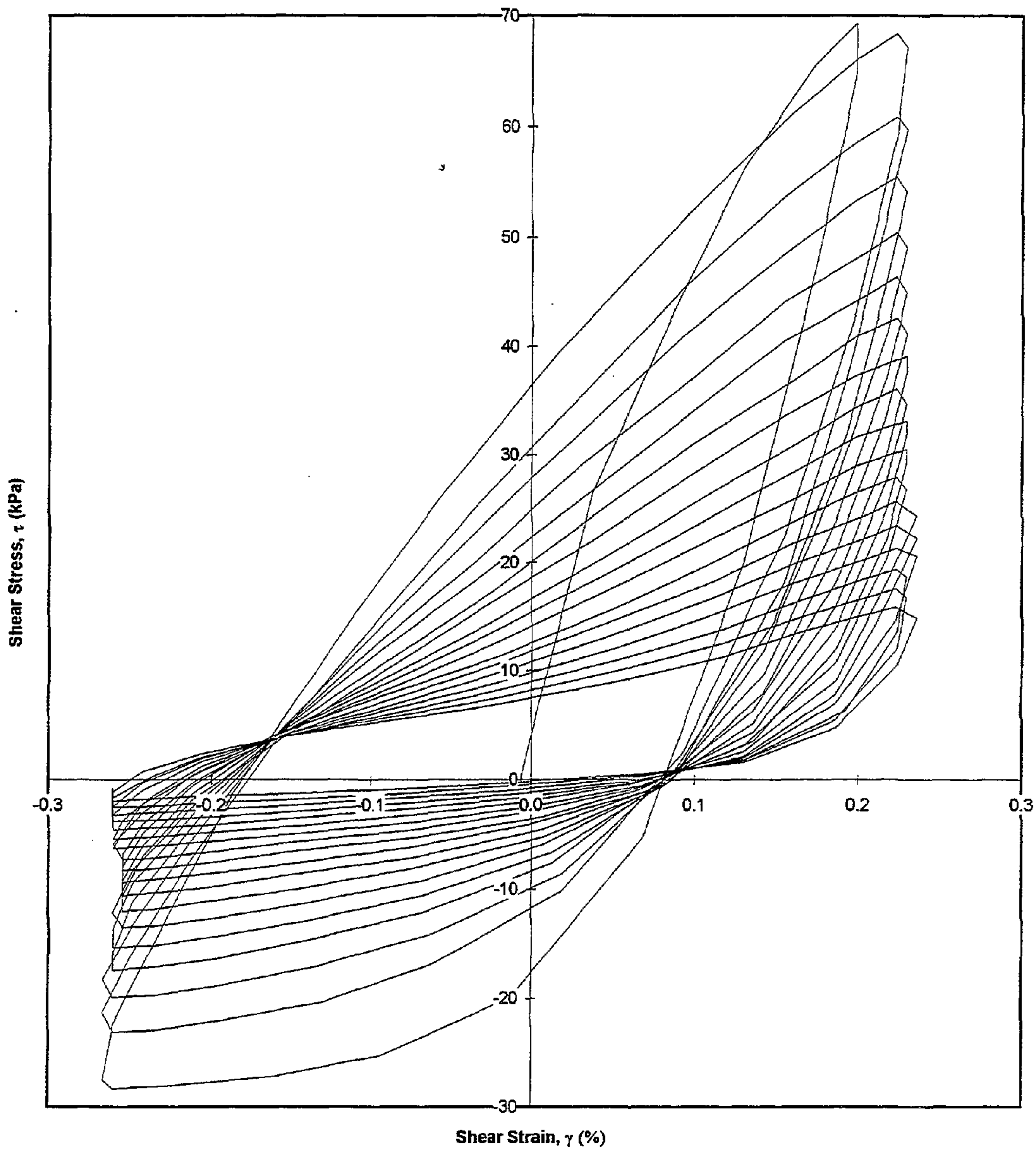

Test I.D.:	MONT20	**Controlled Parameter:**	Strain
Relative Density (%):	40.9	**Initial Effective Stress (kPa):**	100
Applied Shear Strain (%):	0.25	**Frequency (Hz):**	1

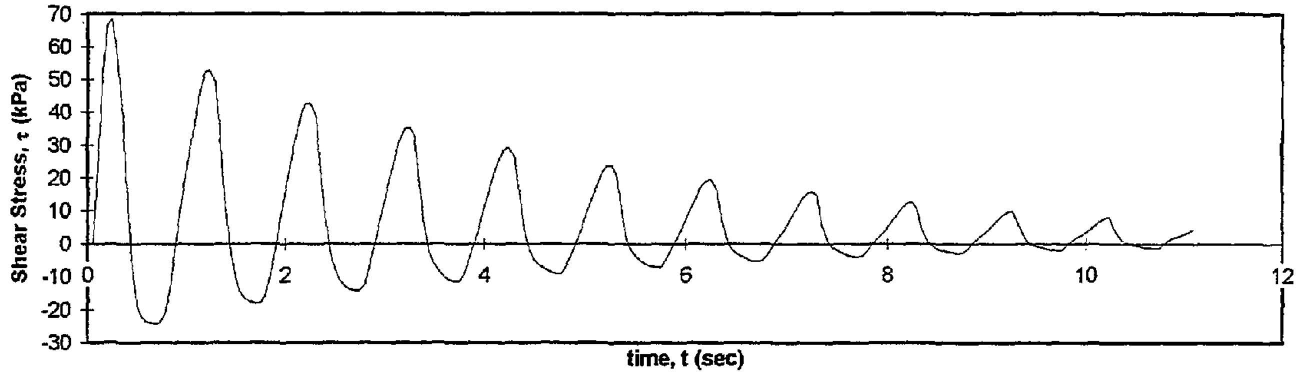

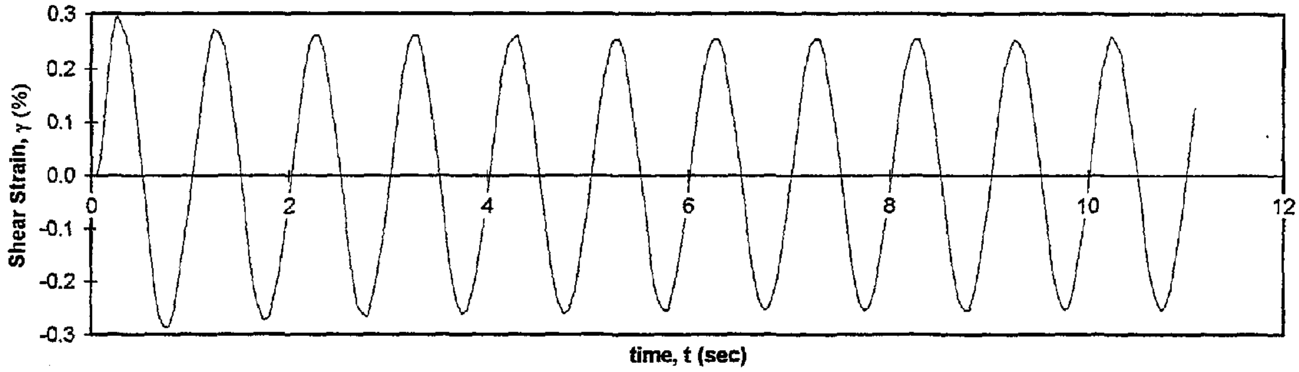

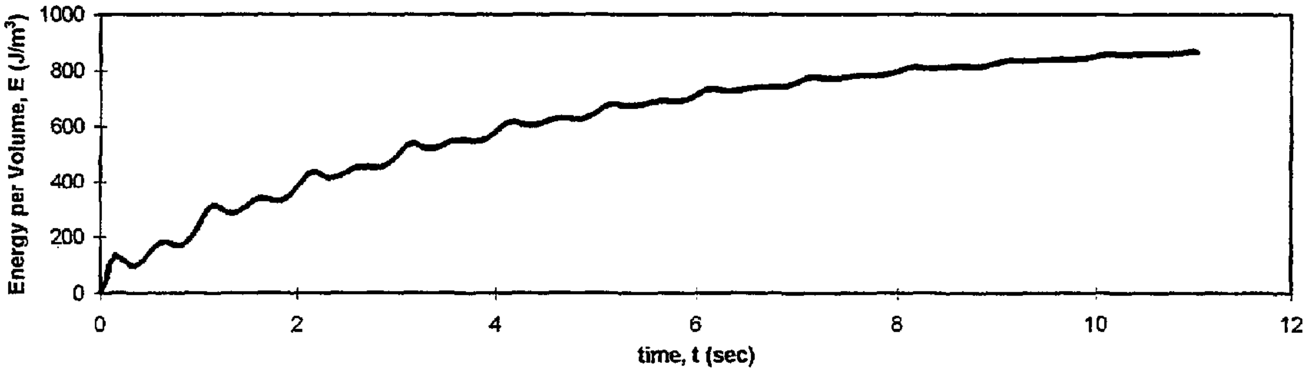

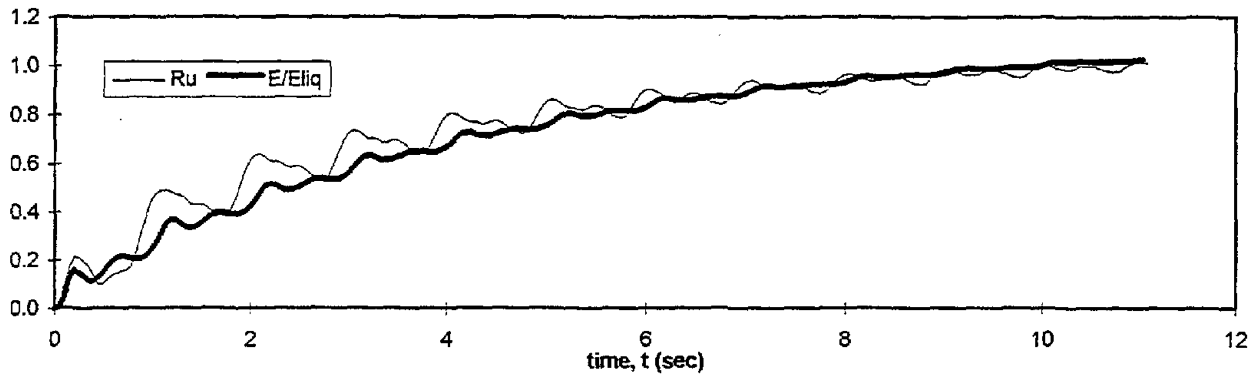

d:\nit\itp\cy_files\MONT20.XLS 8/15/96 11:47 AM

Test I.D.:	MONT20	**Controlled Parameter:**	Strain
Relative Density (%):	40.9	**Initial Effective Stress (kPa):**	100
Applied Shear Strain (%):	0.25	**Frequency (Hz):**	1

Shear Stress vs. Shear Strain

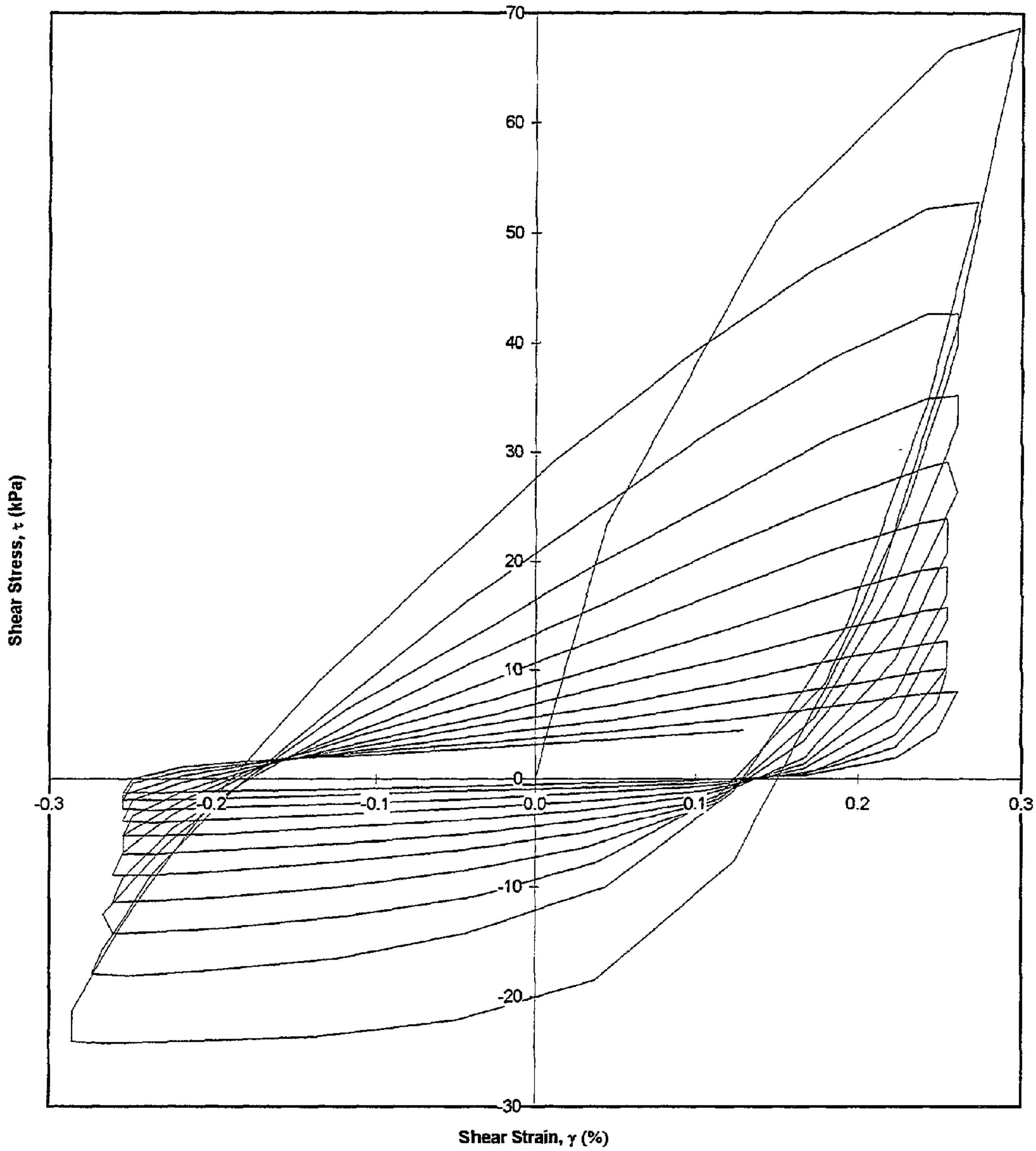

Test I.D.:	MONT21	**Controlled Parameter:**	Strain
Relative Density (%):	41.8	**Initial Effective Stress (kPa):**	100
Applied Shear Strain (%):	0.15	**Frequency (Hz):**	1

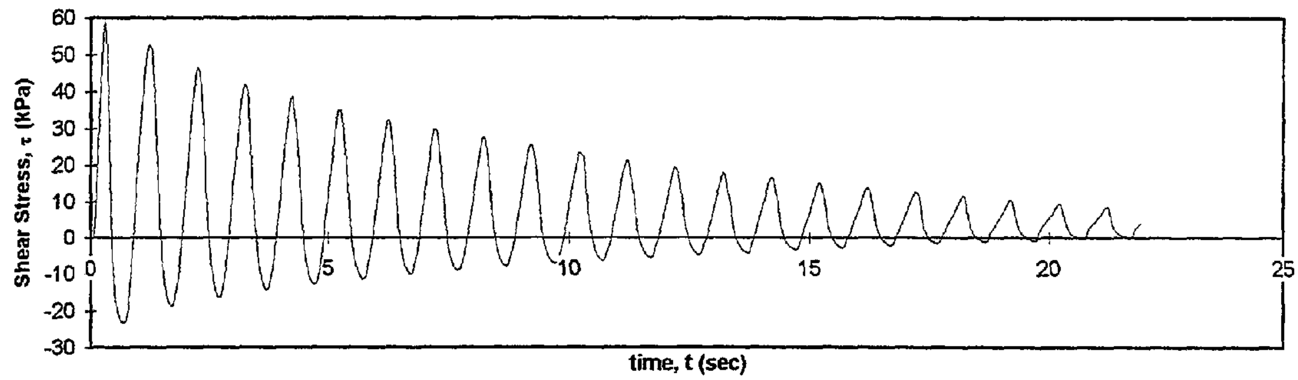

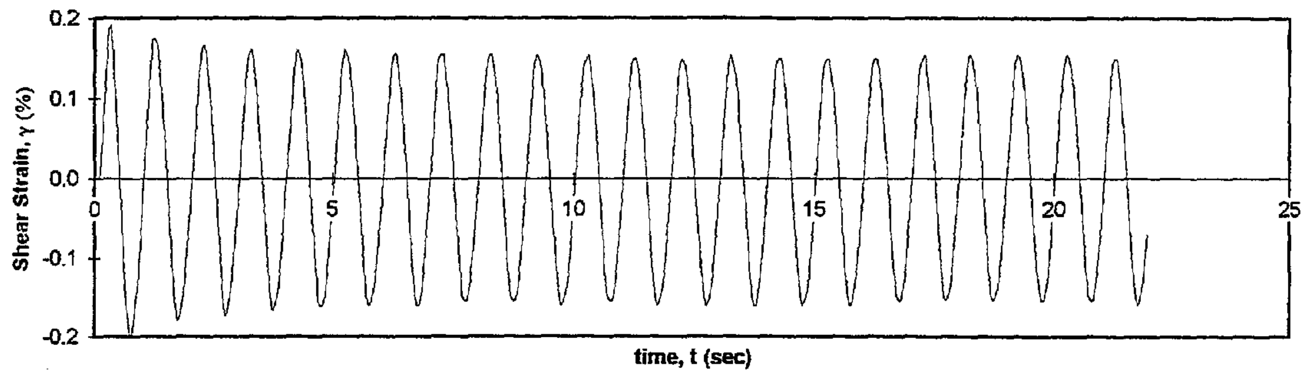

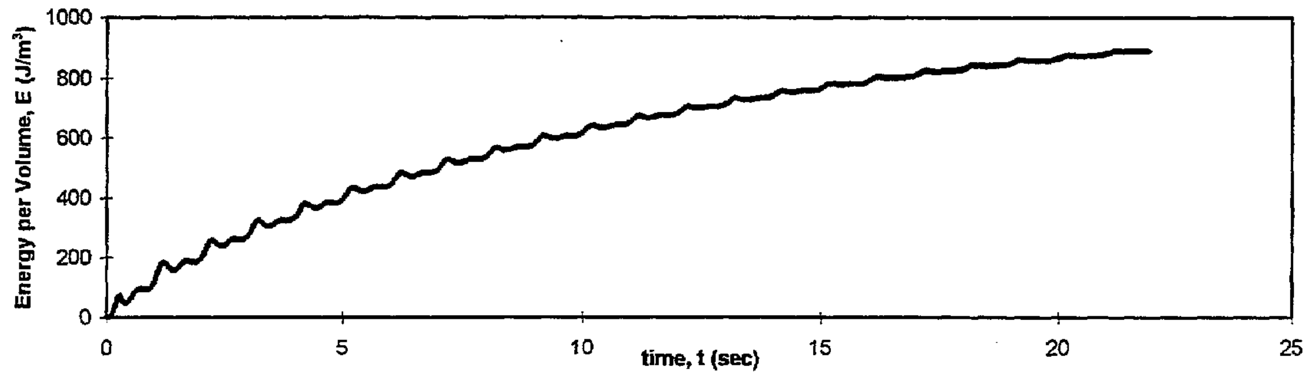

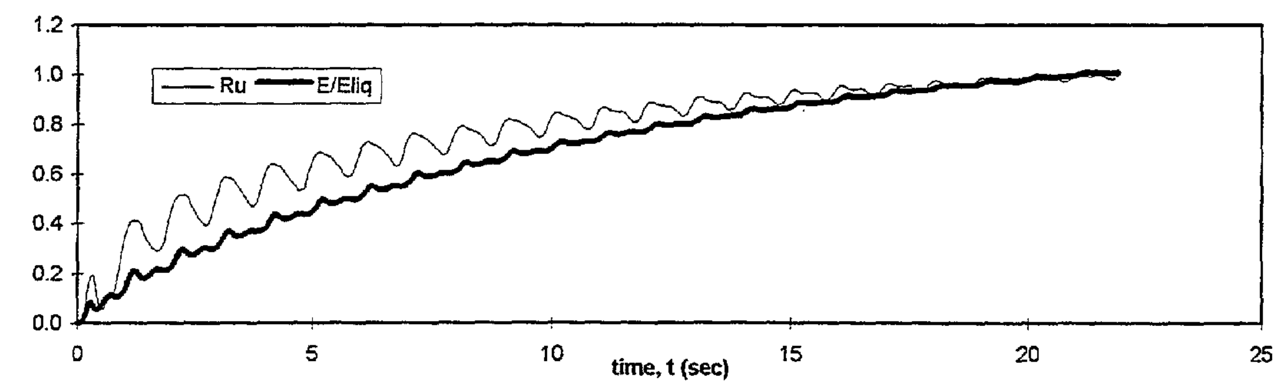

Test I.D.:	MONT21	**Controlled Parameter:**	Strain
Relative Density (%):	41.8	**Initial Effective Stress (kPa):**	100
Applied Shear Strain (%):	0.15	**Frequency (Hz):**	1

Shear Stress vs. Shear Strain

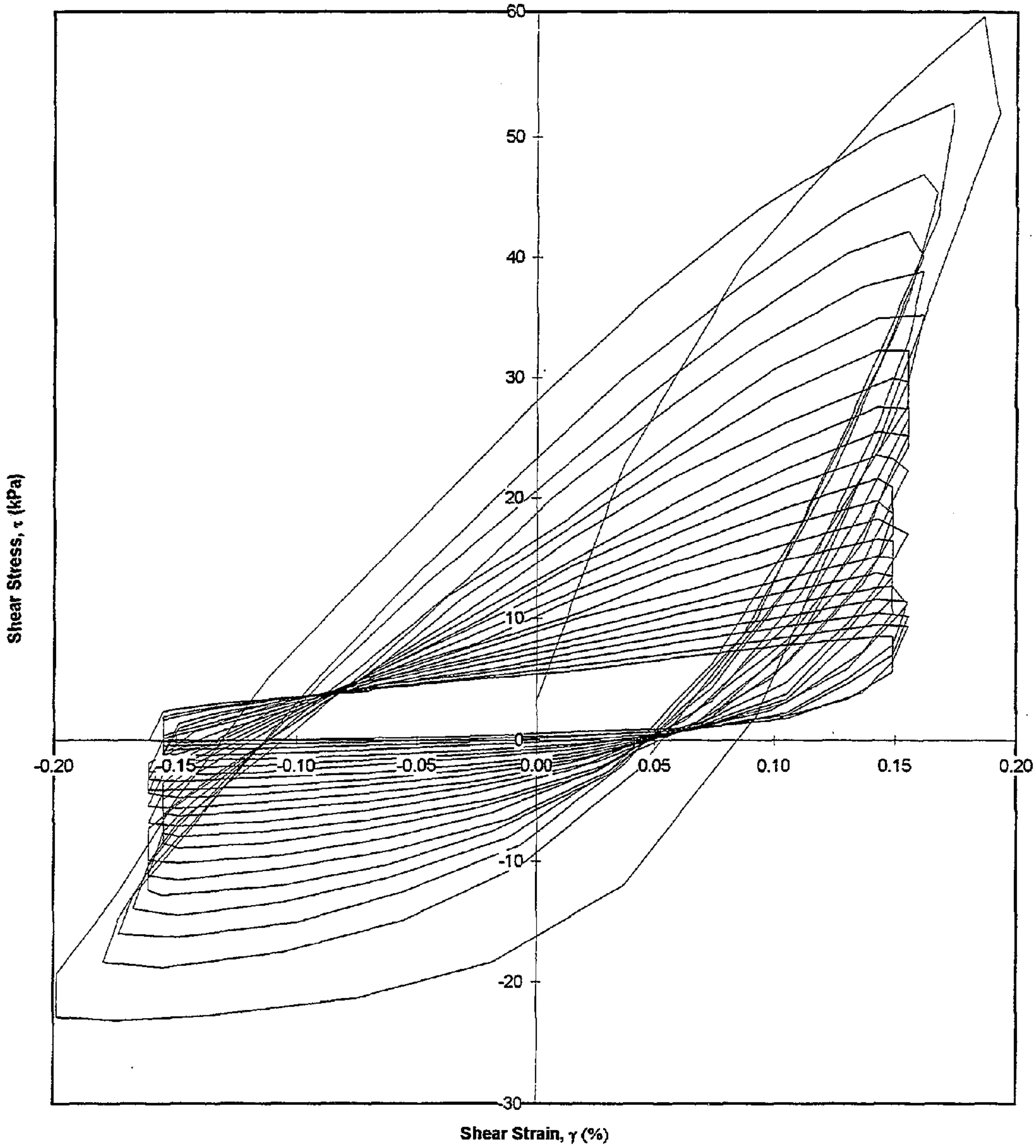

d:\nit\itp\cy_files\MONT21.XLS 8/15/96 11:53 AM

Test I.D.:	MONT22	**Controlled Parameter:**	Strain
Relative Density (%):	42.3	**Initial Effective Stress (kPa):**	100
Applied Shear Strain:	0.08%	**Frequency (Hz):**	1

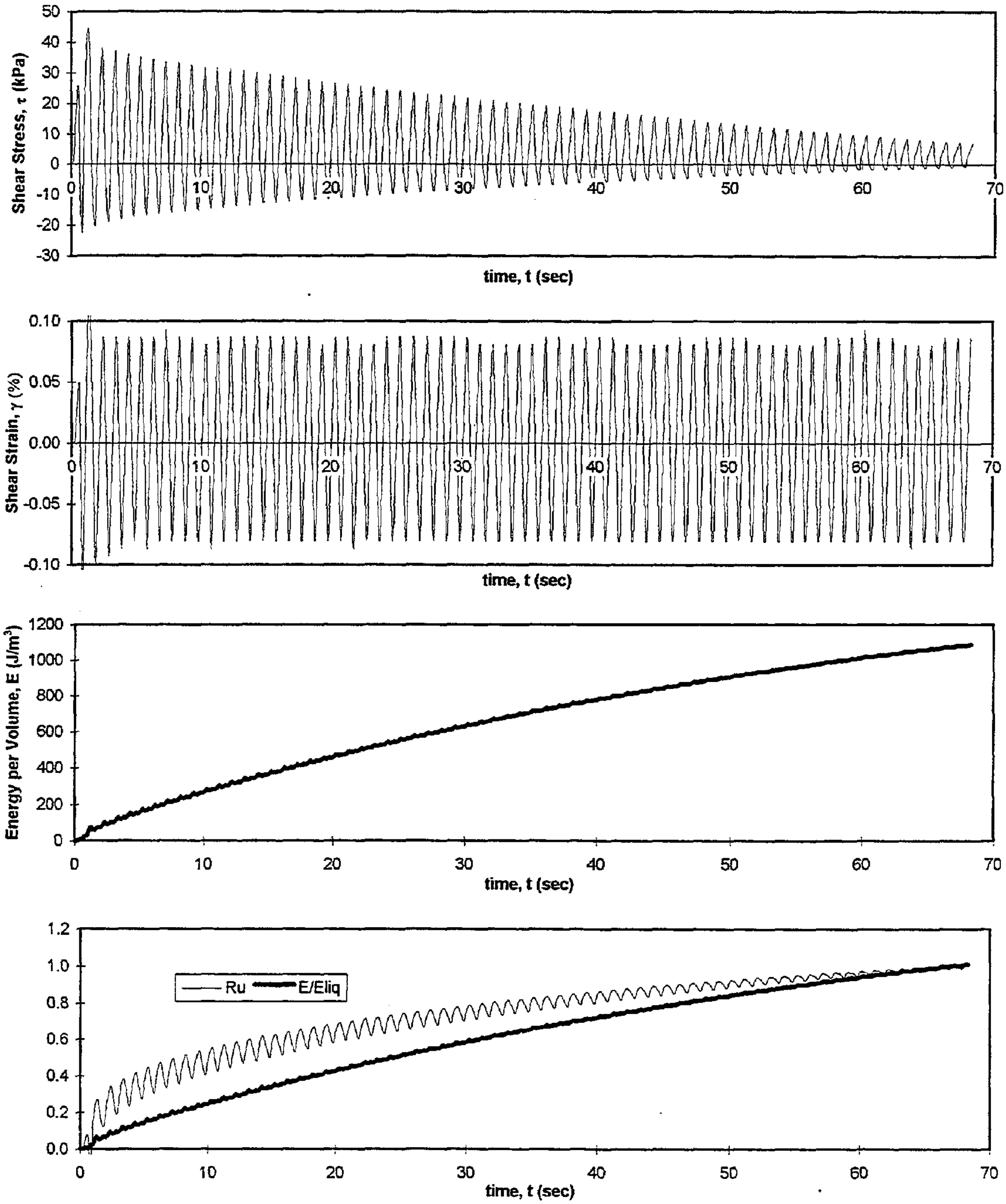

d:\nit\itp\cy_files\MONT22.XLS 8/21/96 9:47 AM

Test I.D.:	MONT22	**Controlled Parameter:**	Strain
Relative Density (%):	42.3	**Initial Effective Stress (kPa):**	100
Applied Shear Strain:	0.08%	**Frequency (Hz):**	1

Shear Stress vs. Shear Strain

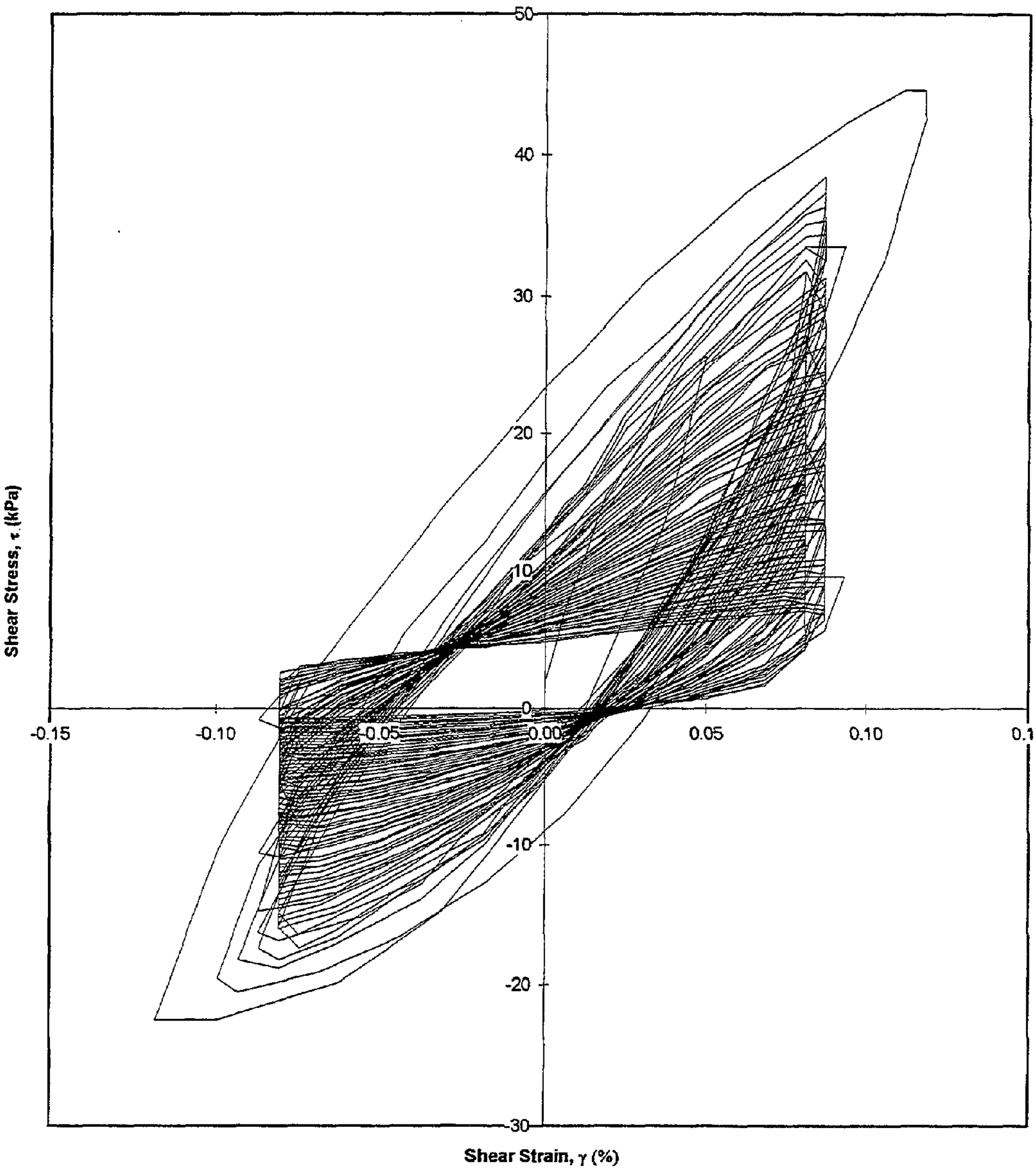

Test I.D.:	MONT24	**Controlled Parameter:**	Stress
Relative Density (%):	51.8	**Initial Effective Stress (kPa):**	100
Applied Stress Ratio:	0.31	**Frequency (Hz):**	1

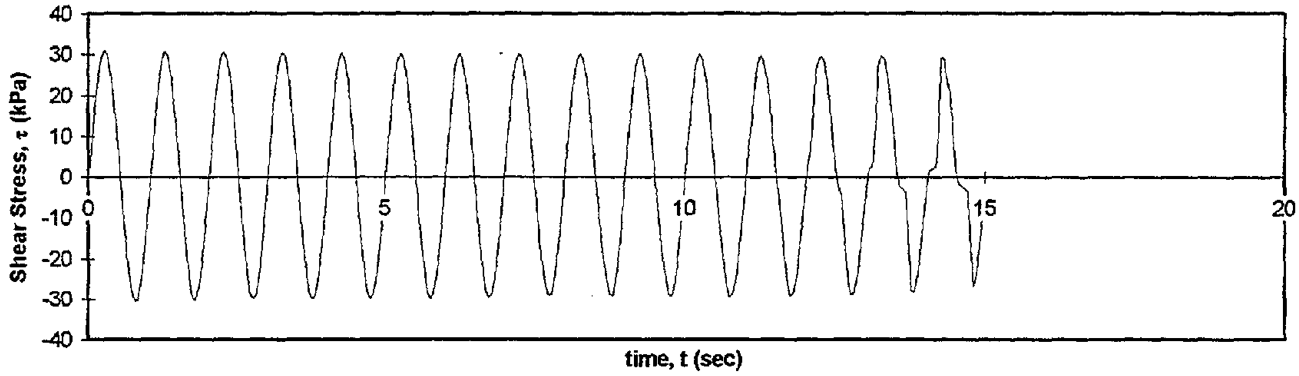

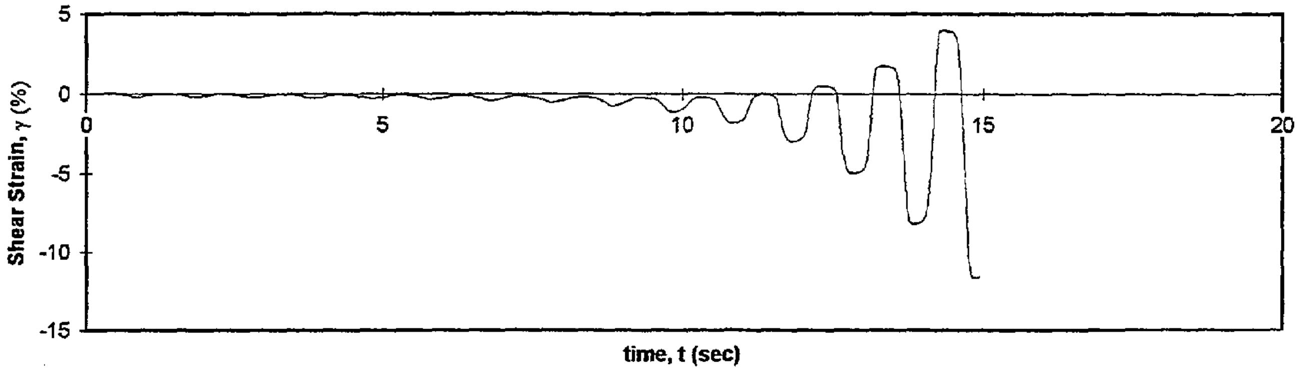

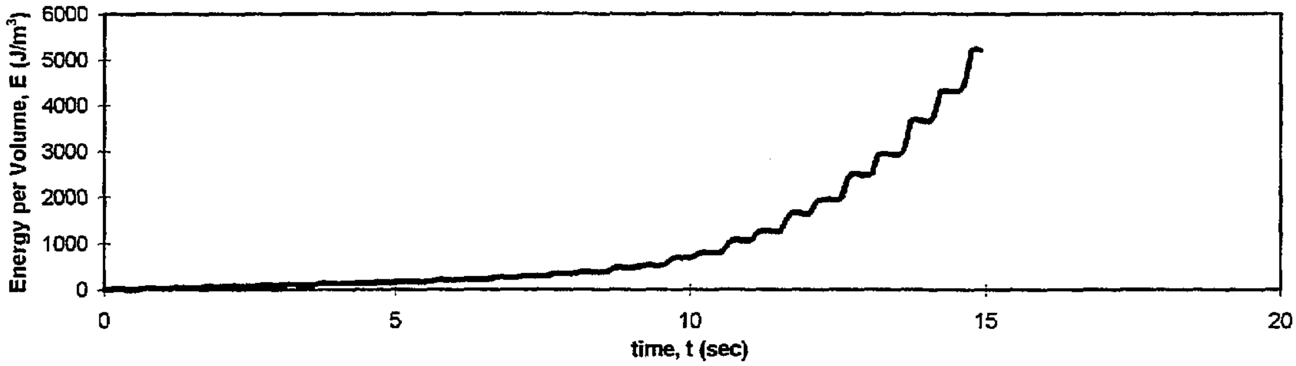

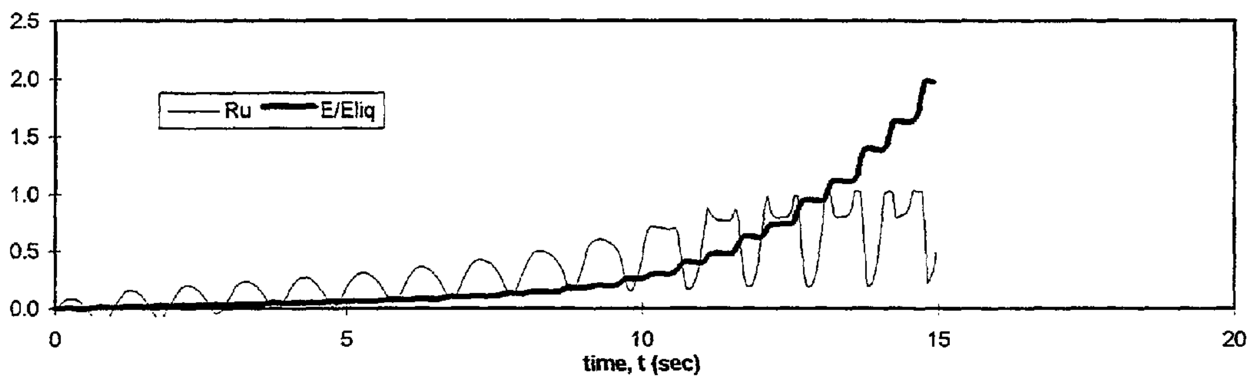

Test I.D.:	MONT24	**Controlled Parameter:**	Stress
Relative Density (%):	51.8	**Initial Effective Stress (kPa):**	100
Applied Stress Ratio:	0.31	**Frequency (Hz):**	1

Shear Stress vs. Shear Strain

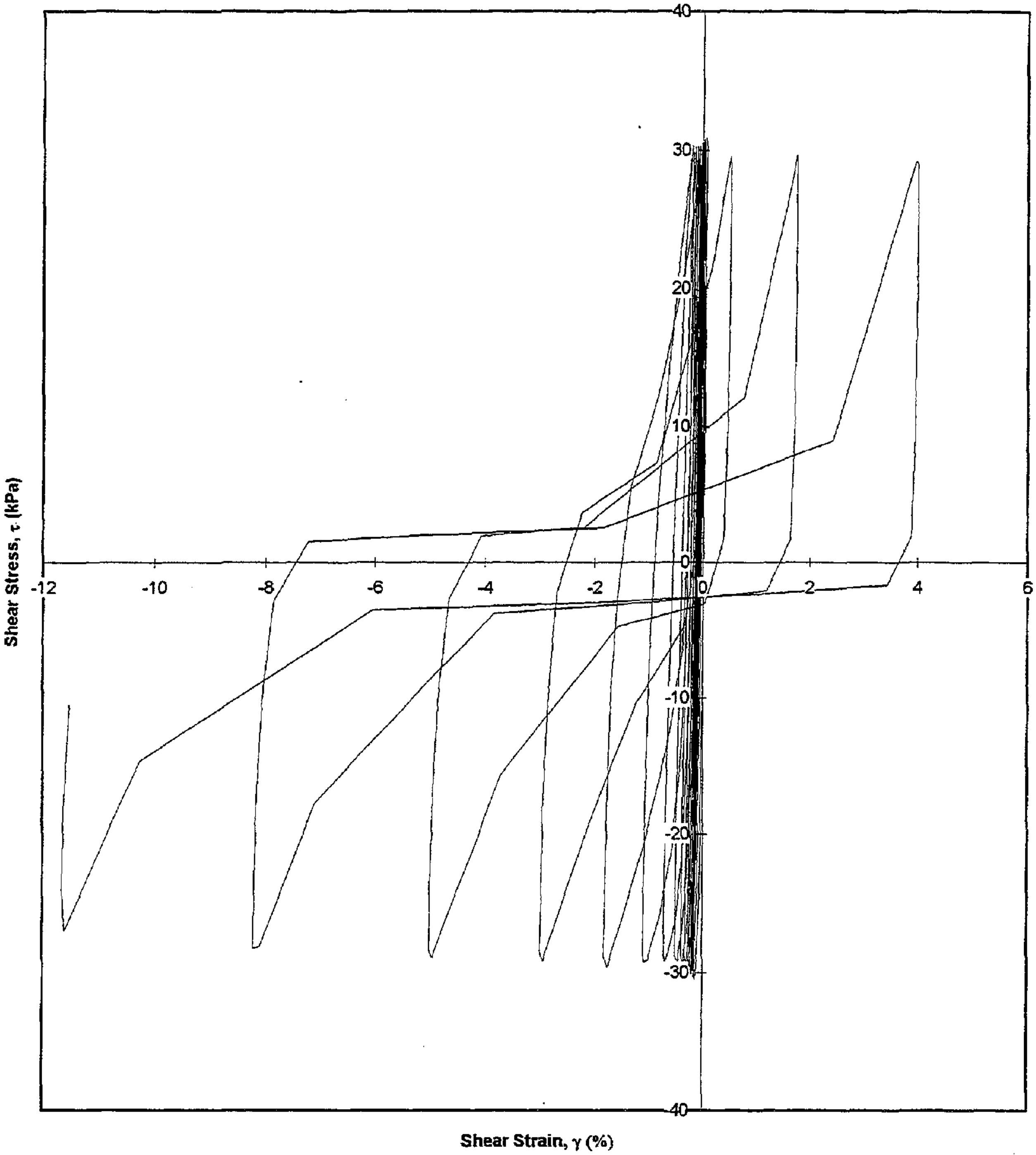

d:\nit\itp\cy_files\MONT24.XLS 8/21/96 9:48 AM

Test I.D.:	MONT25	**Controlled Parameter:**	Stress
Relative Density (%):	50.4	**Initial Effective Stress (kPa):**	100
Applied Stress Ratio:	0.25	**Frequency (Hz):**	1

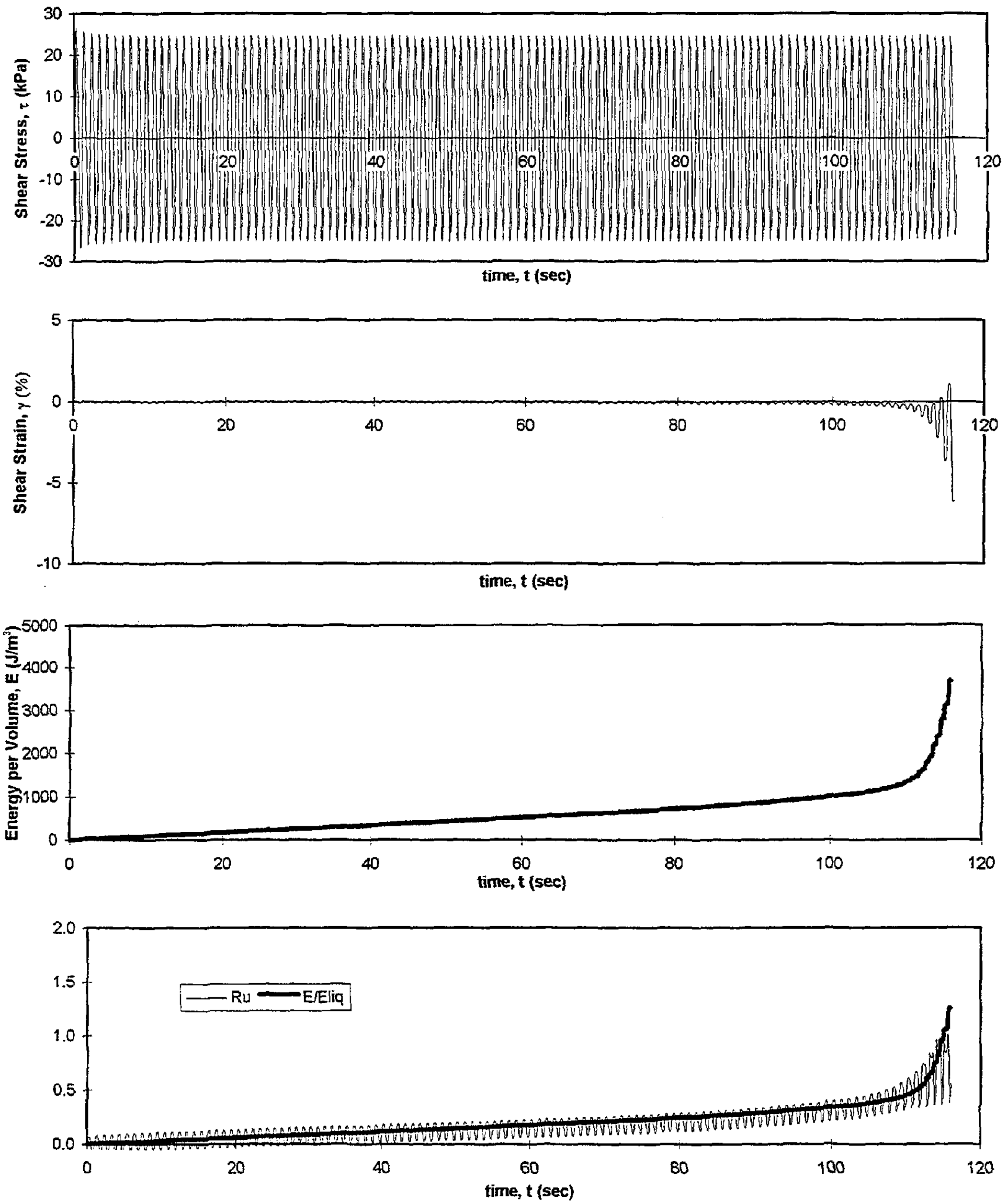

Test I.D.:	MONT25	**Controlled Parameter:**	Stress
Relative Density (%):	50.4	**Initial Effective Stress (kPa):**	100
Applied Stress Ratio:	0.25	**Frequency (Hz):**	1

Shear Stress vs. Shear Strain

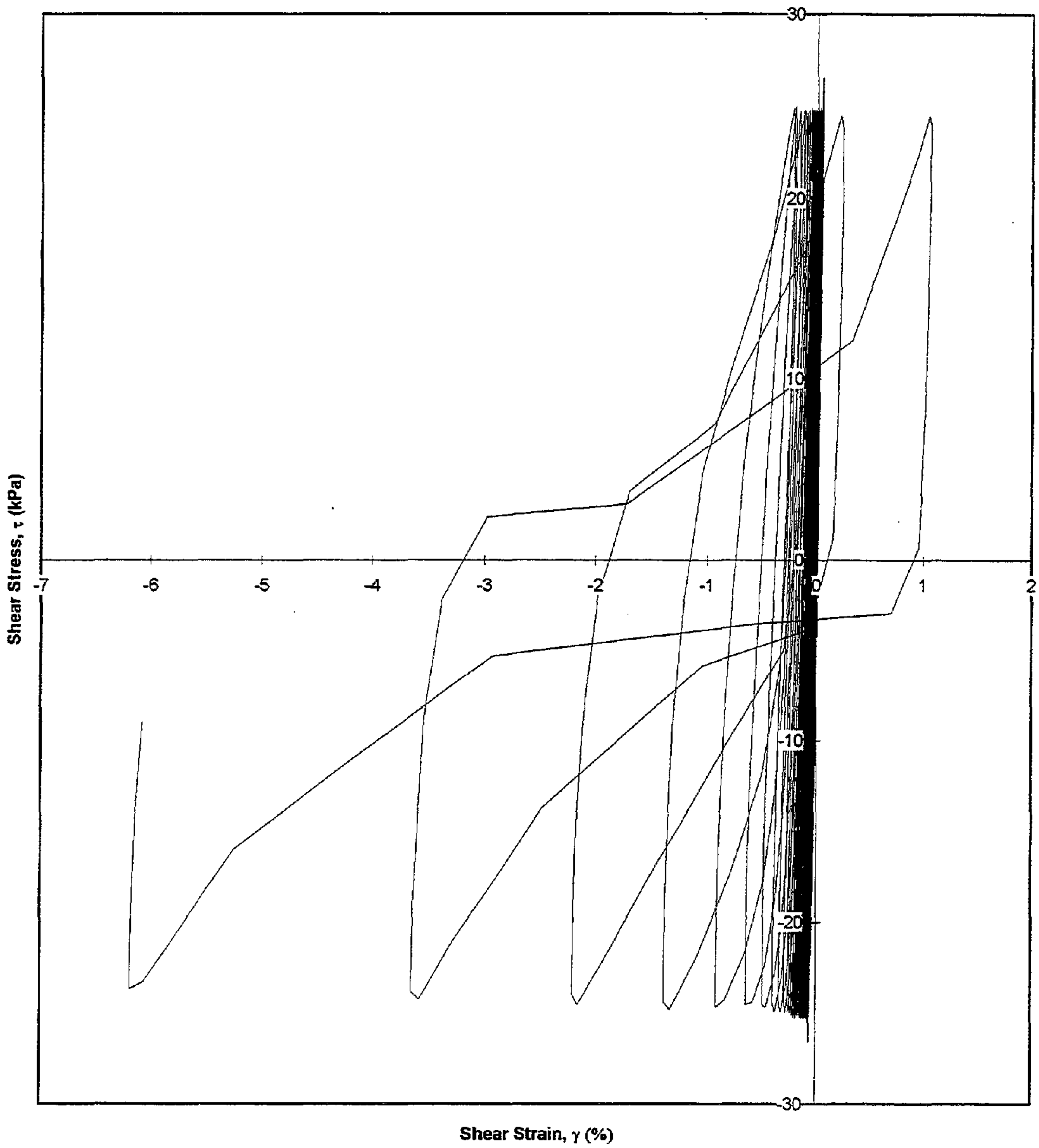

d:\nit\itp\cy_files\MONT25.XLS 8/20/96 8:23 AM

Test I.D.:	MONT26	**Controlled Parameter:**	Stress
Relative Density (%):	49.9	**Initial Effective Stress (kPa):**	100
Applied Stress Ratio:	0.35	**Frequency (Hz):**	1

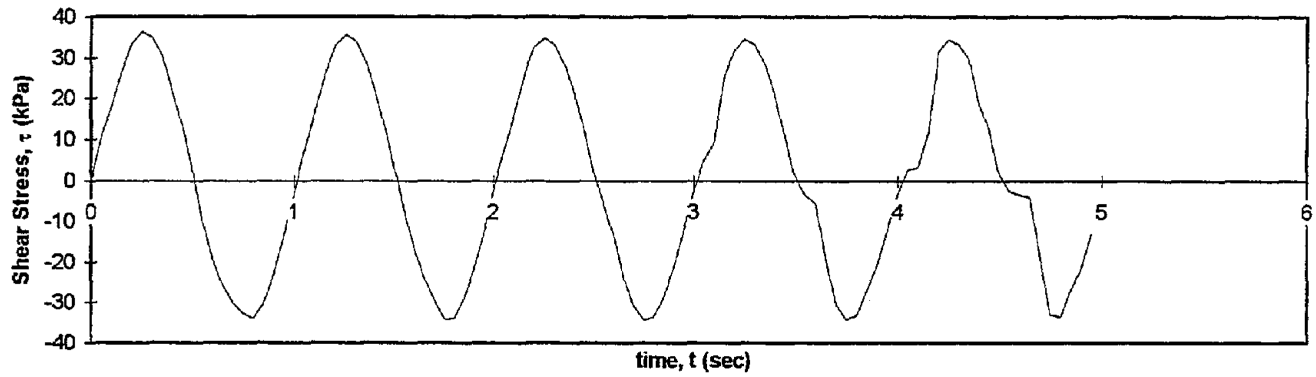

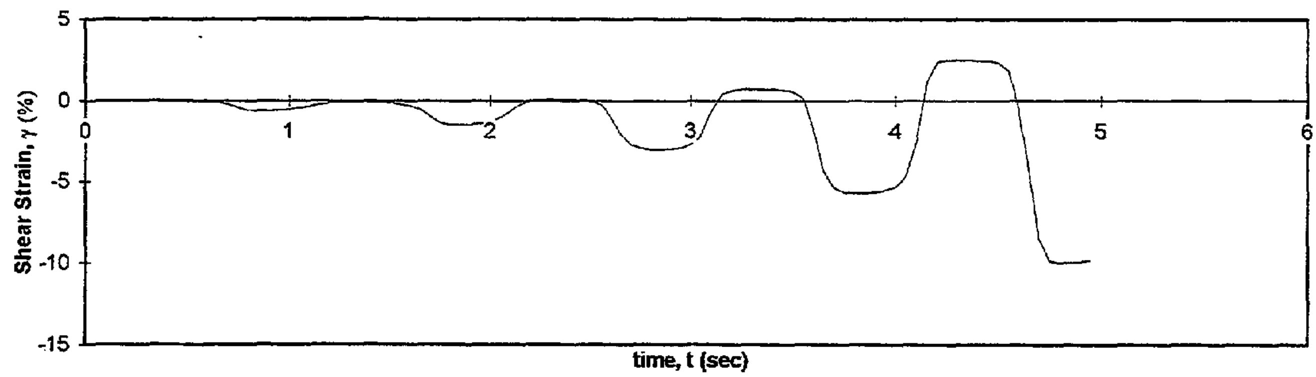

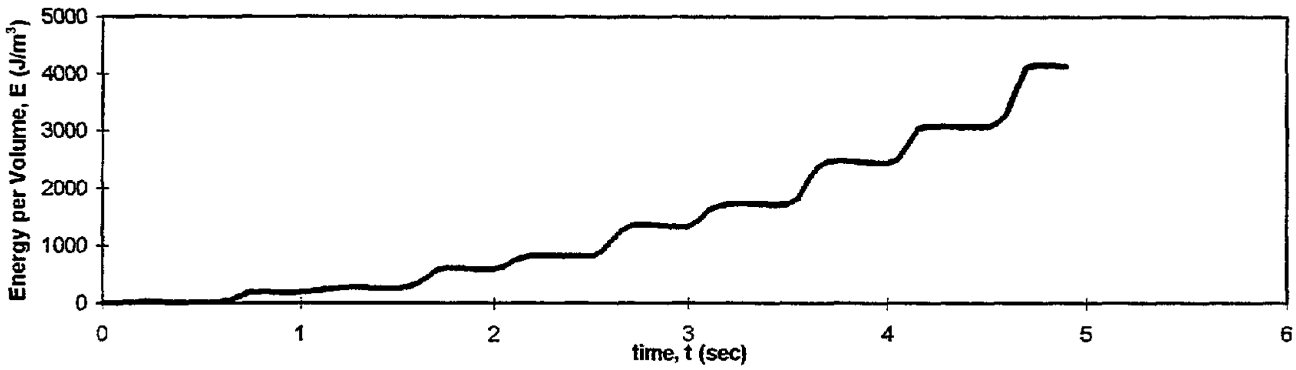

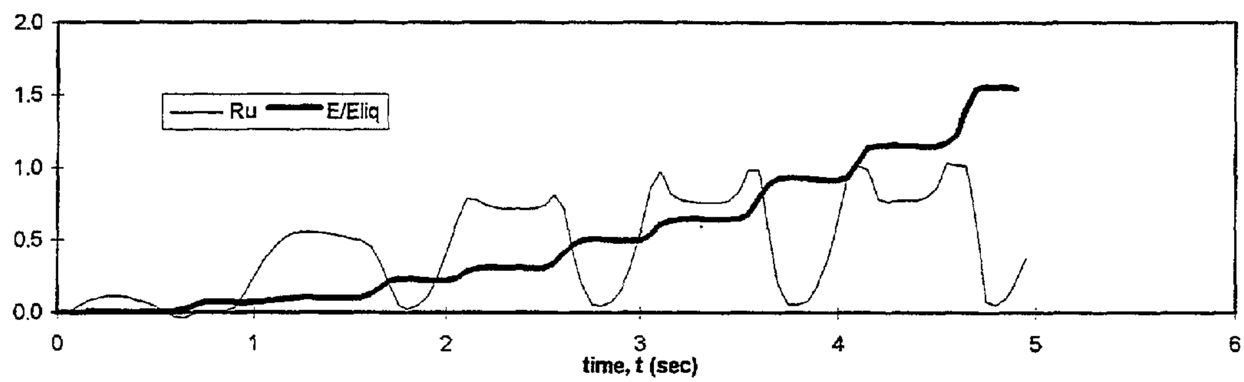

d:\nit\itp\cy_files\MONT26.XLS 8/21/96 8:58 AM

Test I.D.:	MONT26	**Controlled Parameter:**	Stress
Relative Density (%):	49.9	**Initial Effective Stress (kPa):**	100
Applied Stress Ratio:	0.35	**Frequency (Hz):**	1

Shear Stress vs. Shear Strain

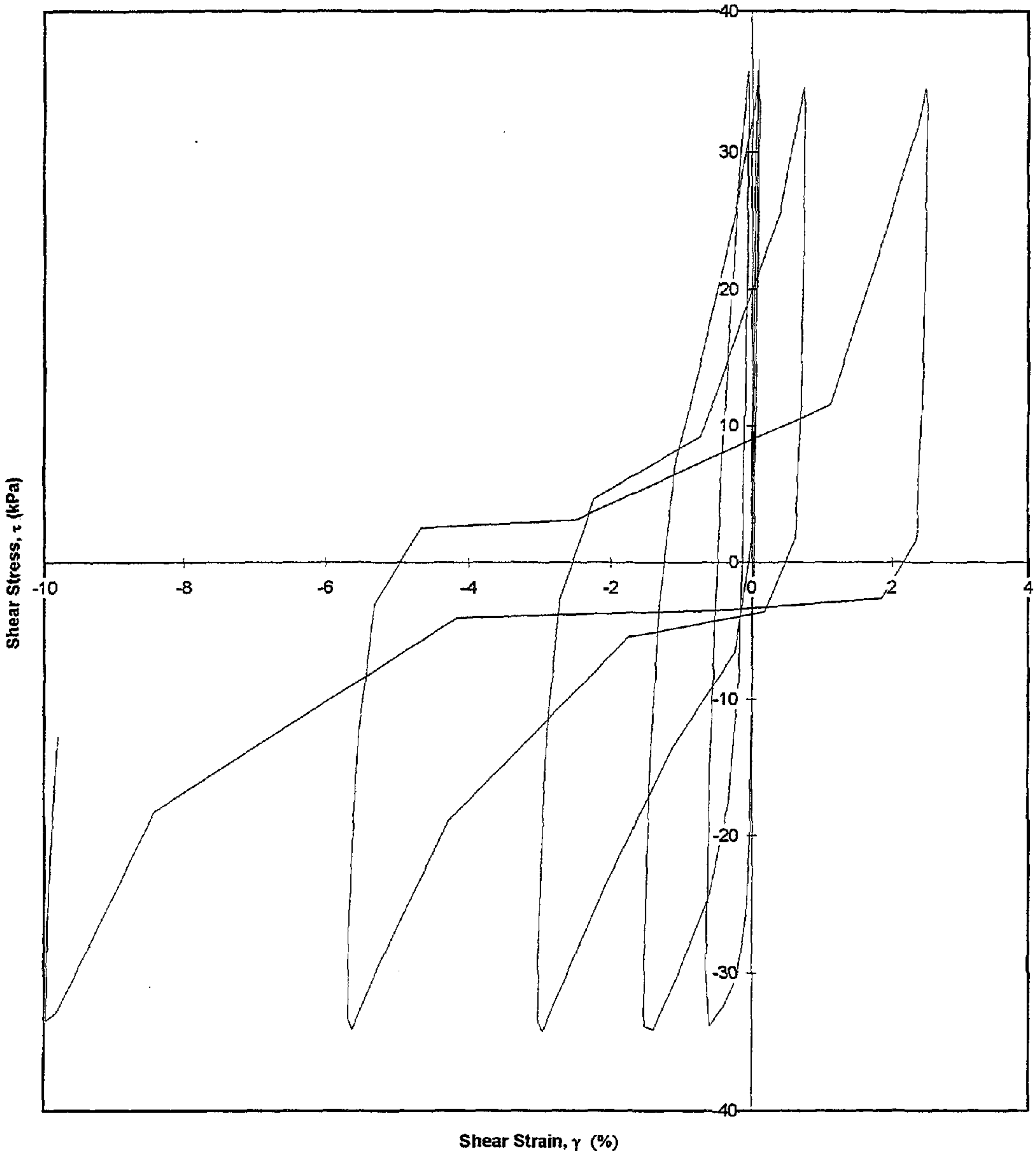

Test I.D.:	MONT30	**Controlled Parameter:**	Strain
Relative Density (%)	41.9	**Initial Effective Stress (kPa):**	100
Applied Shear Strain (%):	0.26	**Frequency (Hz):**	10

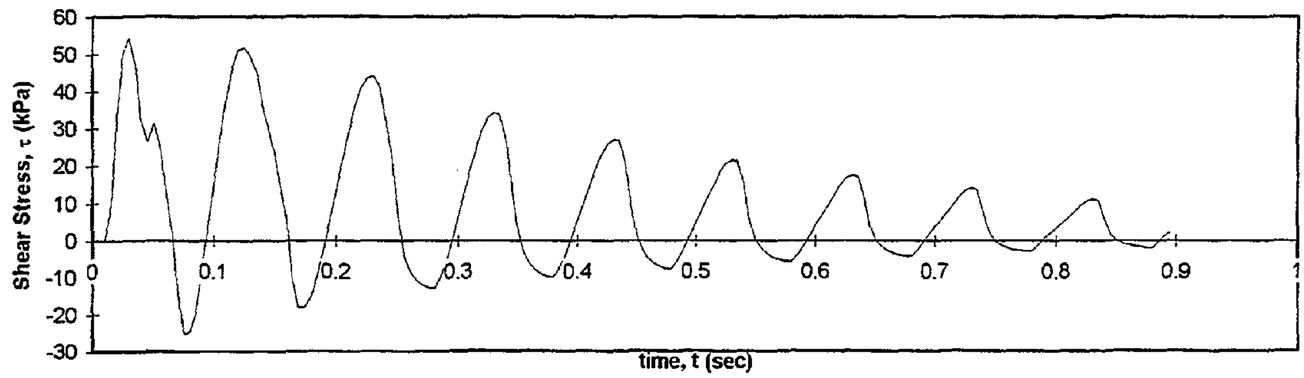

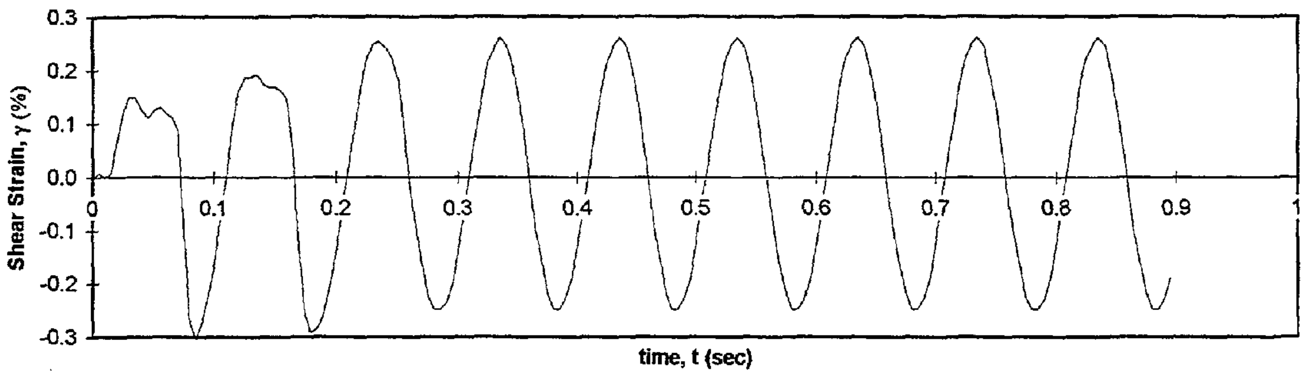

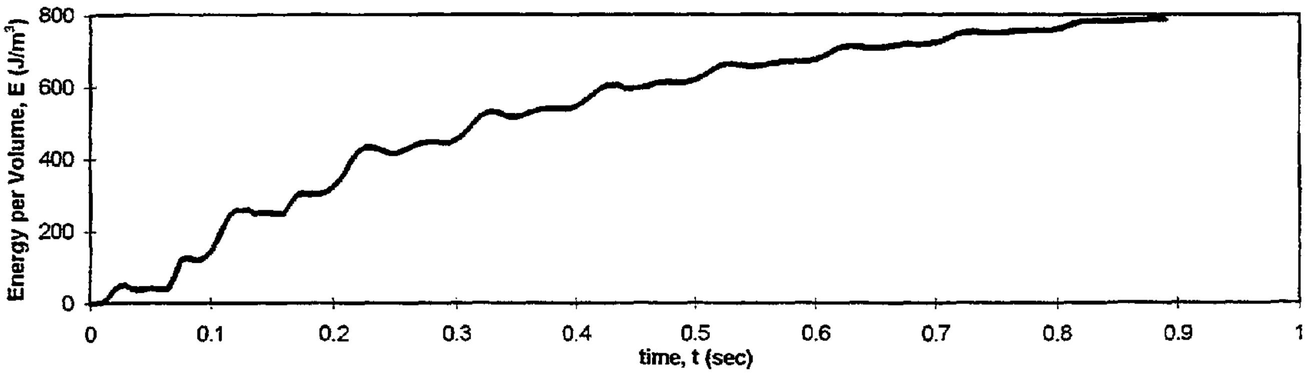

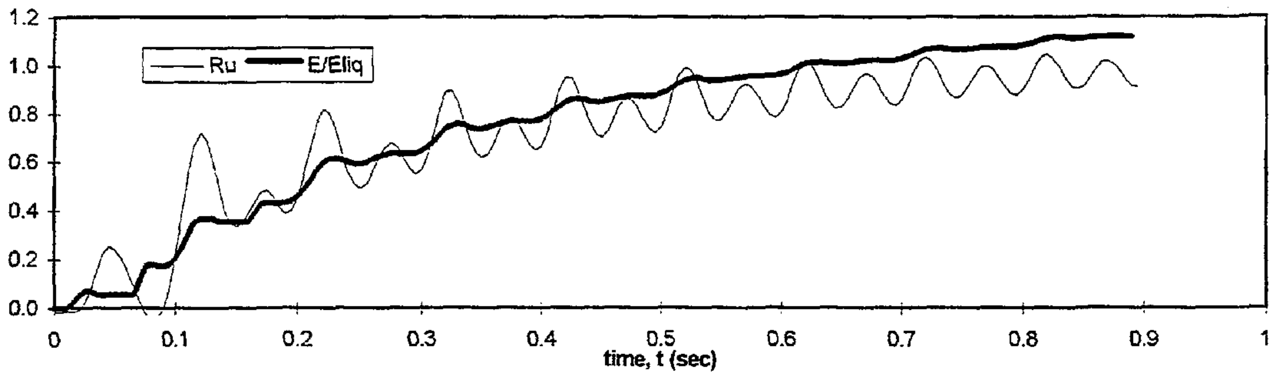

Test I.D.:	MONT30	**Controlled Parameter:**	Strain
Relative Density (%)	41.9	**Initial Effective Stress (kPa):**	100
Applied Shear Strain (%):	0.26	**Frequency (Hz):**	10

Shear Stress vs. Shear Strain

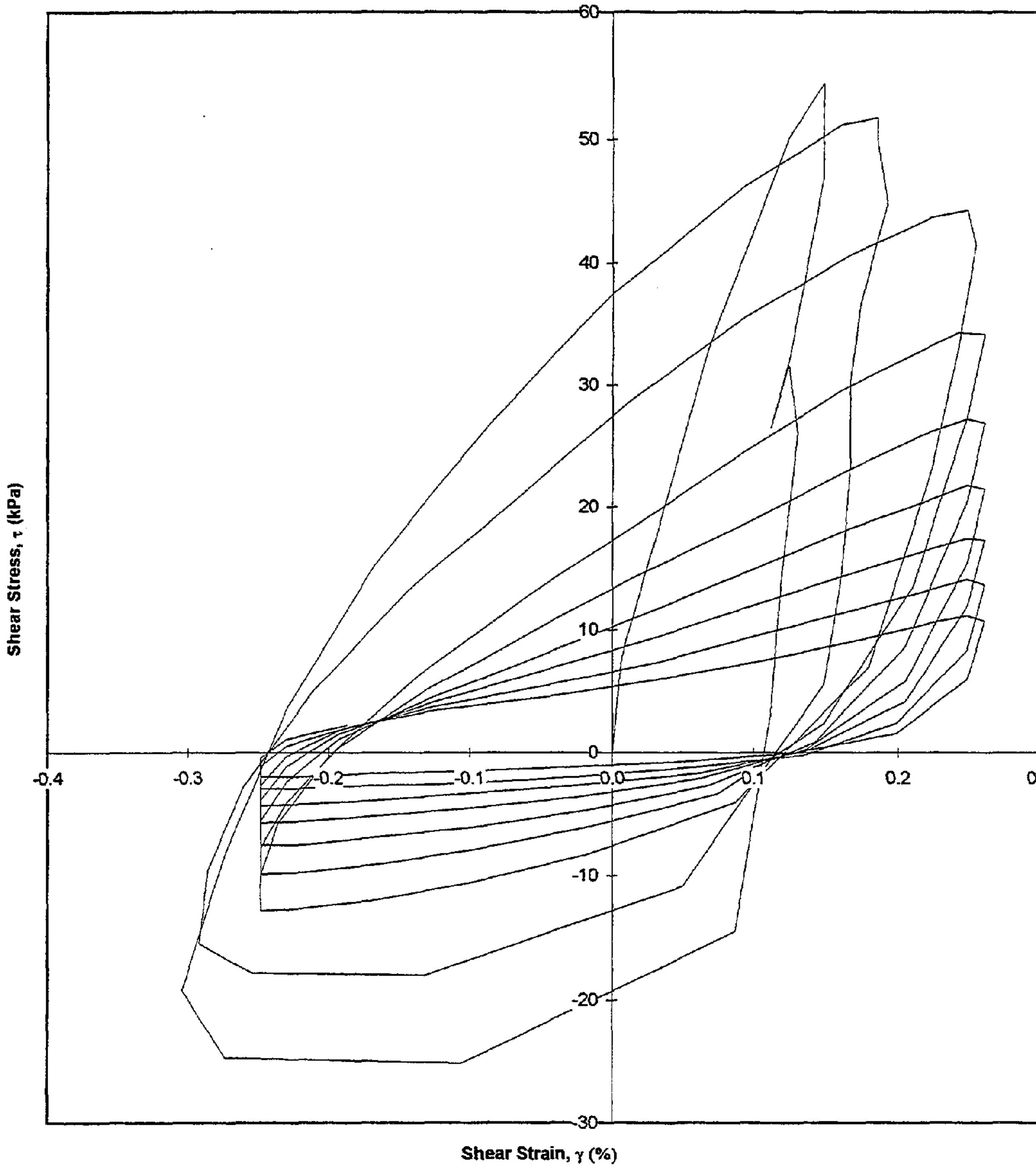

d:\nit\itp\cy_files\MONT30.XLS

8/21/96 9:08 AM

Test I.D.:	MONT33	**Controlled Parameter:**	Strain
Relative Density (%)	40.5	**Initial Effective Stress (kPa):**	100
Applied Shear Strain (%)	0.08	**Frequency (Hz):**	10

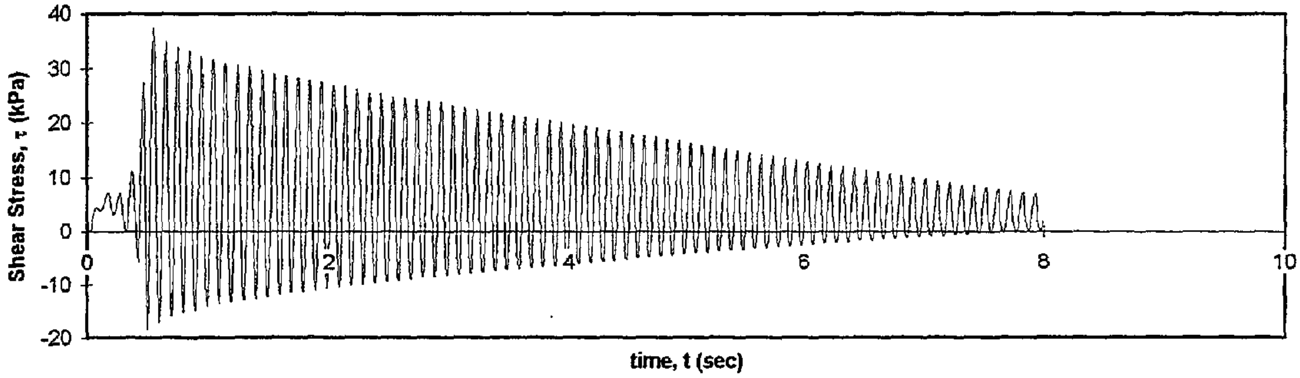

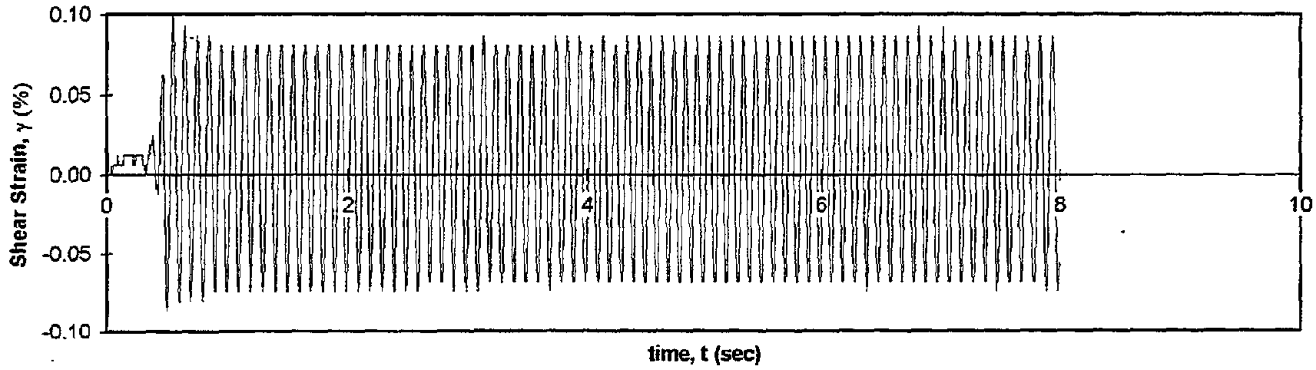

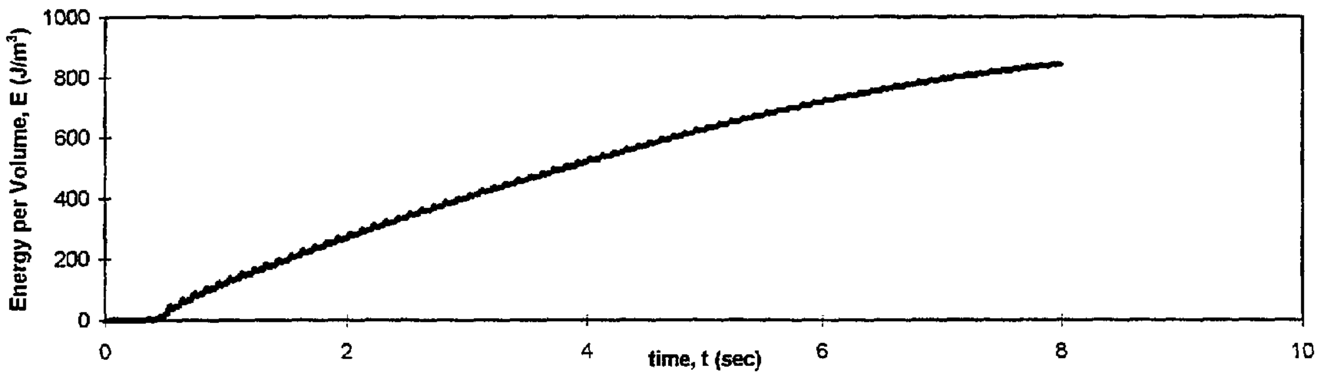

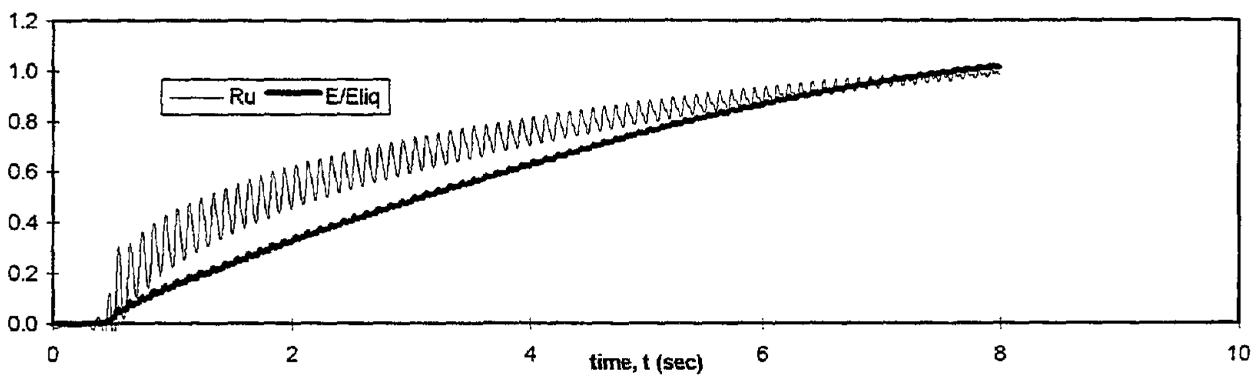

Test I.D.:	MONT33	**Controlled Parameter:**	Strain
Relative Density (%)	40.5	**Initial Effective Stress (kPa):**	100
Applied Shear Strain (%)	0.08	**Frequency (Hz):**	10

Shear Stress vs. Shear Strain

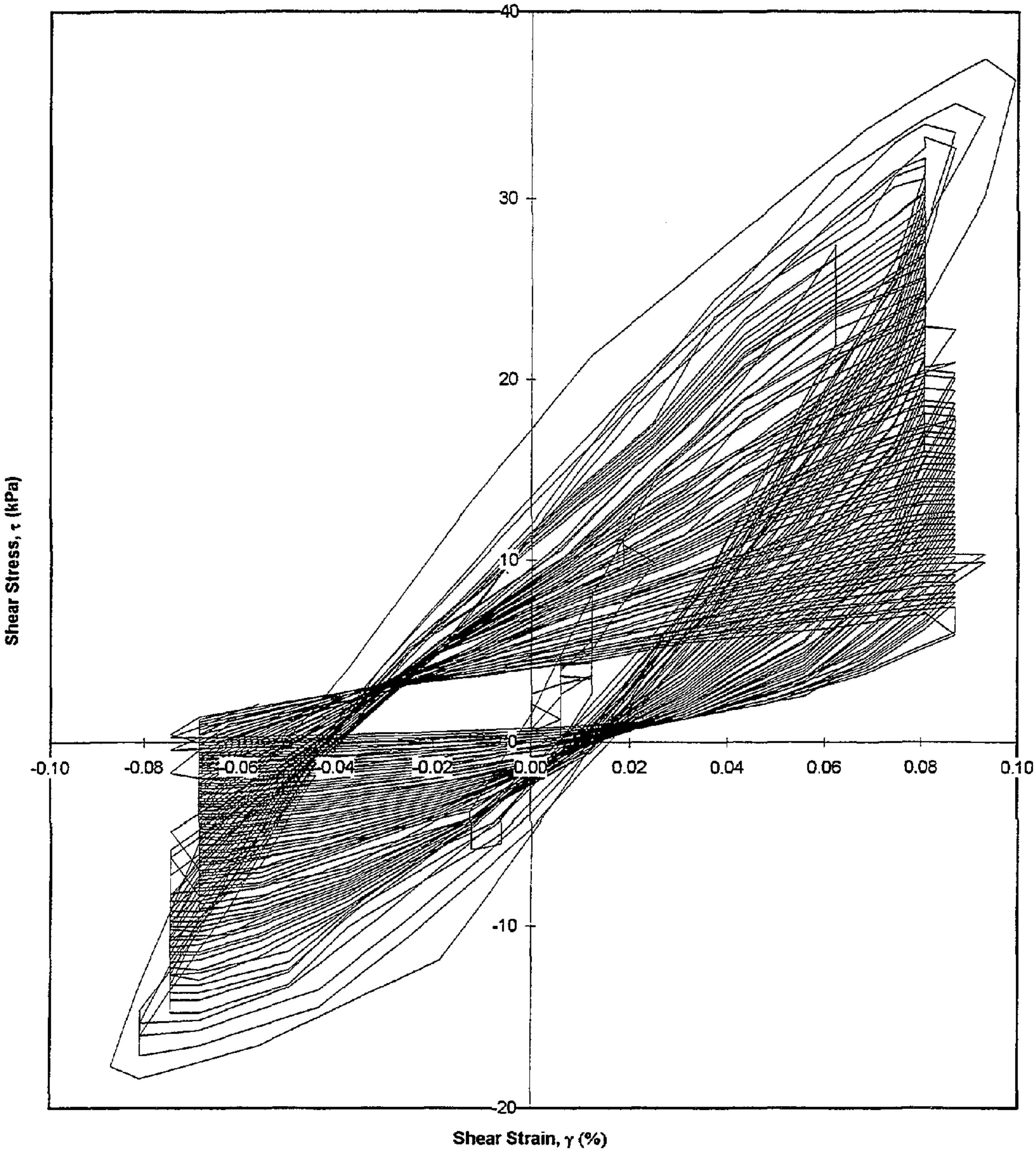

Test I.D.:	MONT35	**Controlled Parameter:**	Stress
Relative Density (%)	61.8	**Initial Effective Stress (kPa):**	100
Applied Stress Ratio:	0.35	**Frequency (Hz):**	0.1

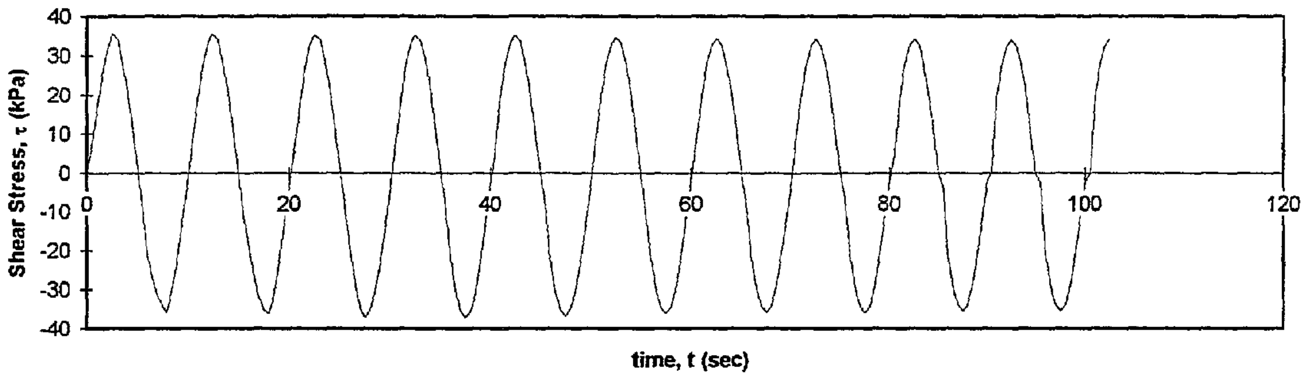

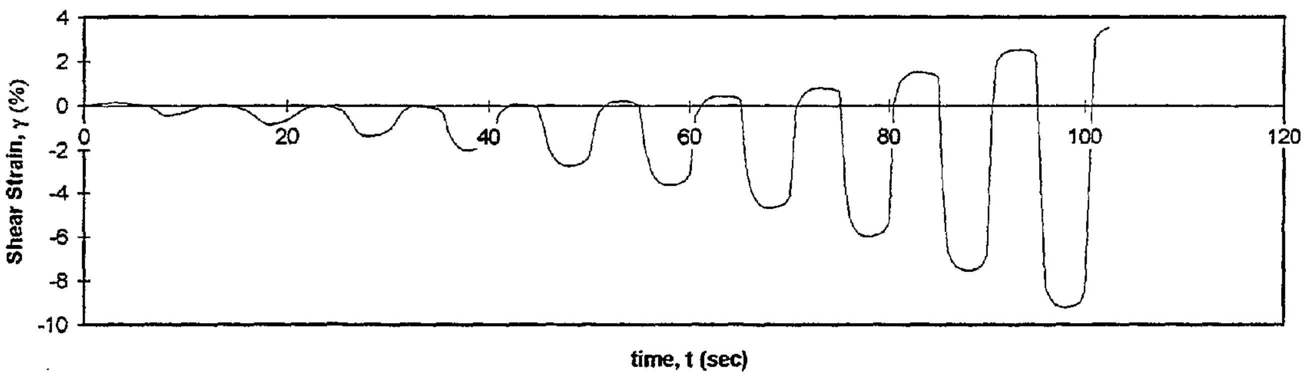

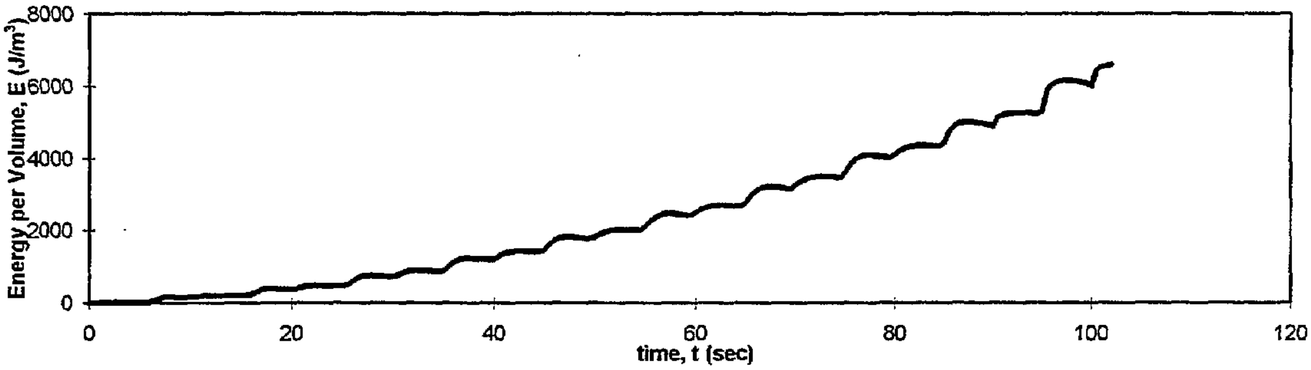

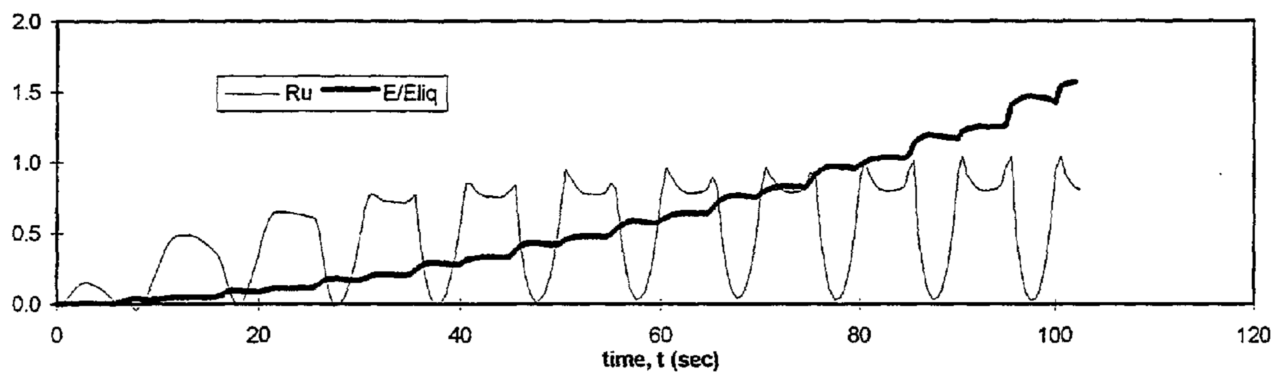

Test I.D.:	MONT35	**Controlled Parameter:**	Stress
Relative Density (%):	61.8	**Initial Effective Stress (kPa):**	100
Applied Stress Ratio:	0.35	**Frequency (Hz):**	0.1

Shear Stress vs. Shear Strain

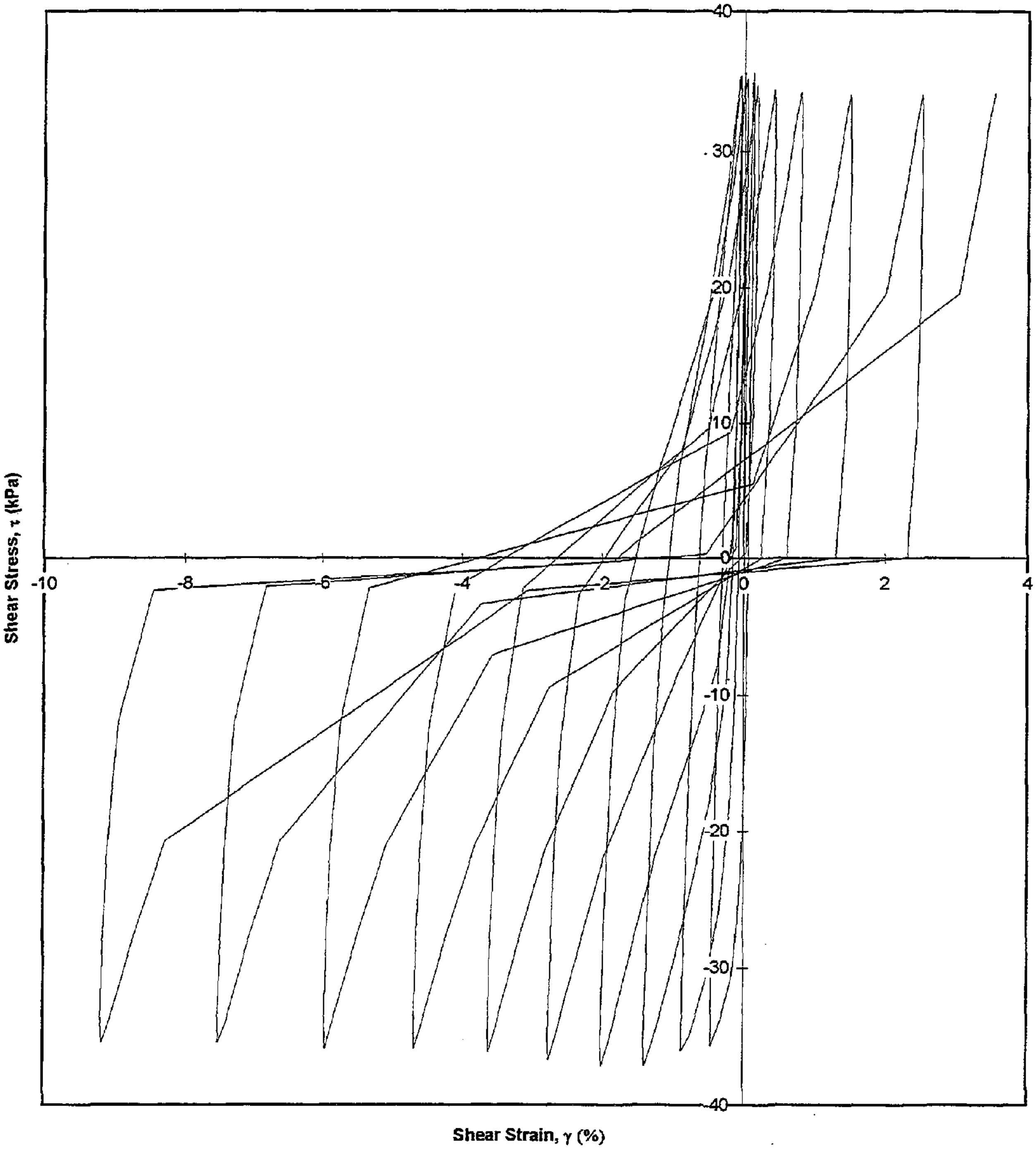

d:\nit\itp\cy_files\MONT35.XLS 8/20/96 10:42 AM

Test I.D.:	MONT37	**Controlled Parameter:**	Strain
Relative Density (%):	61.6	**Initial Effective Stress (kPa):**	100
Applied Shear Strain (%)	0.17	**Frequency (Hz):**	1

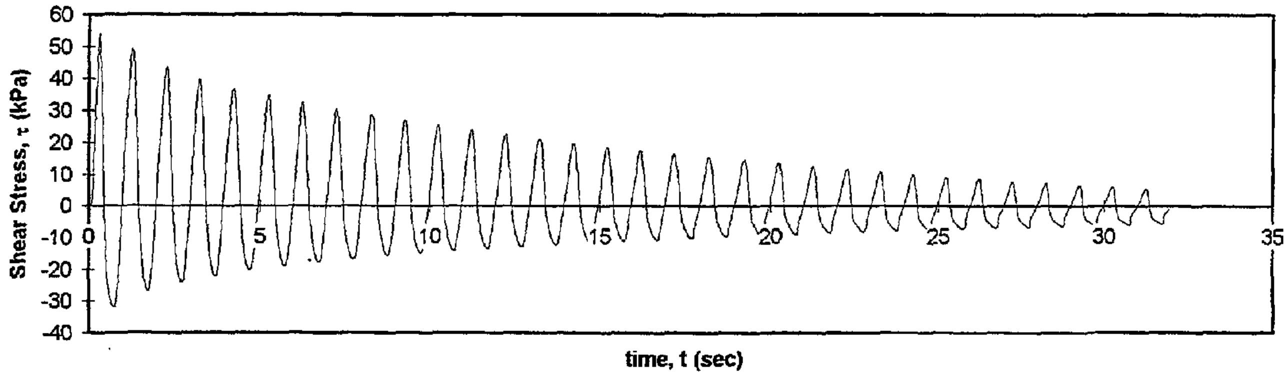

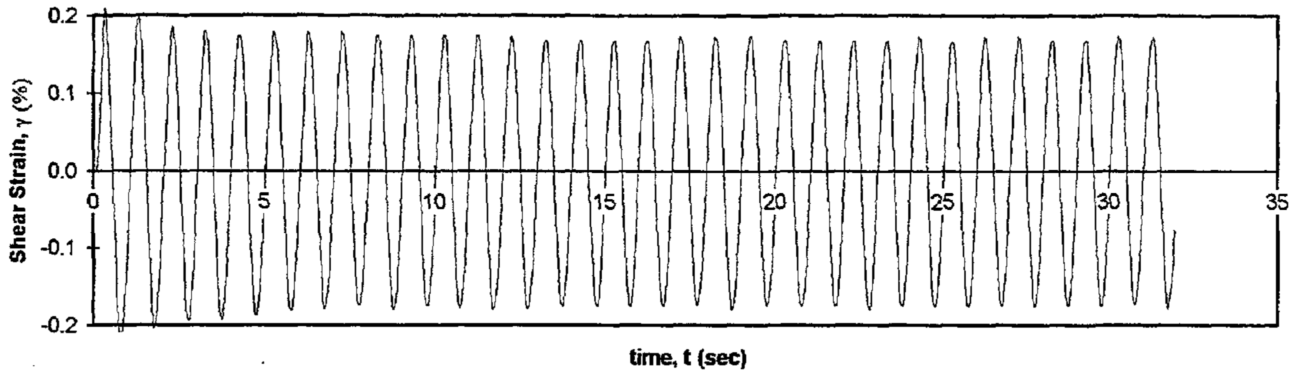

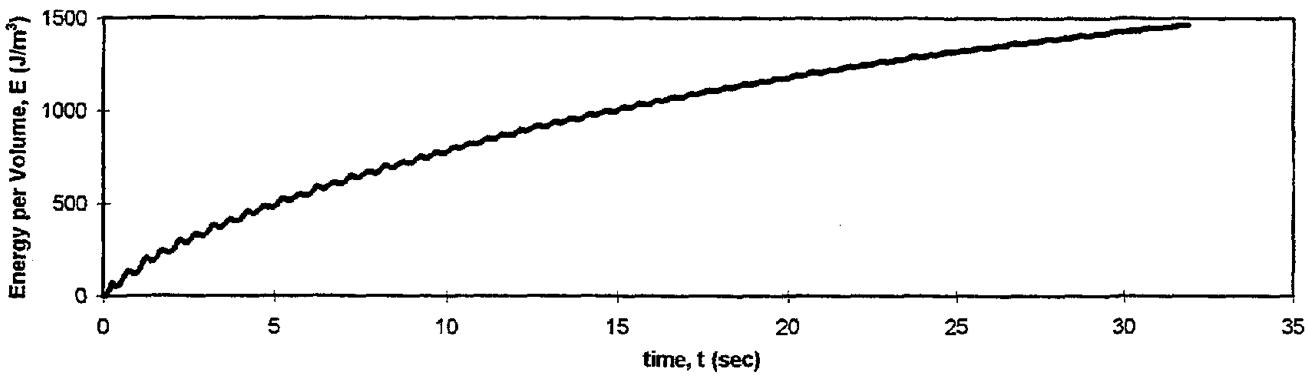

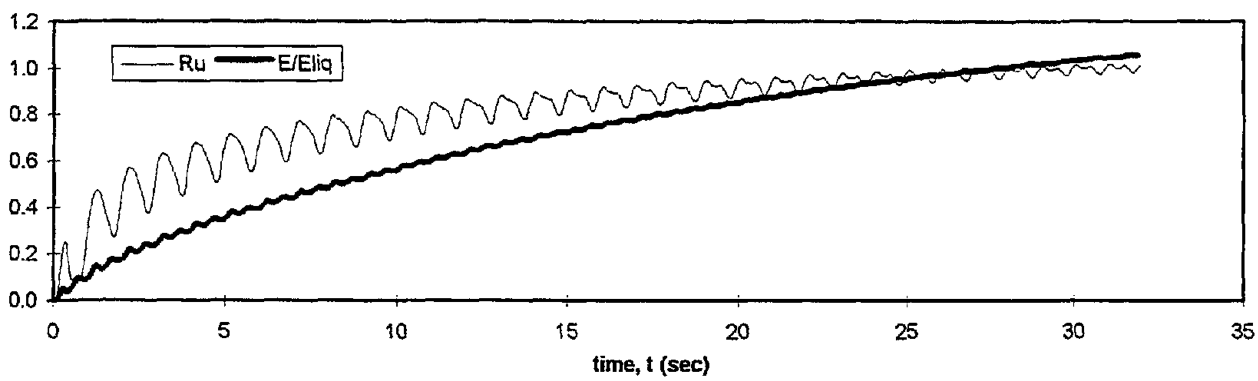

d:\nit\itp\cy_files\MONT37.XLS 8/20/96 10:47 AM

Test I.D.:	MONT37	**Controlled Parameter:**	Strain
Relative Density (%):	61.6	**Initial Effective Stress (kPa):**	100
Applied Shear Strain (%)	0.17	**Frequency (Hz):**	1

Shear Stress vs. Shear Strain

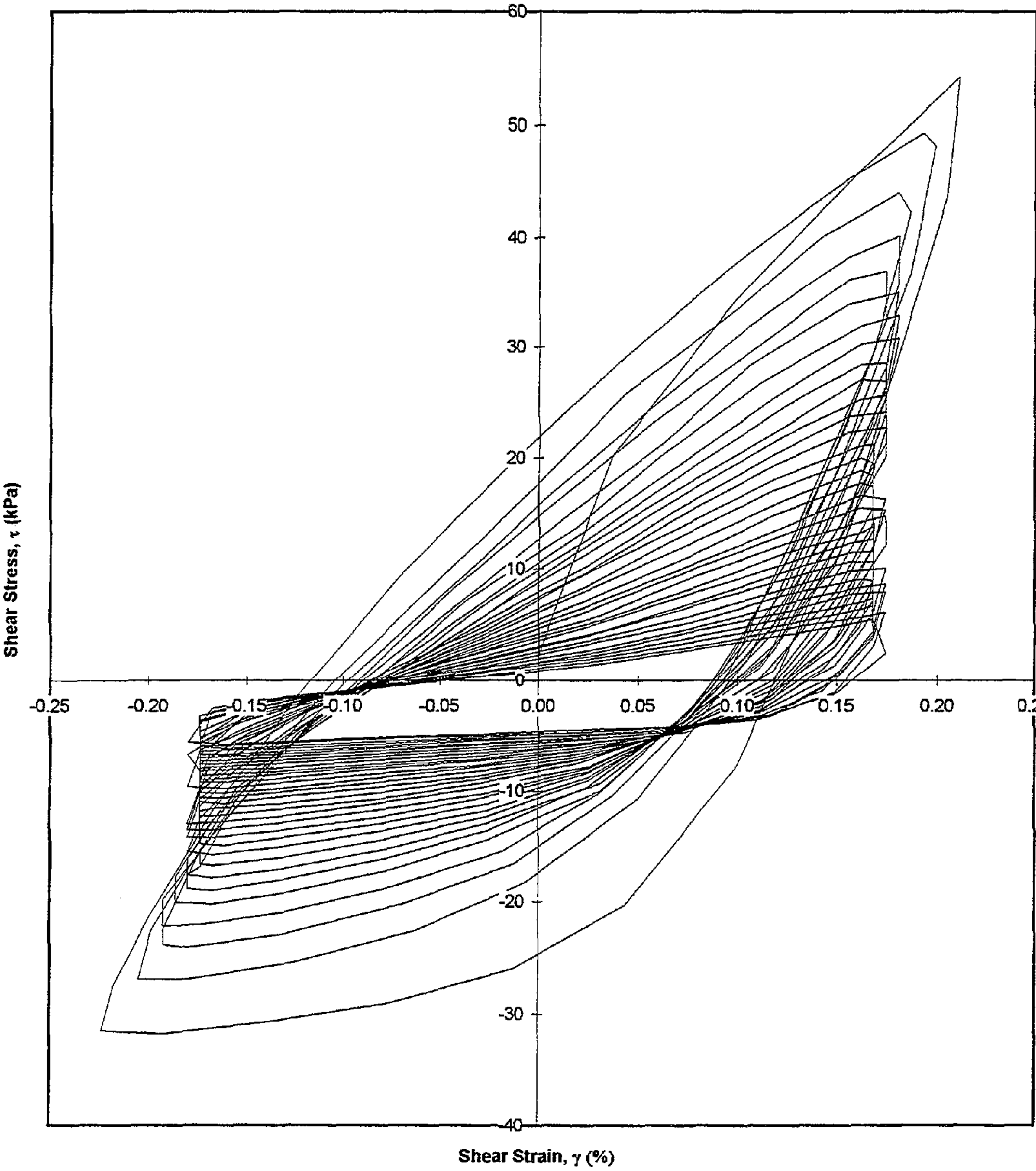

Test I.D.:	MONT38	**Controlled Parameter:**	Strain
Relative Density (%):	61.8	**Initial Effective Stress (kPa):**	100
Applied Shear Strain (%):	0.25	**Frequency (Hz):**	10

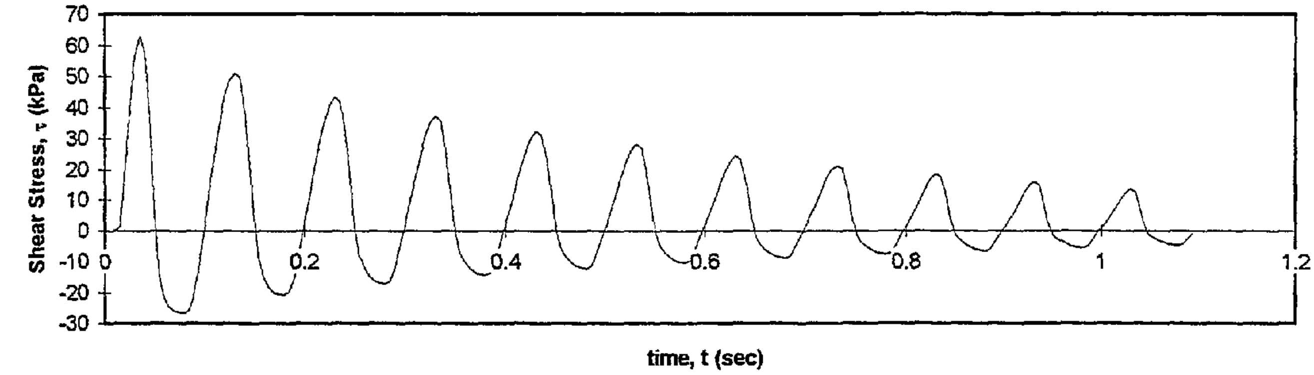

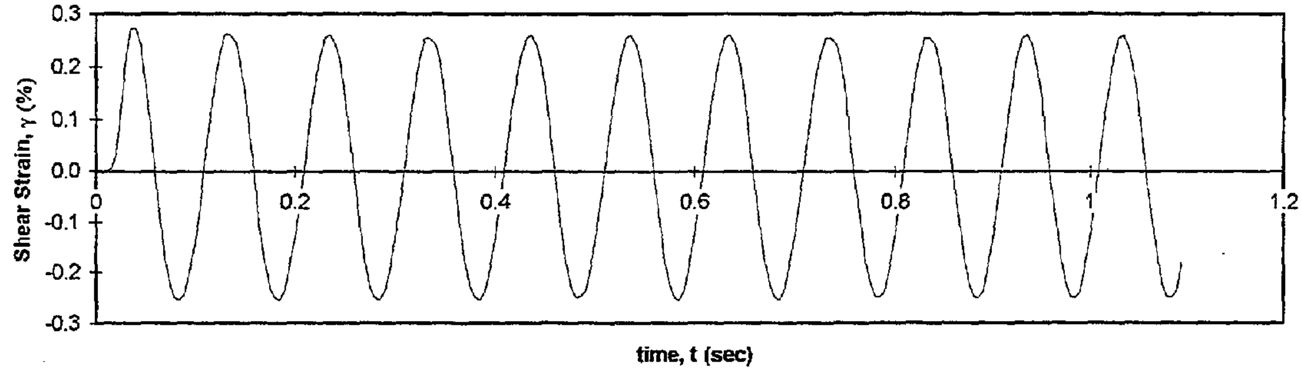

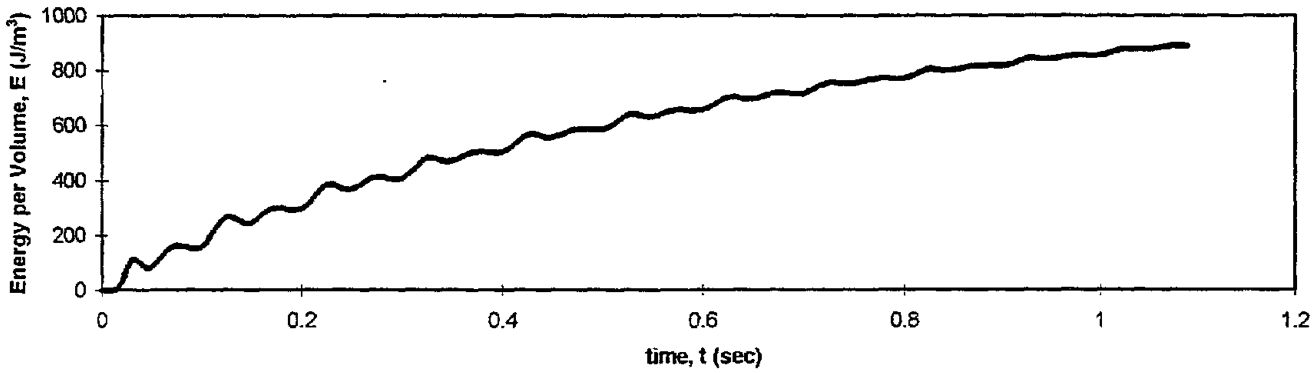

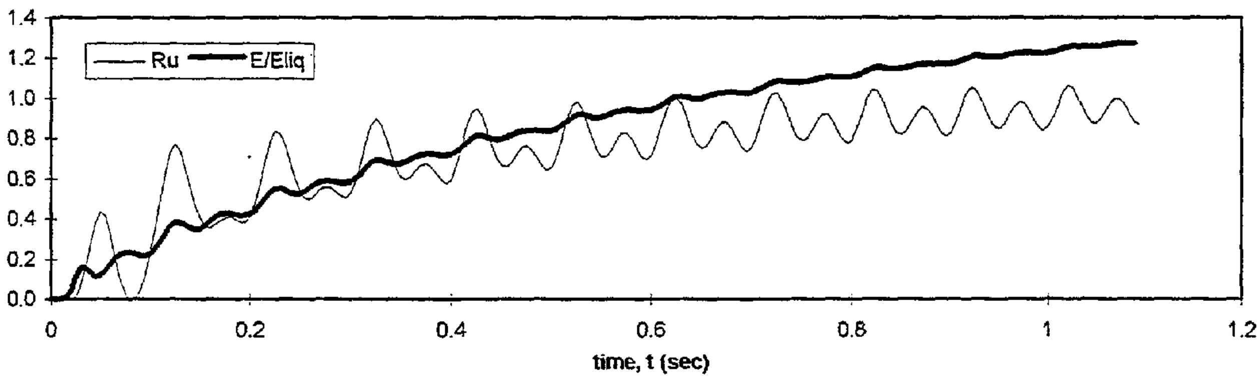

Test I.D.:	MONT38	**Controlled Parameter:**	Strain
Relative Density (%):	61.8	**Initial Effective Stress (kPa):**	100
Applied Shear Strain (%):	0.25	**Frequency (Hz):**	10

Shear Stress vs. Shear Strain

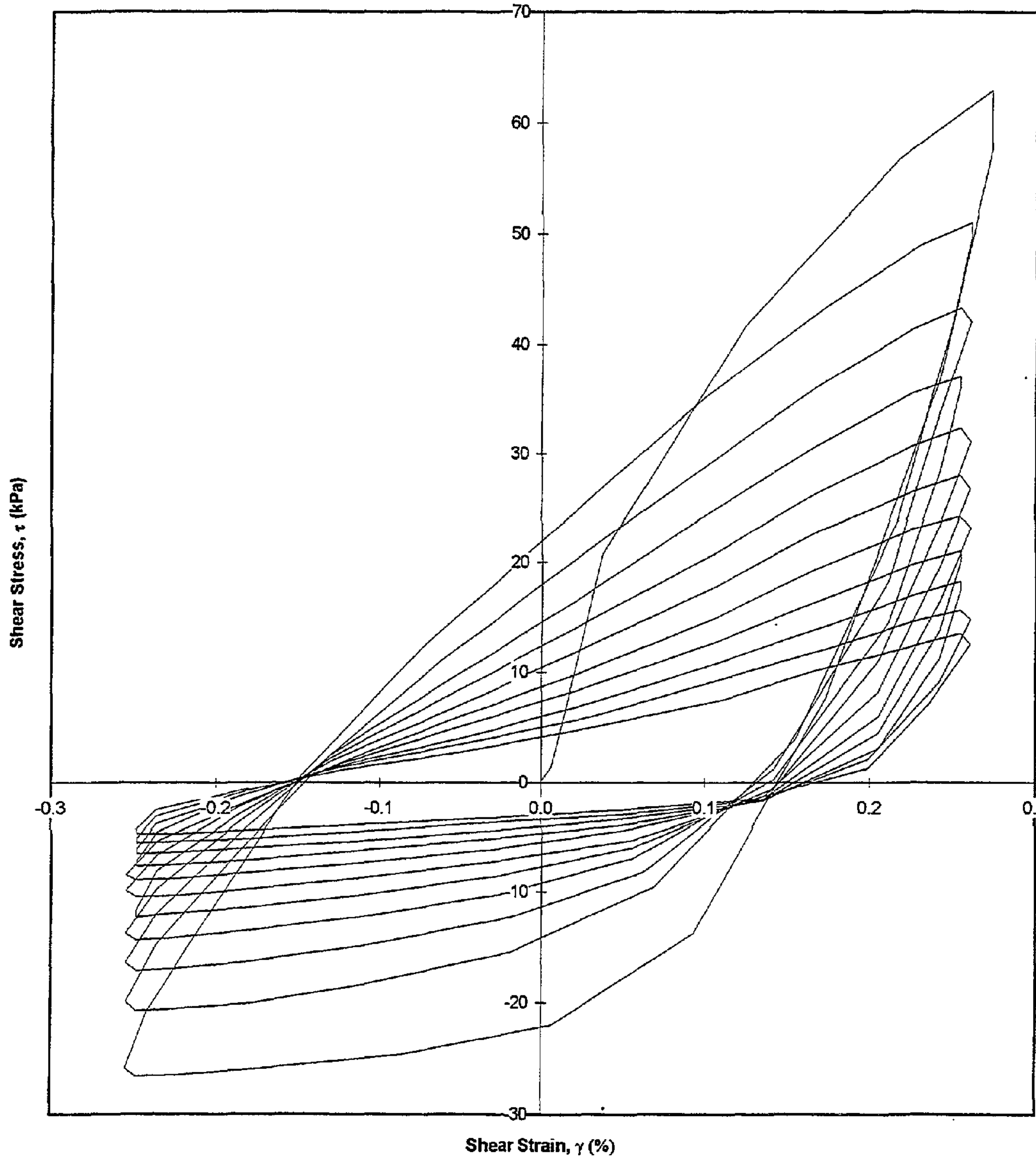

d:\nit\itp\cy_files\MONT38.XLS 8/20/96 10:54 AM

APPENDIX B

LABORATORY TESTS ON SOIL SAMPLES FROM THE SAVANNAH RIVER SITE, PERFORMED AT THE UNIVERSITY OF CALIFORNIA, BERKELEY

Table B.1 - Summary of the Cyclic Triaxial Test Data on SRS Soil Samples Performed at University of California, Berkeley

No.	Test ID	Sample	D_r(%)	E_{liq} (J/m^3)	FC (%)	γ_d (kN/m^3)	Control	σ_c' (kPa)	Freq. (Hz)	Load Shape
1	B23P2BCY	Santee	N/A	14675	33.7	16.0	Stress	400	1	Sinusoidal 2-way
2	B23P2MCY	Santee	N/A	16782	35.6	16.4	Stress	400	1	Sinusoidal 2-way
3	B23P2TCY	Santee	N/A	11402	32.6	16.8	Stress	400	1	Sinusoidal 2-way
4	B23P3BCY	Tobacco Rd.	N/A	4929	16.6	16.4	Stress	200	1	Sinusoidal 2-way
5	B23P3MCY	Tobacco Rd.	N/A	5585	18.5	15.2	Stress	200	1	Sinusoidal 2-way
6	B23P3TCY	Tobacco Rd.	N/A	2924	20.5	16.6	Stress	200	1	Sinusoidal 2-way
7	B12P5BCY	Tobacco Rd.	N/A	14918	27.0	15.8	Stress	300	1	Sinusoidal 2-way
8	B12P5MCY	Tobacco Rd.	N/A	49114	26.8	16.8	Stress	300	1	Sinusoidal 2-way
9	B12P5TCY	Tobacco Rd.	N/A	5450	22.3	18.0	Stress	300	1	Sinusoidal 2-way
10	B12P7BCY	Tobacco Rd.	N/A	7666	15.7	15.9	Stress	375	1	Sinusoidal 2-way
11	B12P7MCY	Tobacco Rd.	N/A	14482	17.0	16.3	Stress	375	1	Sinusoidal 2-way
12	B12P7TCY	Tobacco Rd.	N/A	3852	15.7	16.2	Stress	375	1	Sinusoidal 2-way
13	B2P5BCYC	Tobacco Rd.	N/A	11672	25.4	14.7	Stress	500	1	Sinusoidal 2-way
14	B2P5MCYC	Tobacco Rd.	N/A	23344	29.6	15.4	Stress	500	1	Sinusoidal 2-way
15	B2P5TCYC	Tobacco Rd.	N/A	8819	26.6	16.7	Stress	500	1	Sinusoidal 2-way
16	B23P4BCY	Tobacco Rd.	N/A	21667	11.4	14.6	Stress	750	1	Sinusoidal 2-way
17	B23P4MCY	Tobacco Rd.	N/A	36680	16.5	15.5	Stress	700	1	Sinusoidal 2-way
18	B23P4TCY	Tobacco Rd.	N/A	17968	28.0	N/A	Stress	750	1	Sinusoidal 2-way
19	B29P2TCY	Tobacco Rd.	N/A	23637	23.0	16.7	Stress	750	1	Sinusoidal 2-way
20	B2P6BCY	Tobacco Rd.	N/A	17985	18.9	16.7	Stress	725	1	Sinusoidal 2-way
21	B2P6MCY	Tobacco Rd.	N/A	19831	20.1	16.5	Stress	743	1	Sinusoidal 2-way
22	B2P6TCYC	Tobacco Rd.	N/A	14446	22.4	16.0	Stress	750	1	Sinusoidal 2-way

Test Results Following the Sequence of Test ID's are Attached.

Test I.D.:	B23P2BCY	**Controlled Parameter:**	Stress
Fines Content (%):	33.7	**Initial Effective Stress (kPa):**	400
Dry Density (kN/m^3):	16.04		

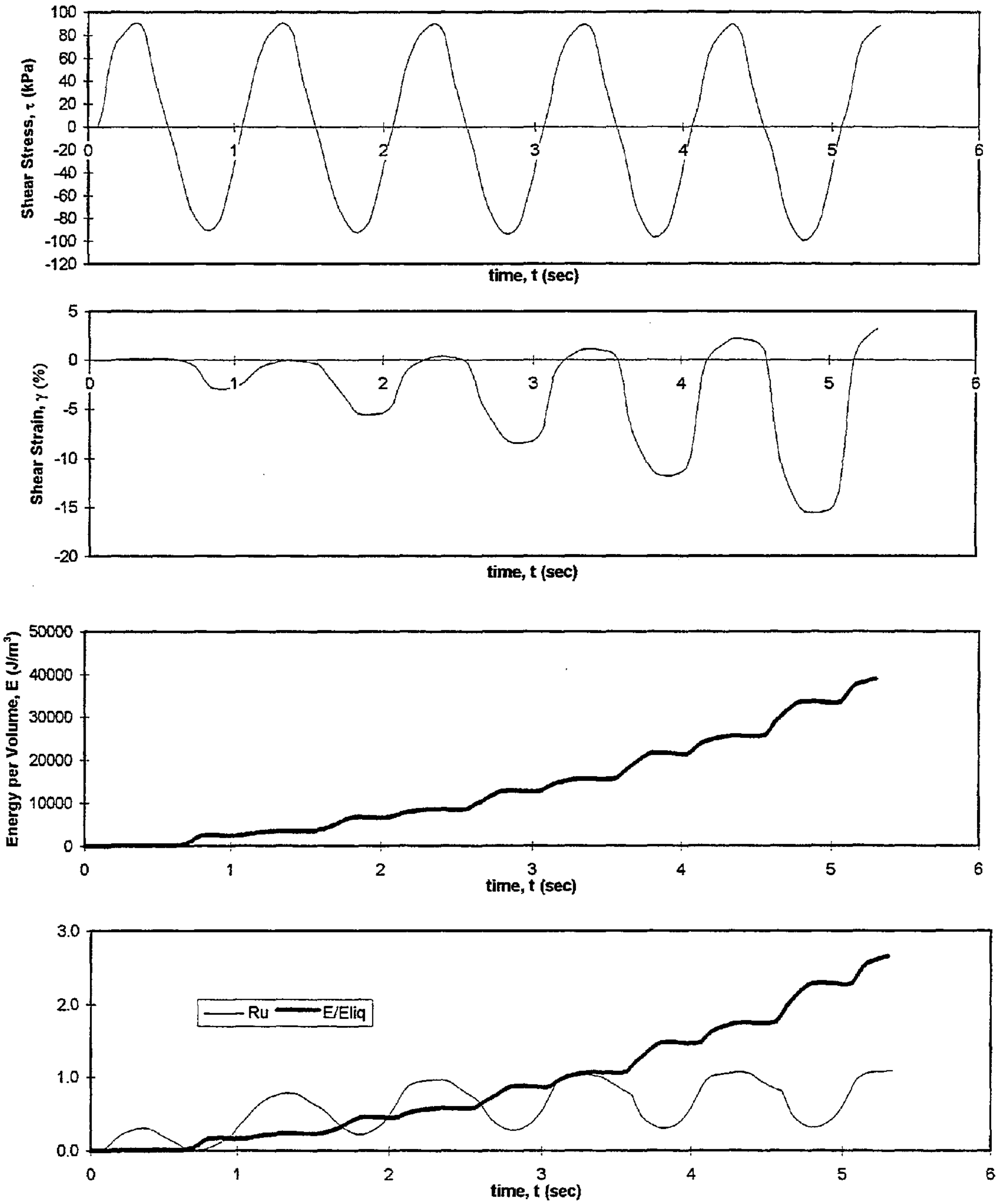

Test I.D.:	B23P2BCY	**Controlled Parameter:**	Stress
Fines Content (%):	33.7	**Initial Effective Stress (kPa):**	400
Dry Density (kN/m³):	16.04		

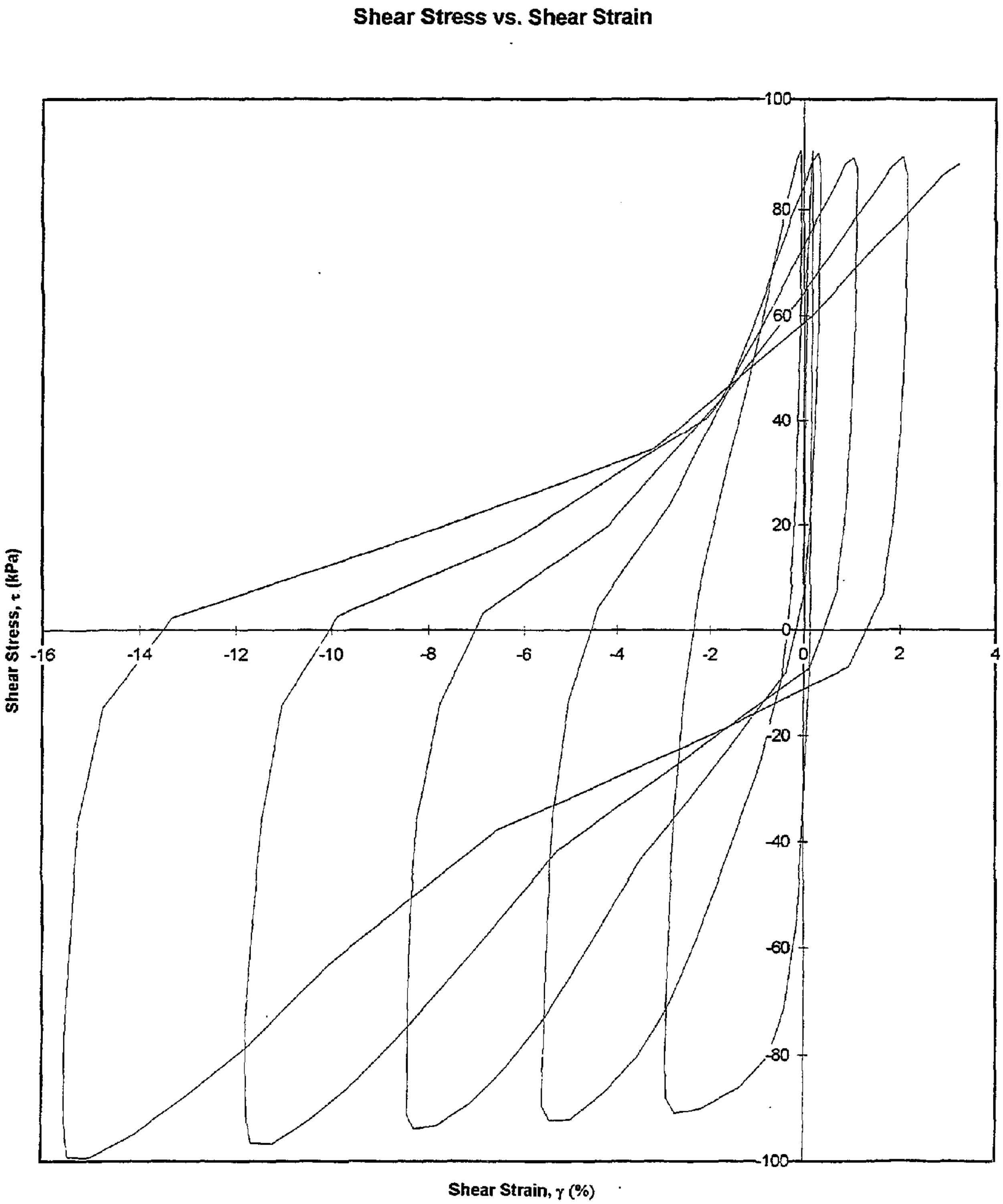

Test I.D.:	B23P2MCY	**Controlled Parameter:**	Stress
Fines Content (%):	35.6	**Initial Effective Stress (kPa):**	400
Dry Density (kN/m³):	16.43		

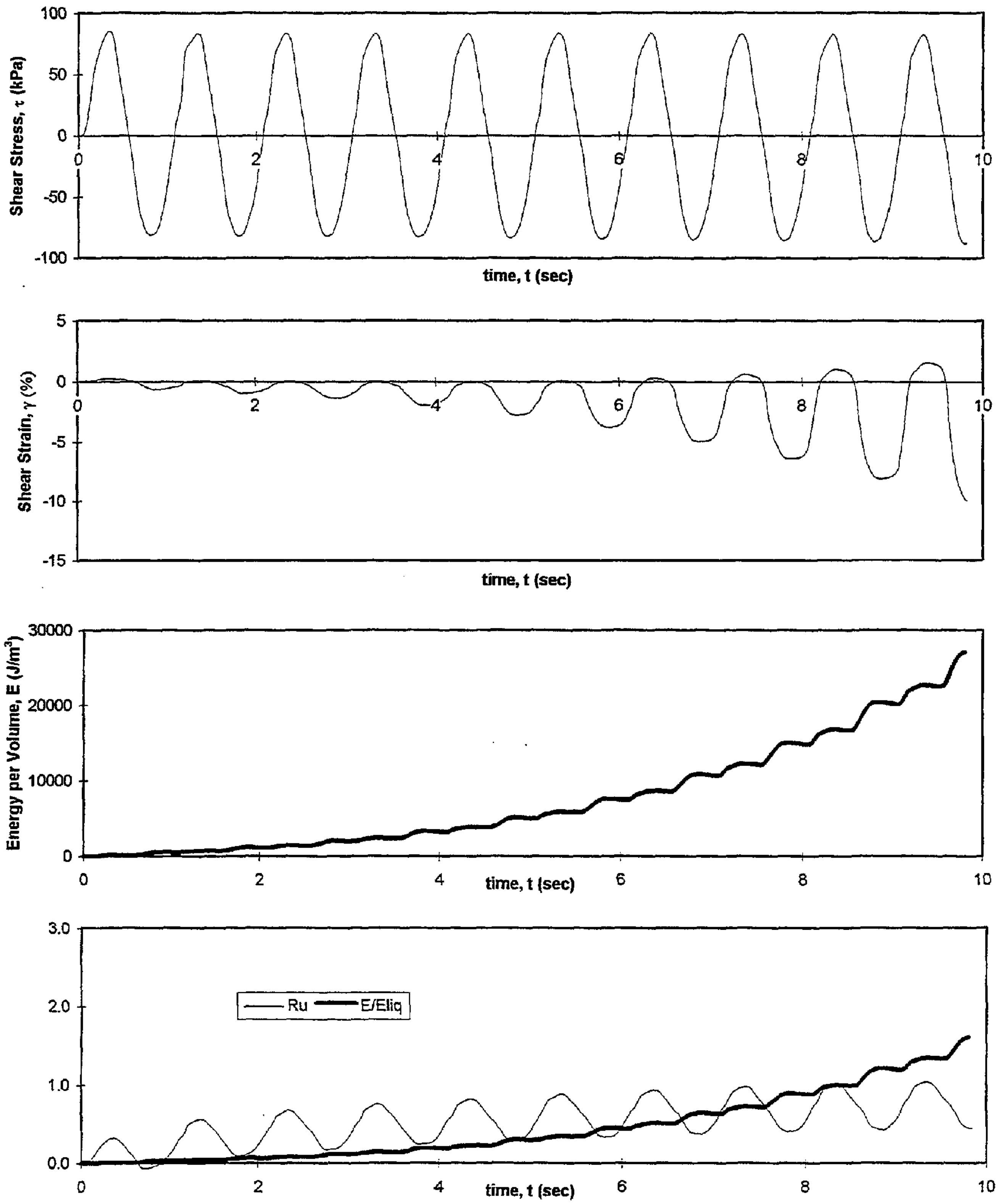

d:\nit\tp\cy_files\B23P2MCY.XLS 8/21/96 9:49 AM

Test I.D.:	B23P2MCY	**Controlled Parameter:**	Stress
Fines Content (%):	35.6	**Initial Effective Stress (kPa):**	400
Dry Density (kN/m³):	16.43		

Shear Stress vs. Shear Strain

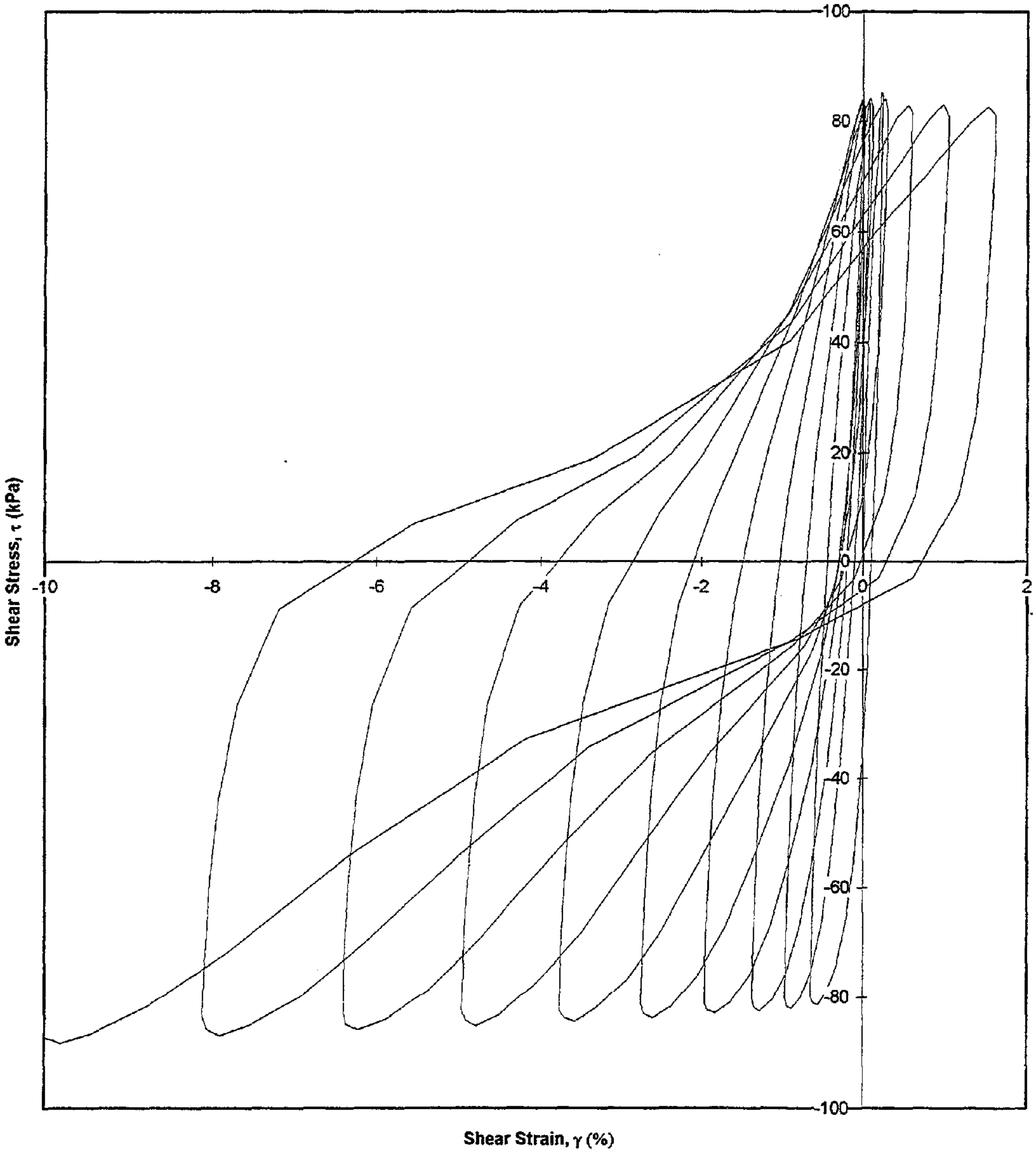

Test I.D.:	B23P2TCY	**Controlled Parameter:**	Stress
Fines Content (%):	32.6	**Initial Effective Stress (kPa):**	400
Dry Density (kN/m^3):	16.75		

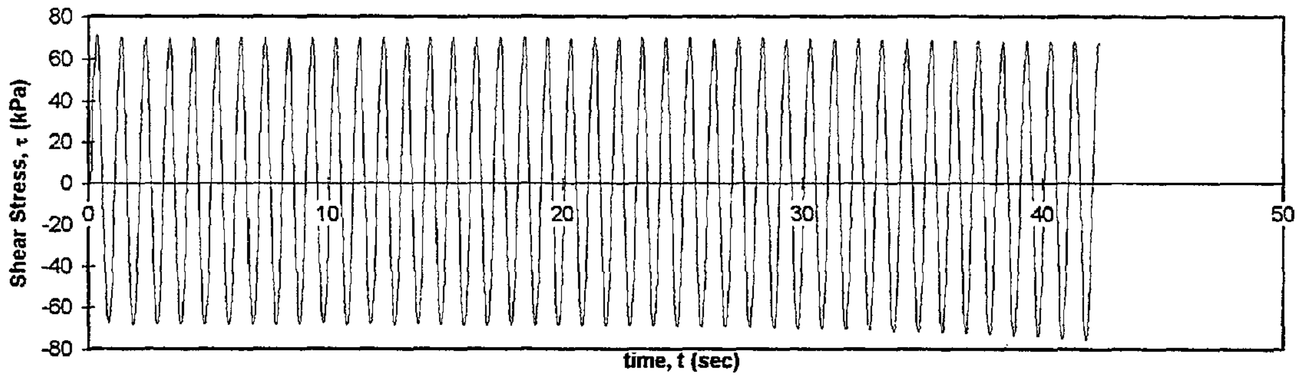

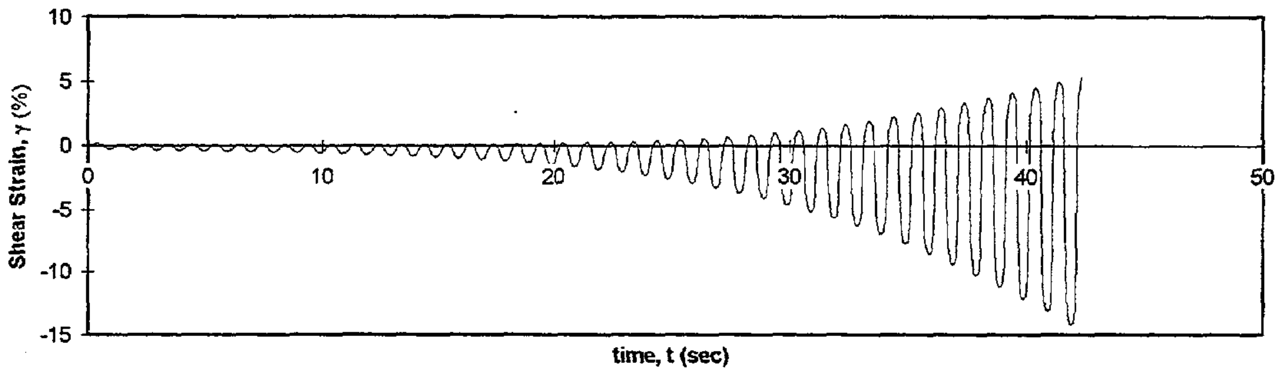

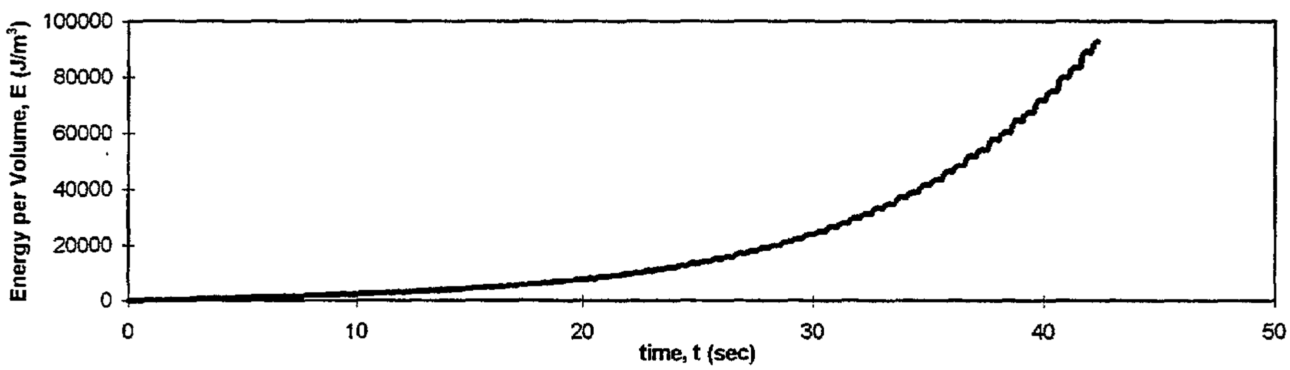

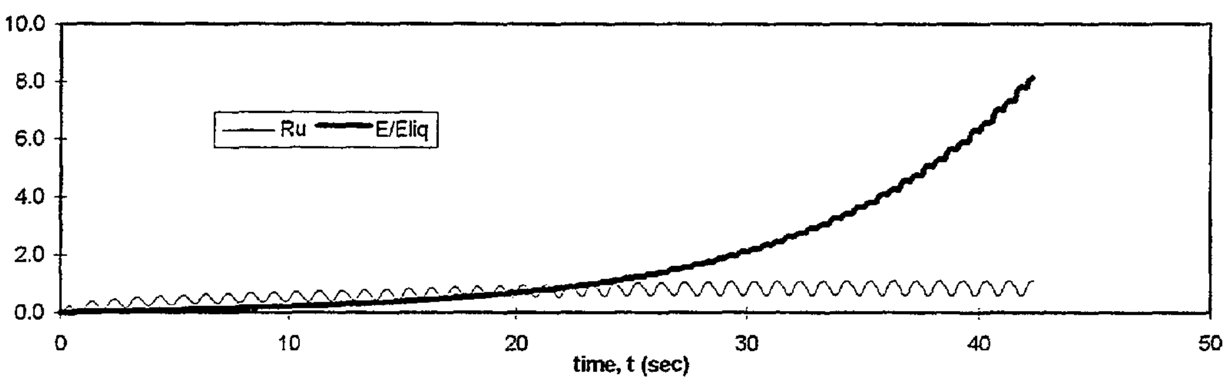

Test I.D.:	B23P2TCY	**Controlled Parameter:**	Stress
Fines Content (%):	32.6	**Initial Effective Stress (kPa):**	400
Dry Density (kN/m³):	16.75		

Shear Stress vs. Shear Strain

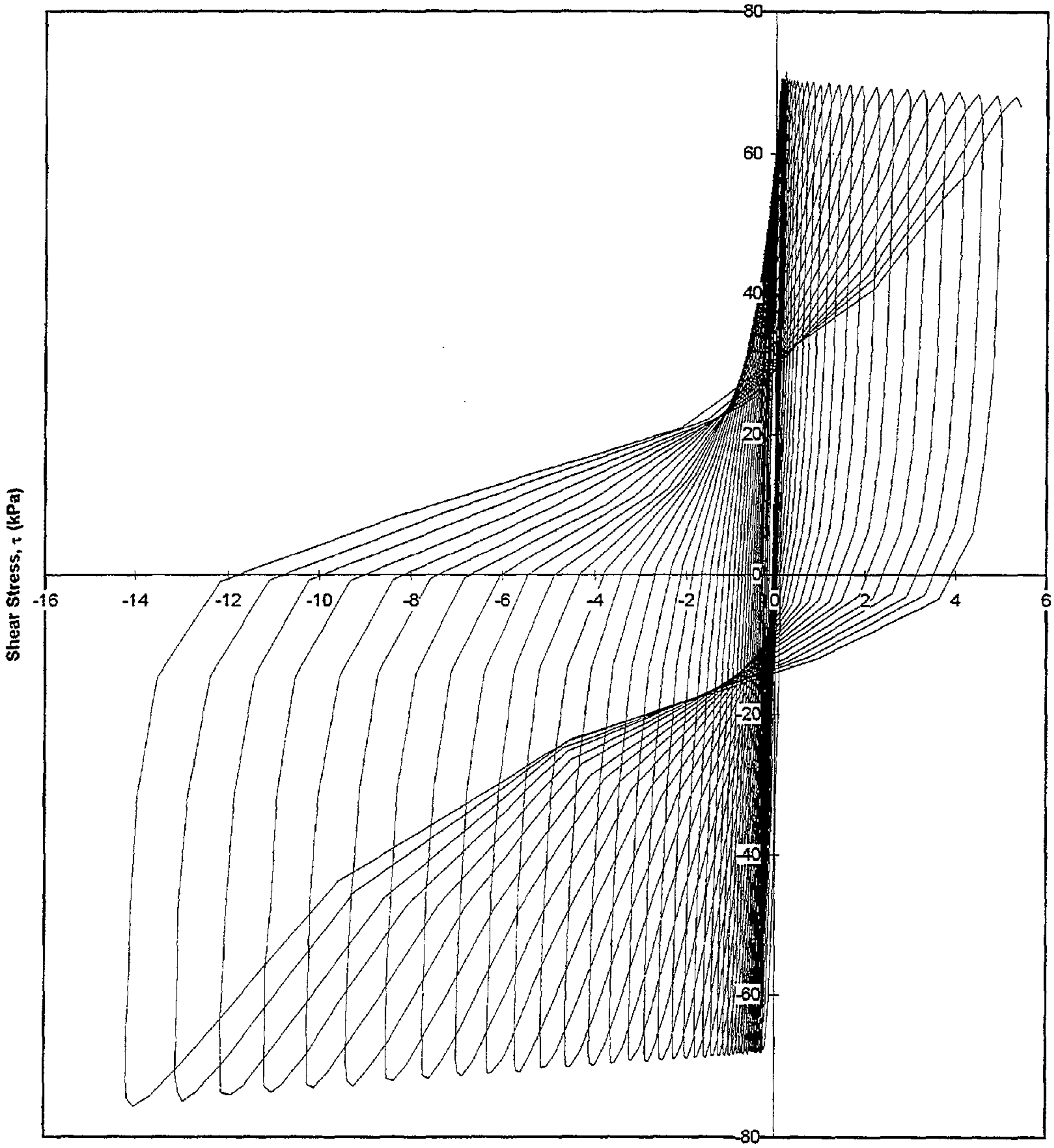

d:\nit\itp\cy_files\B23P2TCY.XLS

8/21/96 7:44 AM

Test I.D.:	B23P3BCY	**Controlled Parameter:**	Stress
Fines Content (%):	16.6	**Initial Effective Stress (kPa):**	200
Dry Density (kN/m³):	16.4		

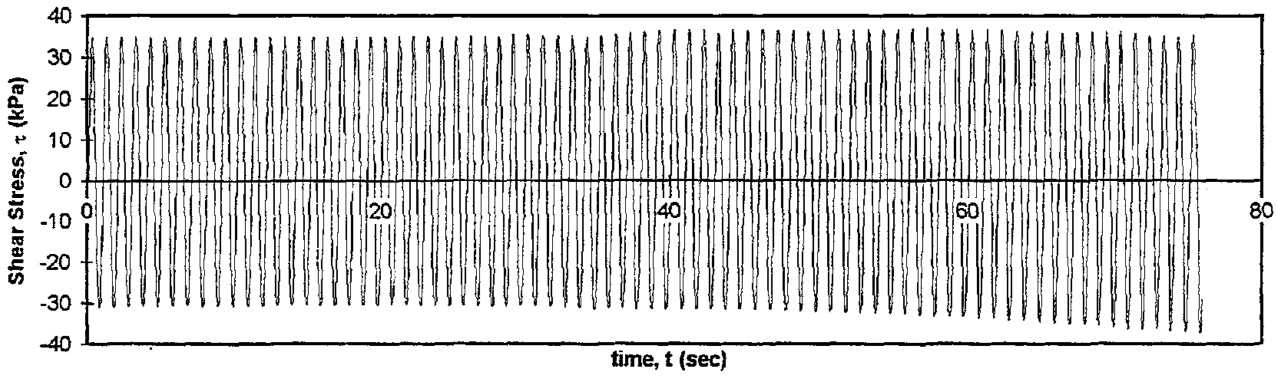

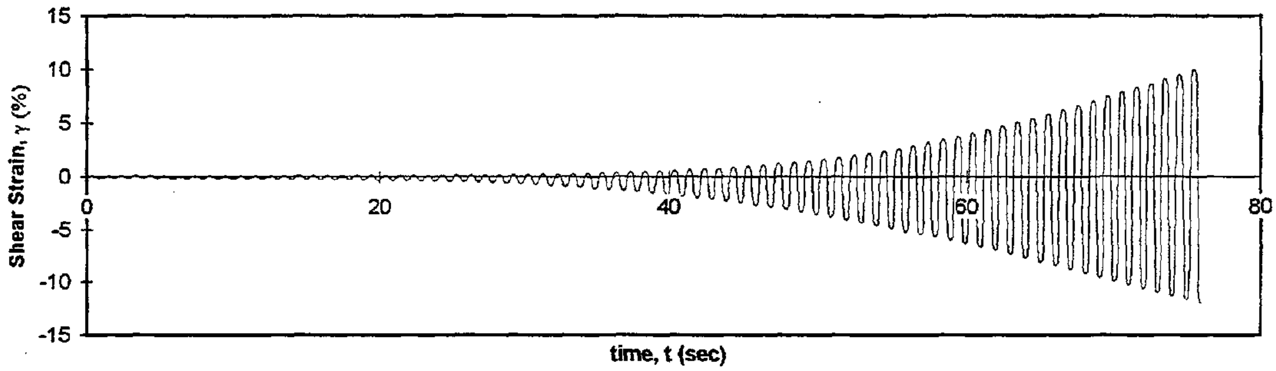

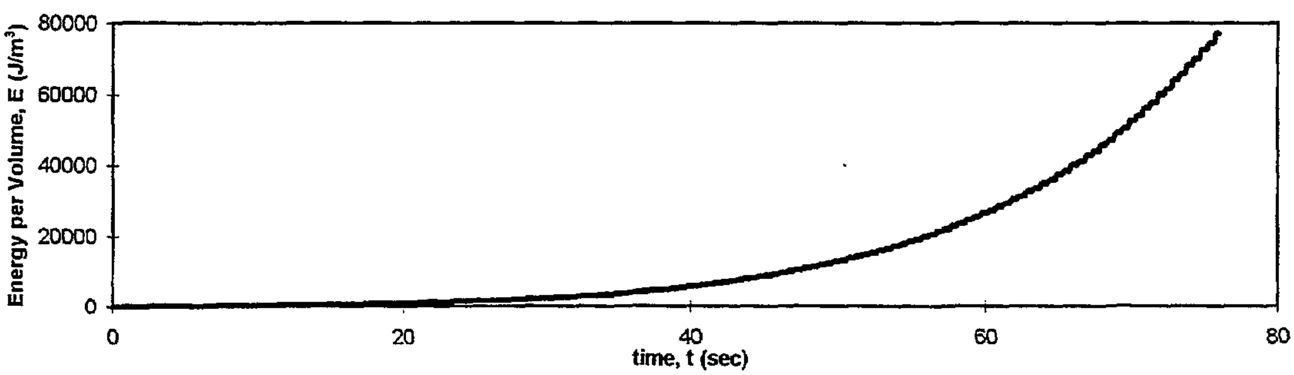

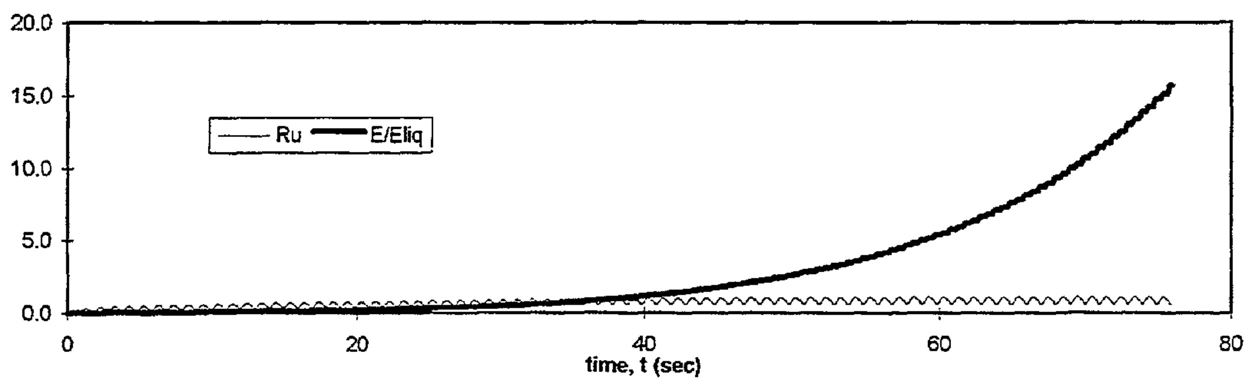

Test I.D.:	B23P3BCY	**Controlled Parameter:**	Stress
Fines Content (%):	16.6	**Initial Effective Stress (kPa):**	200
Dry Density (kN/m^3):	16.4		

Shear Stress vs. Shear Strain

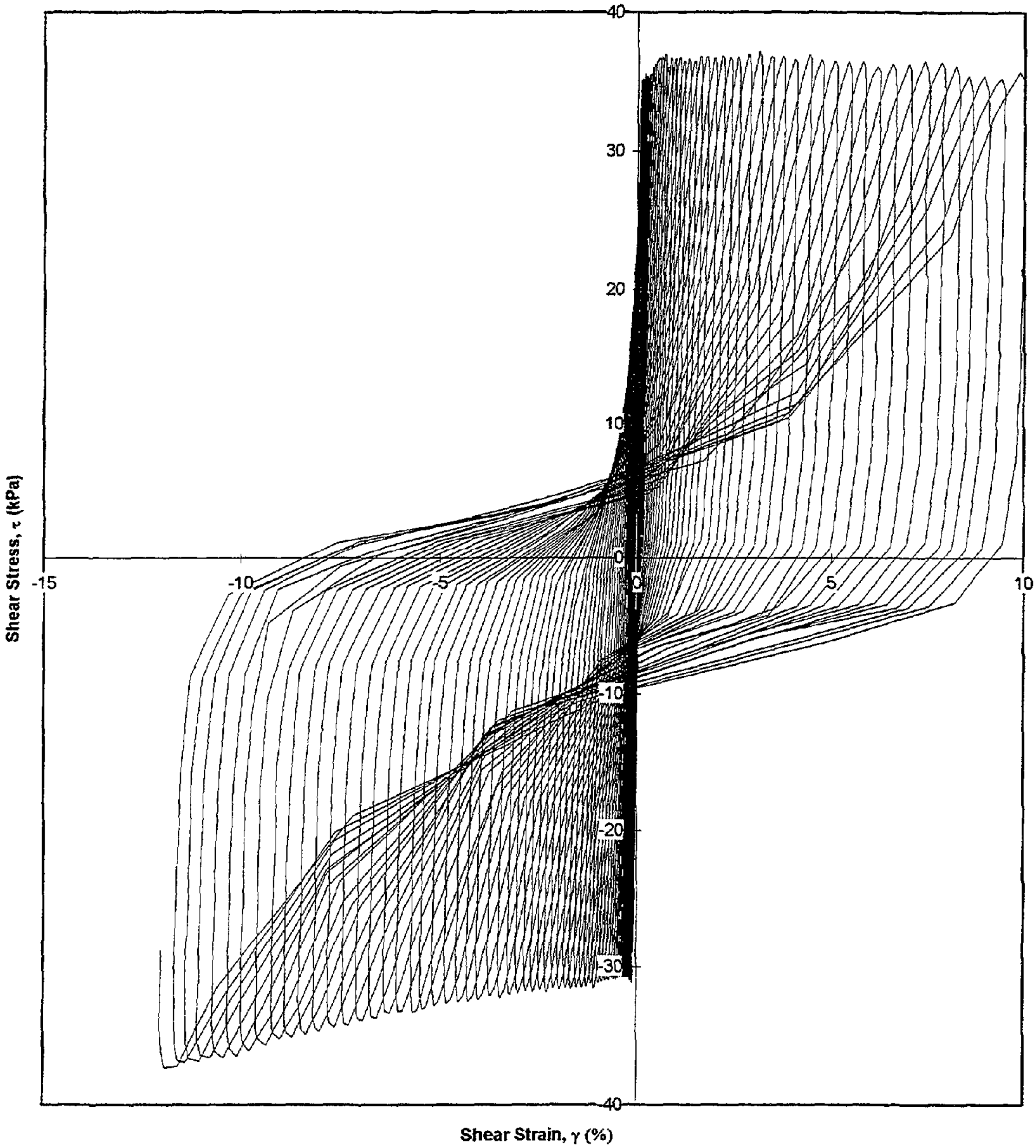

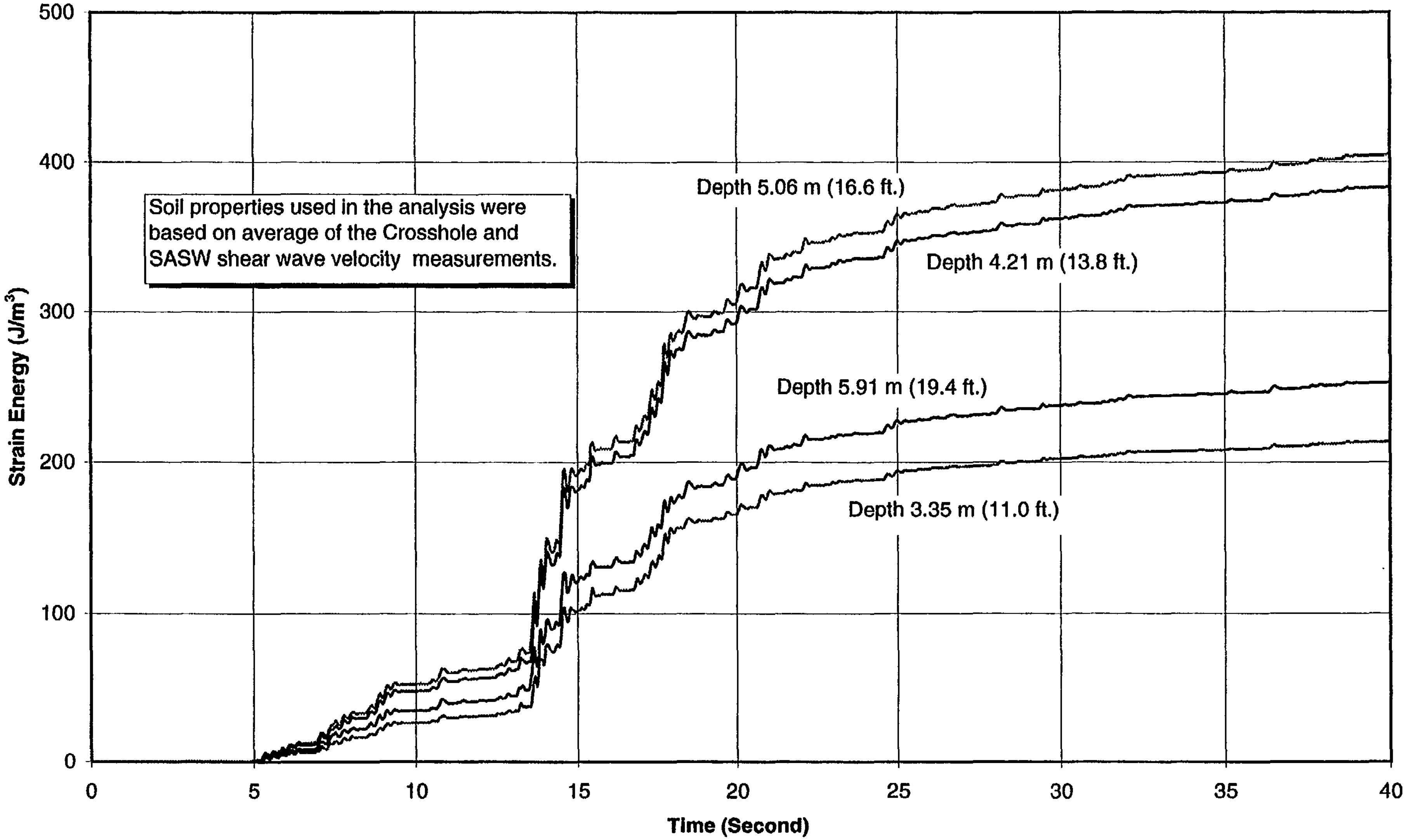

Figure 4.16 - Accumulation of Strain Energy in Liquefied Sand Layer - Wildlife Site, November 24, 1987, 1315 GMT Earthquake in 360° Direction - SHAKE Analysis Output

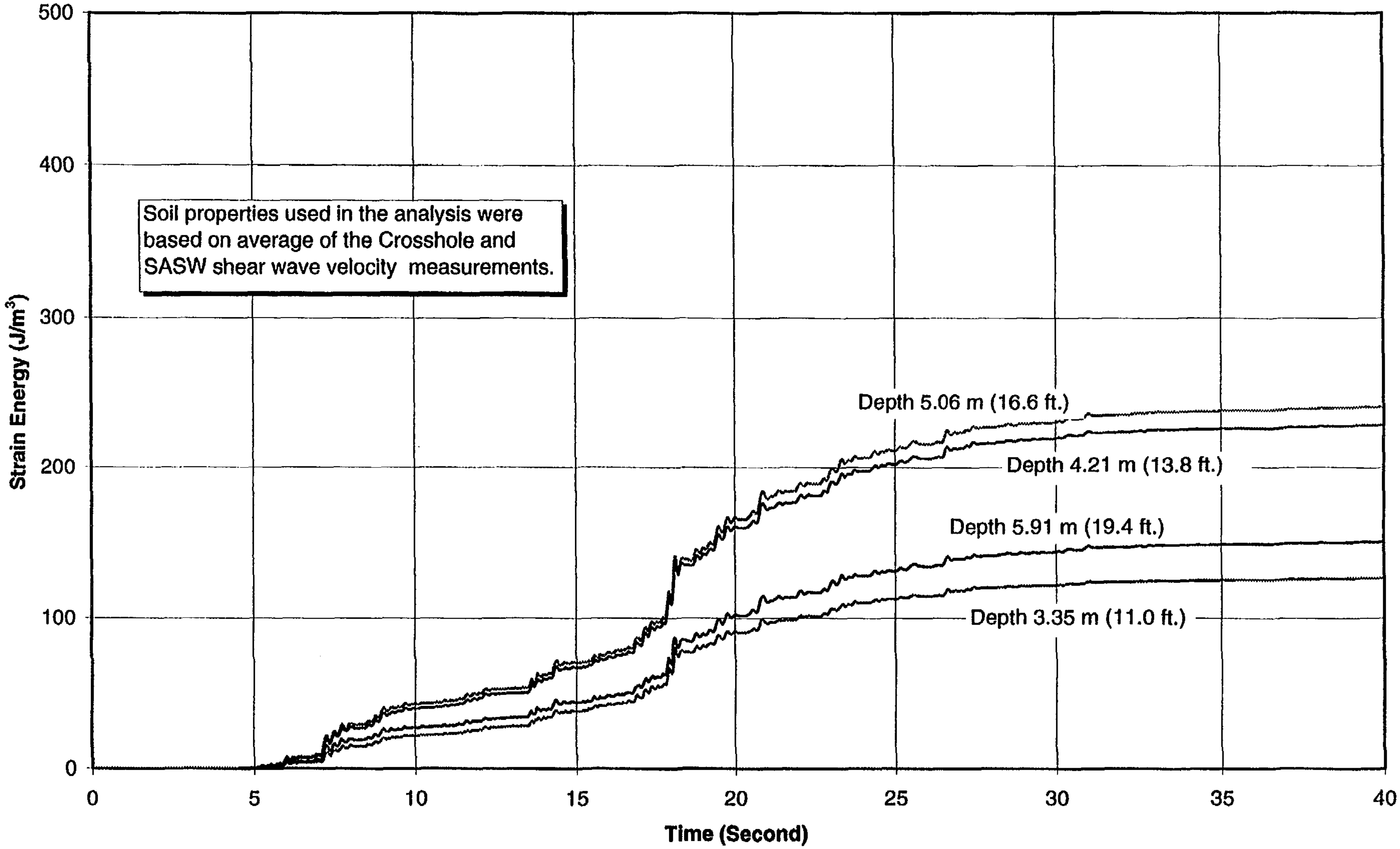

Figure 4.17 - Accumulation of Strain Energy in Liquefied Sand Layer - Wildlife Site, November 24, 1987, 1315 GMT Earthquake in 90° Direction - SHAKE Analysis Output

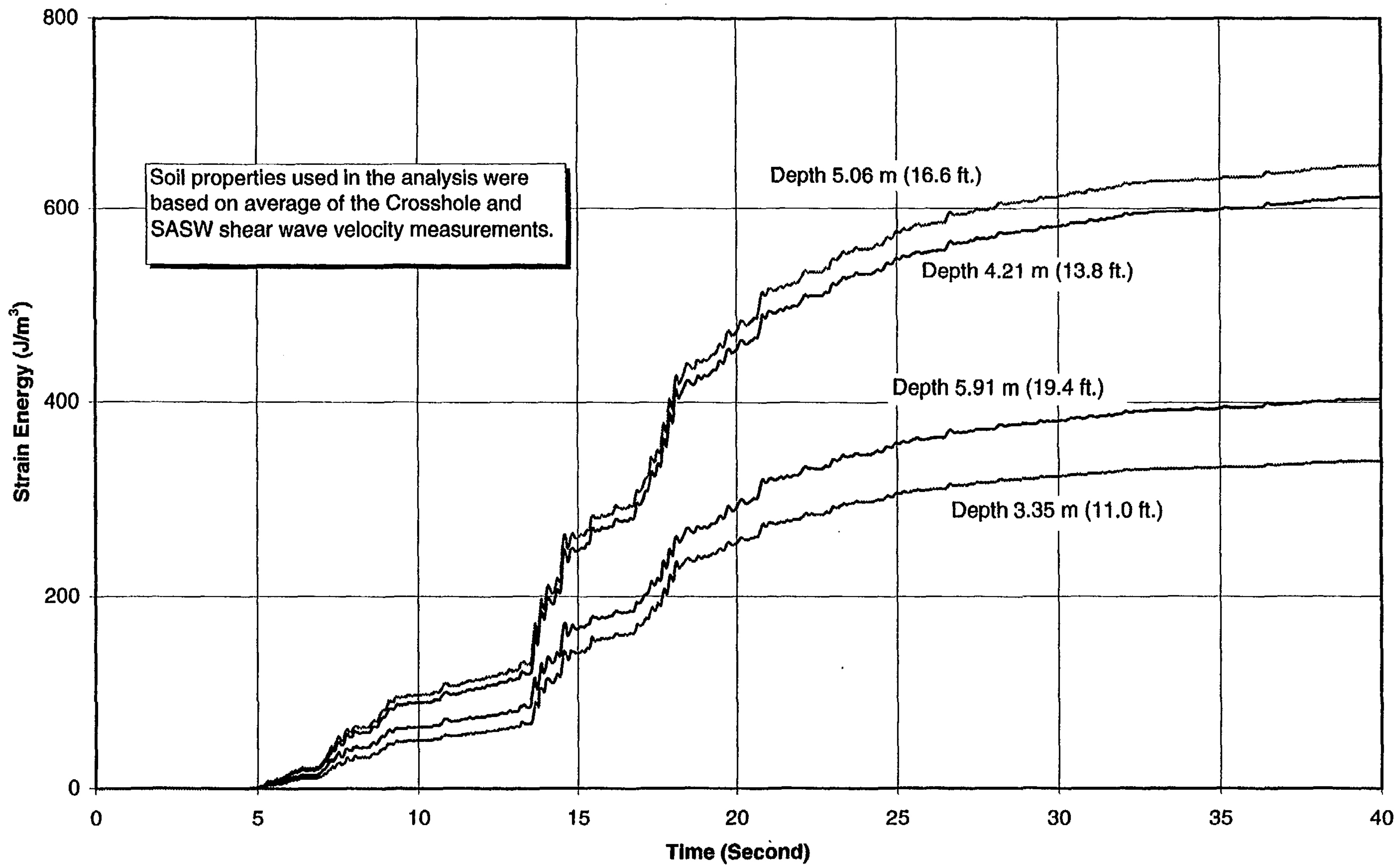

Figure 4.18 - Accumulation of Strain Energy in Liquefied Sand Layer - Wildlife Site, November 24, 1987, 1315 GMT Eathquake - Summation of SHAKE Analysis Output in both 360° and 90° Directions

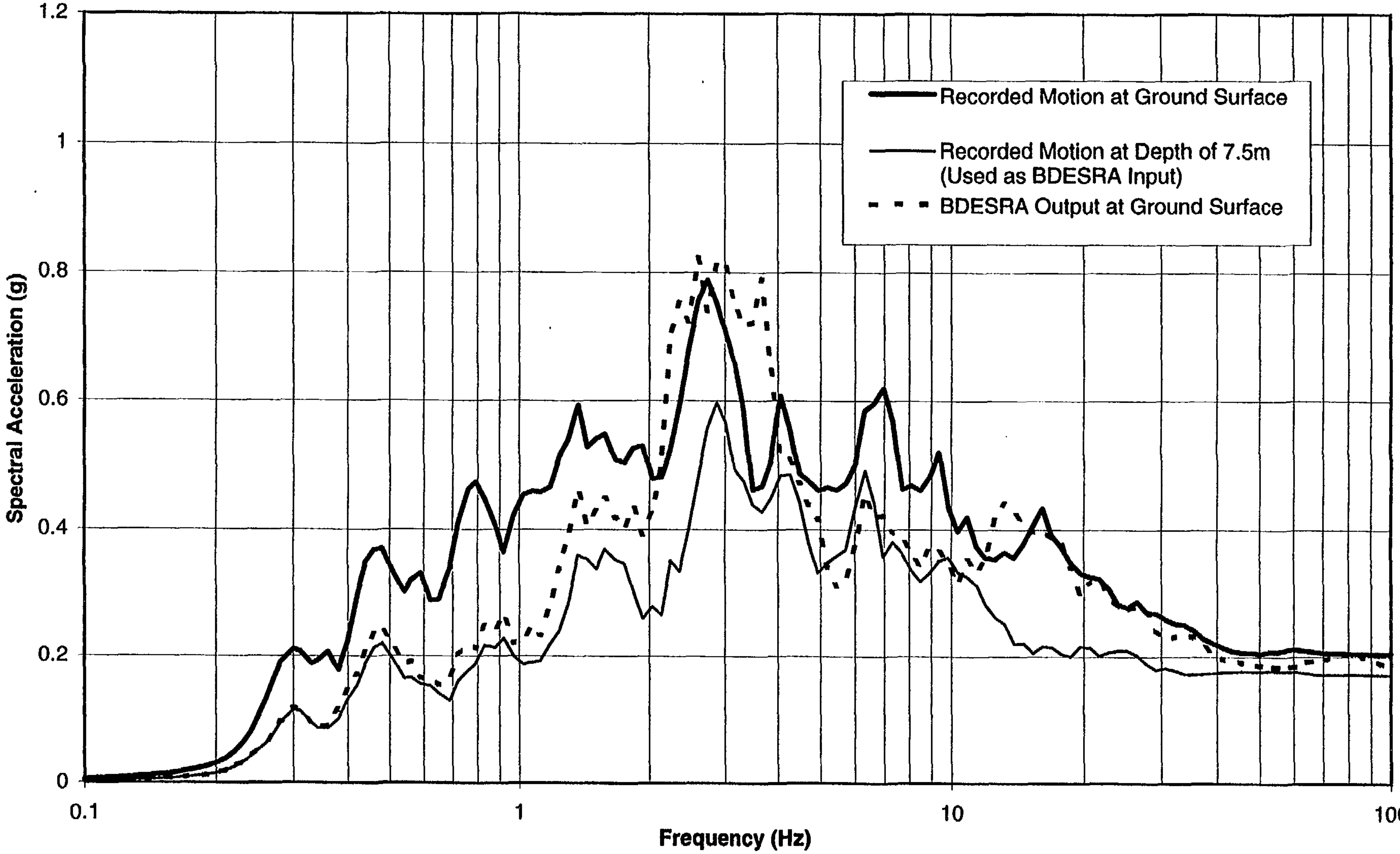

Figure 4.19 - Acceleration Response Spectra at 5% Damping - Wildlife Liquefaction Array, November 24, 1987, 1315 GMT Earthquake - Comparison of Horizontal Motions in 360° Direction - BDESRA Output, Total Stress Analysis

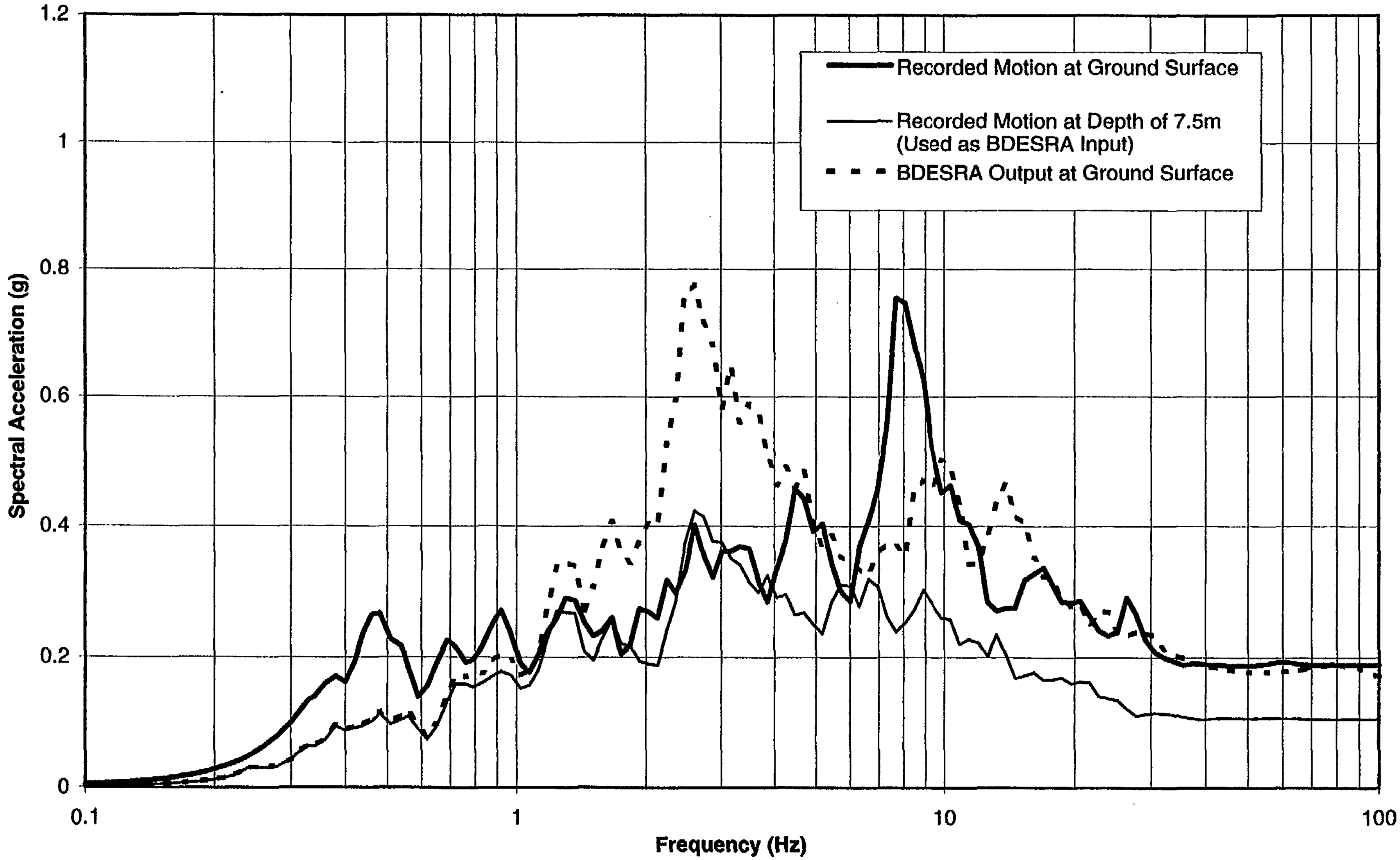

Figure 4.20 - Acceleration Response Spectra at 5% Damping - Wildlife Liquefaction Array, November 24, 1987, 1315 GMT Earthquake - Comparison of Horizontal Motions in 90° Direction - BDESRA Output, Total Stress Analysis

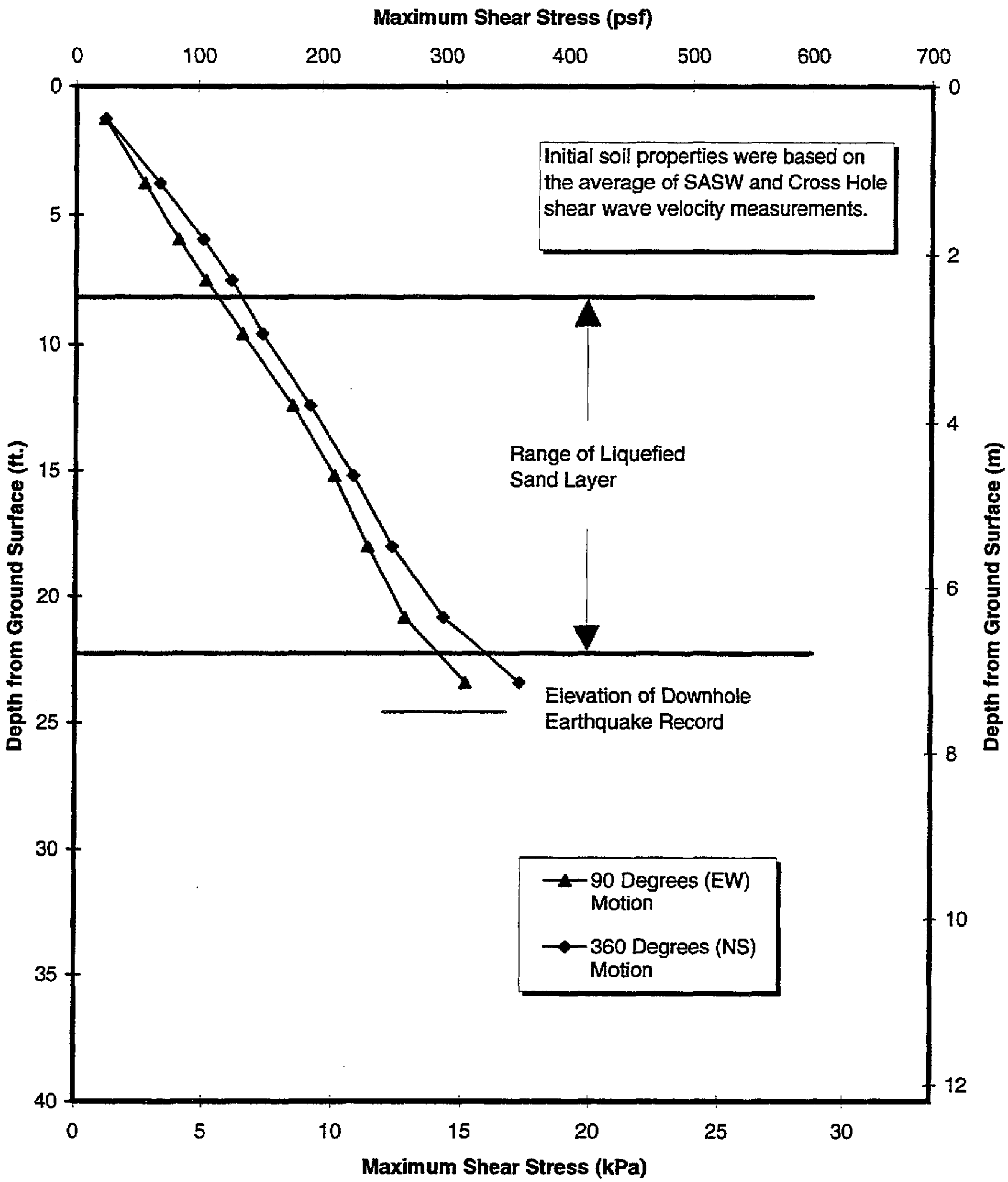

Figure 4.21 - Maximum Shear Stress Distribution over Depth from BDESRA Results of Total Stress Analyses - Wildlife Site, November 24, 1987, 1315 GMT Earthquake

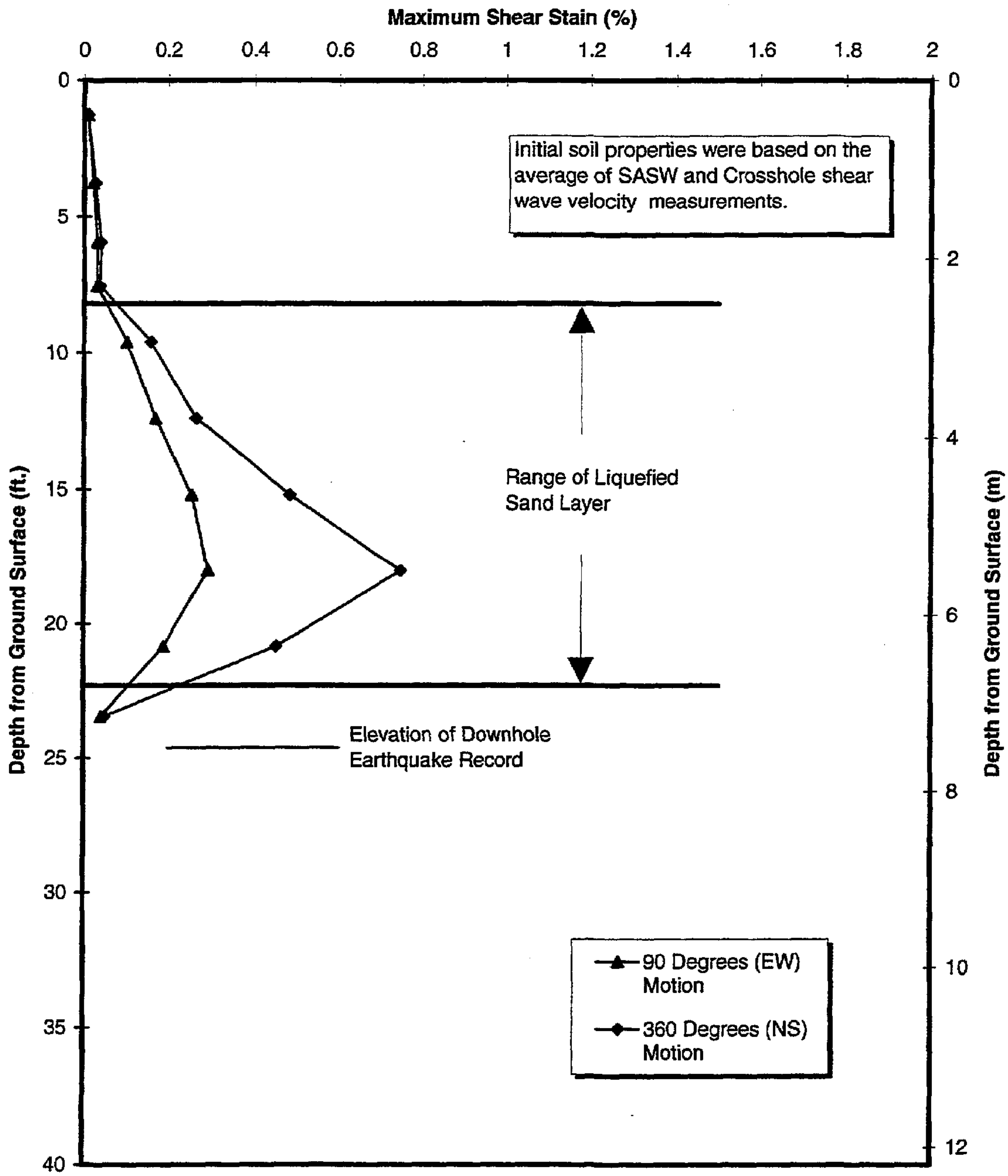

Figure 4.22 - Maximum Shear Strain Distribution over Depth from BDESRA Results of Total Stress Analyses - Wildlife Site, November 24, 1987, 1315 GMT Earthquake

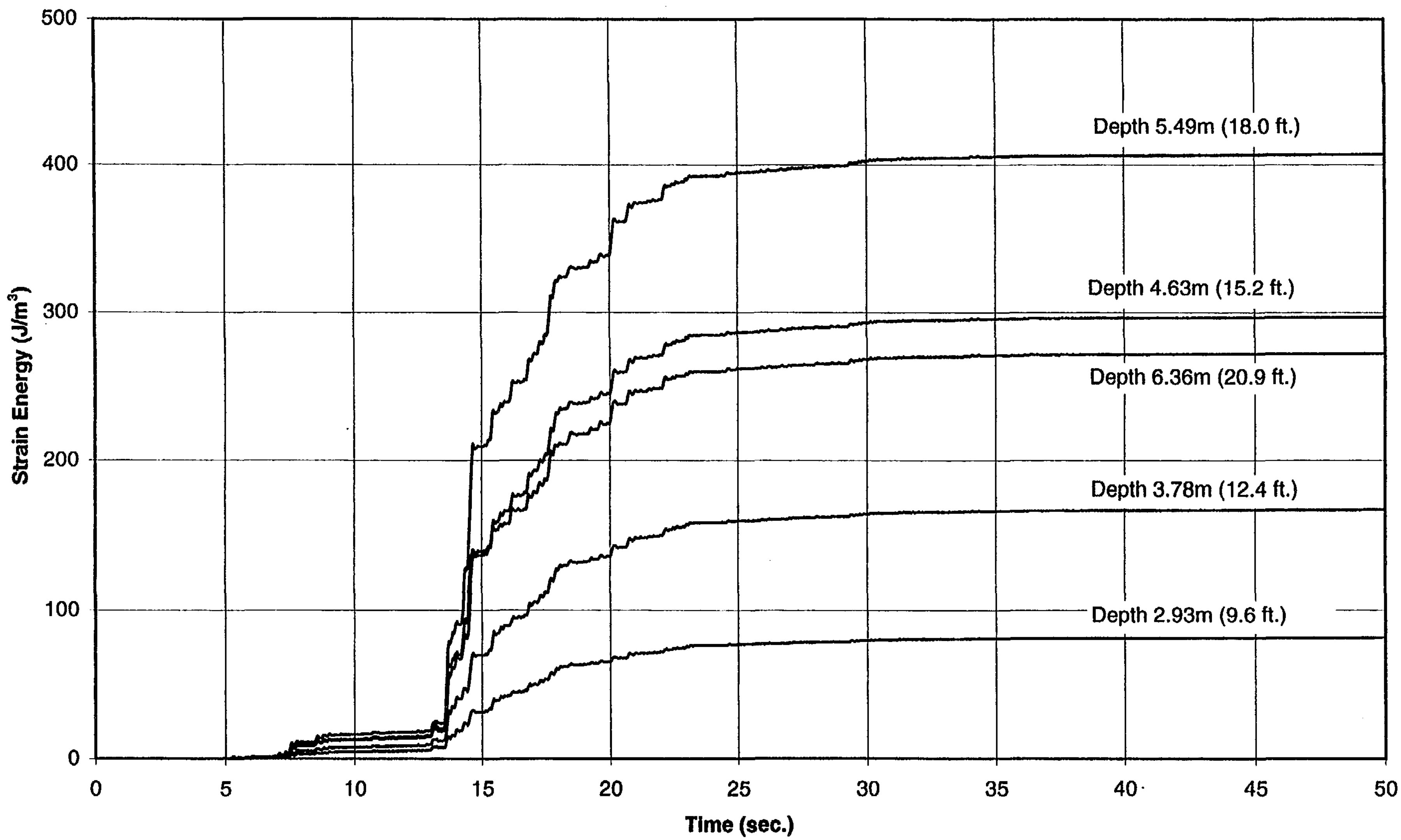

Figure 4.23 - Accumulation of Strain Energy in Liquefied Sand Layer - Wildlife Site, November 24, 1987, 1315 GMT Earthquake in 360° Direction - BDESRA Output, Total Stress Analysis

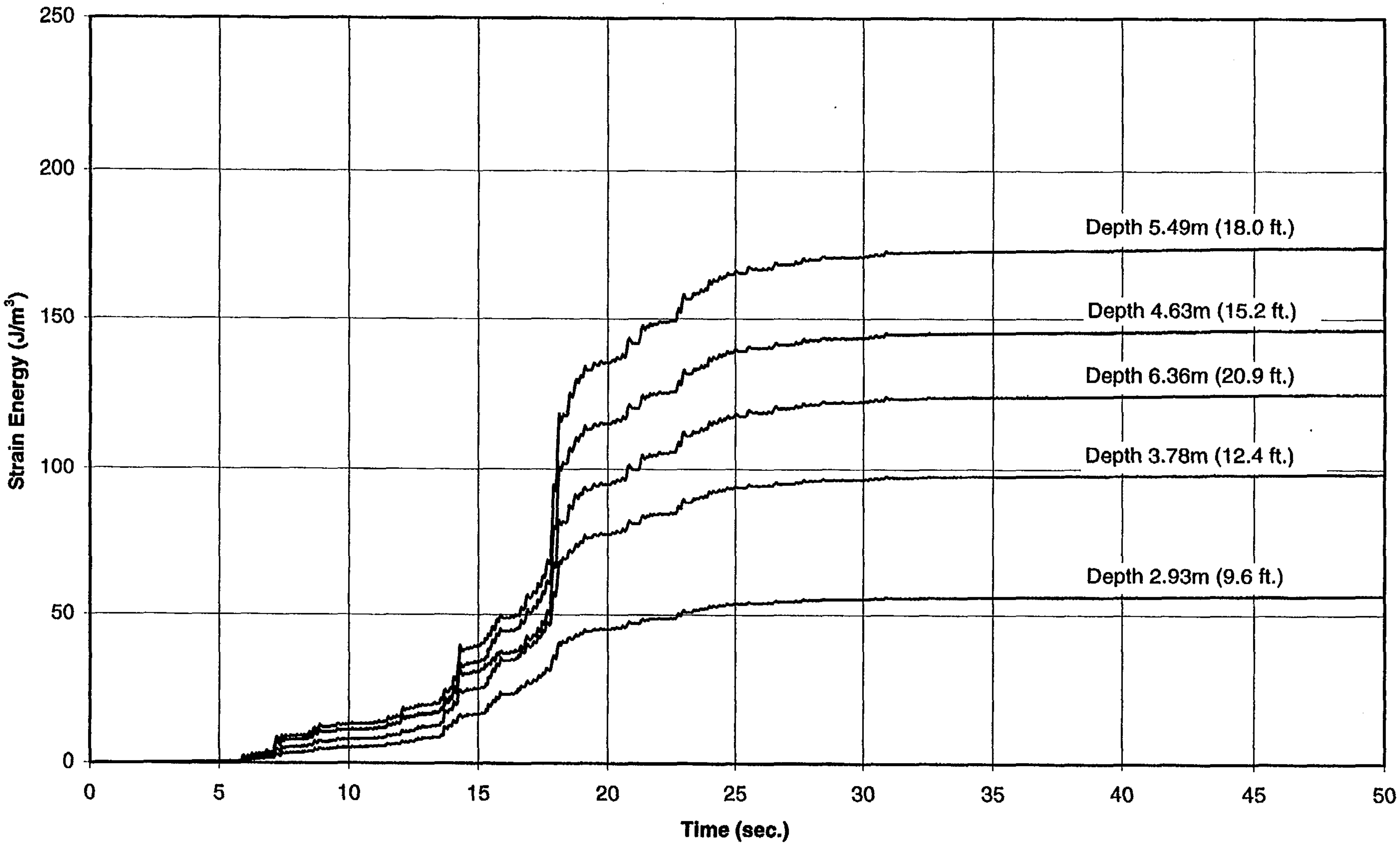

Figure 4.24 - Accumulation of Strain Energy in Liquefied Sand Layer - Wildlife Site, November 24, 1987, 1315 GMT Earthquake in 90° Direction - BDESRA Output, Total Stress Analysis

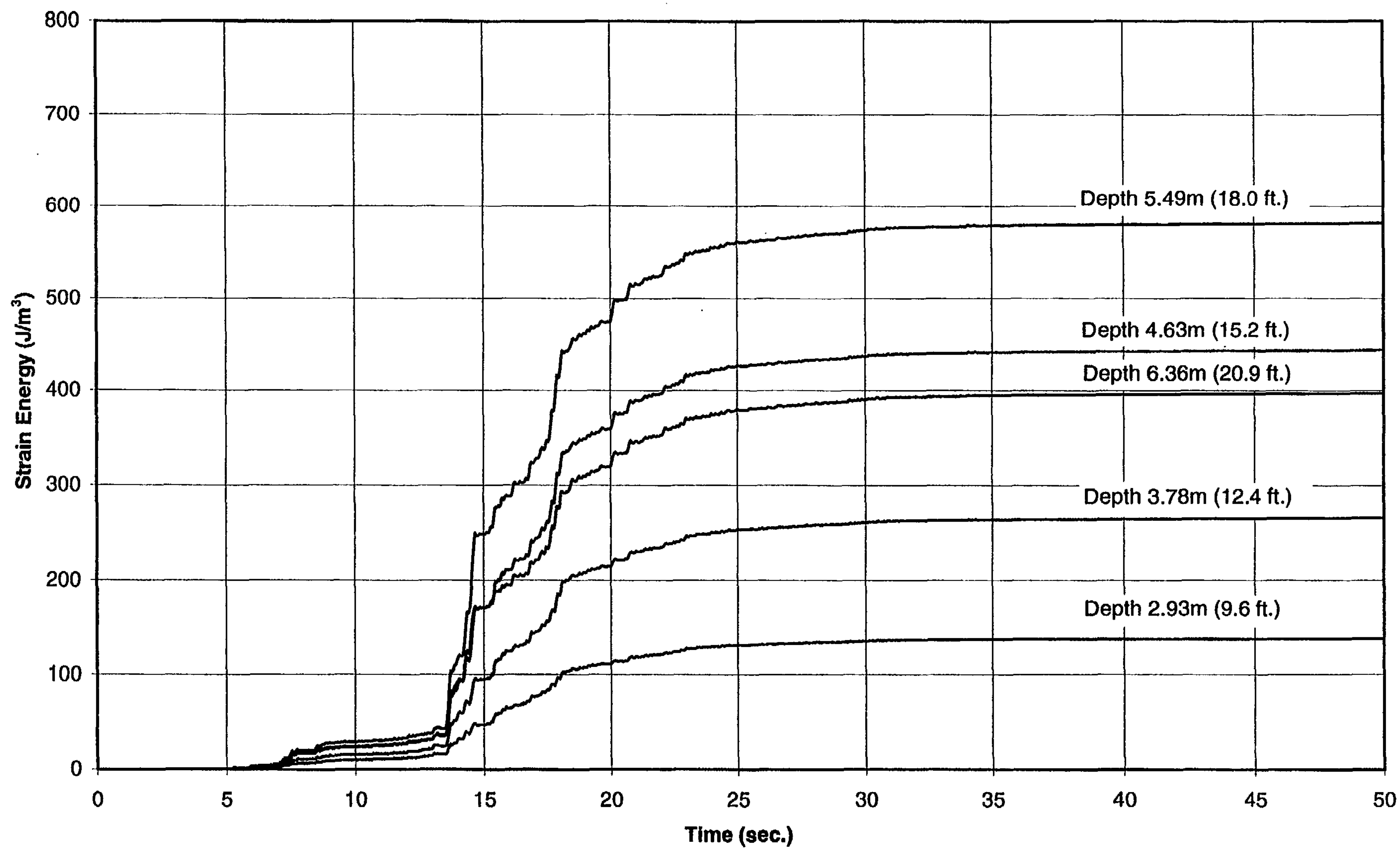

Figure 4.25 - Accumulation of Strain Energy in Liquefied Sand Layer - Wildlife Site, November 24, 1987, 1315 GMT Earthquake - Summation of BDESRA Total Stress Analysis Output in both 360° and 90° Directions

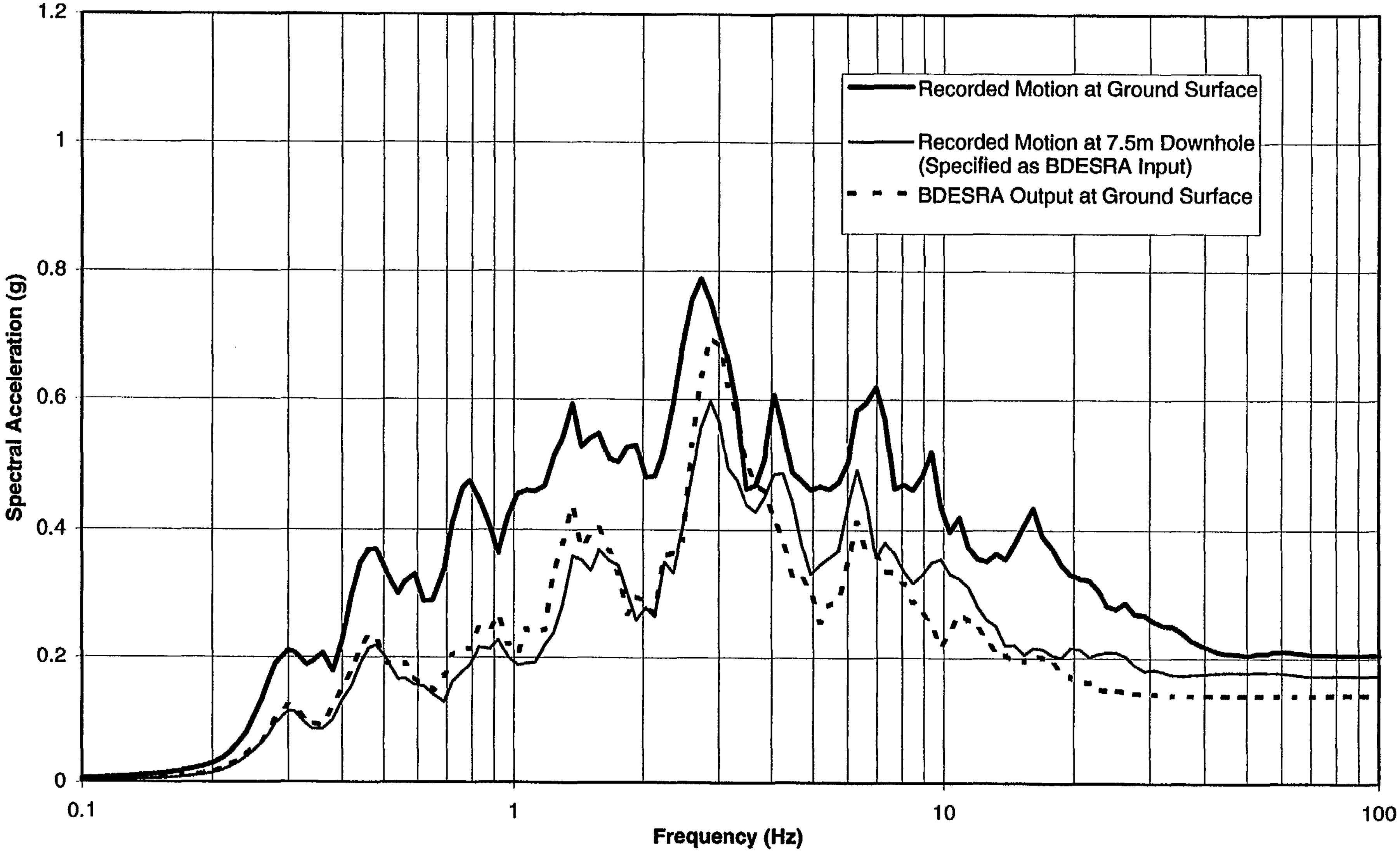

Figure 4.26 - Acceleration Response Spectra at 5% Damping - Wildlife Liquefaction Array, November 24, 1987, 1315 GMT Earthquake - Comparison of Horizontal Motions in 360° Direction - BDESRA Output, Effective Stress Analysis

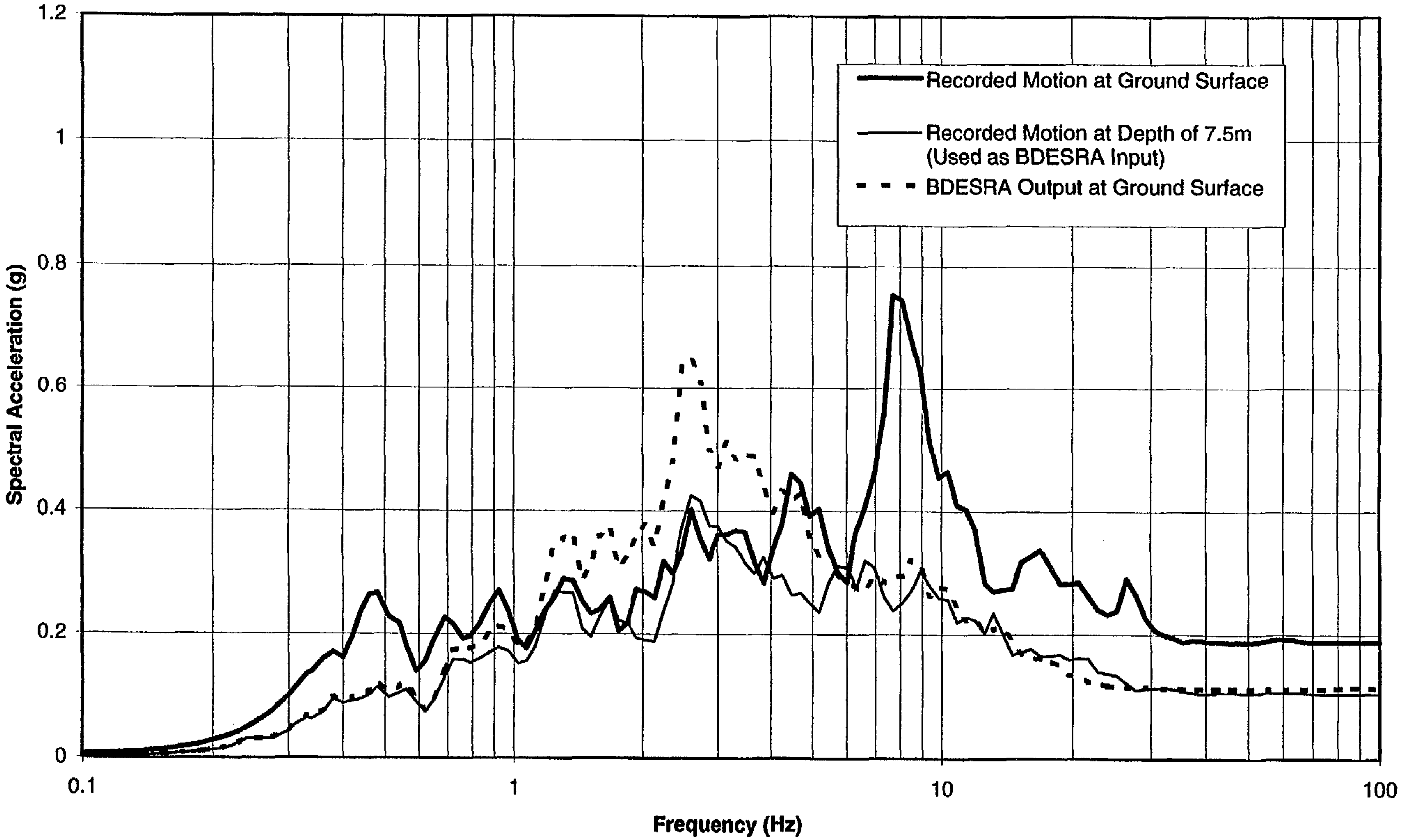

Figure 4.27 - Acceleration Response Spectra at 5% Damping - Wildlife Liquefaction Array, November 24, 1987, 1315 GMT Earthquake - Comparison of Horizontal Motions in 90° Direction - BDESRA Output, Effective Stress Analysis

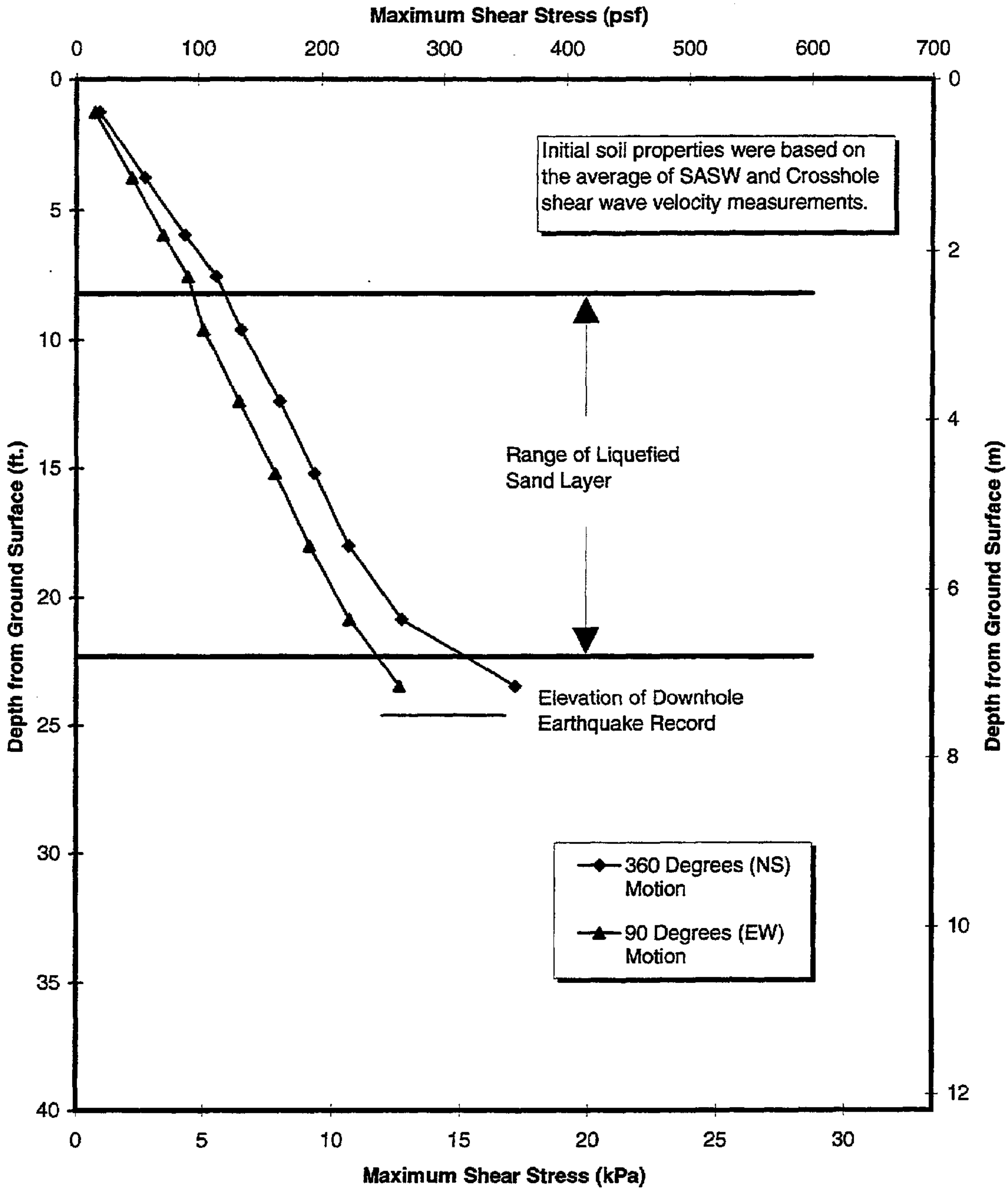

Figure 4.28 - Maximum Shear Stress Distribution over Depth from BDESRA Results of Effective Stress Analyses - Wildlife Site, November 24, 1987, 1315 GMT Earthquake

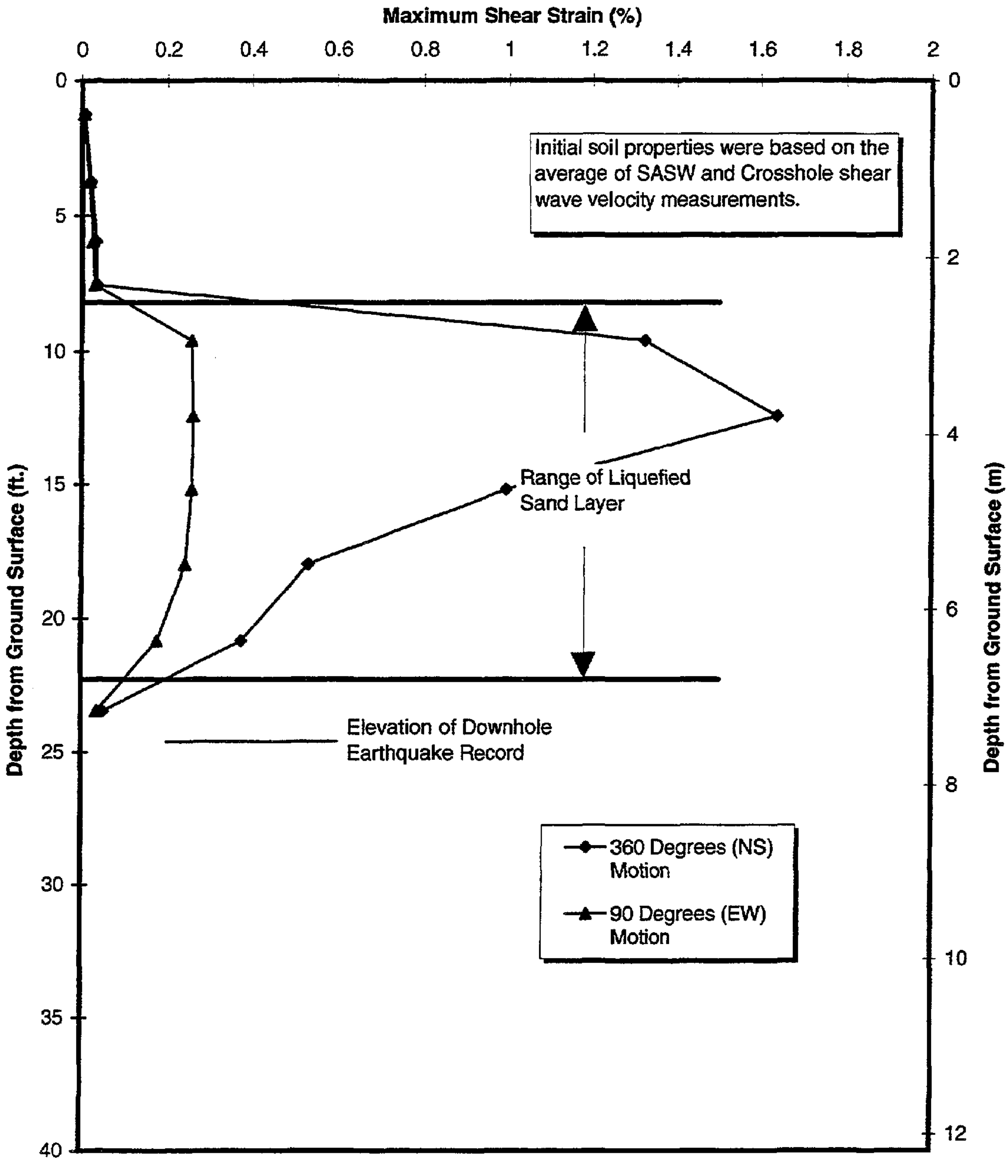

Figure 4.29 - Maximum Shear Strain Distribution over Depth from BDESRA Results of Effective Stress Analyses - Wildlife Site, November 24, 1987, 1315 GMT Earthquake

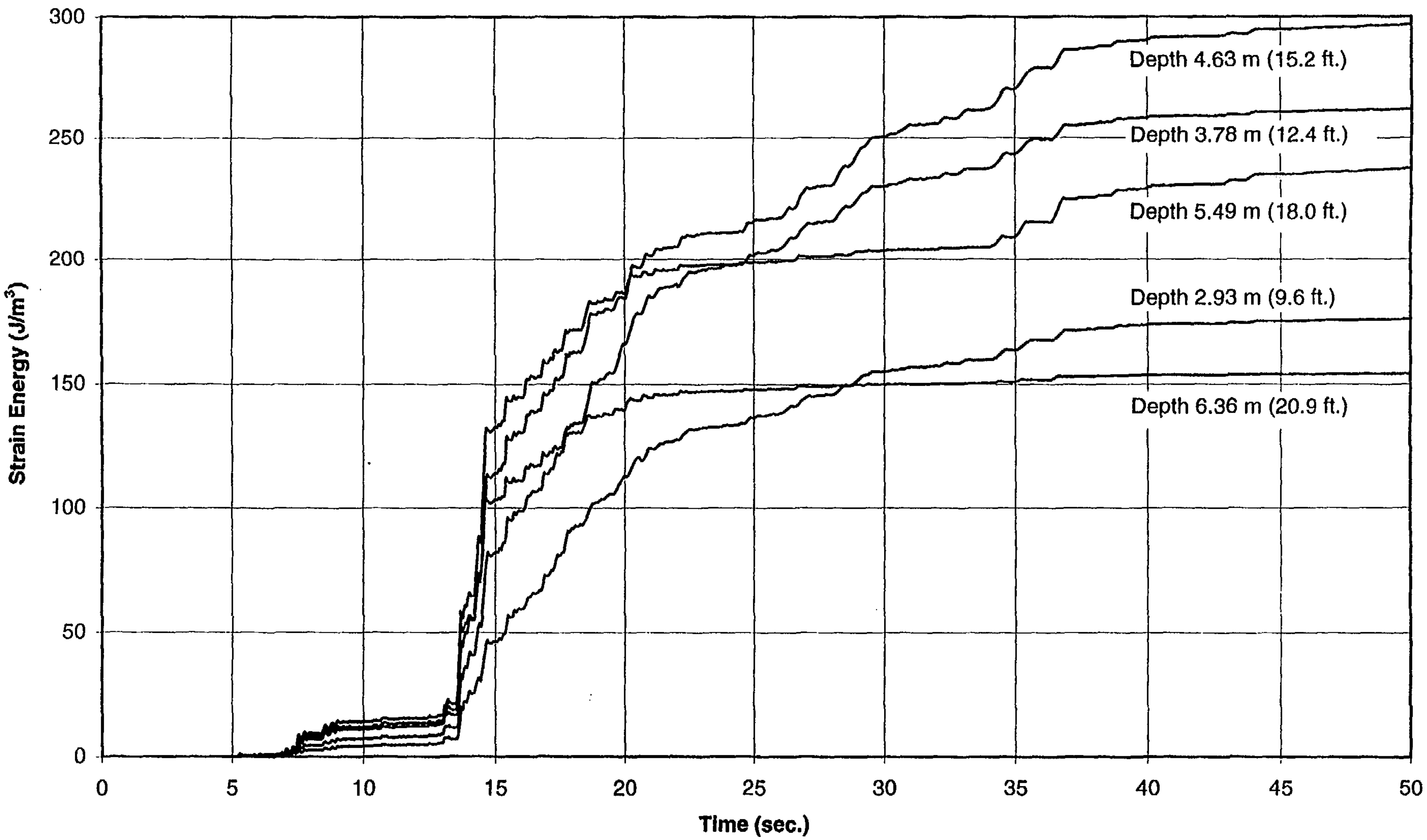

Figure 4.30 - Accumulation of Strain Energy in Liquefied Sand Layer - Wildlife Site, November 24, 1987, 1315 GMT Earthquake in 360° Direction - BDESRA Output, Effective Stress Analysis

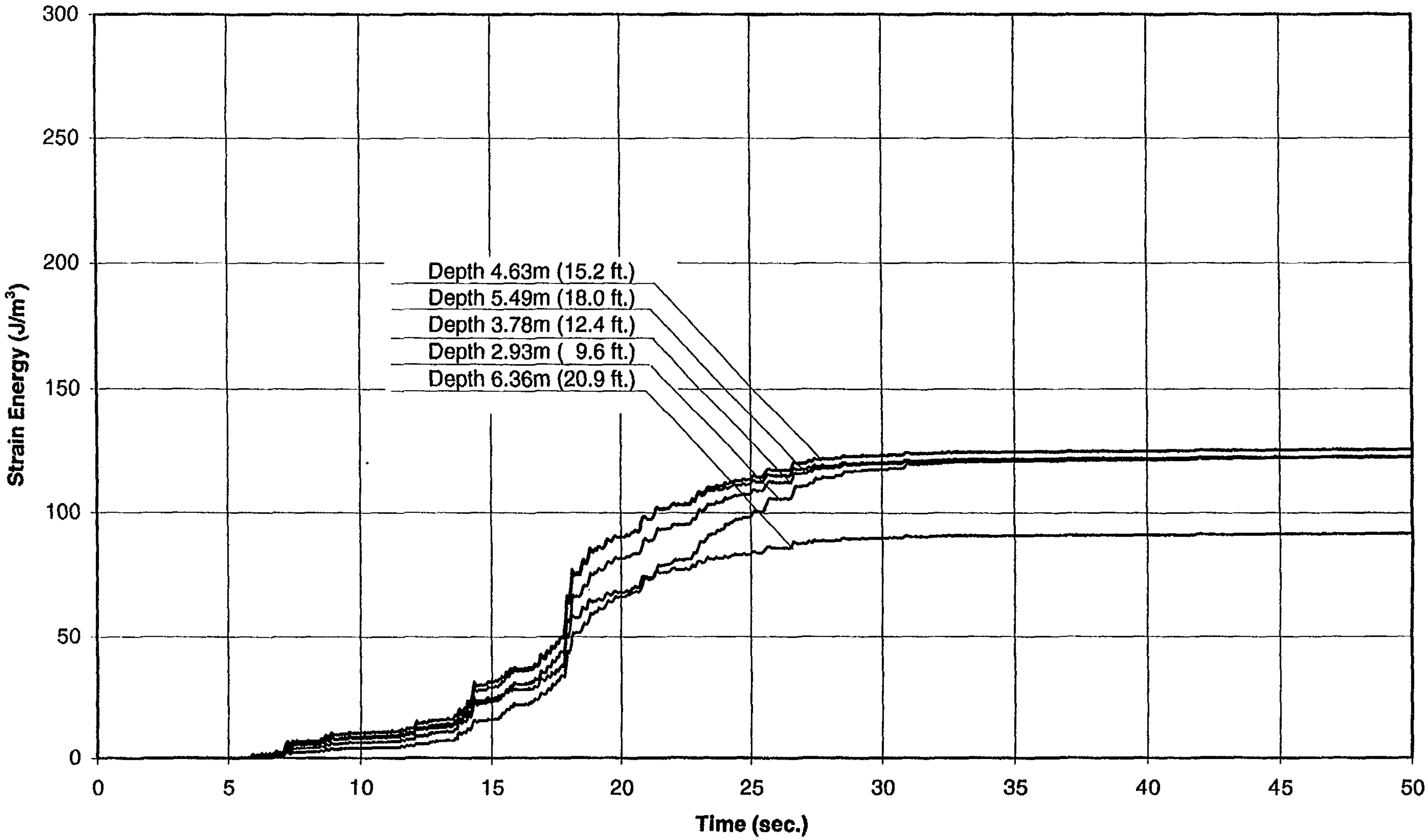

Figure 4.31 - Accumulation of Strain Energy in Liquefied Sand Layer - Wildlife Site, November 24, 1987, 1315 GMT Earthquake in 90° Direction - BDESRA Output, Effective Stress Analysis

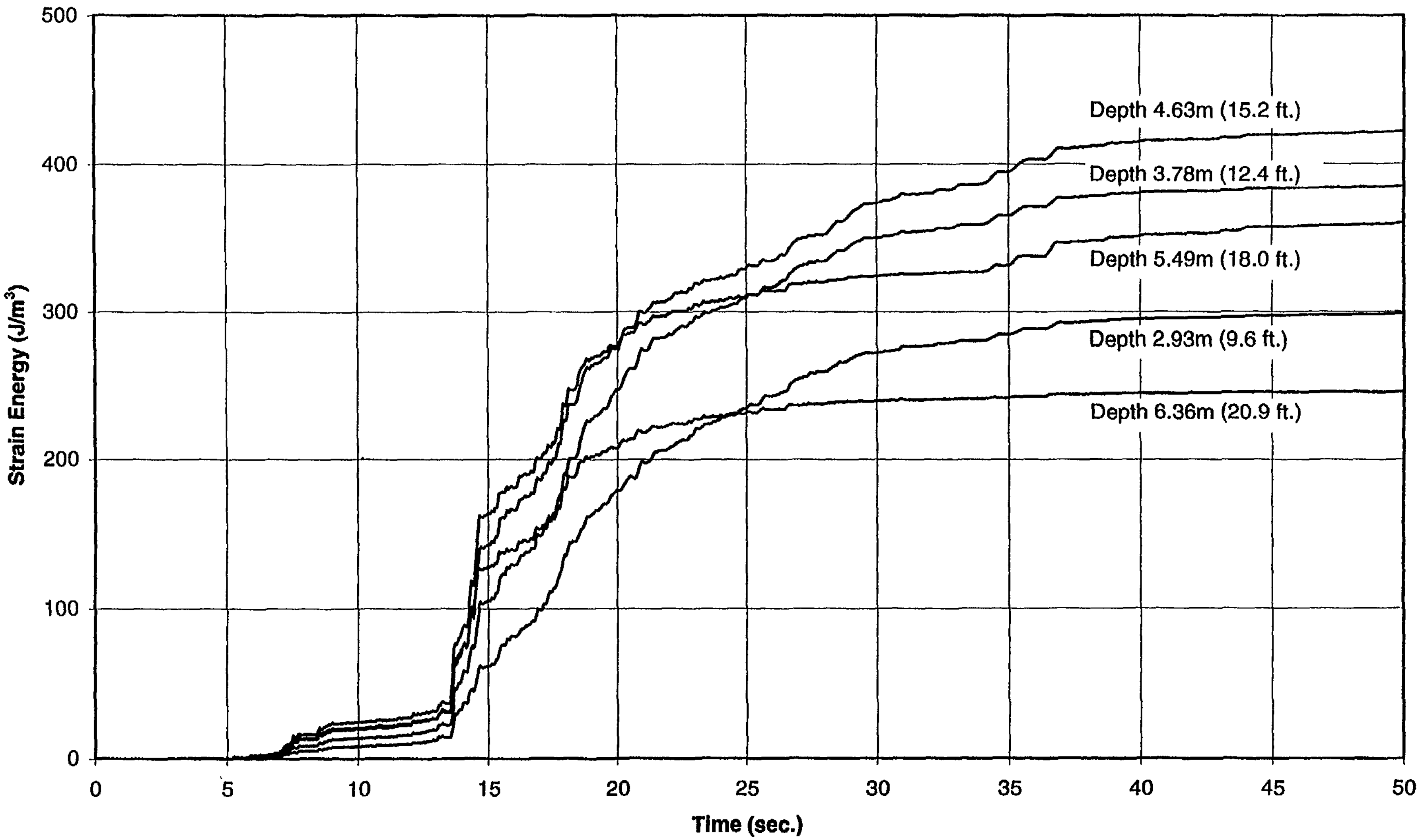

Figure 4.32 - Accumulation of Strain Energy in Liquefied Sand Layer - Wildlife Site, November 24, 1987, 1315 GMT Earthquake - Summation of BDESRA Effective Stress Analysis Output in both 360° and 90° Directions

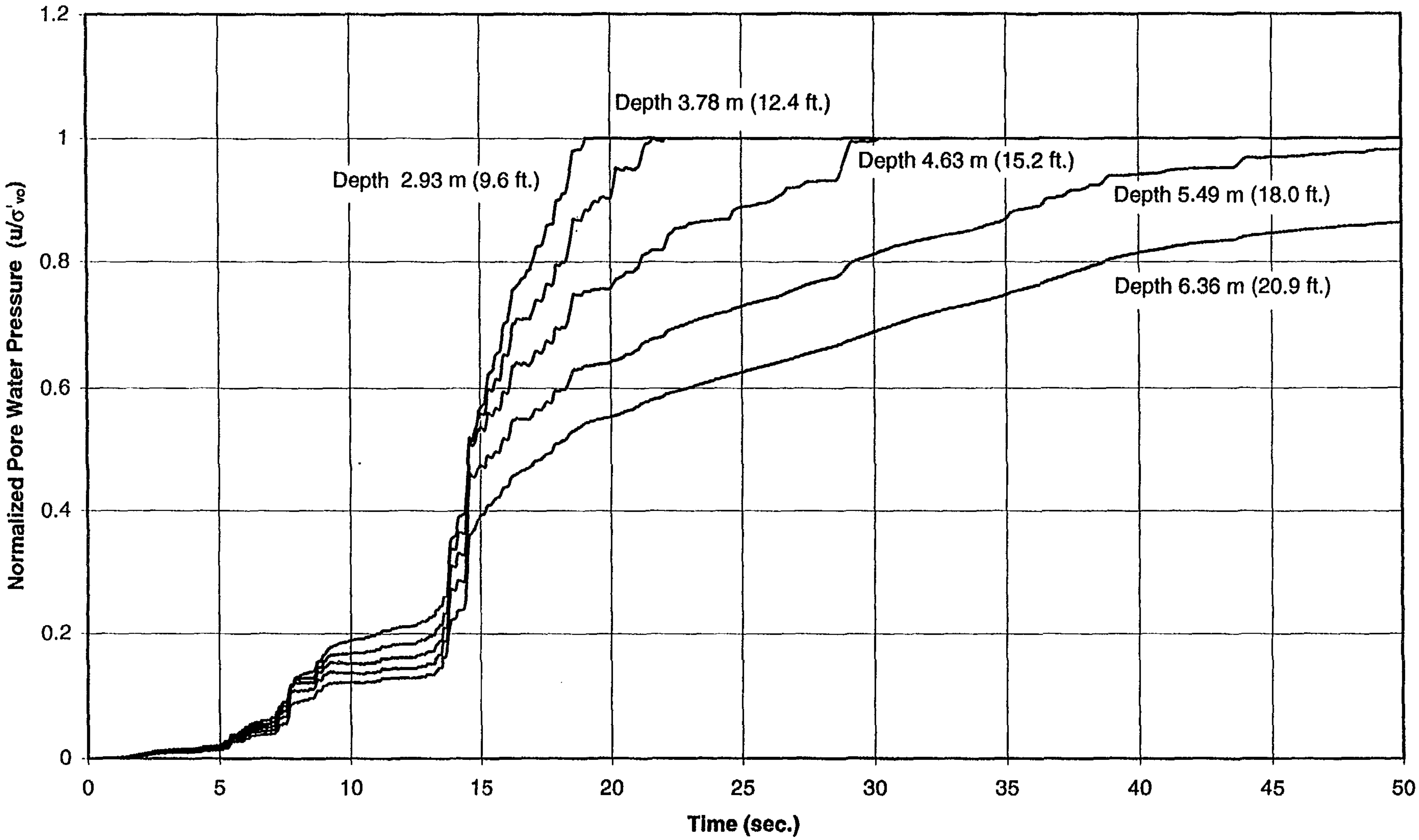

Figure 4.33 - Normalized Pore Water Pressure Generation in Liquefied Sand Layer - Wildlife Site, November 24, 1987, 1315 GMT Earthquake in 360° Direction, BDESRA Output, Effective Stress Analysis

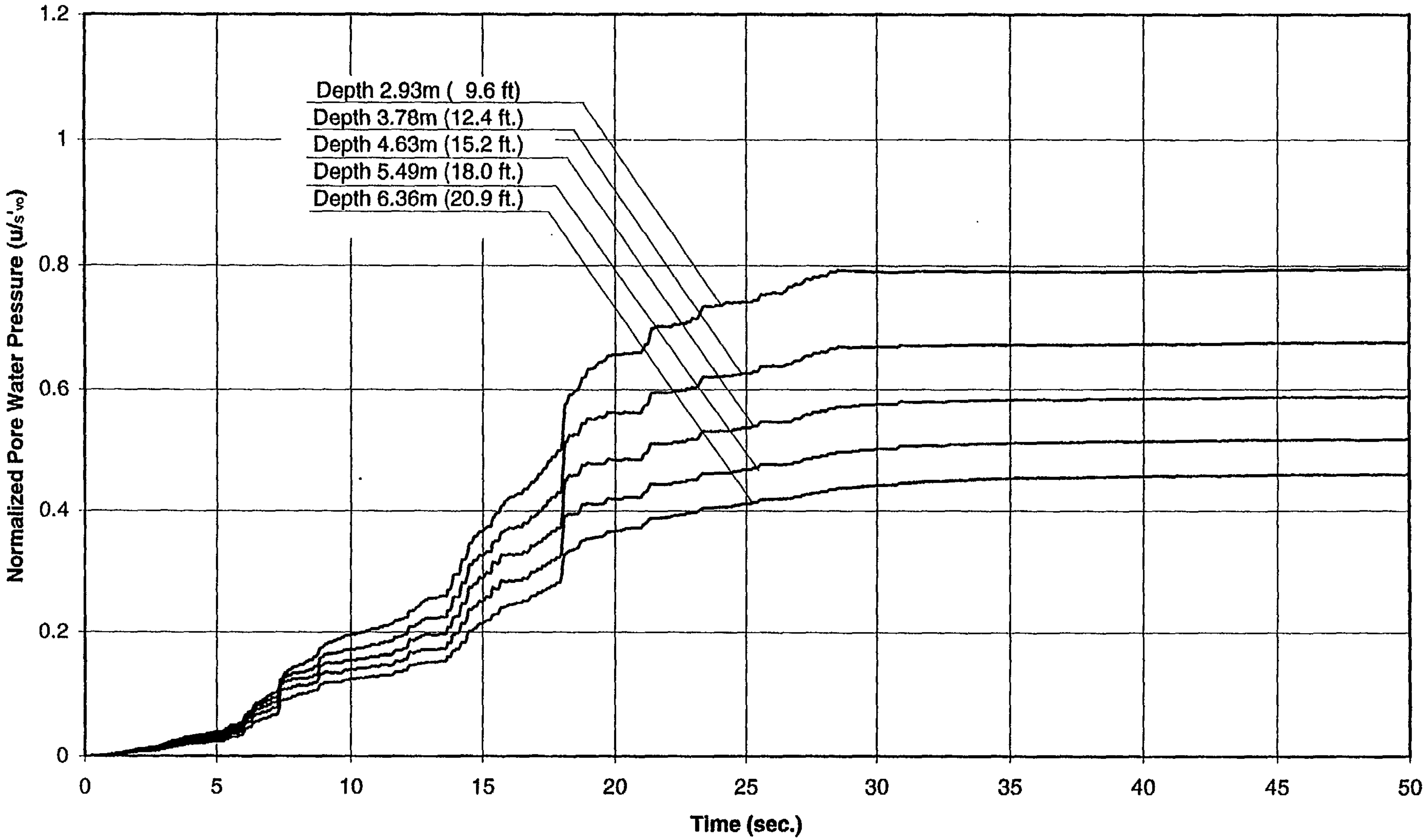

Figure 4.34 - Normalized Pore Water Pressure Generation in Liquefied Sand Layer - Wildlife Site, November 24, 1987, 1315 GMT Earthquake in 90° Direction, BDESRA Output, Effective Stress Analysis

Acceleration at Depth z:

$$a_z = a_{top} + (a_{bottom} - a_{top}) \cdot \frac{z}{h}$$

Shear Stress at Depth z:

$$\tau_z = \frac{1}{2} \cdot \rho \cdot z \cdot (a_{top} + a_z)$$

Shear Strain at Depth z:

$$\gamma = \frac{d_{top} - d_{bottom}}{h}$$

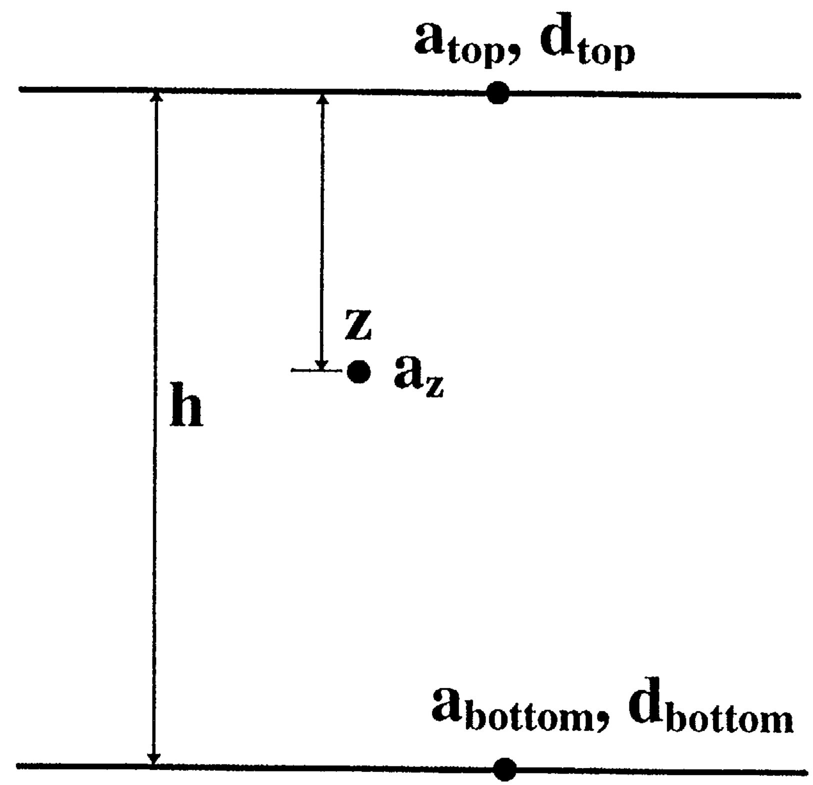

Figure 4.35 - Methodology Adopted in Estimating the Dynamic Stress and Strain Time Histories in a Soil Layer from Field Records (After Zeghal and Elgamal, 1994)

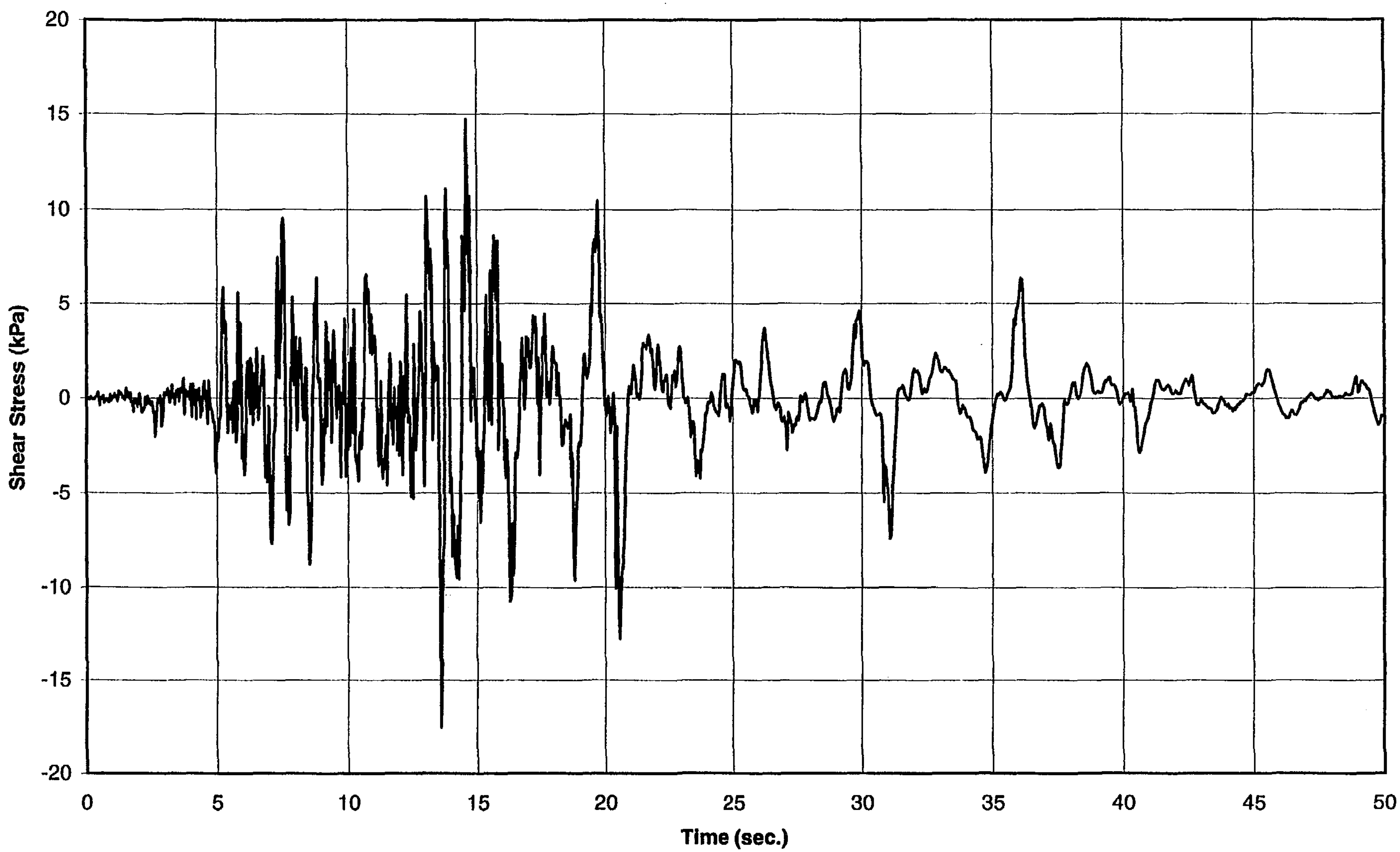

Figure 4.36 - Shear Stress Time History at Depth of 5.06 m (16.6 ft.) - Based on Direct Interpolation of Recorded Motions, Wildlife Site, November 24, 1987, 1315 GMT Earthquake in 360° Direction

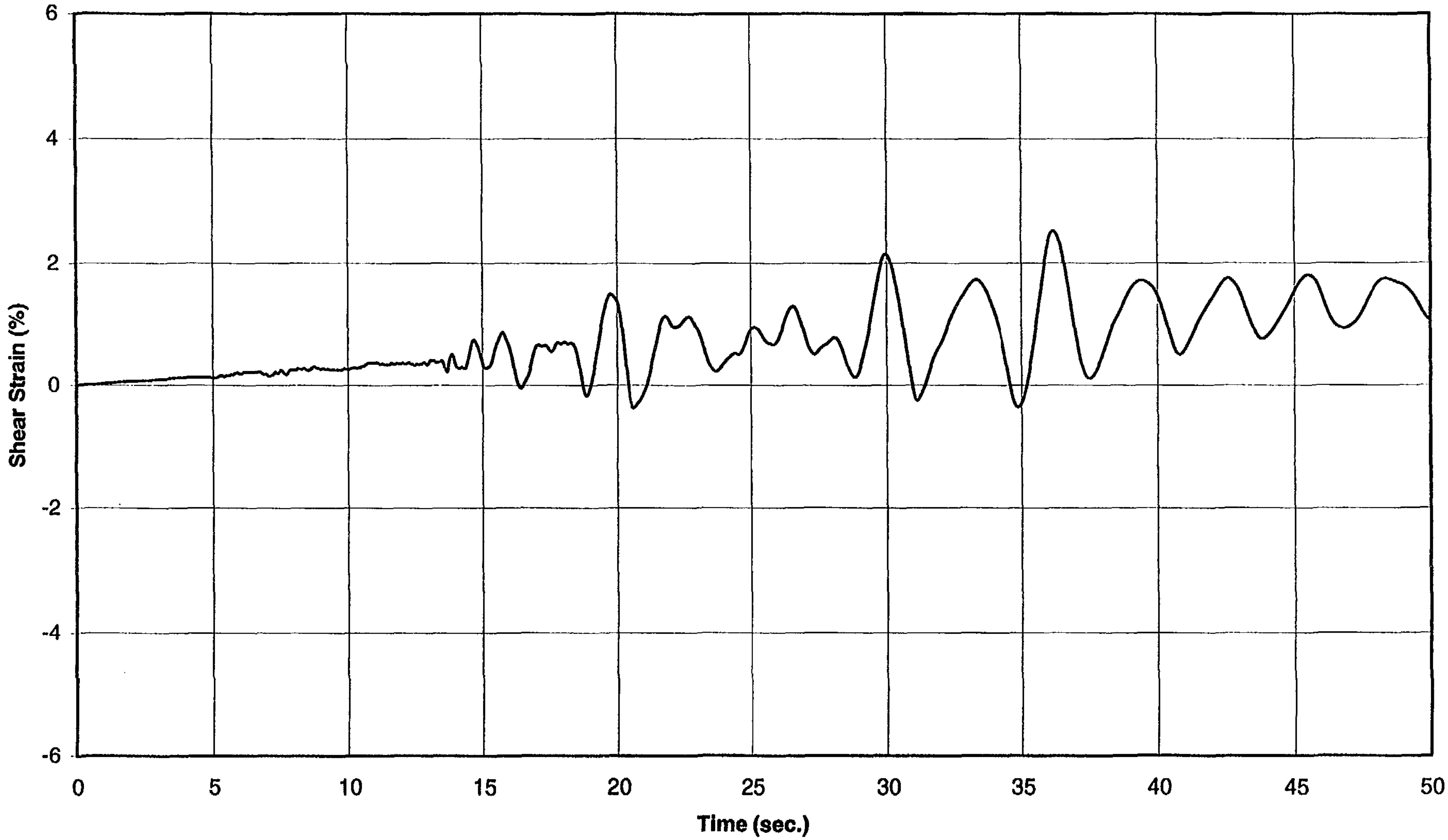

Figure 4.37 - Shear Strain Time History at Depth of 5.06 m (16.6 ft.) - Based on Direct Interpolation of Recorded Motions, Wildlife Site, November 24, 1987, 1315 GMT Earthquake in 360° Direction

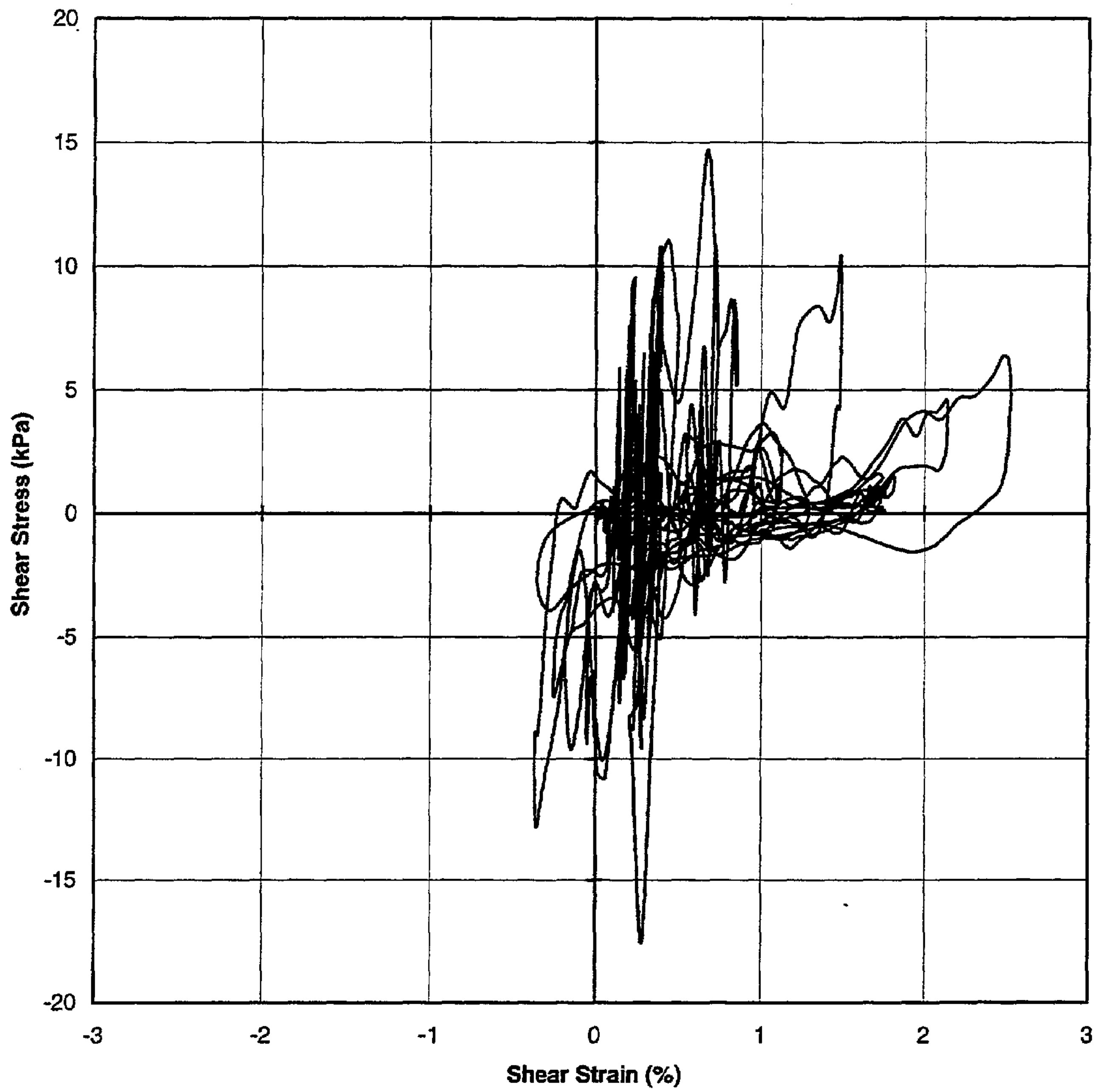

Figure 4.38 - Shear Stress - Shear Strain Hysteresis Loop at Depth of 5.06 m (16.6 ft.) - Based on Direction Interpolation of Recorded Motions, Wildlife Site, November 24, 1987, 1315 GMT Earthquake in 360° Direction.

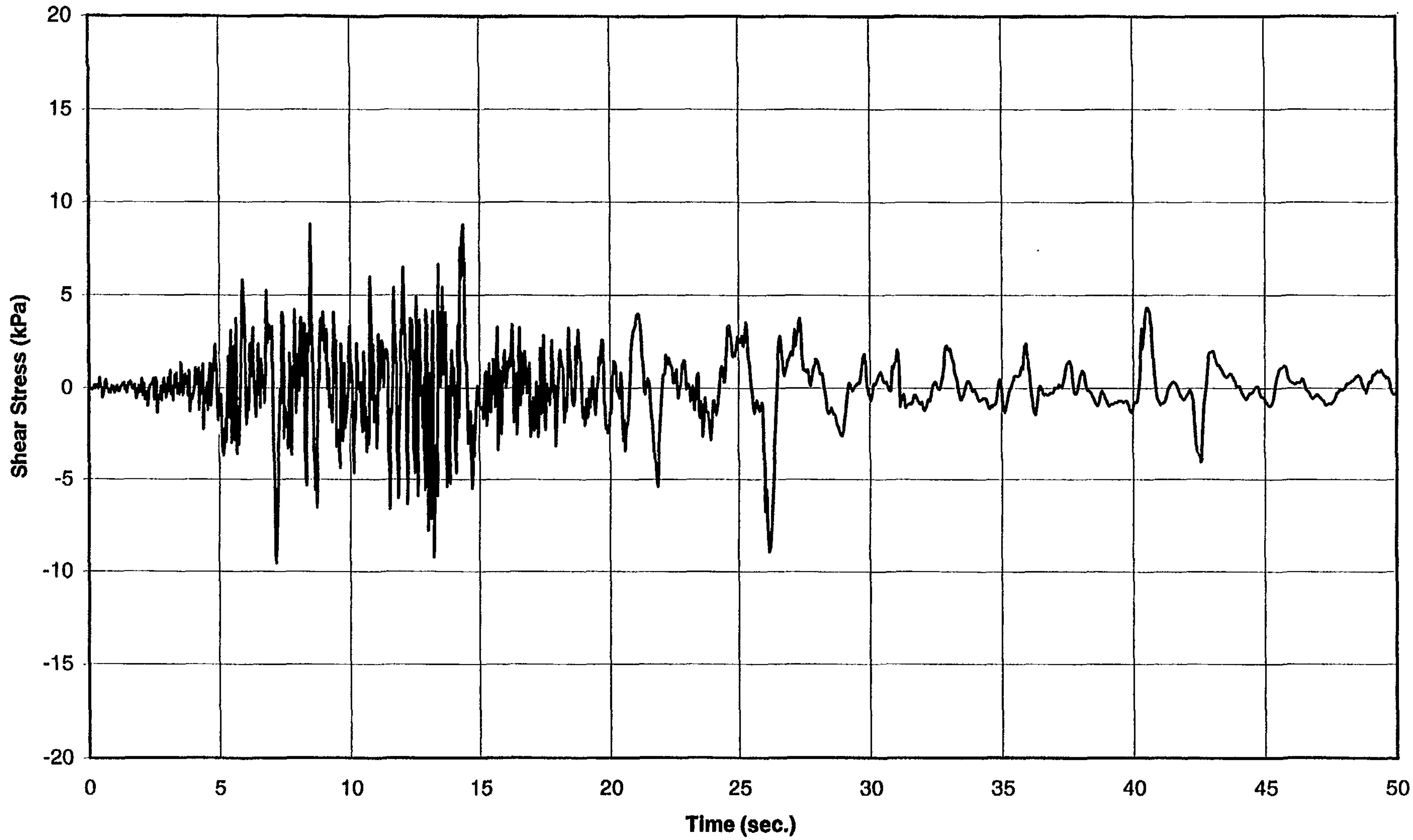

Figure 4.39 - Shear Stress Time History at Depth of 5.06 m (16.6 ft.). - Based on Direct Interpolation of Recorded Motions, Wildlife Site, November 24, 1987, 1315 GMT Earthquake in 90° Direction

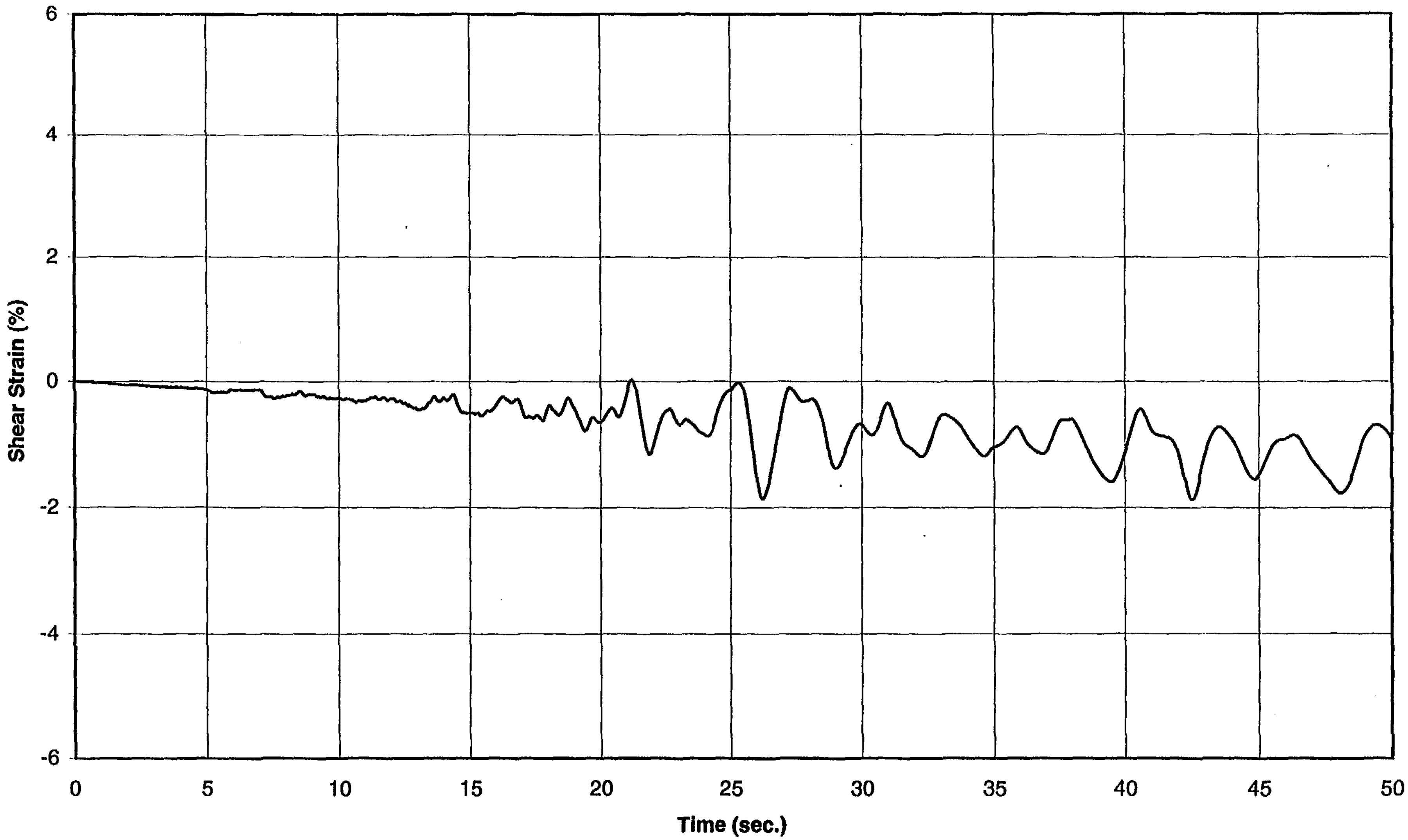

Figure 4.40 - Shear Strain Time History at Depth of 5.06 m (16.6 ft.) - Based on Direct Interpolation of Recorded Motions, Wildlife Site, November 24, 1987, 1315 GMT Earthquake in 90° Direction

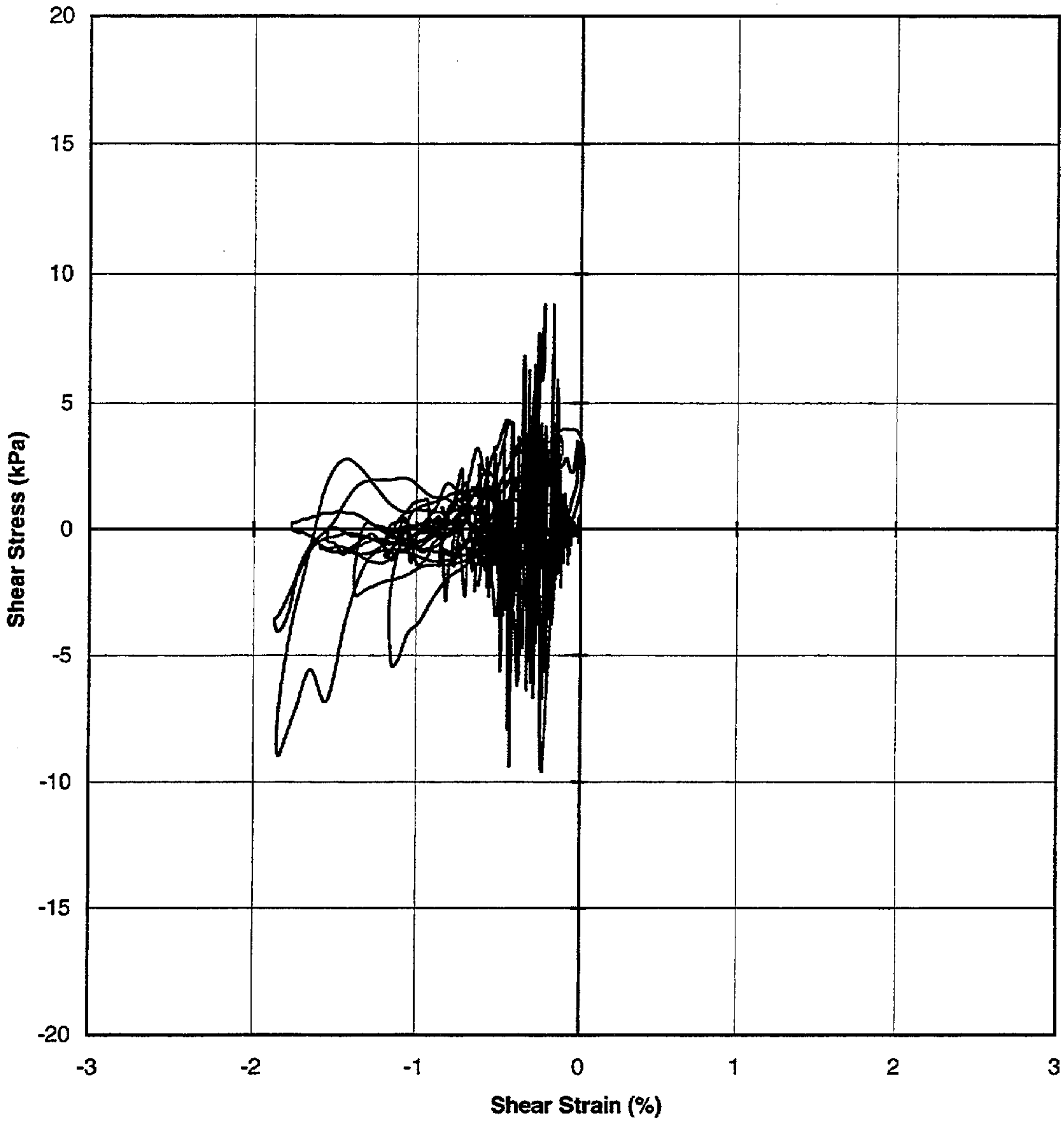

Figure 4.41 - Shear Stress - Shear Strain Hysteresis Loop at Depth of 5.06 m (16.6 ft.) - Based on Direct Interpolation of Recorded Motions, Wildlife Site, November 24, 1987, 1315 GMT Earthquake in 90° Direction

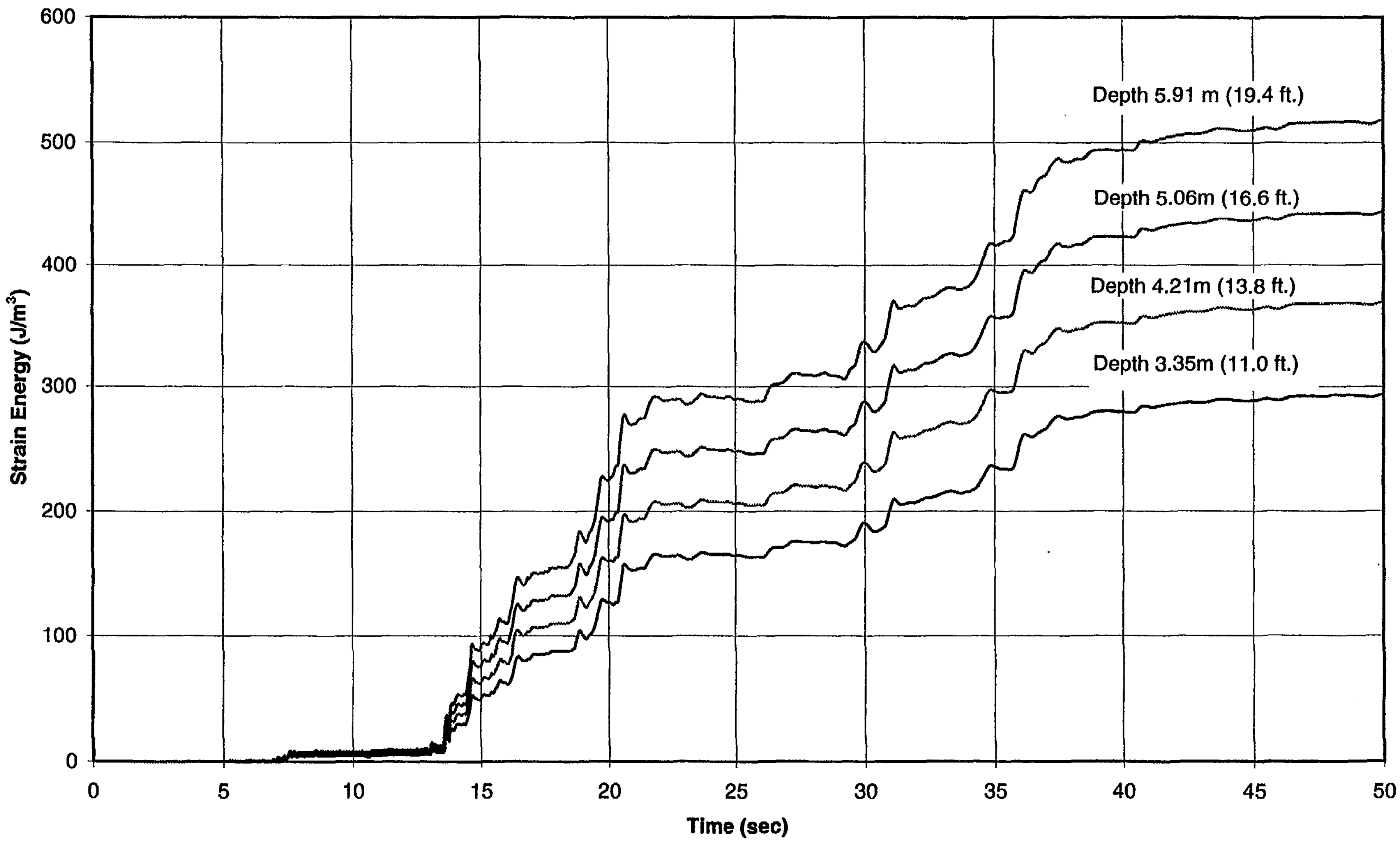

Figure 4.42 - Accumulation of Strain Energy in Liquefied Sand Layer - Based on Direct Interpolation of Recorded Motions, Wildlife Site, November 24, 1987, 1315 GMT Earthquake in 360° Direction

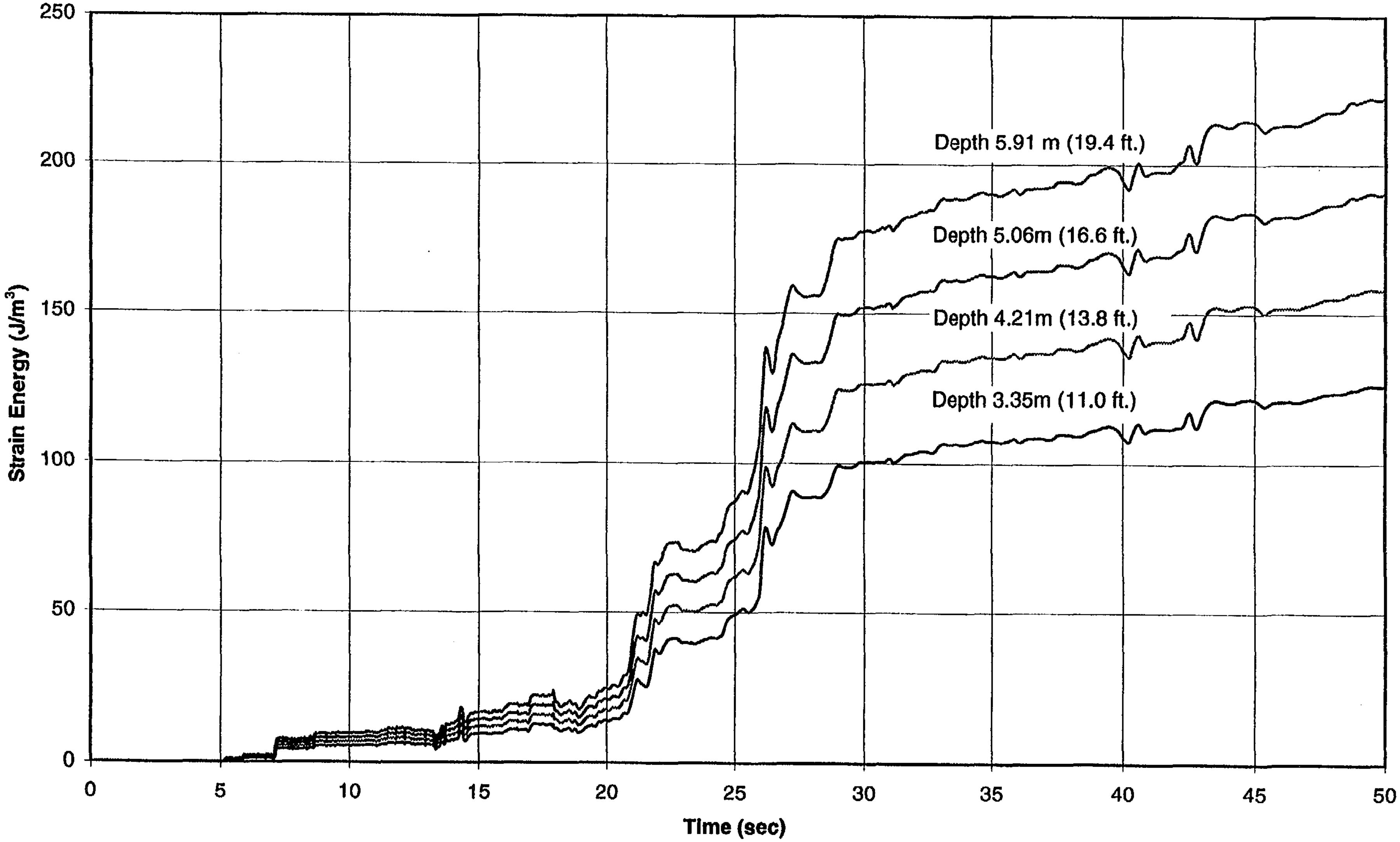

Figure 4.43 - Accumulation of Strain Energy in Liquefied Sand Layer - Based on Direct Interpolation of Recorded Motions, Wildlife Site, November 24, 1987, 1315 GMT Earthquake in 90° Direction

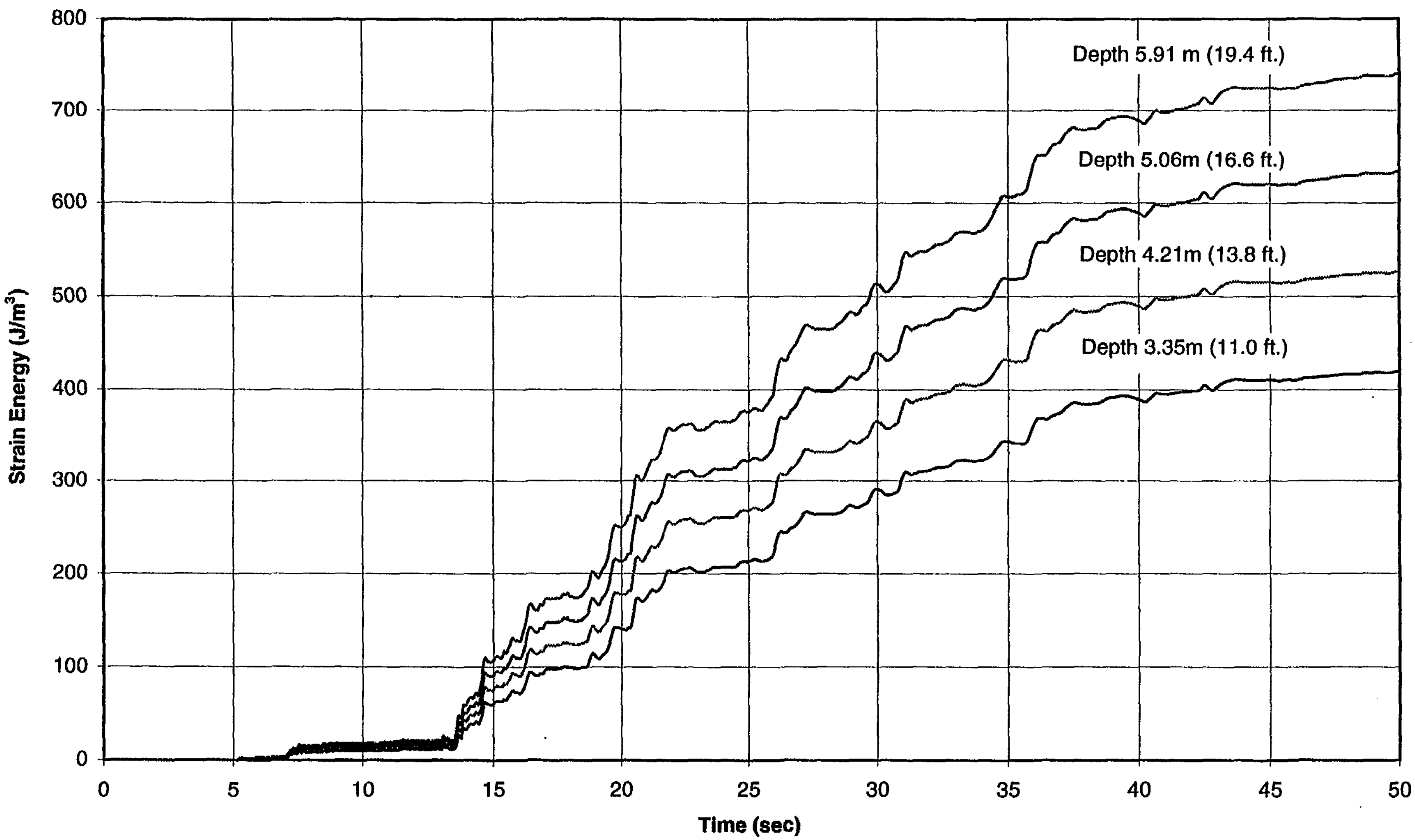

Figure 4.44 - Accumulation of Strain Energy in Liquefied Sand Layer - Based on Direct Interpolation of Recorded Motions, Wildlife Site, November 24, 1987, 1315 GMT Earthquake - Summation of Strain Energy in both 360° and 90° Directions

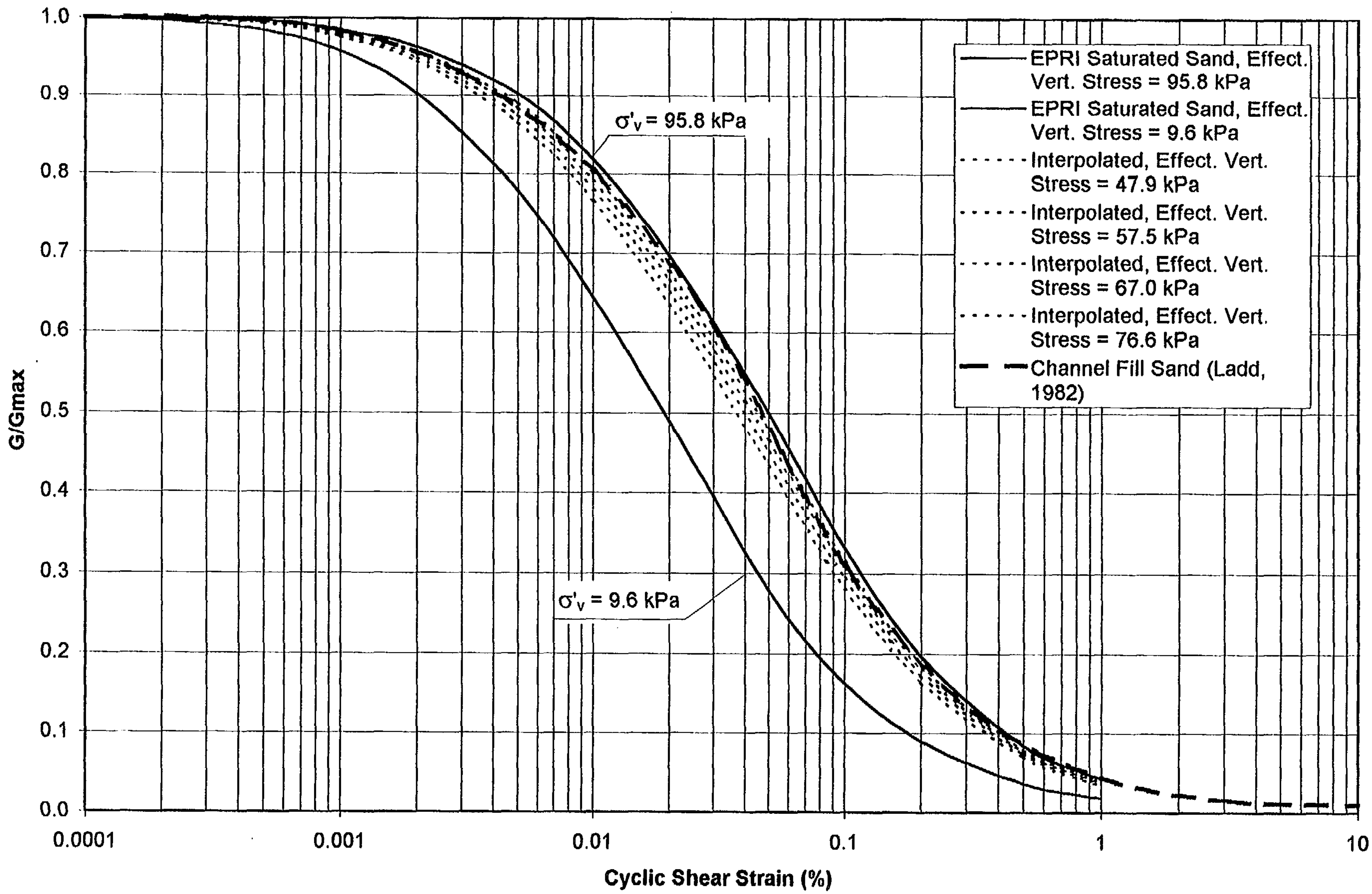

Figure 4.45 - Comparison of Shear Modulus Degradation Curves Used in SHAKE Analyses

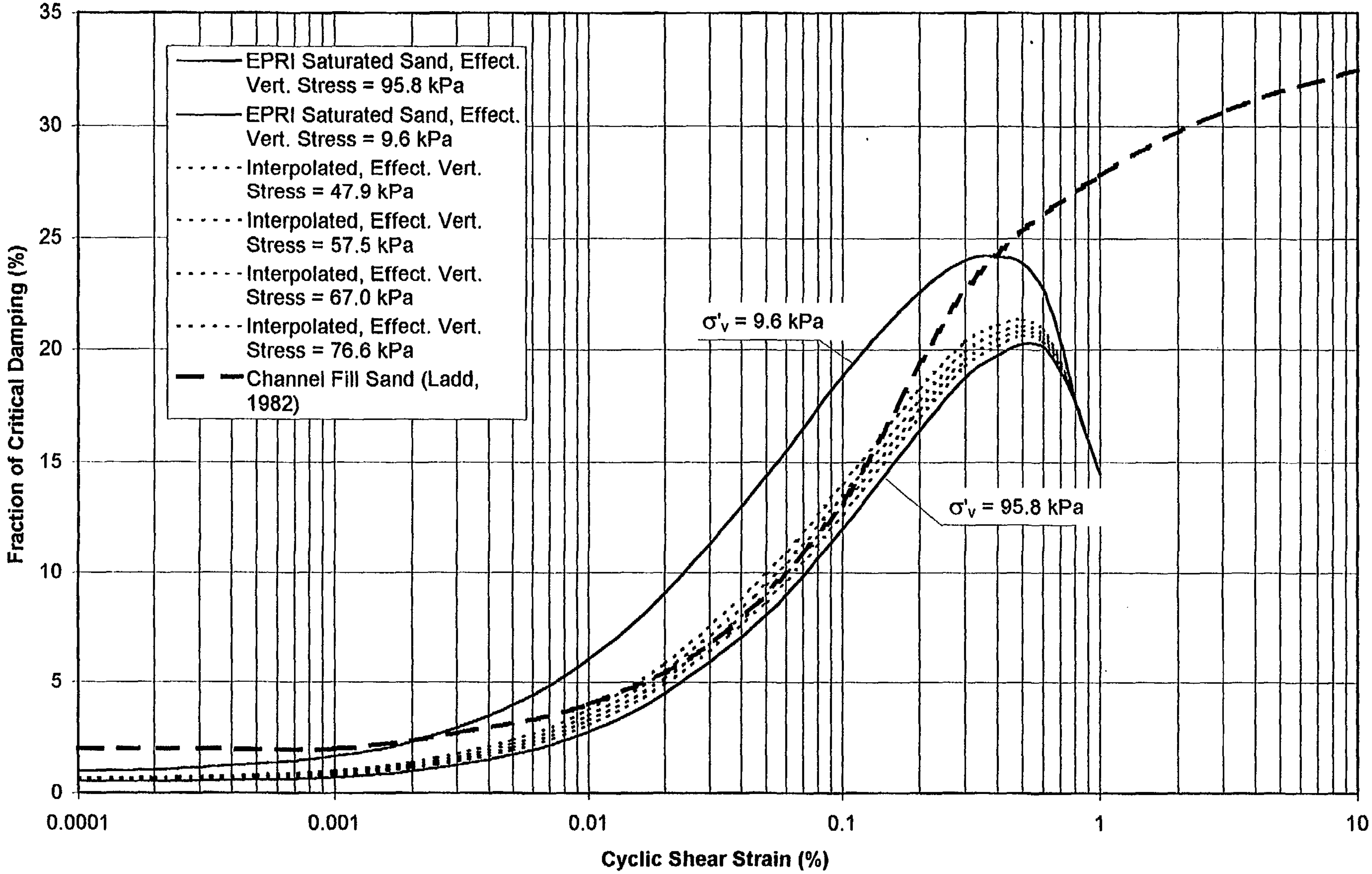

Figure 4.46 - Comparison of Damping Curves Used in SHAKE Analyses

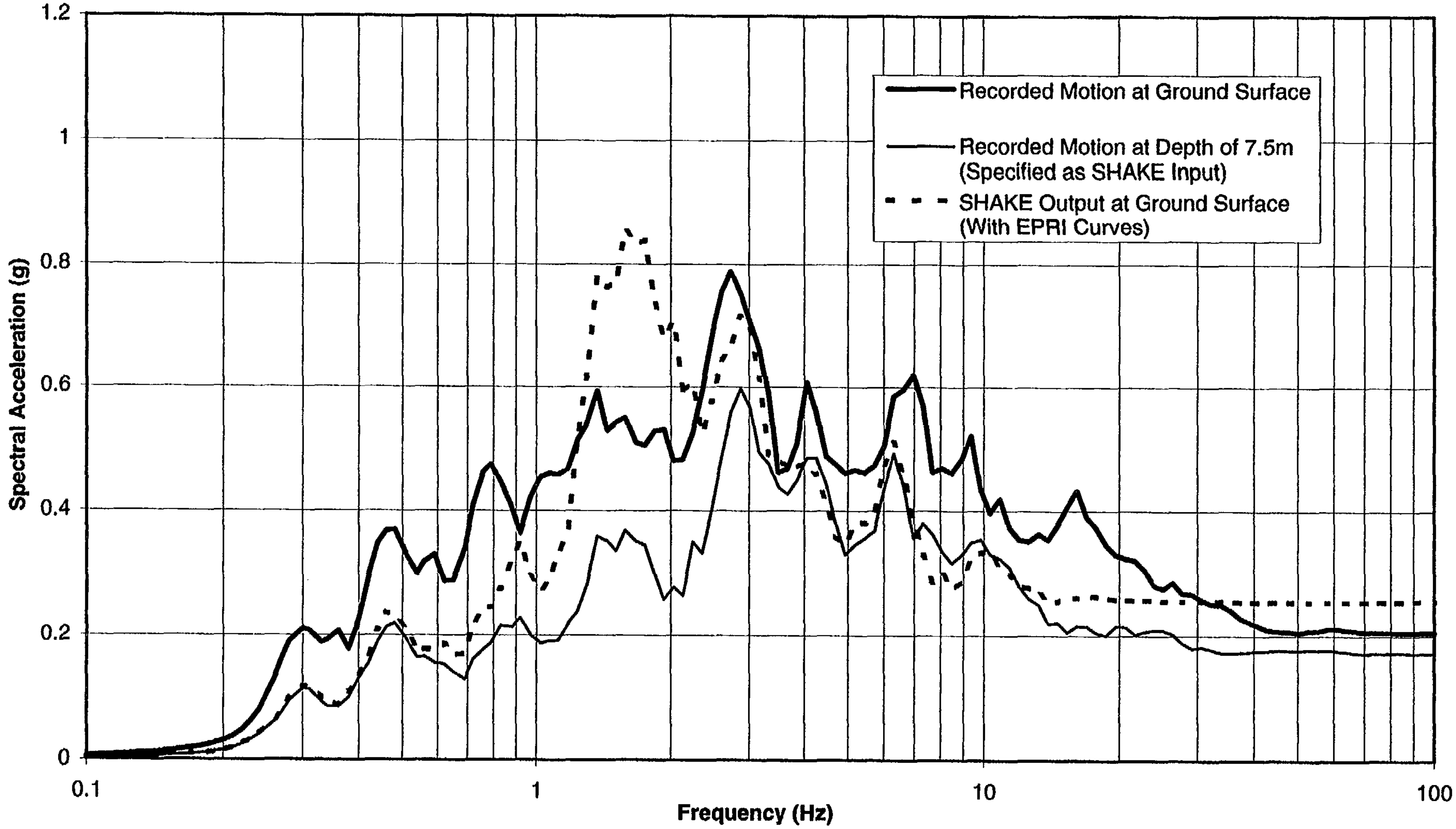

Figure 4.47 - Acceleration Response Spectra at 5% Damping - Wildlife Liquefaction Array, November 24, 1987, 1315 GMT Earthquake - Comparison of Horizontal Motions in 360° Direction - SHAKE Output with EPRI (1993) Soil Curves.

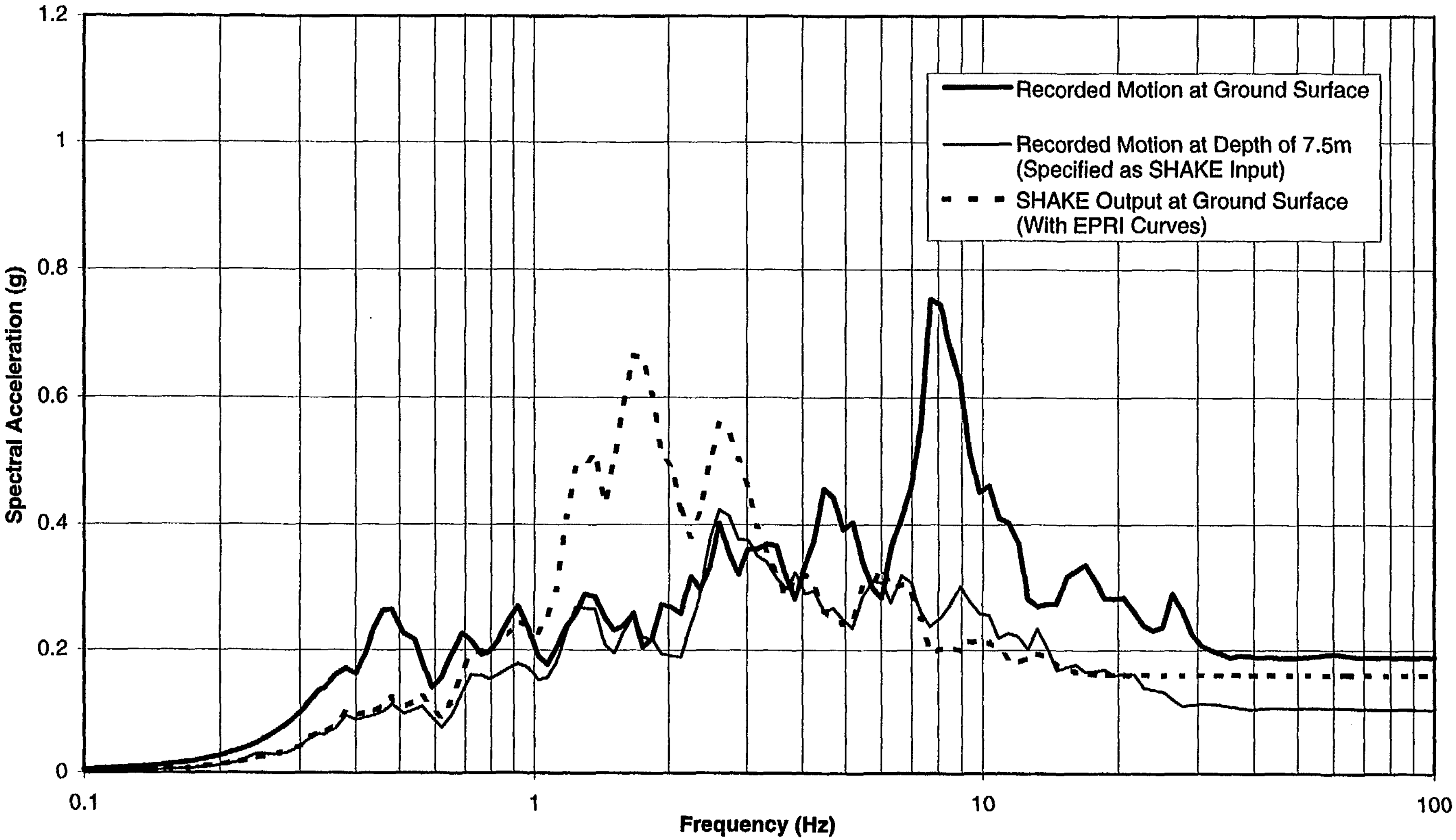

Figure 4.48 - Acceleration Response Spectra at 5% Damping - Wildlife Liquefaction Array, November 24, 1987, 1315 GMT Earthquake - Comparison of Horizontal Motions in 90° Direction - SHAKE Output with EPRI (1993) Soil Curves

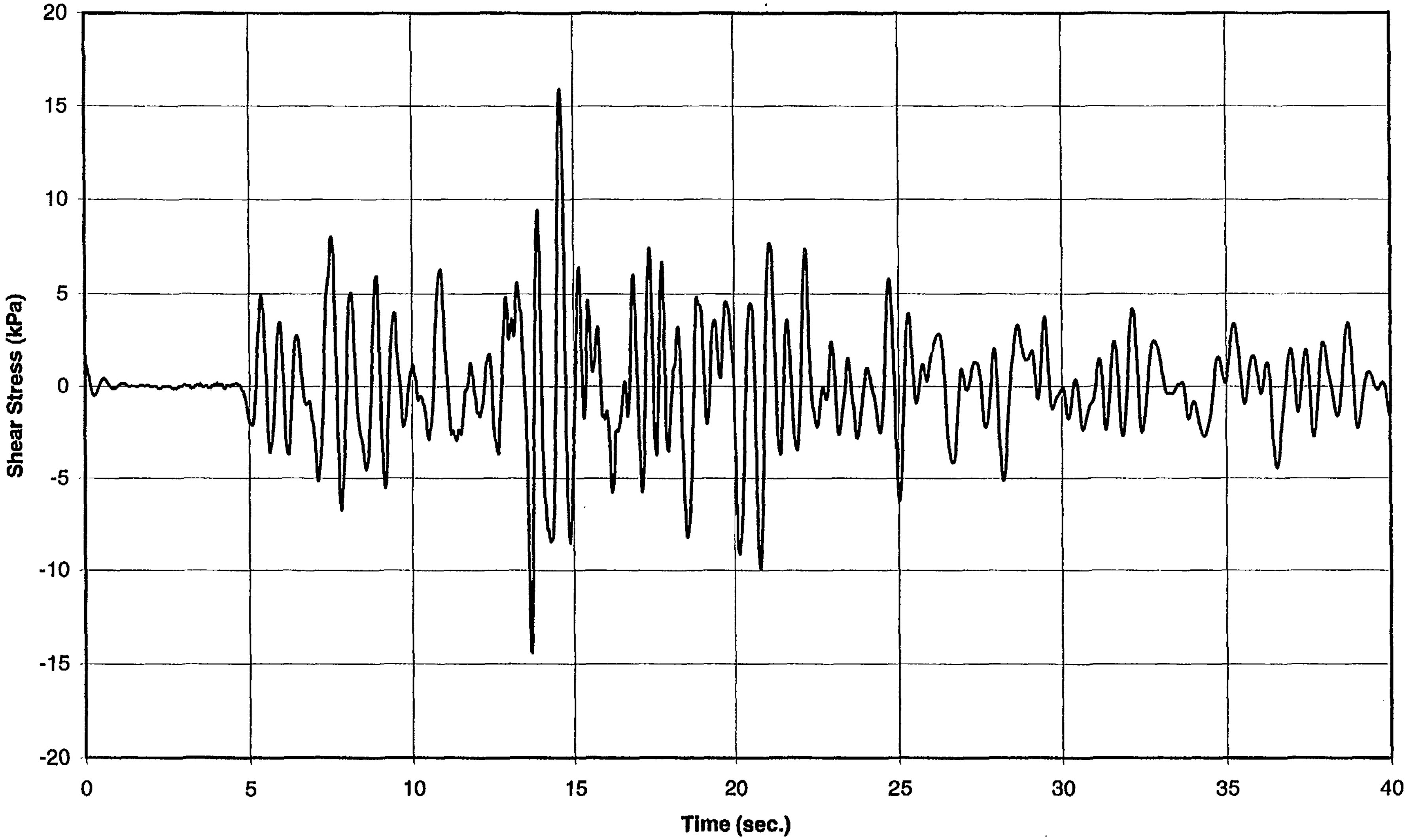

Figure 4.49 - Shear Stress Time History at Depth of 4.21 m (13.8 ft.) from SHAKE Output with EPRI (1993) Soil Curves - Wildlife Site, November 24, 1987, 1315 GMT Earthquake in 360° Direction

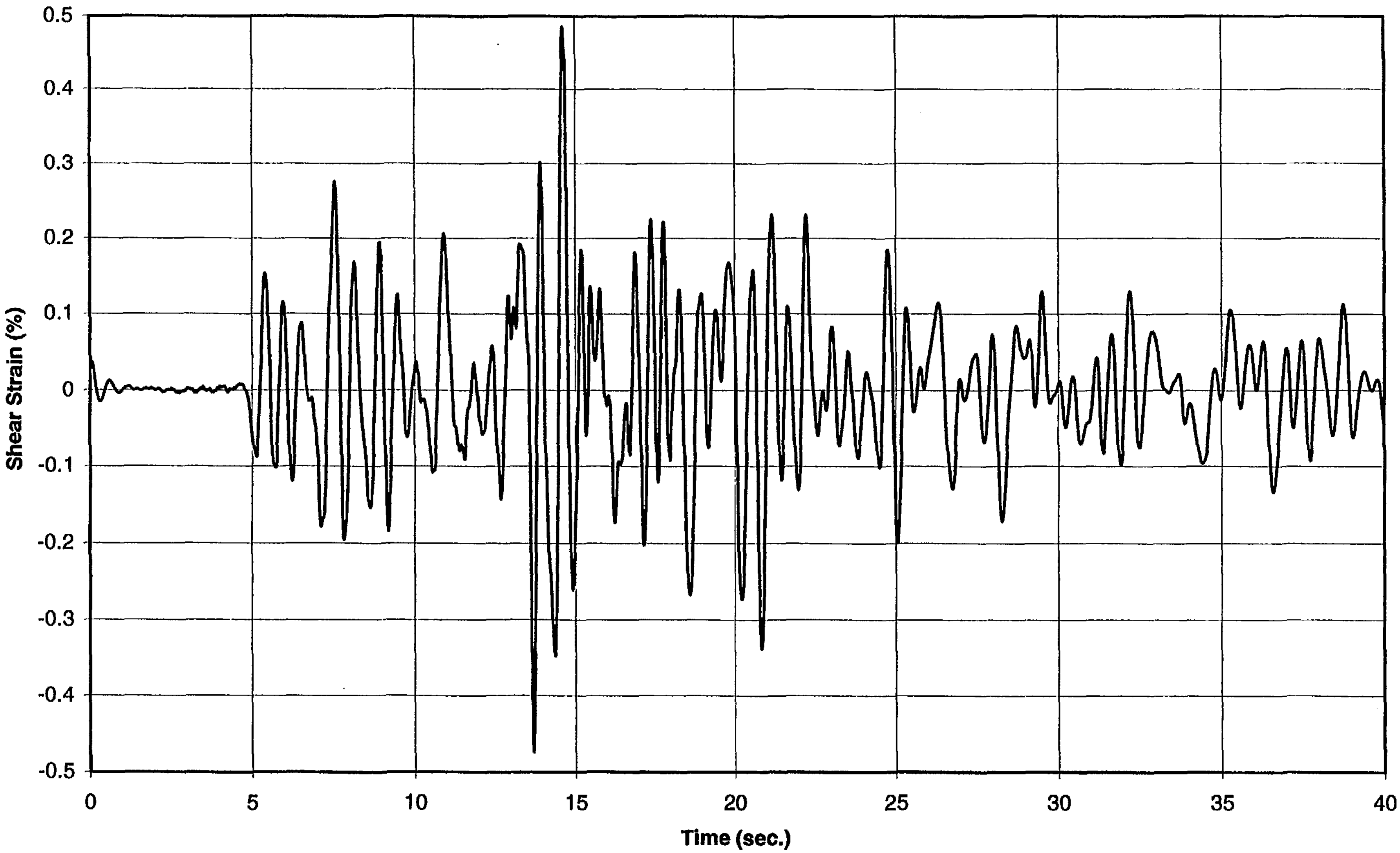

Figure 4.50 - Shear Strain Time History at Depth of 4.21 m (13.8 ft.) from SHAKE Output with EPRI (1993) Soil Curves - Wildlife Site, November 24, 1987, 1315 GMT Earthquake in 360° Direction

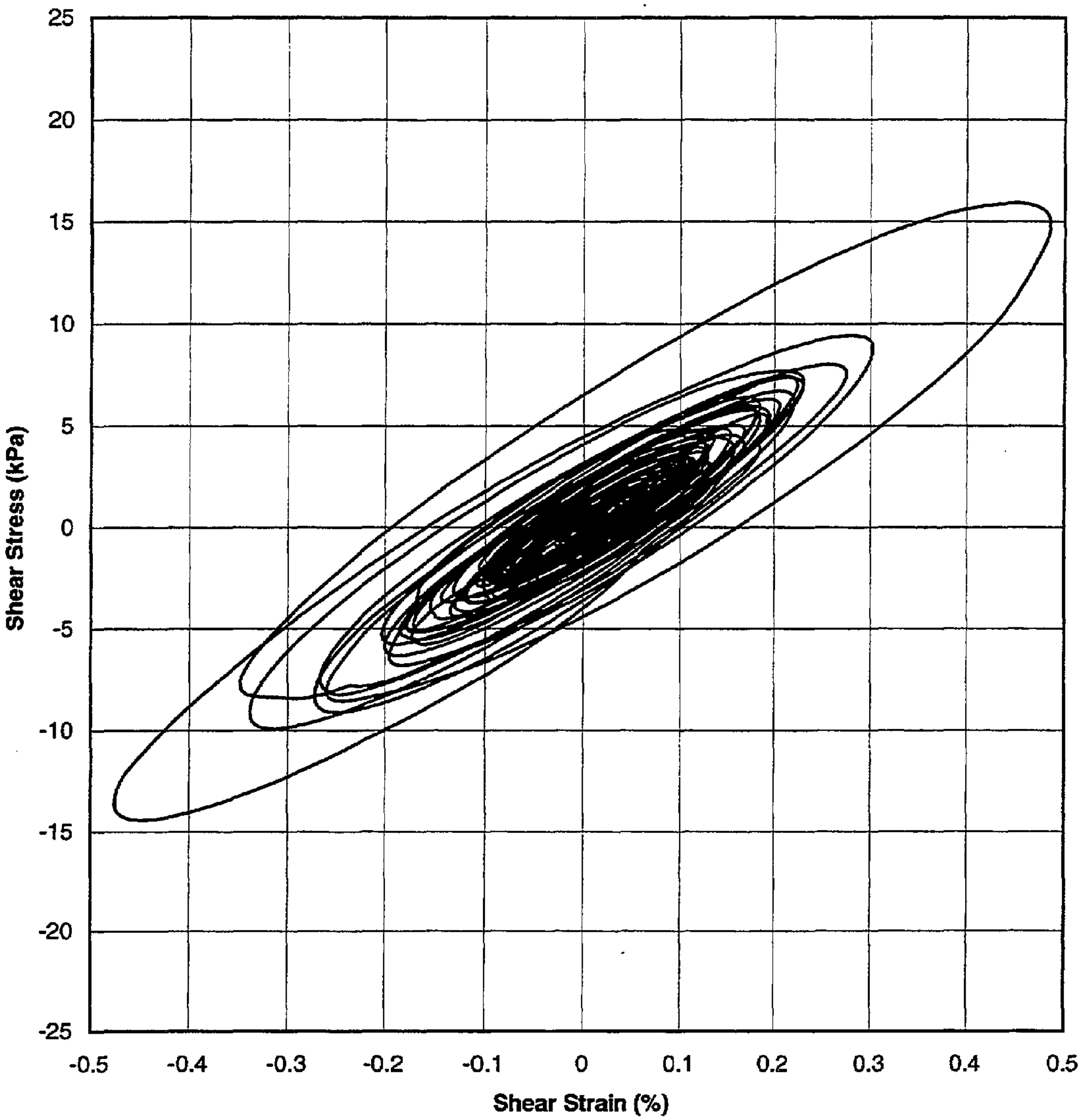

Figure 4.51 - Shear Stress - Shear Strain Hysteresis Loop at Depth of 4.21 m (13.8 ft.). Calculated from SHAKE Output - Wildlife SIte, November 24, 1987, 1315 GMT Earthquake in 360° Direction. Soil Properties Are Based on the Average of SASW and Crosshole Shear Wave Velocity Measurements. The EPRI (1993) G/Gmax and Damping Curves Are Used in the Calculation.

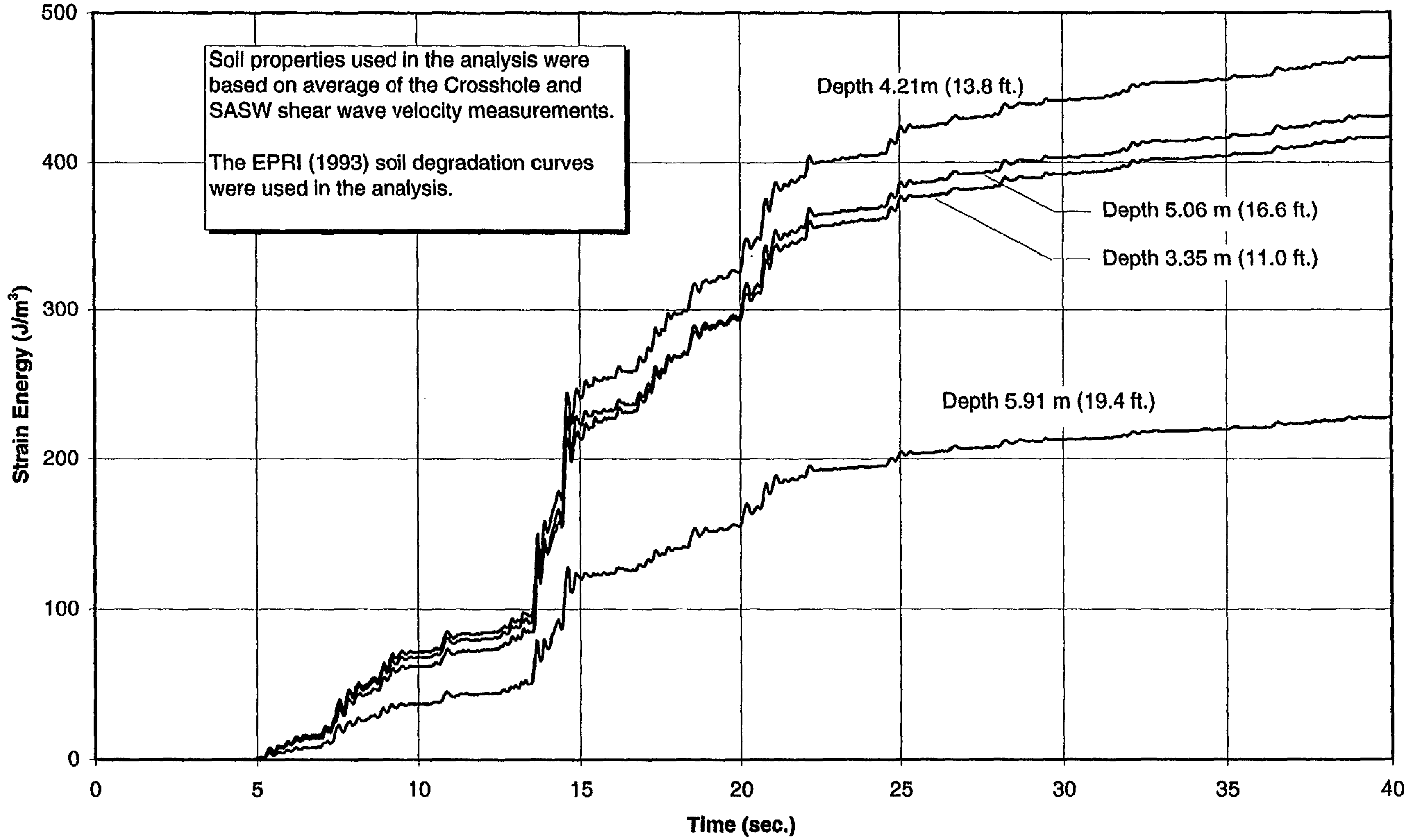

Figure 4.52 - Accumulation of Strain Energy in Liquefied Sand Layer - Wildlife Site, November 24, 1987, 1315 GMT Earthquake in 360° Direction - SHAKE Output Using EPRI (1993) Soil Curves

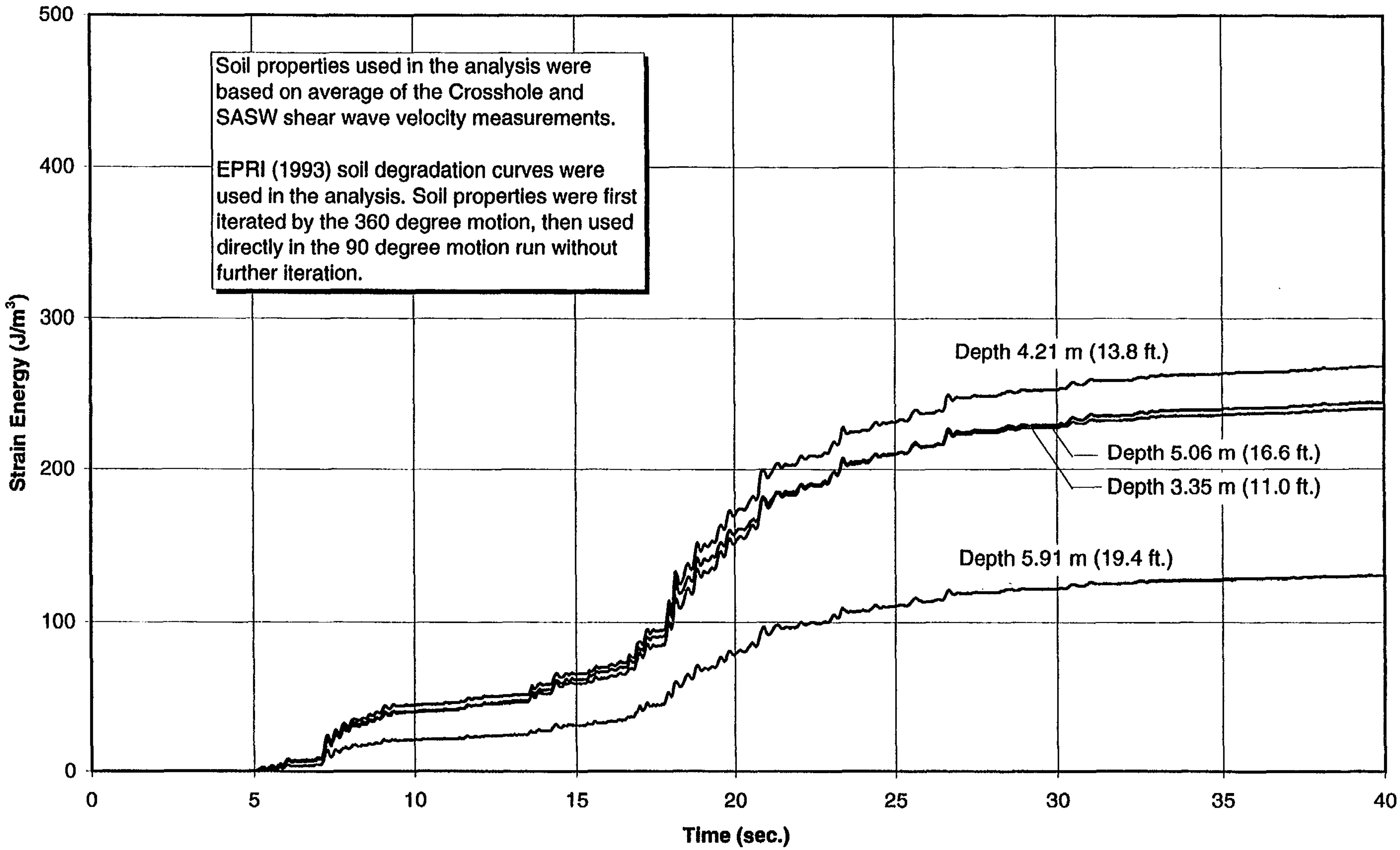

Figure 4.53 - Accumulation of Strain Energy in Liquefied Sand Layer - Wildlife Site, November 24, 1987, 1315 GMT Earthquake in 90° Direction - SHAKE Output Using EPRI (1993) Soil Curves

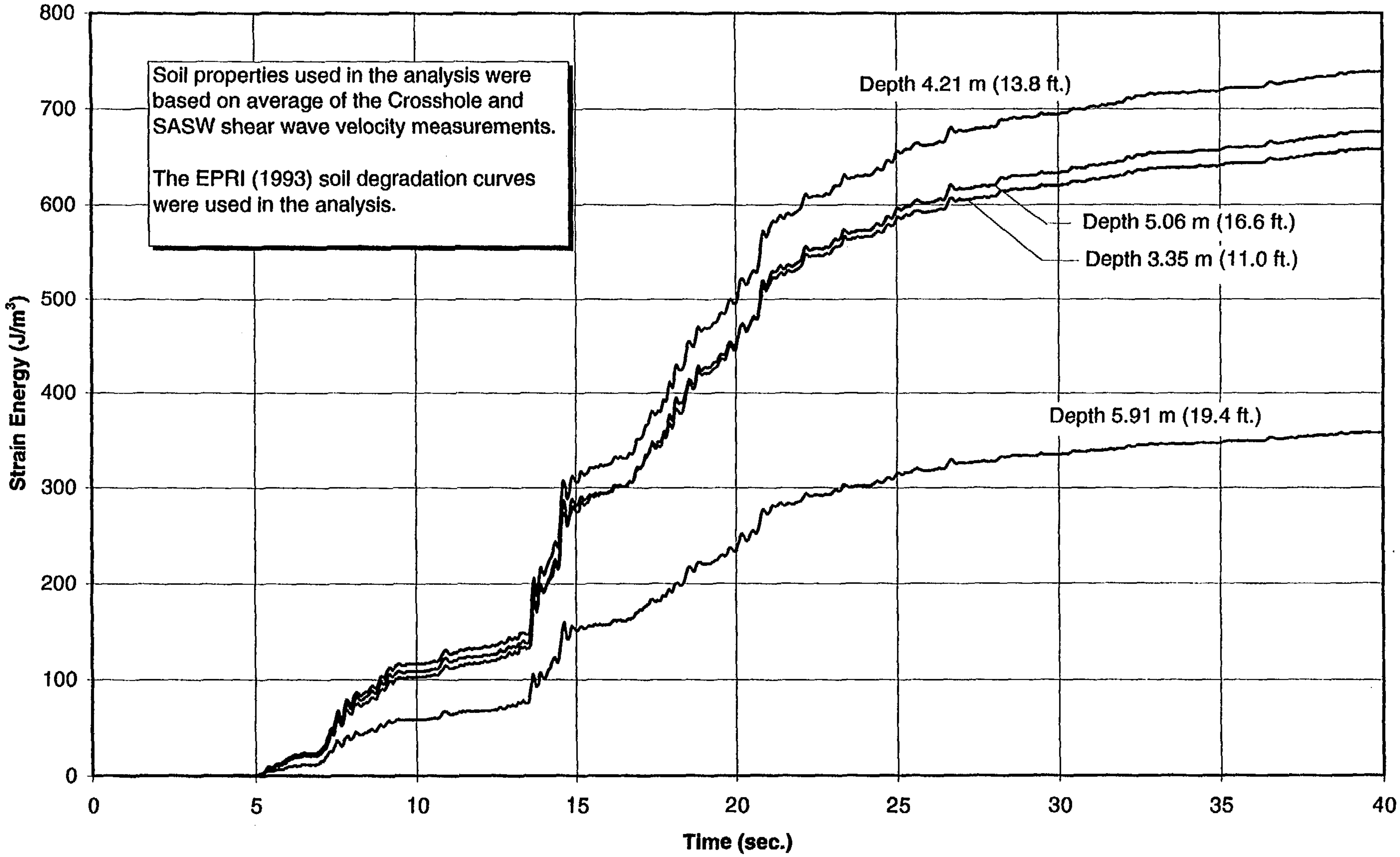

Figure 4.54 - Accumulation of Strain Energy in Liquefied Sand Layer - Wildlife Site, November 24, 1987, 1315 GMT Earthquake - Summation of Strain Energy in both 360° and 90° Directions - SHAKE Output Using EPRI (1993) Soil Curves

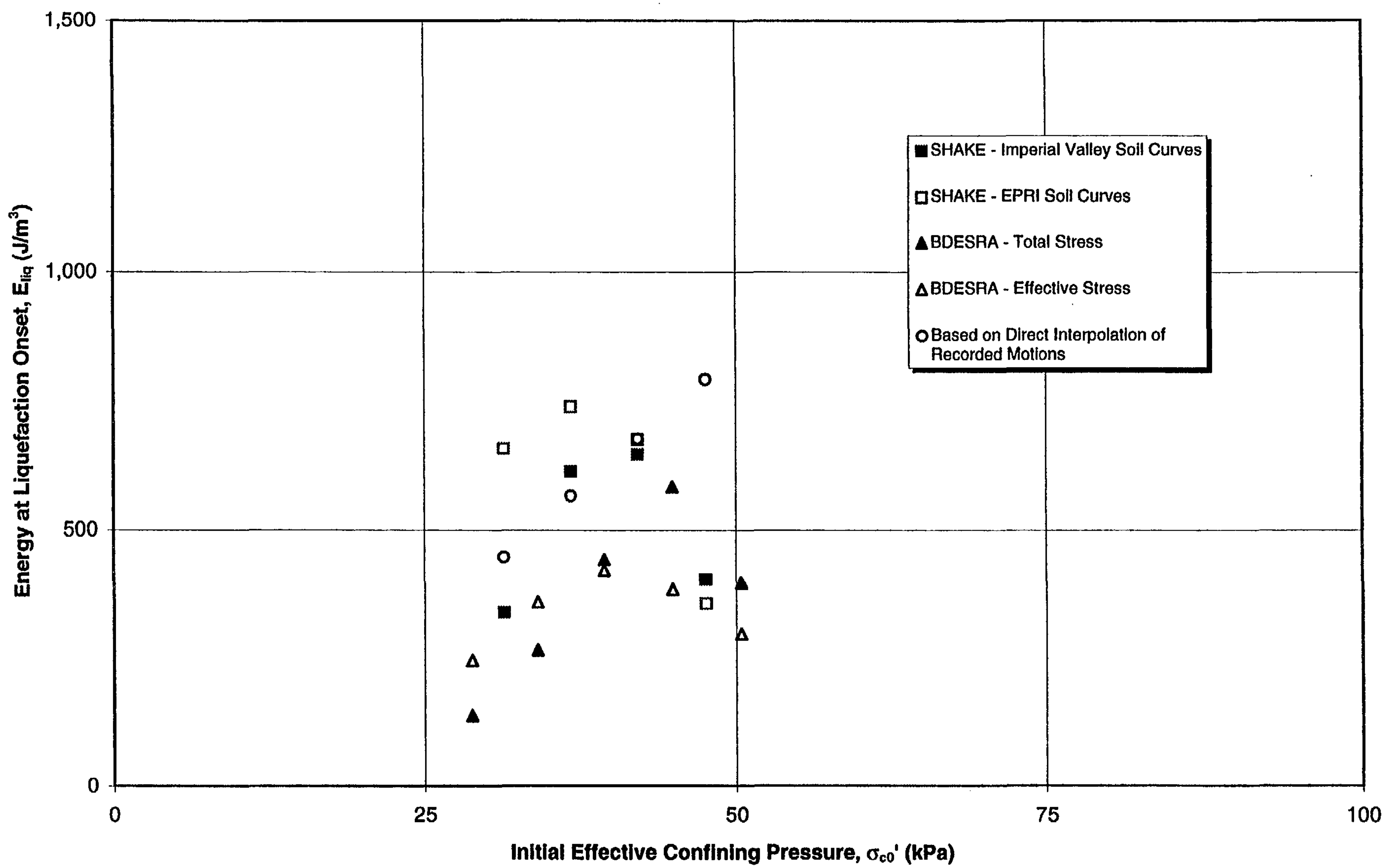

Figure 4.55 - Total Strain Energy at Liquefaction Onset. Calculated from Ground Response Analyses

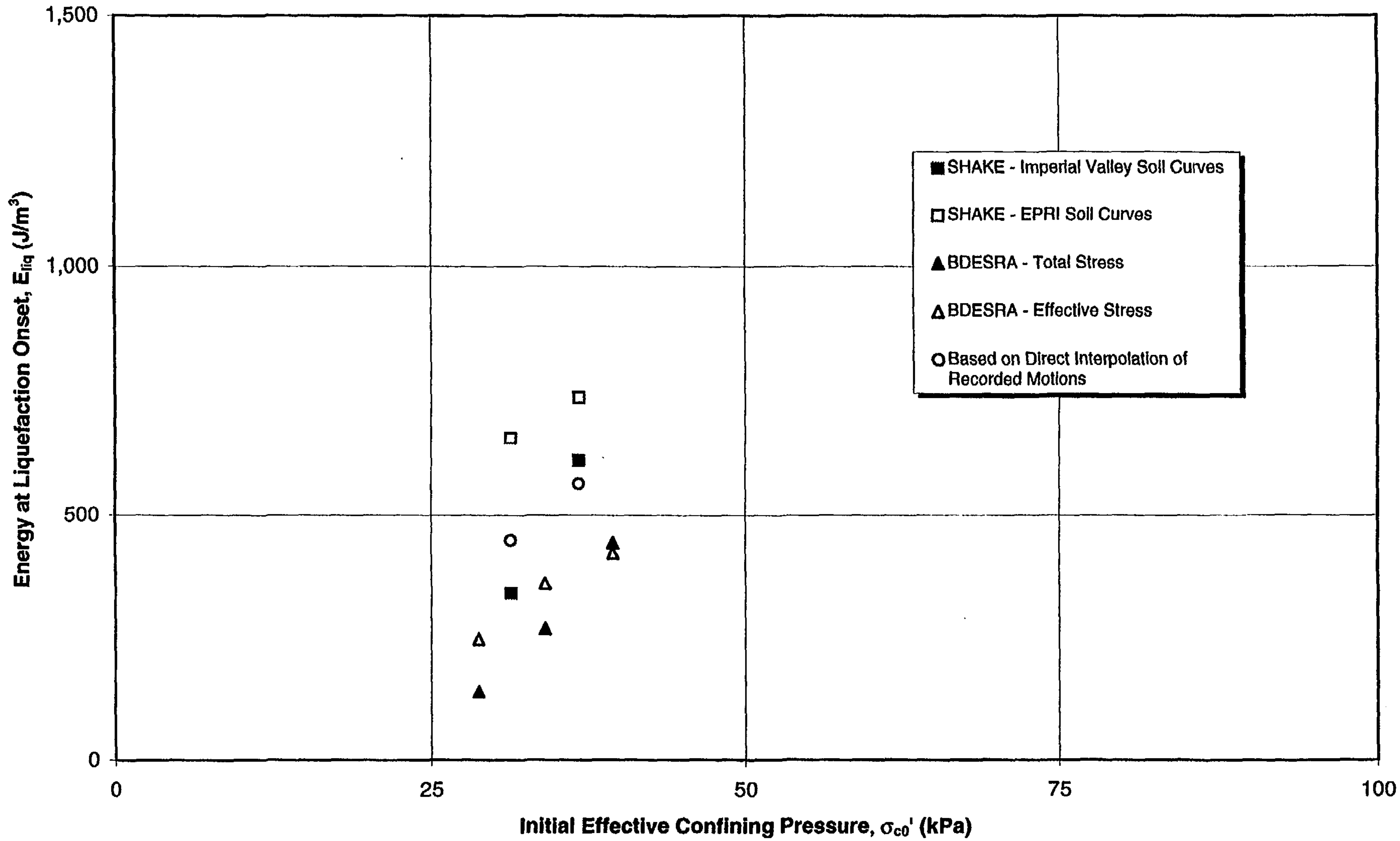

Figure 4.56 - Total Strain Energy at Liquefaction Onset. Calculated from Ground Response Analyses (All Points in Unliquefied Layers Removed)

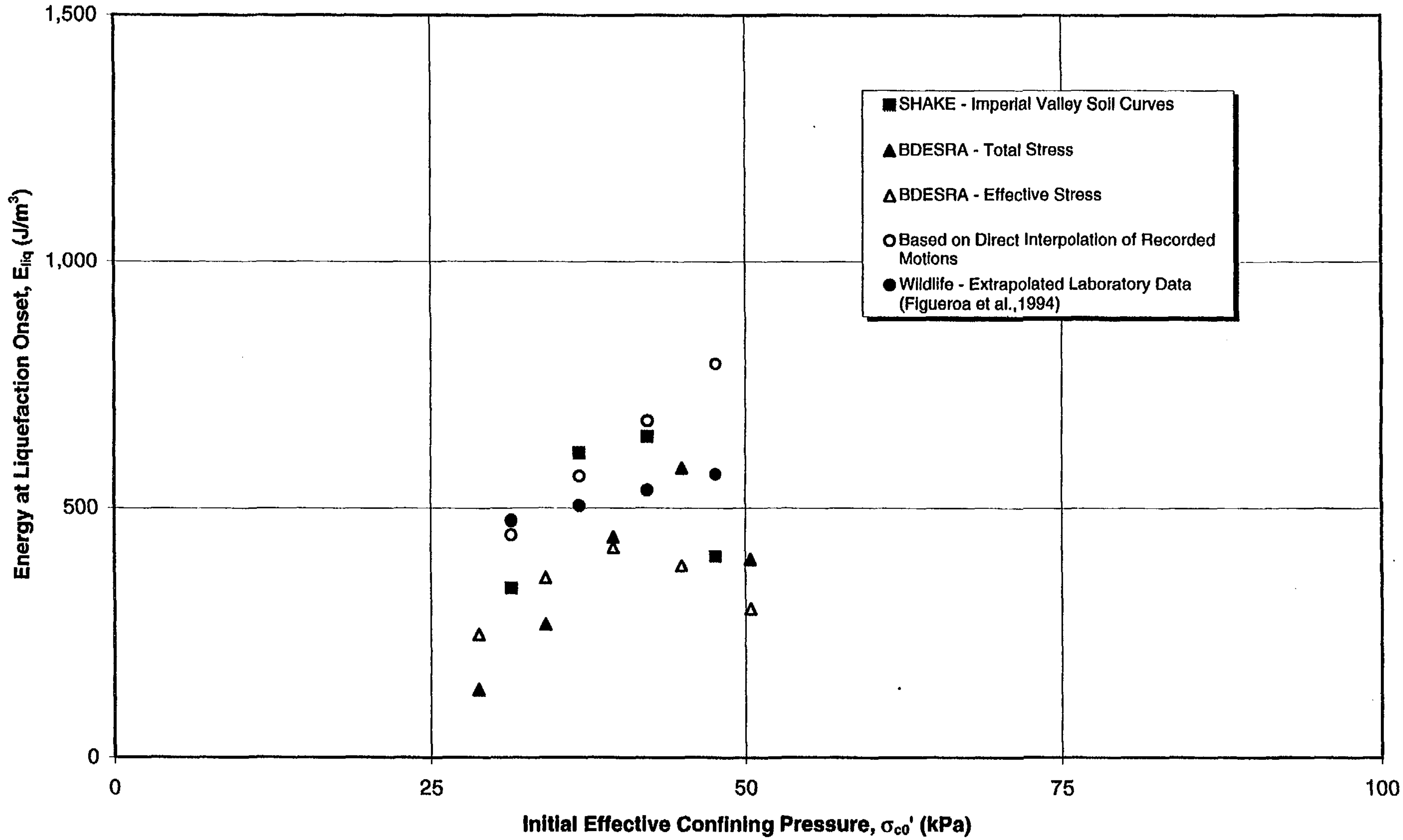

Figure 4.57 - Comparison of Total Strain Energy at Liquefaction Onset: Ground Response Analyses and Laboratory Data - Wildlife Site, November 24, 1987, 1315 GMT Earthquake.

CHAPTER 5

SUMMARY AND RECOMMENDATION

A feasibility study was conducted to determine the applicability of the strain energy method for liquefaction potential evaluation. This study consisted of collection and synthesis of available laboratory test data and evaluation of the strain energy as a measure of soil resistance to liquefaction. The data obtained by several groups of researchers confirm the observation that the strain energy (in normalized form) follows the time history of the pore pressure ratio increase up to the onset of liquefaction. The data also show that by using the relative density for clean sands and the confining pressure for silty sands, development of the generic strain energy relationships for liquefaction resistance is feasible. However, other factors such as the shape and size of the sand particles, the type and the amount of fines content, and the effect of the rate and type of loading on the strain energy need to be investigated and quantified.

The feasibility study also successfully predicts the strain energy required for liquefaction to take place in the field based on the recorded data at the Wildlife Site. The ground response analyses performed for this site, using the conventional methods of the ground response analyses, resulted in consistent results, with a scatter typically expected in such analyses. However, all methods used in the ground response analyses were one-dimensional, and the summation of the strain energy due to shaking in each direction is at best an approximation. Nevertheless, the comparison of the laboratory data with the results of ground response analyses is encouraging. Such favorable comparison suggests also that the goal of developing the strain energy approach for generic application to the evaluation of the soil liquefaction potential should be pursued in future phases of the project.

Based on the results of the feasibility study, it is recommended to:

- Perform laboratory testing, preferably on soil samples from the Wildlife Site at confining pressures in the range of 26 kPa to 50 kPa to cover the low end of the test results.

- Perform ground response analyses using a nonlinear computer program with multi-directional shaking capability to validate or modify the summation of the total strain energy calculated by the methods limited to uni-directional shaking capability as used in the current study.

- Apply the energy based method to liquefaction/no liquefaction sites at Northridge, Kobe in Japan where recorded motions are available, and at the Wildlife Site for the Elmore Ranch earthquake during which no liquefaction occurrence was observed.

The energy method provides a sound approach to the evaluation of liquefaction potential. It is based on the basic principles of the "stress" and "strain" approaches in which the soil capacity to resist liquefaction is measured in terms of the strain energy. It can also handle the special characteristics of the ground motion, such as the near-field effects. The method also has the capability of providing an estimate of the amount of pore pressure build-up before the onset of liquefaction. In this approach, the laboratory data can also be corroborated as more field data from the sites that have or have not liquefied become available.

CHAPTER 6

REFERENCES

Al-Khatib, M. A. (1994). "Liquefaction Assessment by Strain Energy Approach," Doctoral Dissertation Submitted to the Graduate School of Wayne State University, Detroit, Michigan.

Arango, I. (1994). "Methodology for Liquefaction Evaluation of Sites East of the Rockies," Bechtel Corporation, Technical Grant. San Francisco, California, June.

Arango, I., Migues, R. E. (1996), "Investigation of the Seismic Liquefaction of Old Sand Deposits," a Report Prepared for the National Science Foundation Grant No. CMS-9416169, Bechtel Corporation, San Francisco, California, March.

Bennett, M. J., McLaughlin, P. V., Sarmiento, P. V., Youd, T. L. (1984). "Geotechnical Investigation of Liquefaction Sites, Imperial Valley, California," USGS Open-File Report 84-252.

Bierschwale, J. G., Stokoe, K. H. (1984). "Analytical Evaluation of Liquefaction Potential of Sands Subjected to the 1981 Westmoreland Earthquake," Geotechnical Engineering Report GR84-15, Geotechnical Engineering Center, Civil Engineering Department, The University of Texas at Austin, Austin, Texas.

Dobry, R., Elgamal, A. W., Baziar, M. (1989). "Pore Pressure and Acceleration Response of Wildlife Site During the 1987 Earthquake," Proceedings from the 2nd US - Japan Workshop on Liquefaction, Large Ground Deformation and Their Effects on Lifelines, held at the Grand Island Holiday Inn in Grand Island, New York from September 26-28 and at the Cornell University in Ithaca, New York on September 29; also Technical Report NCEER-89-0032.

Dobry, R., Ladd, R. S., Yokel, F. Y., Chung, R. M., Powell, D. (1982). "Prediction of Pore Water Pressure Build-Up and Liquefaction of Sands During Earthquakes by the Cyclic Strain Method," NBS Building Science Series 138, National Bureau of Standards, US Department of Commerce, July.

Electric Power Research Institute (EPRI), (1993). Guidelines for Determining Design Basis Ground Motion," EPRI Report No. TR-102293, November.

Etheredge, R. P., Maley, R., Switzer, J. (1987). Strong-Motion Data from the Superstition Hills Earthquakes of 0154 and 1315 (GMT), November 24, 1987," USGS Open-File Report 87-672, December.

Figueroa, J. L., Saada, A. S., Liang, L., Dahisaria, N. M. (1994). "Evaluation of Soil Liquefaction by Energy Principles," Journal of the Geotechnical Engineering, Vol. 120, No. 9, September.

Figueroa, J. L., Saada, A. S., Liang, L., (1995). "Effect of the Grain Size on the Energy per Unit Volume at the Onset of Liquefaction," Proceedings of the 3rd International Conference on Recent Advances in Geotechnical Earthquake Engineering and Soil Dynamics, April 2-7, St. Louis, Missouri, Vol. 1.

Haag, E. D., Stokoe, K. (1985). "Laboratory Investigation of Static and Dynamic Properties of Sandy Soils Subjected to the 1981 Westmoreland Earthquake," Geotechnical Engineering Report GR85-11, Geotechnical Engineering Center, Civil Engineering Department, The University of Texas at Austin, Austin, Texas.

Holzer, T. L., Bennett, M. J., Youd, T. L. (1989). "Lateral Spreading Field Experiments by the US Geological Survey," Proceedings from the 2nd US - Japan Workshop on Liquefaction, Large Ground Deformation and Their Effects on Lifelines, held at the Grand Island Holiday Inn in Grand Island, New York from September 26-28 and at the Cornell University in Ithaca, New York on September 29; also Technical Report NCEER-89-0032.

Holzer, T. L., Youd, L., Bennett, M. J. (1988). "In Situ Measurement of Pore Pressure Build-Up During Liquefaction," Proceedings of the 20th Joint Meeting of The US - Japan Cooperative Program in Natural Resources, Panel on Wind and Seismic Effects, NIST Report SP 760.

Ishihara, K. (1993). "Liquefaction and Flow Failure During Earthquakes," 33rd Rankine Lecture, Geotechnique, Vol. 43, No. 3, pp. 351-415.

Kagawa, T., Al-Khatib, M. A. (1990). "Use of Shear-Strain Energy for Liquefaction Prediction," Proceedings of 4th US National Conference on Earthquake Engineering, May 20-24, Palm Springs, California, Vol. 3.

Koester, J. P. (1992). "Cyclic Strength and Pore Pressure Generation Characteristics of Fine-Grained Soils," A Thesis Submitted to the Faculty of the Graduate School of the University of Colorado, Denver, Colorado.

Ladd, R. S., (1982). "Geotechnical Laboratory Testing Program for Study and Evaluation of Liquefaction Ground Failure Using Stress and Strain Approaches: Heber Site, October 15, 1979 Imperial Valley Earthquake," Woodward-Clyde Consultants, Wayne, New Jersey, February.

Lee, M. K., Finn, W. L. (1978). "DESRA-2C, Dynamic Effective Stress Analysis of Soil Deposits with Energy Transmitting Boundary Including Assessment of Liquefaction Potential," the University of British Columbia, British Columbia, Canada; Modified by Bechtel Corporation to include Martin-Davidenkov Soil Model, Bechtel Corporation, San Francisco, California.

Magistrale, H., Jones, L., Kanamori, H. (1989). "The Superstition Hills, California, Earthquake of 24 November 1987," Bulletin of the Seismological Society of America, Vol. 79, April.

Matasovic, J., Vucetic, M. (1993). "Analyses of Seismic Records Obtained on November 24, 1987 at the Wildlife Liquefaction Array," Research Report, Civil Engineering Department, University of California, Los Angeles, California, May.

Porcella, R., Etheredge, E., Maley, R., Switzer, J. (1987). "Strong-Motion Data from the Superstition Hills Earthquakes of 0154 and 1315 (GMT), November 24, 1987," USGS Report, 87-672.

Riemer, M. F., Gookin, W. B., Bray, J. D, Arango, I. (1994). "Effects of Loading Frequency and Control on the Liquefaction Behavior of Clean Sands," Geotechnical Engineering report No. UCB/GT/94-07, Geotechnical Engineering, Department of Civil Engineering, University of California, Berkeley.

Riemer, M. F., Seed. R. B. (1994). "Dynamic Testing of Soils from the SRS/ITP Facility," Geotechnical Engineering Report No. UCB/GT/94-02, Geotechnical Engineering, Department of Civil Engineering, University of California, Berkeley, May.

Schnabel, P. B., Lysmer, J., Seed, H. B. (1972), "SHAKE, A Computer Program for Earthquake Response Analyses of Horizontally Layered Sites," Report EERC 72-12, University of California, Berkeley; Modified by Bechtel Corporation, San Francisco, California, 1995.

Seed, H. B., Idriss, I. M., Arango, I. (1983). "Evaluation of Liquefaction Potential Using Field Performance Data," Journal of Geotechnical Engineering, Vol. 109, No. 3, March.

Seed, H. B., Tokimatsu, K., Harder, L. F. (1985). "Influence of SPT Procedures in Soil Liquefaction Resistance Evaluations," Journal of Geotechnical Engineering, Vol. 111, No. 12, February.

Thilakaratne, V., Vucetic, M. (1990). "Analysis of the Seismic Response at the Imperial Wildlife Liquefaction Array in 1987," Proceedings of the 4th US National Conference on Earthquake Engineering, May 20-24, Palm Springs, California, Vol. 3.

Turner, E., Stokoe, K. H. (1982). "Static and Dynamic Properties of the Clayey Soils Subjected to the 1979 Imperial Valley Earthquake," Geotechnical Engineering Report GR82-86, The University of Texas at Austin, Texas, October.

Vucetic, M., Thilakaratne, V. (1989). "Liquefaction at the Wildlife Site - Effect of Soil Stiffness on Seismic Responses," Proceedings of the 4th International Conference on Soil Dynamics and Earthquake Engineering, Mexico City, October.

Wald, D J., Helmberger, D. V., Hartzell, S. H. (1990). "Rupture Process of the 1987 Superstition Hills Earthquake from the Inversion of Strong-Motion Data," Bulletin of the Seismological Society of America, Vol. 80, No. 5, October.

Youd, T. L., Holtzer, T. L., Bennett, M. J. (1989). "Liquefaction Lessons Learned from the Imperial Valley, California," Proceedings of the 12th International Conference on Soil Mechanics and Foundation Engineering, Rio de Janeiro.

Zeghal, M., Elgamal, A. W. (1994). "Analysis of Site Liquefaction Using Earthquake Records," Journal of Geotechnical Engineering, Vol. 120, No. 6, June.

APPENDIX A

LABORATORY TESTS ON MONTEREY NO. 0 SAND, PERFORMED AT THE UNIVERSITY OF CALIFORNIA, BERKELEY

Table A.1 - Summary of the Cyclic Triaxial Test Data on Monterey No. 0 Sand Performed at University of California, Berkeley

No.	Test ID	Sample	D_r(%)	E_{liq} (J/m^3)	FC (%)	γ_d (kN/m^3)	Control	σ_c' (kPa)	Freq. (Hz)	Load Shape
1	MONT4	Monterey No.0	61.8	2677	2	15.6	Stress	100	1	Sinusoidal 2-way
2	MONT10	Monterey No.0	61.0	1933	2	15.5	Stress	100	1	Sinusoidal 2-way
3	MONT11	Monterey No.0	60.6	988	2	15.5	Stress	100	10	Sinusoidal 2-way
4	MONT12	Monterey No.0	61.0	2481	2	15.5	Stress	100	1	Sinusoidal 2-way
5	MONT14	Monterey No.0	60.2	1583	2	15.5	Stress	100	20	Sinusoidal 2-way
6	MONT15	Monterey No.0	60.5	1245	2	15.5	Stress	100	10	Sinusoidal 2-way
7	MONT17	Monterey No.0	61.0	1878	2	15.5	Strain	100	1	Sinusoidal 2-way
8	MONT18	Monterey No.0	61.0	1187	2	15.5	Strain	100	10	Sinusoidal 2-way
9	MONT19	Monterey No.0	60.6	1483	2	15.5	Strain	100	15	Sinusoidal 2-way
10	MONT20	Monterey No.0	40.9	851	2	15.0	Strain	100	1	Sinusoidal 2-way
11	MONT21	Monterey No.0	41.8	880	2	15.0	Strain	100	1	Sinusoidal 2-way
12	MONT22	Monterey No.0	42.3	1078	2	15.0	Strain	100	1	Sinusoidal 2-way
13	MONT24	Monterey No.0	51.8	2736	2	15.3	Stress	100	1	Sinusoidal 2-way
14	MONT25	Monterey No.0	50.4	2985	2	15.3	Stress	100	1	Sinusoidal 2-way
15	MONT26	Monterey No.0	49.9	2769	2	15.2	Stress	100	1	Sinusoidal 2-way
16	MONT30	Monterey No.0	41.9	708	2	15.0	Strain	100	10	Sinusoidal 2-way
17	MONT33	Monterey No.0	40.5	829	2	15.0	Strain	100	10	Sinusoidal 2-way
18	MONT35	Monterey No.0	61.8	4211	2	15.6	Stress	100	0.1	Sinusoidal 2-way
19	MONT37	Monterey No.0	61.6	1388	2	15.5	Strain	100	1	Sinusoidal 2-way
20	MONT38	Monterey No.0	61.8	704	2	15.6	Strain	100	10	Sinusoidal 2-way

Test Results Following the Sequence of Test ID's are Attached.

Test I.D.:	MONT4	**Controlled Parameter:**	Stress
Relative Density (%):	61.8	**Initial Effective Stress (kPa):**	100
Applied Stress Ratio:	0.31	**Frequency (Hz):**	1

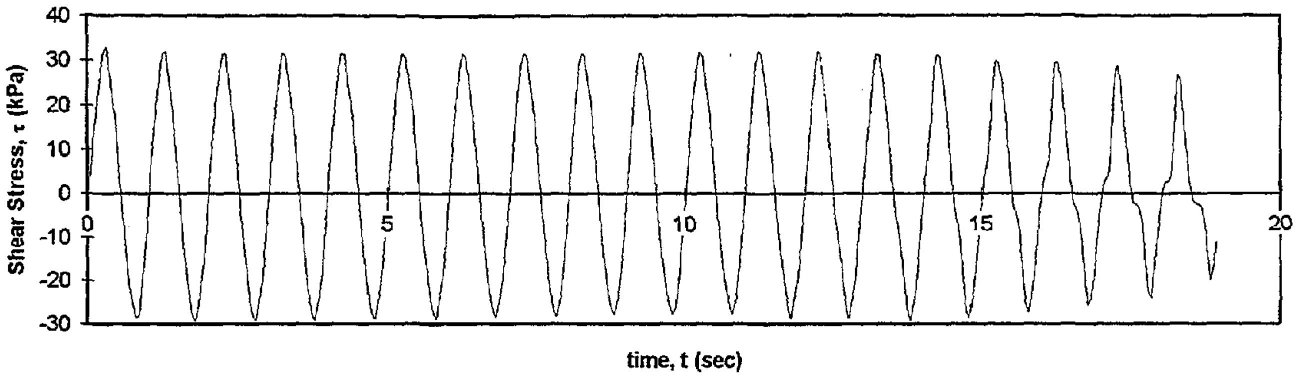

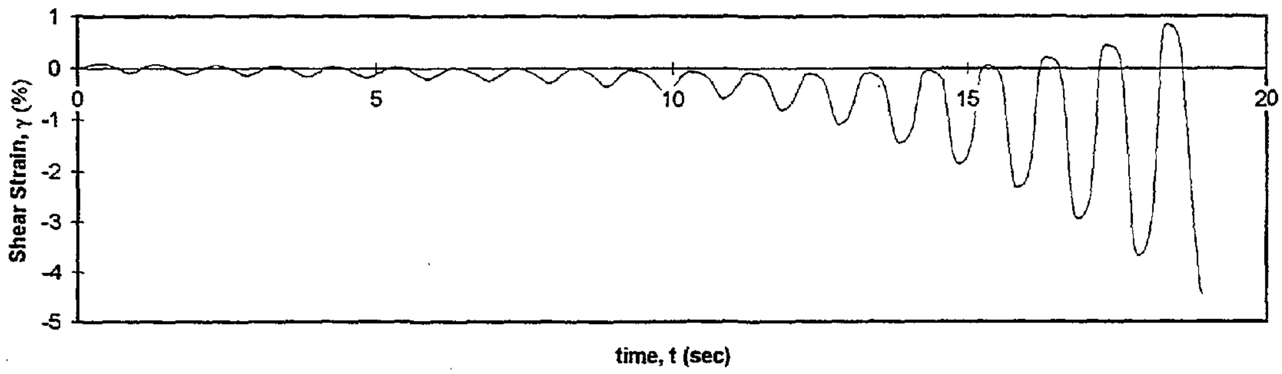

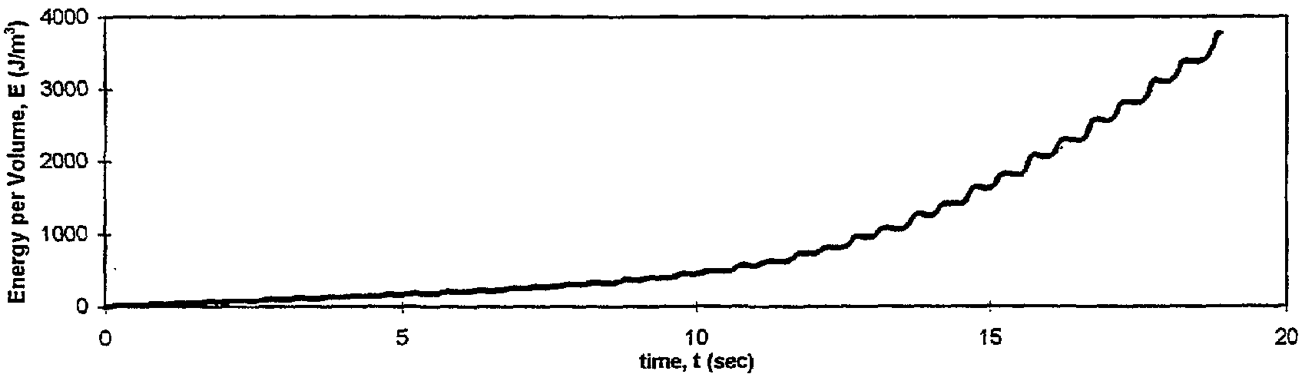

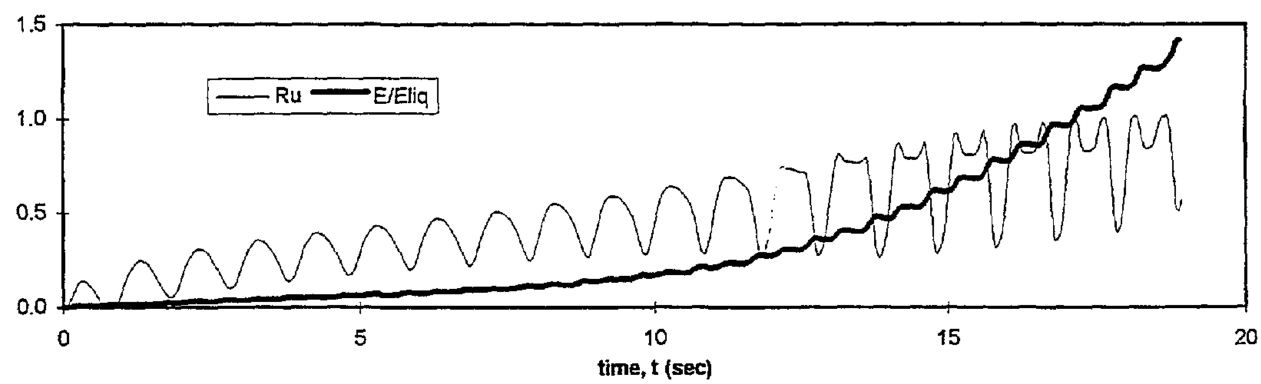

Test I.D.:	MONT4	**Controlled Parameter:**	Stress
Relative Density (%)	61.8	**Initial Effective Stress (kPa):**	100
Applied Stress Ratio:	0.31	**Frequency (Hz):**	1

Shear Stress vs. Shear Strain

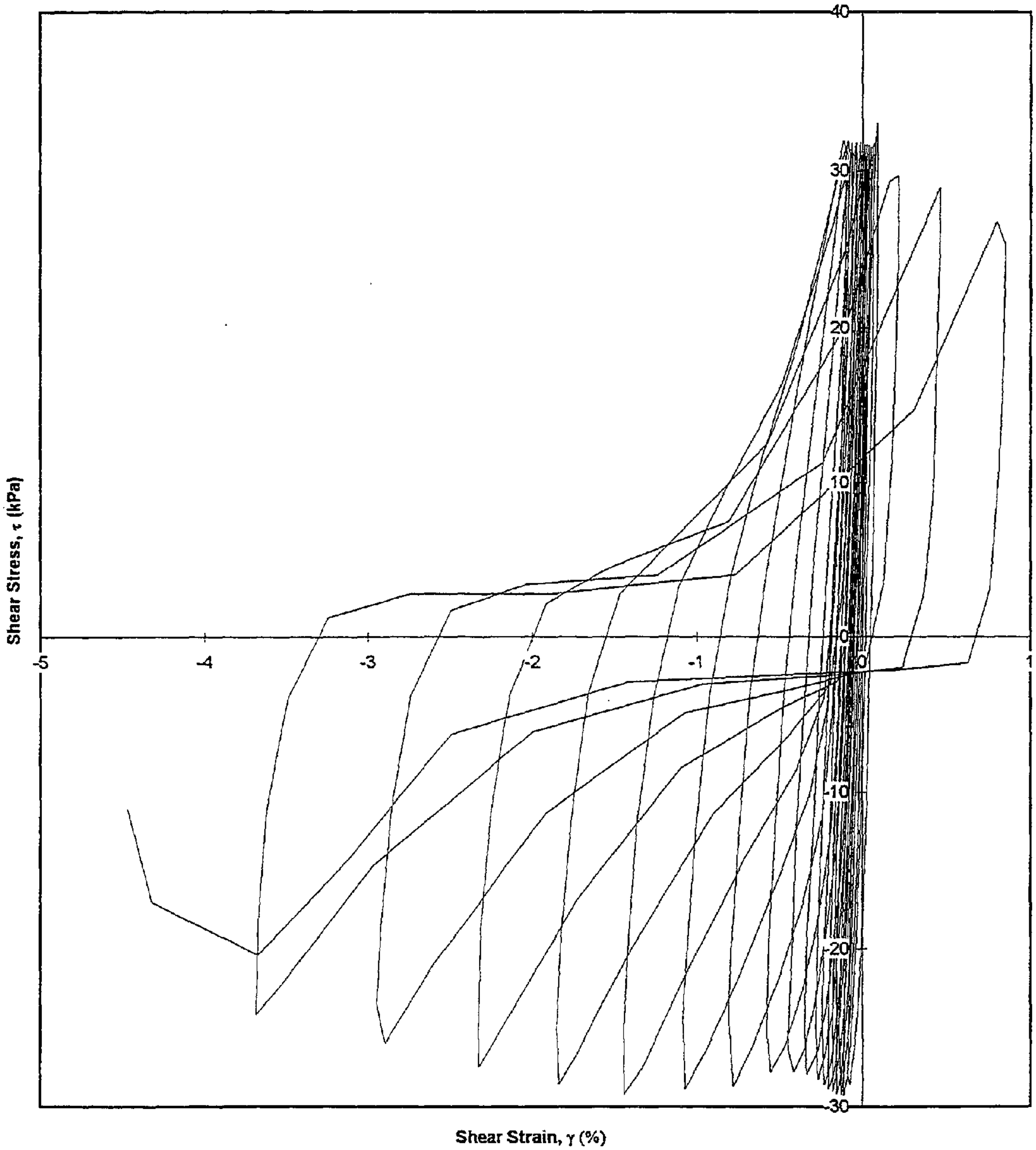

Test I.D.:	MONT10	**Controlled Parameter:**	Stress
Relative Density (%):	61	**Initial Effective Stress (kPa):**	100
Applied Stress Ratio:	0.27	**Frequency (Hz):**	1

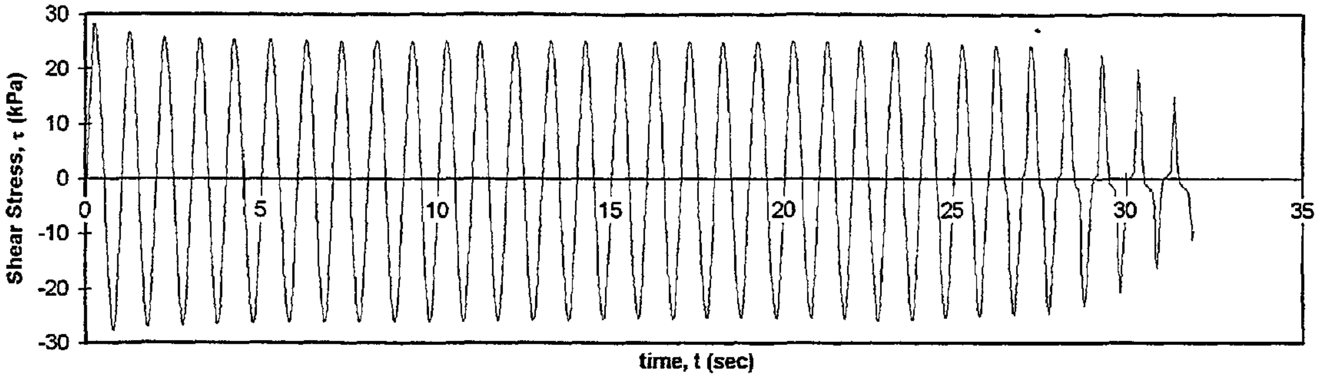

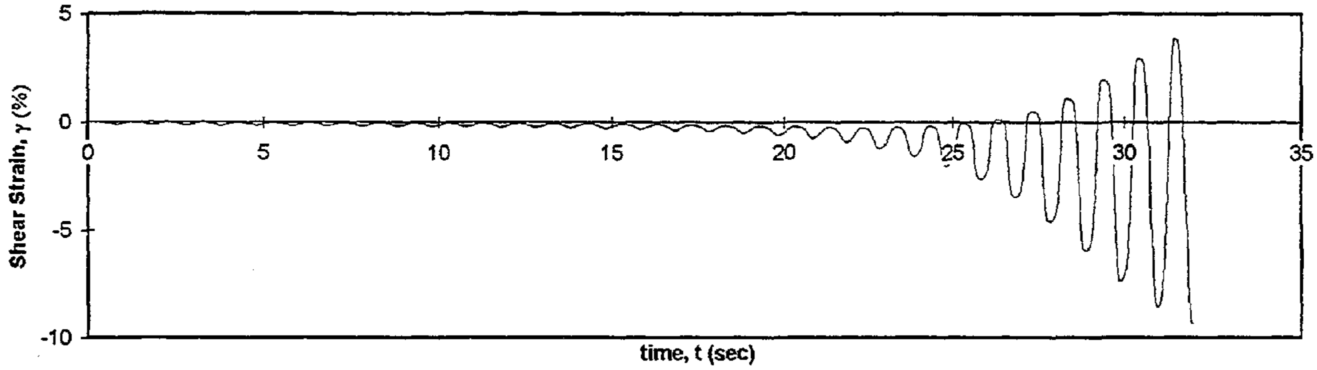

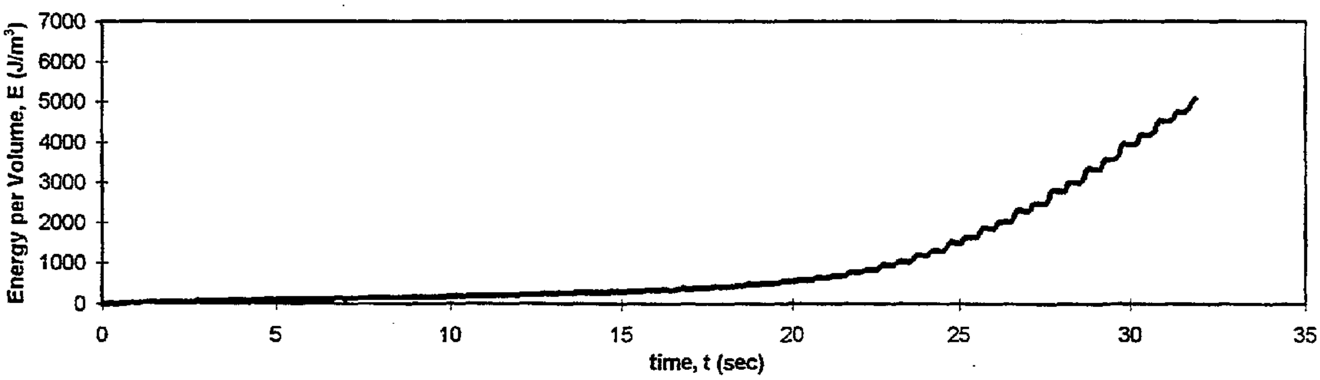

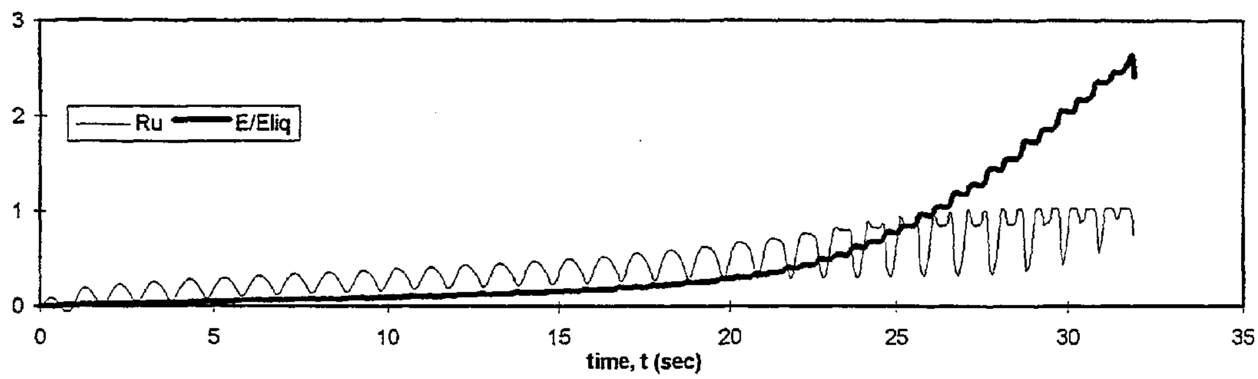

Test I.D.:	MONT10	**Controlled Parameter:**	Stress
Relative Density (%):	61	**Initial Effective Stress (kPa):**	100
Applied Stress Ratio:	0.27	**Frequency (Hz):**	1

Shear Stress vs. Shear Strain

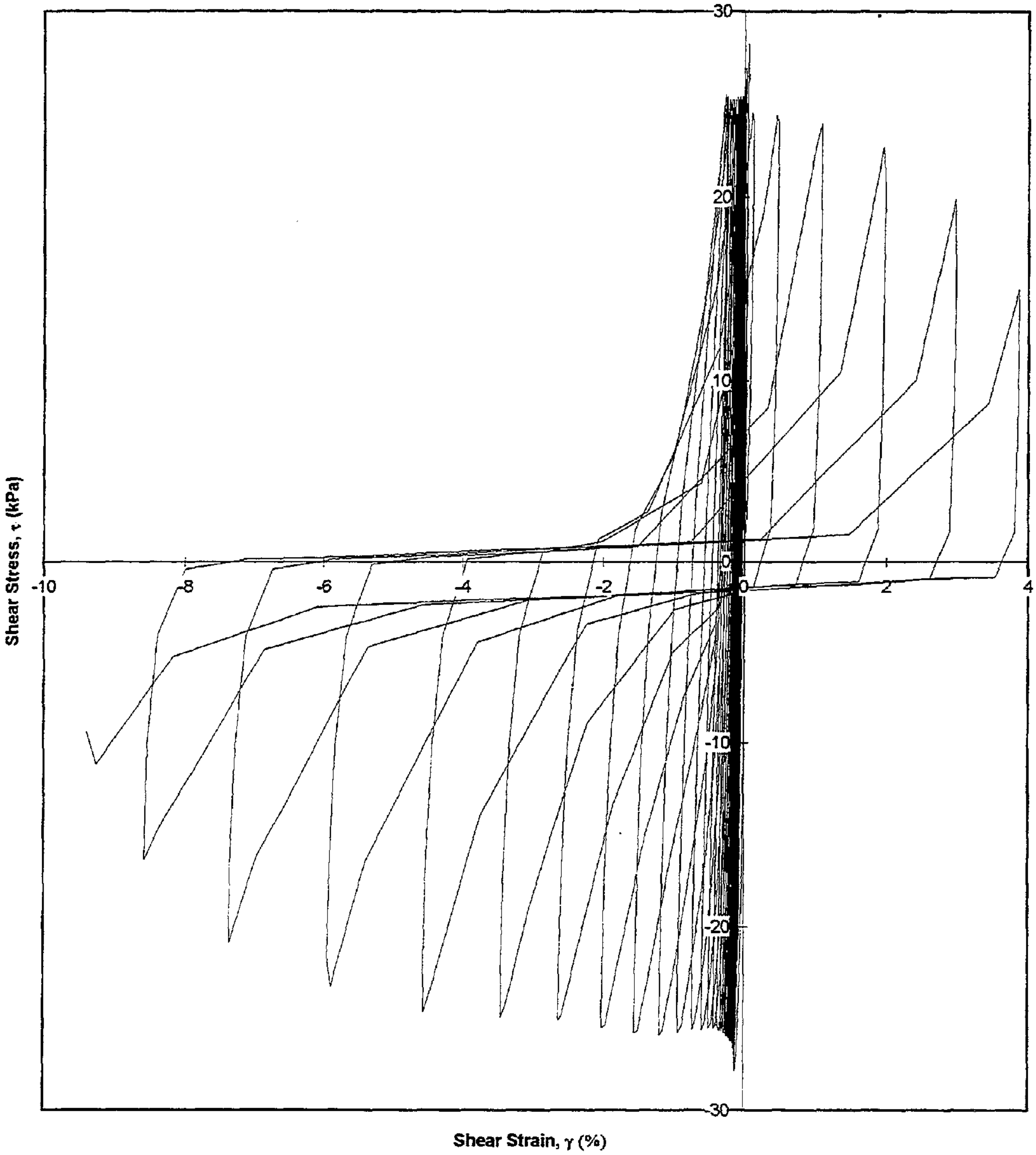

d:\nit\itp\cy_files\MONT10.XLS

8/21/96 9:46 AM

Test I.D.:	MONT11	**Controlled Parameter:**	Stress
Relative Density (%):	60.6	**Initial Effective Stress (kPa):**	100
Applied Stress Ratio:	0.3	**Frequency (Hz):**	10

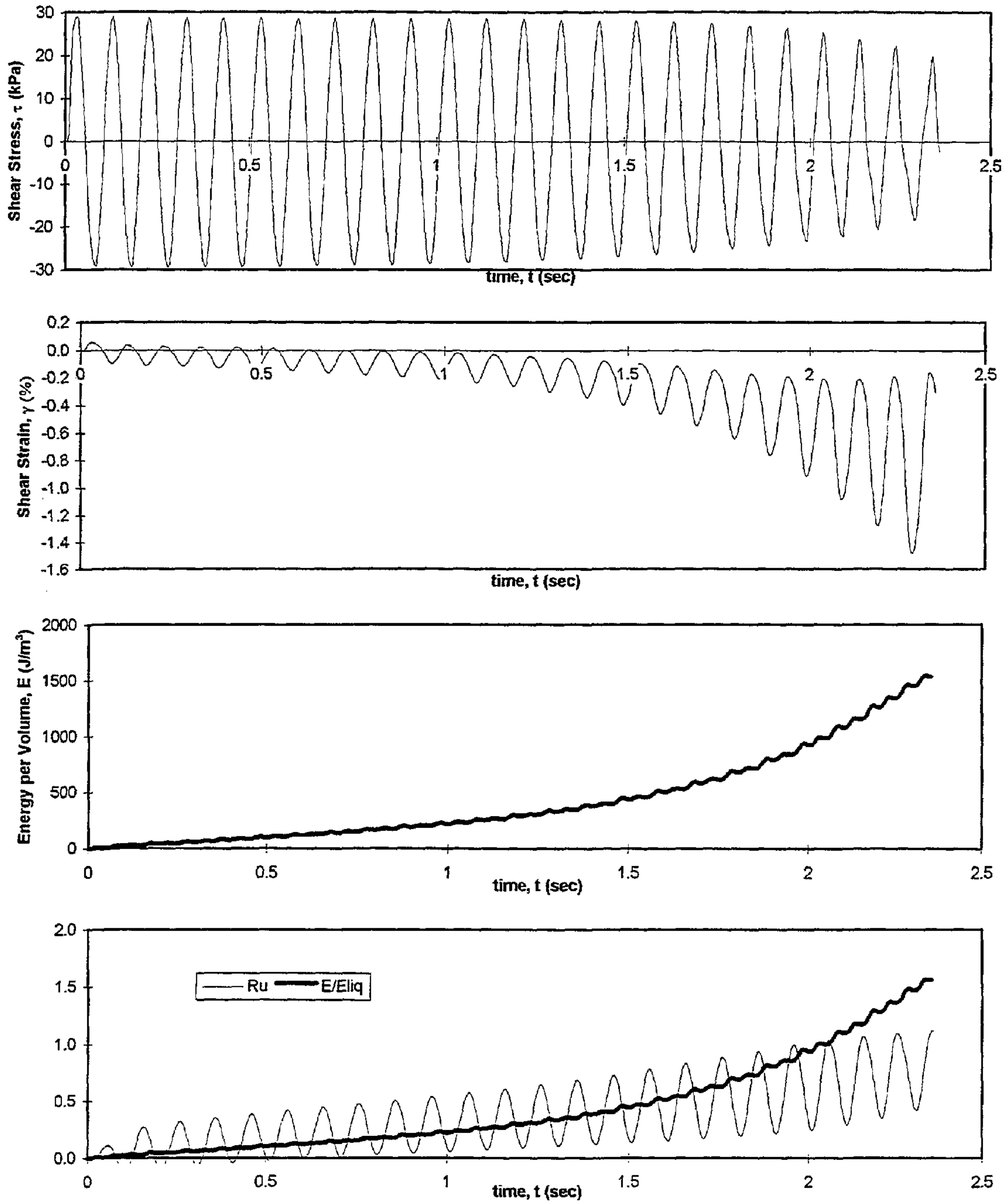

Test I.D.:	MONT11	**Controlled Parameter:**	Stress
Relative Density (%):	60.6	**Initial Effective Stress (kPa):**	100
Applied Stress Ratio:	0.3	**Frequency (Hz):**	10

Shear Stress vs. Shear Strain

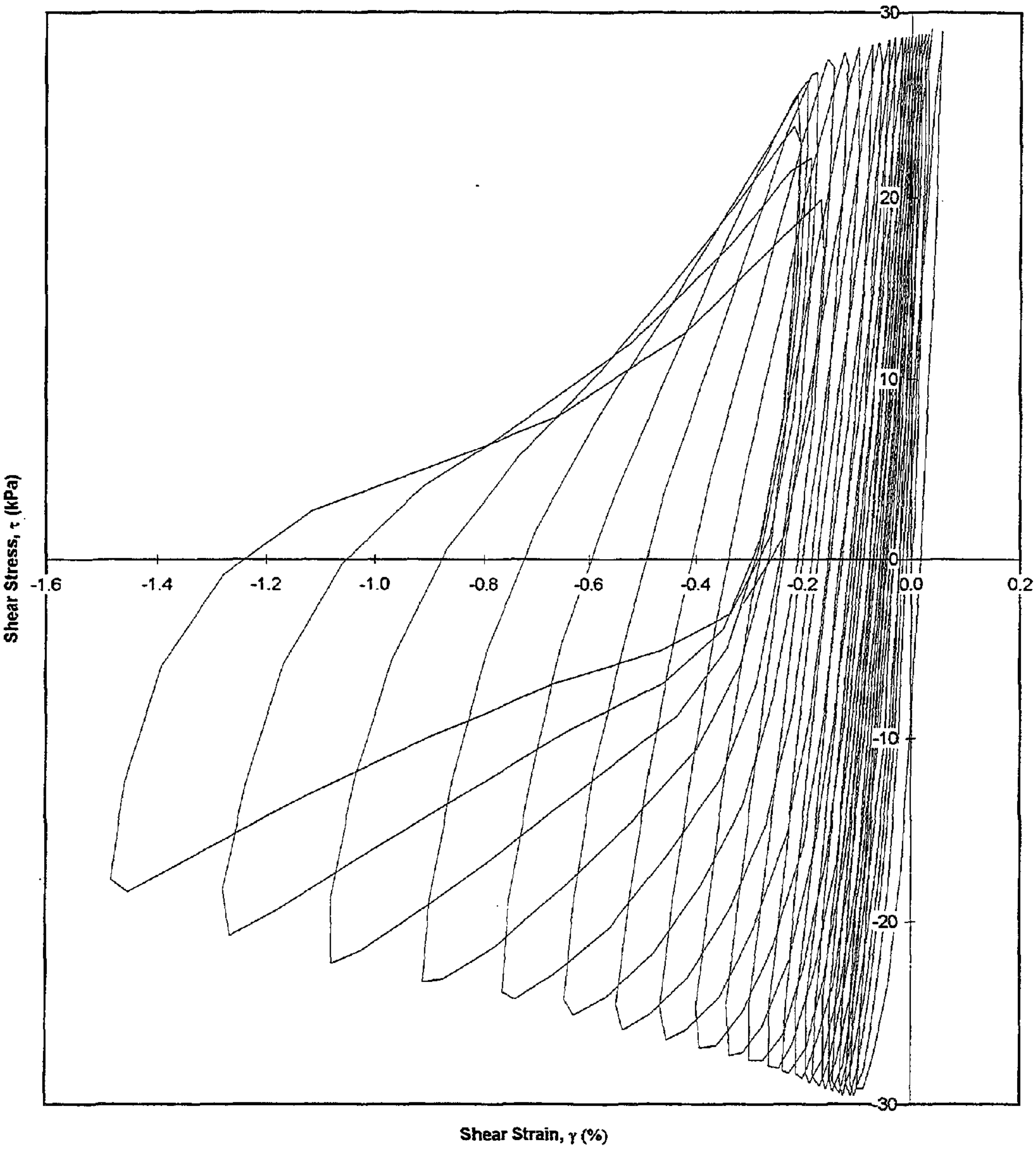

Test I.D.:	MONT12	**Controlled Parameter:**	Stress
Relative Density (%):	61	**Initial Effective Stress (kPa):**	100
Applied Stress Ratio:	0.23	**Frequency (Hz):**	1

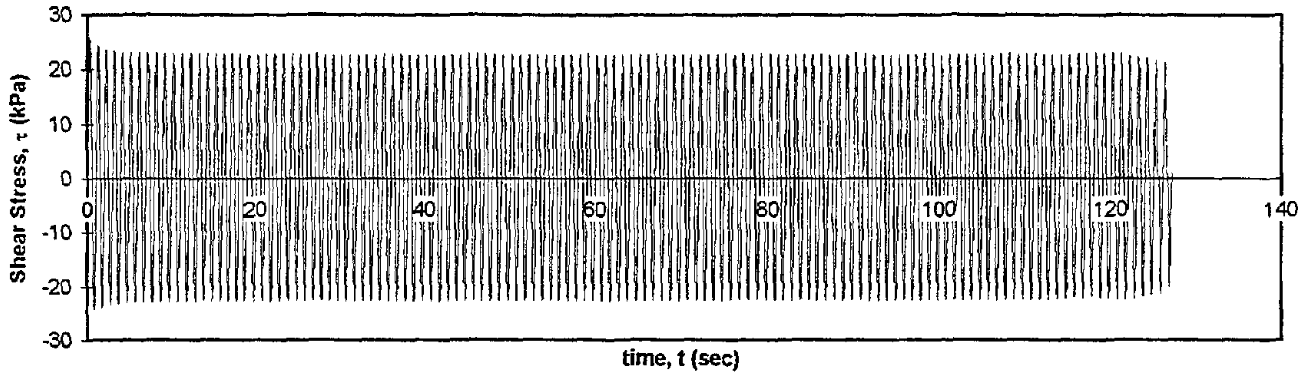

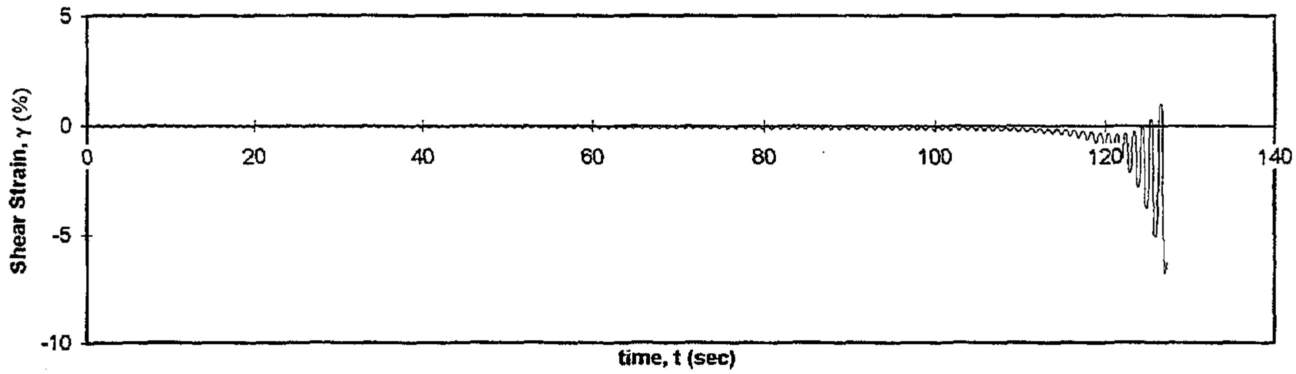

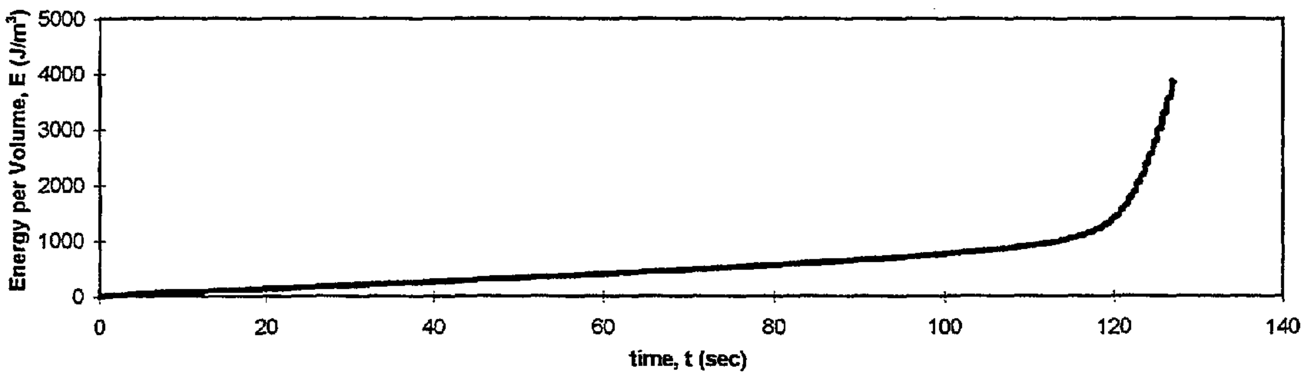

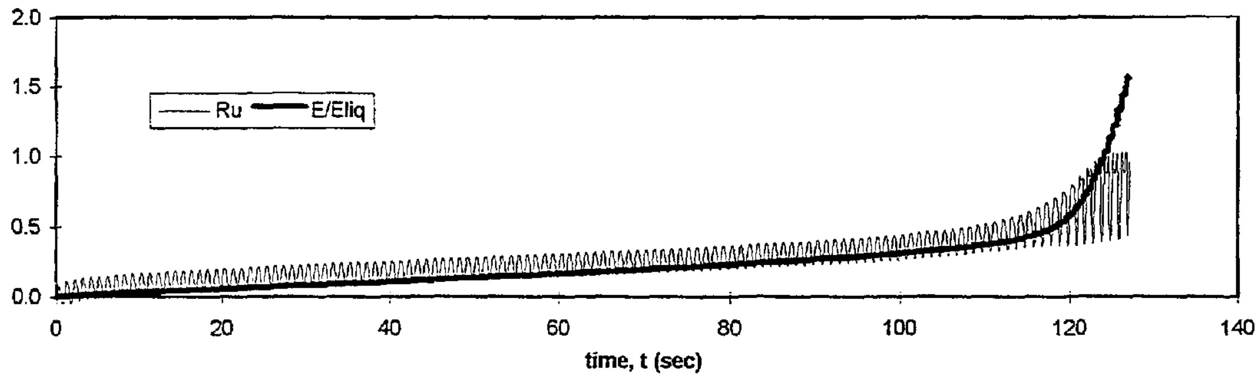

d:\nit\itp\cy_files\MONT12.XLS 8/15/96 11:22 AM

Test I.D.:	MONT12	**Controlled Parameter:**	Stress
Relative Density (%):	61	**Initial Effective Stress (kPa):**	100
Applied Stress Ratio:	0.23	**Frequency (Hz):**	1

Shear Stress vs. Shear Strain

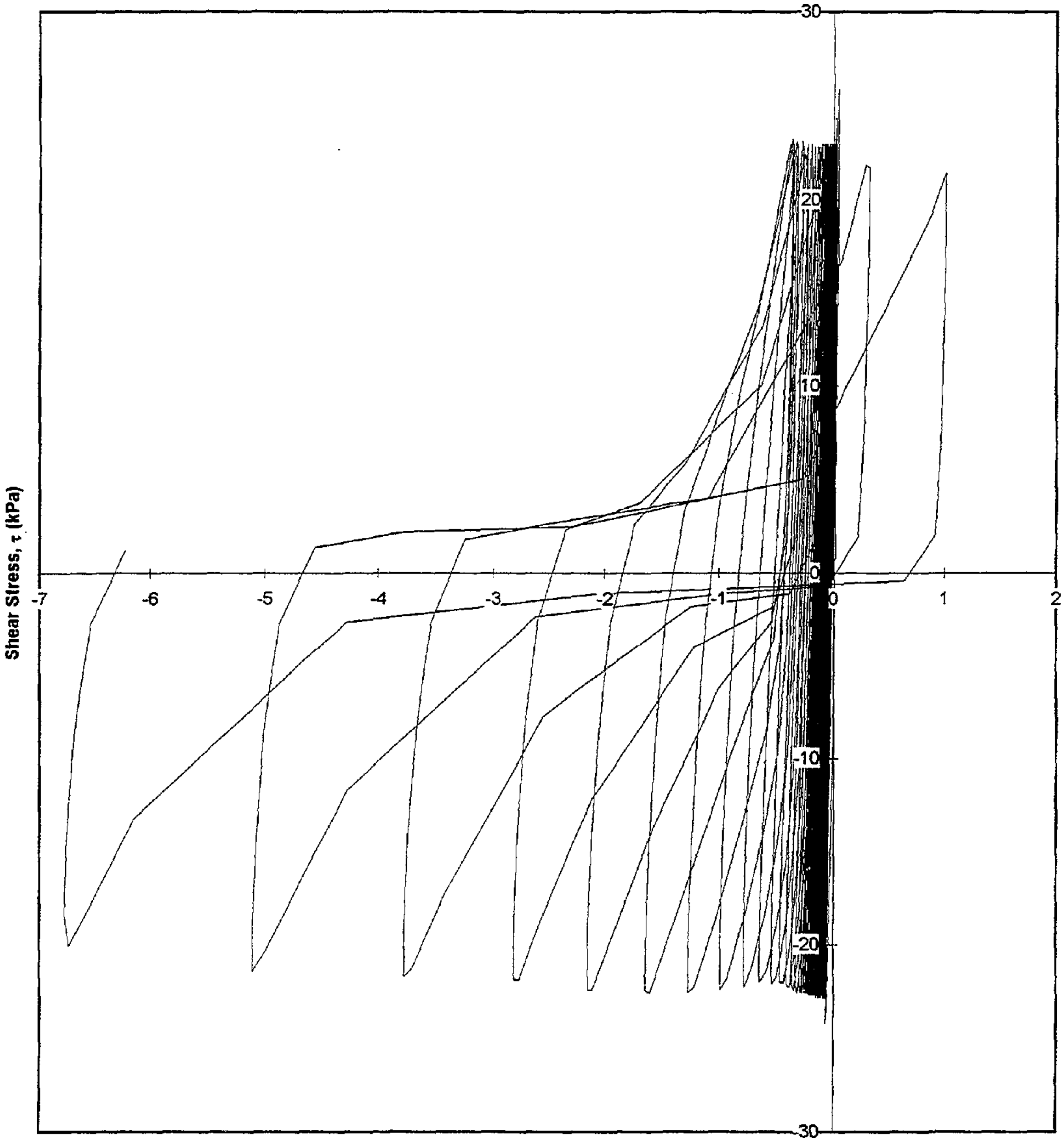

Test I.D.:	MONT14	**Controlled Parameter:**	Stress
Relative Density (%):	60.2	**Initial Effective Stress (kPa):**	100
Applied Stress Ratio:	0.3	**Frequency (Hz):**	20

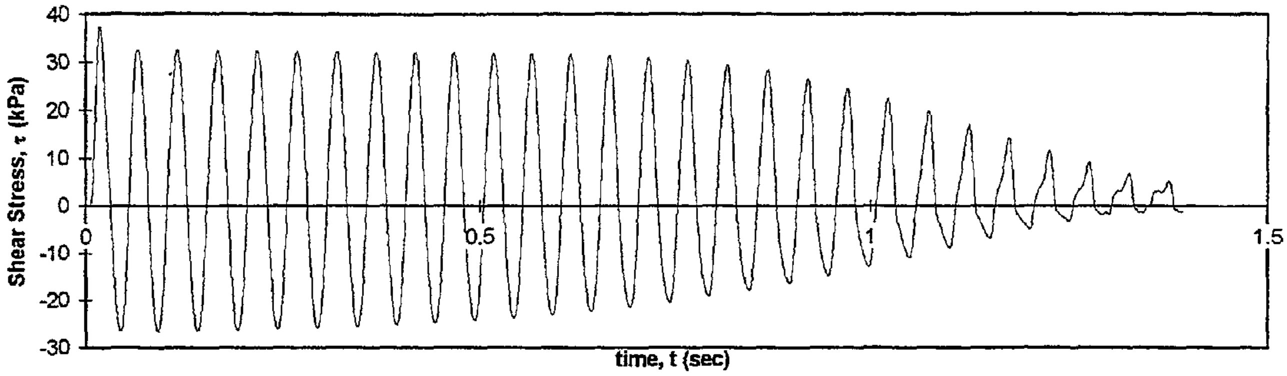

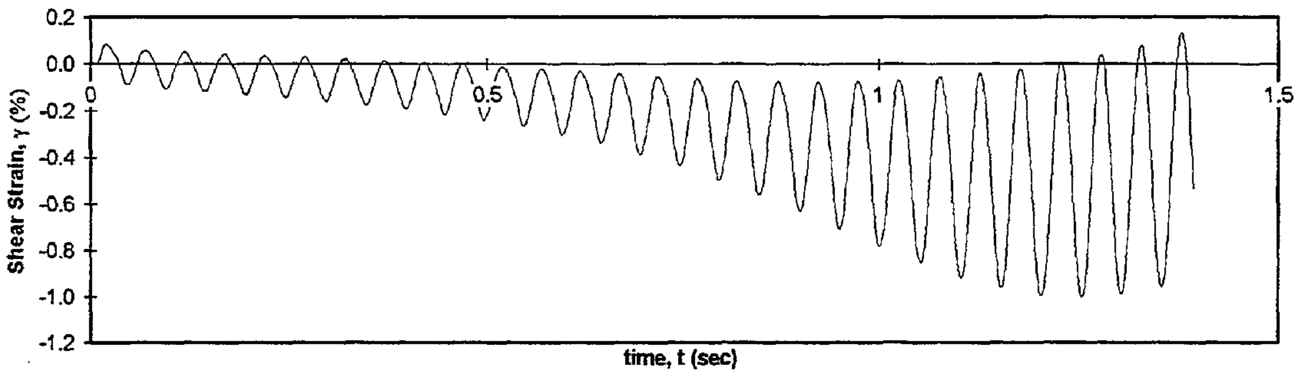

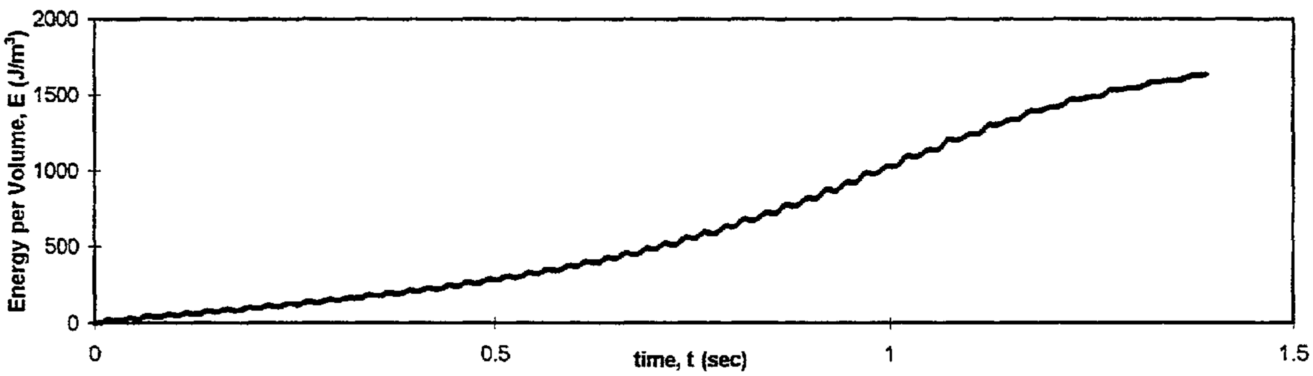

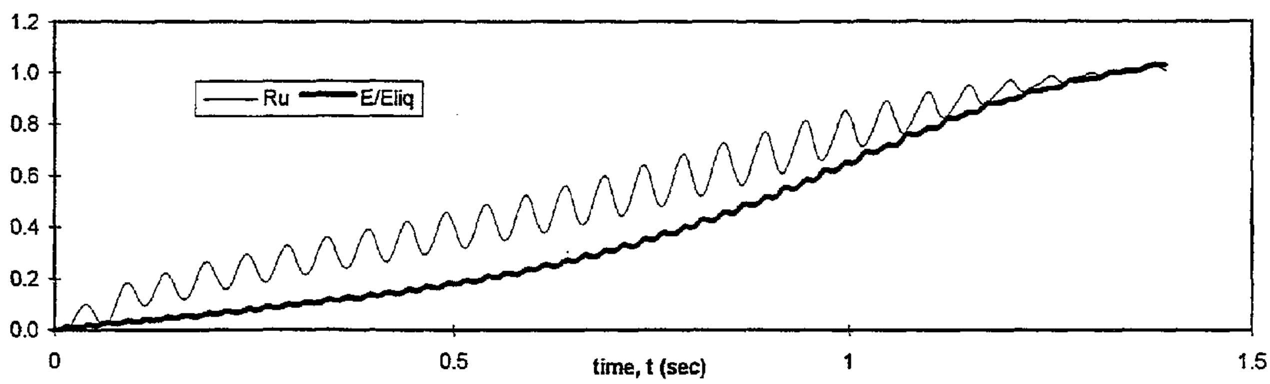

d:\nit\itp\cy_files\MONT14.XLS 8/15/96 11:24 AM

Test I.D.:	MONT14	**Controlled Parameter:**	Stress
Relative Density (%):	60.2	**Initial Effective Stress (kPa):**	100
Applied Stress Ratio:	0.3	**Frequency (Hz):**	20

Shear Stress vs. Shear Strain

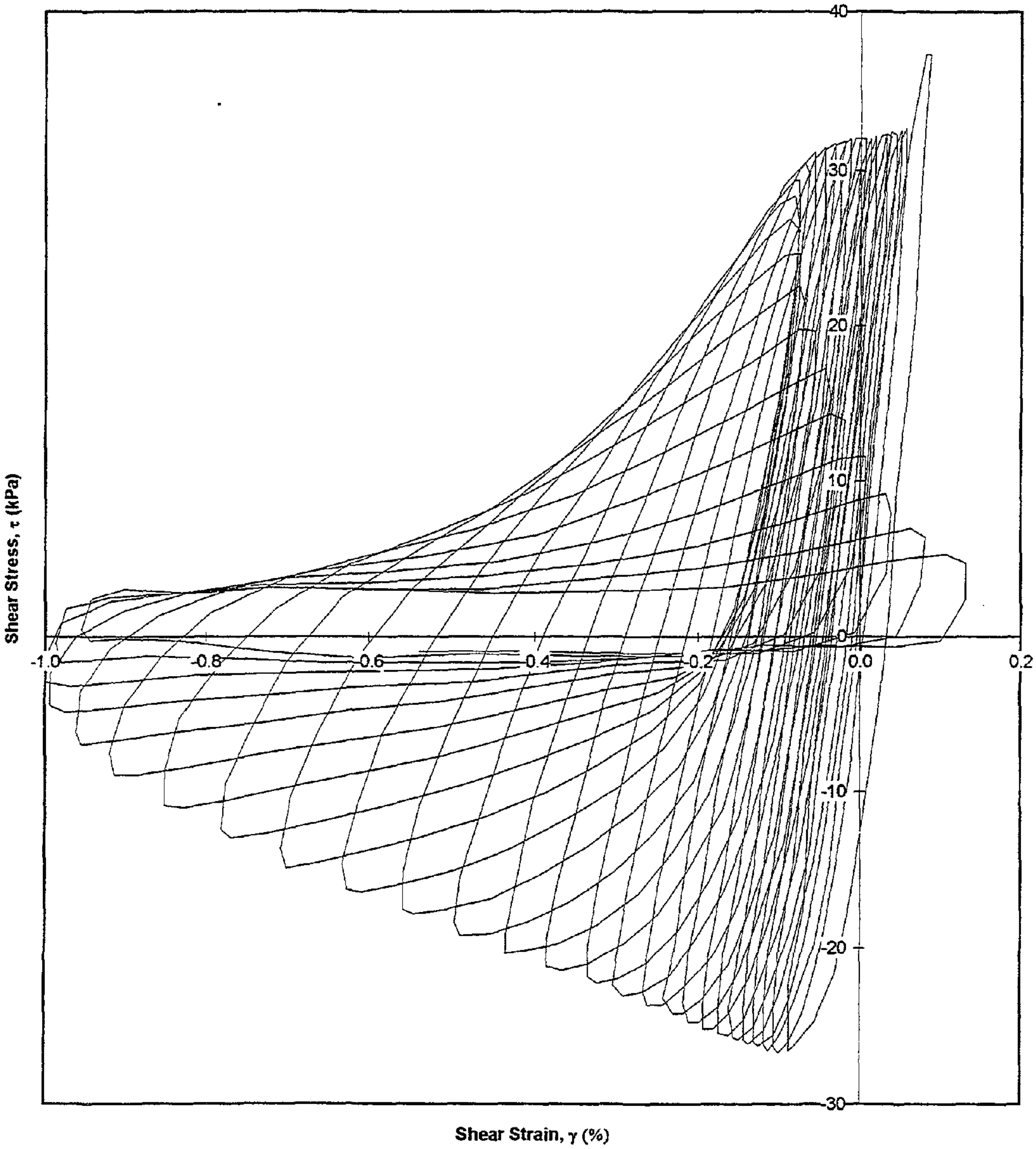

d:\nit\itp\cy_files\MONT14.XLS 8/15/96 11:24 AM

Test I.D.:	MONT15	**Controlled Parameter:**	Stress
Relative Density (%):	60.5	**Initial Effective Stress (kPa):**	100
Applied Stress Ratio:	0.22	**Frequency (Hz):**	10

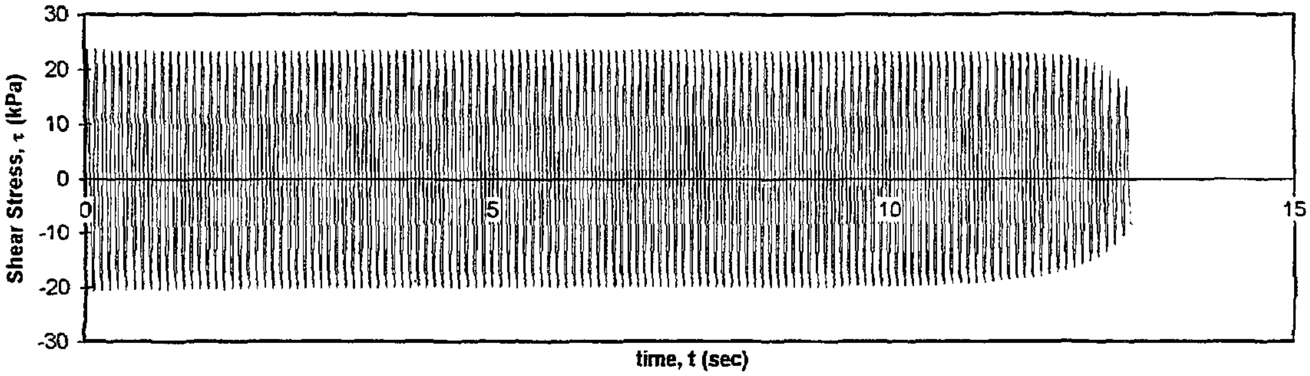

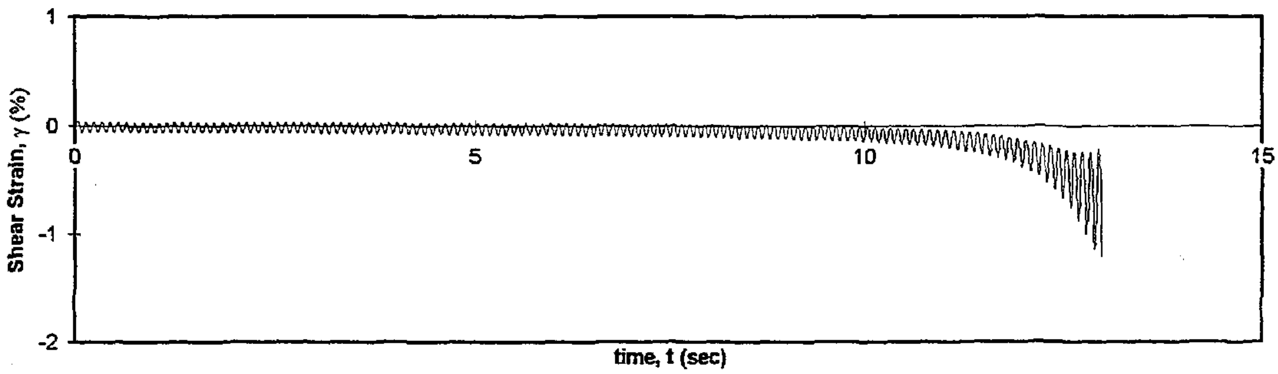

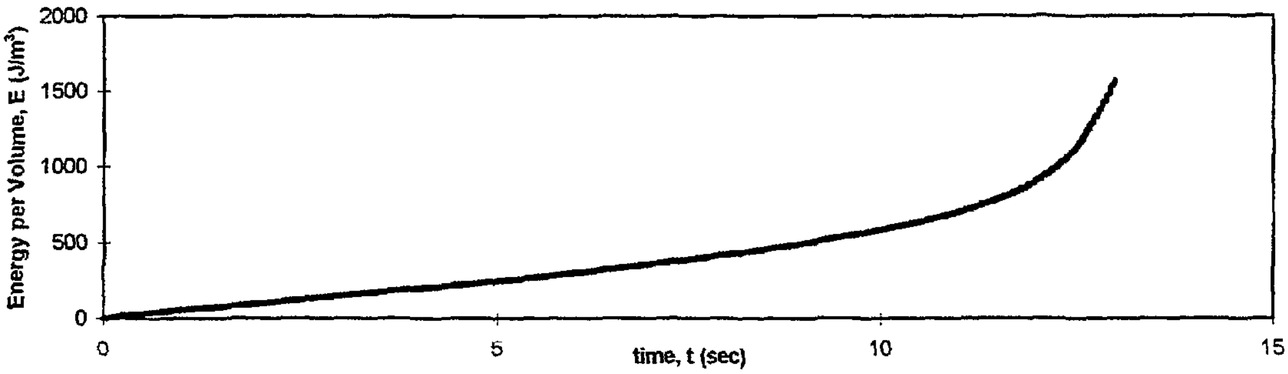

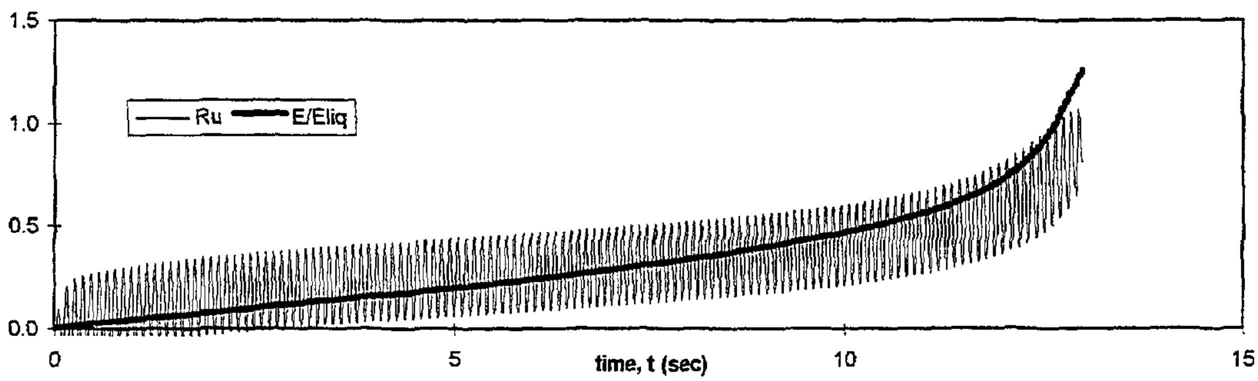

d:\nit\itp\cy_files\MONT15.XLS 8/15/96 11:28 AM

Test I.D.:	MONT15	**Controlled Parameter:**	Stress
Relative Density (%):	60.5	**Initial Effective Stress (kPa):**	100
Applied Stress Ratio:	0.22	**Frequency (Hz):**	10

Shear Stress vs. Shear Strain

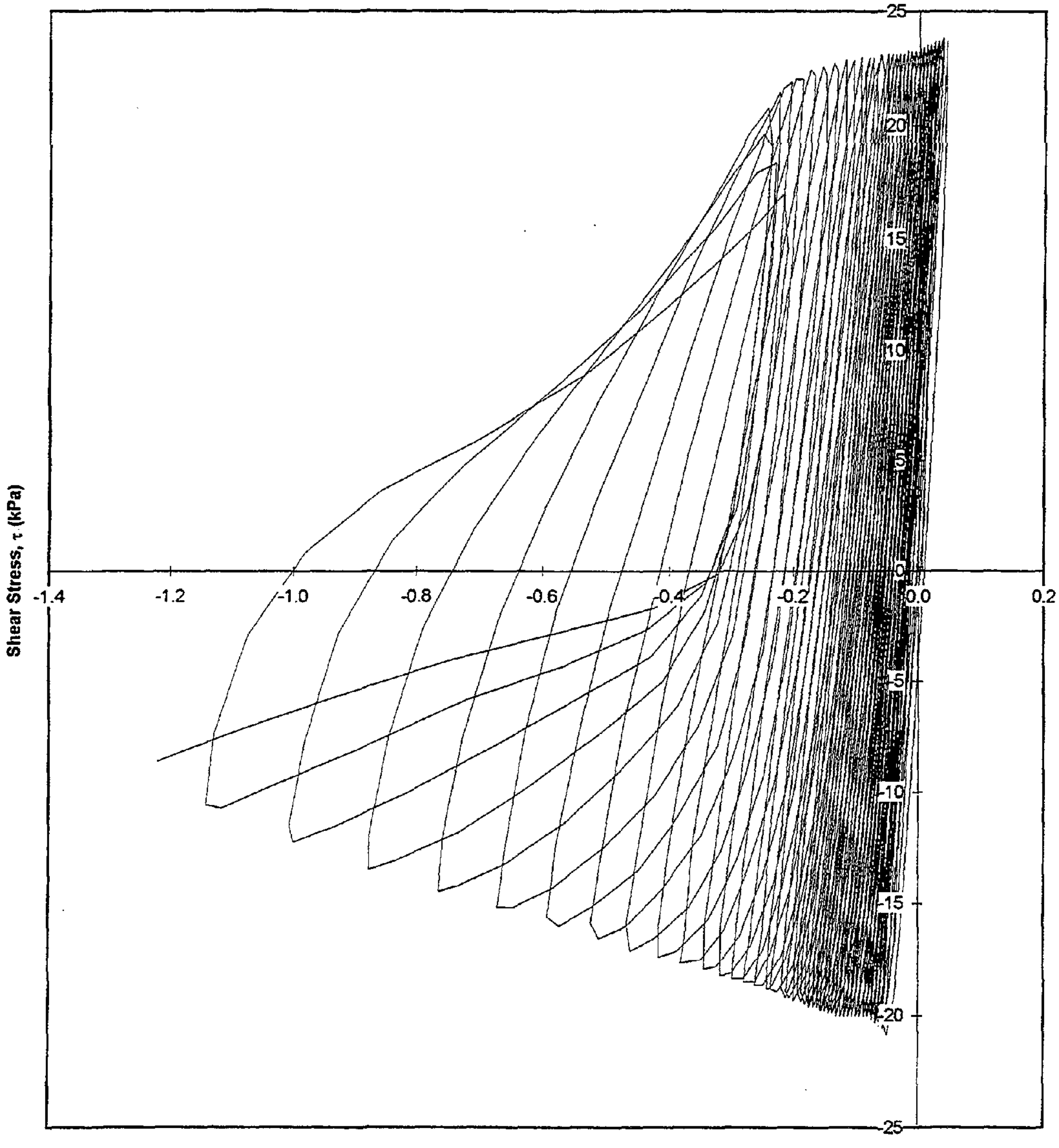

d:\nit\itp\cy_files\MONT15.XLS 8/15/96 11:28 AM

Test I.D.:	MONT17	**Controlled Parameter:**	Strain
Relative Density (%):	61	**Initial Effective Stress (kPa):**	100
Applied Shear Strain (%):	0.25	**Frequency (Hz):**	1

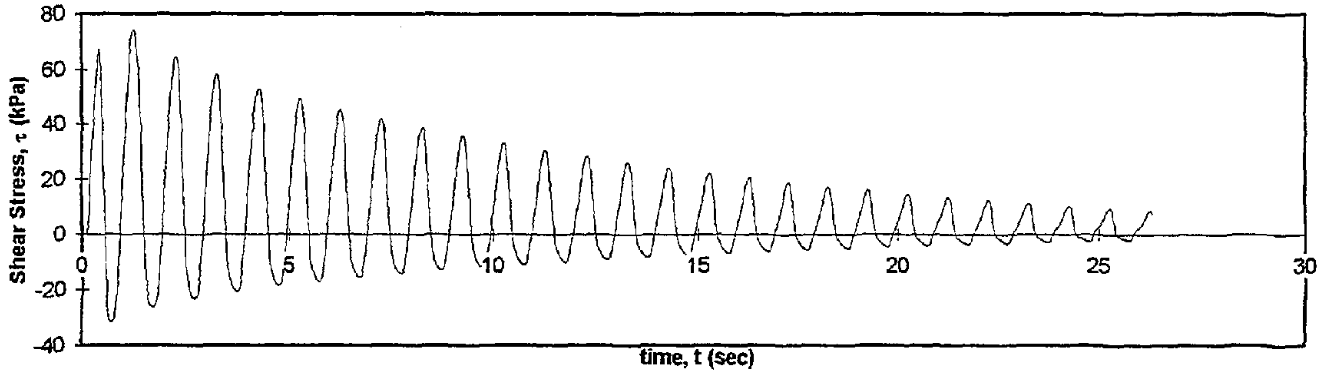

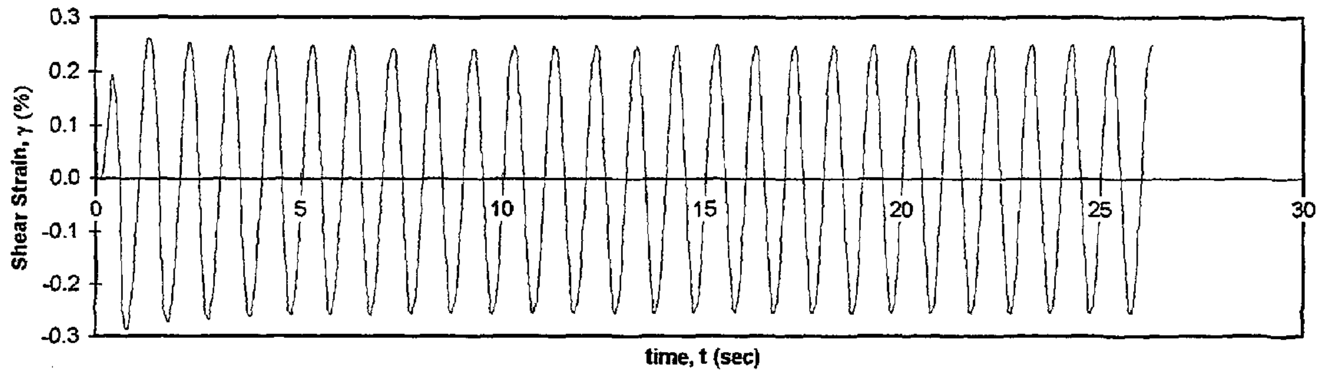

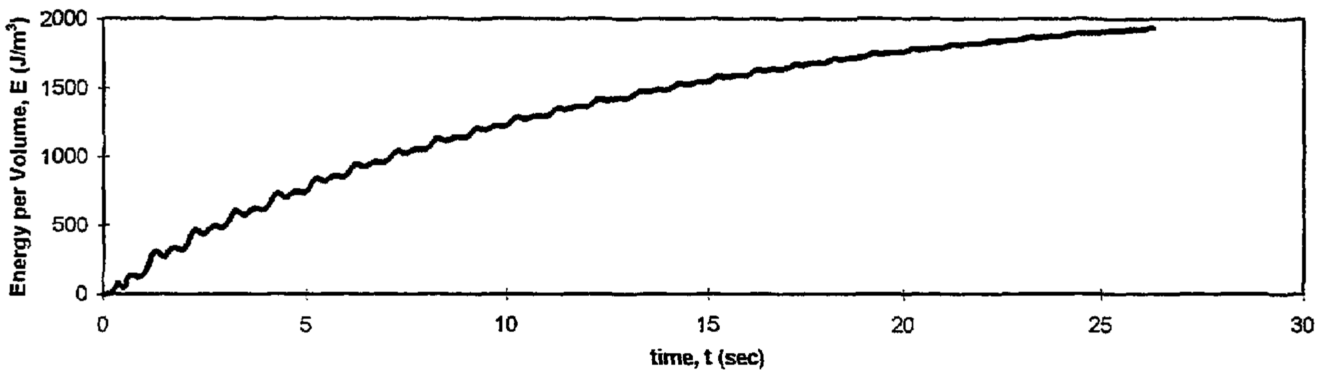

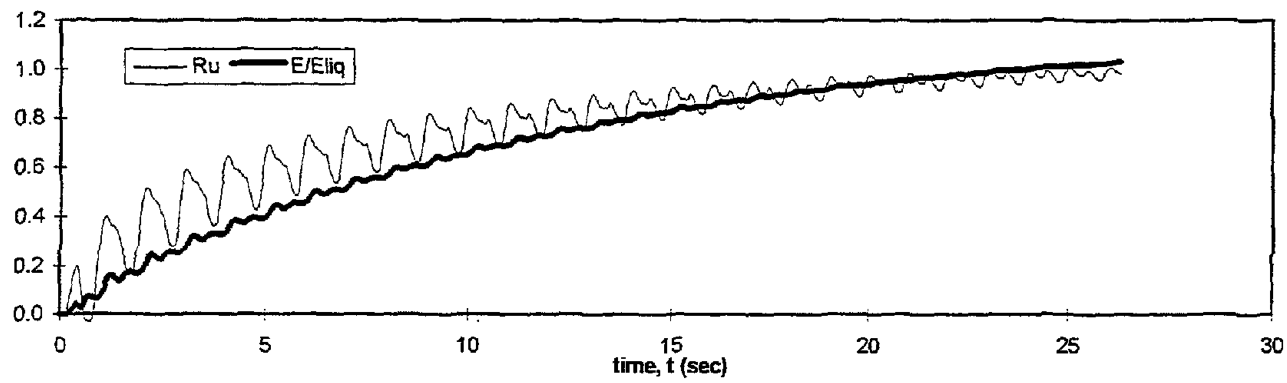

Test I.D.:	MONT17	**Controlled Parameter:**	Strain
Relative Density (%):	61	**Initial Effective Stress (kPa):**	100
Applied Shear Strain (%):	0.25	**Frequency (Hz):**	1

Shear Stress vs. Shear Strain

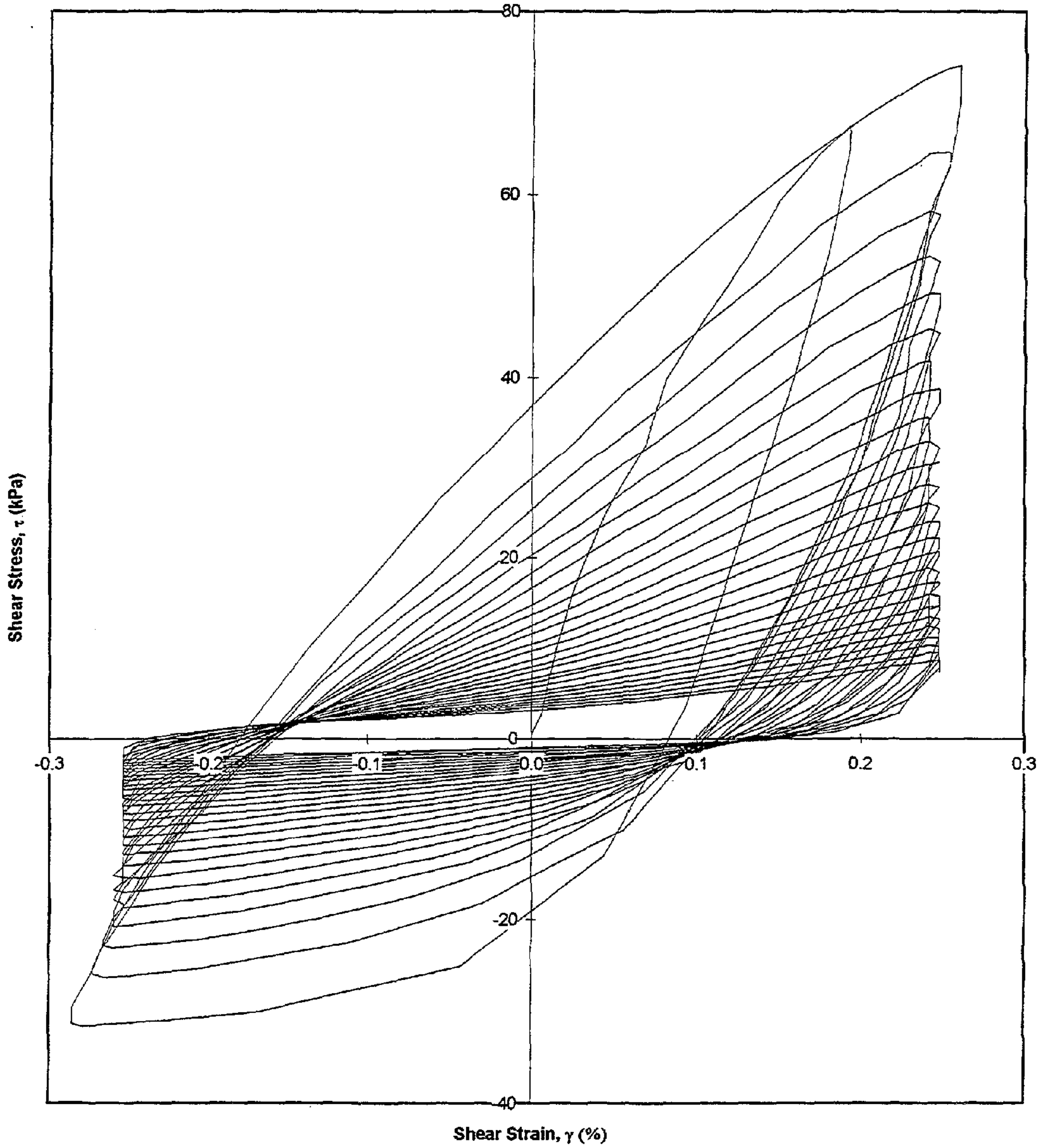

d:\nit\itp\cy_files\MONT17.XLS 8/15/96 11:31 AM

Test I.D.:	MONT18	**Controlled Parameter:**	Strain
Relative Density (%):	61	**Initial Effective Stress (kPa):**	100
Applied Shear Strain (%):	0.25	**Frequency (Hz):**	10

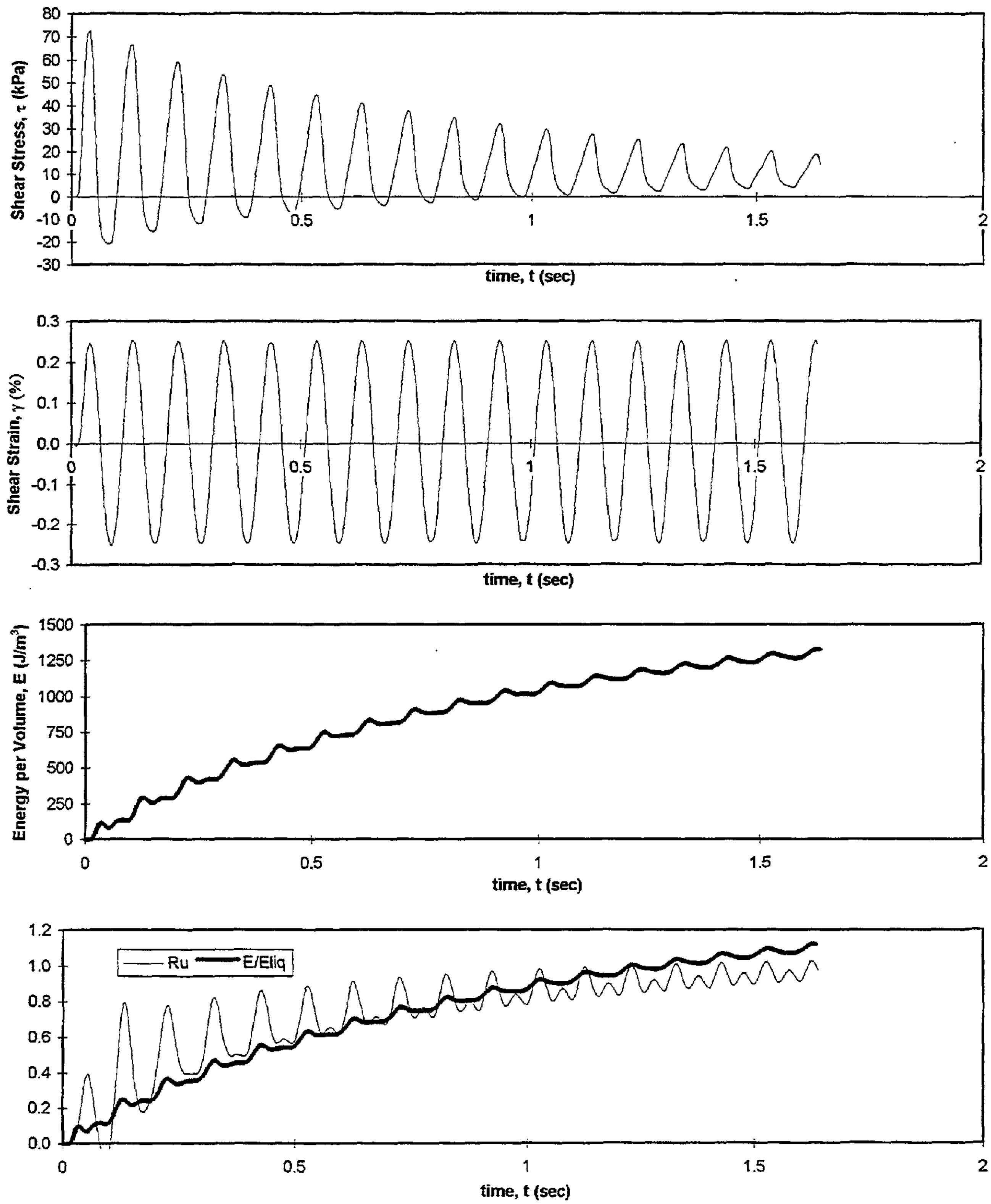

d:\nit\itp\cy_files\MONT18.XLS 8/15/96 11:37 AM

Test I.D.:	MONT18	**Controlled Parameter:**	Strain
Relative Density (%):	61	**Initial Effective Stress (kPa):**	100
Applied Shear Strain (%):	0.25	**Frequency (Hz):**	10

Shear Stress vs. Shear Strain

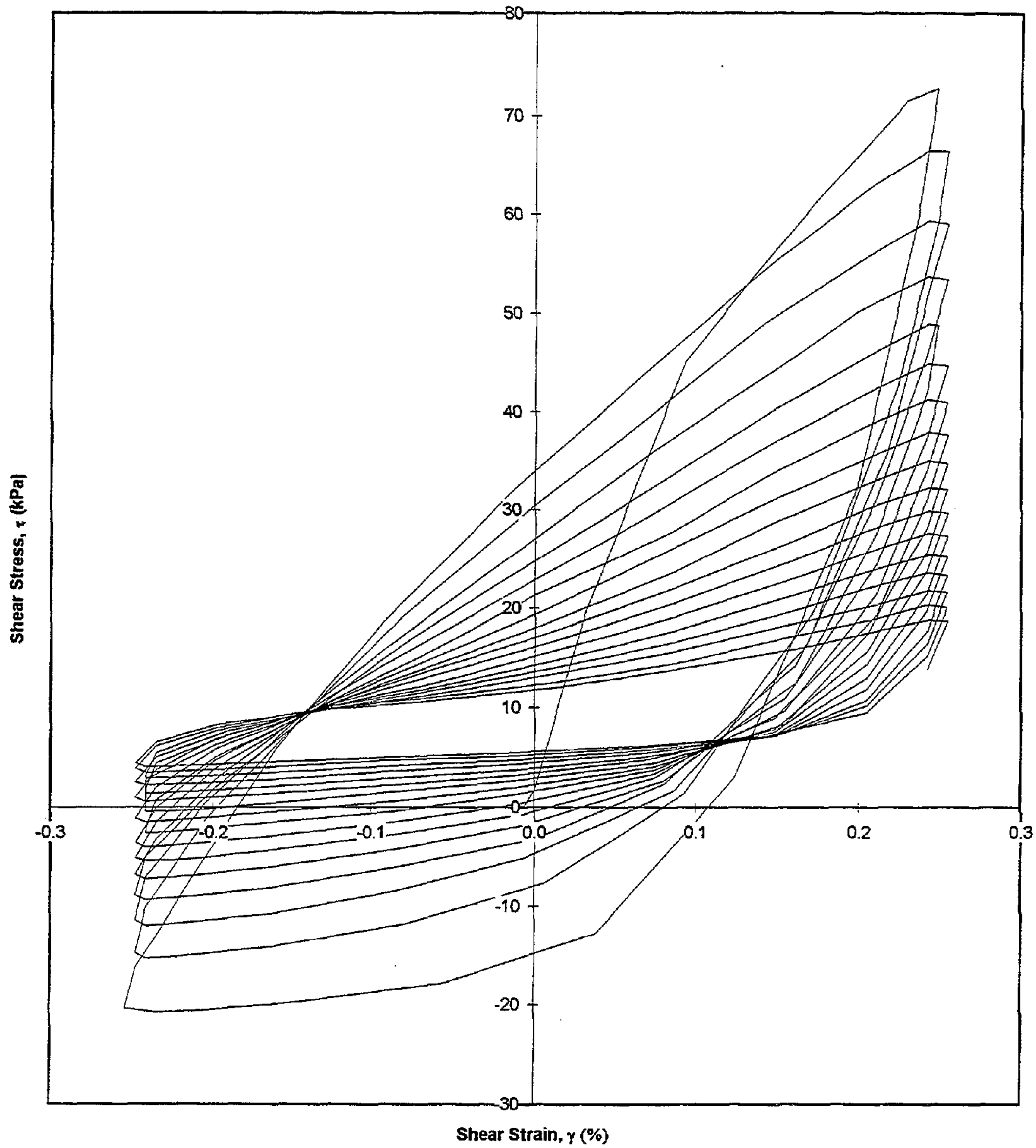

d:\nit\itp\cy_files\MONT18.XLS 8/15/96 11:37 AM

Test I.D.:	MONT19	**Controlled Parameter:**	Strain
Relative Density (%):	60.6	**Initial Effective Stress (kPa):**	100
Applied Shear Strain (%):	0.25	**Frequency (Hz):**	15

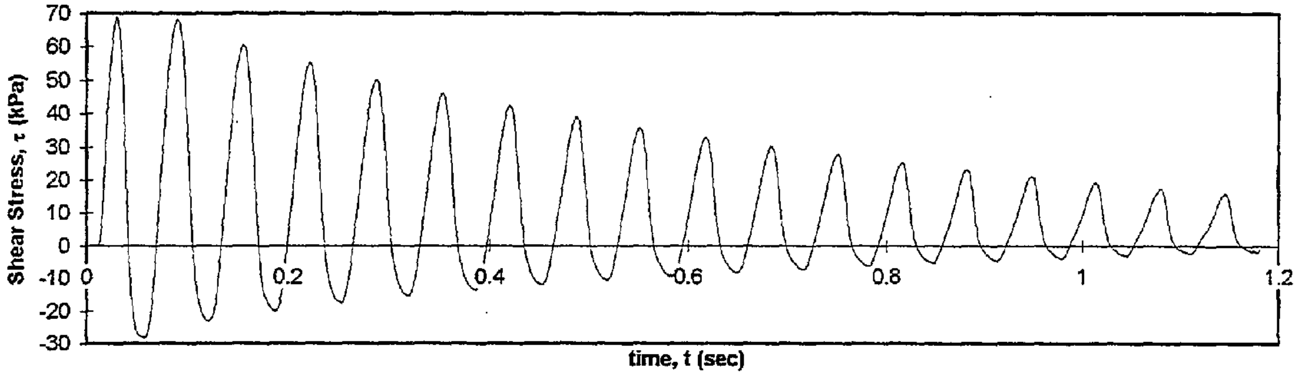

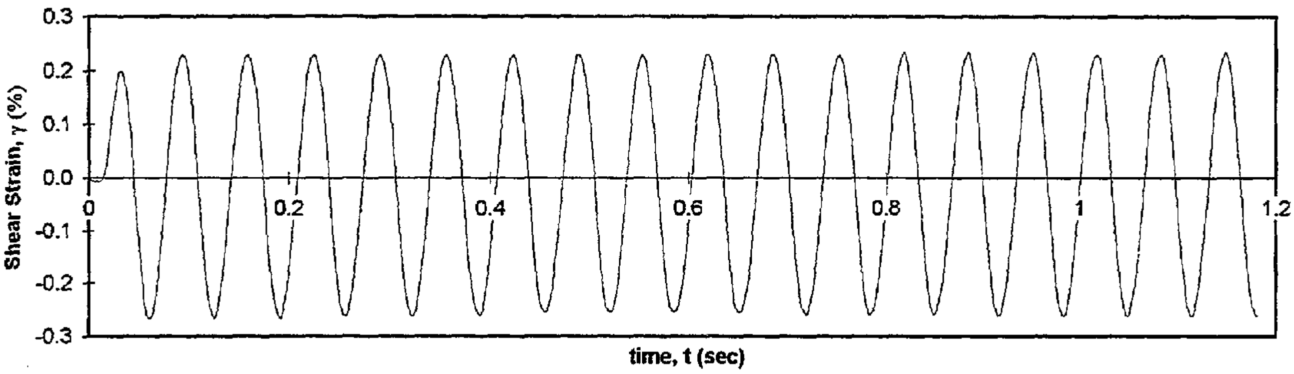

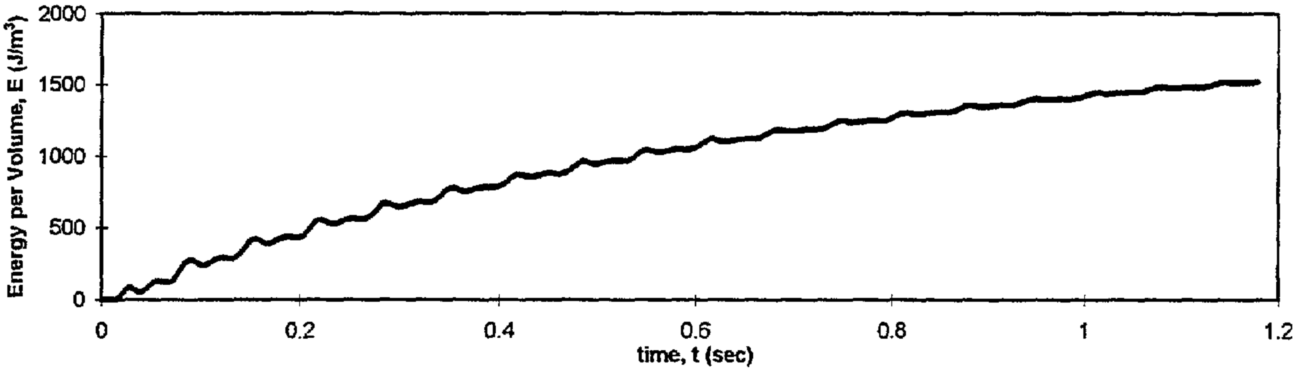

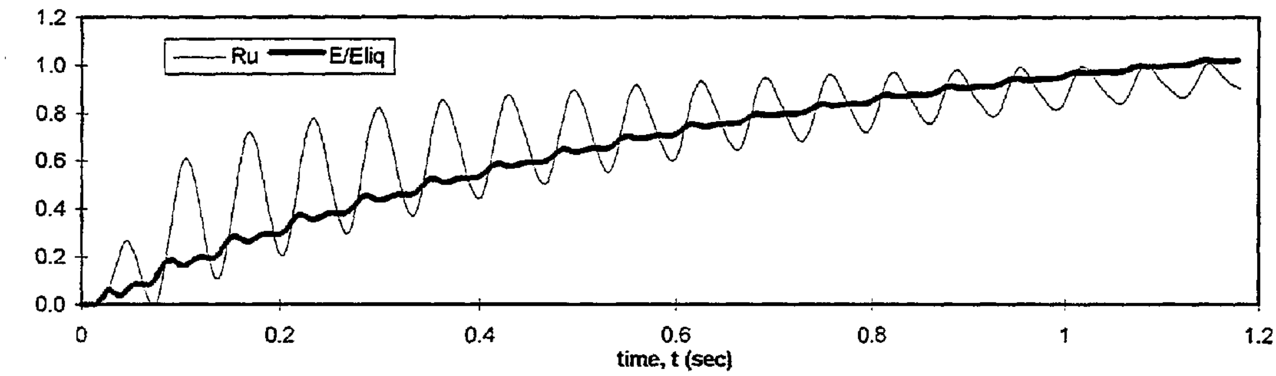

Test I.D.:	MONT19	**Controlled Parameter:**	Strain
Relative Density (%):	60.6	**Initial Effective Stress (kPa):**	100
Applied Shear Strain (%):	0.25	**Frequency (Hz):**	15

Shear Stress vs. Shear Strain

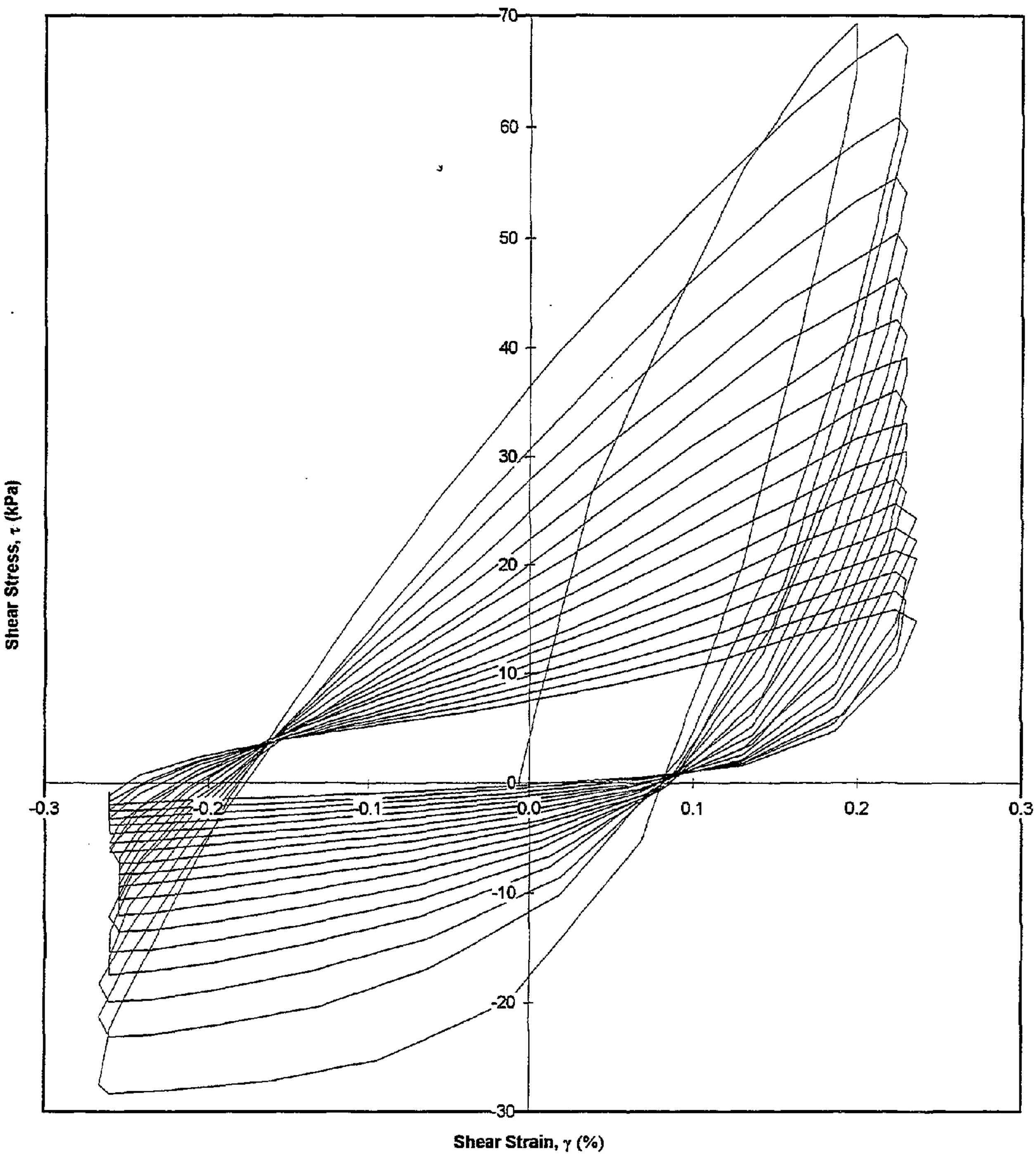

Test I.D.:	MONT20	**Controlled Parameter:**	Strain
Relative Density (%):	40.9	**Initial Effective Stress (kPa):**	100
Applied Shear Strain (%):	0.25	**Frequency (Hz):**	1

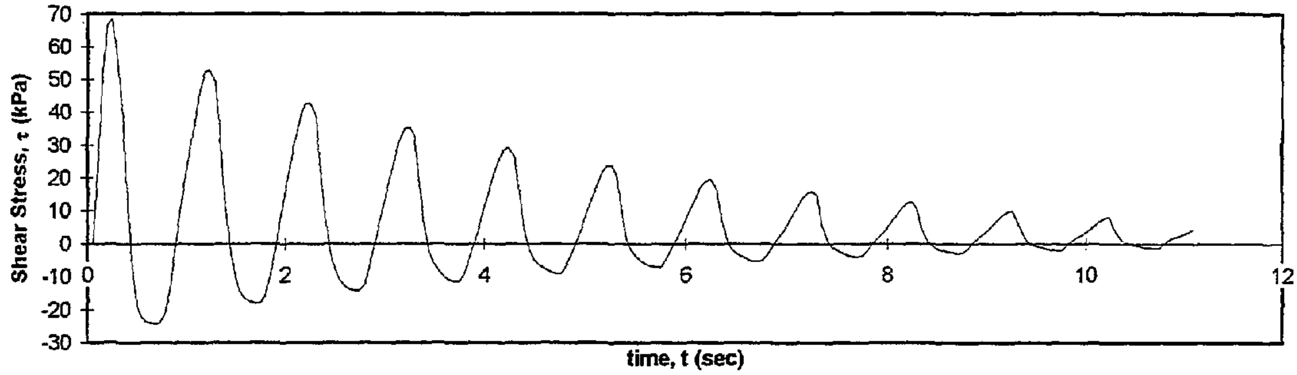

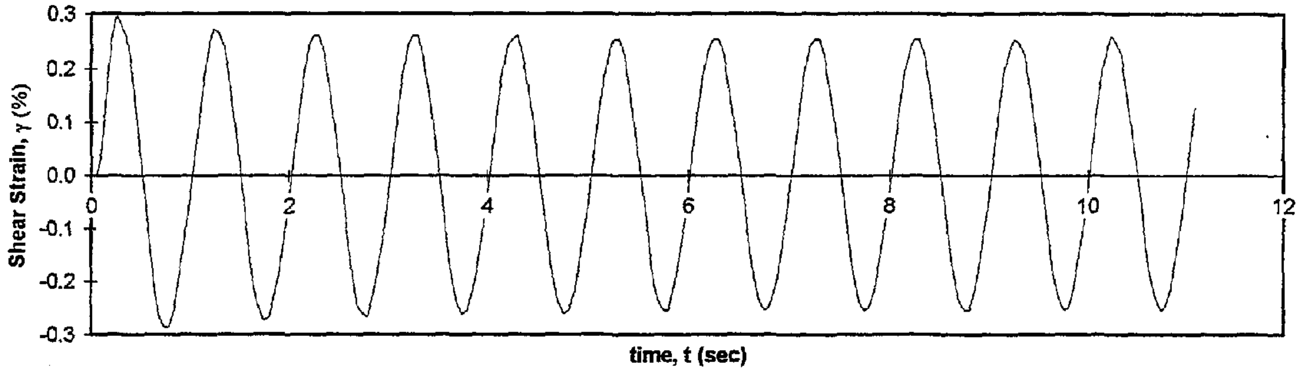

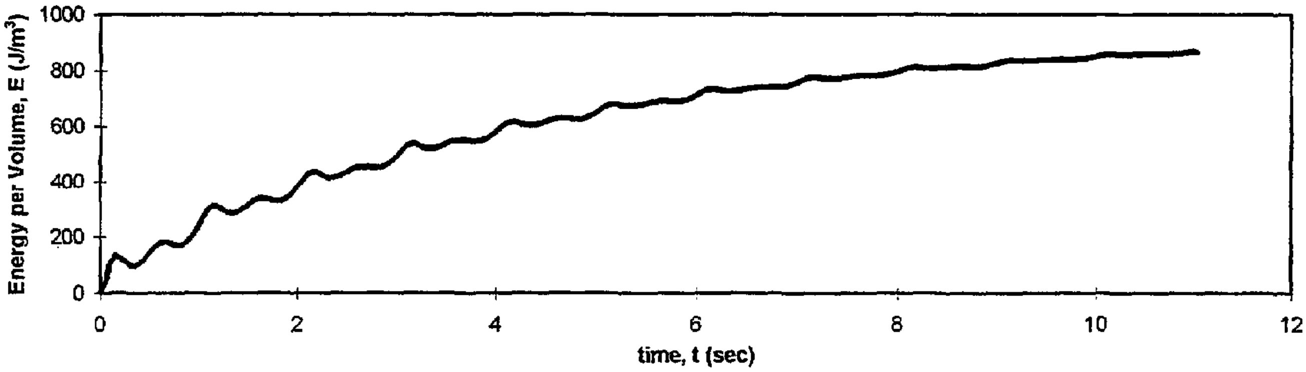

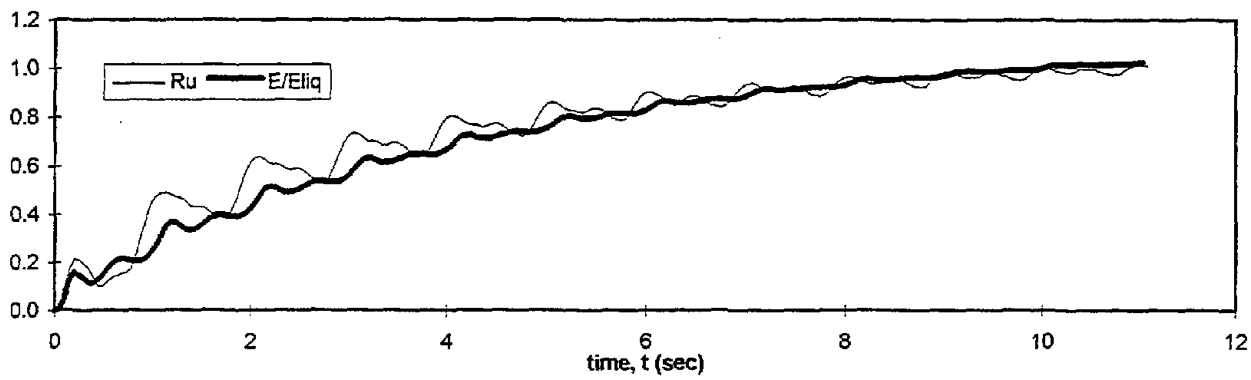

Test I.D.:	MONT20	**Controlled Parameter:**	Strain
Relative Density (%):	40.9	**Initial Effective Stress (kPa):**	100
Applied Shear Strain (%):	0.25	**Frequency (Hz):**	1

Shear Stress vs. Shear Strain

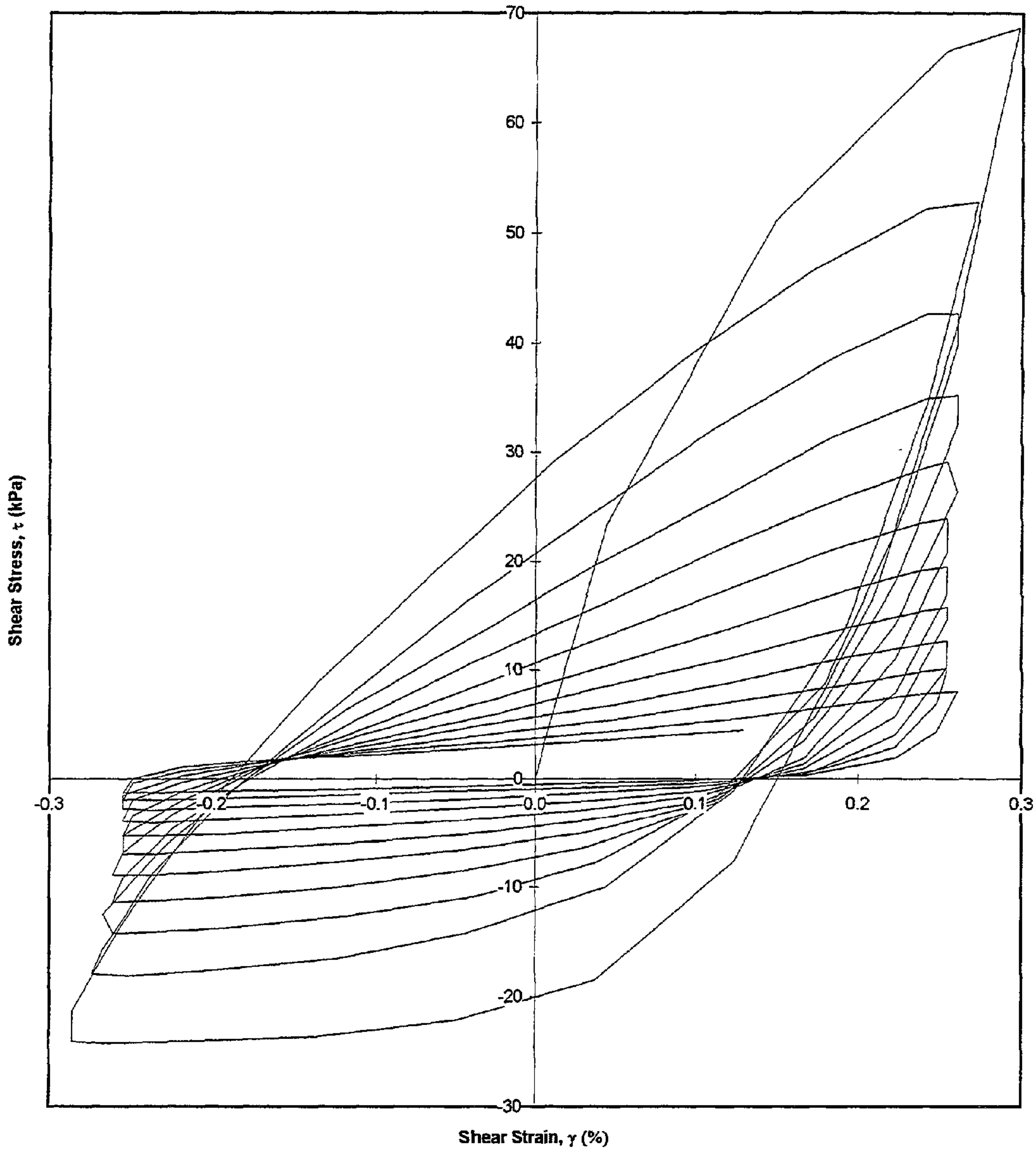

d:\nit\itp\cy_files\MONT20.XLS

8/15/96 11:47 AM

Test I.D.:	MONT21	**Controlled Parameter:**	Strain
Relative Density (%):	41.8	**Initial Effective Stress (kPa):**	100
Applied Shear Strain (%):	0.15	**Frequency (Hz):**	1

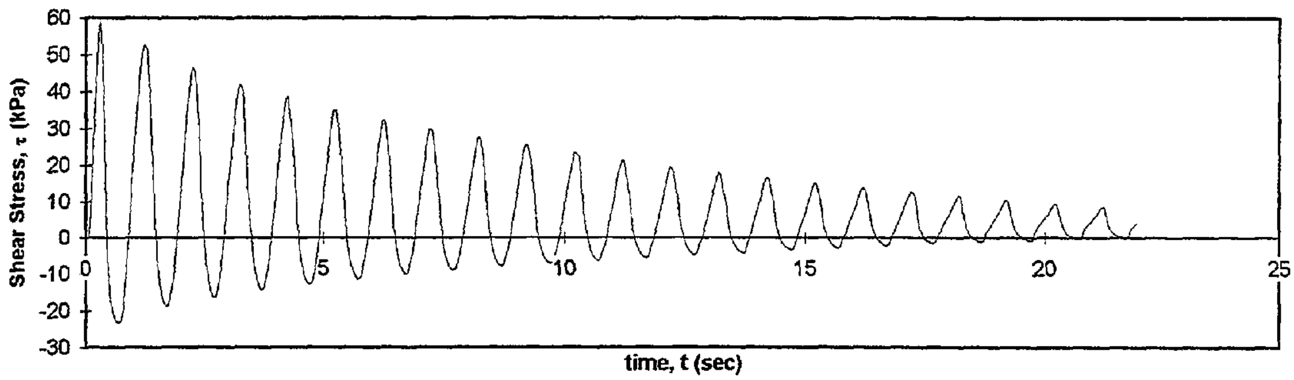

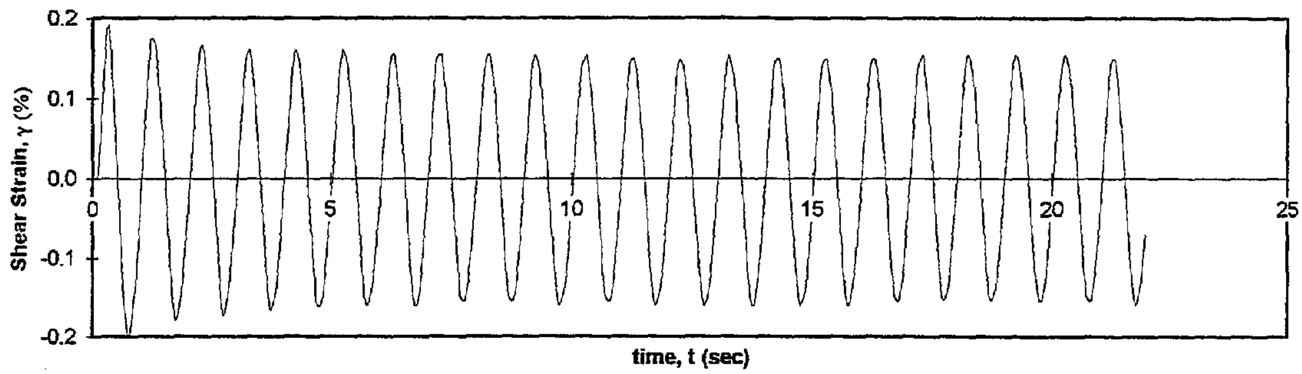

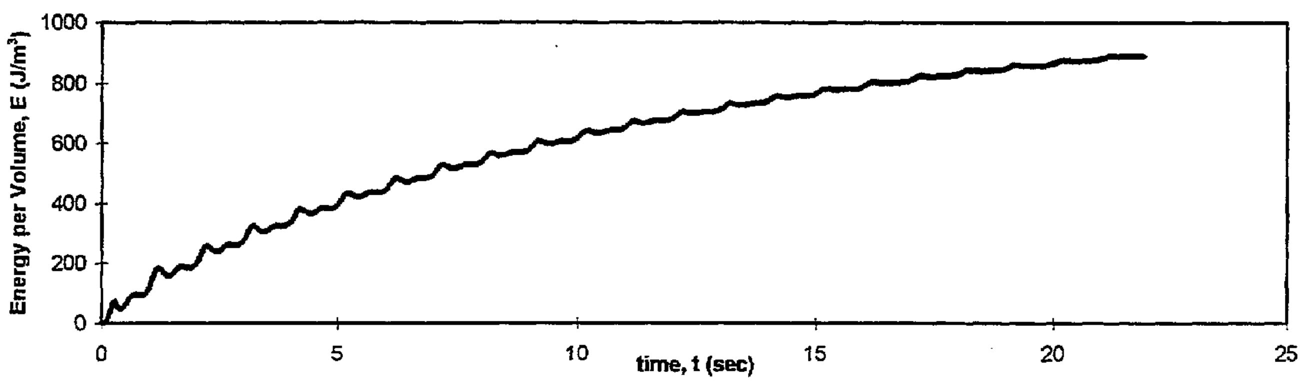

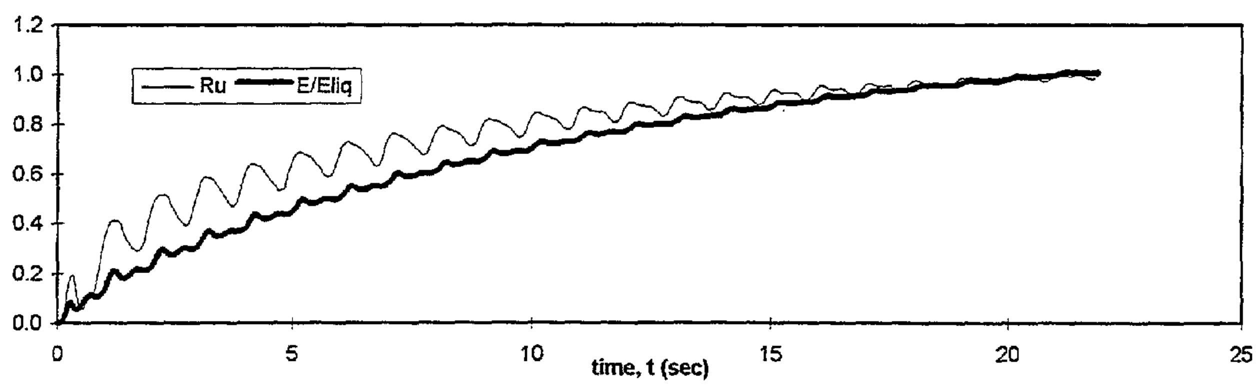

Test I.D.:	MONT21	**Controlled Parameter:**	Strain
Relative Density (%):	41.8	**Initial Effective Stress (kPa):**	100
Applied Shear Strain (%):	0.15	**Frequency (Hz):**	1

Shear Stress vs. Shear Strain

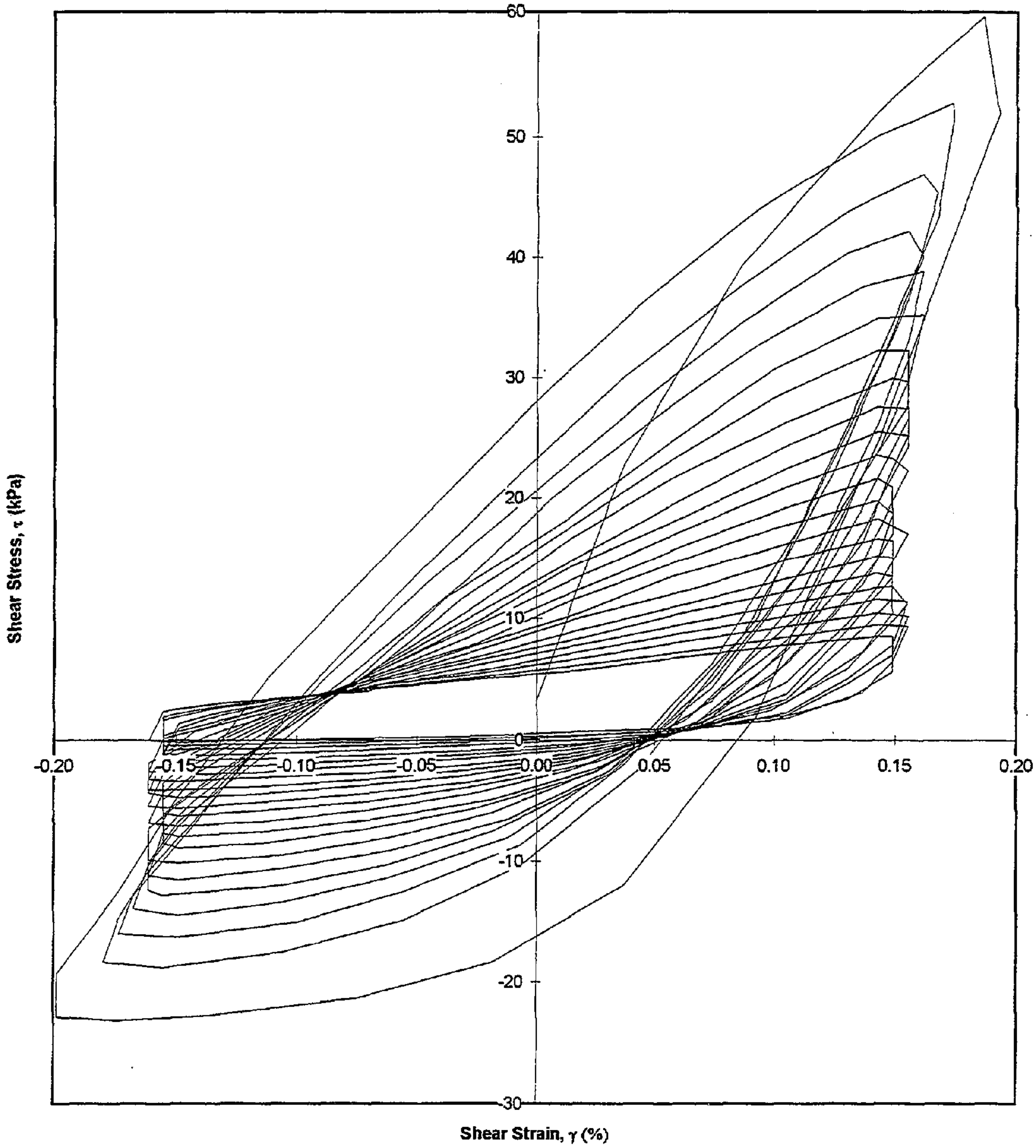

d:\nit\itp\cy_files\MONT21.XLS 8/15/96 11:53 AM

Test I.D.:	MONT22	**Controlled Parameter:**	Strain
Relative Density (%):	42.3	**Initial Effective Stress (kPa):**	100
Applied Shear Strain:	0.08%	**Frequency (Hz):**	1

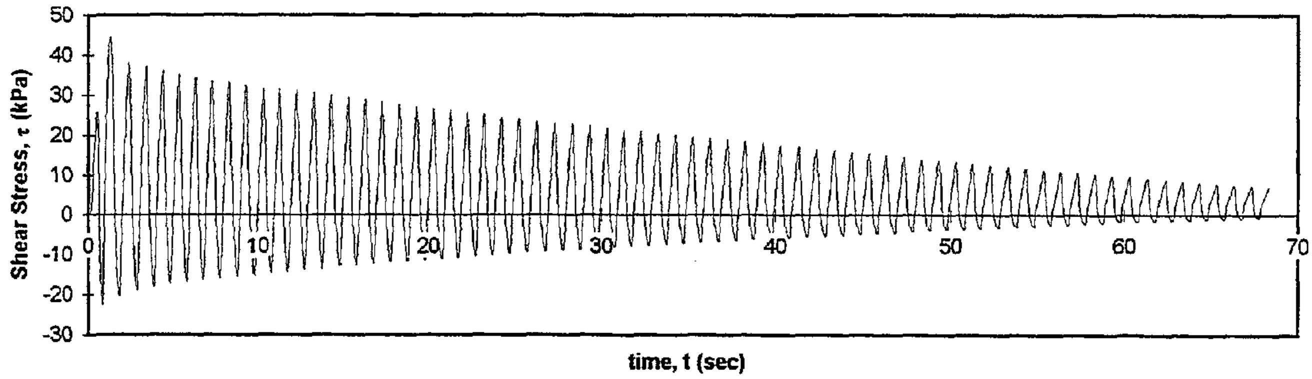

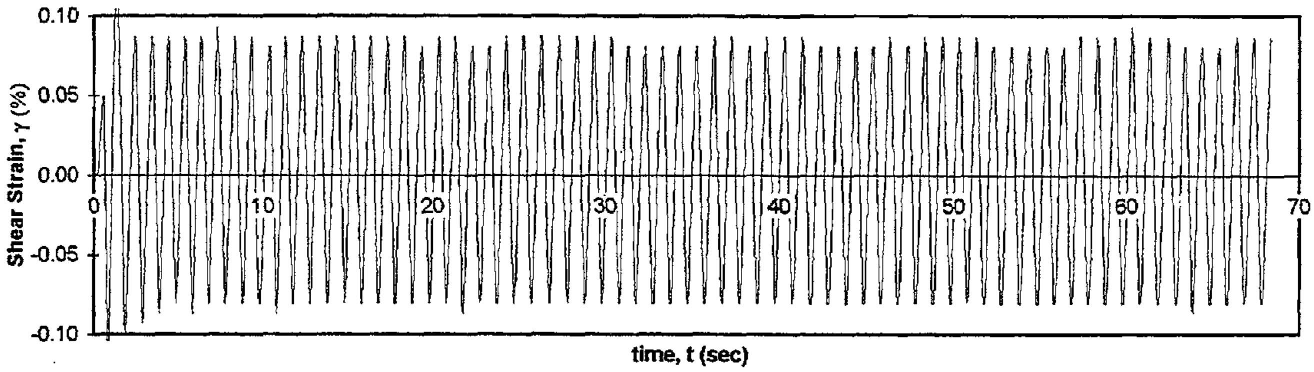

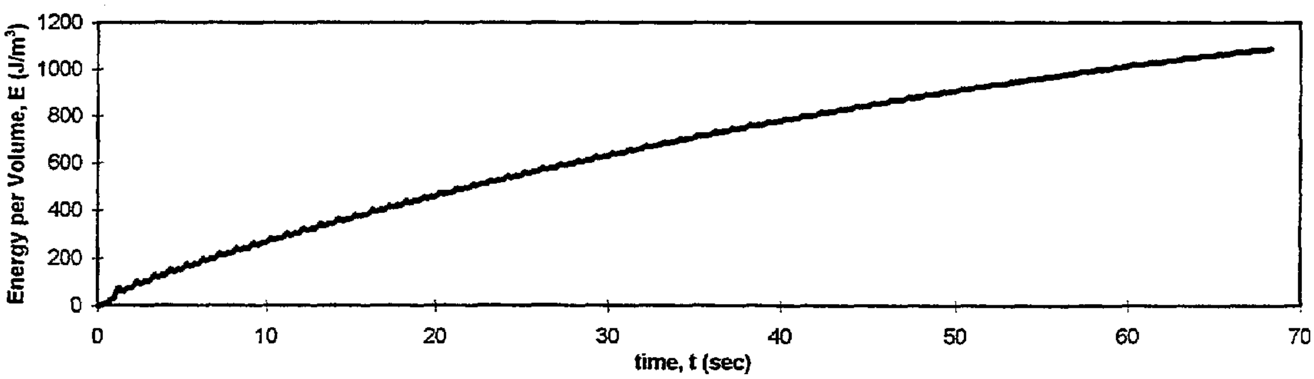

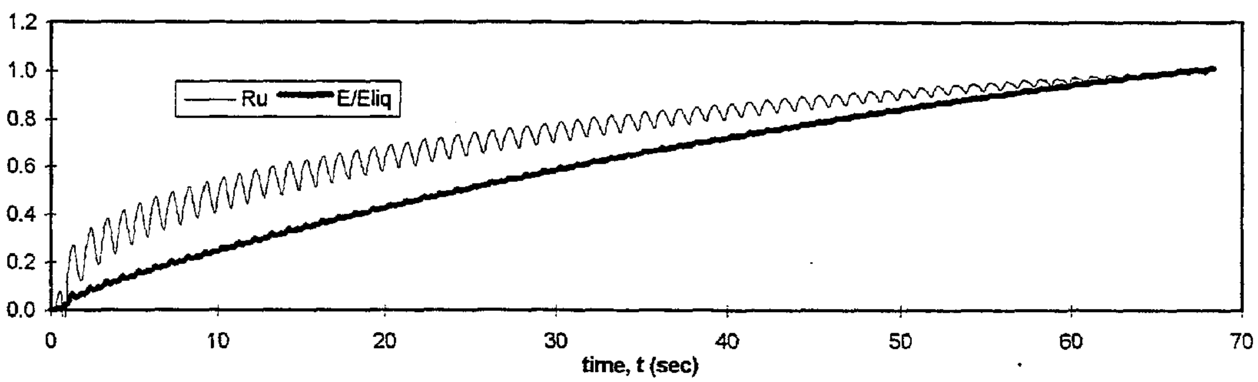

Test I.D.:	MONT22	**Controlled Parameter:**	Strain
Relative Density (%):	42.3	**Initial Effective Stress (kPa):**	100
Applied Shear Strain:	0.08%	**Frequency (Hz):**	1

Shear Stress vs. Shear Strain

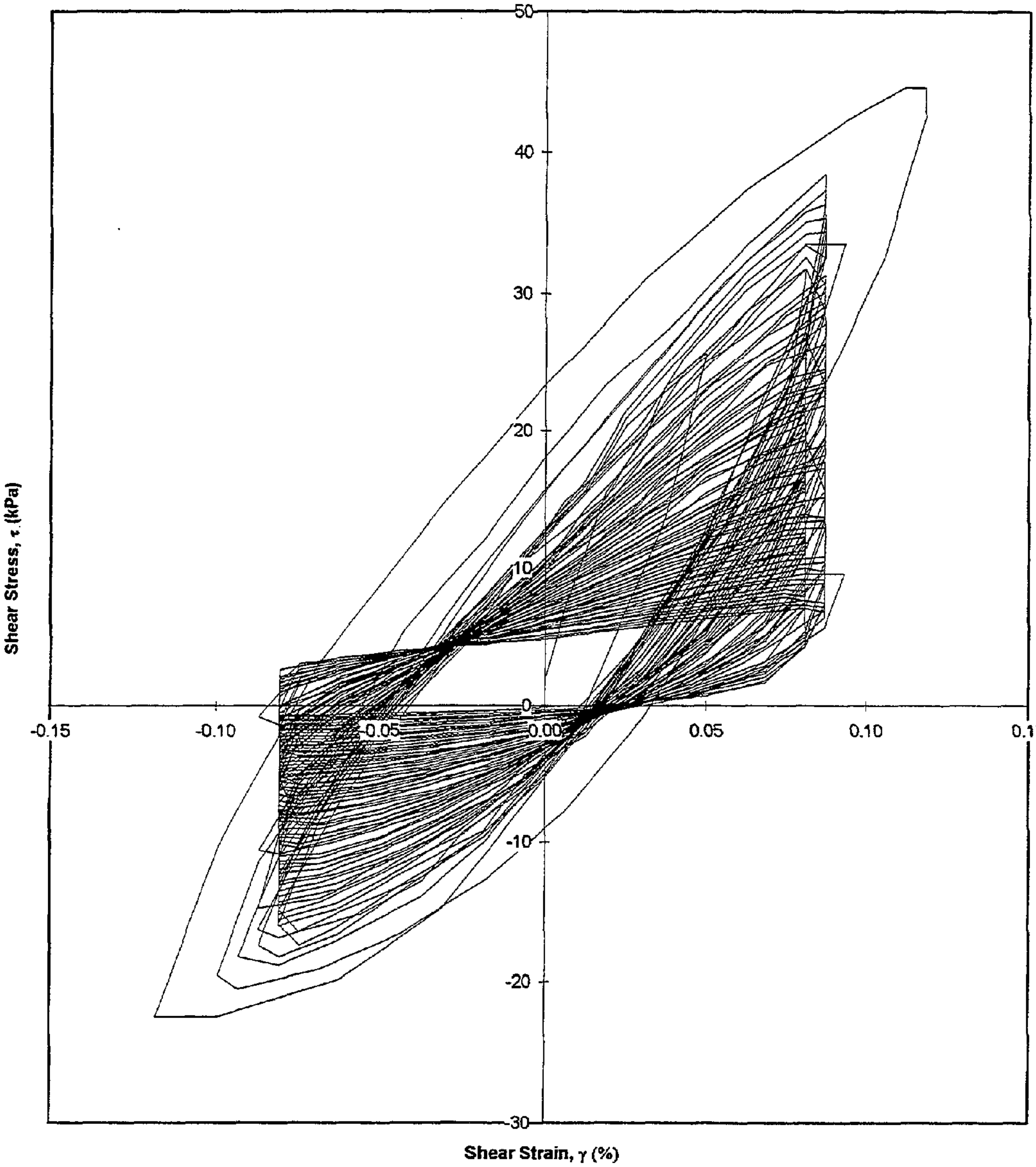

d:\nit\itp\cy_files\MONT22.XLS 8/21/96 9:47 AM

Test I.D.:	MONT24	**Controlled Parameter:**	Stress
Relative Density (%):	51.8	**Initial Effective Stress (kPa):**	100
Applied Stress Ratio:	0.31	**Frequency (Hz):**	1

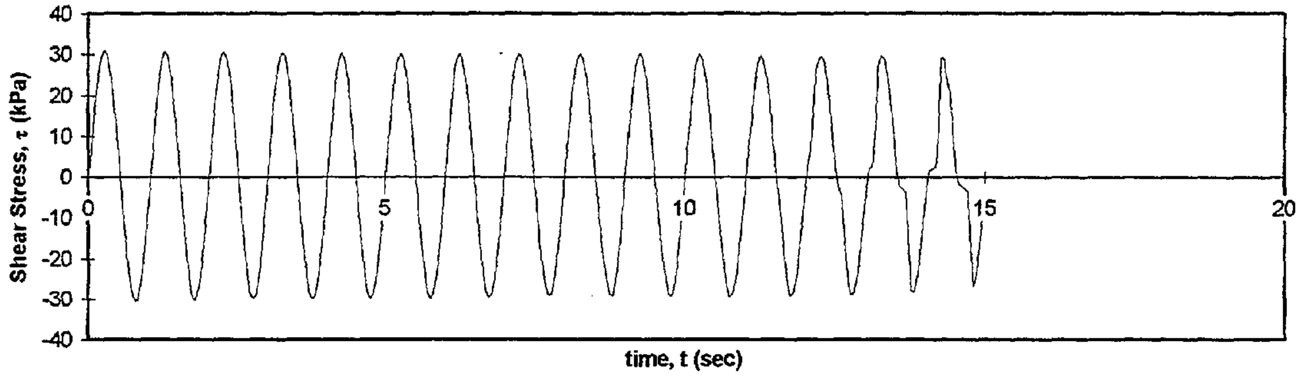

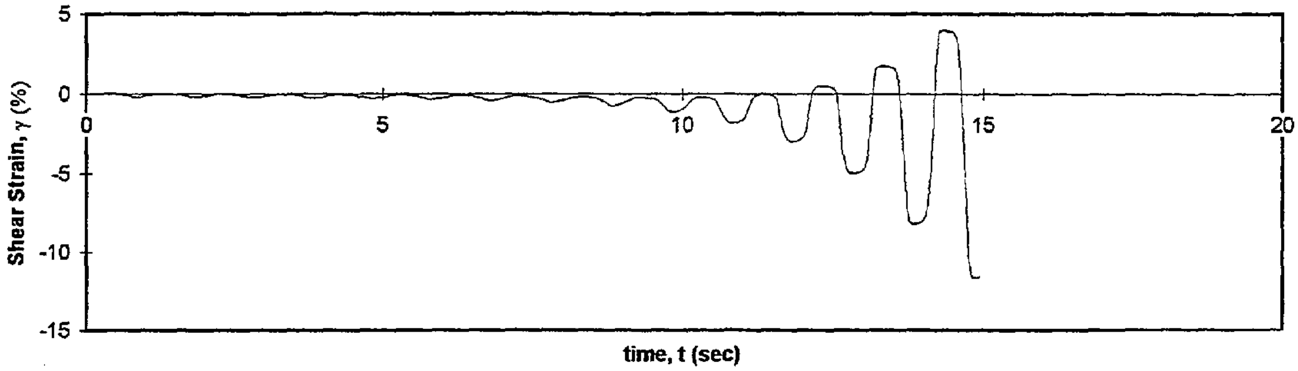

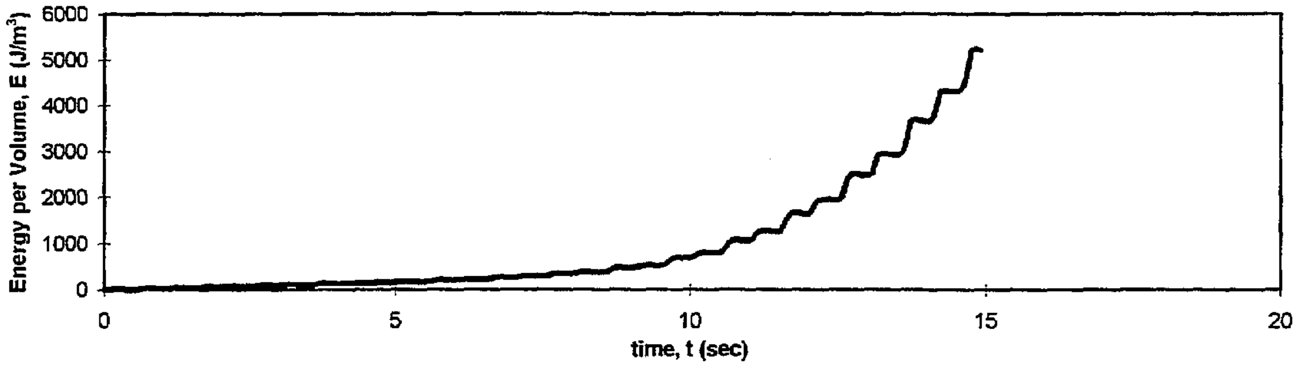

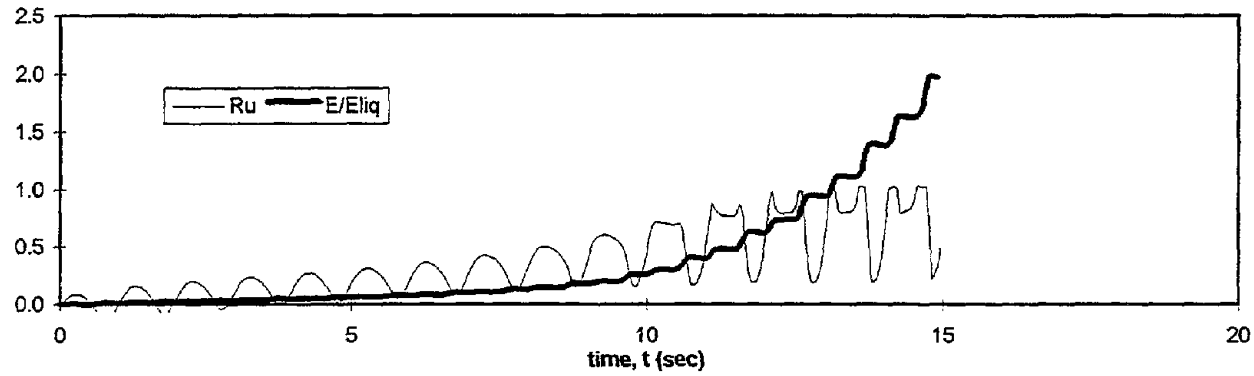

Test I.D.:	MONT24	**Controlled Parameter:**	Stress
Relative Density (%):	51.8	**Initial Effective Stress (kPa):**	100
Applied Stress Ratio:	0.31	**Frequency (Hz):**	1

Shear Stress vs. Shear Strain

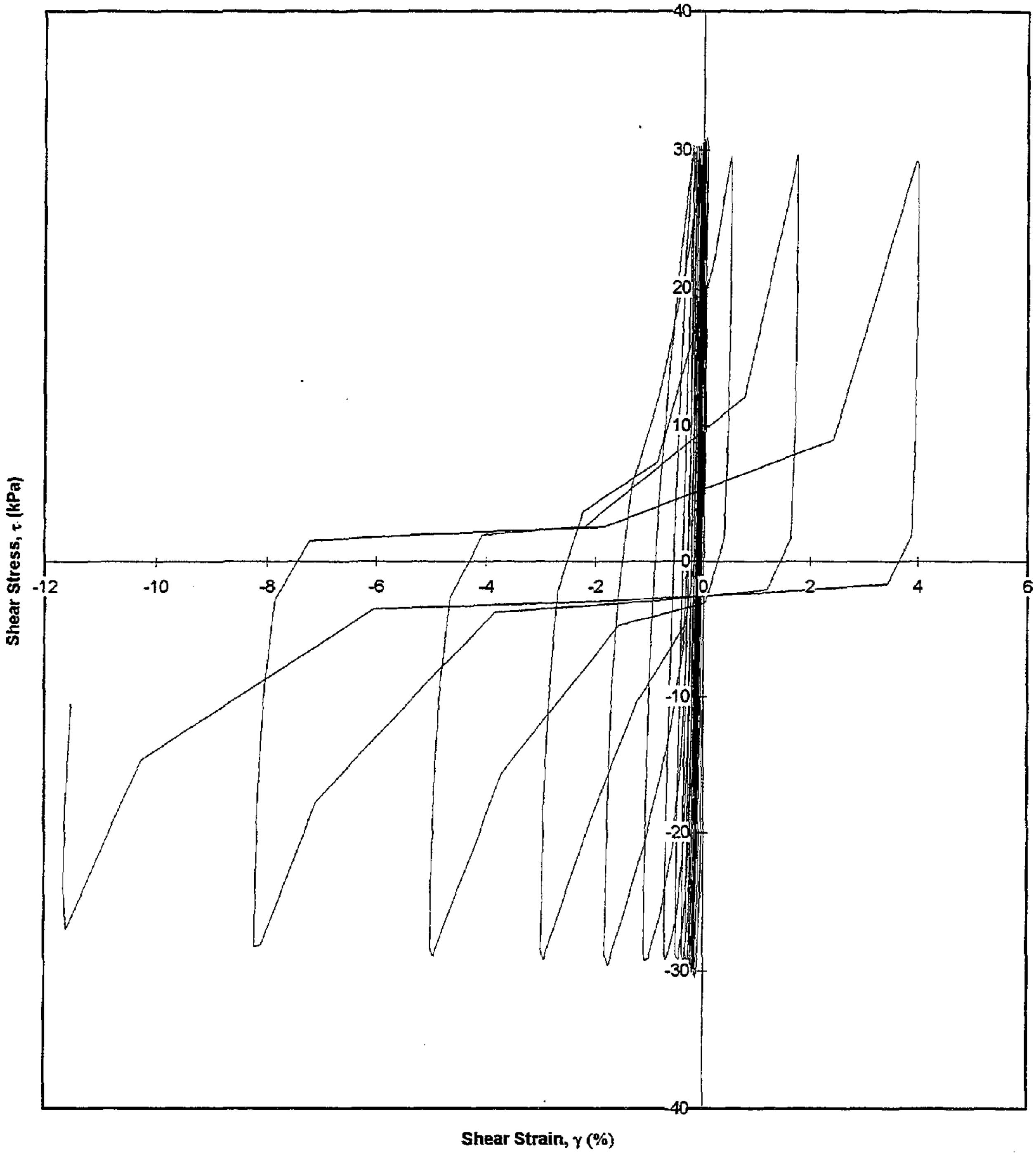

Test I.D.:	MONT25	**Controlled Parameter:**	Stress
Relative Density (%):	50.4	**Initial Effective Stress (kPa):**	100
Applied Stress Ratio:	0.25	**Frequency (Hz):**	1

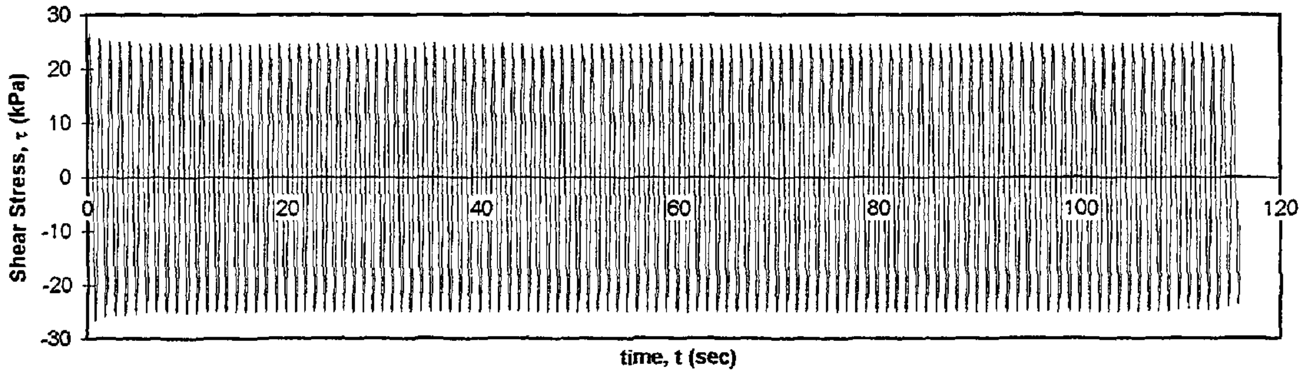

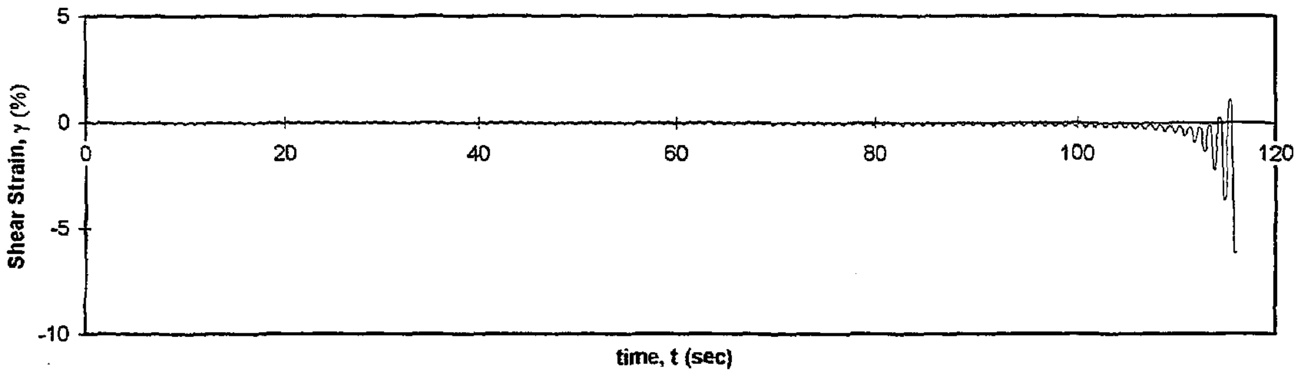

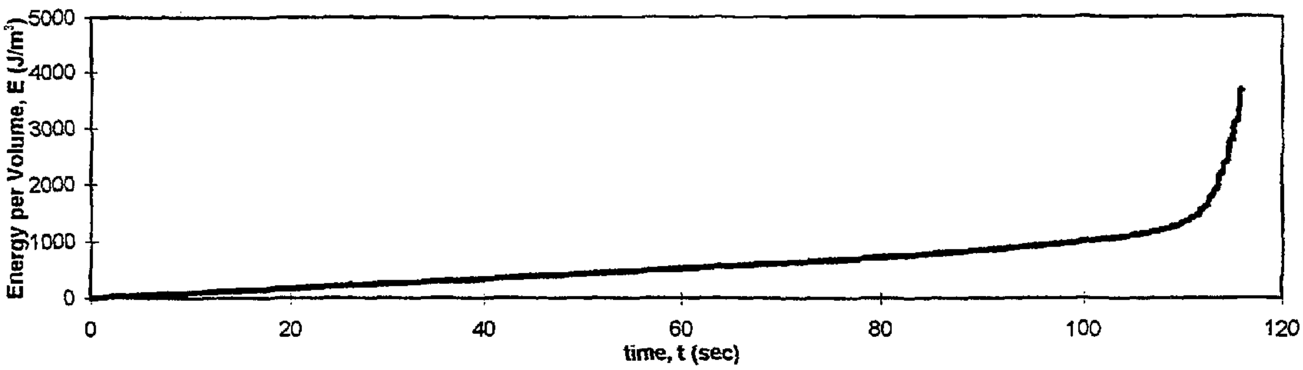

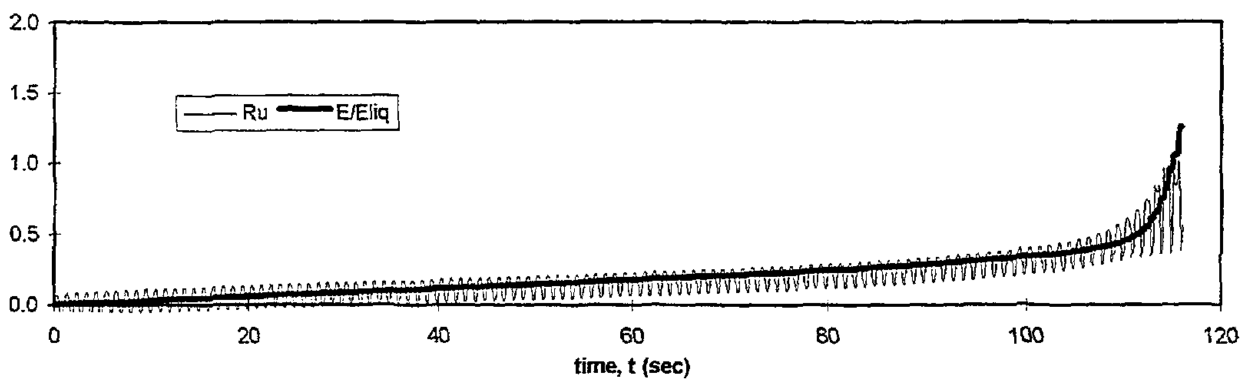

Test I.D.:	MONT25	**Controlled Parameter:**	Stress
Relative Density (%):	50.4	**Initial Effective Stress (kPa):**	100
Applied Stress Ratio:	0.25	**Frequency (Hz):**	1

Shear Stress vs. Shear Strain

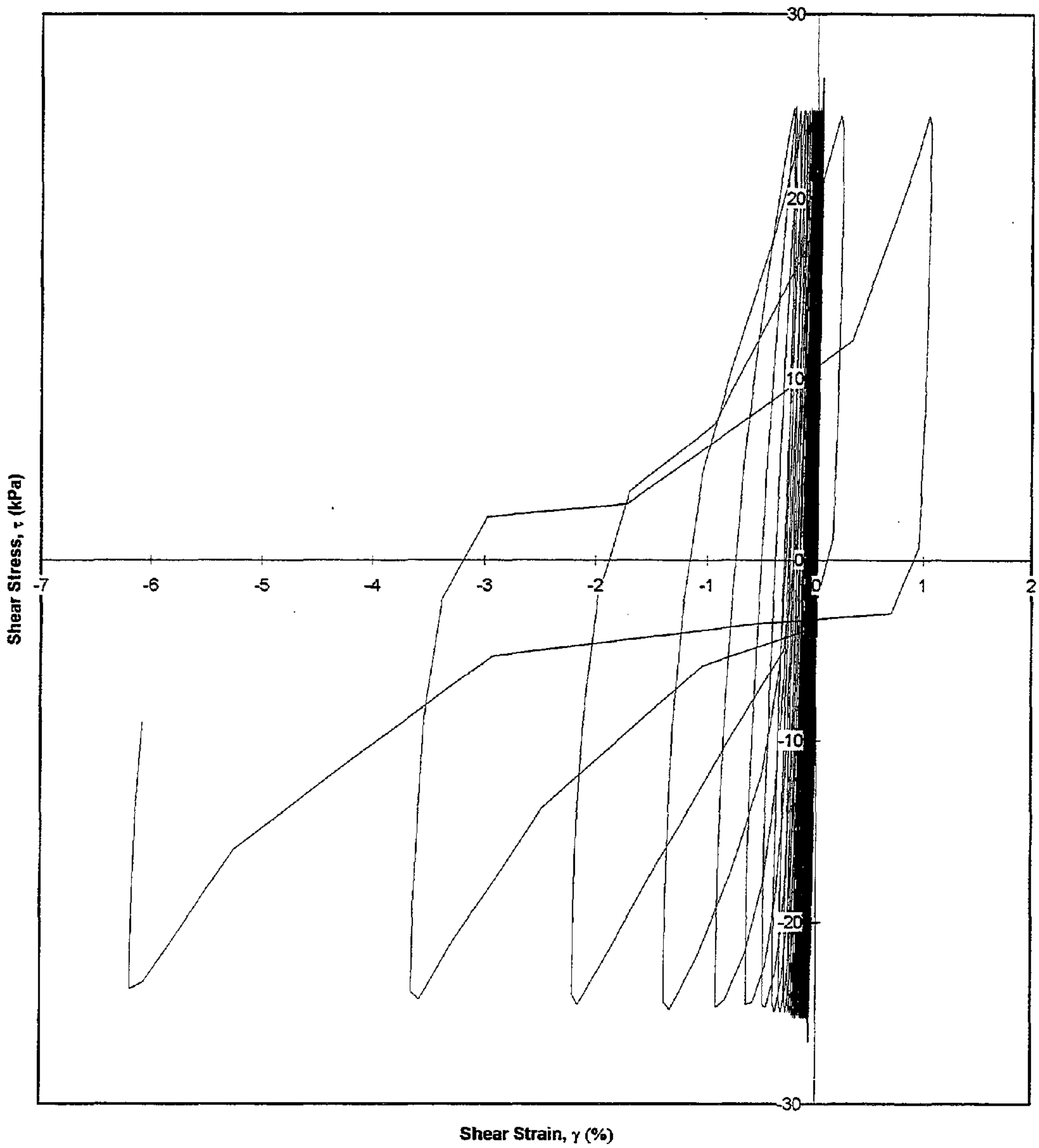

Test I.D.:	MONT26	**Controlled Parameter:**	Stress
Relative Density (%):	49.9	**Initial Effective Stress (kPa):**	100
Applied Stress Ratio:	0.35	**Frequency (Hz):**	1

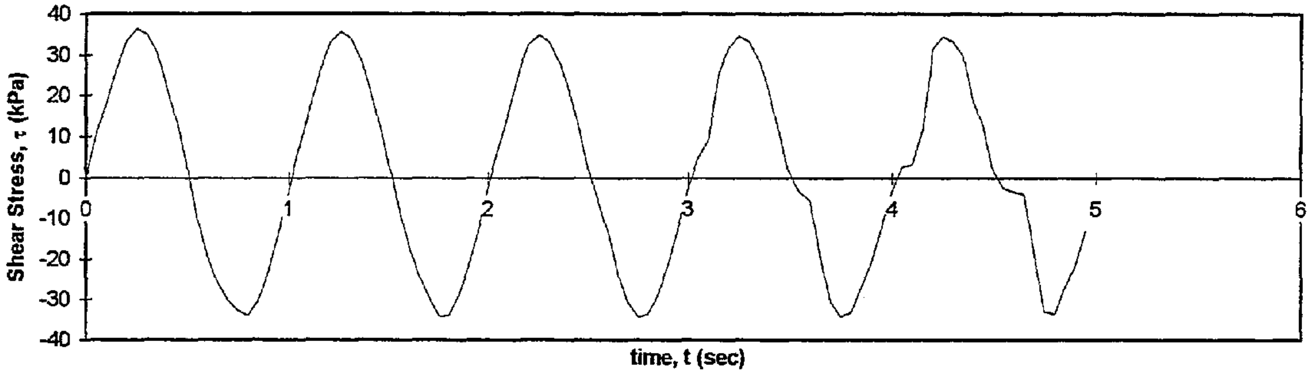

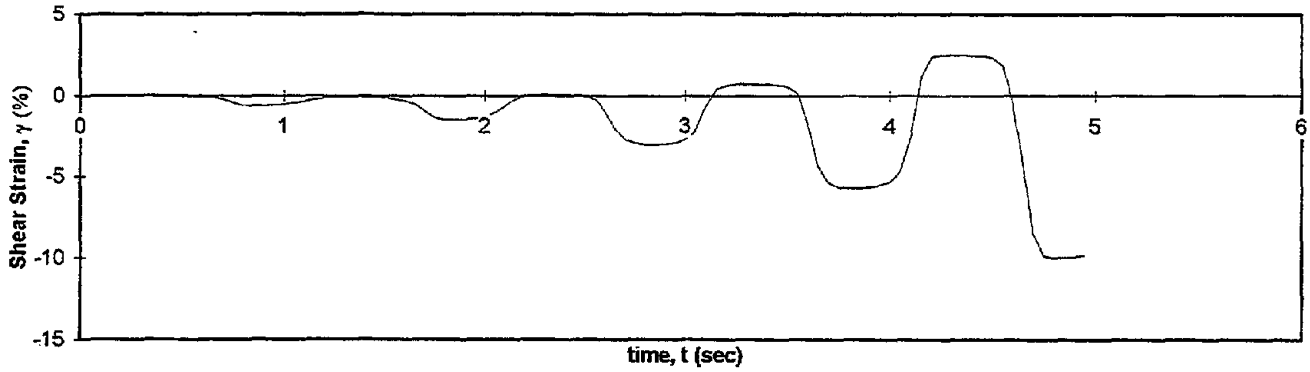

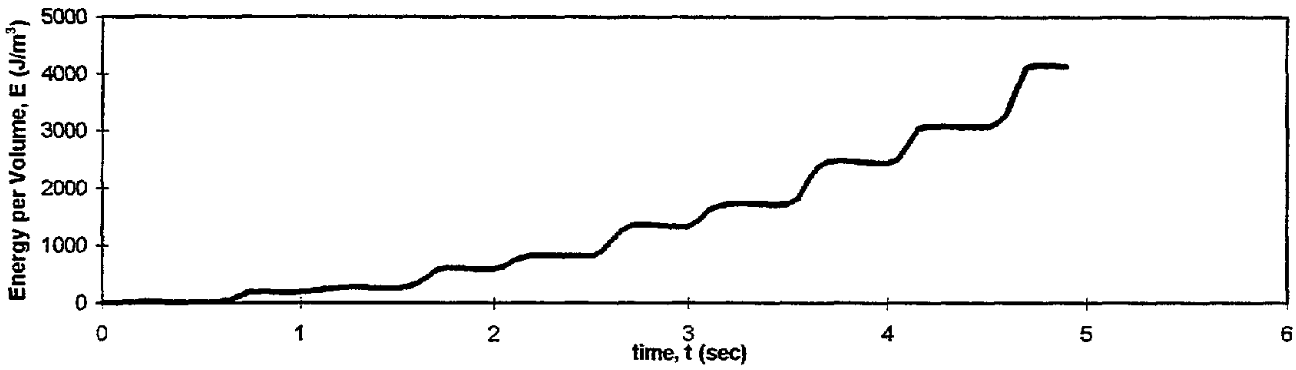

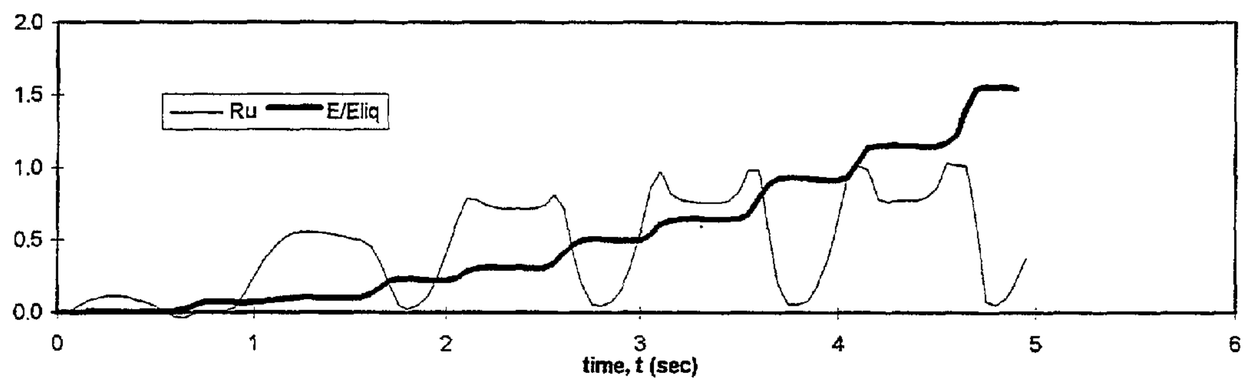

Test I.D.:	MONT26	**Controlled Parameter:**	Stress
Relative Density (%):	49.9	**Initial Effective Stress (kPa):**	100
Applied Stress Ratio:	0.35	**Frequency (Hz):**	1

Shear Stress vs. Shear Strain

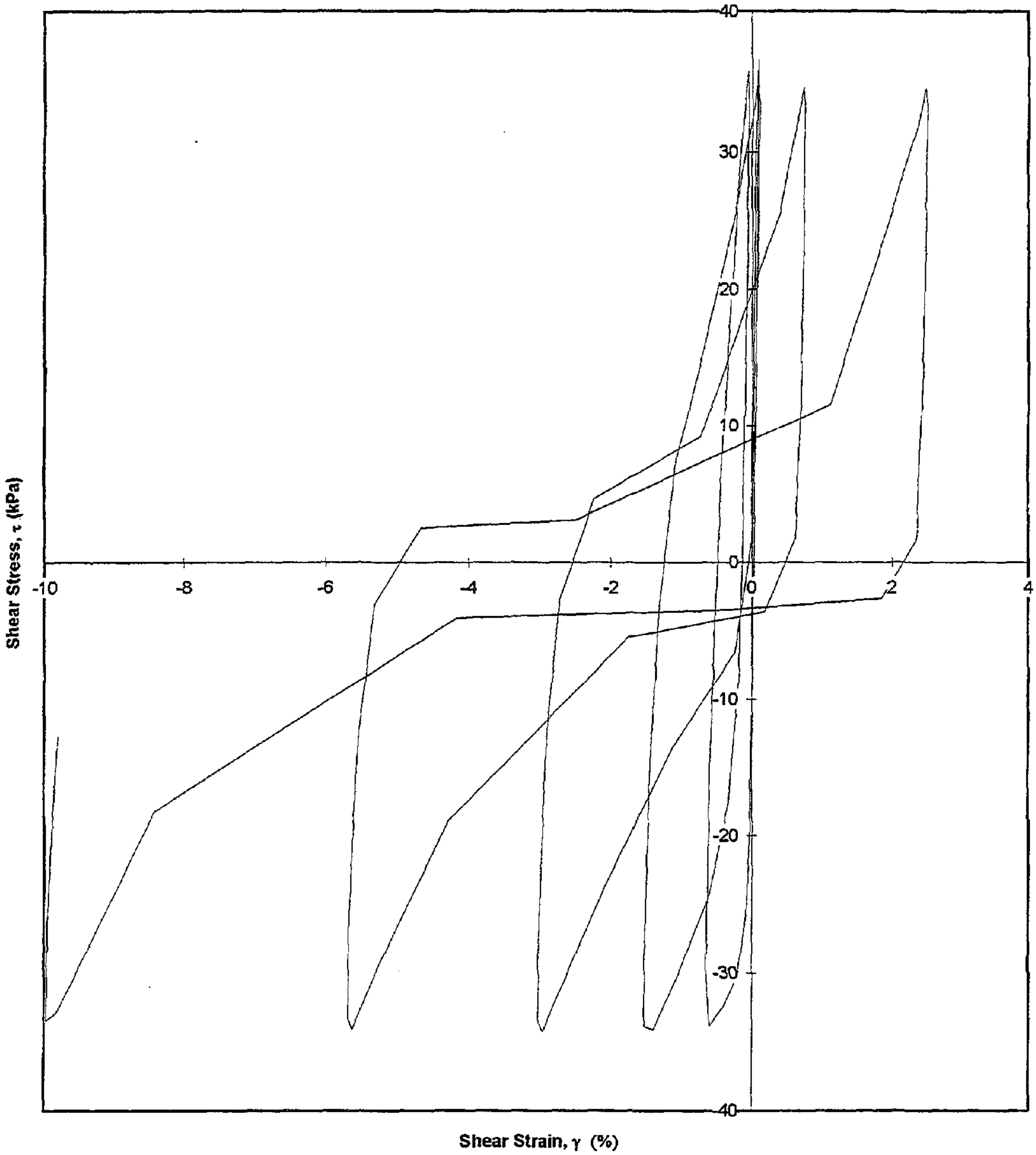

Test I.D.:	MONT30	**Controlled Parameter:**	Strain
Relative Density (%)	41.9	**Initial Effective Stress (kPa):**	100
Applied Shear Strain (%):	0.26	**Frequency (Hz):**	10

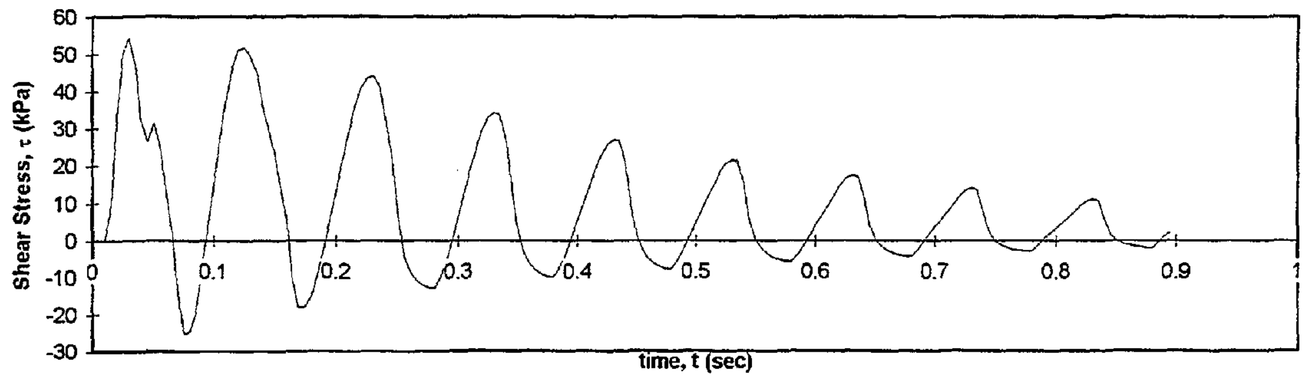

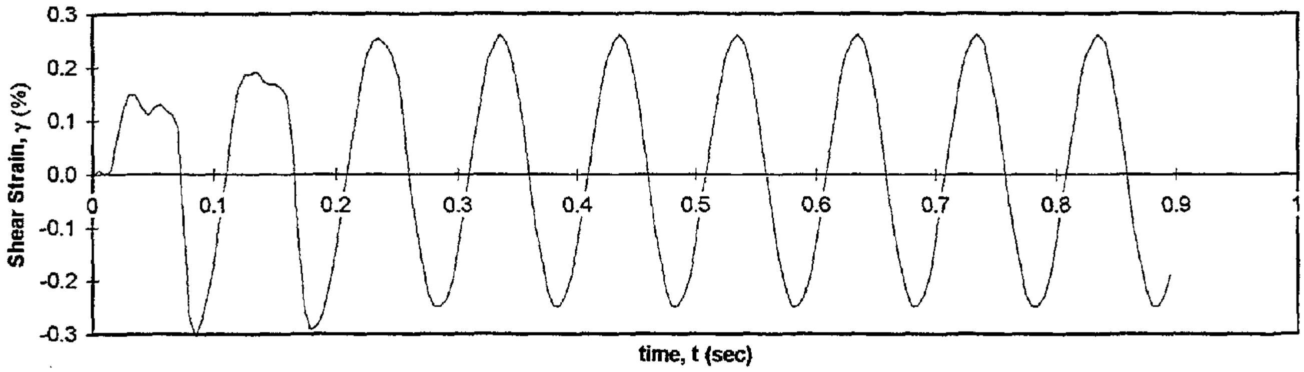

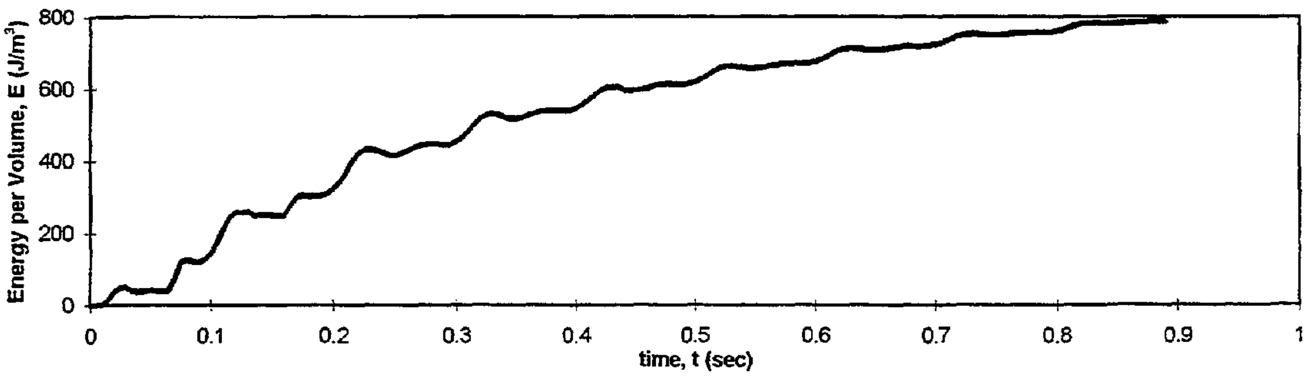

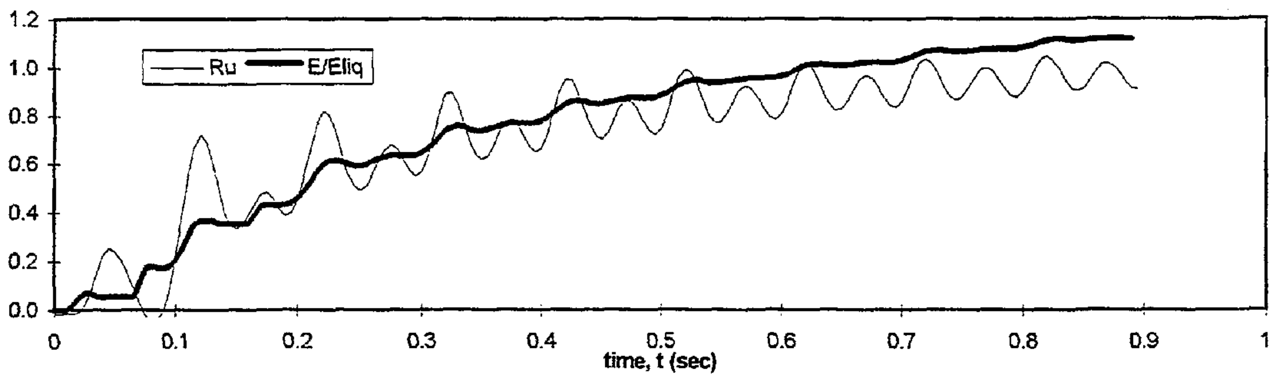

d:\nit\itp\cy_files\MONT30.XLS 8/21/96 9:08 AM

Test I.D.:	MONT30	**Controlled Parameter:**	Strain
Relative Density (%)	41.9	**Initial Effective Stress (kPa):**	100
Applied Shear Strain (%):	0.26	**Frequency (Hz):**	10

Shear Stress vs. Shear Strain

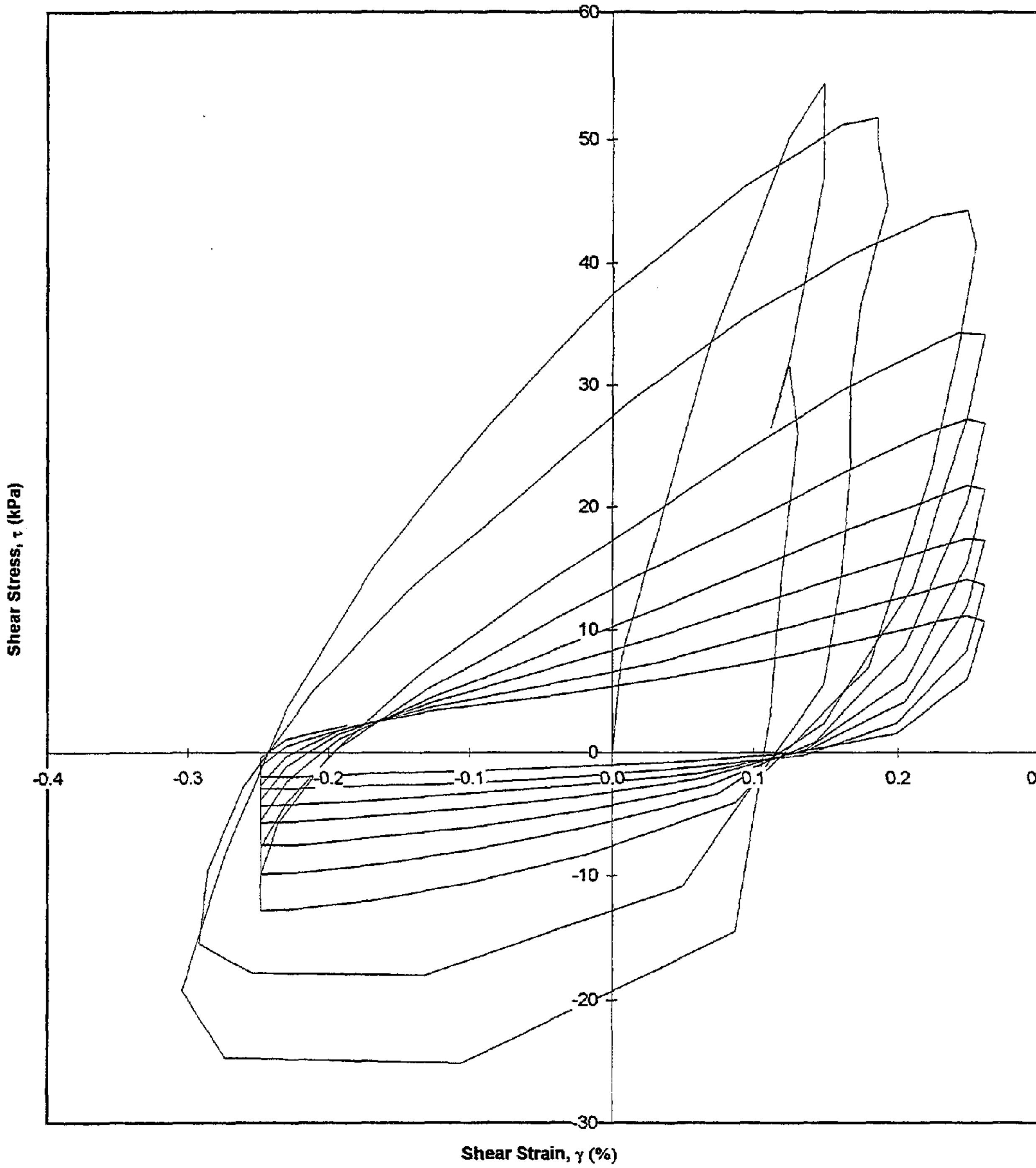

d:\nit\itp\cy_files\MONT30.XLS 8/21/96 9:08 AM

Test I.D.:	MONT33	**Controlled Parameter:**	Strain
Relative Density (%)	40.5	**Initial Effective Stress (kPa):**	100
Applied Shear Strain (%)	0.08	**Frequency (Hz):**	10

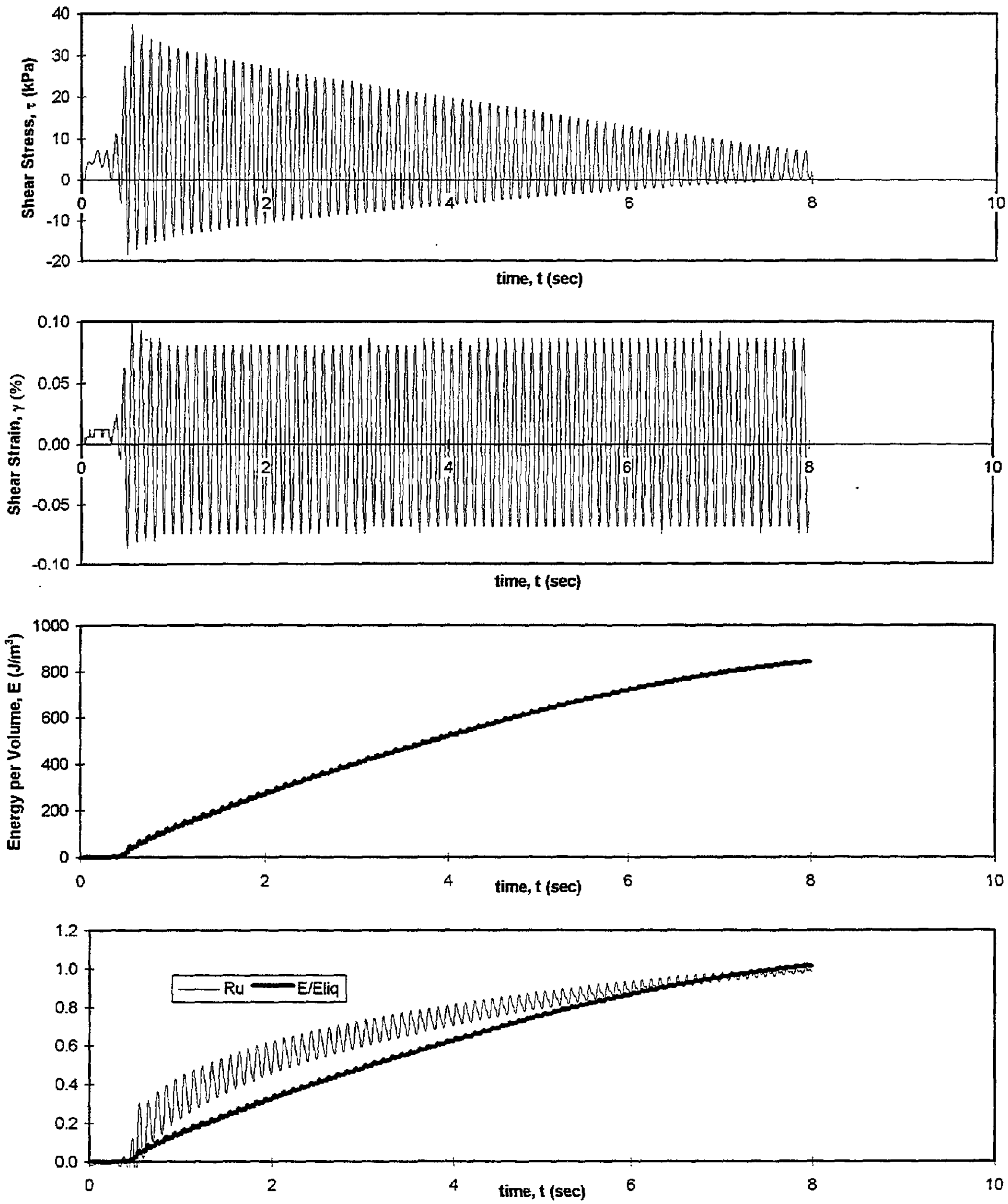

d:\nit\itp\cy_files\MONT33.XLS 8/20/96 9:22 AM

Test I.D.:	MONT33	**Controlled Parameter:**	Strain
Relative Density (%)	40.5	**Initial Effective Stress (kPa):**	100
Applied Shear Strain (%)	0.08	**Frequency (Hz):**	10

Shear Stress vs. Shear Strain

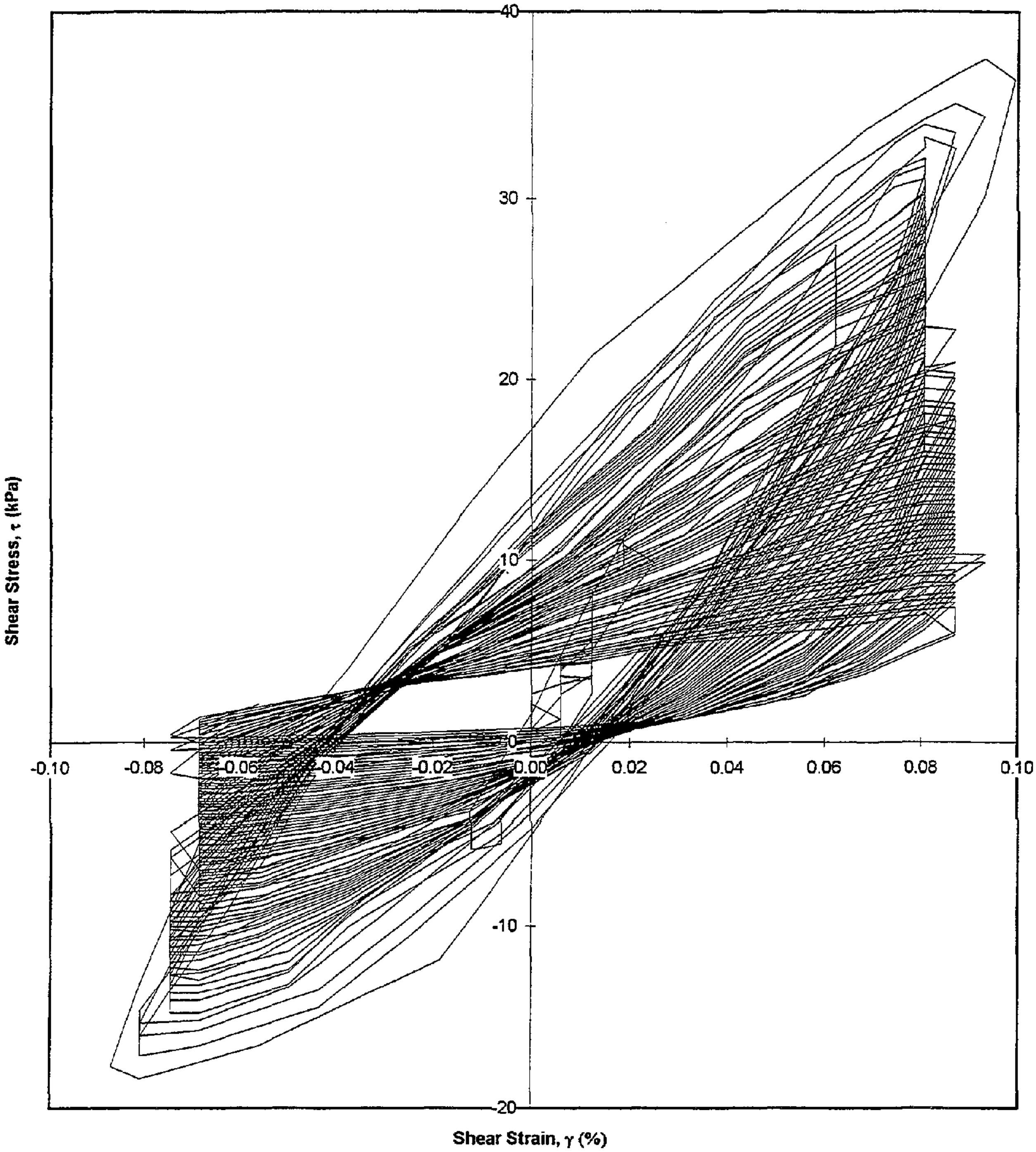

Test I.D.:	MONT35	**Controlled Parameter:**	Stress
Relative Density (%)	61.8	**Initial Effective Stress (kPa):**	100
Applied Stress Ratio:	0.35	**Frequency (Hz):**	0.1

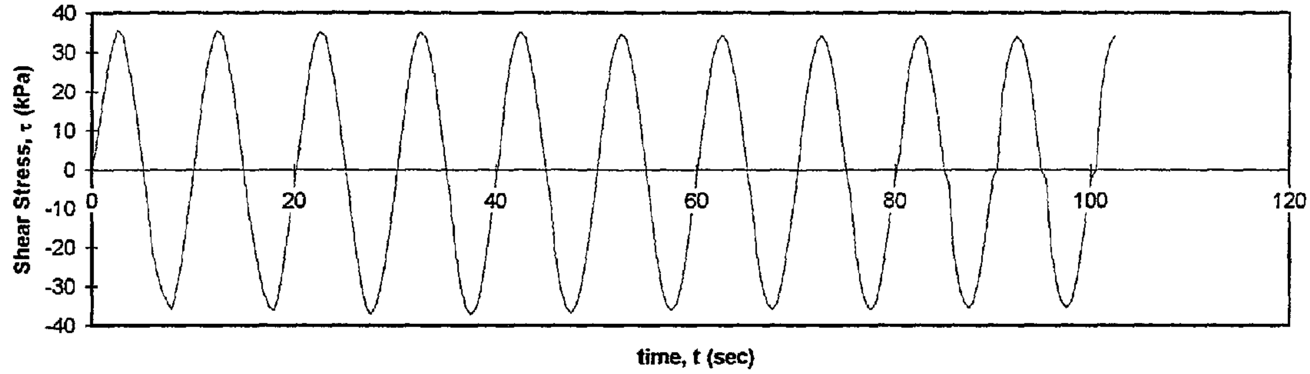

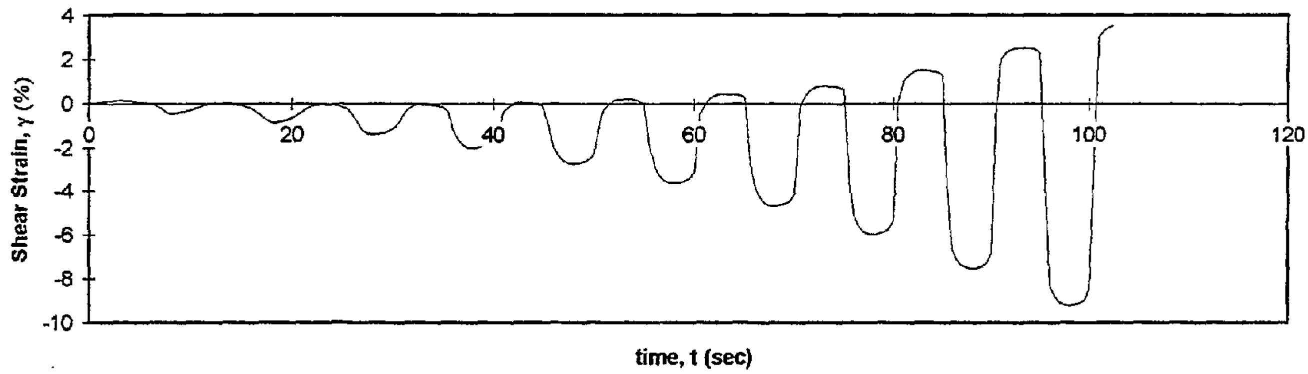

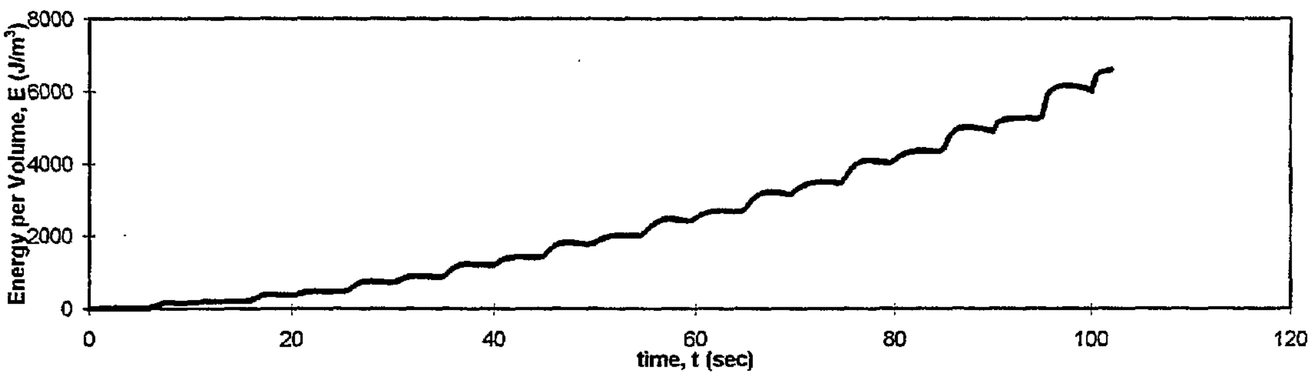

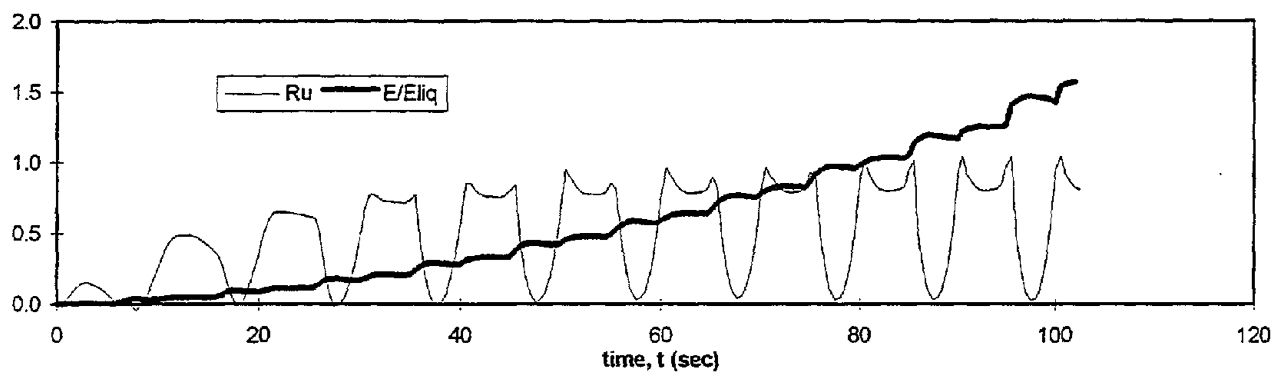

d:\nit\itp\cy_files\MONT35.XLS 8/20/96 10:42 AM

Test I.D.:	MONT35	**Controlled Parameter:**	Stress
Relative Density (%):	61.8	**Initial Effective Stress (kPa):**	100
Applied Stress Ratio:	0.35	**Frequency (Hz):**	0.1

Shear Stress vs. Shear Strain

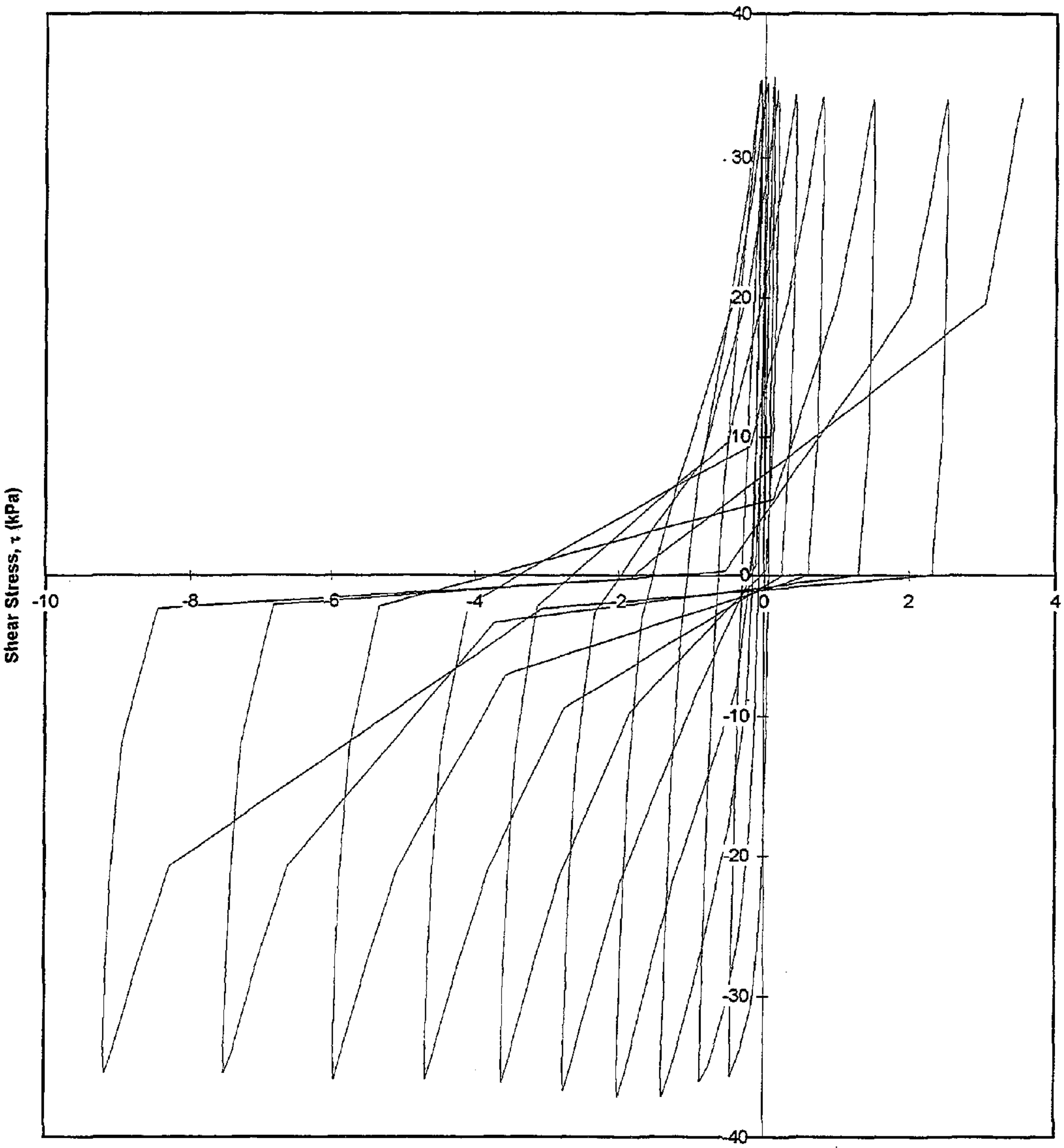

d:\nit\itp\cy_files\MONT35.XLS 8/20/96 10:42 AM

Test I.D.:	MONT37	**Controlled Parameter:**	Strain
Relative Density (%):	61.6	**Initial Effective Stress (kPa):**	100
Applied Shear Strain (%)	0.17	**Frequency (Hz):**	1

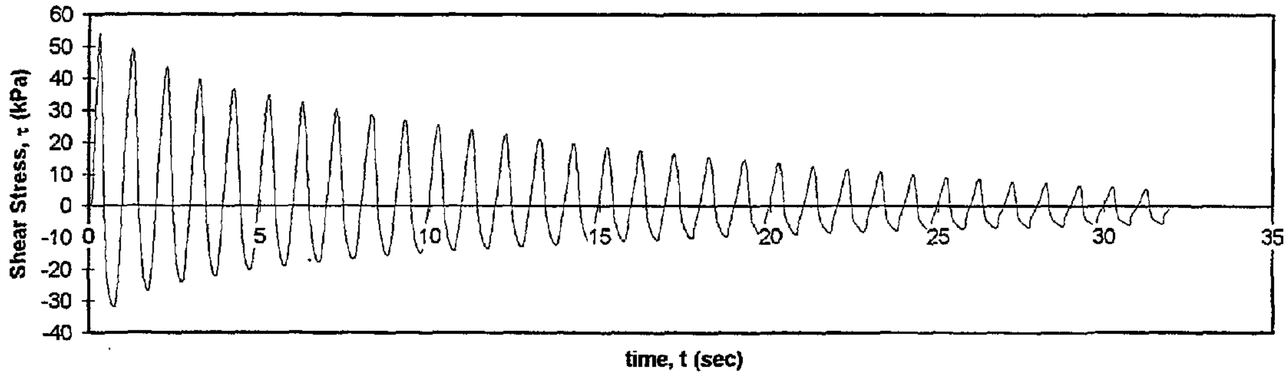

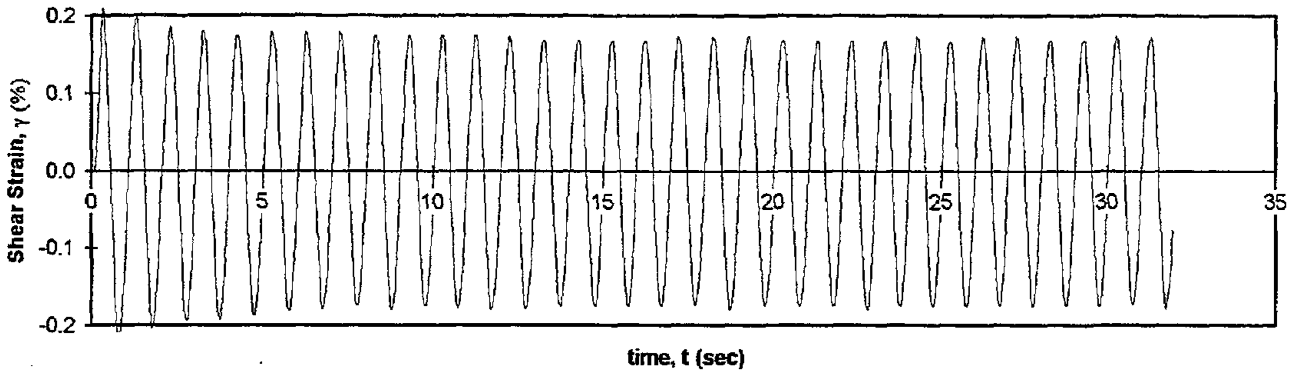

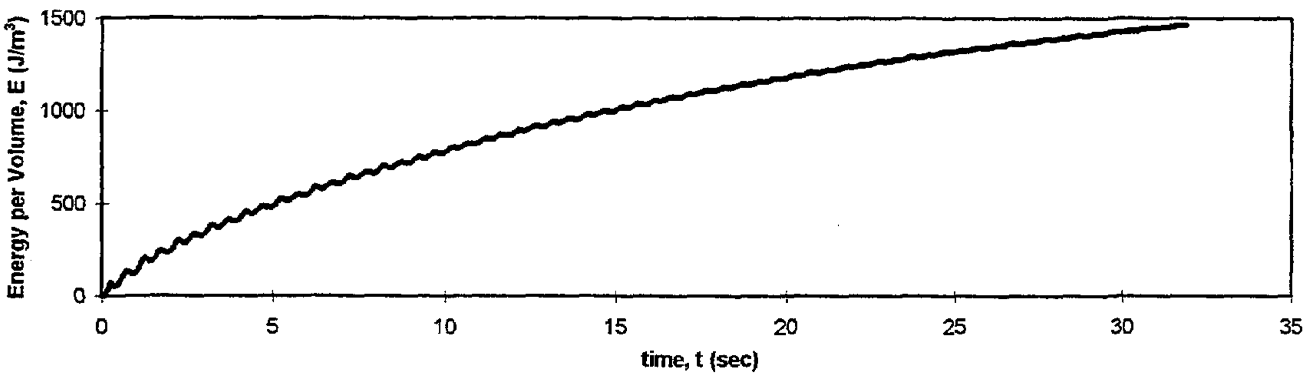

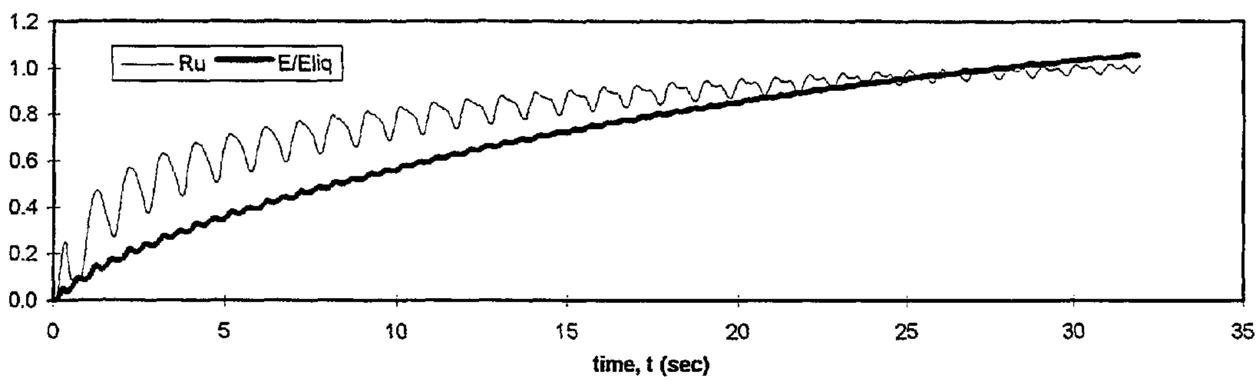

Test I.D.:	MONT37	**Controlled Parameter:**	Strain
Relative Density (%):	61.6	**Initial Effective Stress (kPa):**	100
Applied Shear Strain (%)	0.17	**Frequency (Hz):**	1

Shear Stress vs. Shear Strain

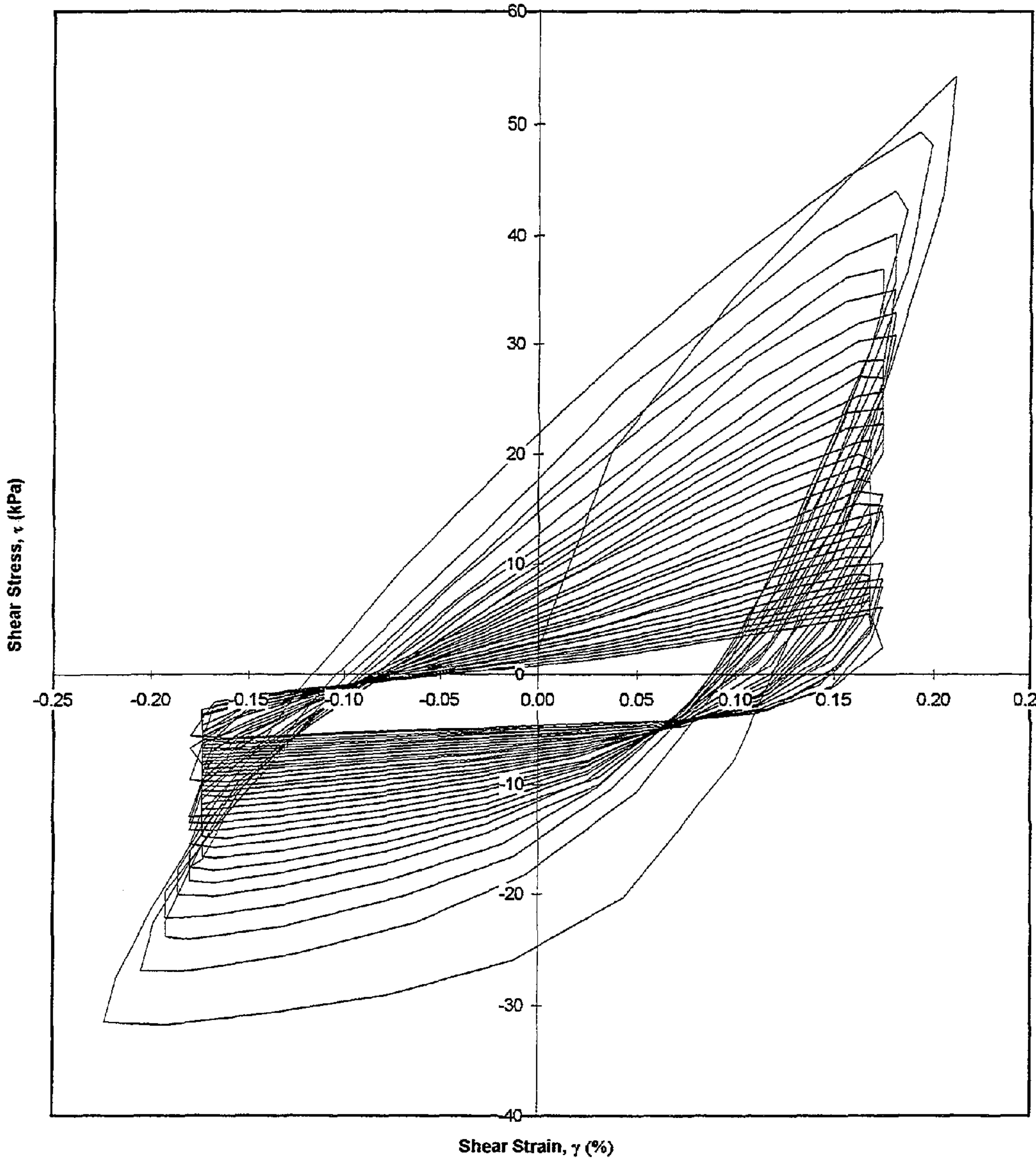

Test I.D.:	MONT38	**Controlled Parameter:**	Strain
Relative Density (%):	61.8	**Initial Effective Stress (kPa):**	100
Applied Shear Strain (%):	0.25	**Frequency (Hz):**	10

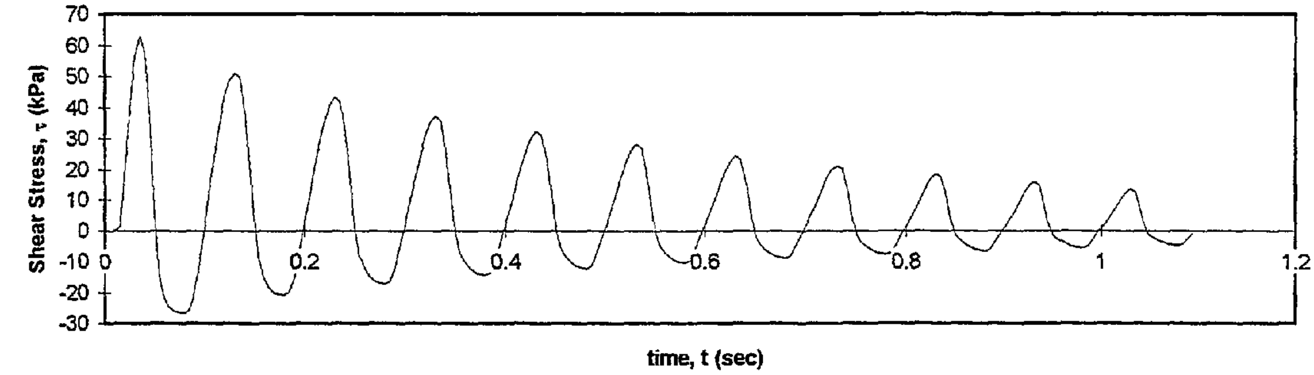

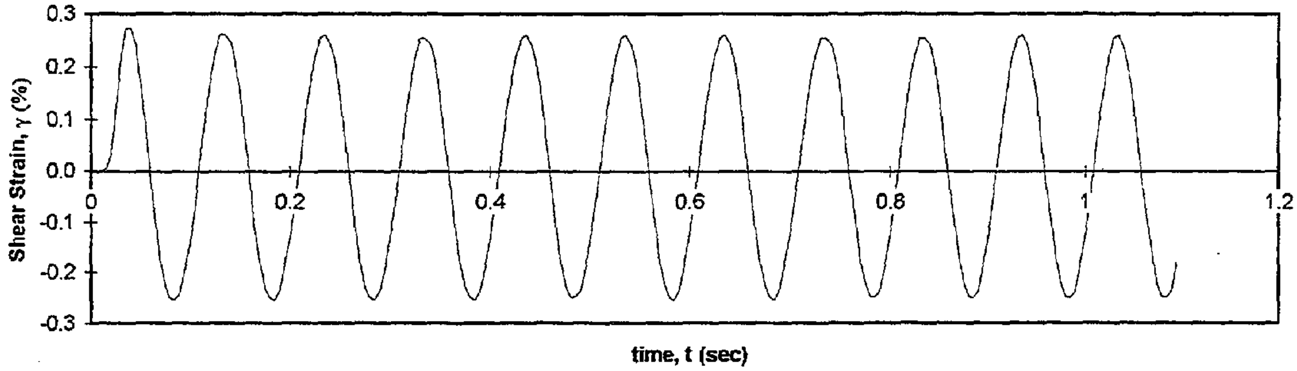

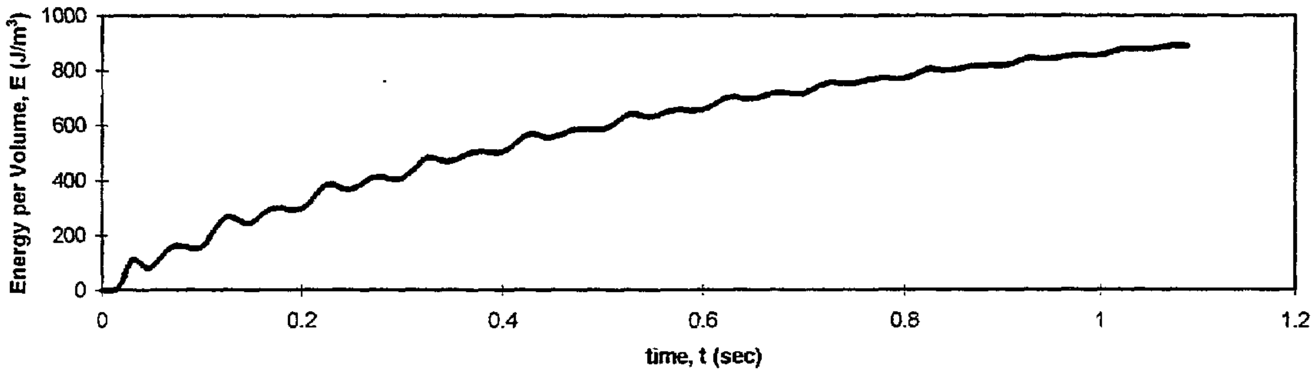

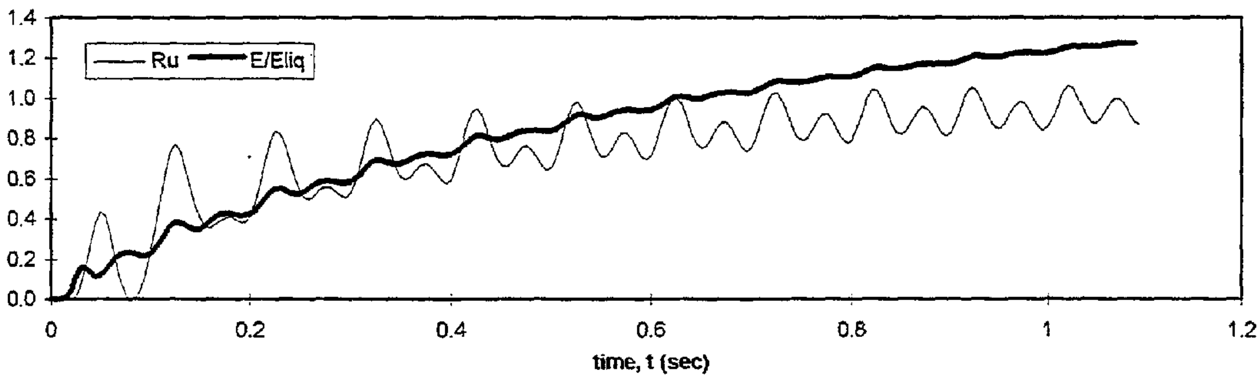

Test I.D.:	MONT38	**Controlled Parameter:**	Strain
Relative Density (%):	61.8	**Initial Effective Stress (kPa):**	100
Applied Shear Strain (%):	0.25	**Frequency (Hz):**	10

Shear Stress vs. Shear Strain

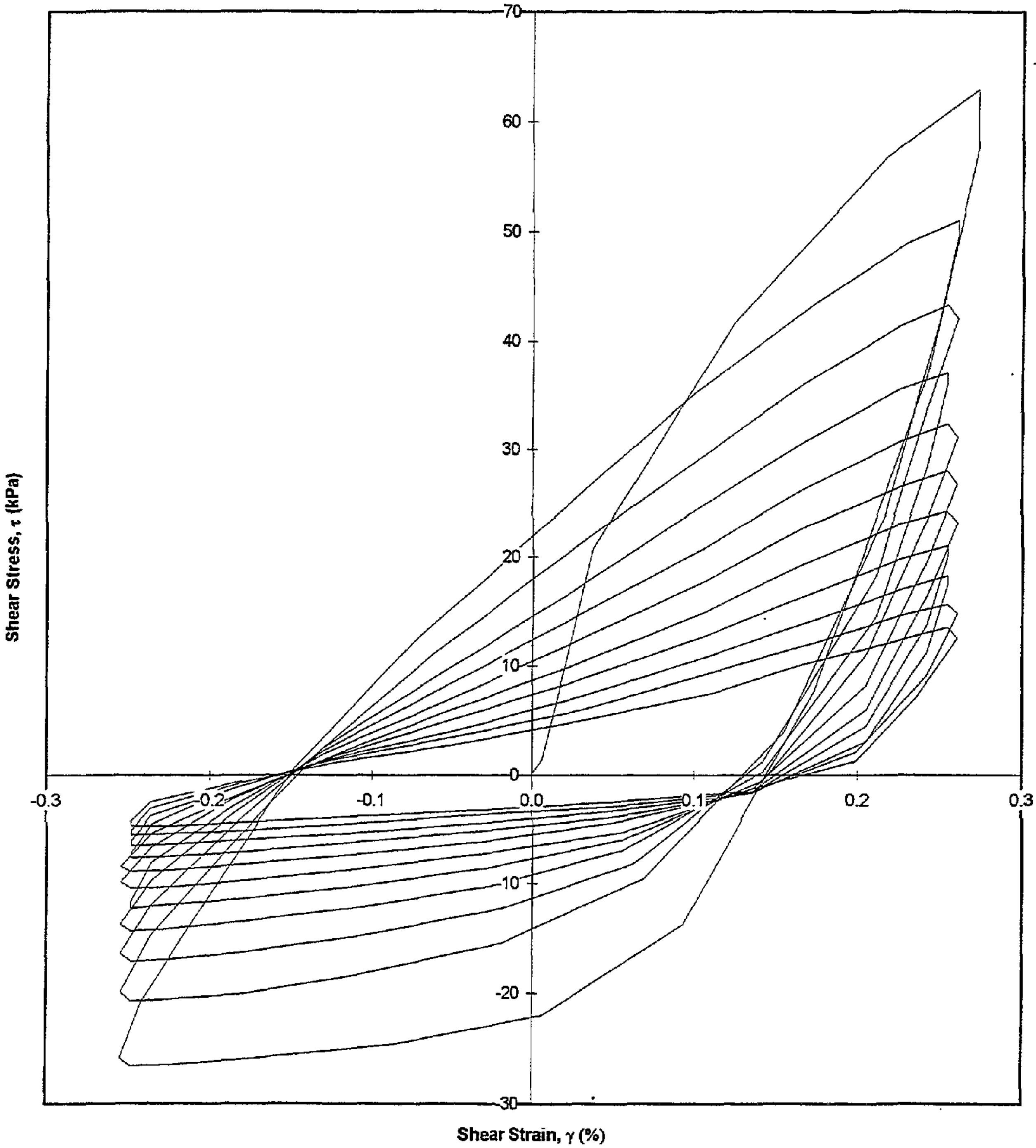

d:\nit\itp\cy_files\MONT38.XLS

8/20/96 10:54 AM

APPENDIX B

LABORATORY TESTS ON SOIL SAMPLES FROM THE SAVANNAH RIVER SITE, PERFORMED AT THE UNIVERSITY OF CALIFORNIA, BERKELEY

Table B.1 - Summary of the Cyclic Triaxial Test Data on SRS Soil Samples Performed at University of California, Berkeley

No.	Test ID	Sample	D_r(%)	E_{liq} (J/m^3)	FC (%)	γ_d (kN/m^3)	Control	σ_c' (kPa)	Freq. (Hz)	Load Shape
1	B23P2BCY	Santee	N/A	14675	33.7	16.0	Stress	400	1	Sinusoidal 2-way
2	B23P2MCY	Santee	N/A	16782	35.6	16.4	Stress	400	1	Sinusoidal 2-way
3	B23P2TCY	Santee	N/A	11402	32.6	16.8	Stress	400	1	Sinusoidal 2-way
4	B23P3BCY	Tobacco Rd.	N/A	4929	16.6	16.4	Stress	200	1	Sinusoidal 2-way
5	B23P3MCY	Tobacco Rd.	N/A	5585	18.5	15.2	Stress	200	1	Sinusoidal 2-way
6	B23P3TCY	Tobacco Rd.	N/A	2924	20.5	16.6	Stress	200	1	Sinusoidal 2-way
7	B12P5BCY	Tobacco Rd.	N/A	14918	27.0	15.8	Stress	300	1	Sinusoidal 2-way
8	B12P5MCY	Tobacco Rd.	N/A	49114	26.8	16.8	Stress	300	1	Sinusoidal 2-way
9	B12P5TCY	Tobacco Rd.	N/A	5450	22.3	18.0	Stress	300	1	Sinusoidal 2-way
10	B12P7BCY	Tobacco Rd.	N/A	7666	15.7	15.9	Stress	375	1	Sinusoidal 2-way
11	B12P7MCY	Tobacco Rd.	N/A	14482	17.0	16.3	Stress	375	1	Sinusoidal 2-way
12	B12P7TCY	Tobacco Rd.	N/A	3852	15.7	16.2	Stress	375	1	Sinusoidal 2-way
13	B2P5BCYC	Tobacco Rd.	N/A	11672	25.4	14.7	Stress	500	1	Sinusoidal 2-way
14	B2P5MCYC	Tobacco Rd.	N/A	23344	29.6	15.4	Stress	500	1	Sinusoidal 2-way
15	B2P5TCYC	Tobacco Rd.	N/A	8819	26.6	16.7	Stress	500	1	Sinusoidal 2-way
16	B23P4BCY	Tobacco Rd.	N/A	21667	11.4	14.6	Stress	750	1	Sinusoidal 2-way
17	B23P4MCY	Tobacco Rd.	N/A	36680	16.5	15.5	Stress	700	1	Sinusoidal 2-way
18	B23P4TCY	Tobacco Rd.	N/A	17968	28.0	N/A	Stress	750	1	Sinusoidal 2-way
19	B29P2TCY	Tobacco Rd.	N/A	23637	23.0	16.7	Stress	750	1	Sinusoidal 2-way
20	B2P6BCY	Tobacco Rd.	N/A	17985	18.9	16.7	Stress	725	1	Sinusoidal 2-way
21	B2P6MCY	Tobacco Rd.	N/A	19831	20.1	16.5	Stress	743	1	Sinusoidal 2-way
22	B2P6TCYC	Tobacco Rd.	N/A	14446	22.4	16.0	Stress	750	1	Sinusoidal 2-way

Test Results Following the Sequence of Test ID's are Attached.

Test I.D.:	B23P2BCY	**Controlled Parameter:**	Stress
Fines Content (%):	33.7	**Initial Effective Stress (kPa):**	400
Dry Density (kN/m³):	16.04		

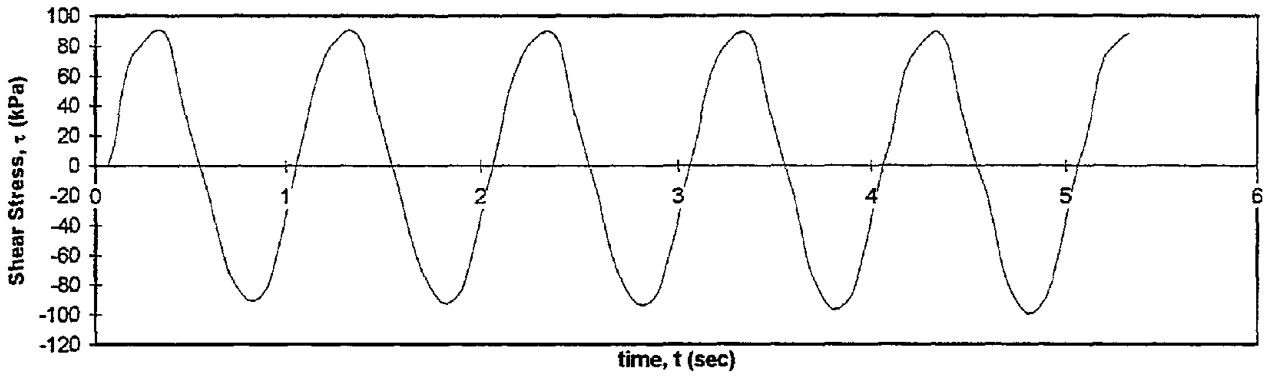

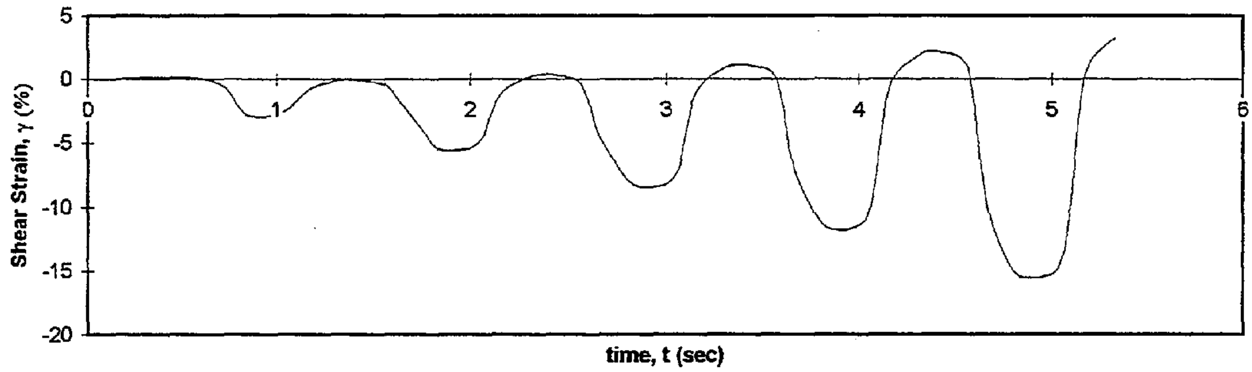

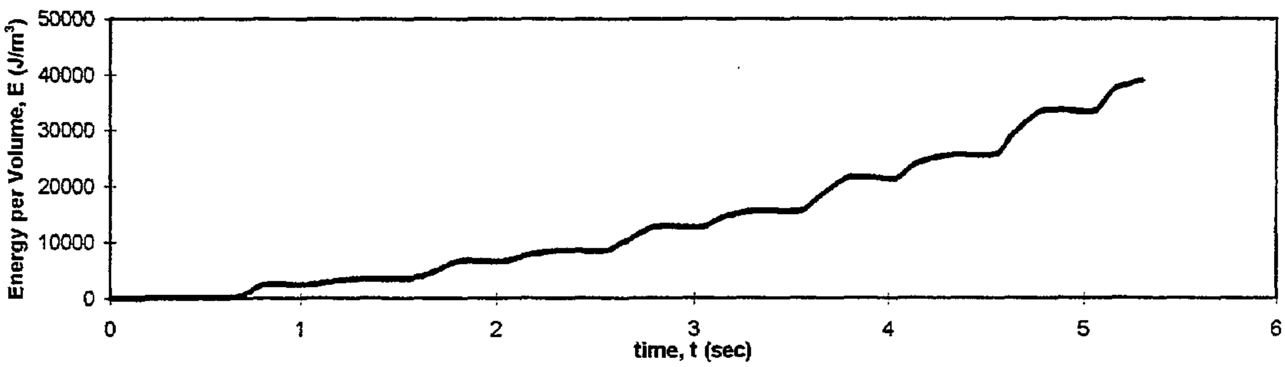

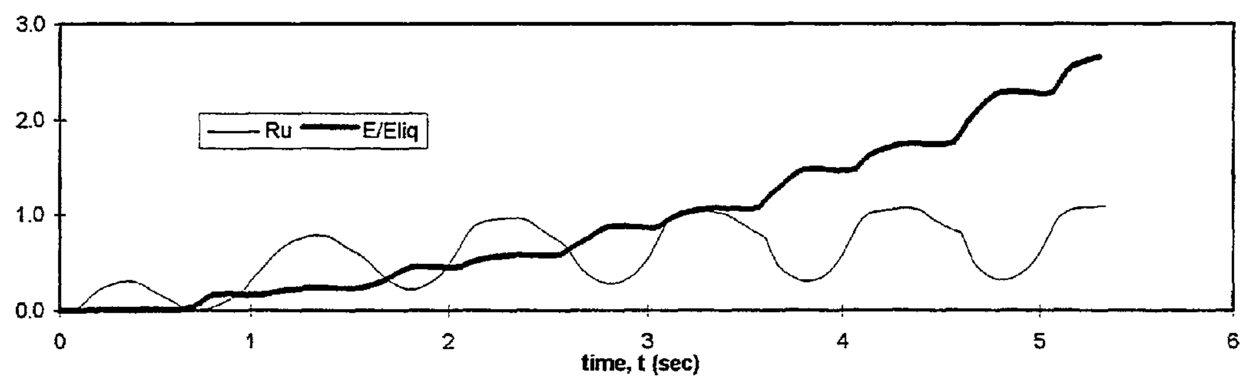

Test I.D.:	B23P2BCY	**Controlled Parameter:**	Stress
Fines Content (%):	33.7	**Initial Effective Stress (kPa):**	400
Dry Density (kN/m^3):	16.04		

Shear Stress vs. Shear Strain

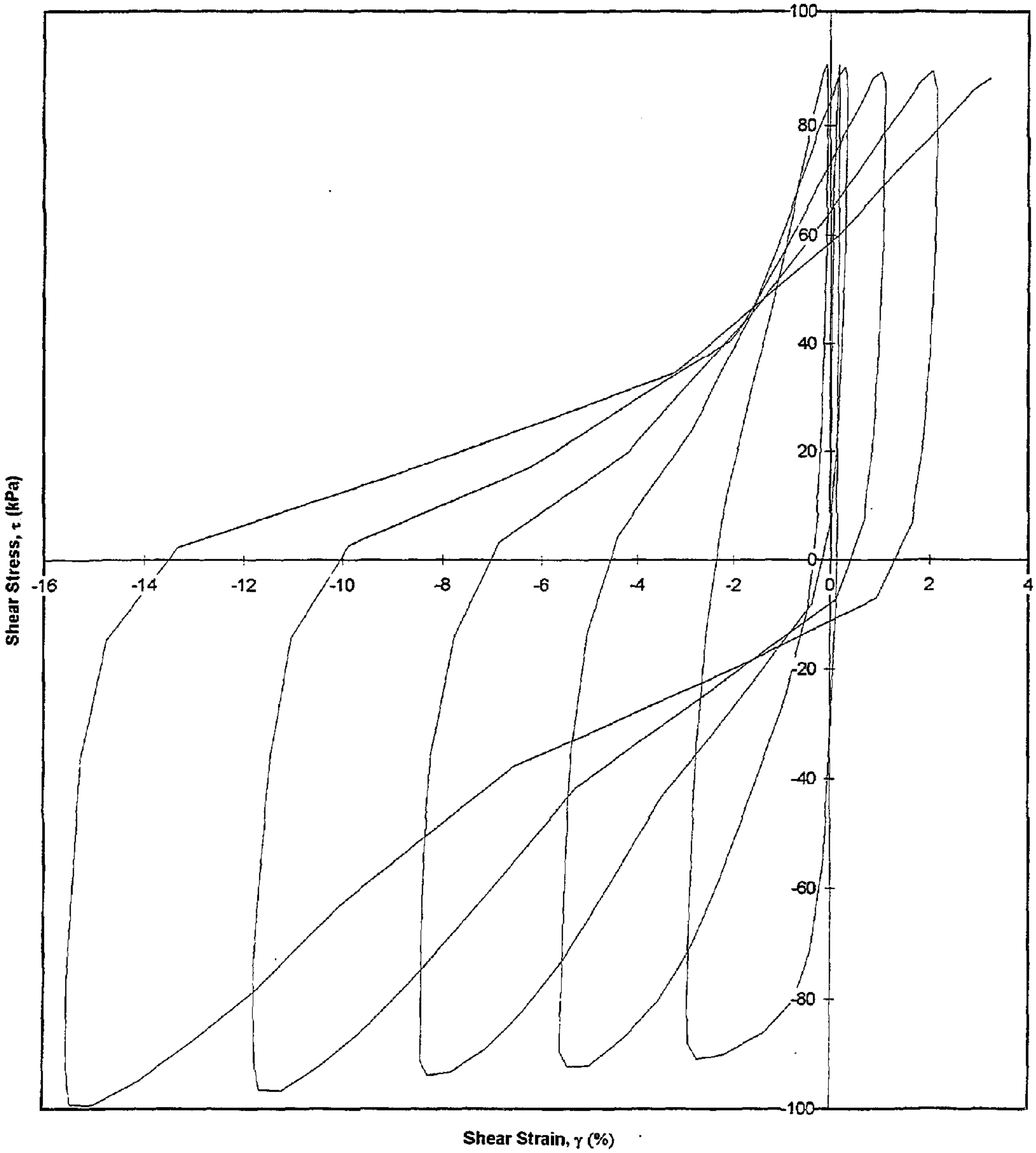

Test I.D.:	B23P2MCY	**Controlled Parameter:**	Stress
Fines Content (%):	35.6	**Initial Effective Stress (kPa):**	400
Dry Density (kN/m^3):	16.43		

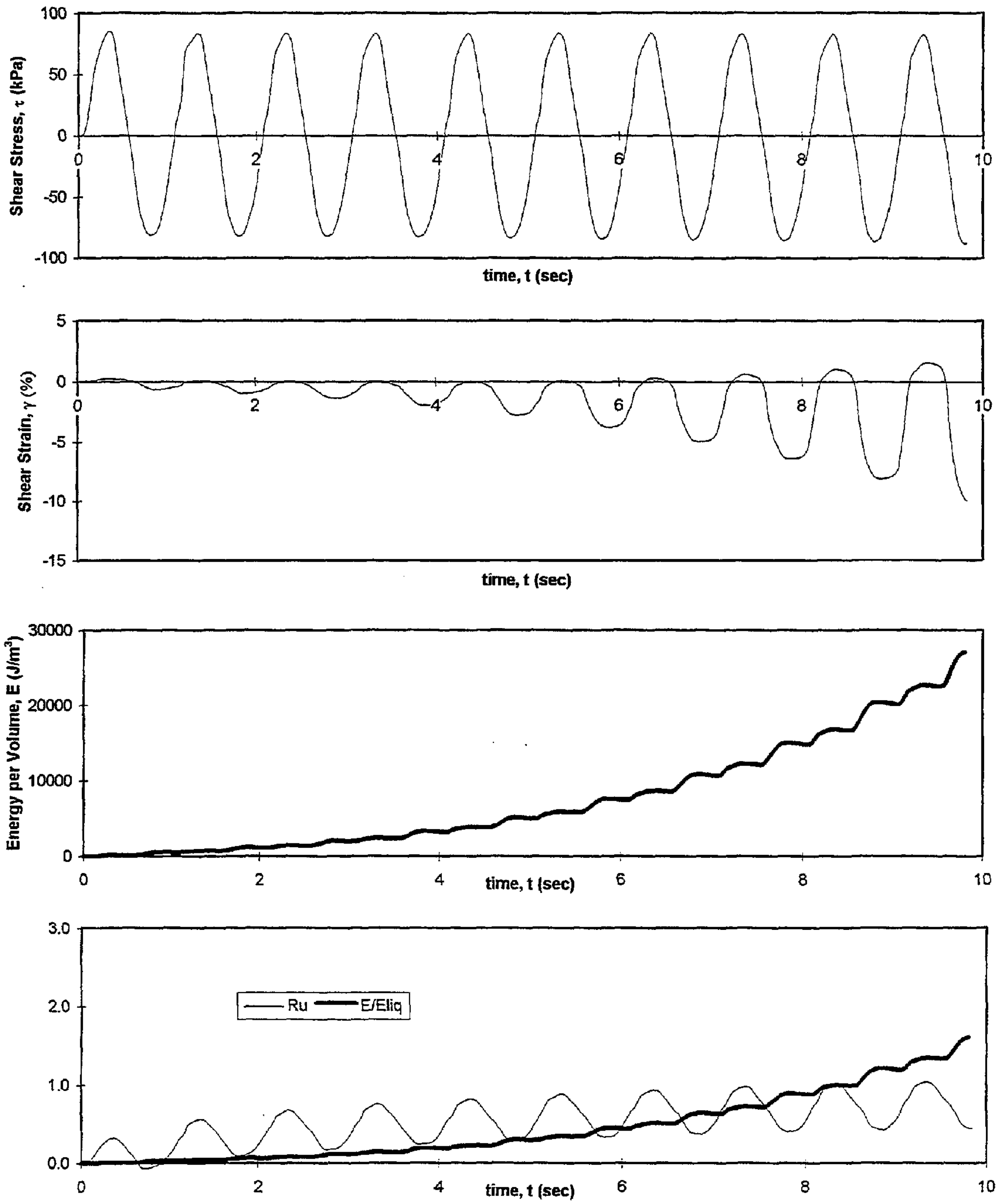

Test I.D.:	B23P2MCY	**Controlled Parameter:**	Stress
Fines Content (%):	35.6	**Initial Effective Stress (kPa):**	400
Dry Density (kN/m³):	16.43		

Shear Stress vs. Shear Strain

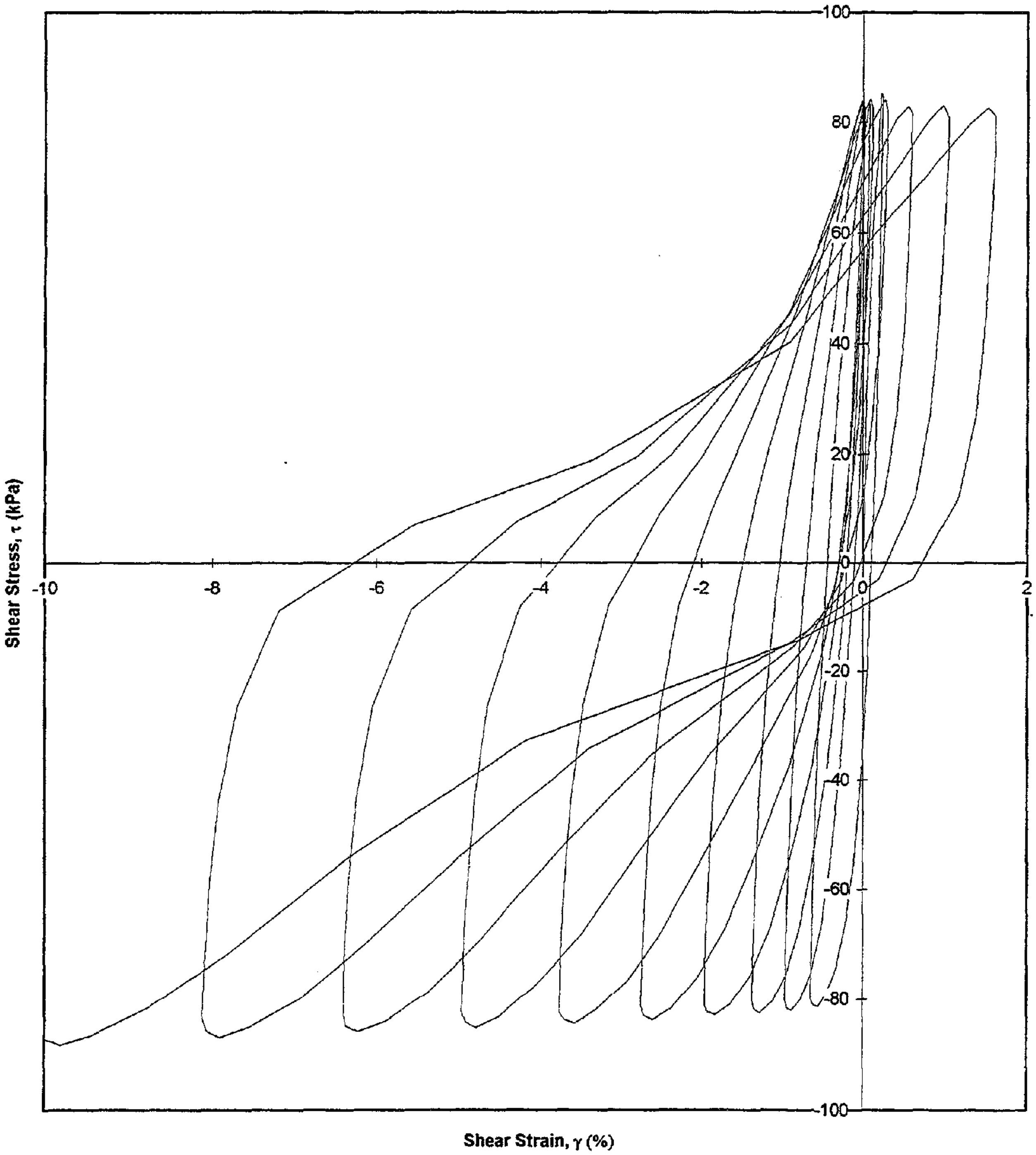

d:\nit\itp\cy_files\B23P2MCY.XLS

8/21/96 9:49 AM

Test I.D.:	B23P2TCY	**Controlled Parameter:**	Stress
Fines Content (%):	32.6	**Initial Effective Stress (kPa):**	400
Dry Density (kN/m³):	16.75		

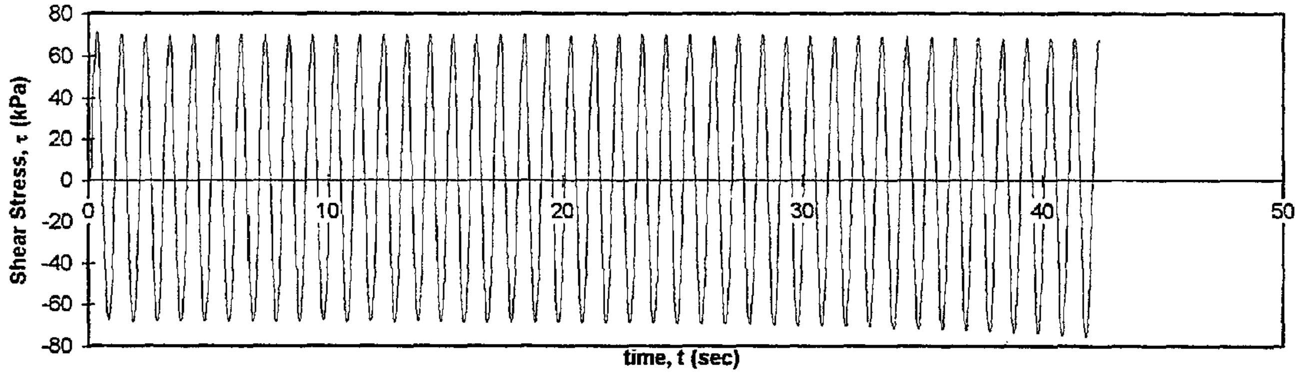

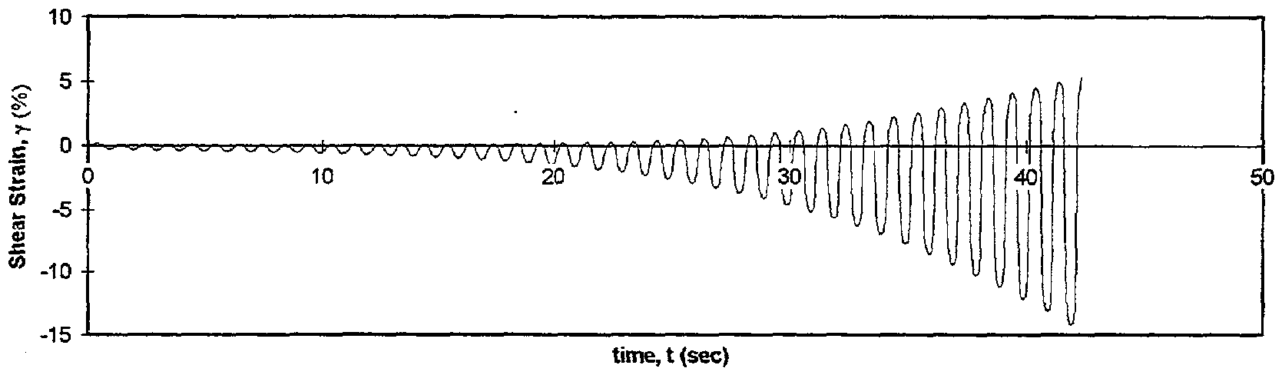

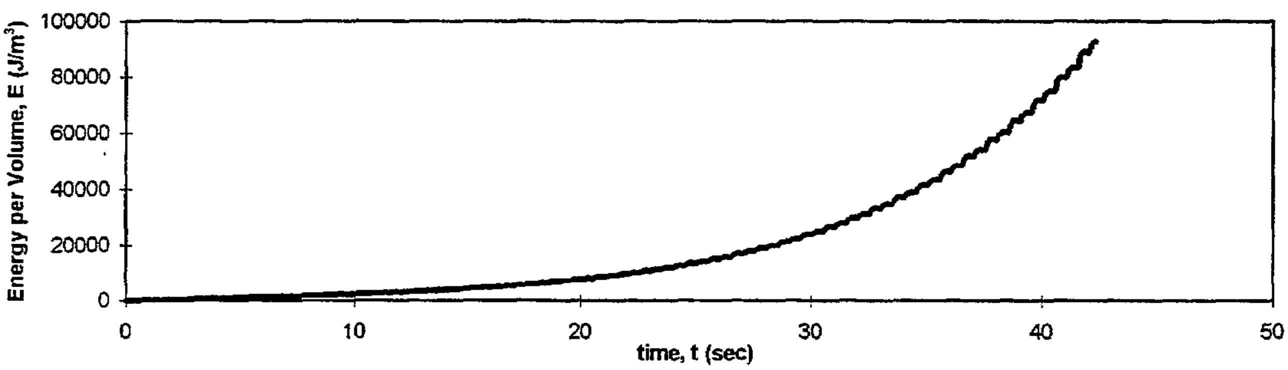

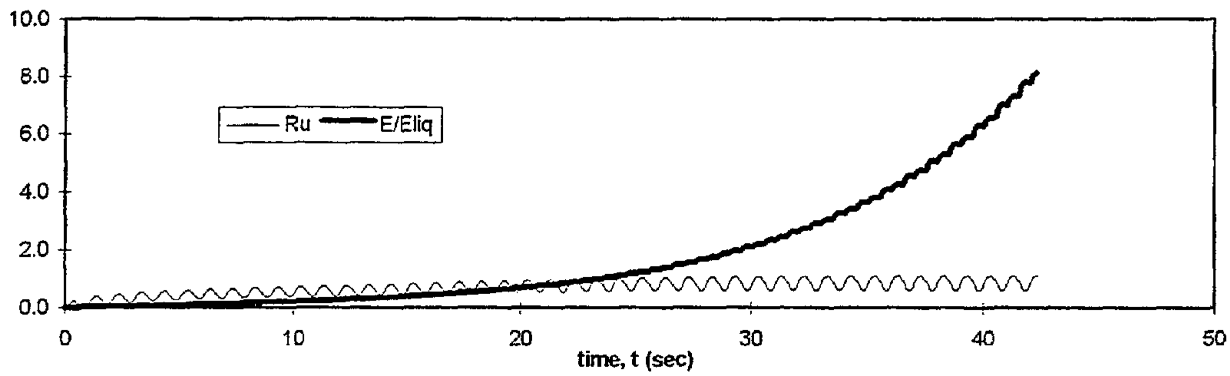

Test I.D.:	B23P2TCY	**Controlled Parameter:**	Stress
Fines Content (%):	32.6	**Initial Effective Stress (kPa):**	400
Dry Density (kN/m^3):	16.75		

Shear Stress vs. Shear Strain

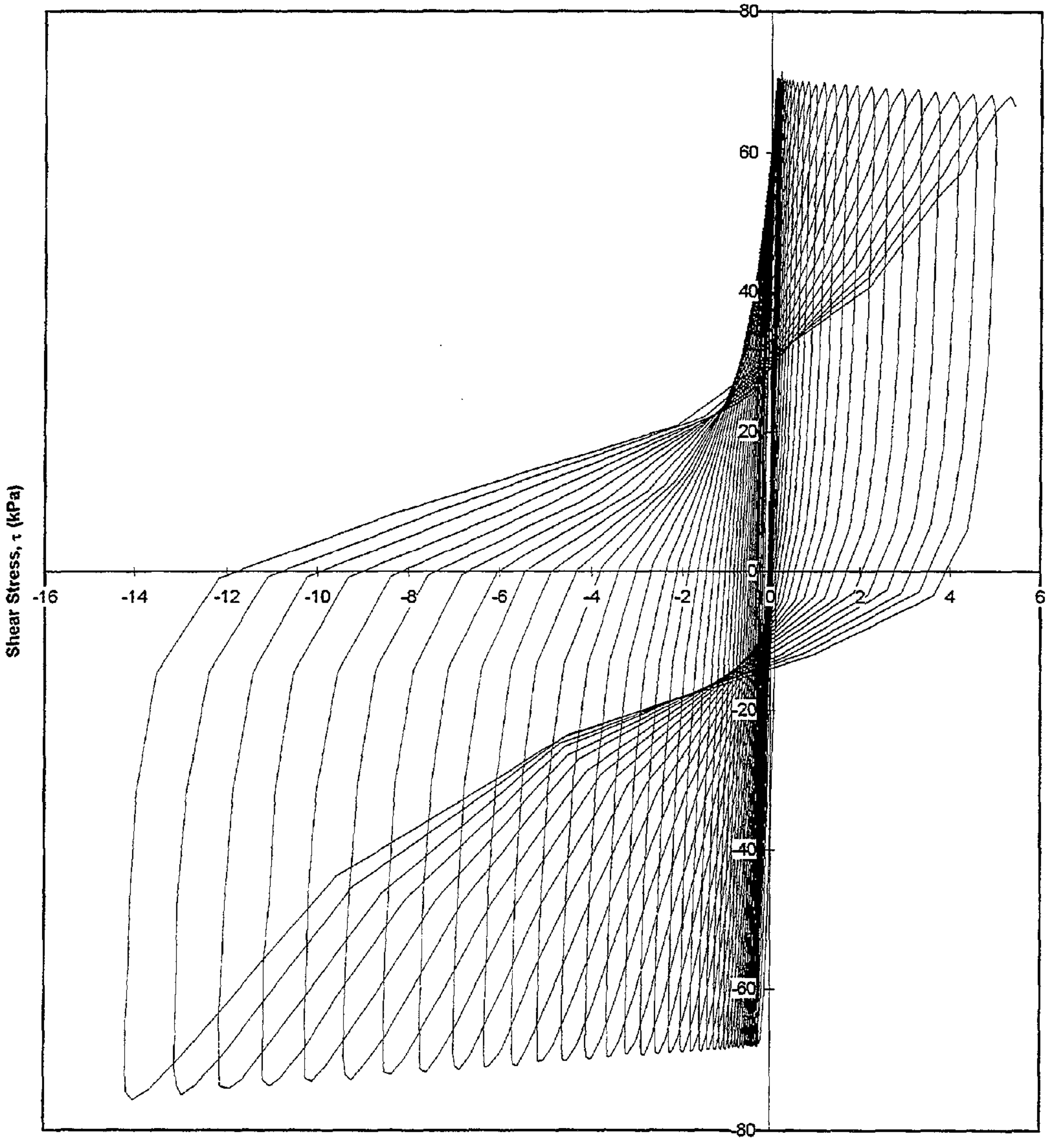

d:\nit\itp\cy_files\B23P2TCY.XLS

8/21/96 7:44 AM

Test I.D.:	B23P3BCY	**Controlled Parameter:**	Stress
Fines Content (%):	16.6	**Initial Effective Stress (kPa):**	200
Dry Density (kN/m³):	16.4		

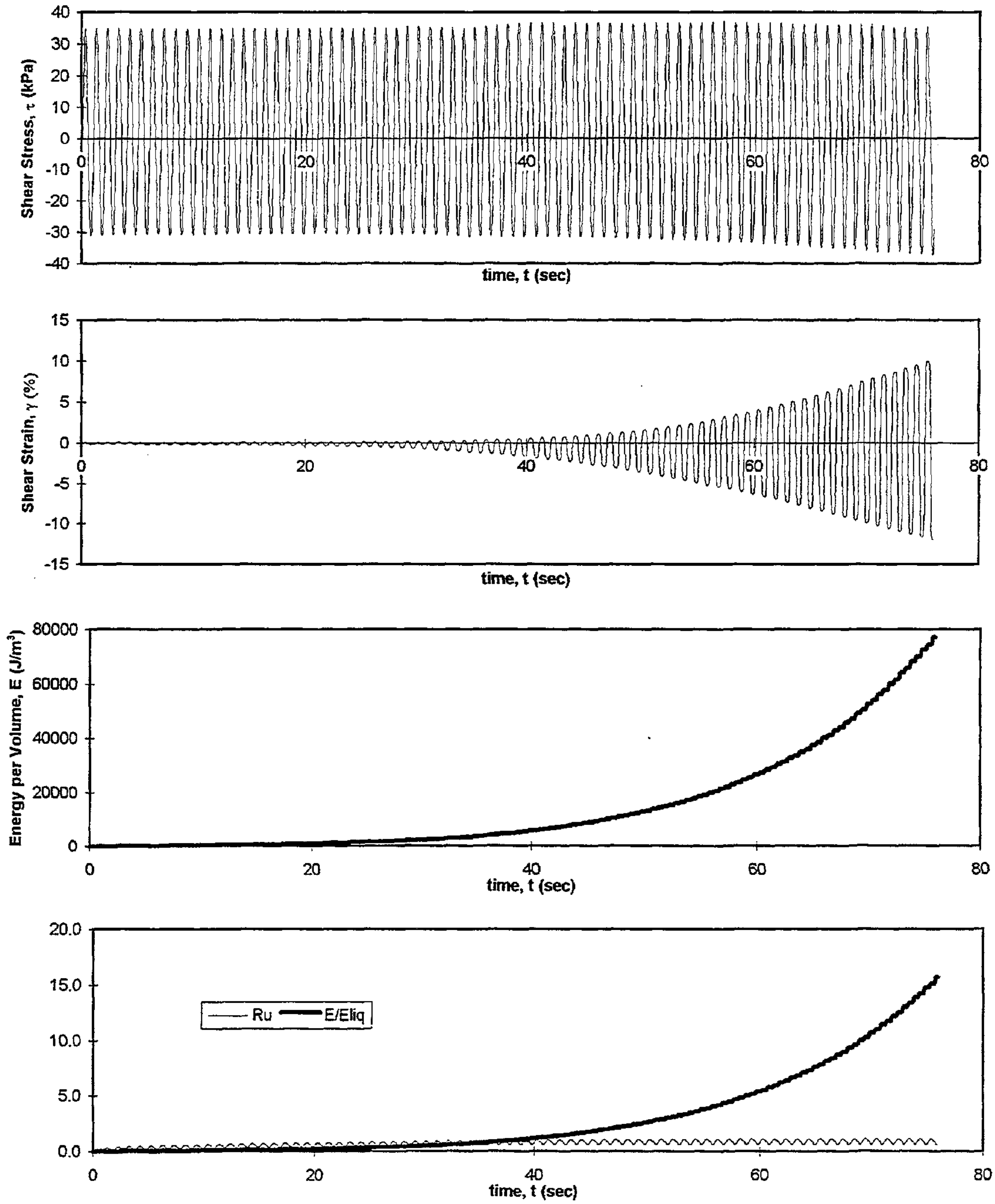

Test I.D.:	B23P3BCY	**Controlled Parameter:**	Stress
Fines Content (%):	16.6	**Initial Effective Stress (kPa):**	200
Dry Density (kN/m^3):	16.4		

Shear Stress vs. Shear Strain

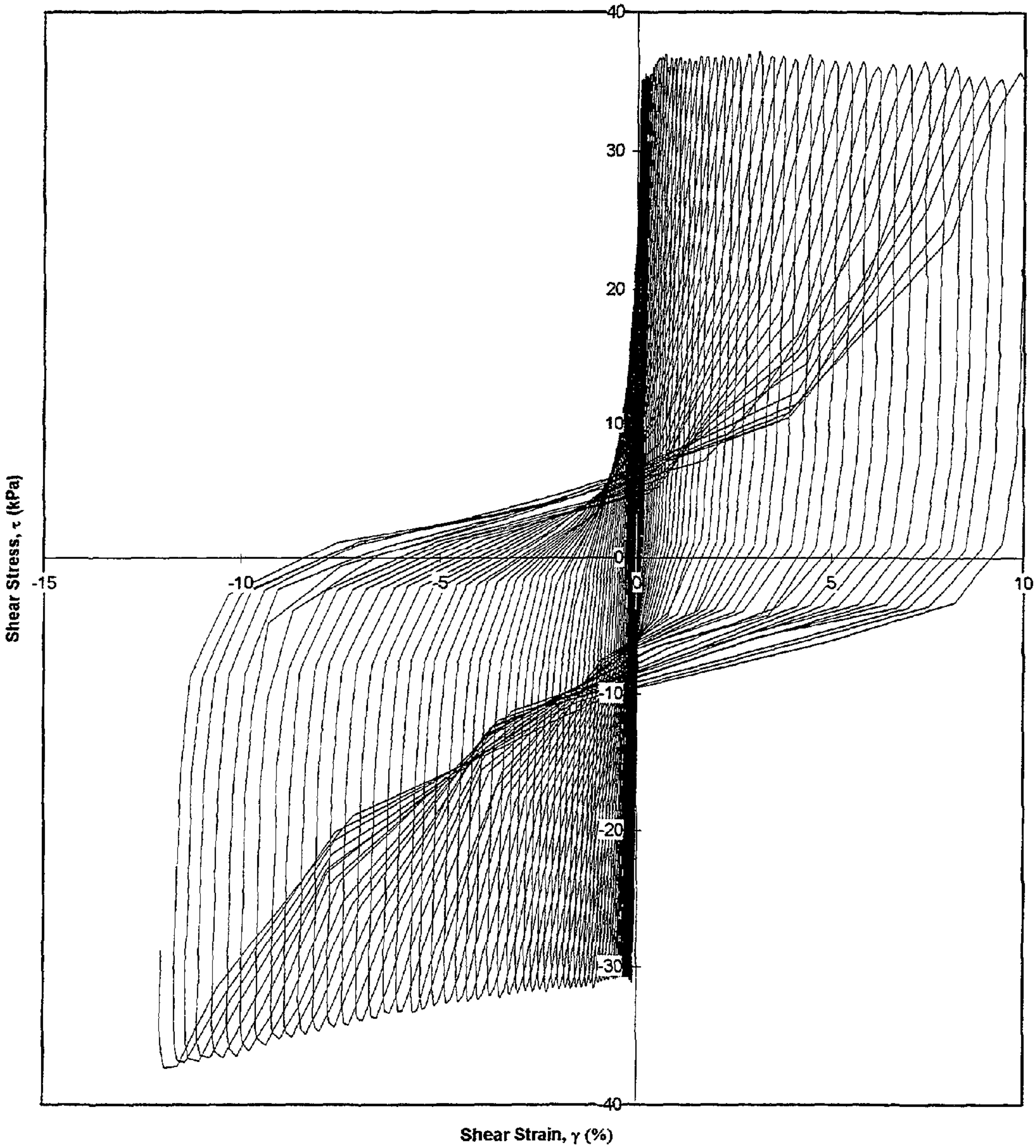

d:\nit\itp\cy_files\B23P3BCY.XLS 8/21/96 7:48 AM

Test I.D.:	B23P3MCY	**Controlled Parameter:**	Stress
Fines Content (%):	18.5	**Initial Effective Stress (kPa):**	200
Dry Density (kN/m³):	15.22		

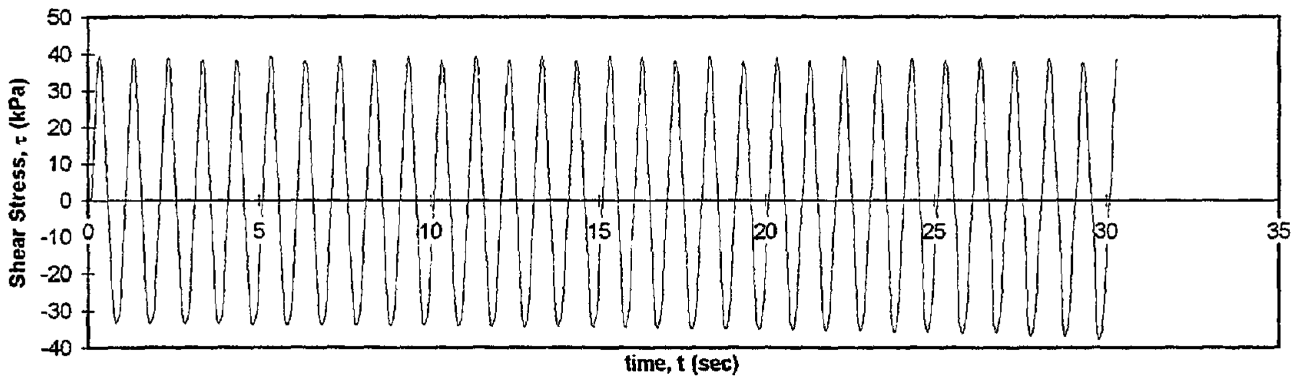

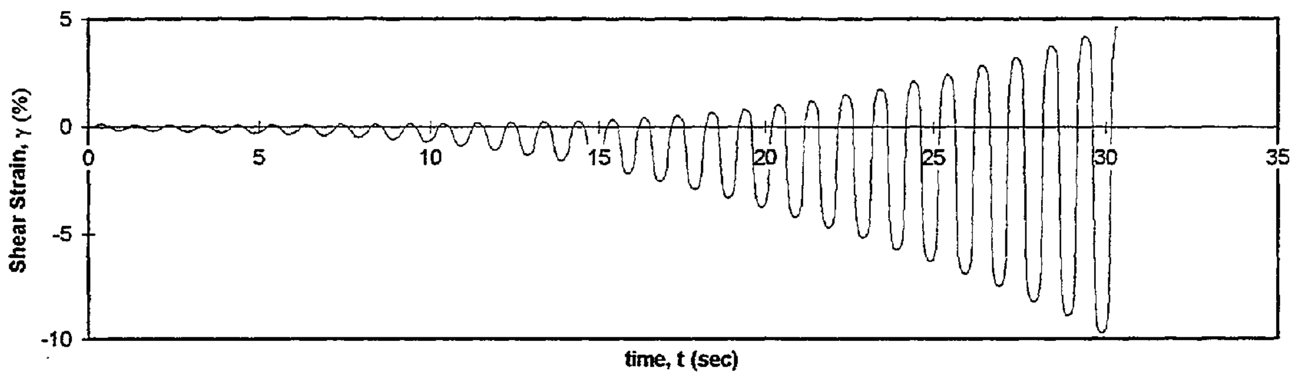

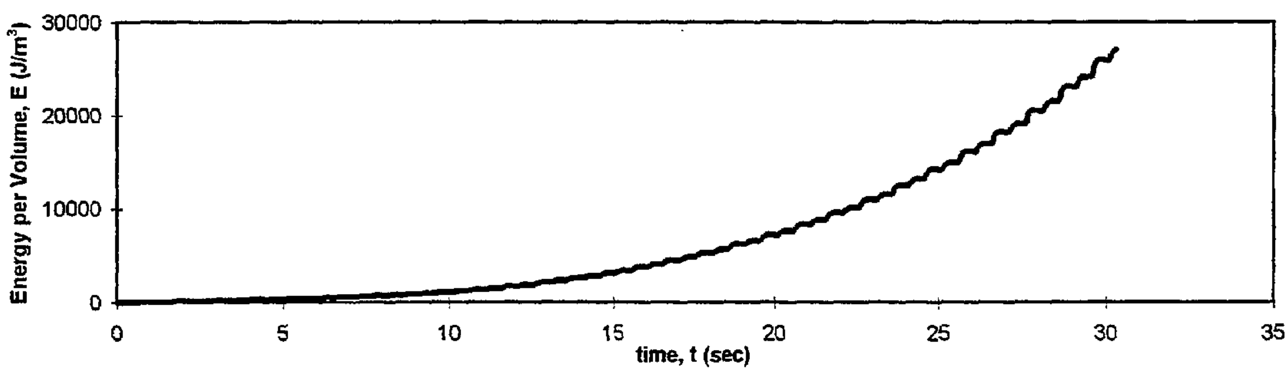

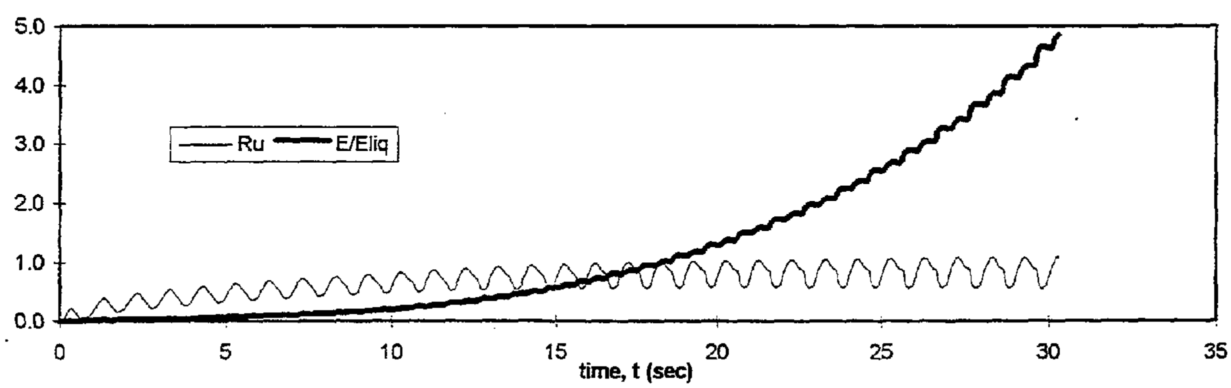

Test I.D.:	B23P3MCY	**Controlled Parameter:**	Stress
Fines Content (%):	18.5	**Initial Effective Stress (kPa):**	200
Dry Density (kN/m³):	15.22		

Shear Stress vs. Shear Strain

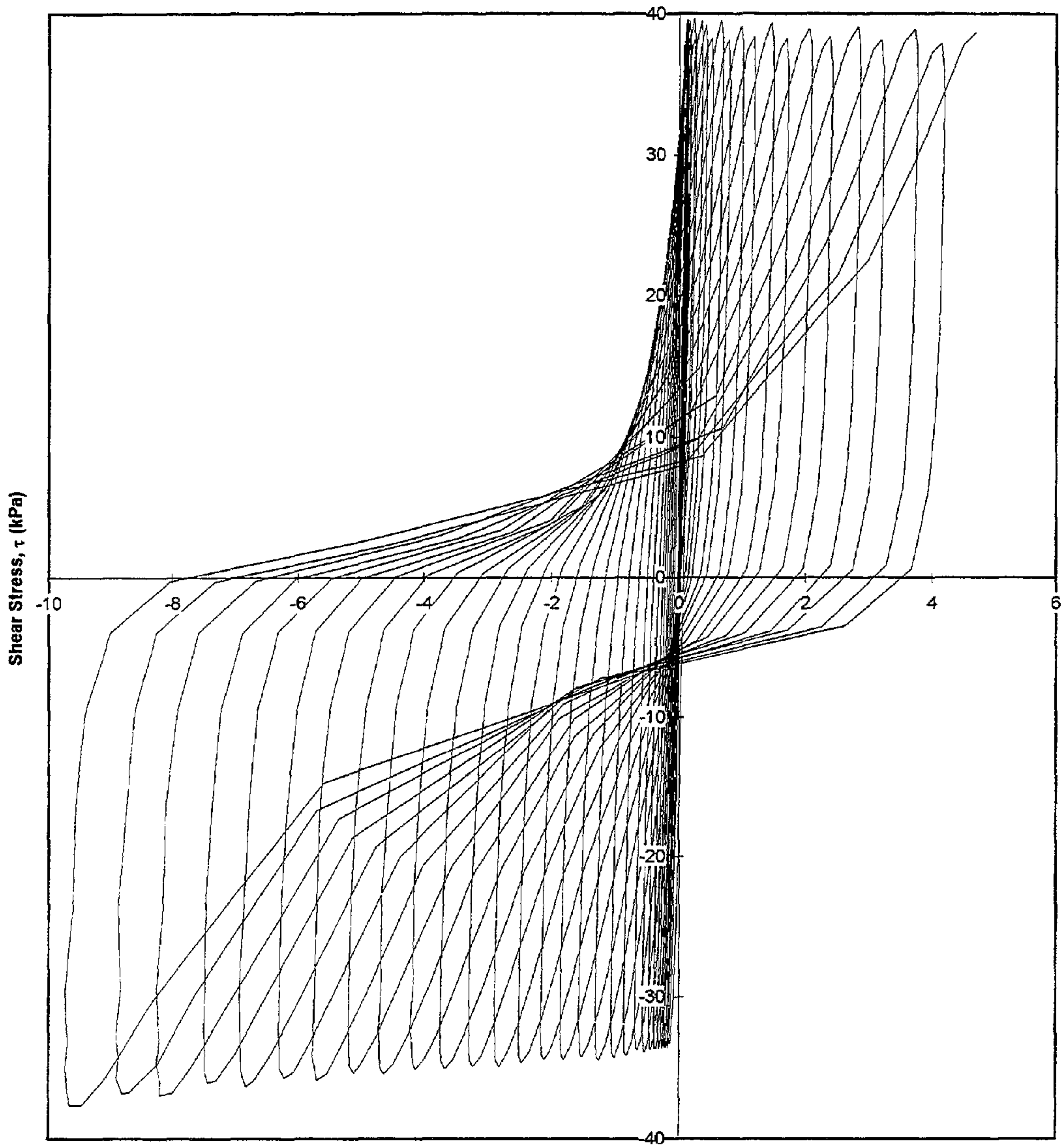

d:\nit\itp\cy_files\B23P3MCY.XLS 8/21/96 7:52 AM

Test I.D.:	B23P3TCY	**Controlled Parameter:**	Stress
Fines Content (%):	20.5	**Initial Effective Stress (kPa):**	200
Dry Density (kN/m³):	16.63		

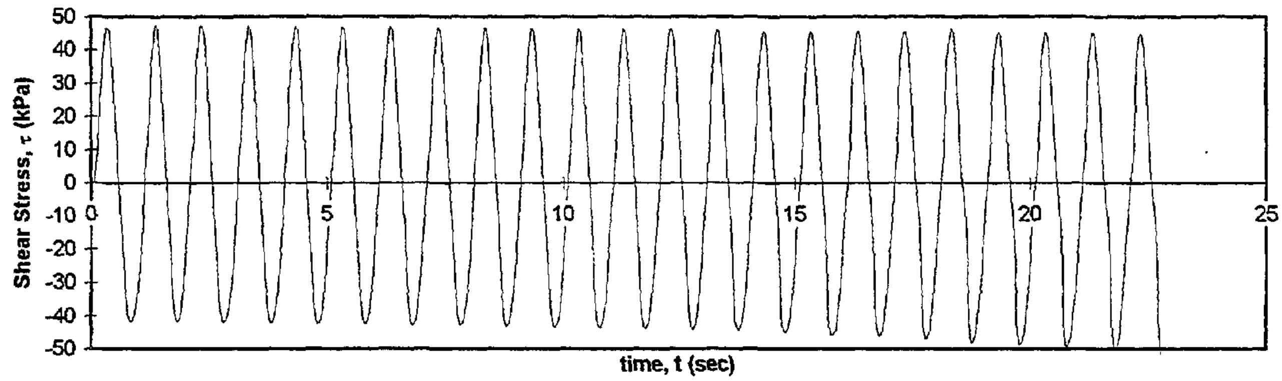

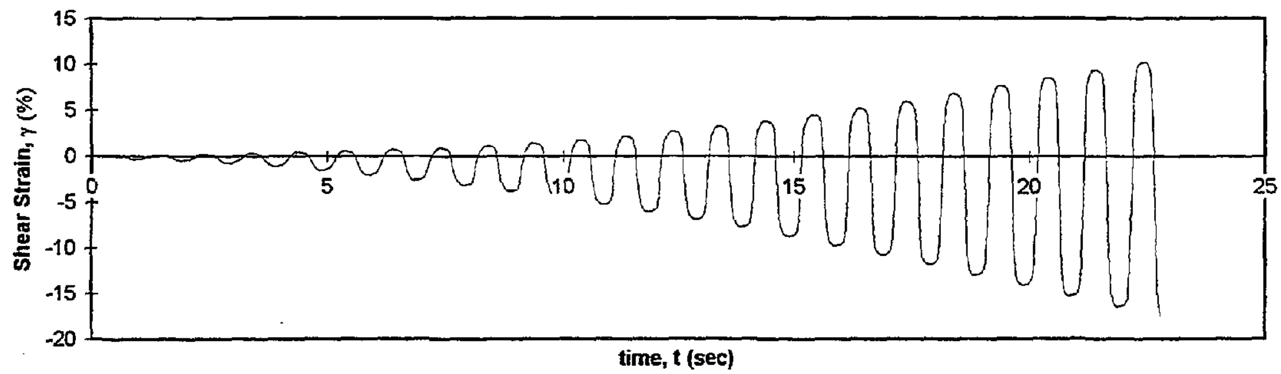

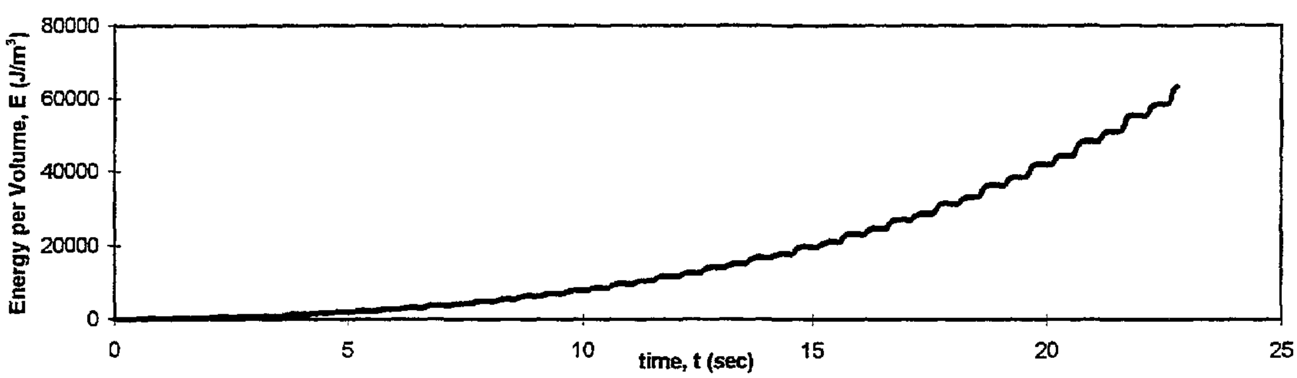

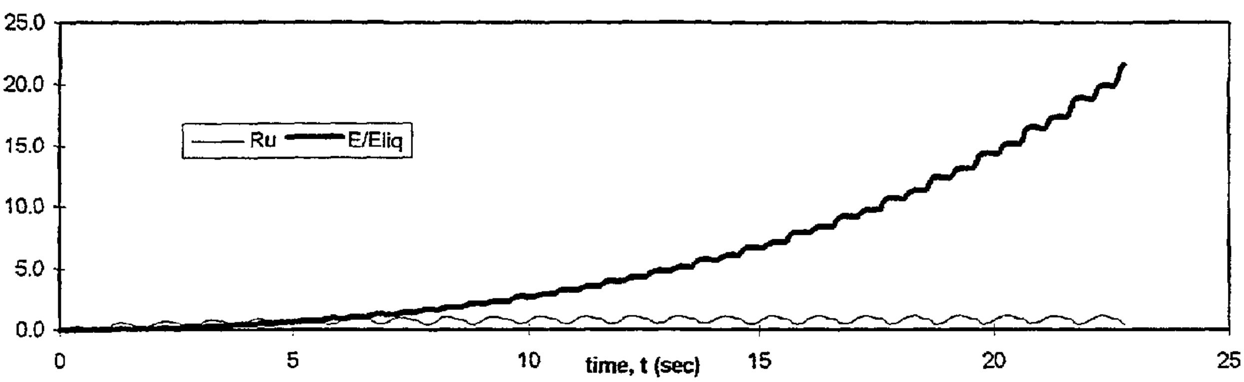

d:\nit\itp\cy_files\B23P3TCY.XLS 8/21/96 7:57 AM

Test I.D.:	B23P3TCY	**Controlled Parameter:**	Stress
Fines Content (%):	20.5	**Initial Effective Stress (kPa):**	200
Dry Density (kN/m^3):	16.63		

Shear Stress vs. Shear Strain

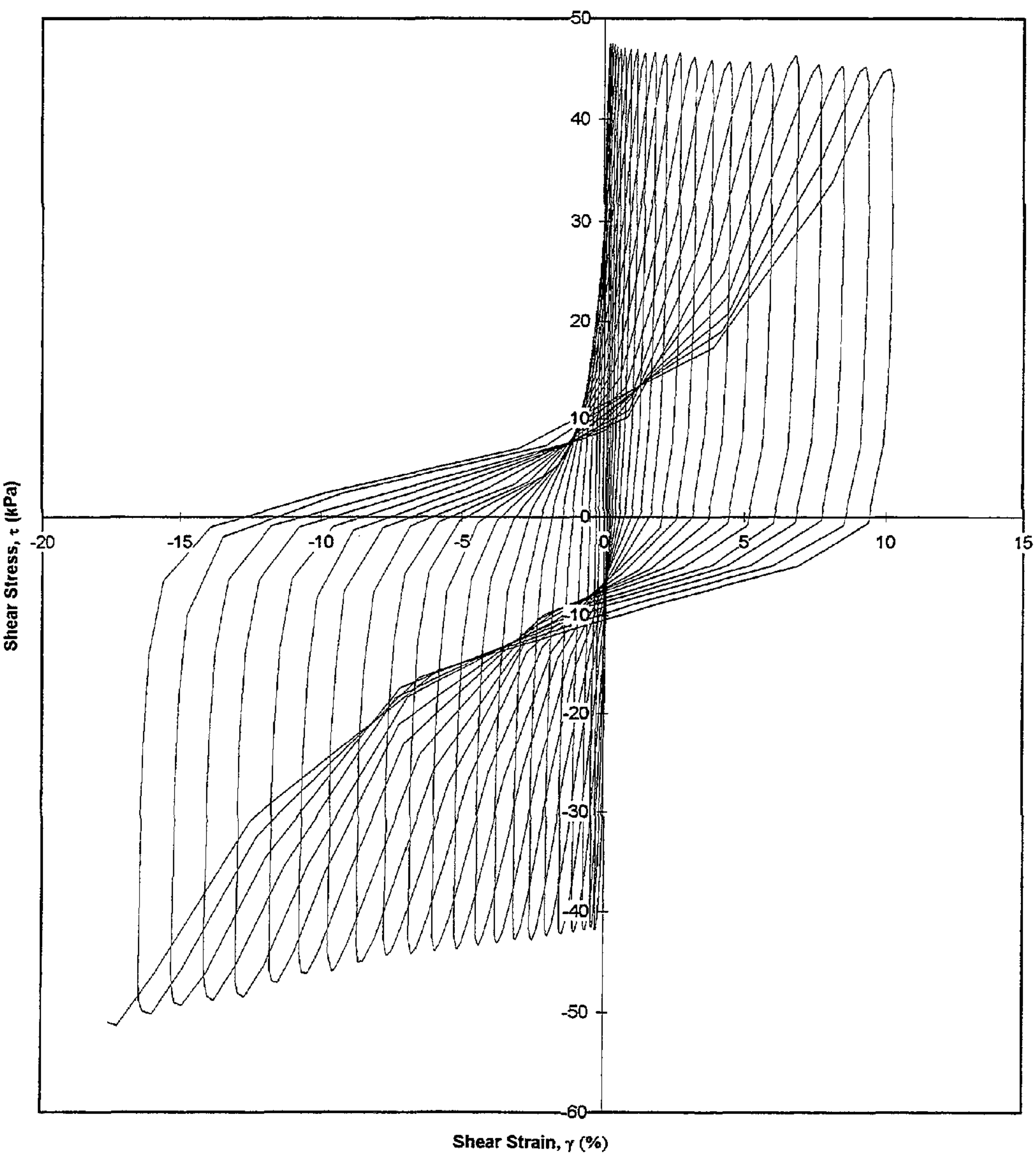

d:\nit\itp\cy_files\B23P3TCY.XLS 8/21/96 7:57 AM

Test I.D.:	B12P5BCY	**Controlled Parameter:**	Stress
Fines Content (%):	27	**Initial Effective Stress (kPa):**	300
Dry Density (kN/m³):	15.82		

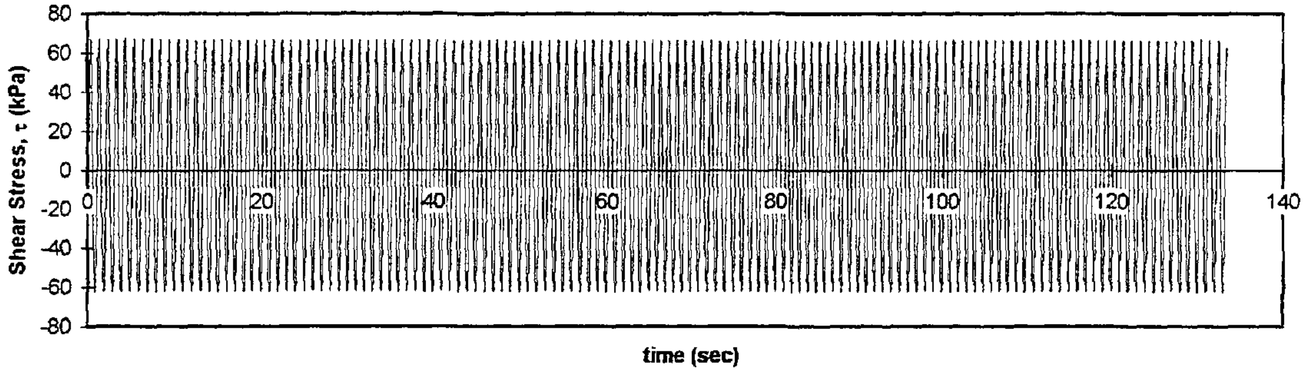

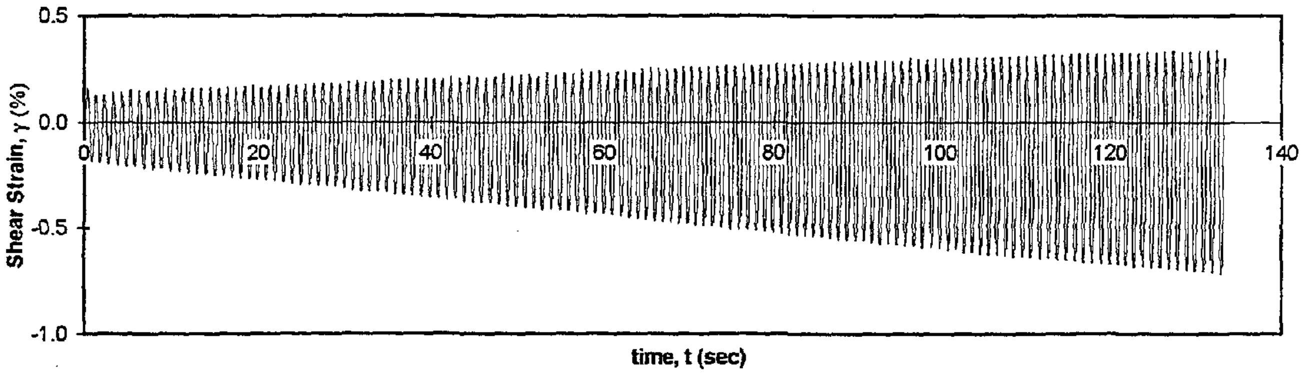

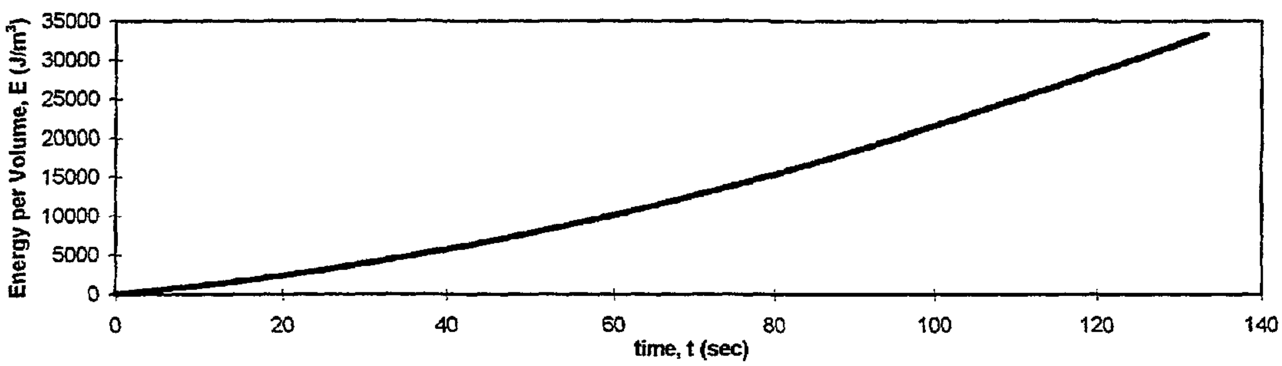

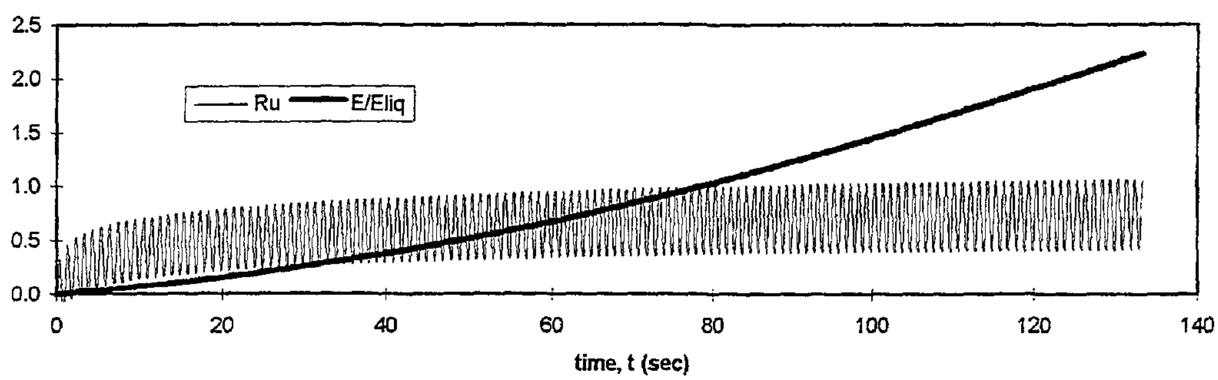

Test I.D.:	B12P5BCY	**Controlled Parameter:**	Stress
Fines Content (%):	27	**Initial Effective Stress (kPa):**	300
Dry Density (kN/m^3):	15.82		

Shear Stress vs. Shear Strain

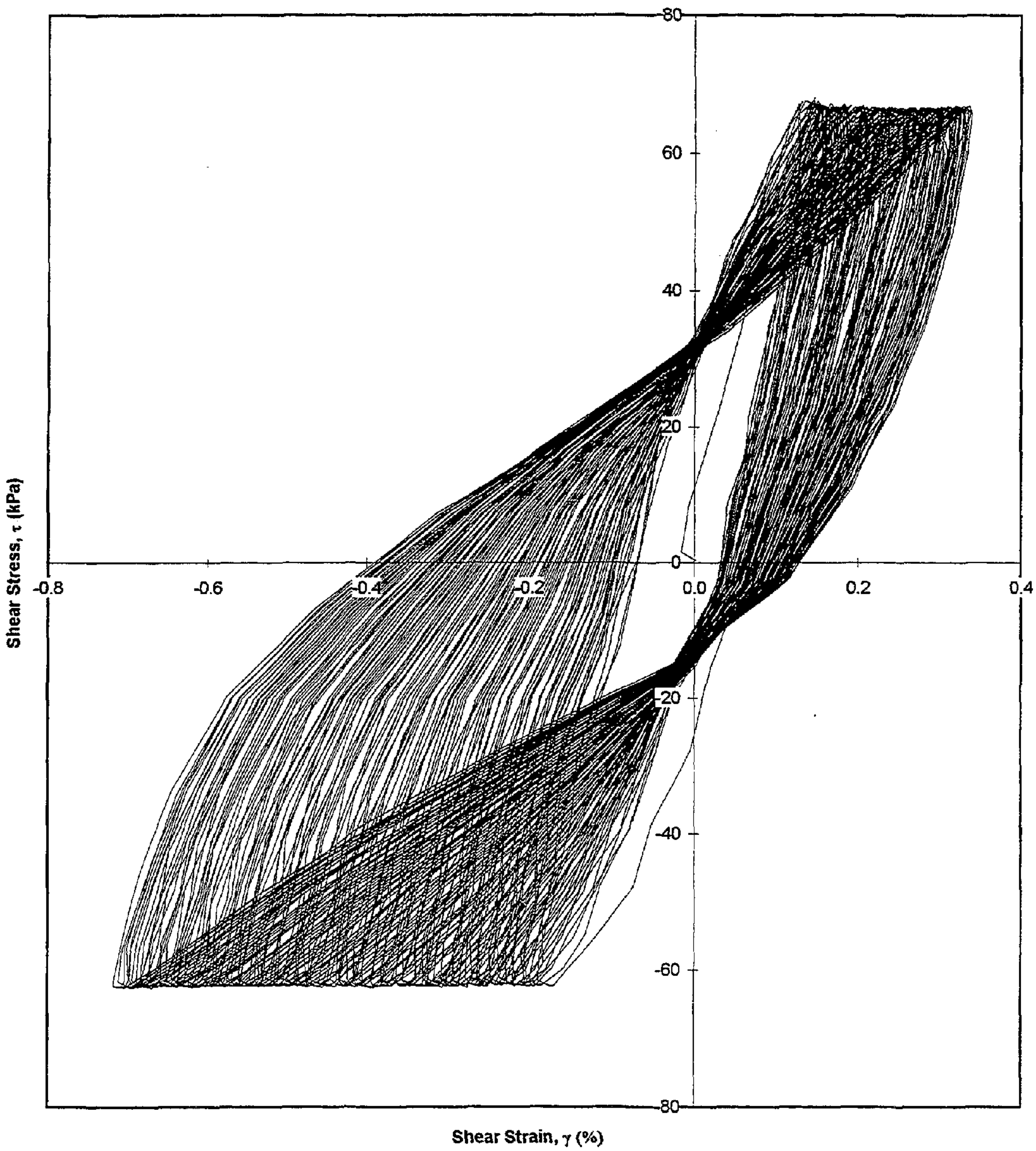

Test I.D.:	B12P5MCY	**Controlled Parameter:**	Stress
Fines Content (%):	26.8	**Initial Effective Stress (kPa):**	300
Dry Density (kN/m³):	16.78		

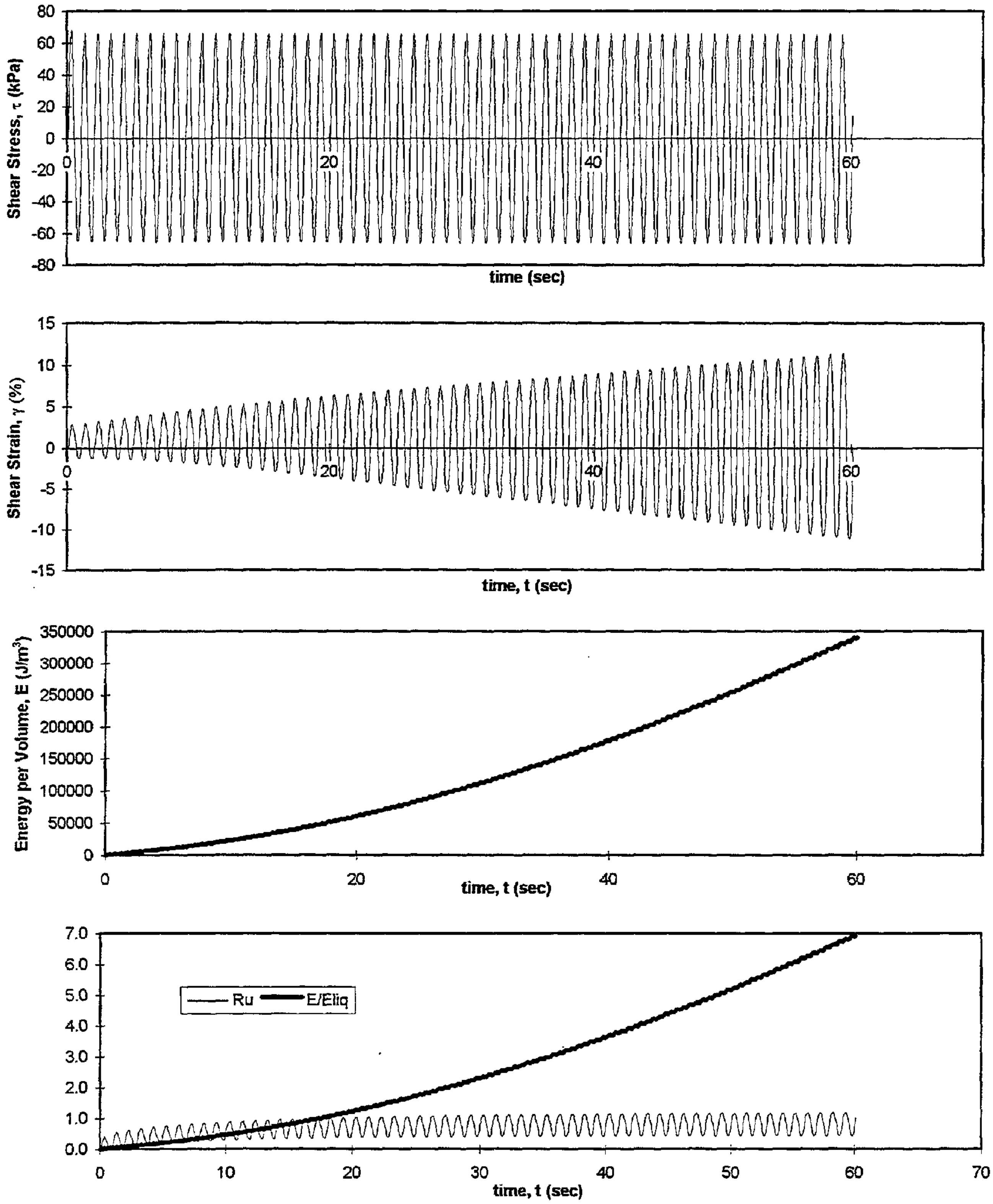

d:\nit\itp\cy_files\B12P5MCY.XLS 8/20/96 4:42 PM

Test I.D.:	B12P5MCY	**Controlled Parameter:**	Stress
Fines Content (%):	26.8	**Initial Effective Stress (kPa):**	300
Dry Density (kN/m³):	16.78		

Shear Stress vs. Shear Strain

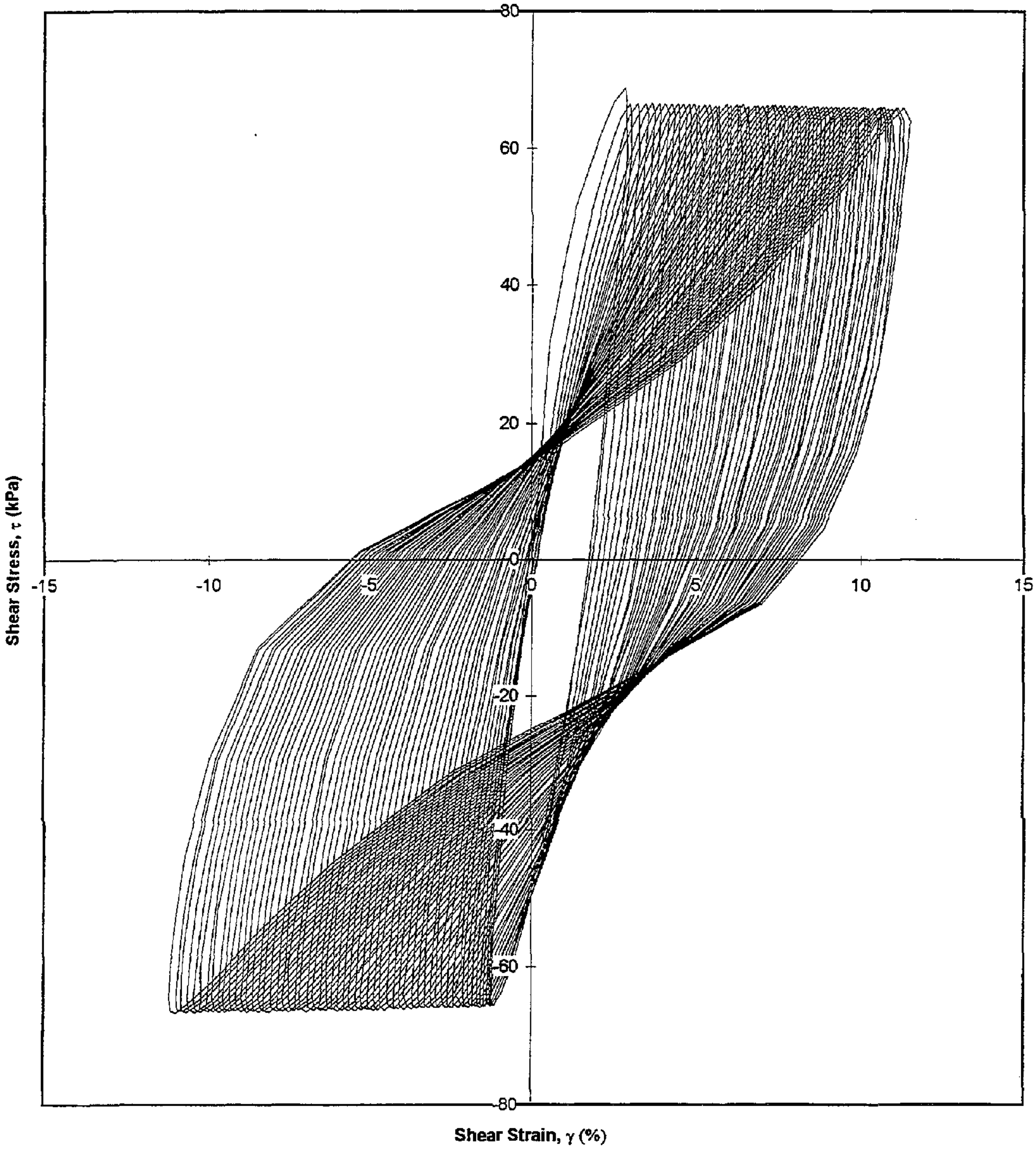

Test I.D.:	B12P5TCY	**Controlled Parameter:**	Stress
Fines Content (%):	22.3	**Initial Effective Stress (kPa):**	300
Dry Density (kN/m^3):	18.02		

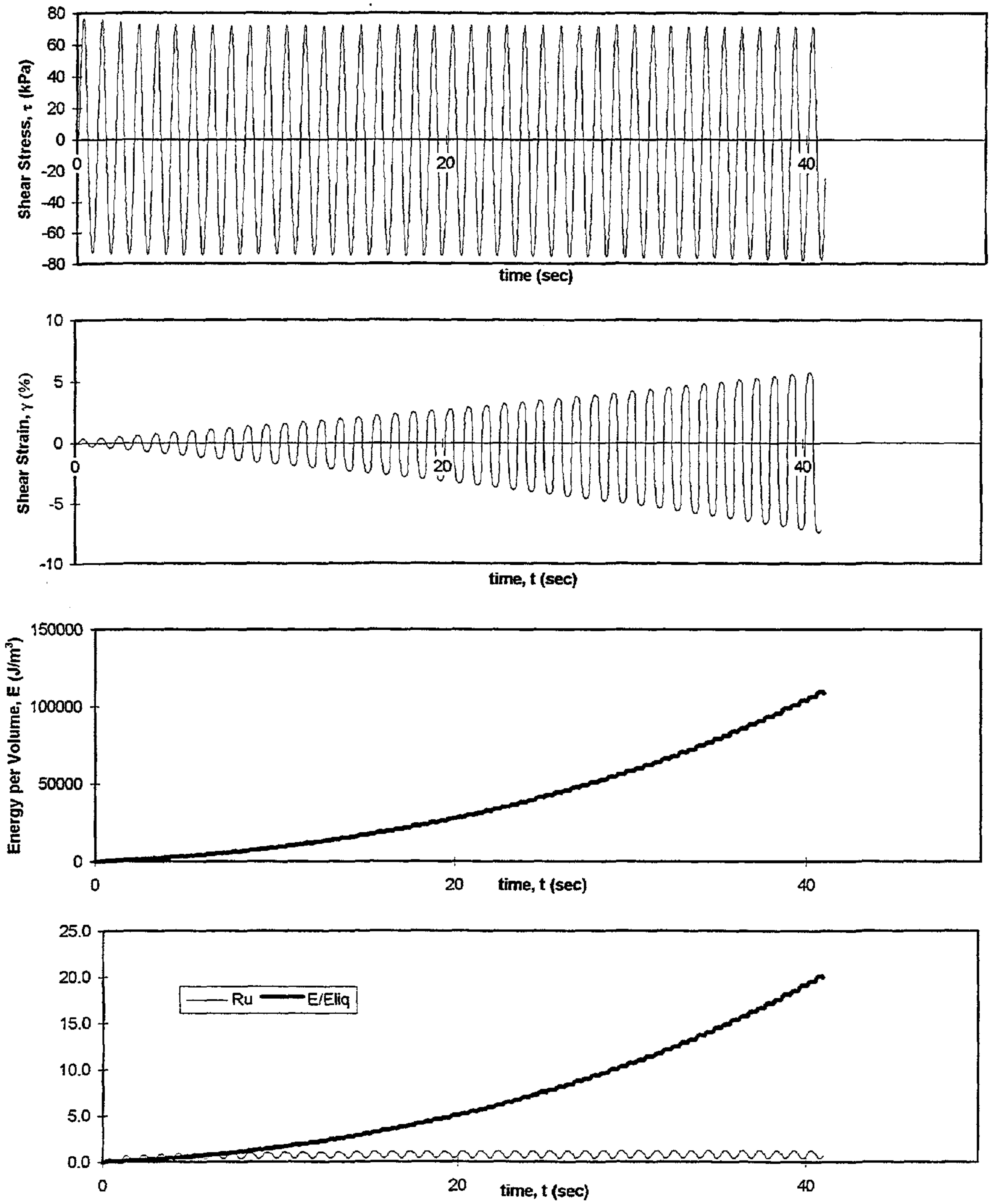

d:\nit\itp\cy_files\B12P5TCY.XLS 8/20/96 4:45 PM

Test I.D.:	B12P5TCY	**Controlled Parameter:**	Stress
Fines Content (%):	22.3	**Initial Effective Stress (kPa):**	300
Dry Density (kN/m³):	18.02		

Shear Stress vs. Shear Strain

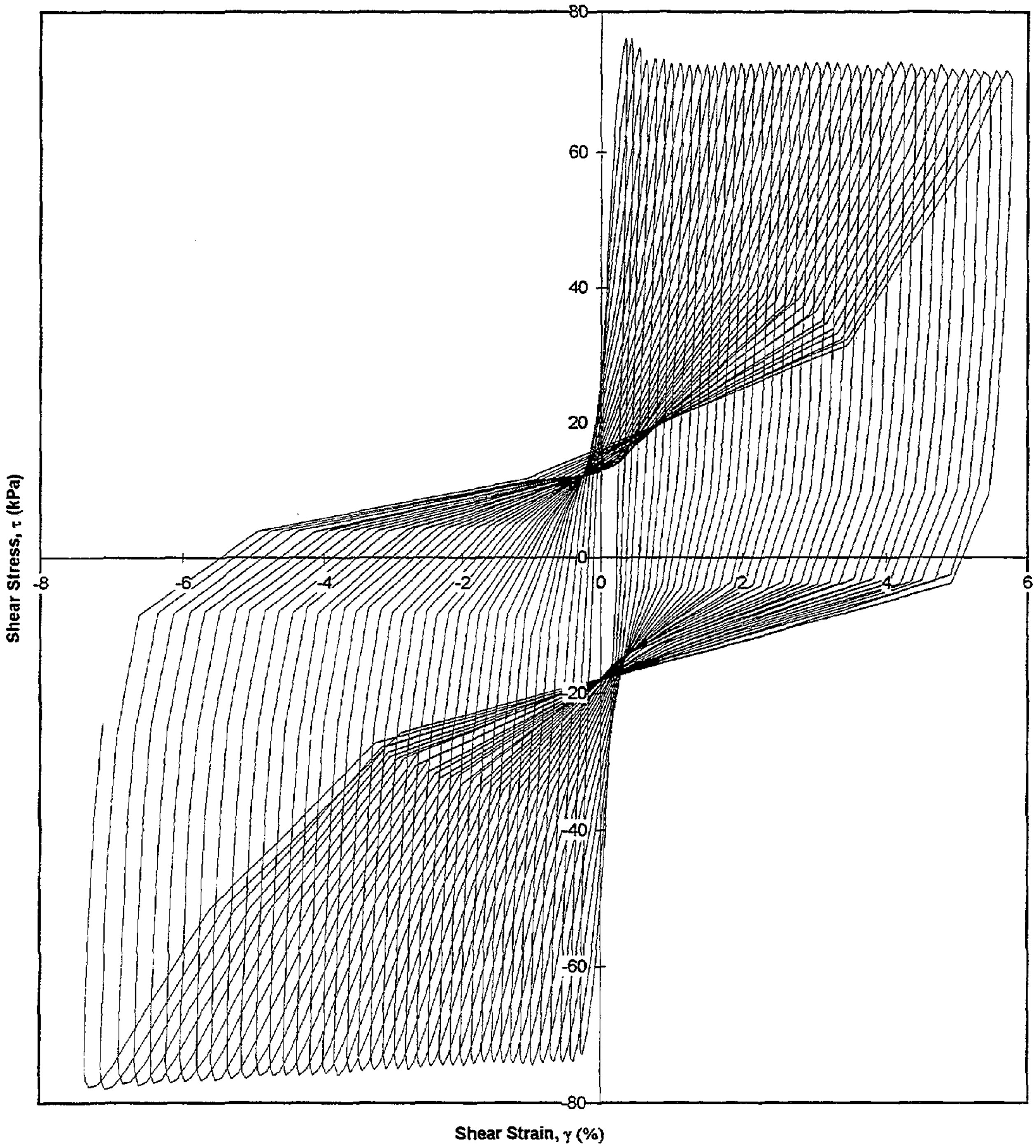

Test I.D.:	B12P7BCY	**Controlled Parameter:**	Stress
Fines Content (%):	15.7	**Initial Effective Stress (kPa):**	375
Dry Density (kN/m³):	15.91		

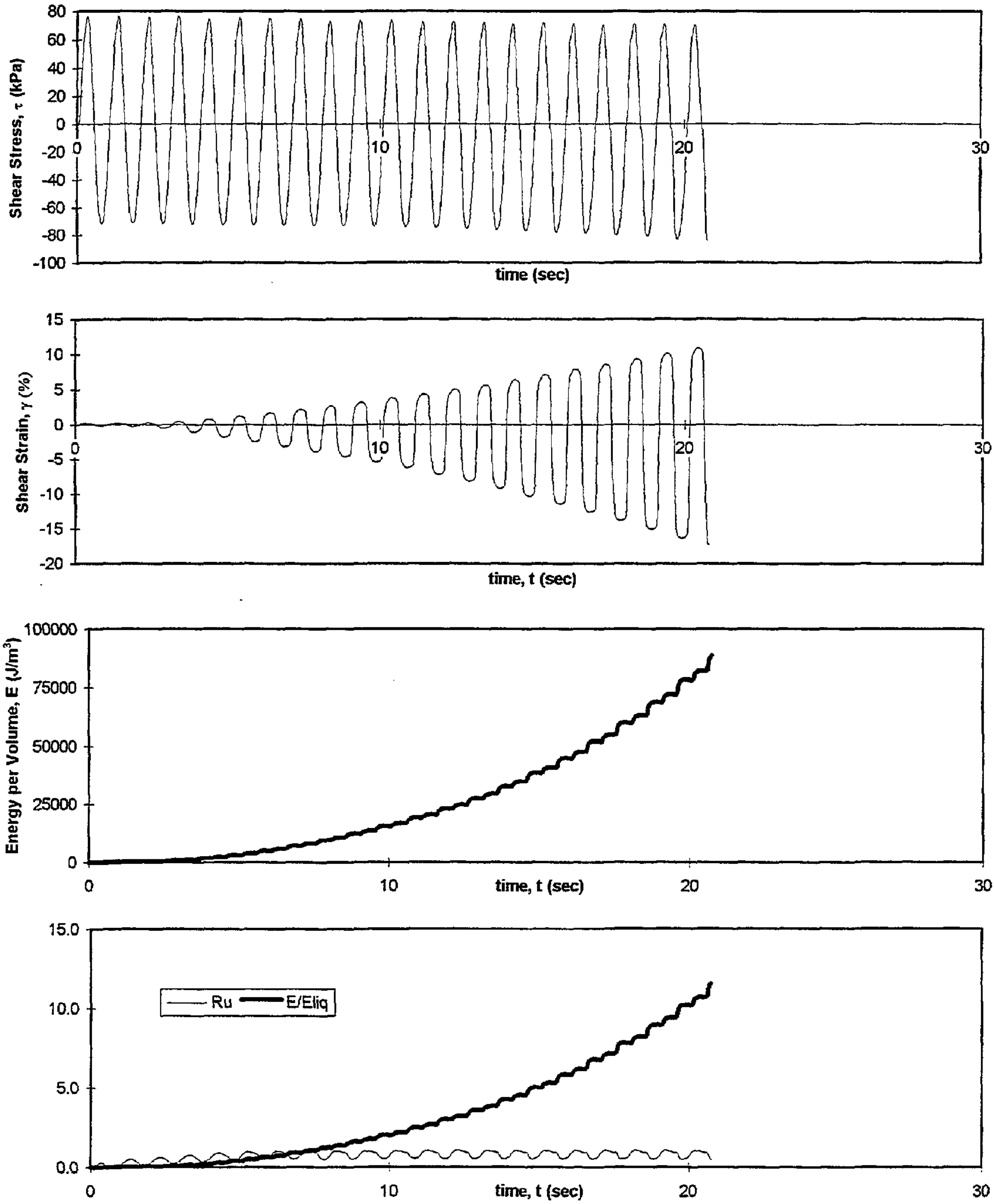

Test I.D.:	B12P7BCY	**Controlled Parameter:**	Stress
Fines Content (%):	15.7	**Initial Effective Stress (kPa):**	375
Dry Density (kN/m^3):	15.91		

Shear Stress vs. Shear Strain

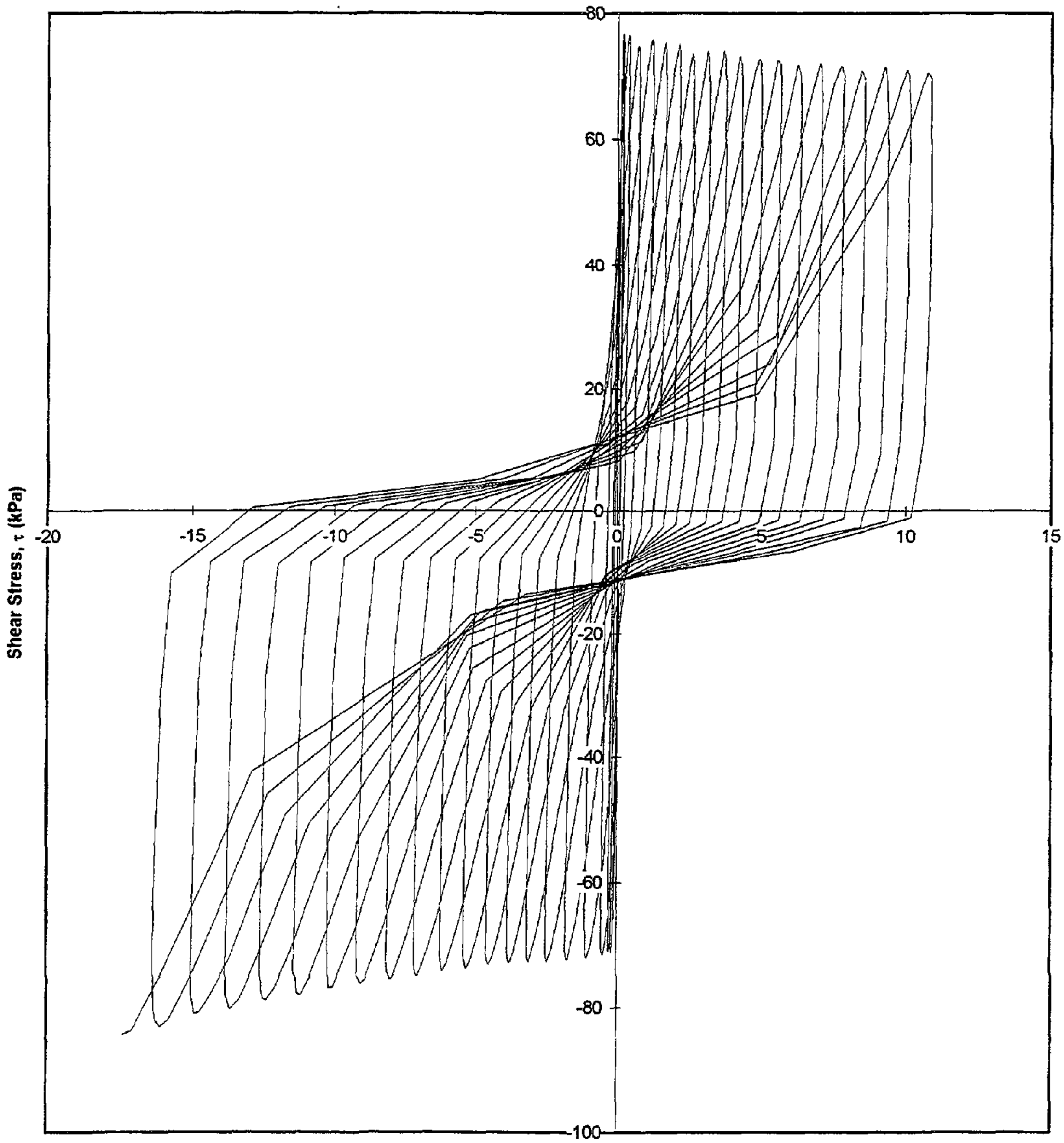

d:\nit\itp\cy_files\B12P7BCY.XLS 8/20/96 4:50 PM

Test I.D.:	B12P7MCY	**Controlled Parameter:**	Stress
Fines Content (%):	17	**Initial Effective Stress (kPa):**	375
Dry Density (kN/m³):	16.25		

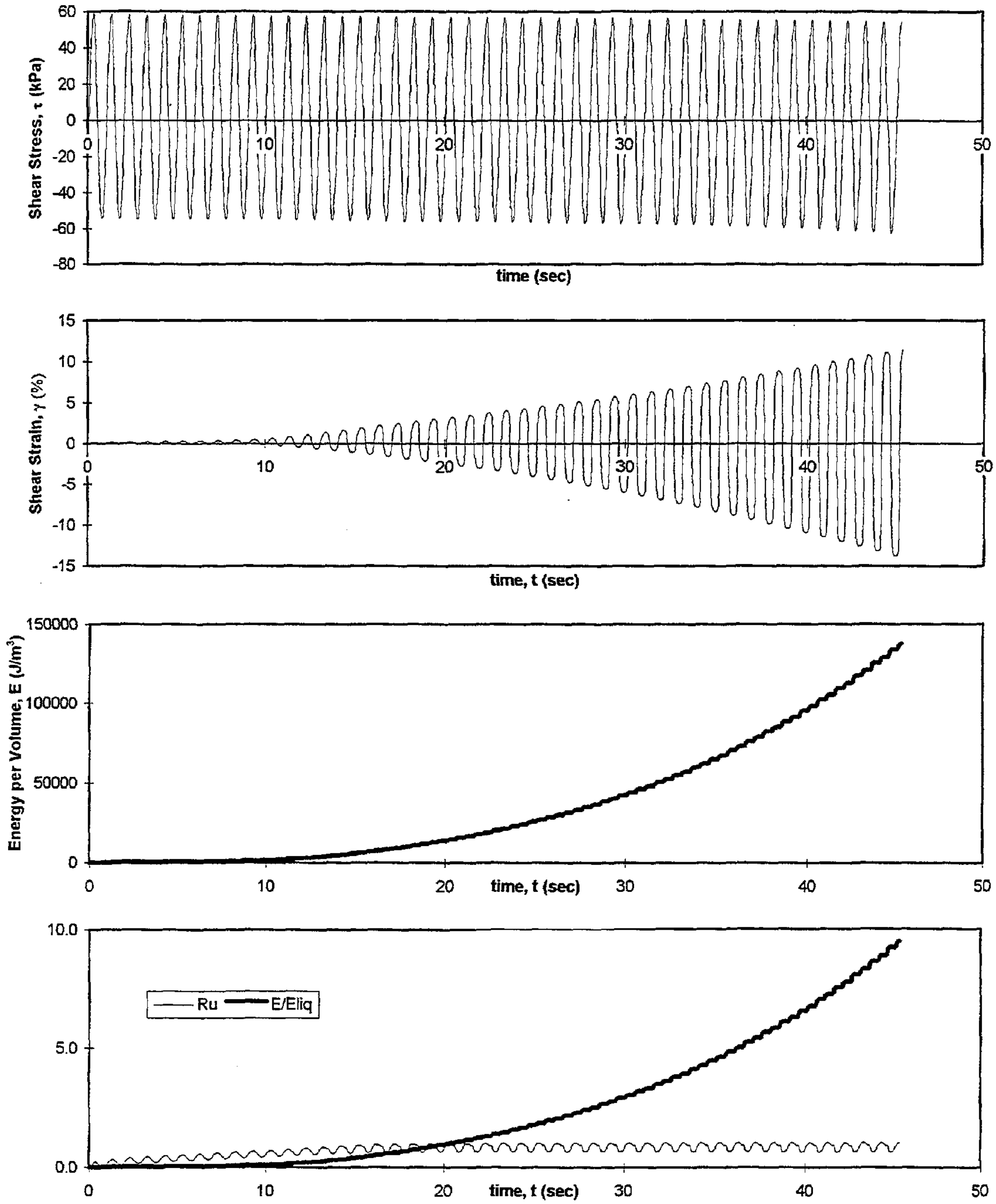

d:\nit\itp\cy_files\B12P7MCY.XLS 8/20/96 4:54 PM

Test I.D.:	B12P7MCY	**Controlled Parameter:**	Stress
Fines Content (%):	17	**Initial Effective Stress (kPa):**	375
Dry Density (kN/m^3):	16.25		

Shear Stress vs. Shear Strain

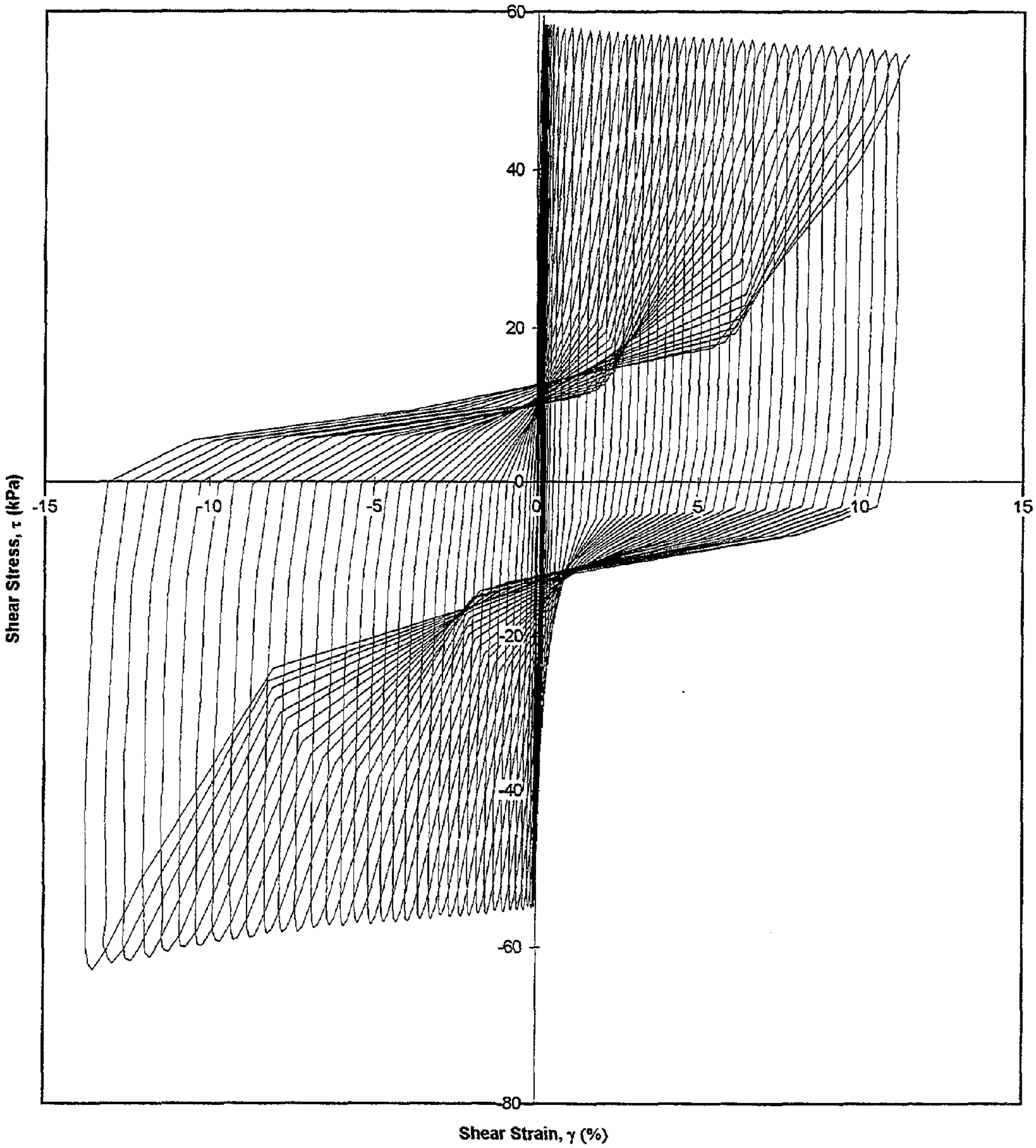

d:\nit\itp\cy_files\B12P7MCY.XLS 8/20/96 4:54 PM

Test I.D.:	B12P7TCY	**Controlled Parameter:**	Stress
Fines Content (%):	15.7	**Initial Effective Stress (kPa):**	375
Dry Density (kN/m³):	16.24		

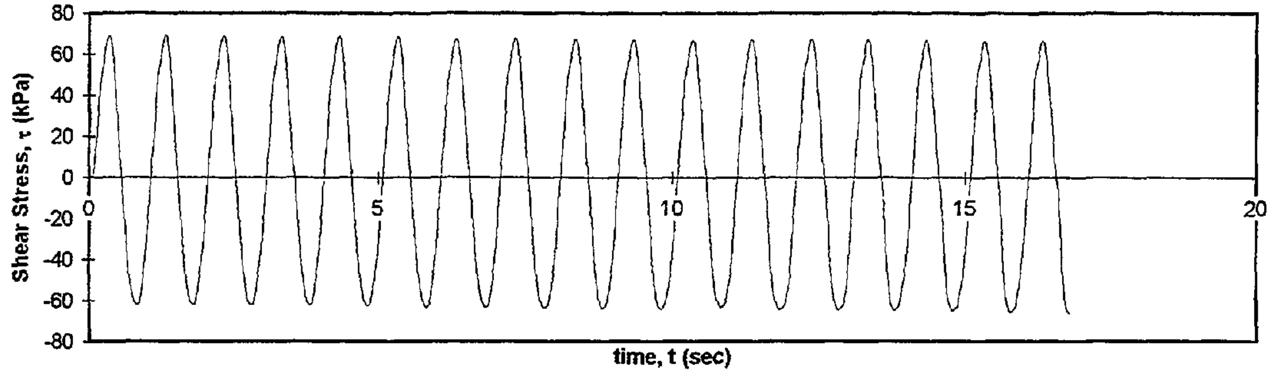

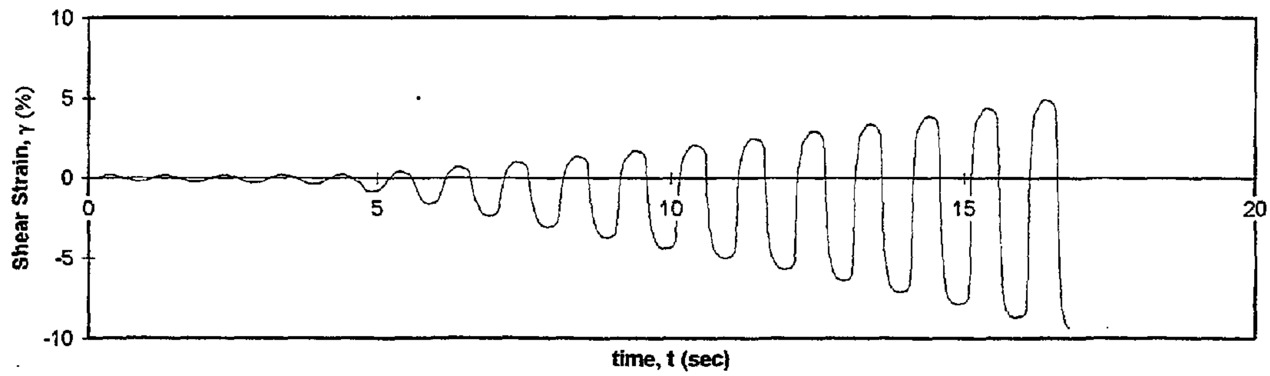

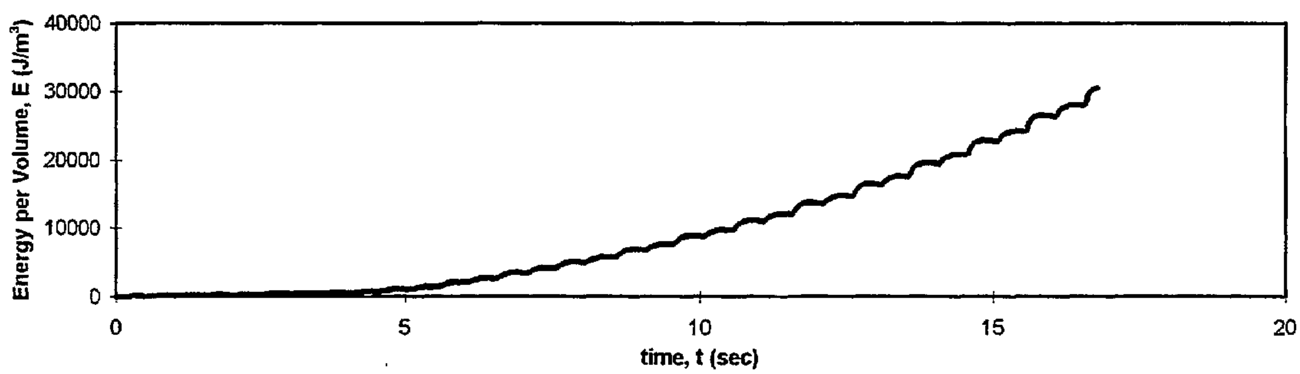

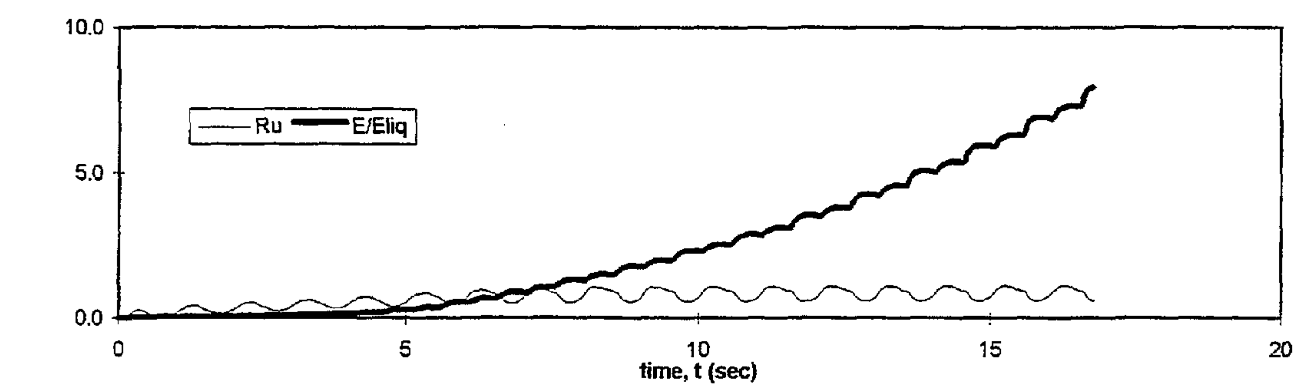

Test I.D.:	B12P7TCY	**Controlled Parameter:**	Stress
Fines Content (%):	15.7	**Initial Effective Stress (kPa):**	375
Dry Density (kN/m^3):	16.24		

Shear Stress vs. Shear Strain

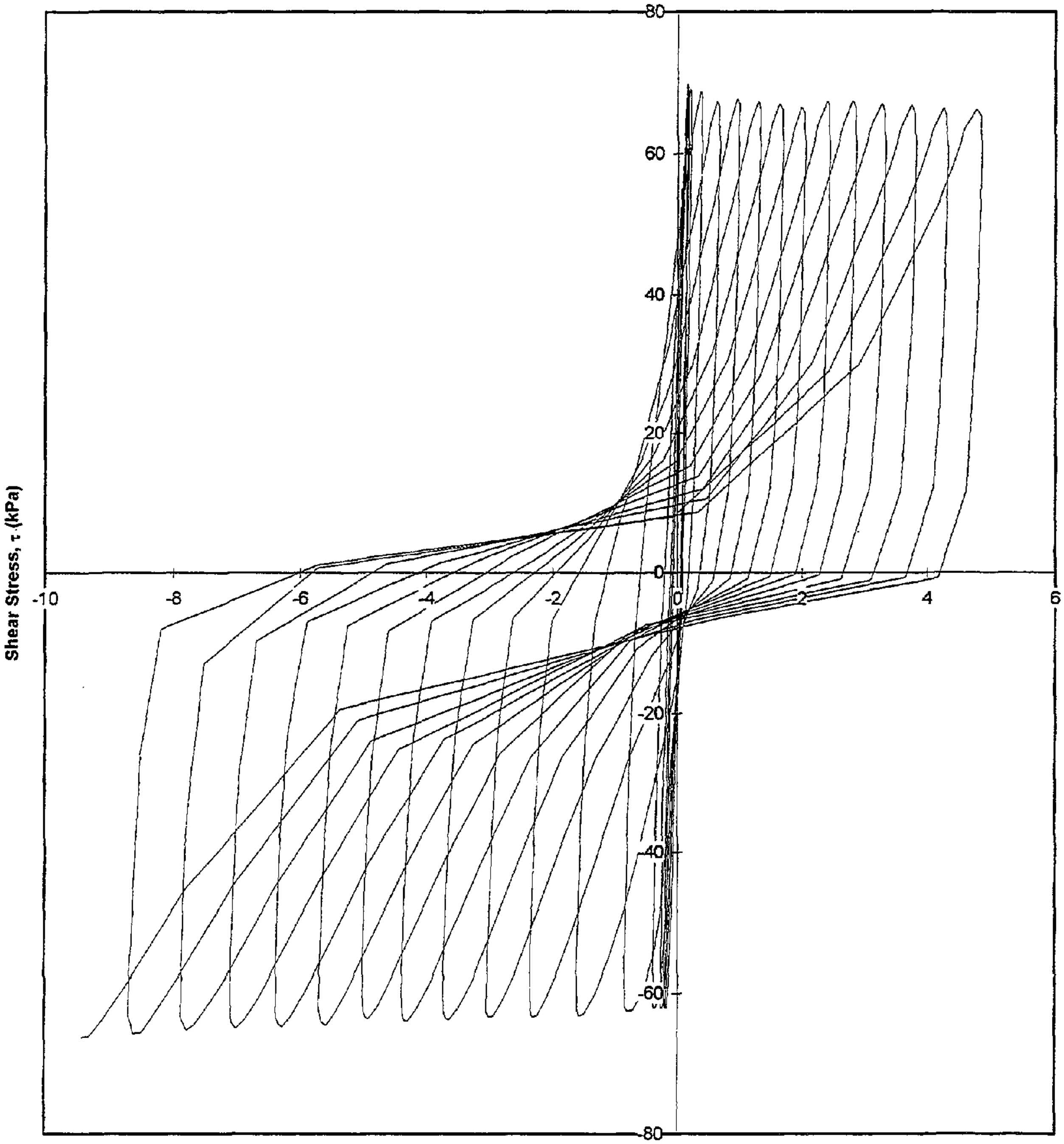

d:\nit\itp\cy_files\B12P7TCY.XLS

8/21/96 9:48 AM

Test I.D.:	B2P5BCYC	**Controlled Parameter:**	Stress
Fines Content (%):	25.4	**Initial Effective Stress (kPa):**	500
Dry Density (kN/m³):	14.65		

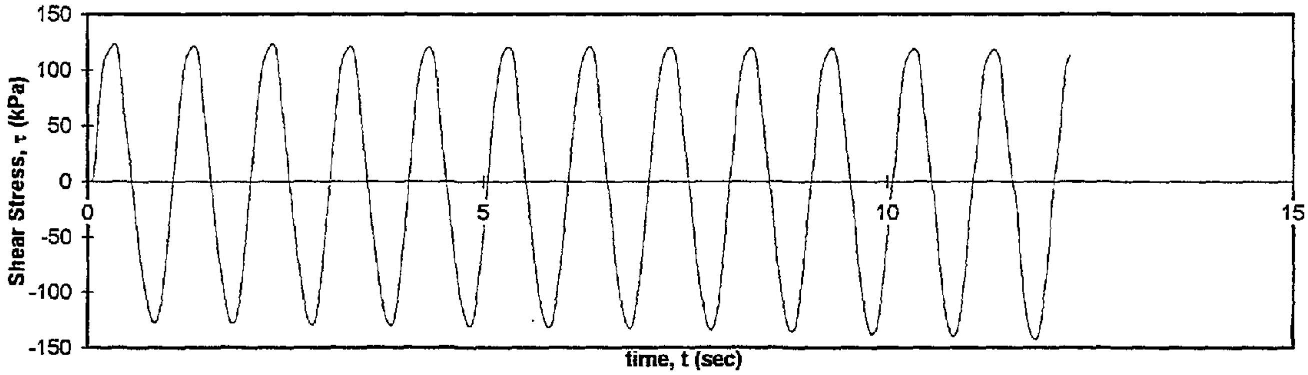

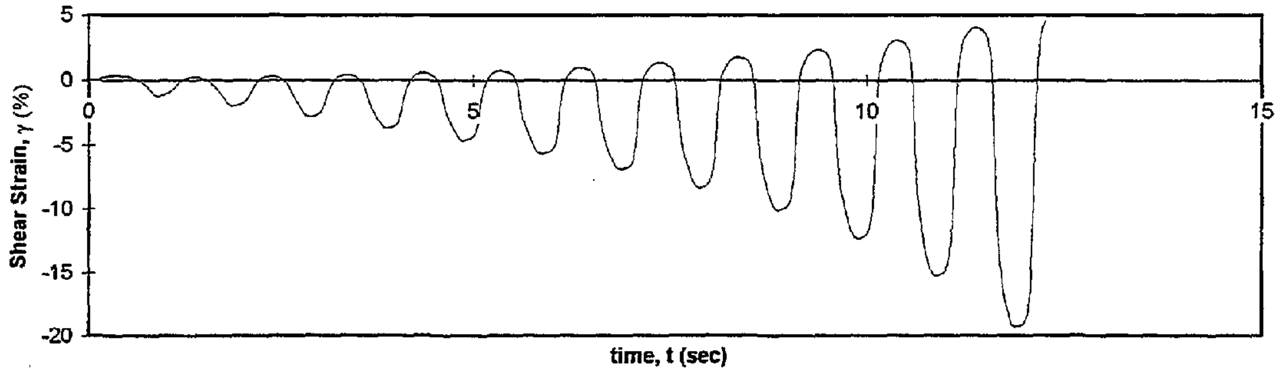

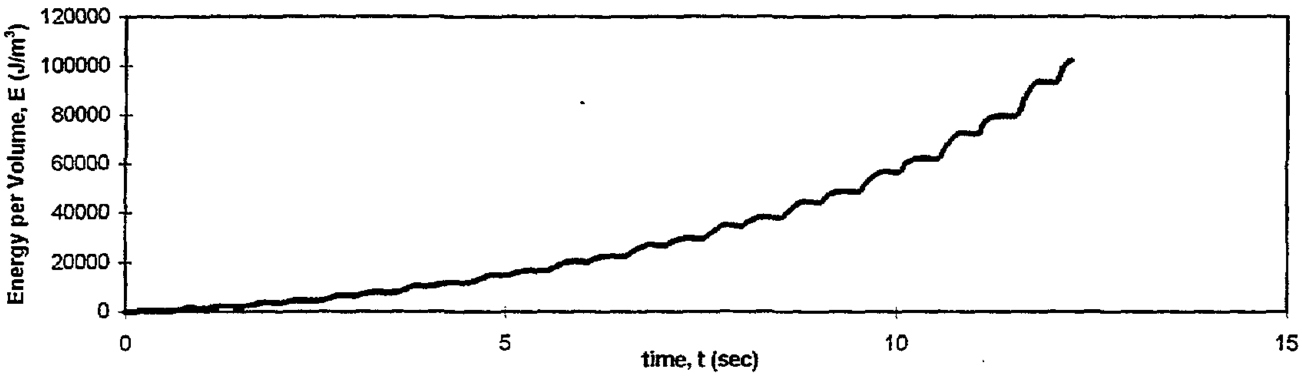

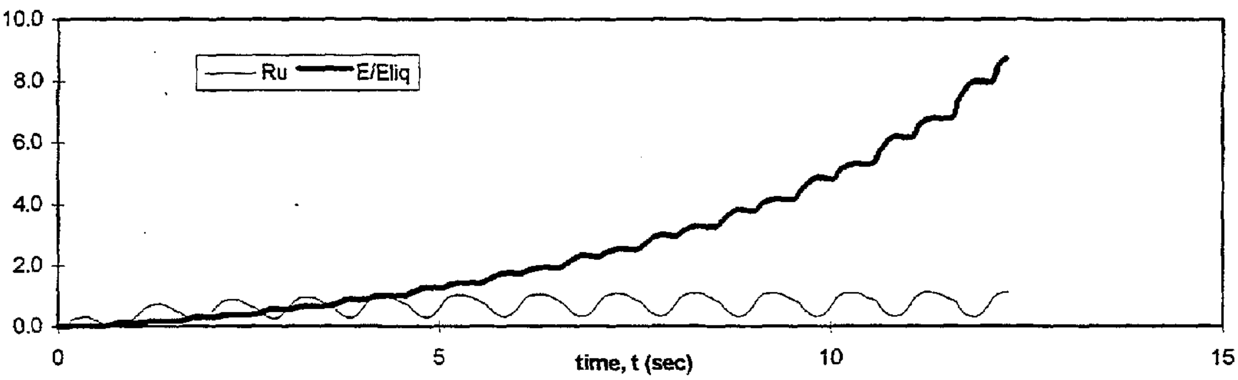

Test I.D.:	B2P5BCYC	**Controlled Parameter:**	Stress
Fines Content (%):	25.4	**Initial Effective Stress (kPa):**	500
Dry Density (kN/m³):	14.65		

Shear Stress vs. Shear Strain

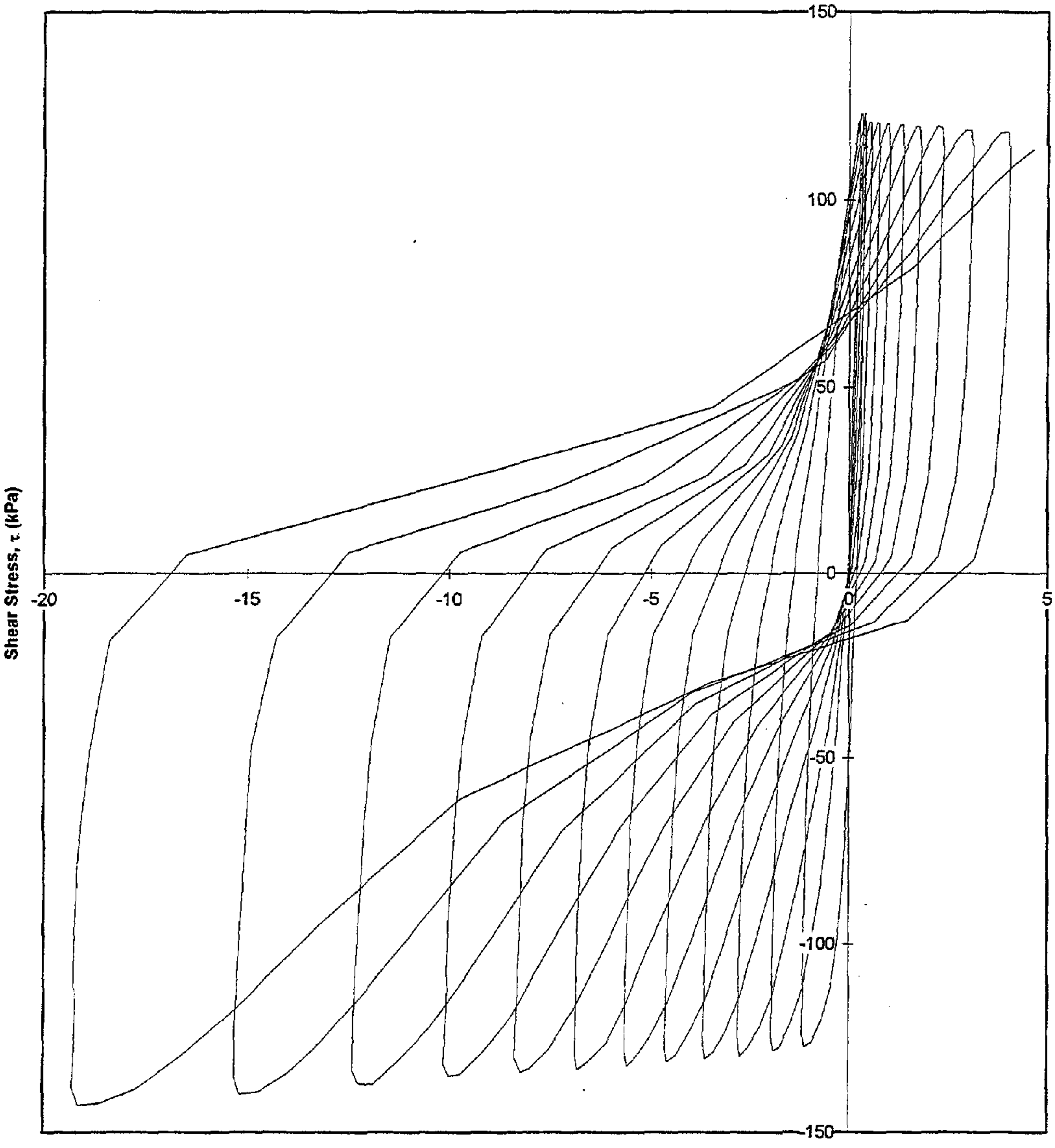

Test I.D.:	B2P5MCYC	**Controlled Parameter:**	Stress
Fines Content (%):	29.6	**Initial Effective Stress (kPa):**	500
Dry Density (kN/m^3):	15.37		

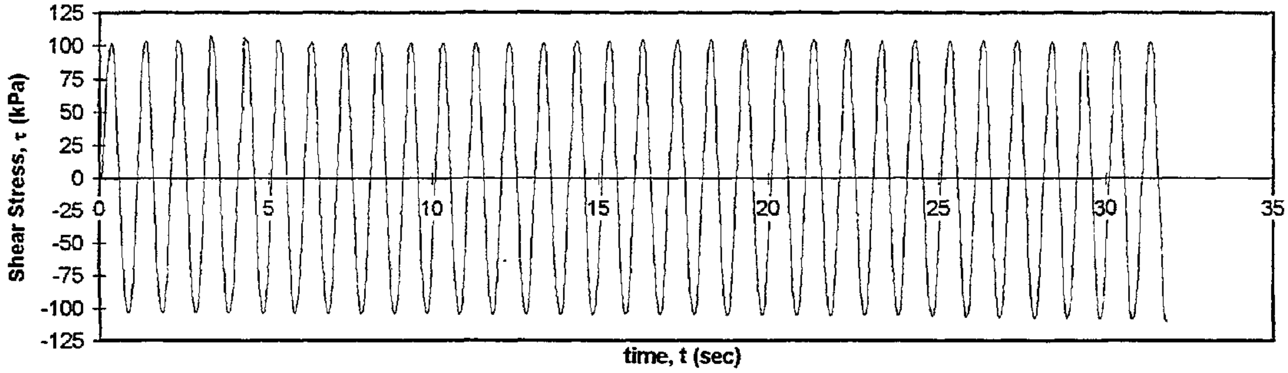

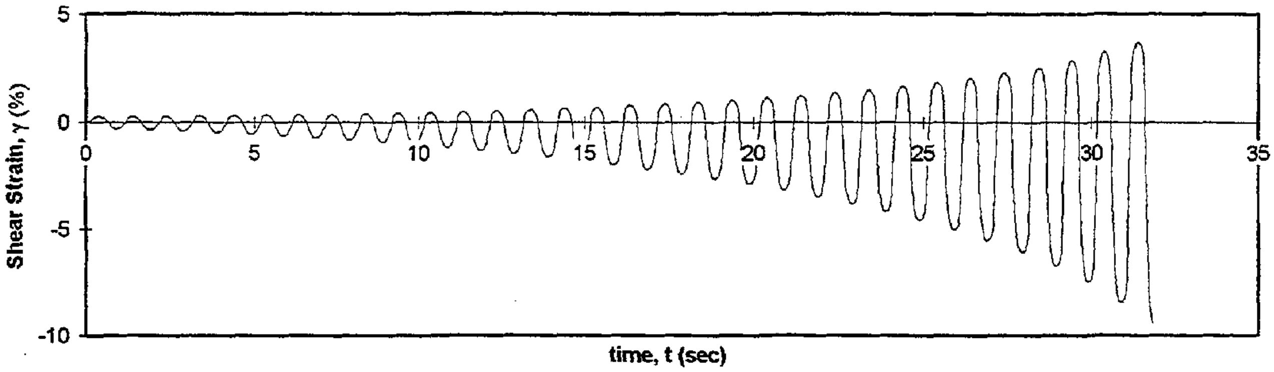

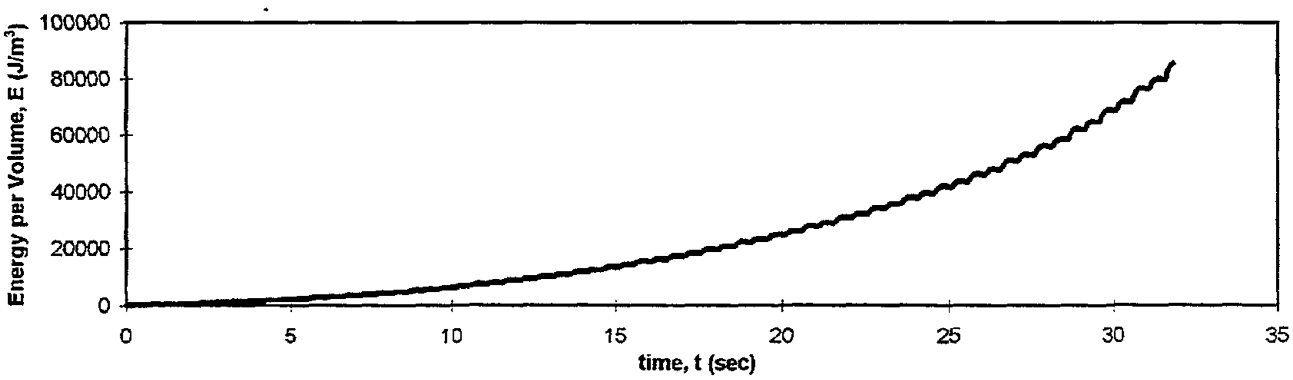

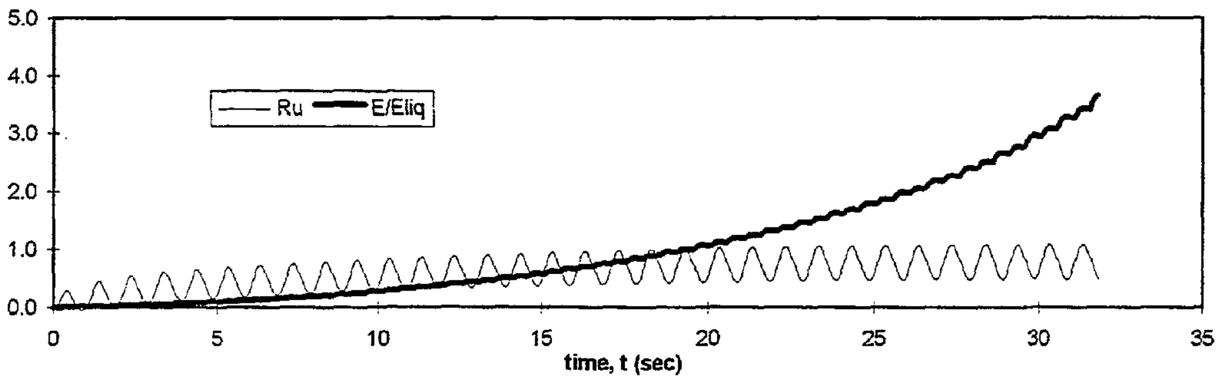

Test I.D.:	B2P5MCYC	**Controlled Parameter:**	Stress
Fines Content (%):	29.6	**Initial Effective Stress (kPa):**	500
Dry Density (kN/m^3):	15.37		

Shear Stress vs. Shear Strain

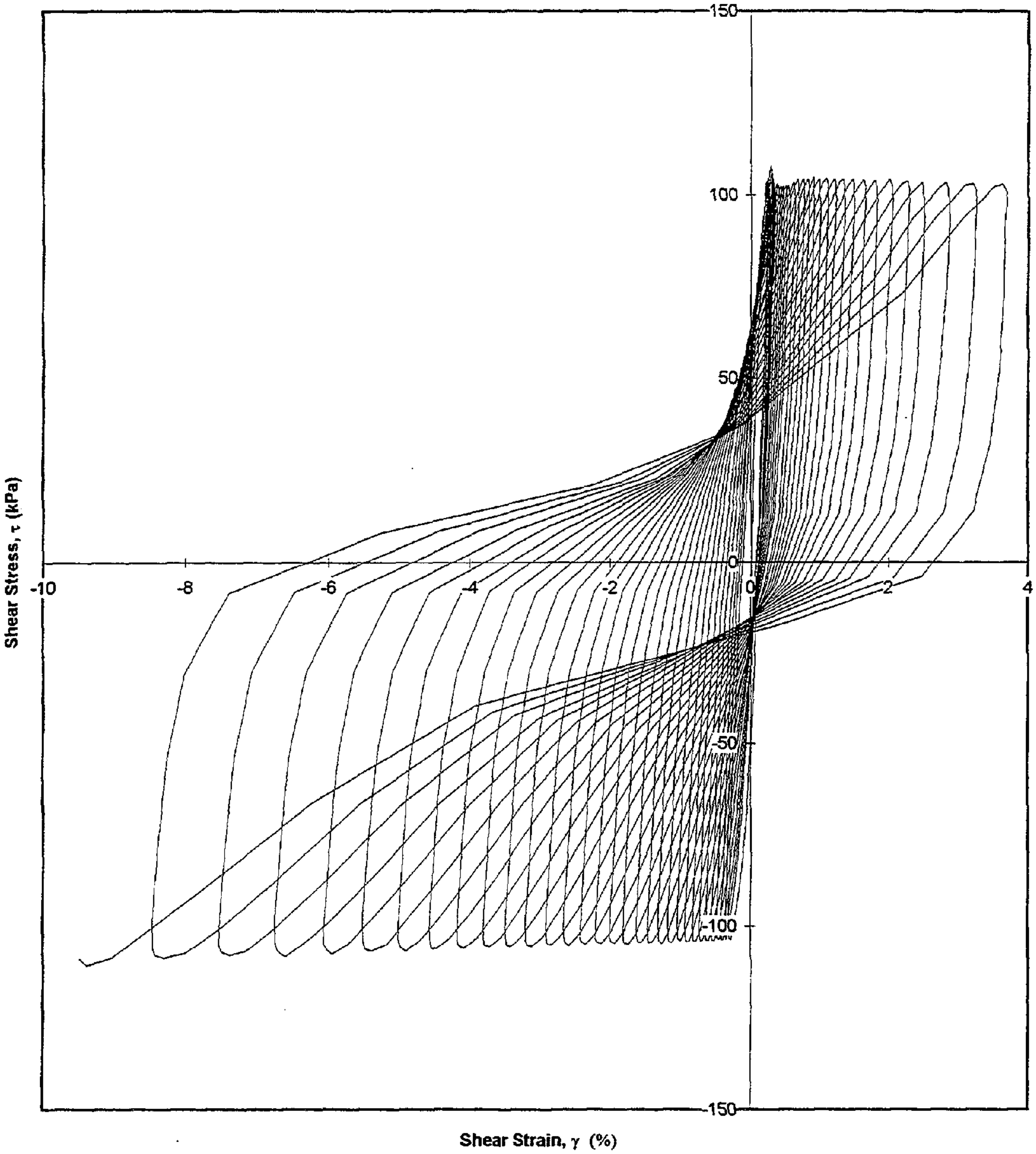

Test I.D.:	B2P5TCYC	**Controlled Parameter:**	Stress
Fines Content (%):	26.6	**Initial Effective Stress (kPa):**	500
Dry Density (kN/m³):	16.71		

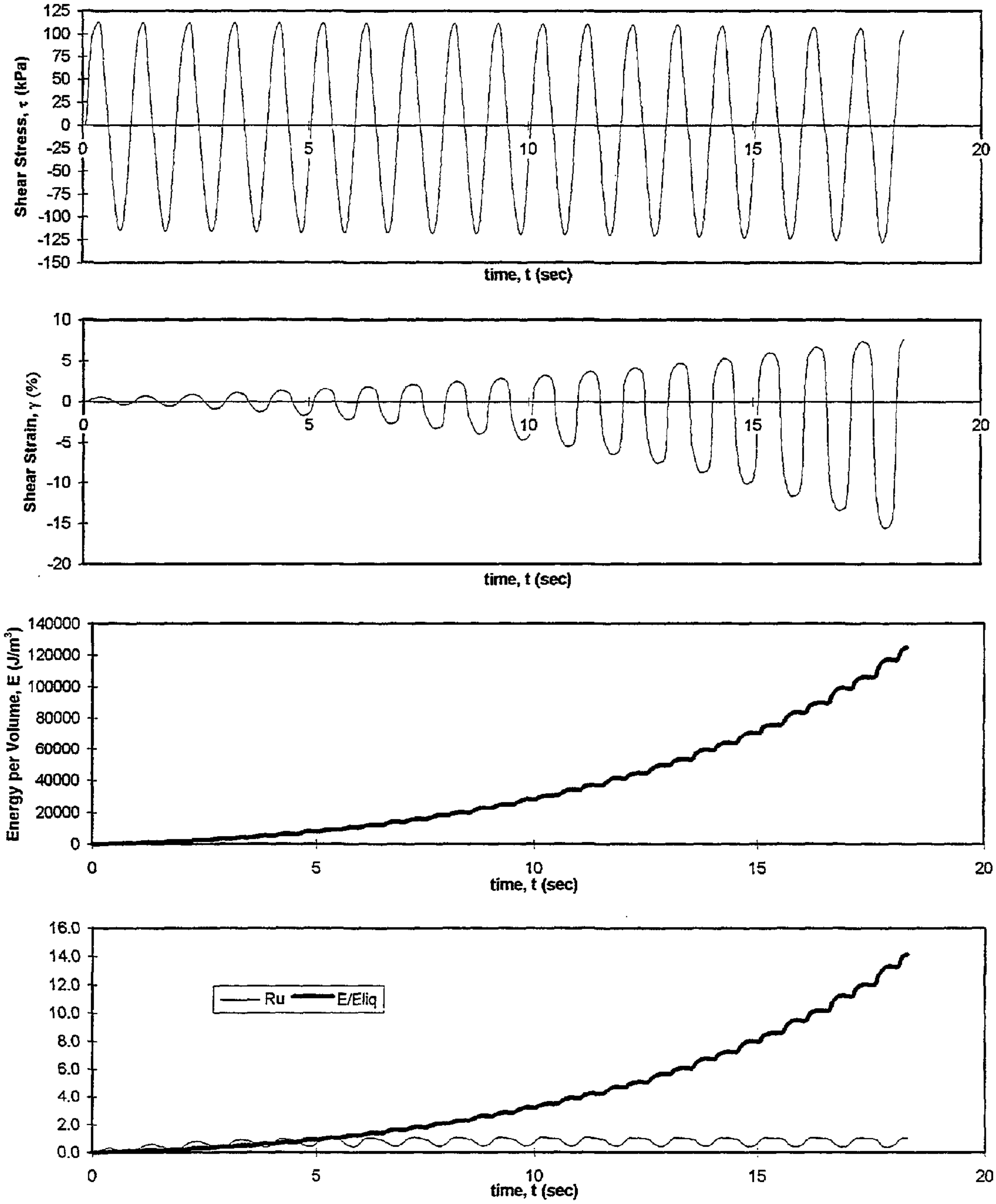

d:\nit\itp\cy_files\B2P5TCYC.XLS 8/21/96 8:25 AM

Test I.D.:	B2P5TCYC	**Controlled Parameter:**	Stress
Fines Content (%):	26.6	**Initial Effective Stress (kPa):**	500
Dry Density (kN/m^3):	16.71		

Shear Stress vs. Shear Strain

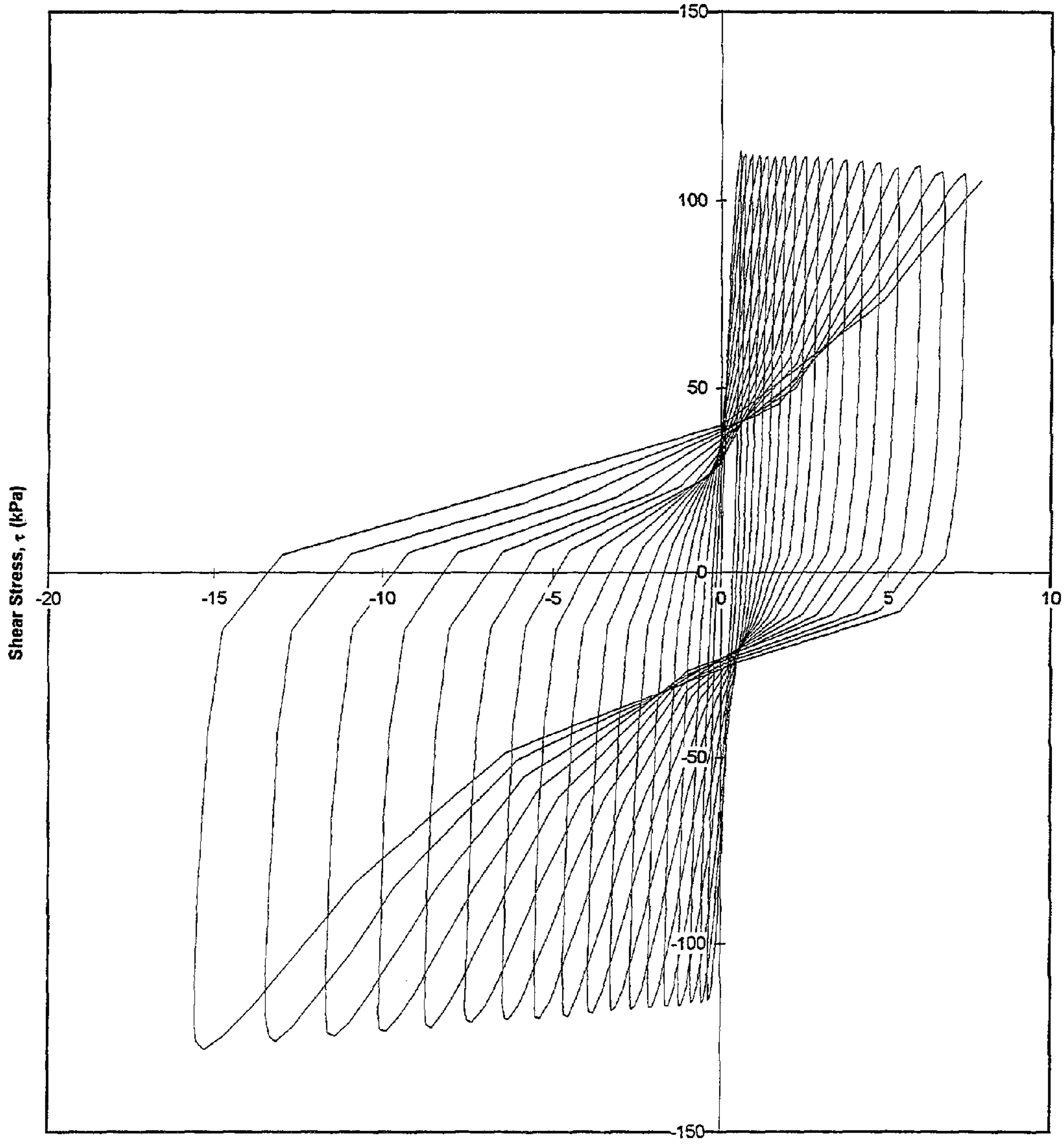

d:\nit\itp\cy_files\B2P5TCYC.XLS 8/21/96 8:25 AM

Test I.D.:	B23P4BCY	**Controlled Parameter:**	Stress
Fines Content (%):	11.4	**Initial Effective Stress (kPa):**	750
Dry Density (kN/m³):	14.6		

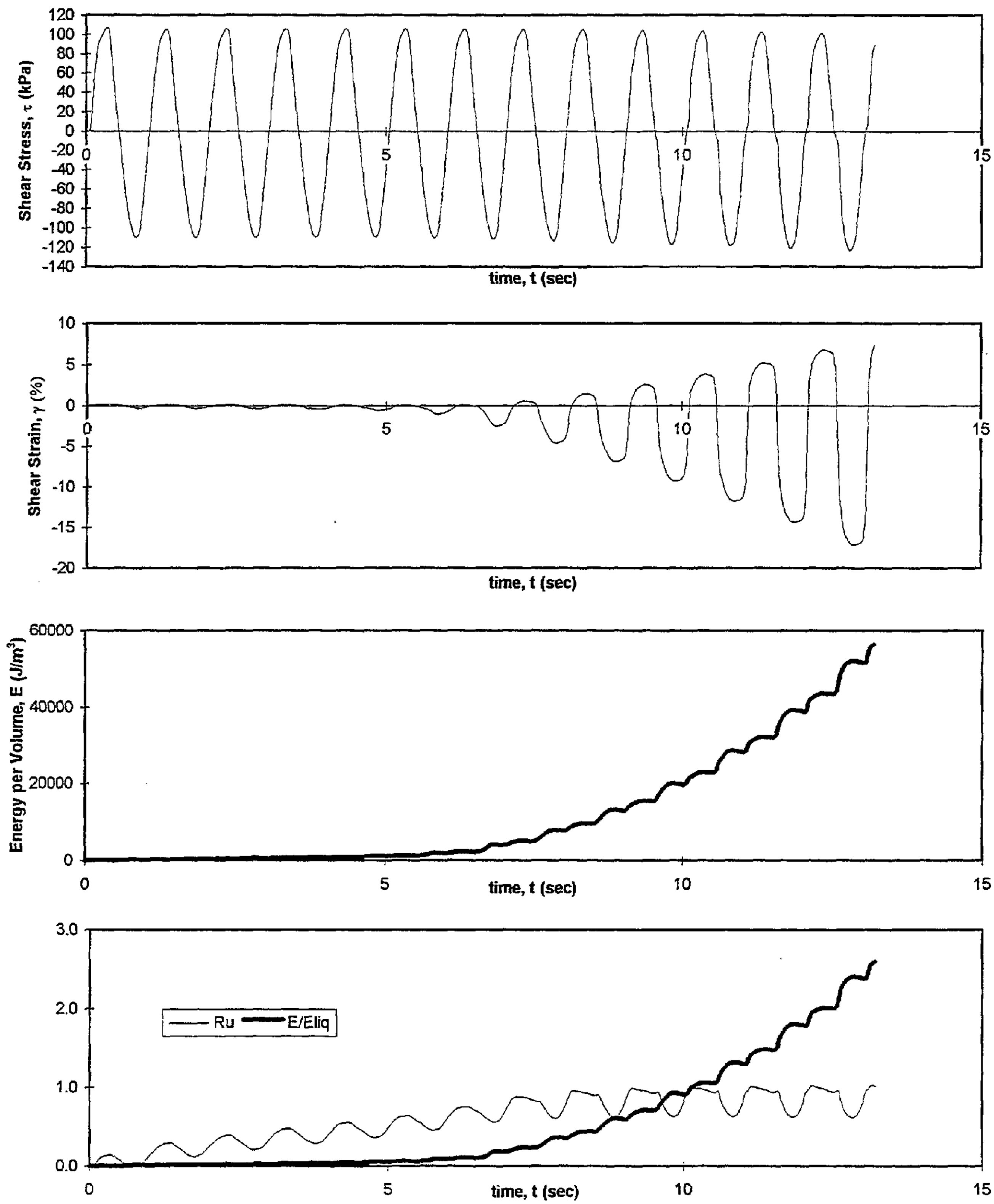

Test I.D.:	B23P4BCY	**Controlled Parameter:**	Stress
Fines Content (%):	11.4	**Initial Effective Stress (kPa):**	750
Dry Density (kN/m^3):	14.6		

Shear Stress vs. Shear Strain

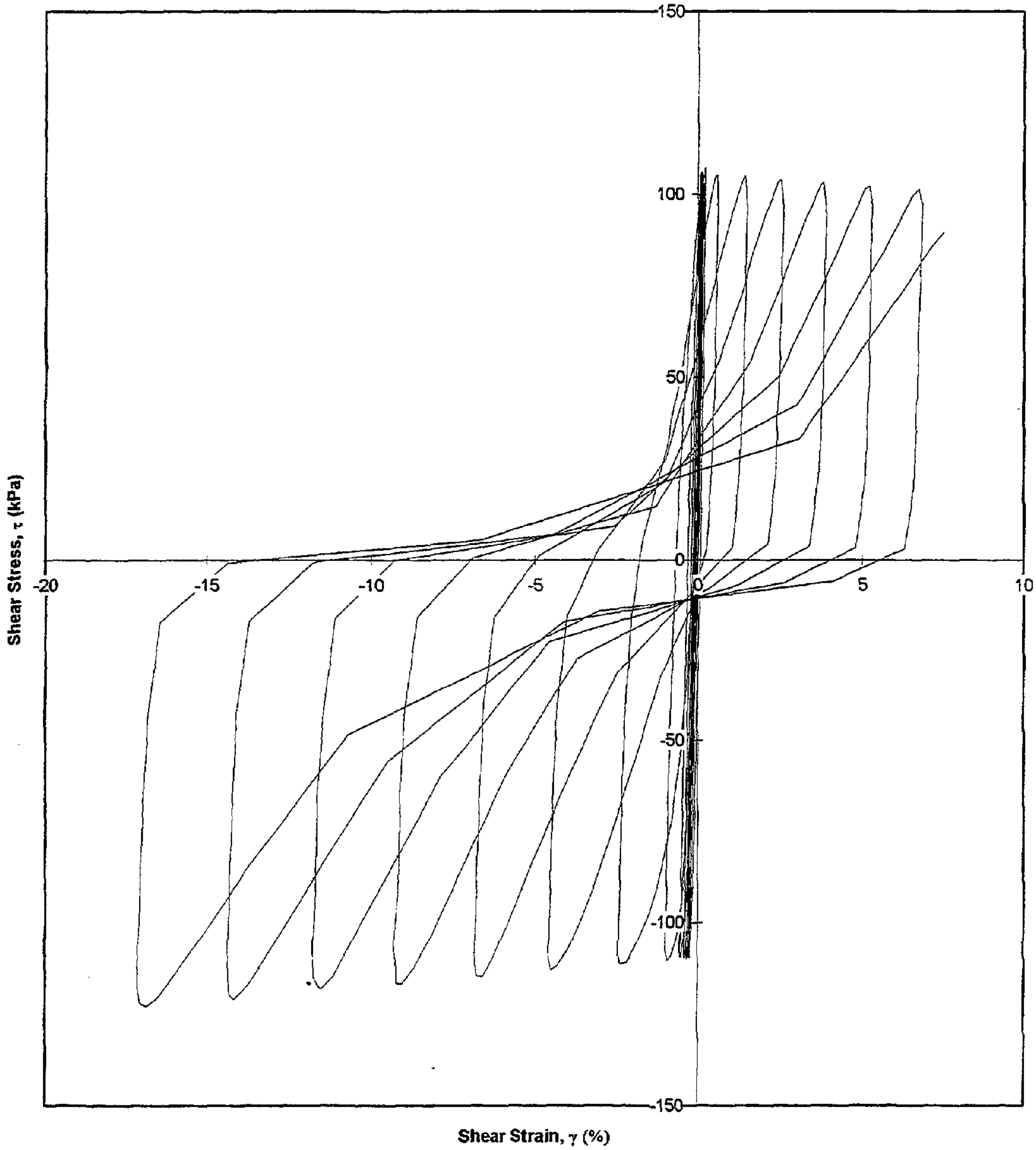

d:\nit\itp\cy_files\B23P4BCY.XLS 8/21/96 8:01 AM

Test I.D.:	B23P4MCY	**Controlled Parameter:**	Stress
Fines Content (%):	16.5	**Initial Effective Stress (kPa):**	700
Dry Density (kN/m^3):	15.53		

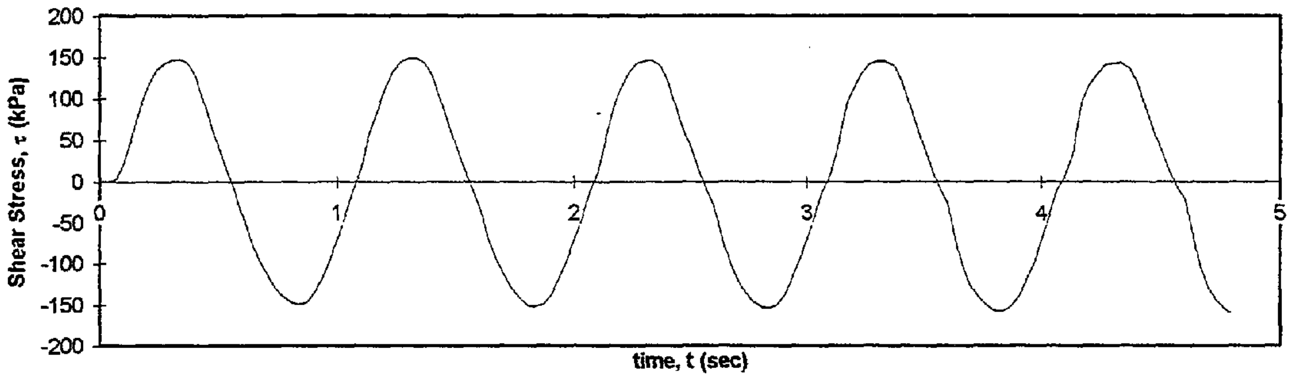

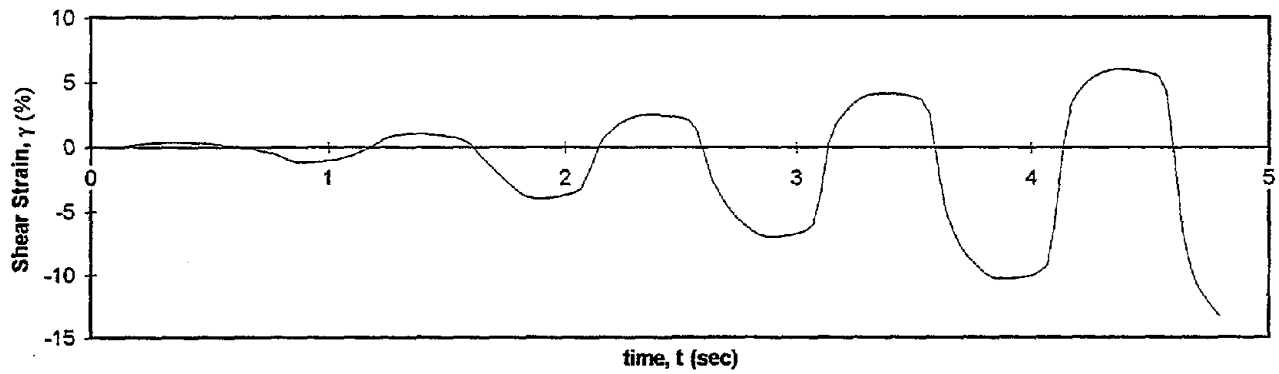

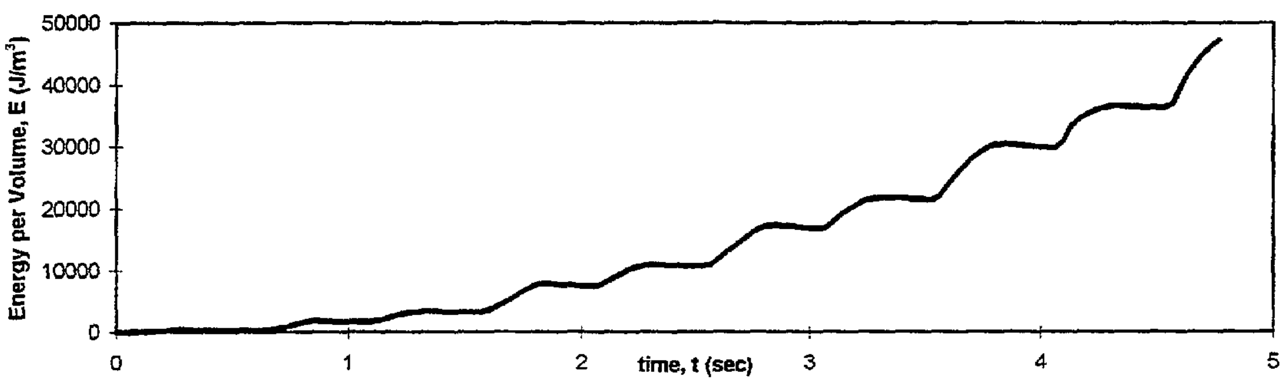

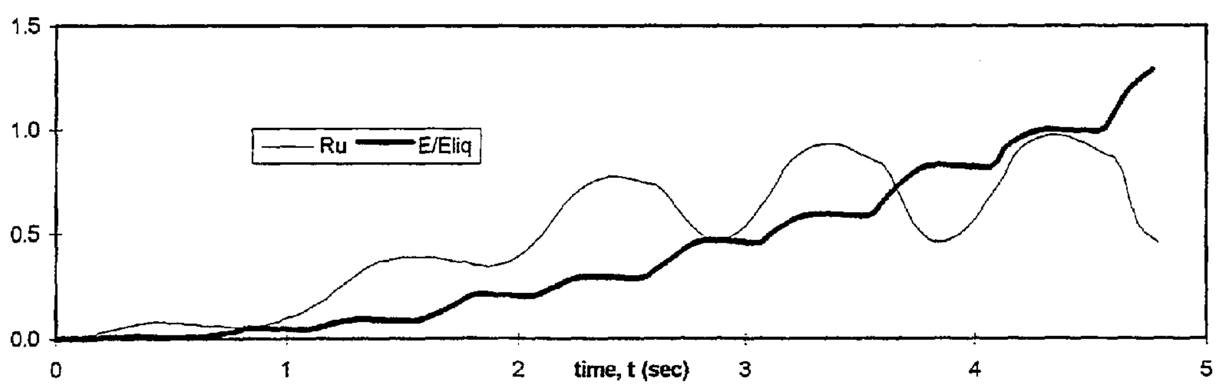

Test I.D.:	B23P4MCY	**Controlled Parameter:**	Stress
Fines Content (%):	16.5	**Initial Effective Stress (kPa):**	700
Dry Density (kN/m^3):	15.53		

Shear Stress vs. Shear Strain

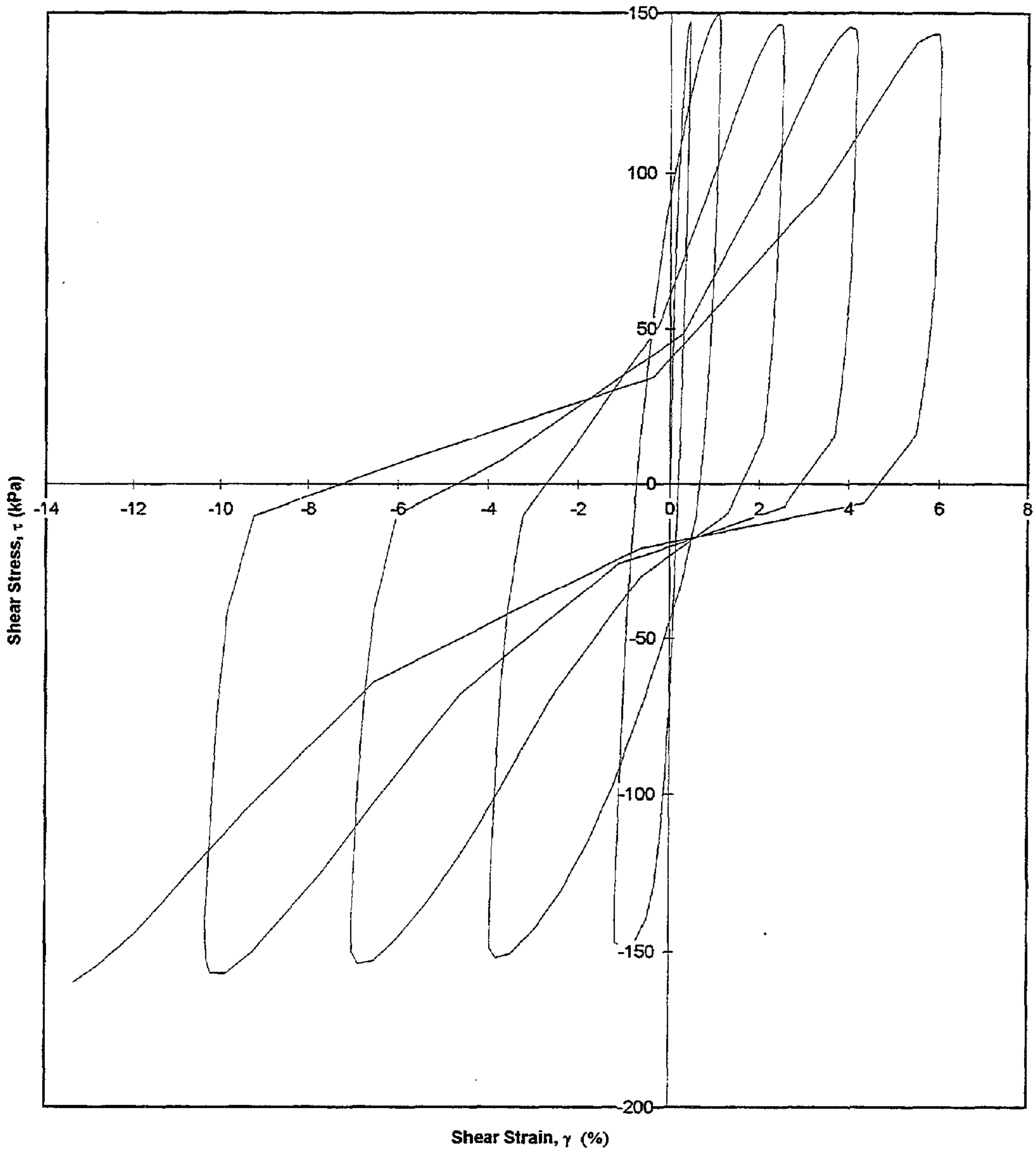

Test I.D.:	B23P4TCY	**Controlled Parameter:**	Stress
Fines Content (%):	28	**Initial Effective Stress (kPa):**	750
Dry Density (kN/m³):	N/A		

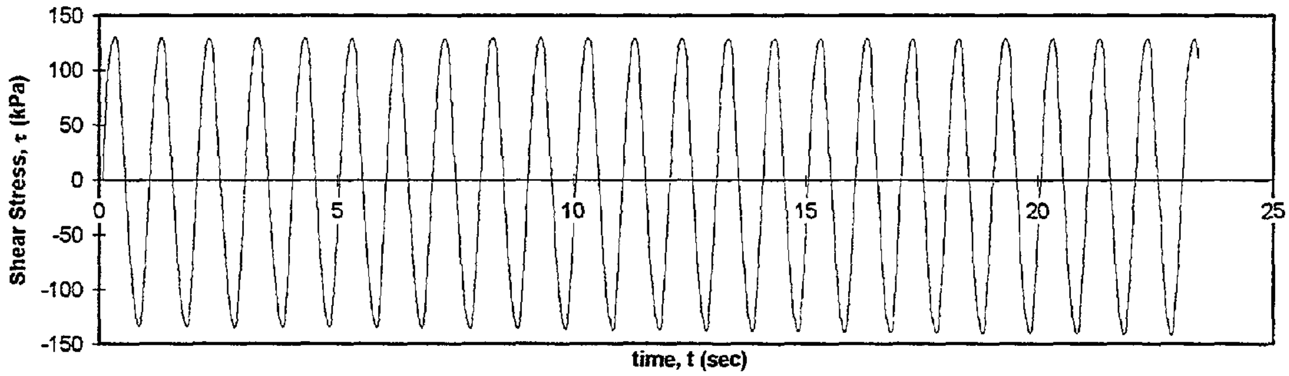

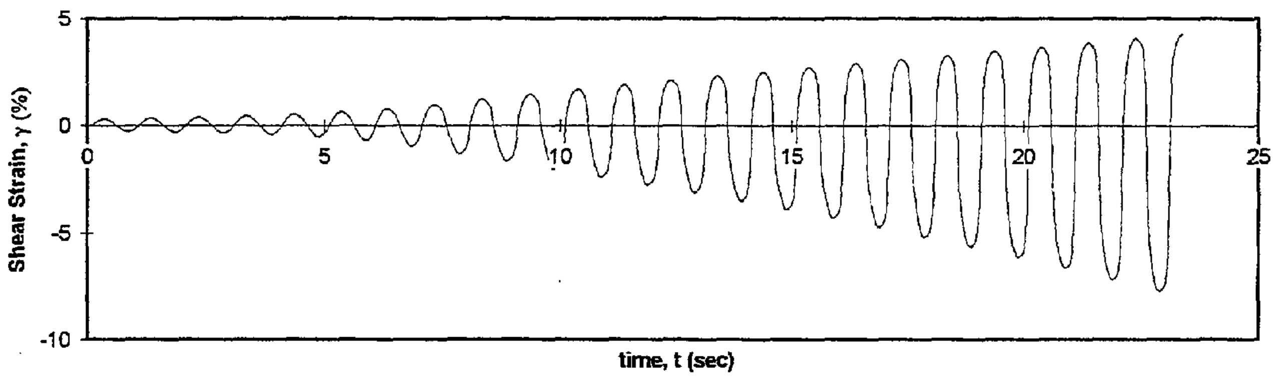

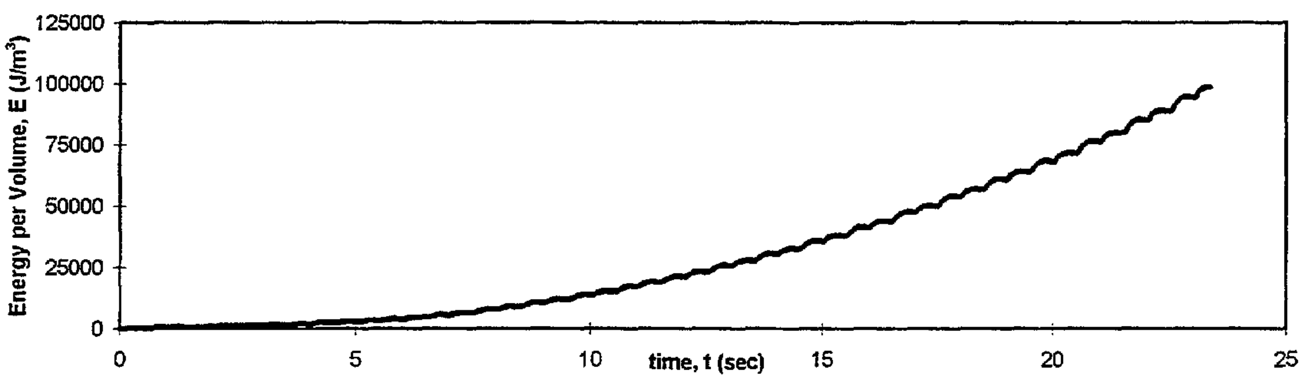

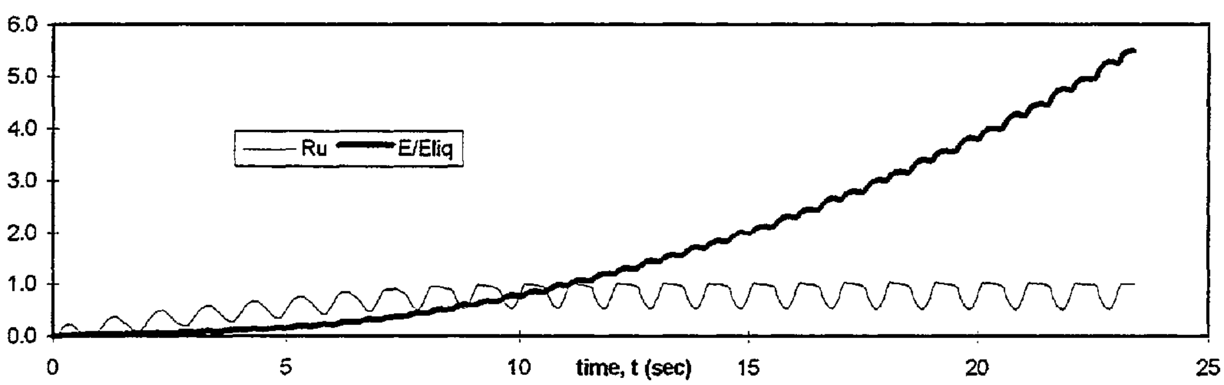

Test I.D.:	B23P4TCY	**Controlled Parameter:**	Stress
Fines Content (%):	28	**Initial Effective Stress (kPa):**	750
Dry Density (kN/m³):	N/A		

Shear Stress vs. Shear Strain

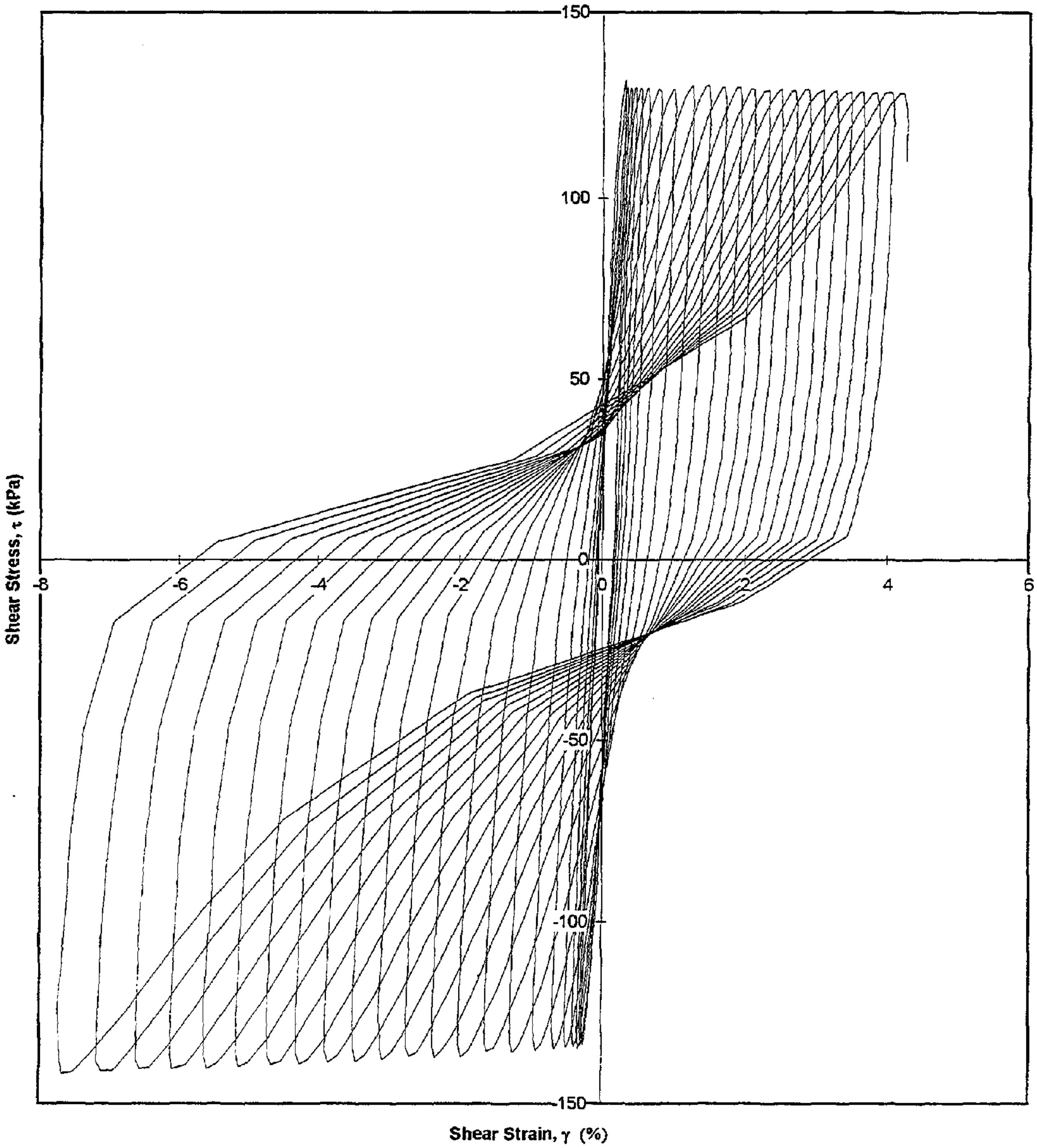

d:\nit\itp\cy_files\B23P4TCY.XLS 8/21/96 8:09 AM

Test I.D.:	B29P2TCY	**Controlled Parameter:**	Stress
Fines Content (%):	23	**Initial Effective Stress (kPa):**	750
Dry Density (kN/m³):	16.7		

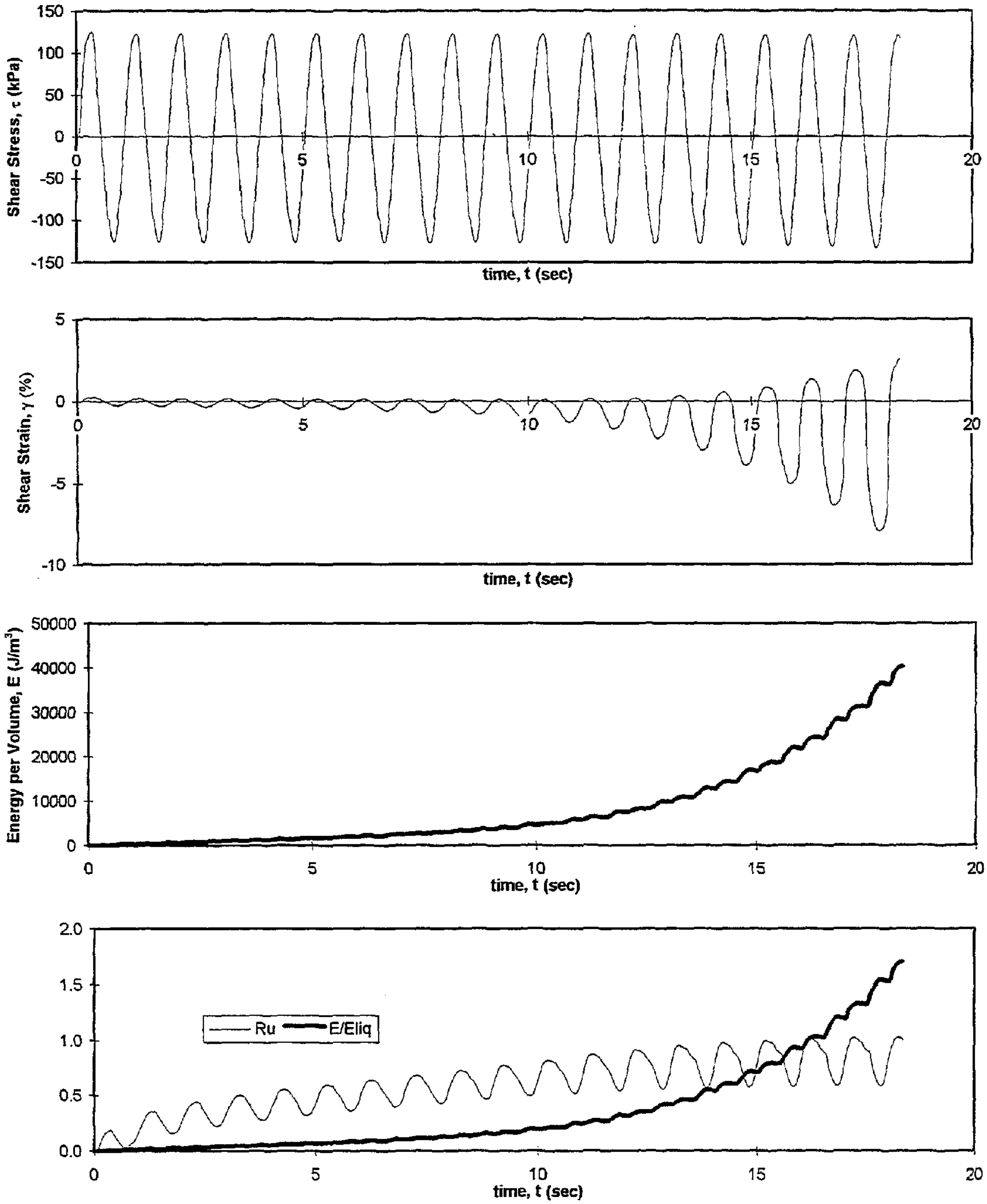

Test I.D.:	B29P2TCY	**Controlled Parameter:**	Stress
Fines Content (%):	23	**Initial Effective Stress (kPa):**	750
Dry Density (kN/m³):	16.7		

Shear Stress vs. Shear Strain

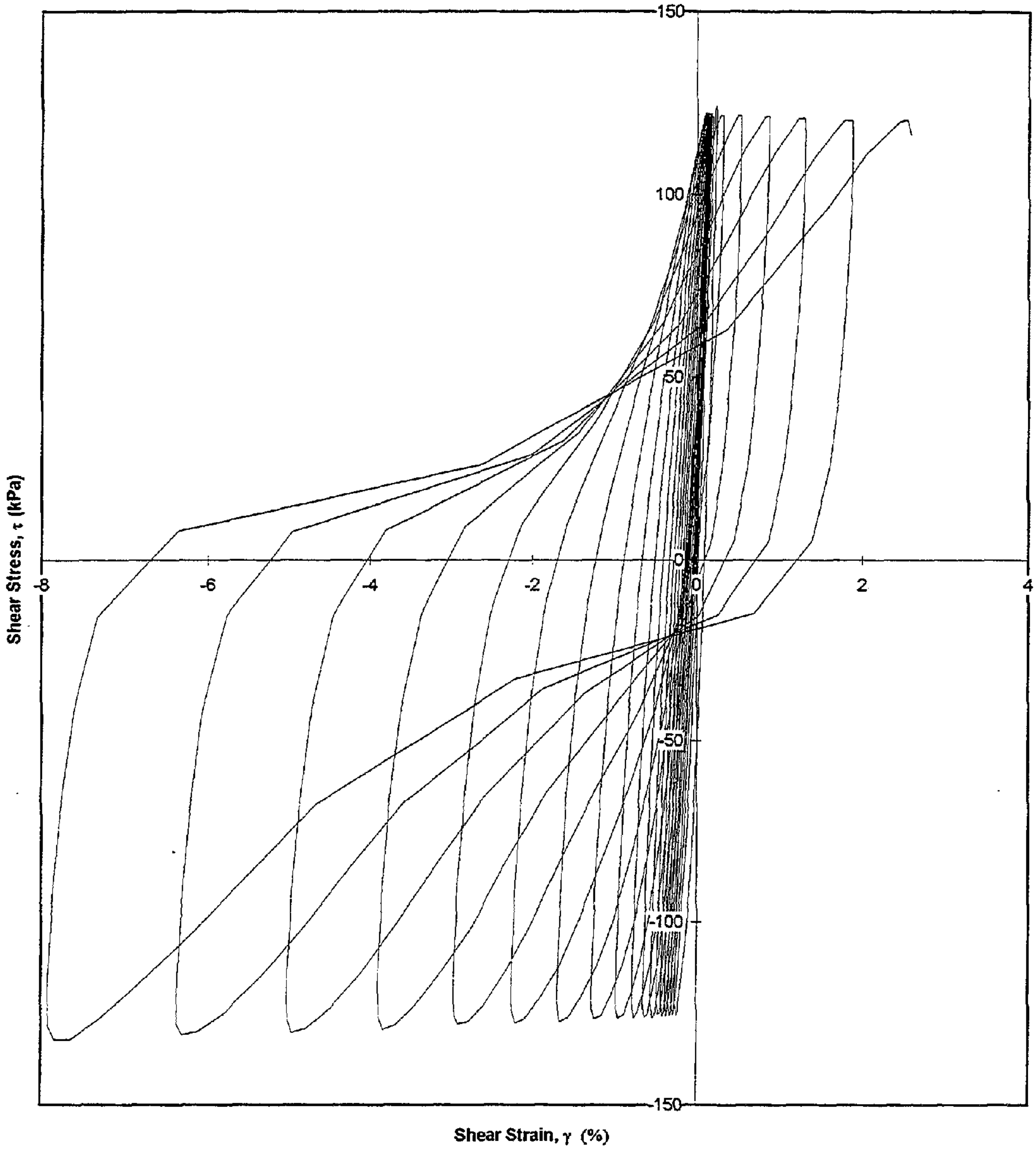

Test I.D.:	B2P6BCY	**Controlled Parameter:**	Stress
Fines Content (%):	18.9	**Initial Effective Stress (kPa):**	725
Dry Density (kN/m³):	16.73		

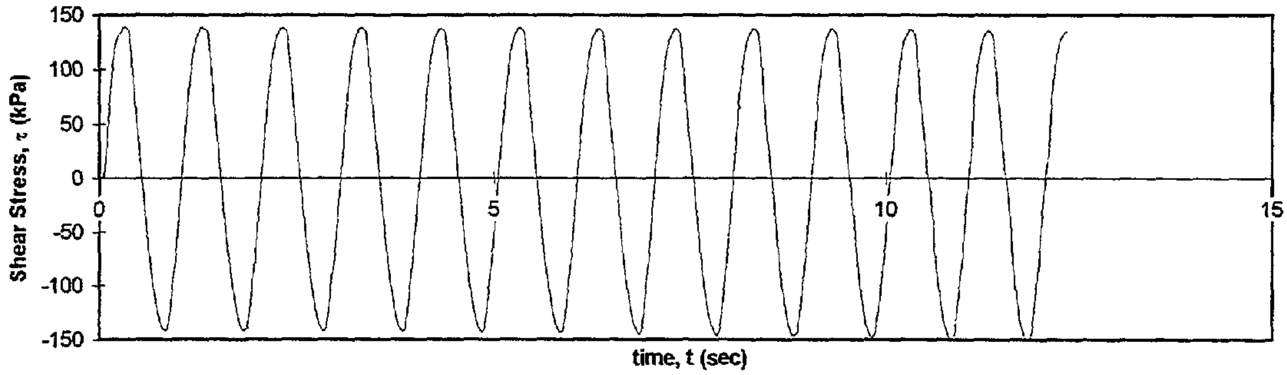

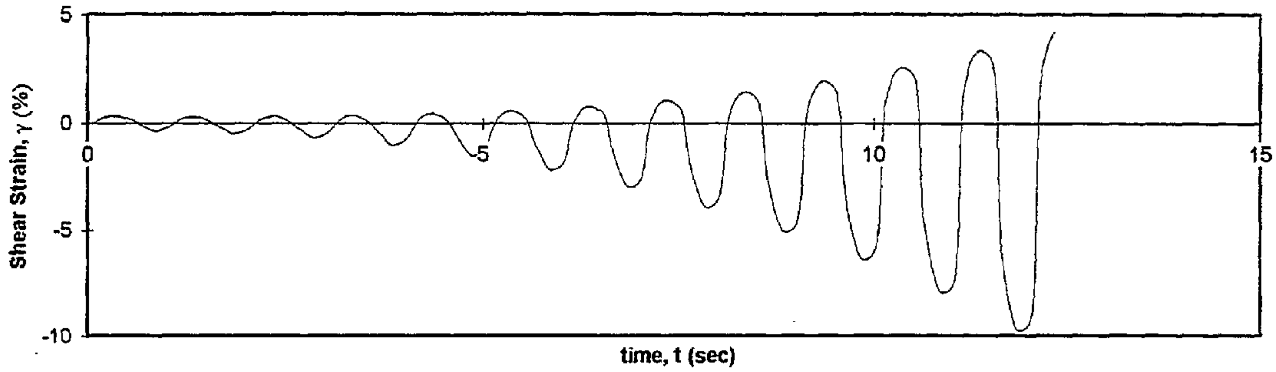

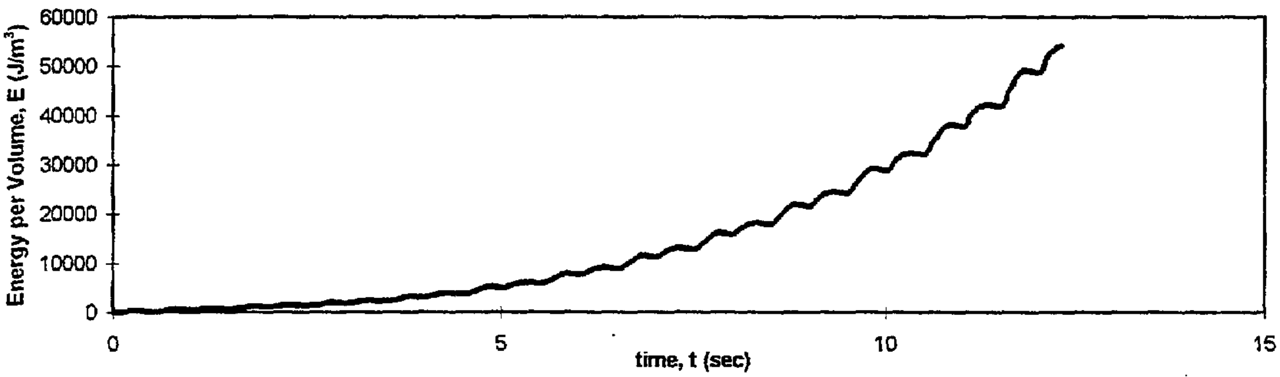

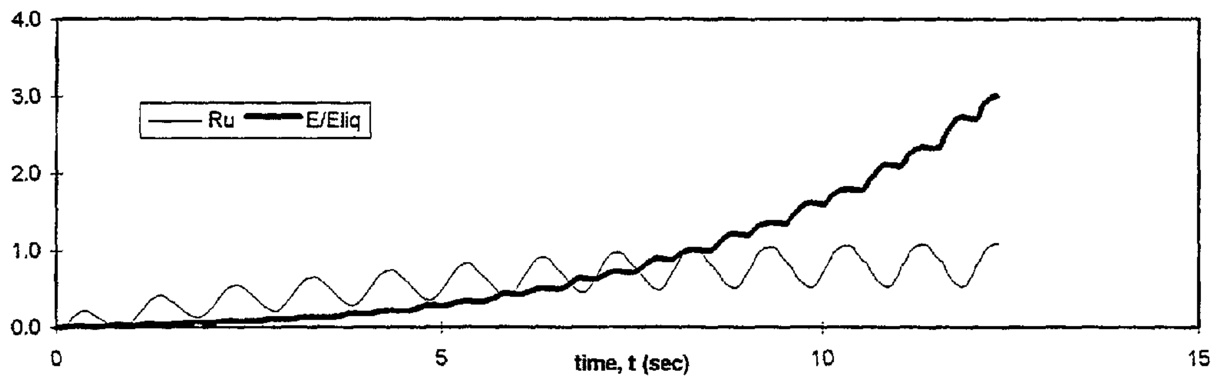

Test I.D.:	B2P6BCY	**Controlled Parameter:**	Stress
Fines Content (%):	18.9	**Initial Effective Stress (kPa):**	725
Dry Density (kN/m^3):	16.73		

Shear Stress vs. Shear Strain

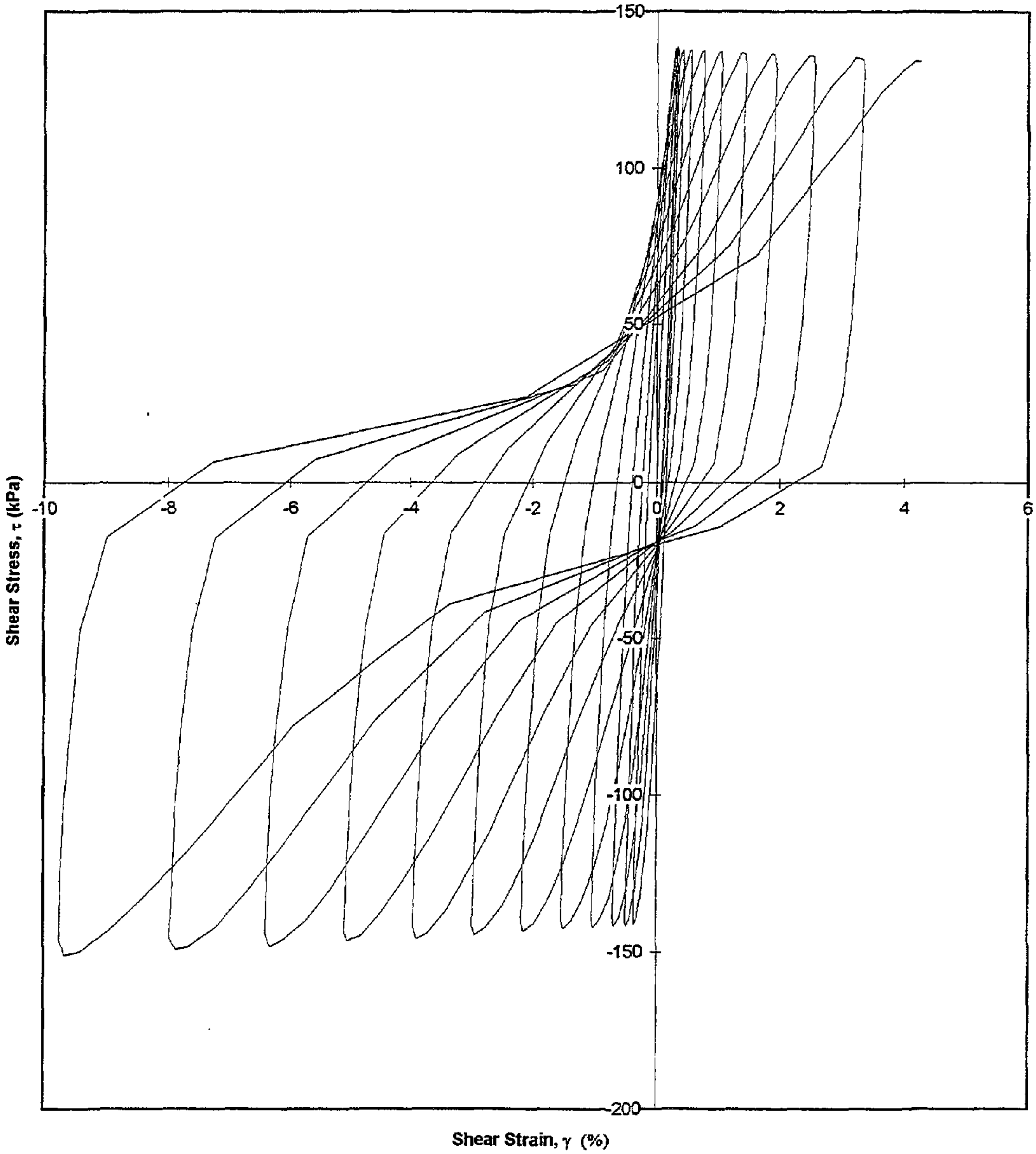

d:\nit\itp\cy_files\B2P6BCY.XLS 8/21/96 8:29 AM

Test I.D.:	B2P6MCY	**Controlled Parameter:**	Stress
Fines Content (%):	20.1	**Initial Effective Stress (kPa):**	743
Dry Density (kN/m³):	16.5		

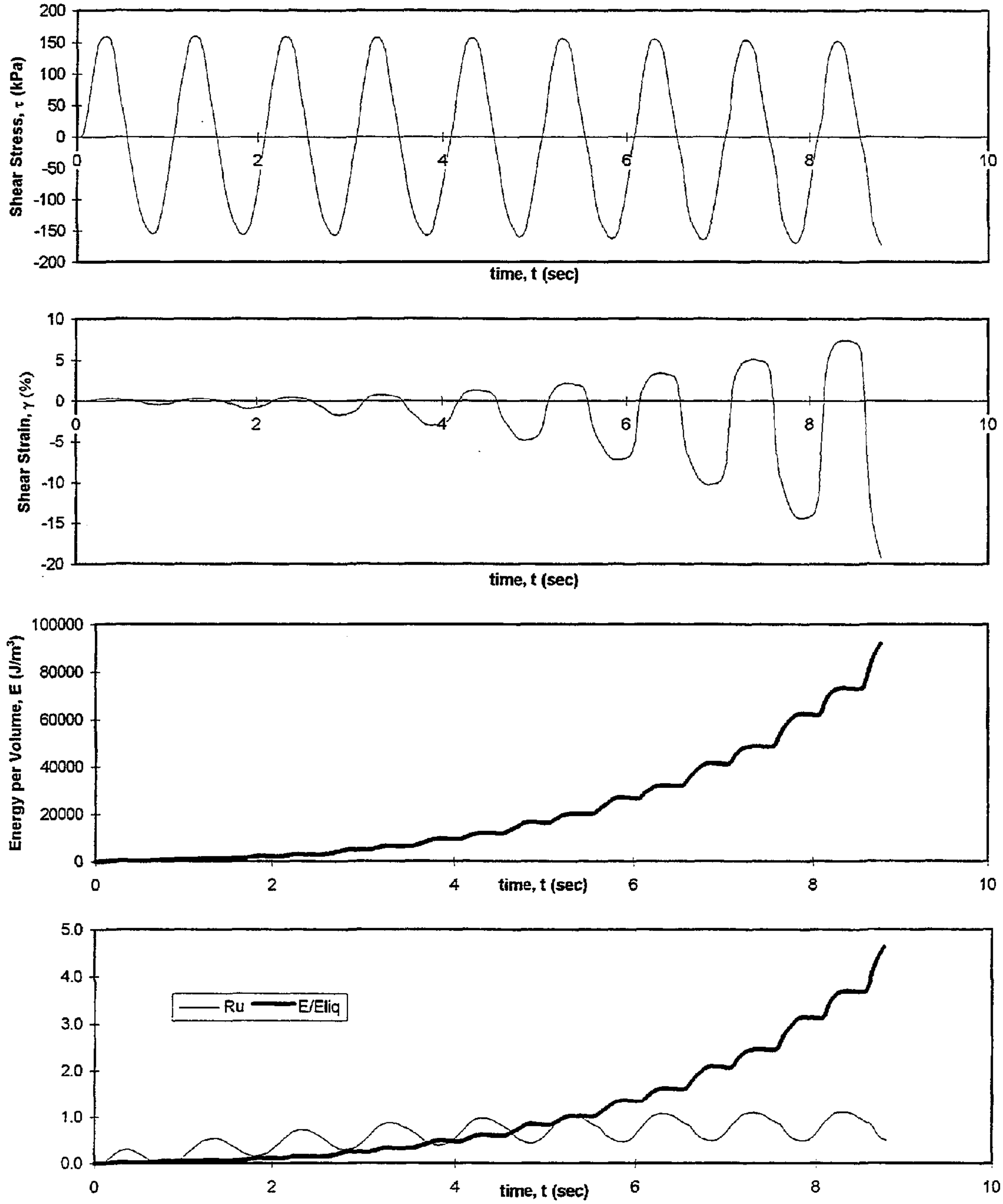

Test I.D.:	B2P6MCY	**Controlled Parameter:**	Stress
Fines Content (%):	20.1	**Initial Effective Stress (kPa):**	743
Dry Density (kN/m^3):	16.5		

Shear Stress vs. Shear Strain

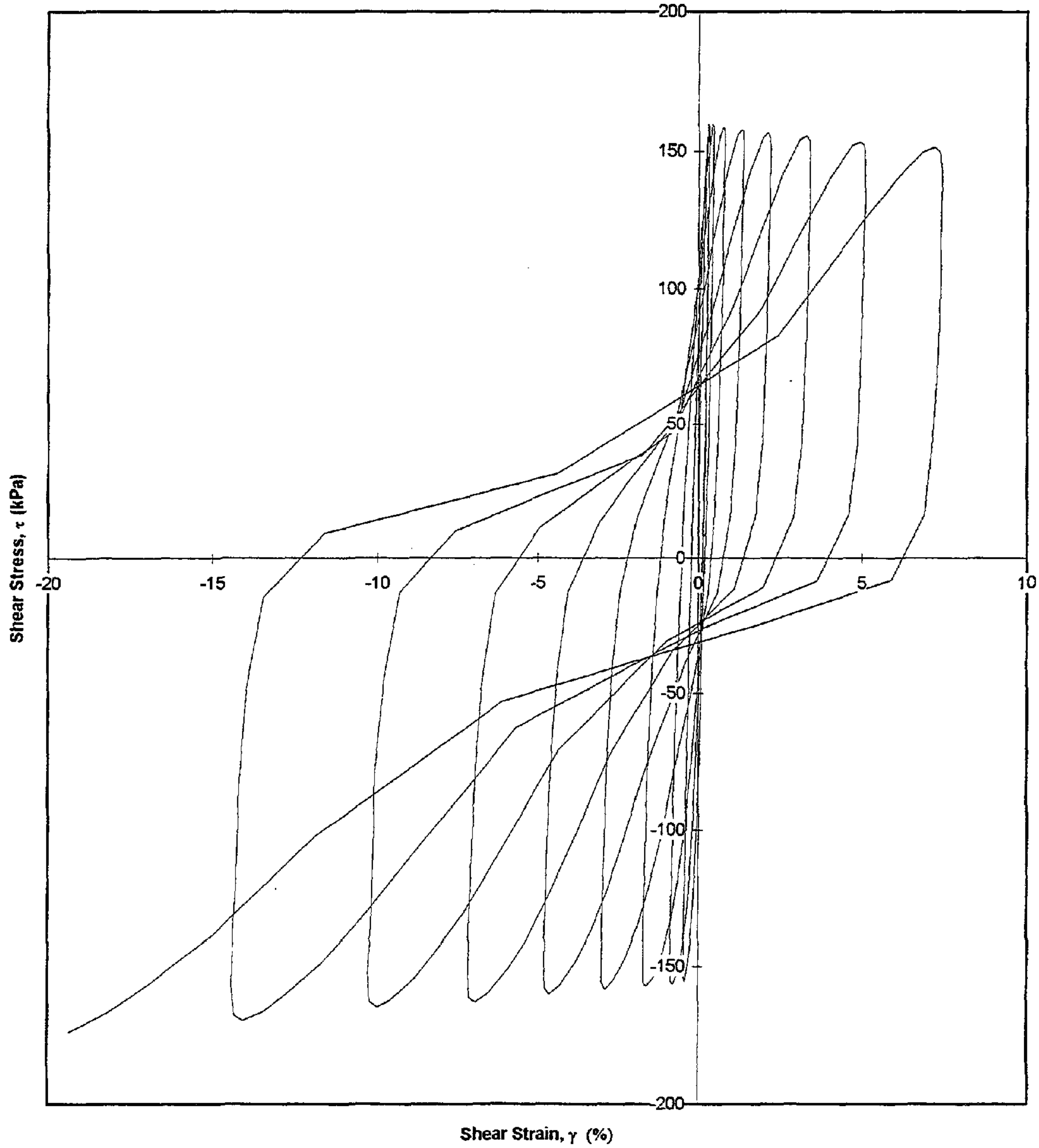

Test I.D.:	B2P6TCYC	**Controlled Parameter:**	Stress
Fines Content (%):	22.4	**Initial Effective Stress (kPa):**	750
Dry Density (kN/m^3):	16.03		

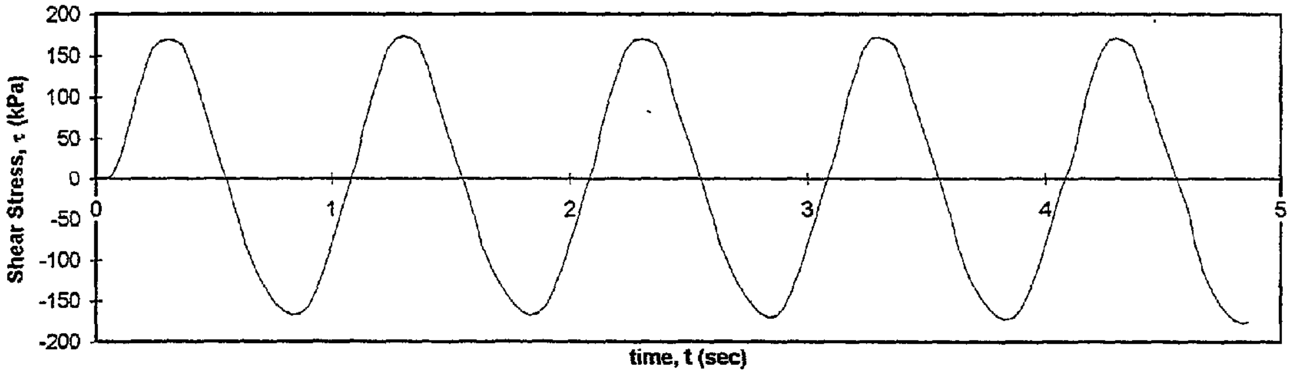

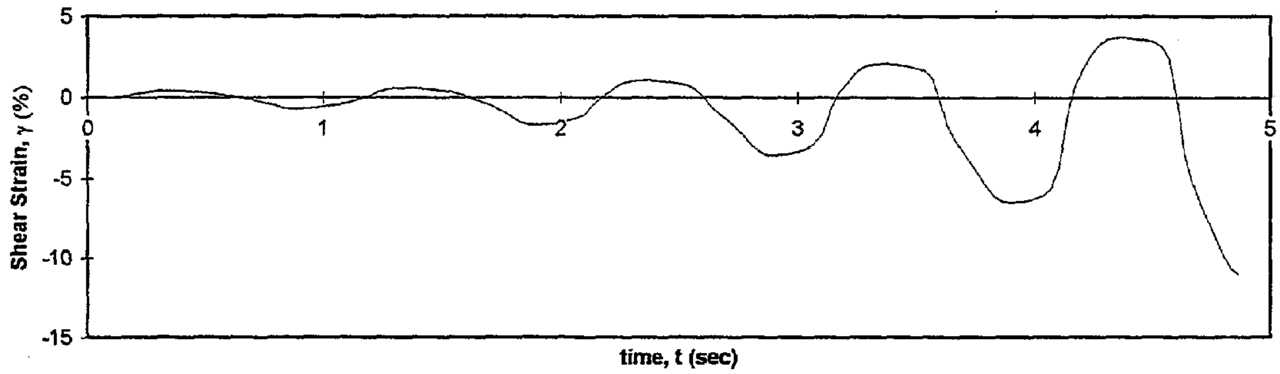

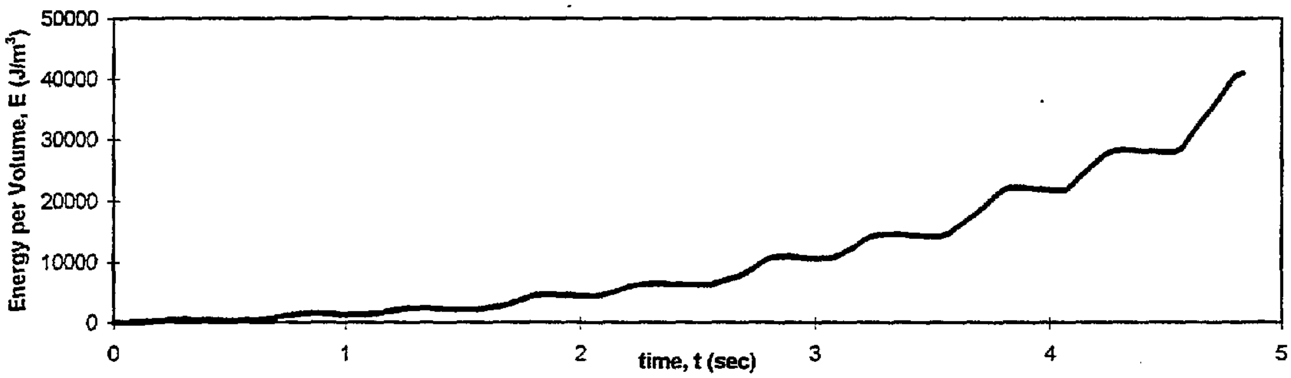

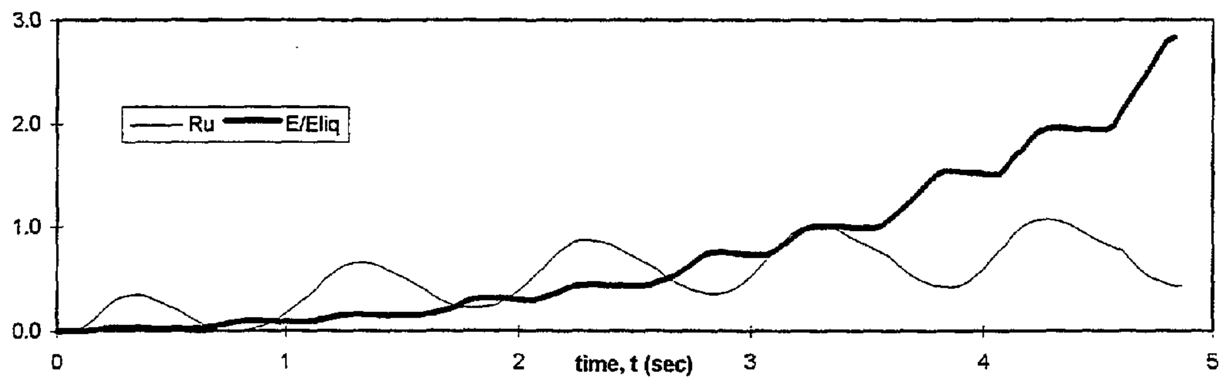

Test I.D.:	B2P6TCYC	**Controlled Parameter:**	Stress
Fines Content (%):	22.4	**Initial Effective Stress (kPa):**	750
Dry Density (kN/m^3):	16.03		

Shear Stress vs. Shear Strain

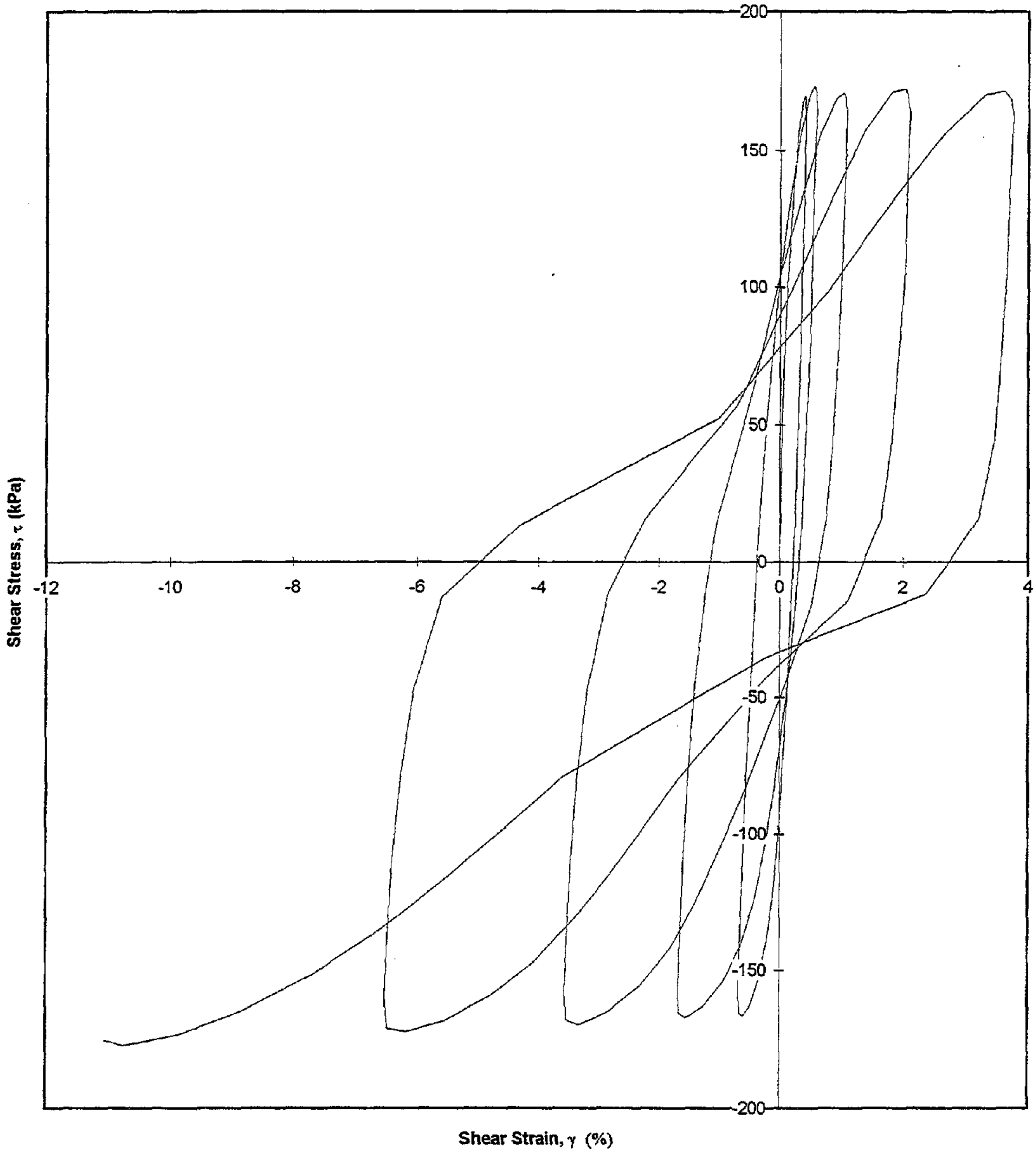

APPENDIX C

LABORATORY TESTS ON SOIL SAMPLES, PERFORMED AT THE UNIVERSITY OF COLORADO

Table C.1 - Summary of the Cyclic Torsional Test Data on Clean and Silty Sands Performed at University of Colorado

No.	Test ID	Sample	D_r(%)	E_{liq} (J/m^3)	FC (%)	γ_d (kN/m^3)	P. I.	Control	σ_c' (kPa)	Freq. (Hz)	Load Shape
1	UOFC5	F11	32.6	3728	0	14.5		Stress	199.9	0.1	Sinusoidal 2-way
2	UOFC7	F11	41.0	12495	0	14.7		Stress	204.8	0.1	Sinusoidal 2-way
3	UOFC9	F11	42.0	16997	0	14.8		Stress	304.1	0.1	Sinusoidal 2-way
4	UOFC13	F43	N/A	3450	20	15.3	10.0	Stress	299.9	0.1	Sinusoidal 2-way
5	UOFC14	F46	N/A	4753	20	15.2	25.0	Stress	199.9	0.1	Sinusoidal 2-way
6	UOFC15	F46	N/A	2485	20	15.2	25.0	Stress	201.3	0.1	Sinusoidal 2-way
7	UOFC17	F64	N/A	3427	45	16.2	15.0	Stress	203.4	0.1	Sinusoidal 2-way
8	UOFC18	F64	N/A	3993	45	16.2	15.0	Stress	190.3	0.1	Sinusoidal 2-way
9	UOFC23	F11	45.3	7437	0	14.9		Stress	199.9	0.1	Sinusoidal 2-way

Test Results Following the Sequence of Test ID's are Attached.

Test I.D.:	UOFC5	**Controlled Parameter:**	Stress
Fines Content (%):	Clean Sand	**Initial Effective Stress (kPa):**	200
Relative Density (%):	32.6		

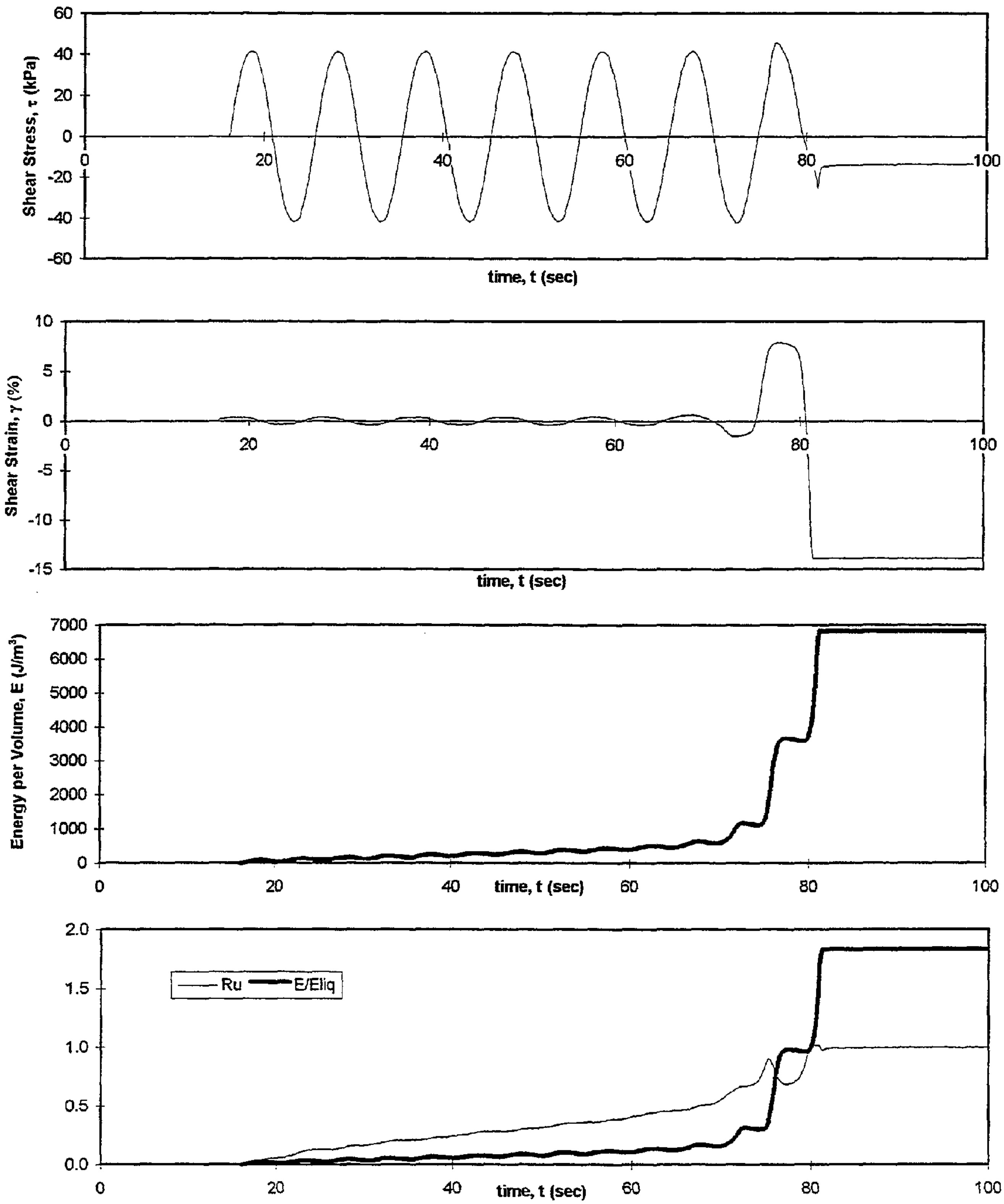

d:\nit\itp\cy_files\UOFC5.XLS 8/19/96 4:18 PM

Test I.D.:	UOFC5	**Controlled Parameter:**	Stress
Fines Content (%):	Clean Sand	**Initial Effective Stress (kPa):**	200
Relative Density (%):	32.6		

Shear Stress vs. Shear Strain

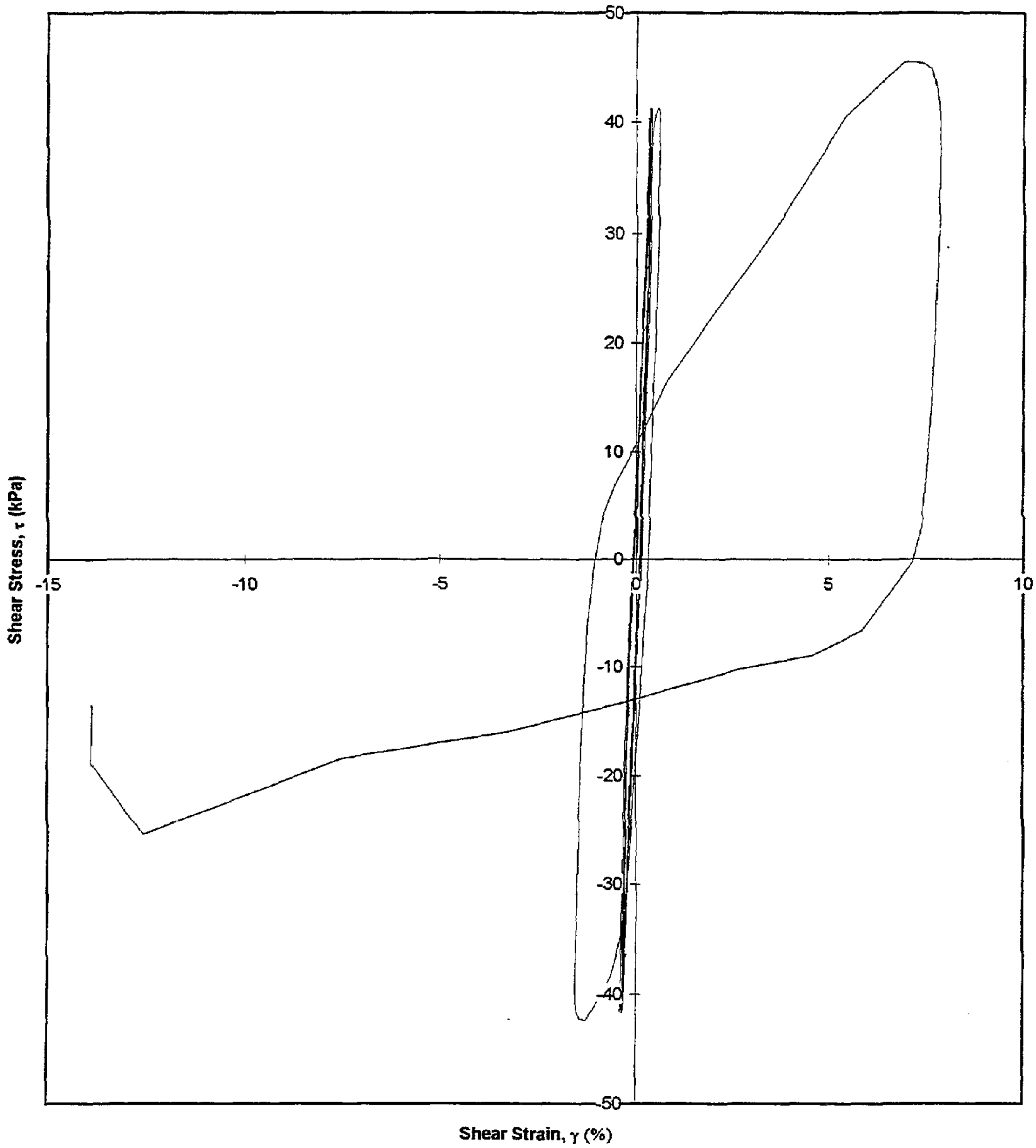

Test I.D.:	UOFC7	**Controlled Parameter:**	Stress
Fines Content (%):	Clean Sand	**Initial Effective Stress (kPa):**	205
Relative Density (%):	41		

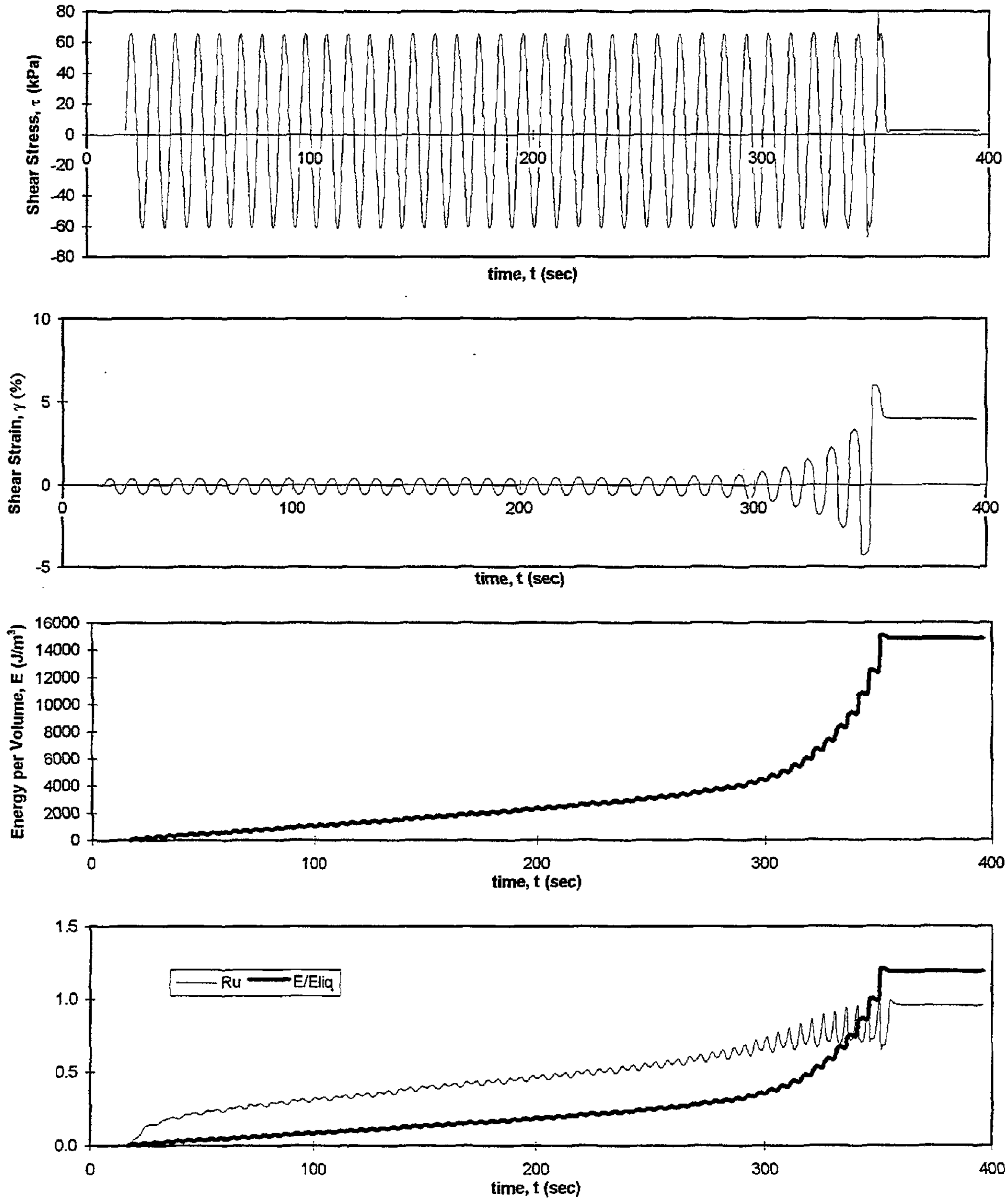

d:\nit\itp\cy_files\UOFC7.XLS 8/21/96 9:22 AM

Test I.D.:	UOFC7	**Controlled Parameter:**	Stress
Fines Content (%):	Clean Sand	**Initial Effective Stress (kPa):**	205
Relative Density (%):	41		

Shear Stress vs. Shear Strain

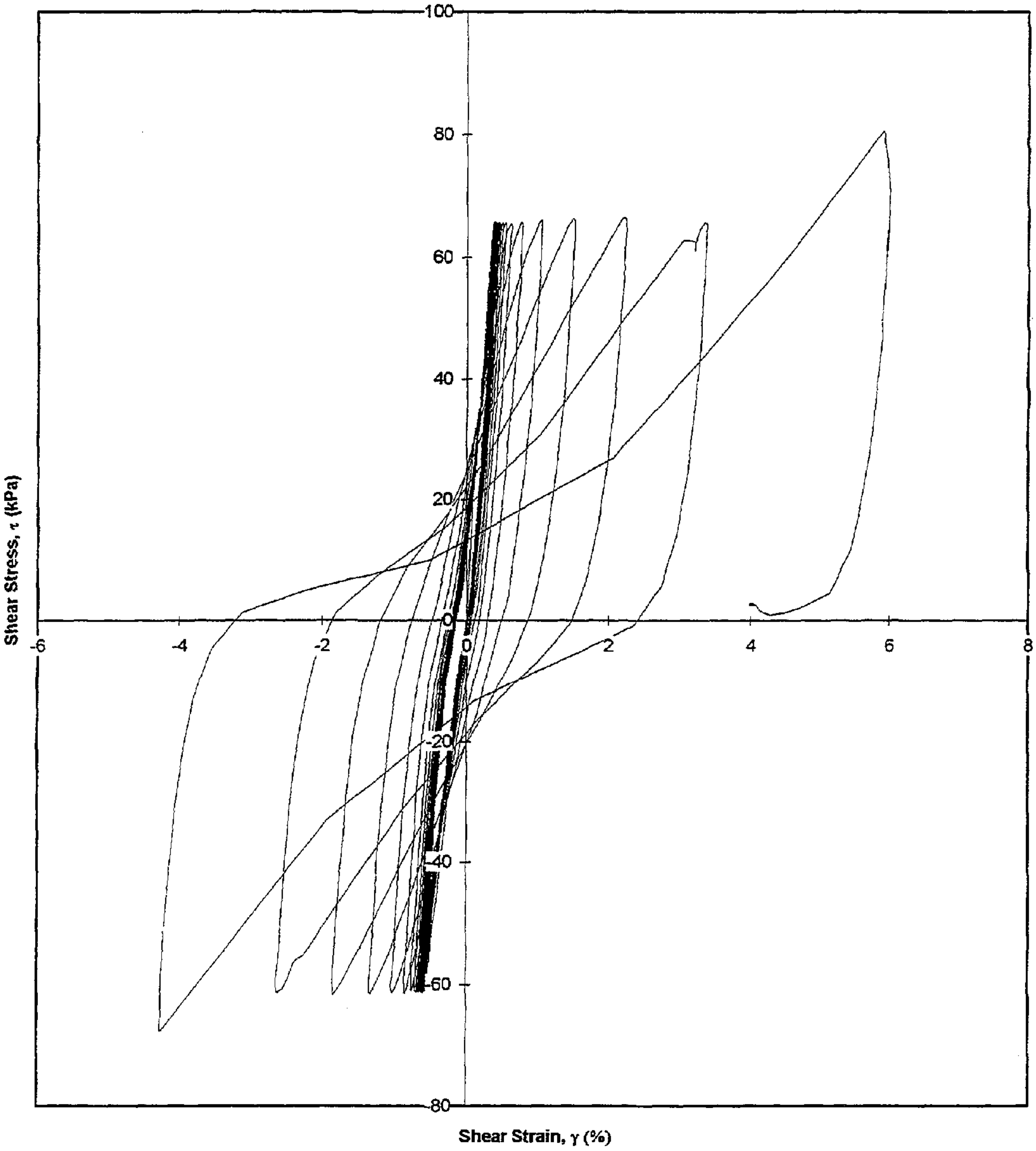

Test I.D.:	UOFC9	**Controlled Parameter:**	Stress
Fines Content (%):	Clean Sand	**Initial Effective Stress (kPa):**	304
Relative Density (%):	42		

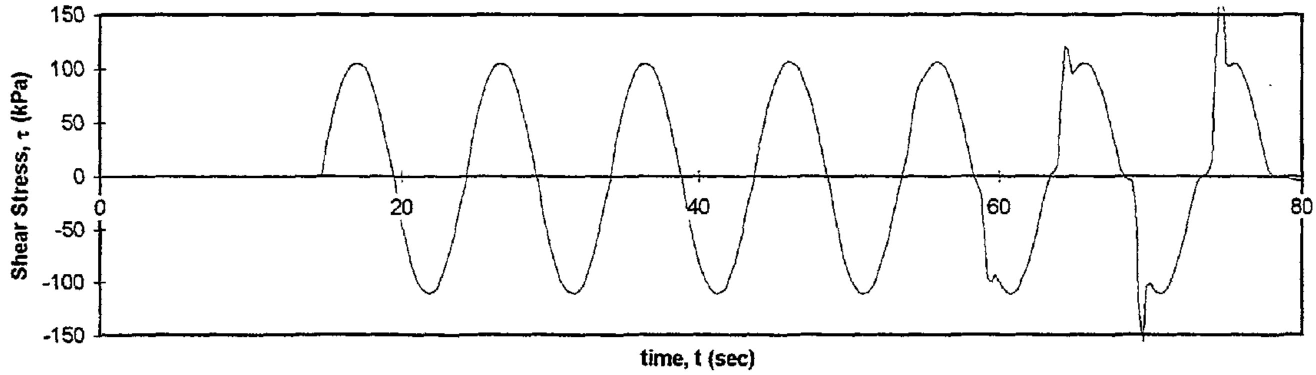

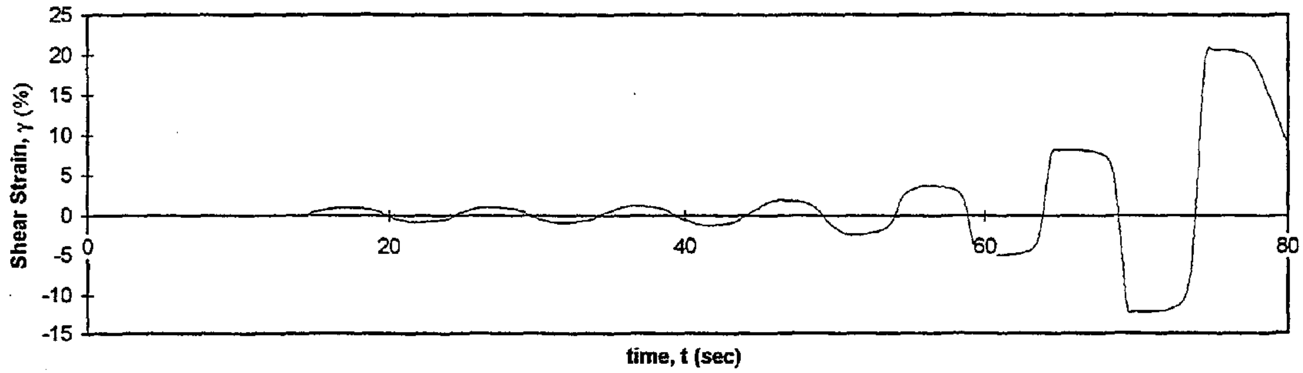

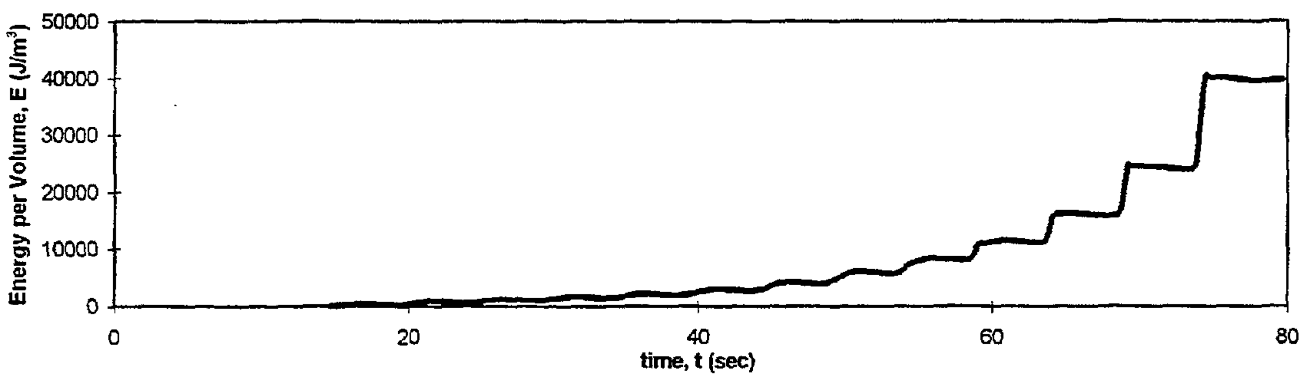

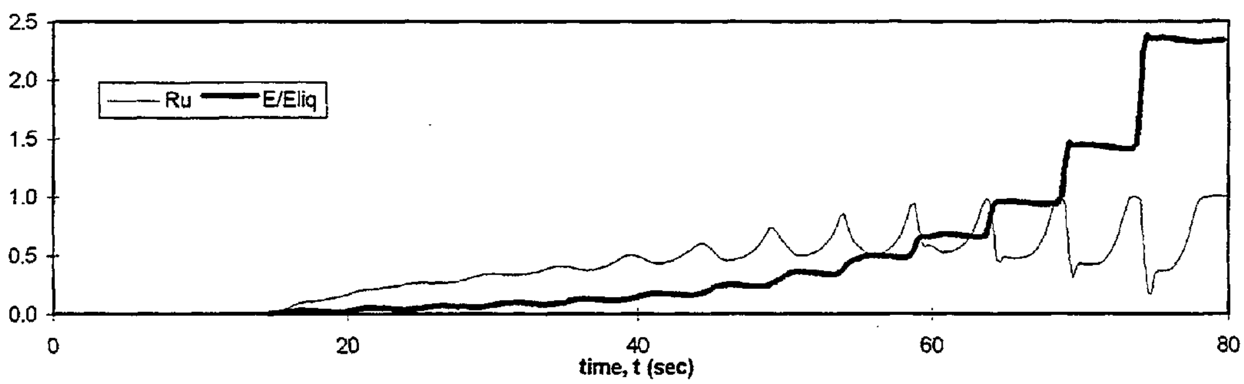

d:\nit\itp\cy_files\UOFC9.XLS 8/21/96 9:23 AM

Test I.D.:	UOFC9	**Controlled Parameter:**	Stress
Fines Content (%):	Clean Sand	**Initial Effective Stress (kPa):**	304
Relative Density (%):	42		

Shear Stress vs. Shear Strain

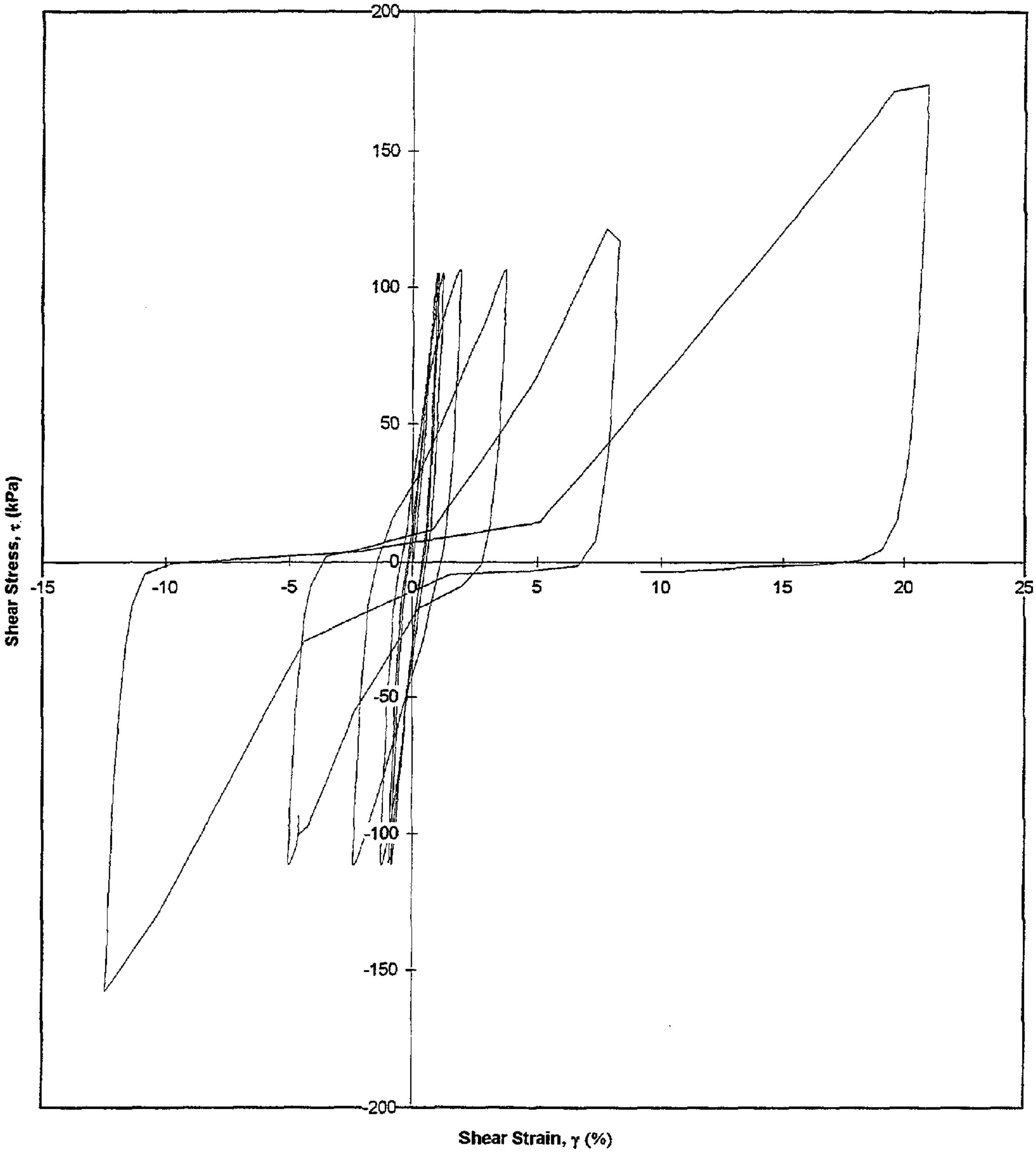

Test I.D.:	UOFC13	**Controlled Parameter:**	Stress
Fines Content (%):	20	**Initial Effective Stress (kPa):**	300
Dry Density (kN/m³)	15.26		

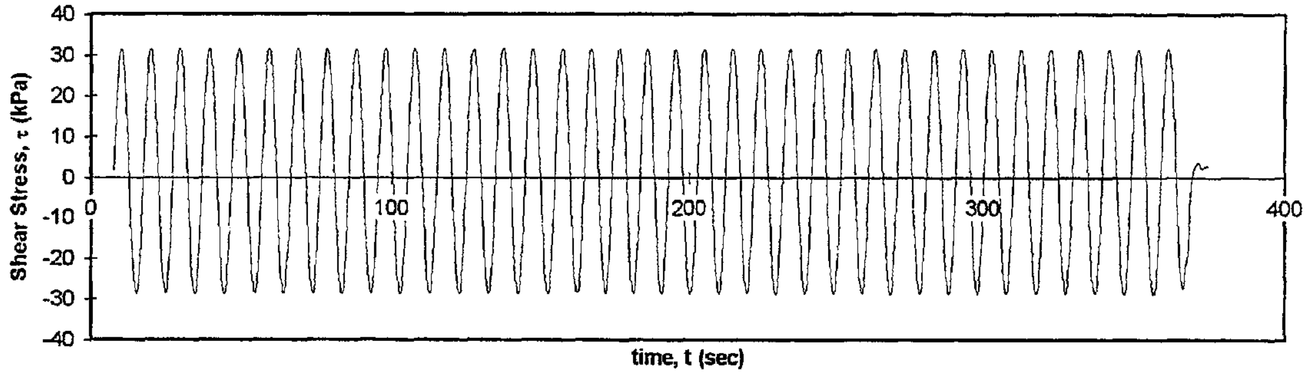

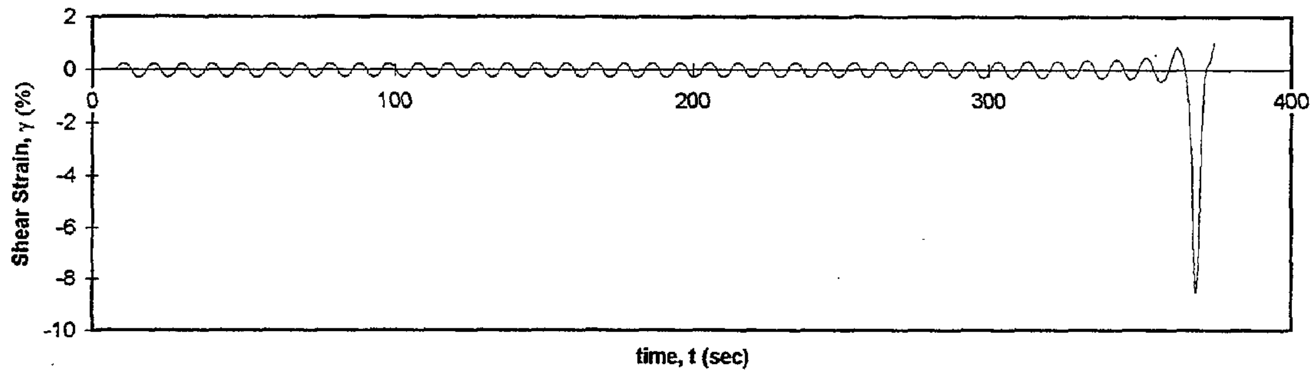

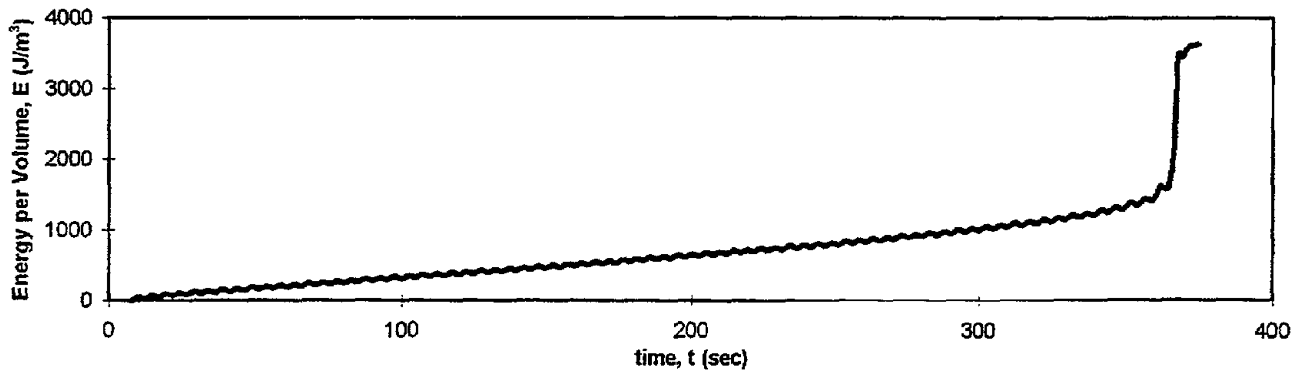

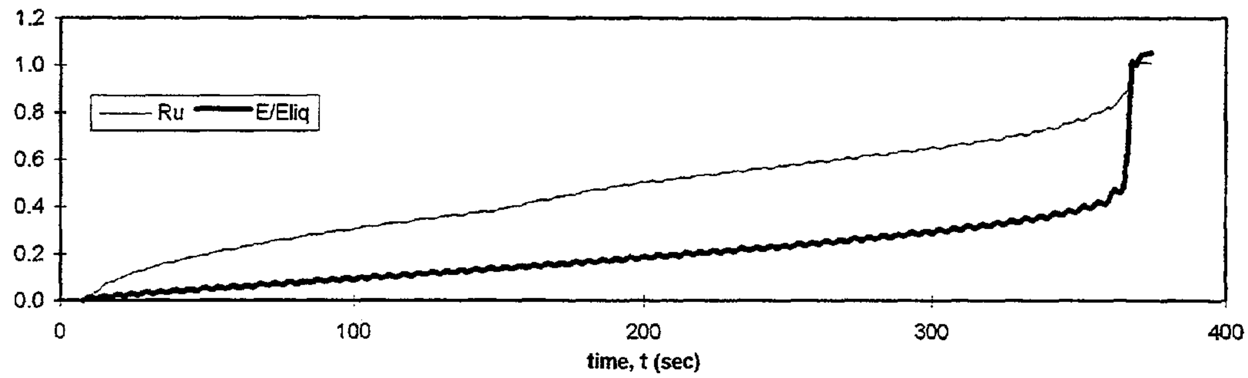

Test I.D.:	UOFC13	**Controlled Parameter:**	Stress
Fines Content (%):	20	**Initial Effective Stress (kPa):**	300
Dry Density (kN/m^3)	15.26		

Shear Stress vs. Shear Strain

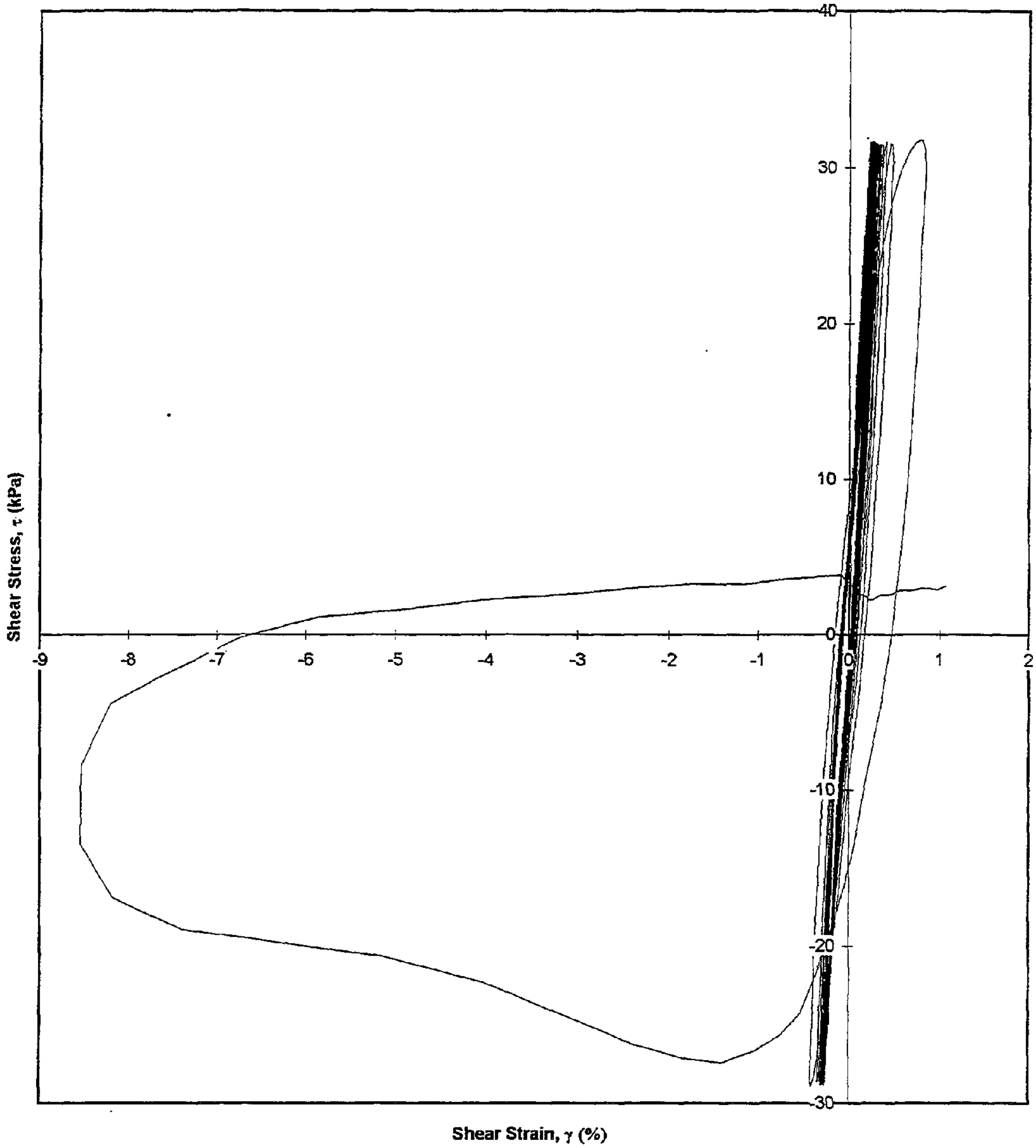

Test I.D.:	UOFC14	**Controlled Parameter:**	Stress
Fines Content (%):	20	**Initial Effective Stress (kPa):**	200
Dry Density (kN/m³)	15.18		

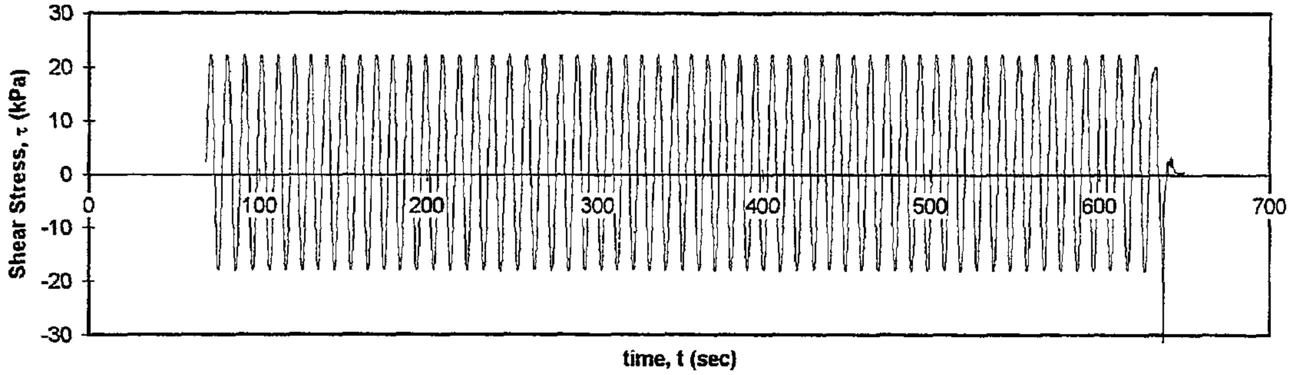

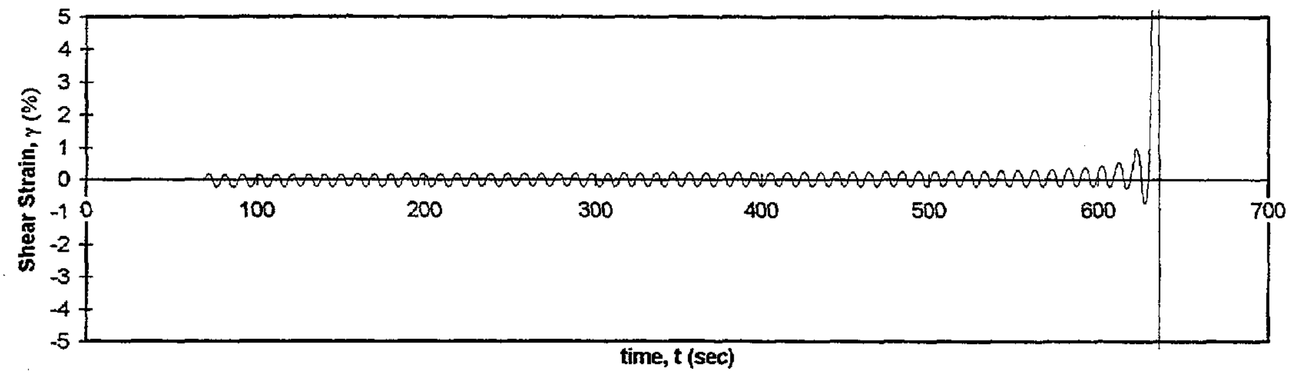

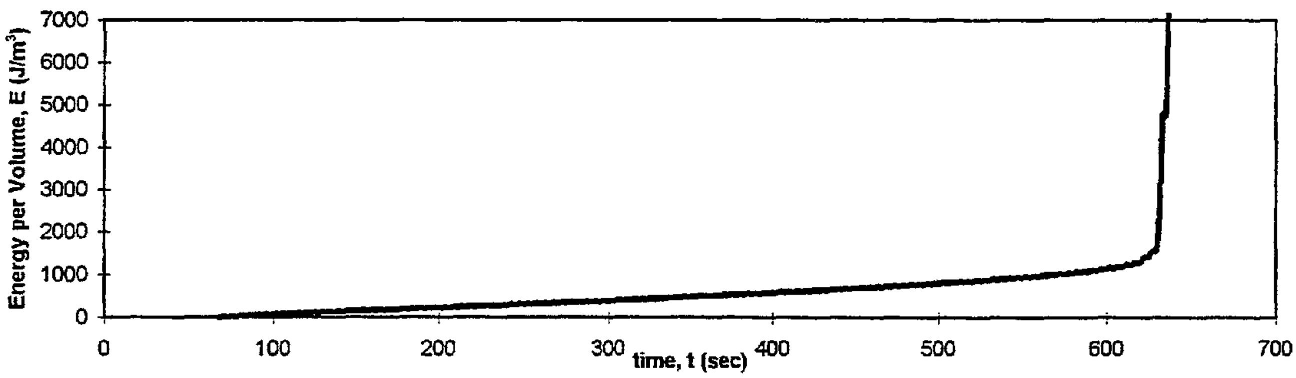

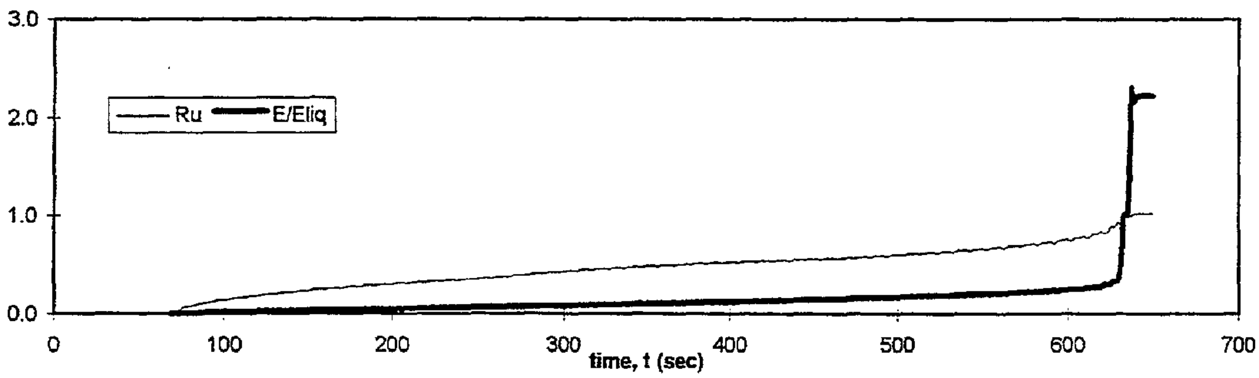

Test I.D.:	UOFC14	**Controlled Parameter:**	Stress
Fines Content (%):	20	**Initial Effective Stress (kPa):**	200
Dry Density (kN/m^3)	15.18		

Shear Stress vs. Shear Strain

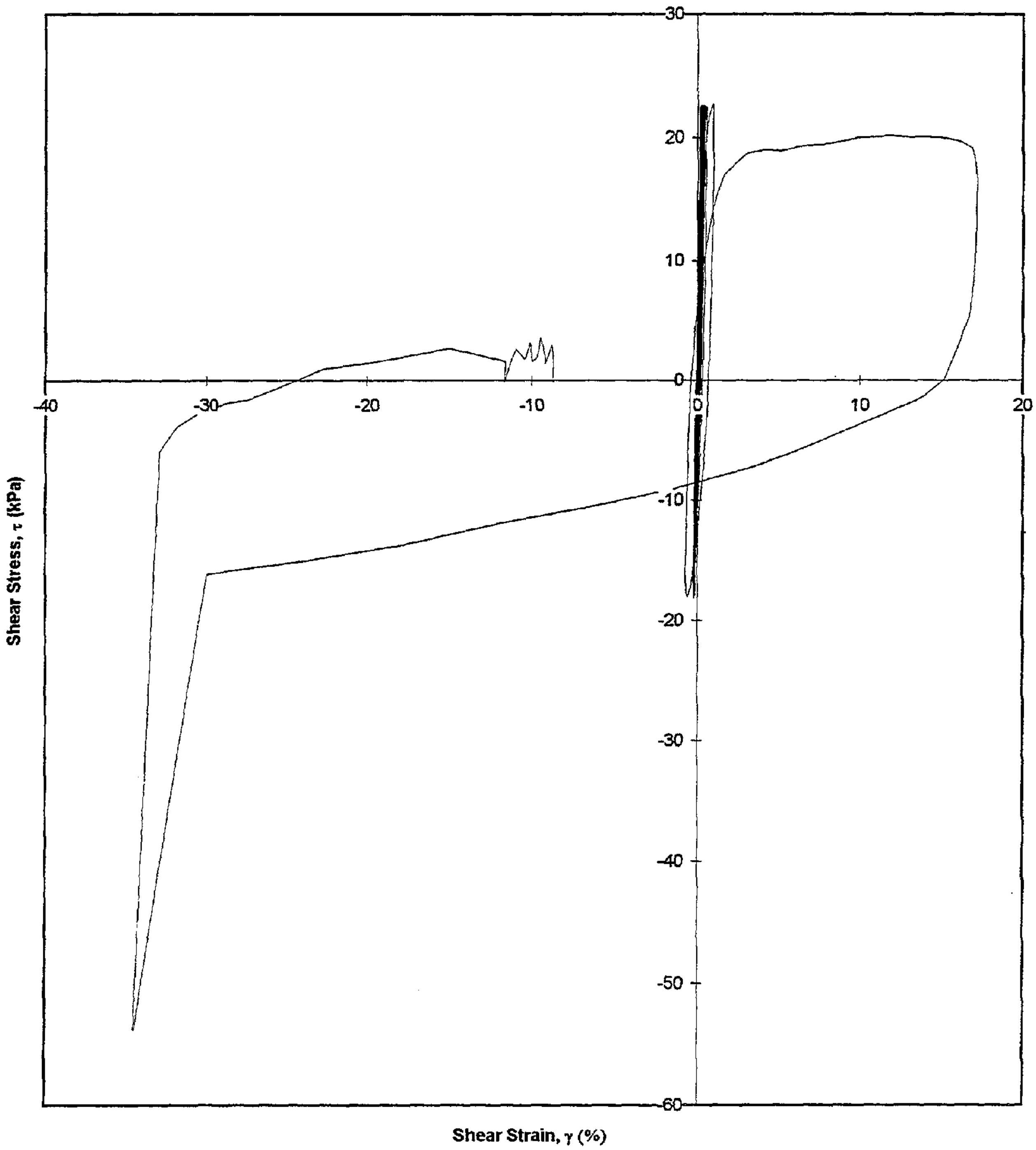

Test I.D.:	UOFC15	**Controlled Parameter:**	Stress
Fines Content (%):	20	**Initial Effective Stress (kPa):**	200
Dry Density (kN/m³)	15.25		

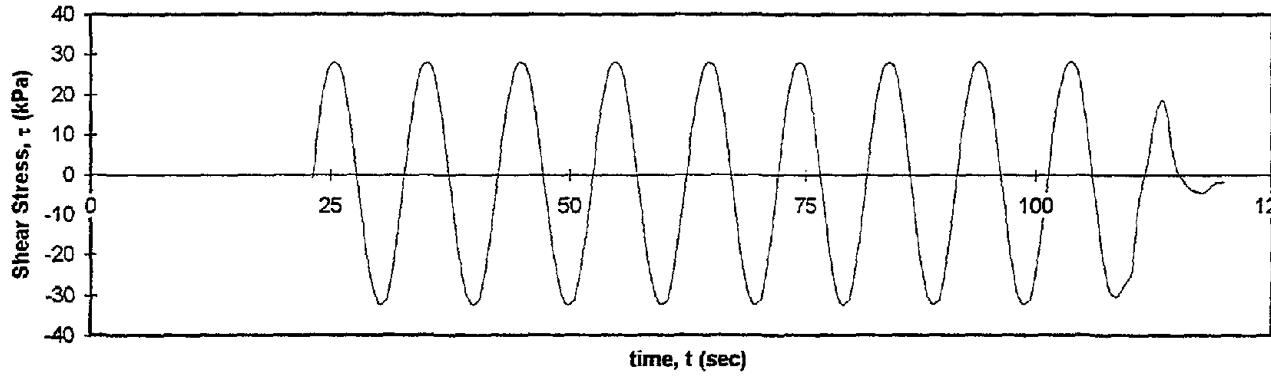

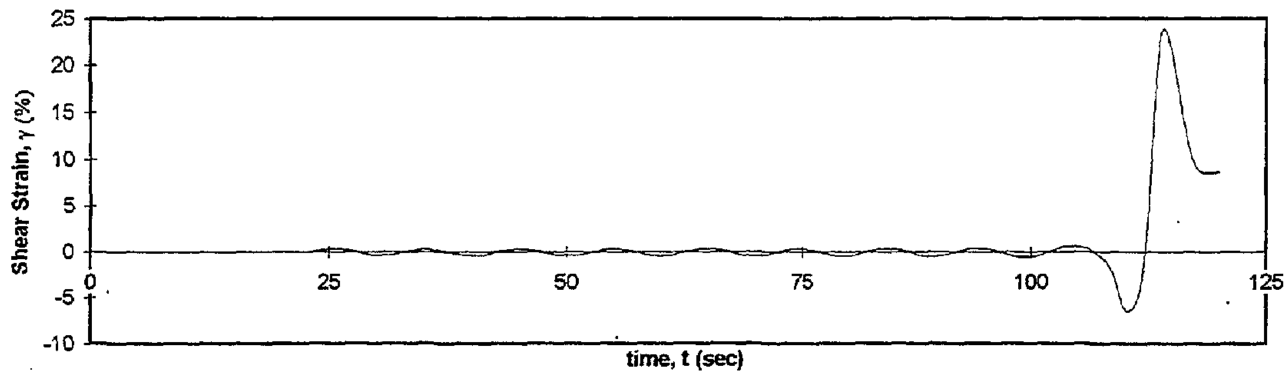

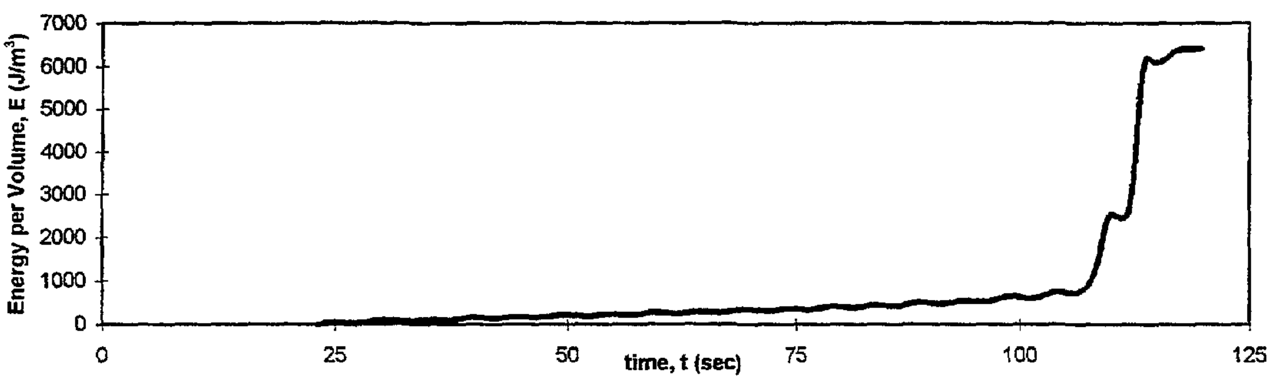

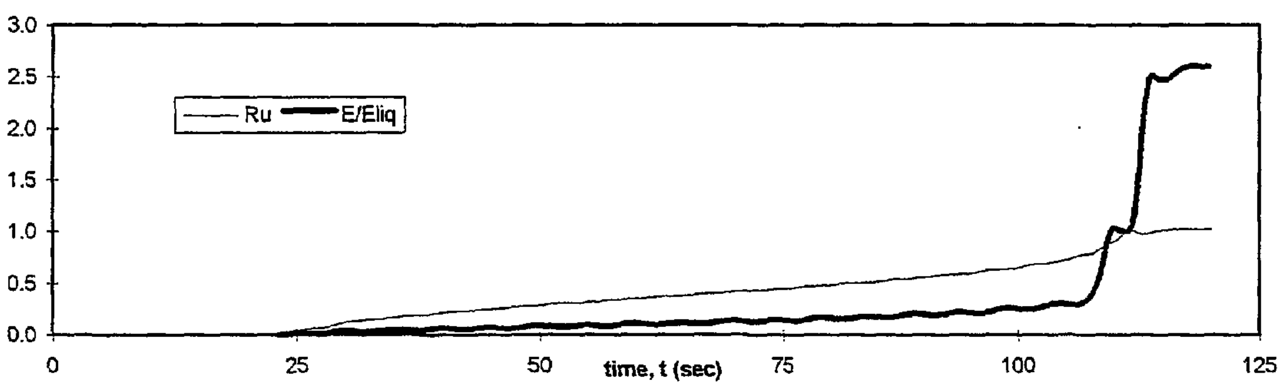

d:\nit\itp\cy_files\UOFC15.XLS 8/20/96 7:35 AM

Test I.D.:	UOFC15	**Controlled Parameter:**	Stress
Fines Content (%):	20	**Initial Effective Stress (kPa):**	200
Dry Density (kN/m^3)	15.25		

Shear Stress vs. Shear Strain

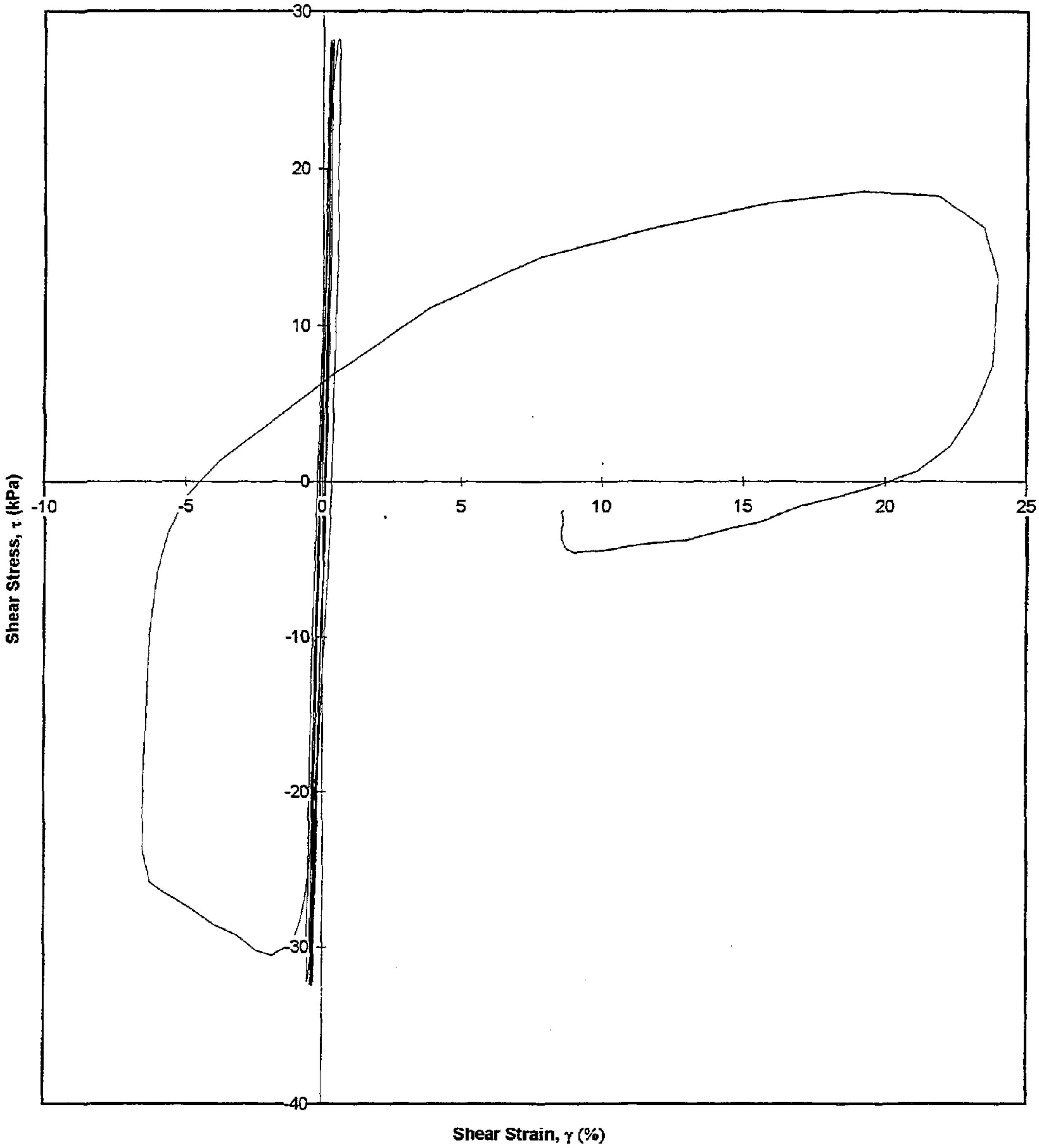

Test I.D.:	UOFC17	**Controlled Parameter:**	Stress
Fines Content (%):	45	**Initial Effective Stress (kPa):**	203.4
Dry Density (kN/m^3)	16.18		

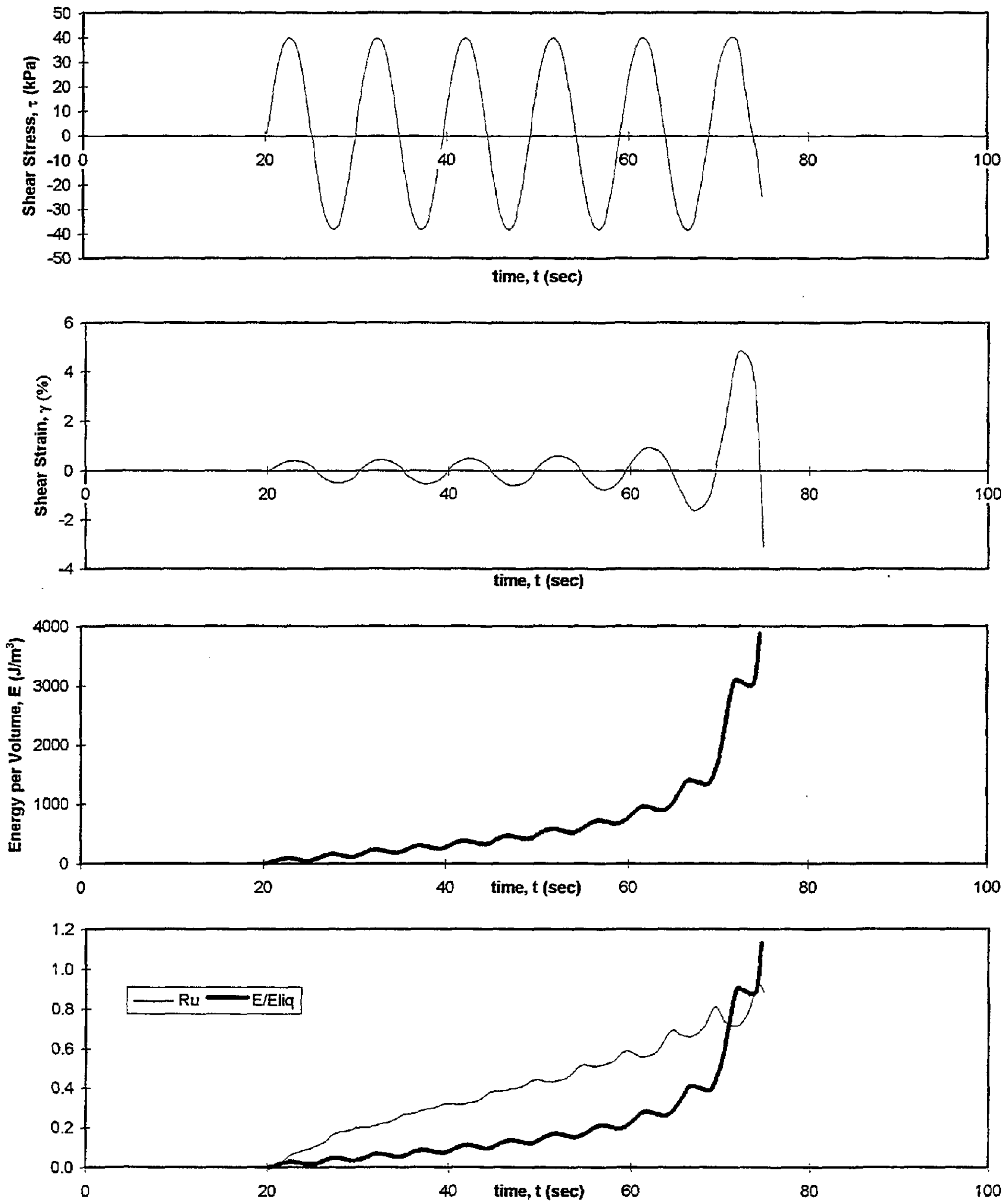

Test I.D.:	UOFC17	**Controlled Parameter:**	Stress
Fines Content (%):	45	**Initial Effective Stress (kPa):**	203.4
Dry Density (kN/m³)	16.18		

Shear Stress vs. Shear Strain

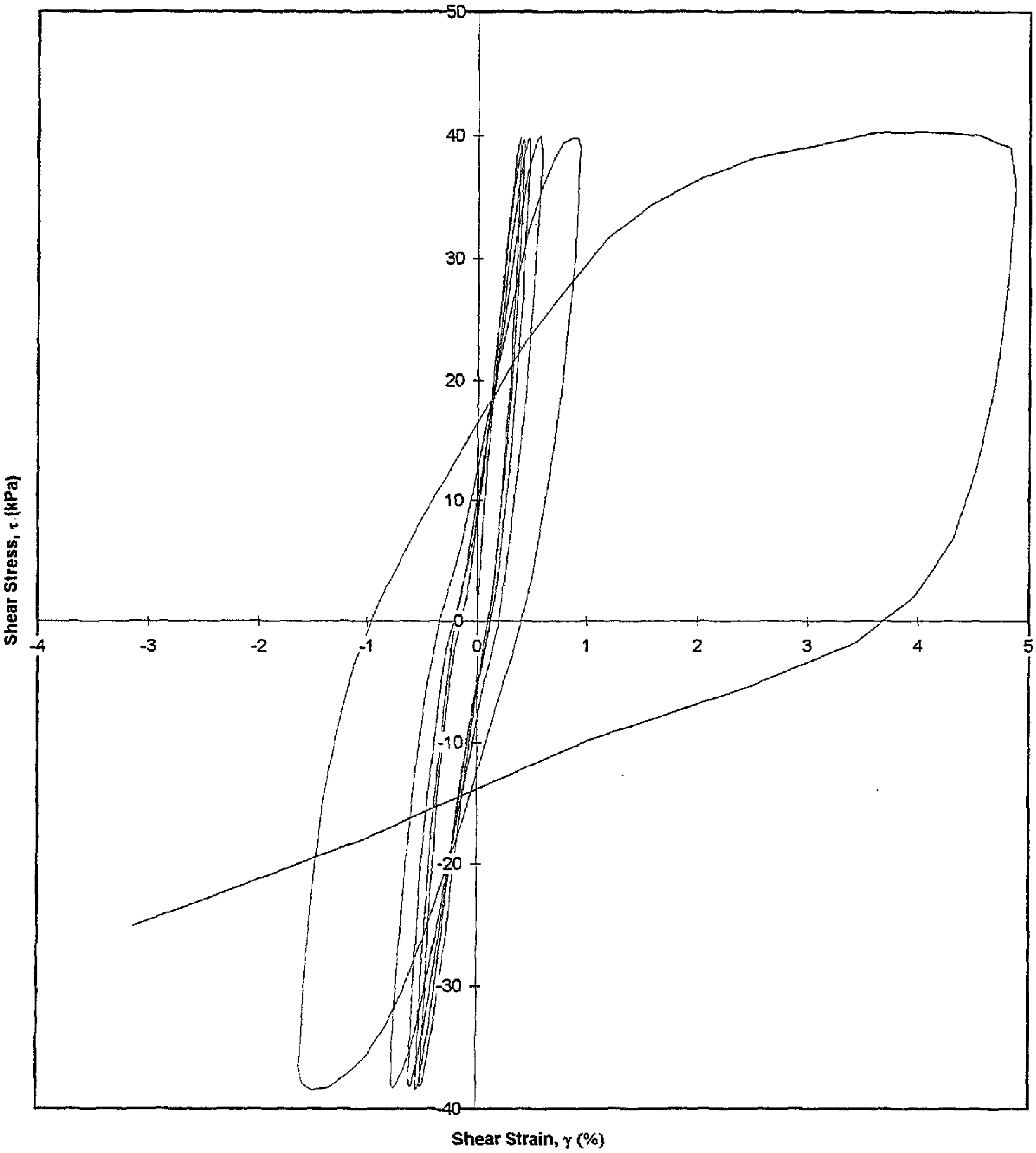

d:\nit\itp\cy_files\UOFC17.XLS 8/20/96 7:40 AM

Test I.D.:	UOFC18	**Controlled Parameter:**	Stress
Fines Content (%):	45	**Initial Effective Stress (kPa):**	190
Dry Density (kN/m³)	16.18		

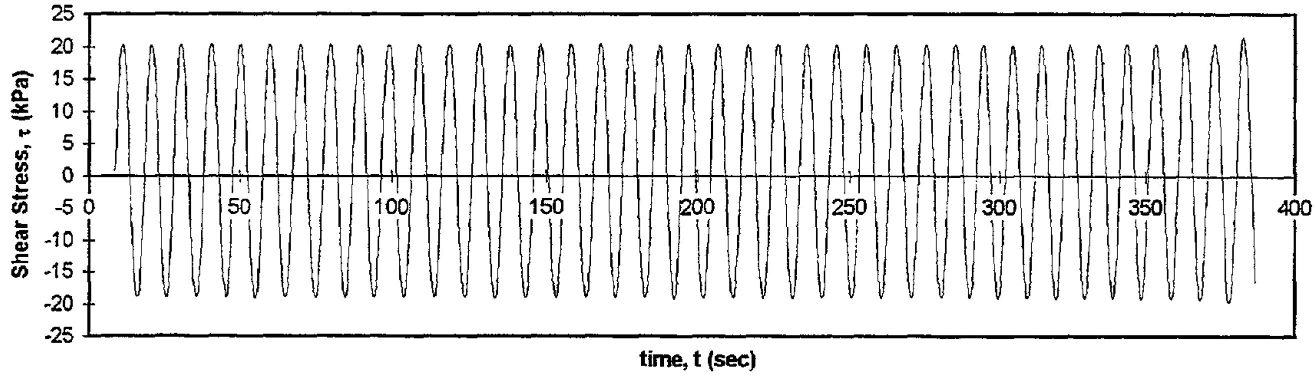

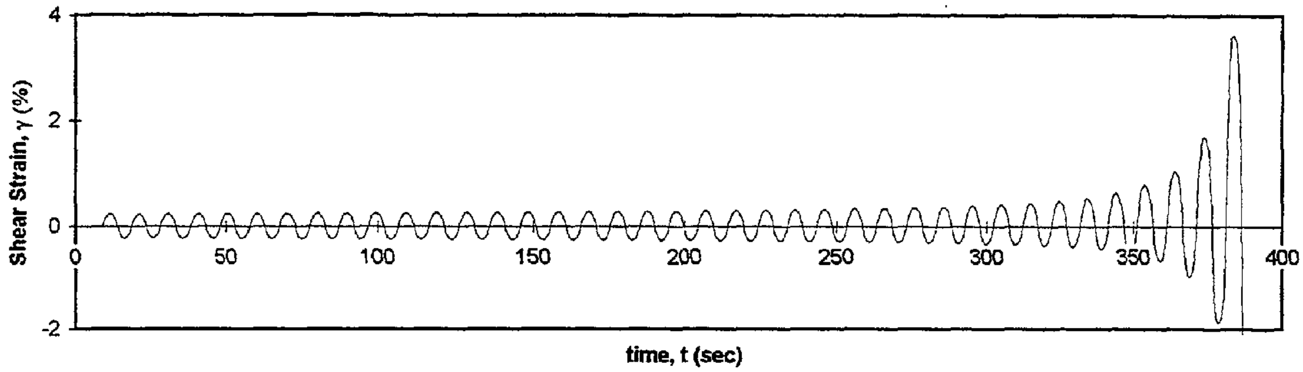

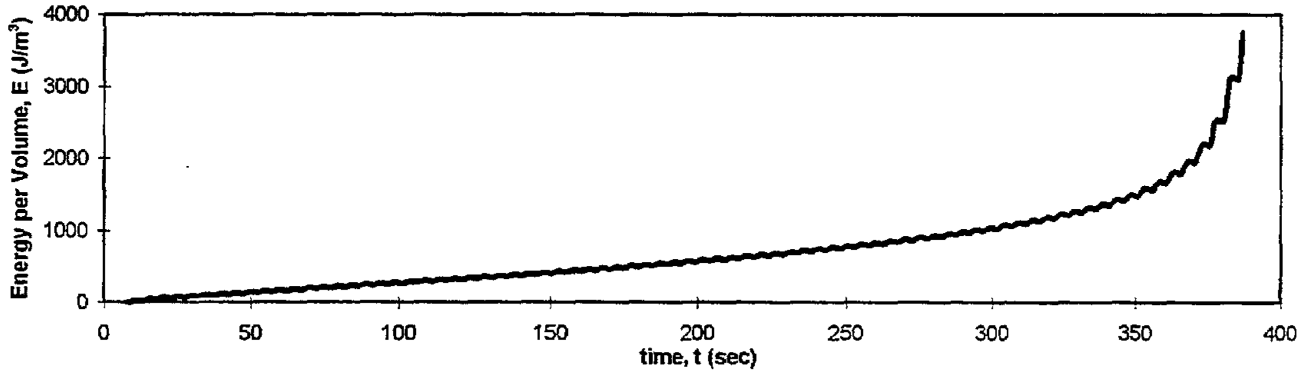

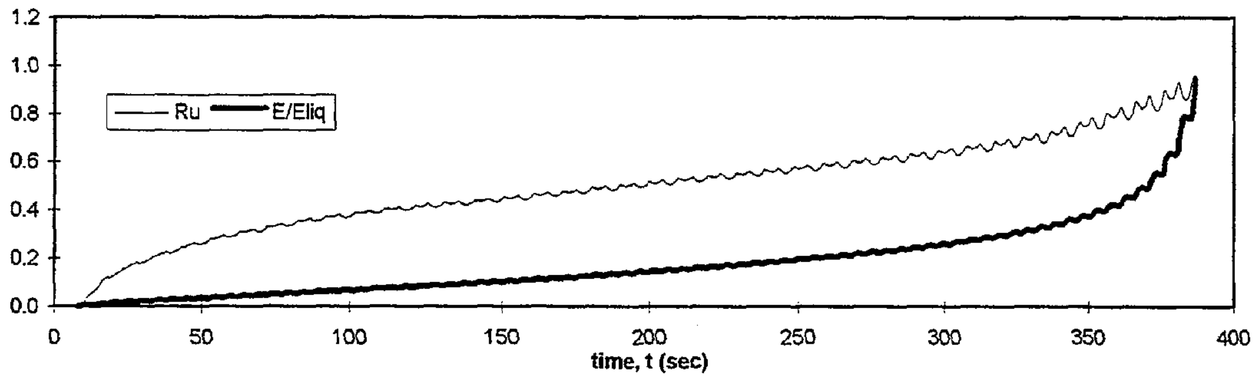

Test I.D.:	UOFC18	**Controlled Parameter:**	Stress
Fines Content (%):	45	**Initial Effective Stress (kPa):**	190
Dry Density (kN/m³)	16.18		

Shear Stress vs. Shear Strain

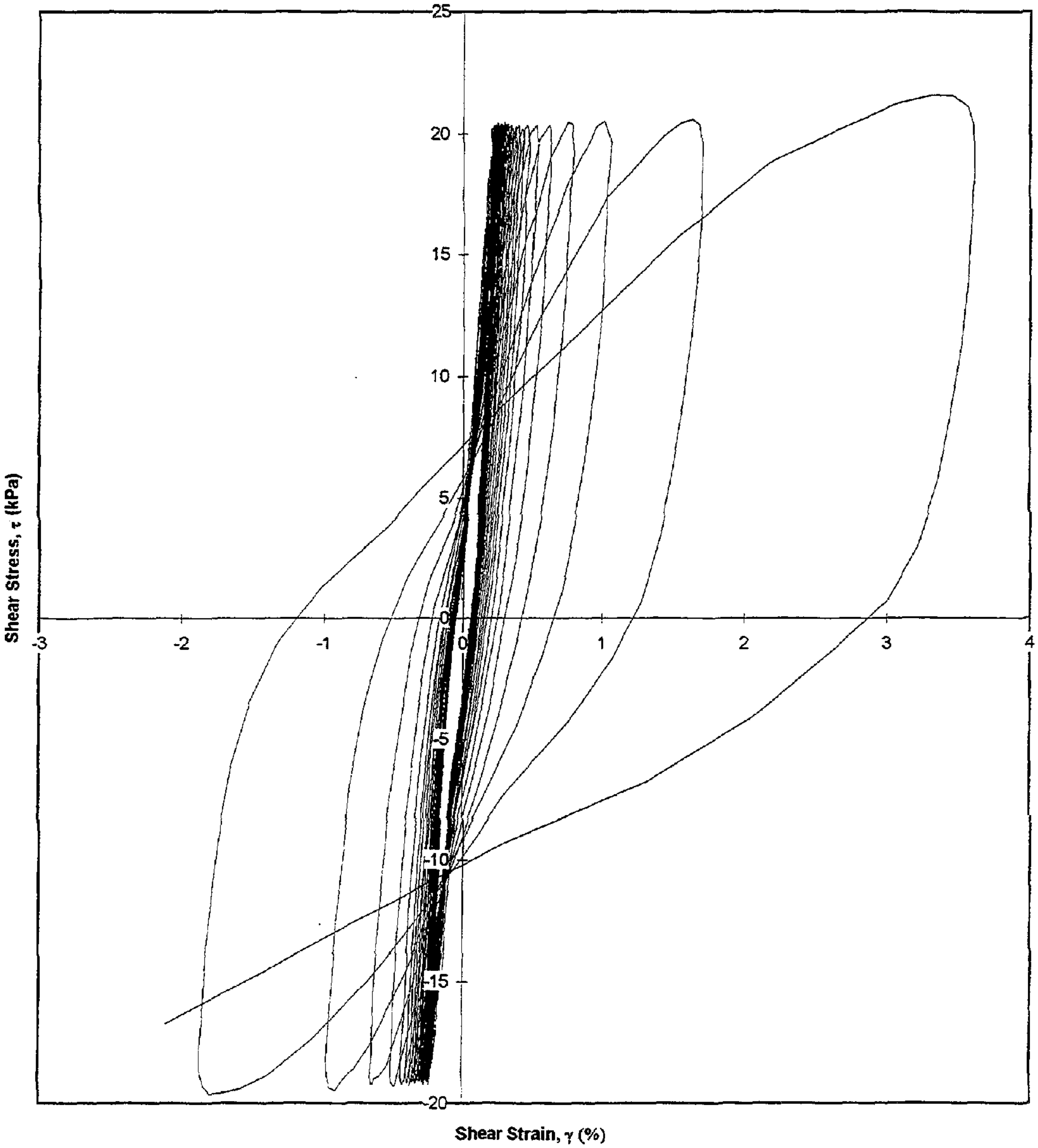

d:\nit\itp\cy_files\UOFC18.XLS

8/21/96 9:25 AM

Test I.D.:	UOFC23	**Controlled Parameter:**	Stress
Fines Content (%):	Clean Sand	**Initial Effective Stress (kPa):**	200
Relative Density(%):	45.3		

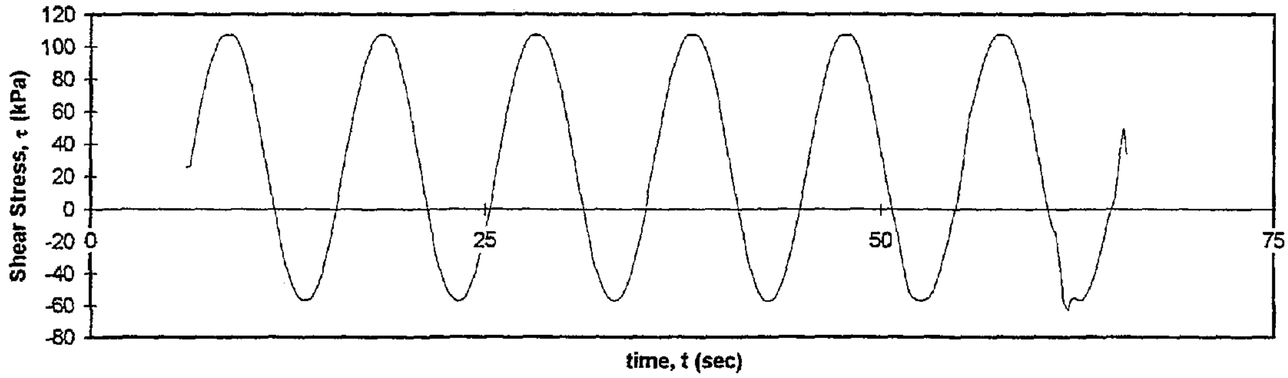

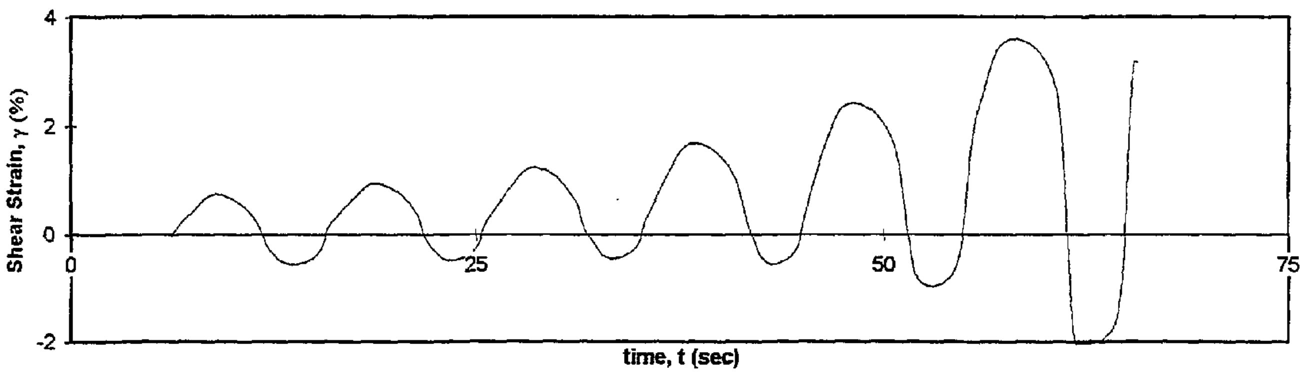

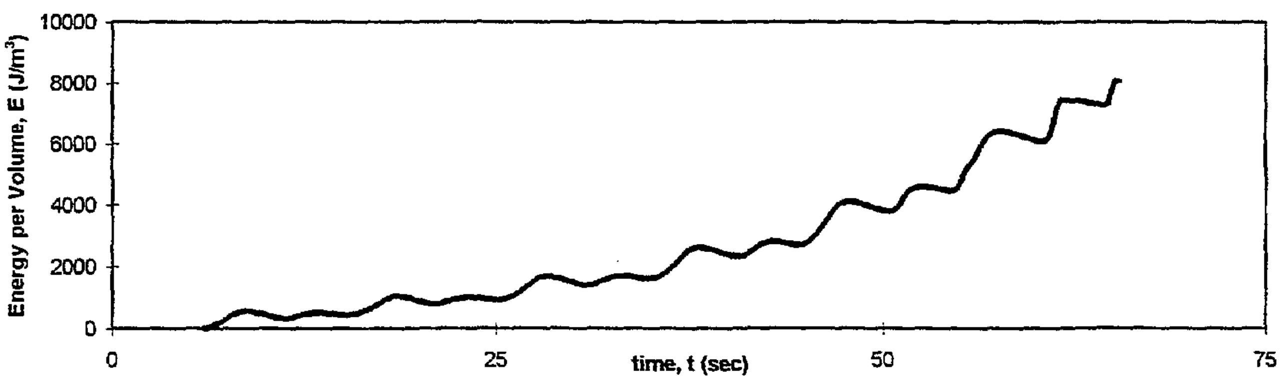

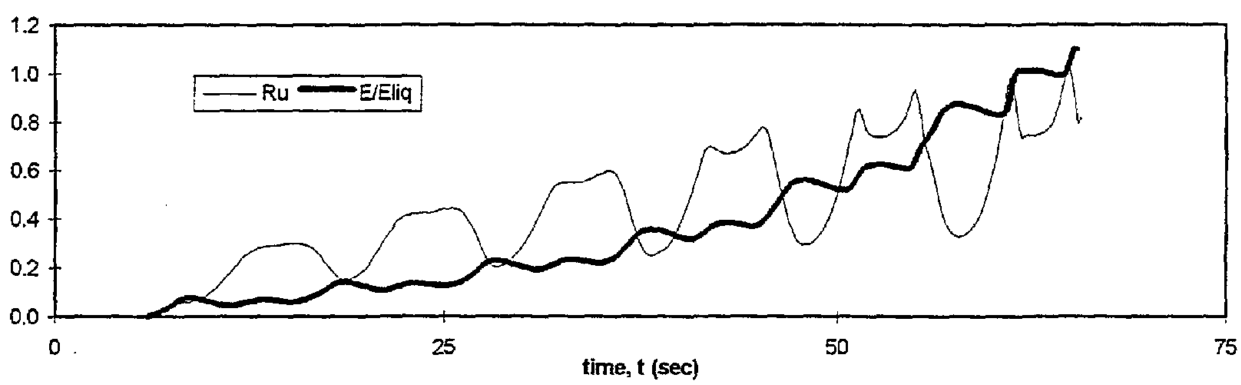

Test I.D.:	UOFC23	**Controlled Parameter:**	Stress
Fines Content (%):	Clean Sand	**Initial Effective Stress (kPa):**	200
Relative Density (%):	45.3		

Shear Stress vs. Shear Strain

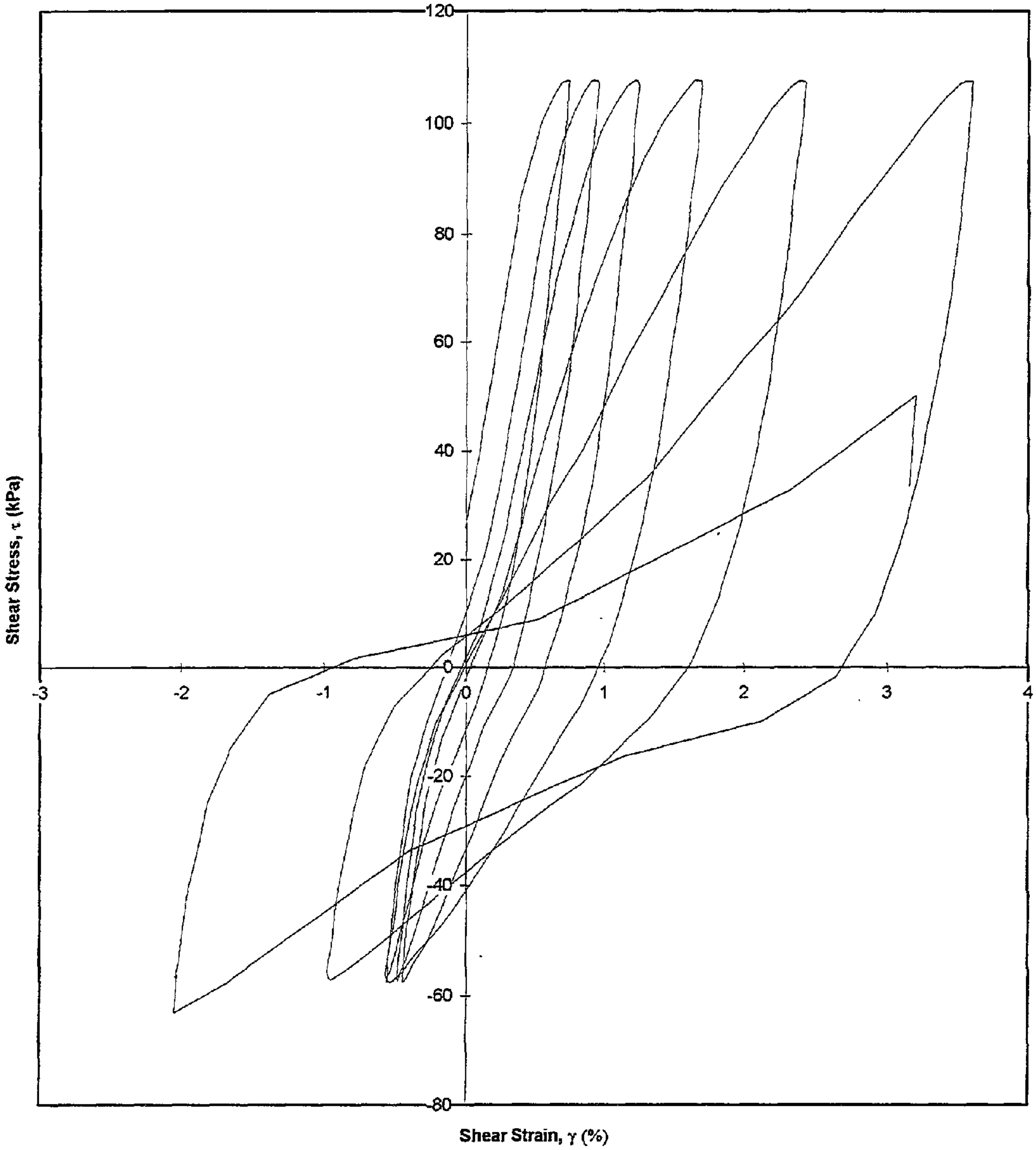

APPENDIX D

LABORATORY DATA ON SOIL SAMPLES FROM THE NORTHRIDGE SITE, PERFORMED AT THE UNIVERSITY OF CALIFORNIA, BERKELEY

Table D.1 - Summary of the Cyclic Triaxial Test Data on Northridge Samples Performed at University of California, Berkeley

No.	Test ID	Sample	D_r(%)	E_{liq} (J/m^3)	FC (%)	γ_d (kN/m^3)	Control	σ_c' (kPa)	Freq. (Hz)	Load Shape
1	BTC2CY1	Northridge Sand	58.3	5930	5	14.5	Stress	100	1	Sinusoidal 2-way
2	BTC2CY2	Northridge Sand	78.4	2247	5	15.5	Stress	100	1	Sinusoidal 2-way
3	BTC3CY1	Northridge Sand	82.3	5146	5	15.7	Stress	100	1	Sinusoidal 2-way
4	BTC3CY2	Northridge Sand	89.9	3813	5	16.1	Stress	100	1	Sinusoidal 2-way
5	BTC3CY3	Northridge Sand	97.2	36156	5	16.5	Stress	100	1	Sinusoidal 2-way
6	BTC4CY1	Northridge Sand	93.7	7874	5	16.3	Stress	100	1	Sinusoidal 2-way
7	BTC4CY2	Northridge Sand	100.0	6647	5	16.7	Stress	100	1	Sinusoidal 2-way
8	BTC6CY1	Northridge Sand	35.2	3206	5	13.5	Stress	100	1	Sinusoidal 2-way

Test Results Following the Sequence of Test ID's are Attached.

Test I.D.:	BTC2CY1	**Controlled Parameter:**	Stress
Fines Content (%):	5	**Initial Effective Stress (kPa):**	100
Dry Density (kN/m³)	14.51		

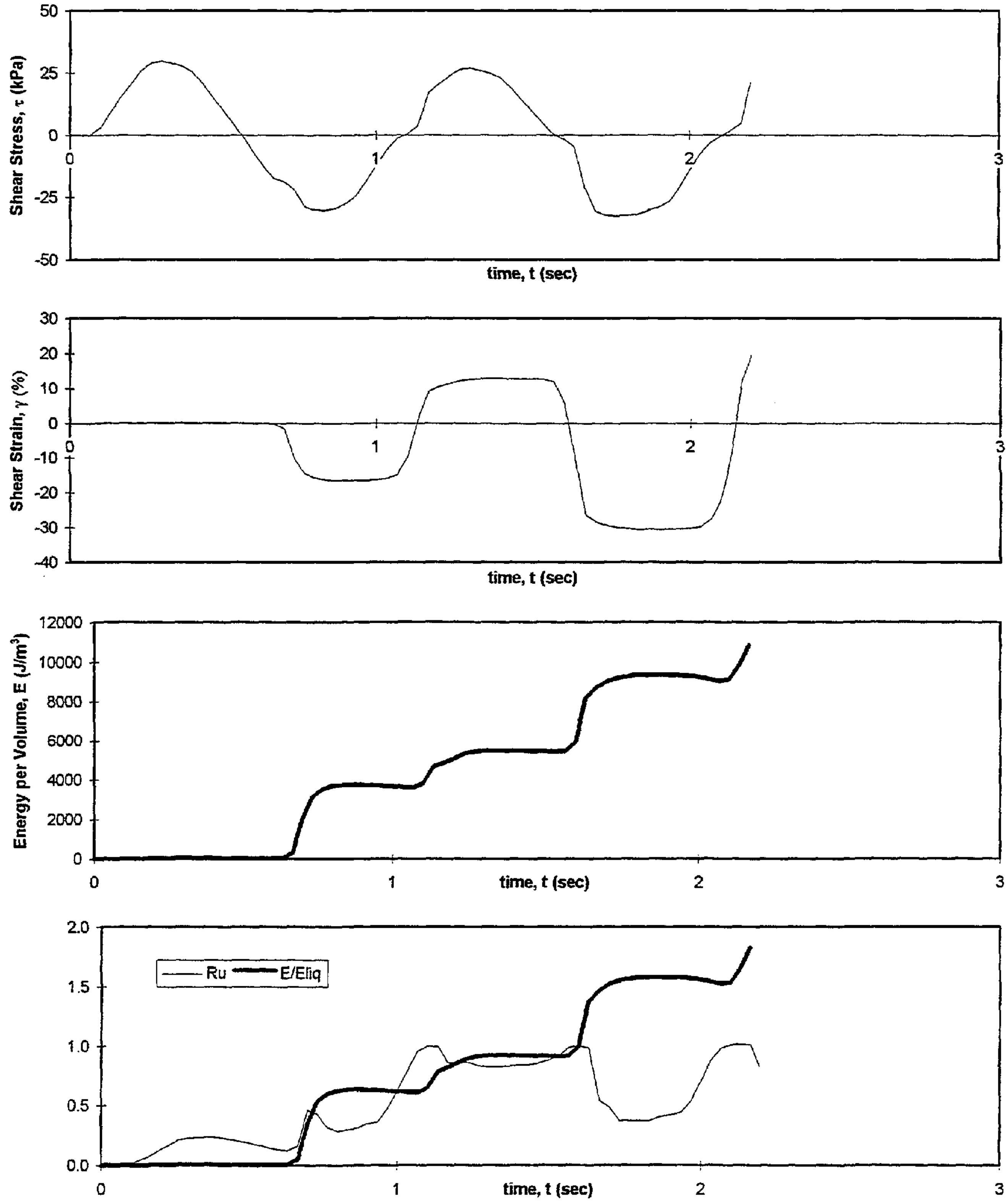

Test I.D.:	BTC2CY1	**Controlled Parameter:**	Stress
Fines Content (%):	5	**Initial Effective Stress (kPa):**	100
Dry Density (kN/m^3)	14.51		

Shear Stress vs. Shear Strain

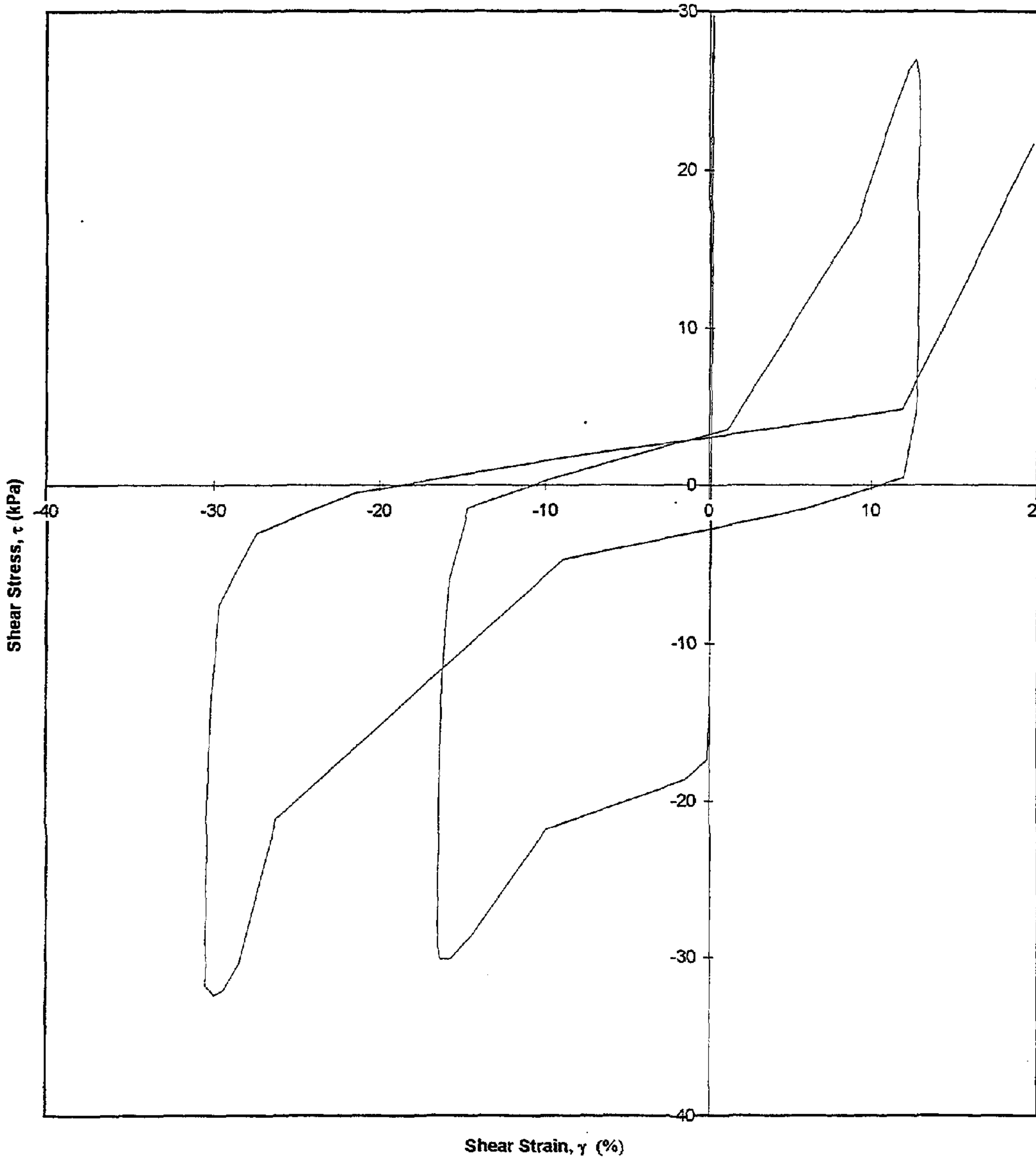

Test I.D.:	BTC2CY2	**Controlled Parameter:**	Stress
Fines Content (%):	5	**Initial Effective Stress (kPa):**	100
Dry Density (kN/m³)	15.5		

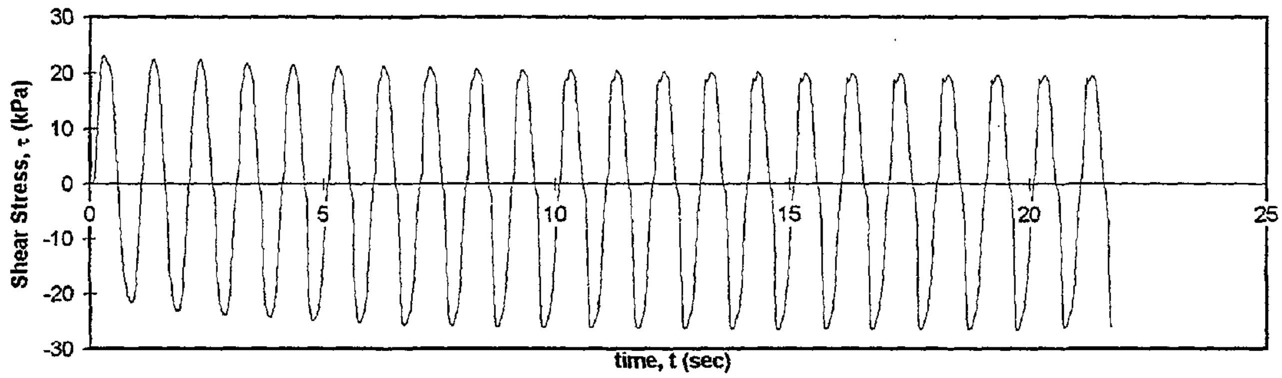

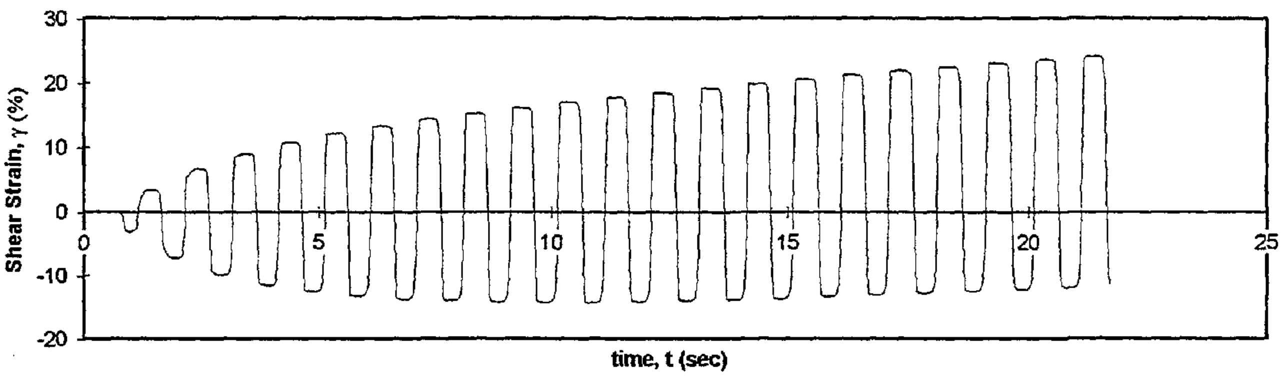

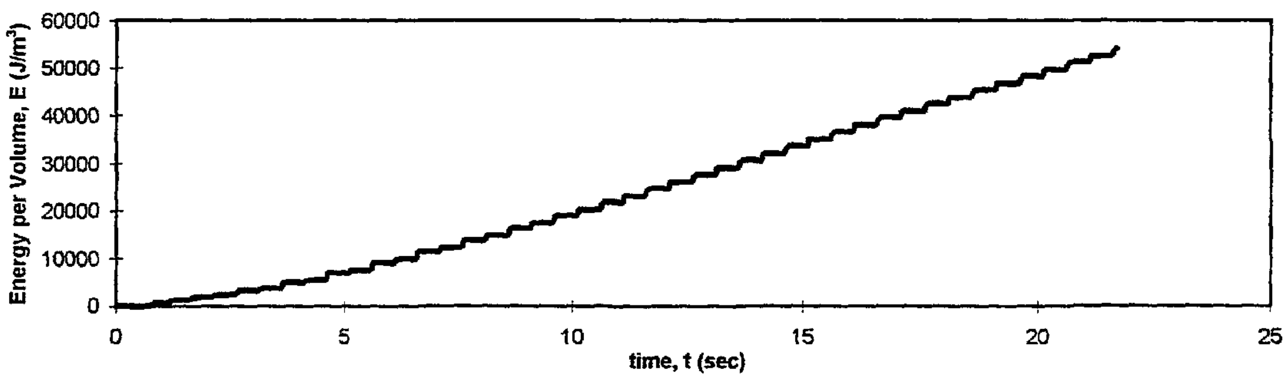

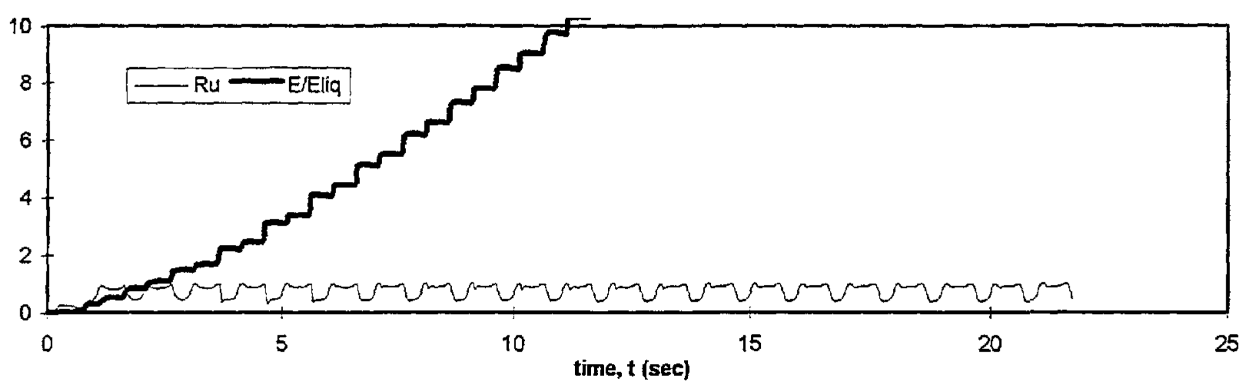

Test I.D.:	BTC2CY2	**Controlled Parameter:**	Stress
Fines Content (%):	5	**Initial Effective Stress (kPa):**	100
Dry Density (kN/m^3)	15.5		

Shear Stress vs. Shear Strain

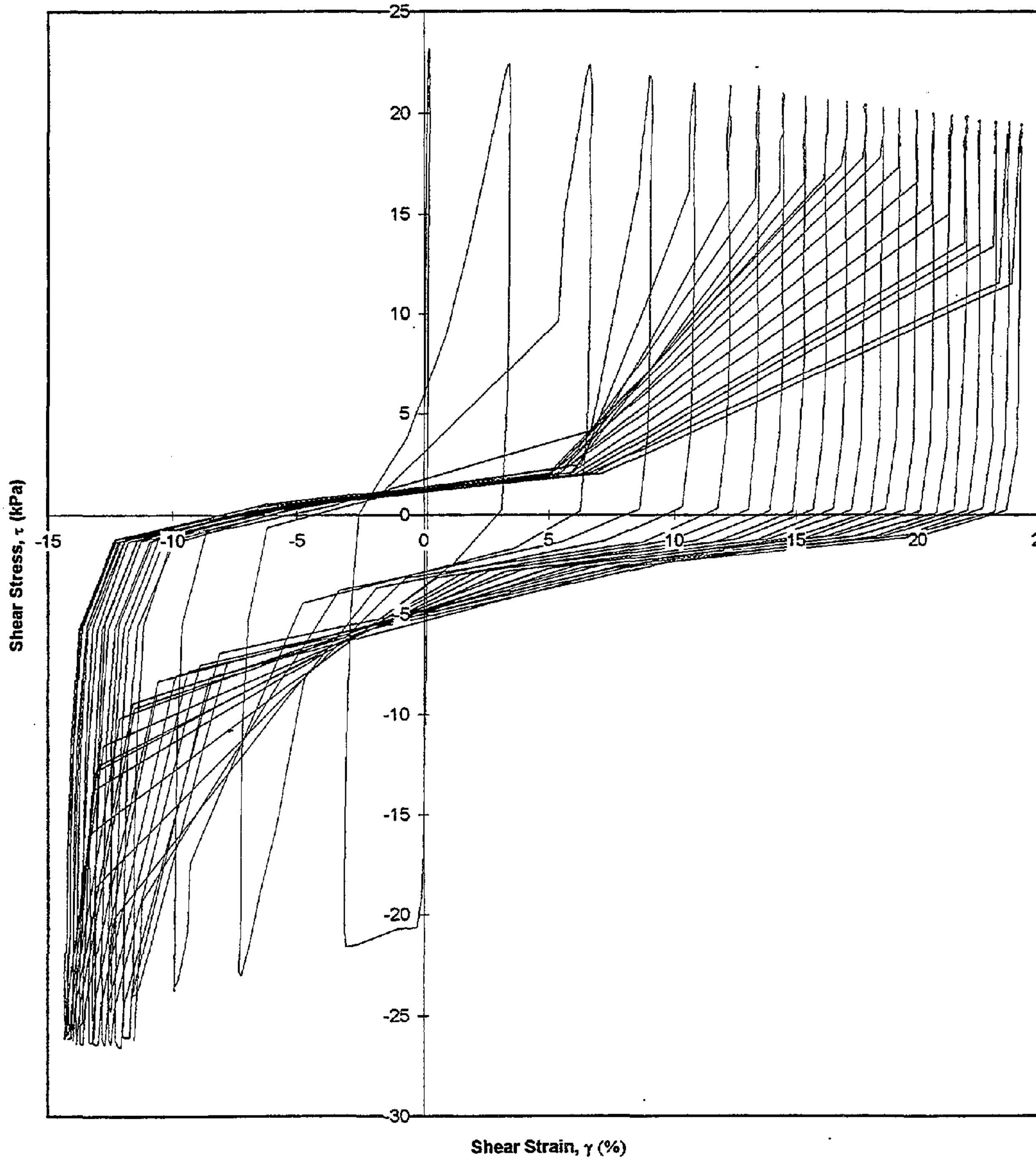

Test I.D.:	BTC3CY1	**Controlled Parameter:**	Stress
Fines Content (%):	5	**Initial Effective Stress (kPa):**	100
Dry Density (kN/m³)	15.7		

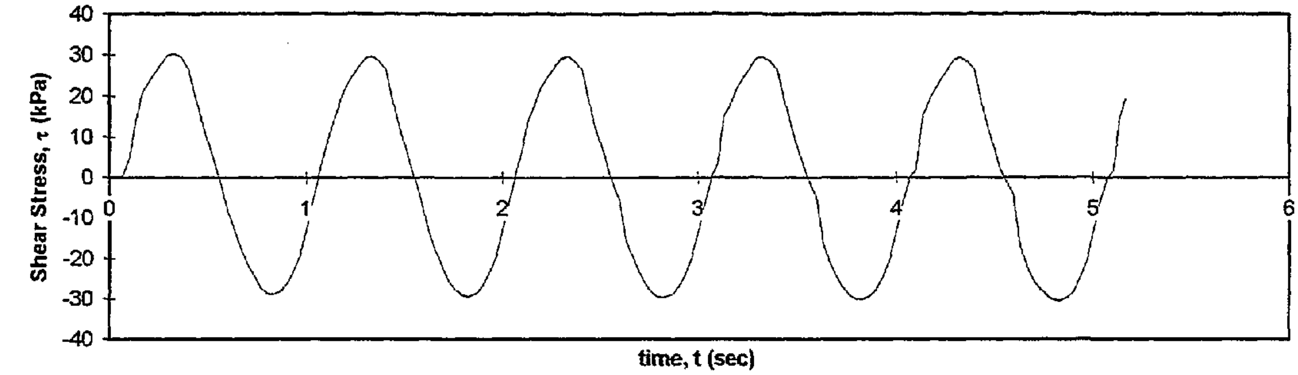

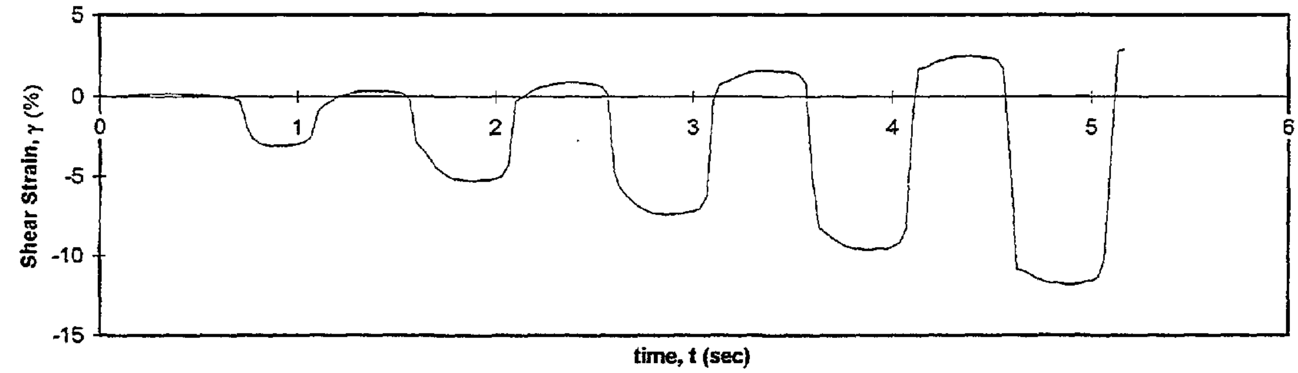

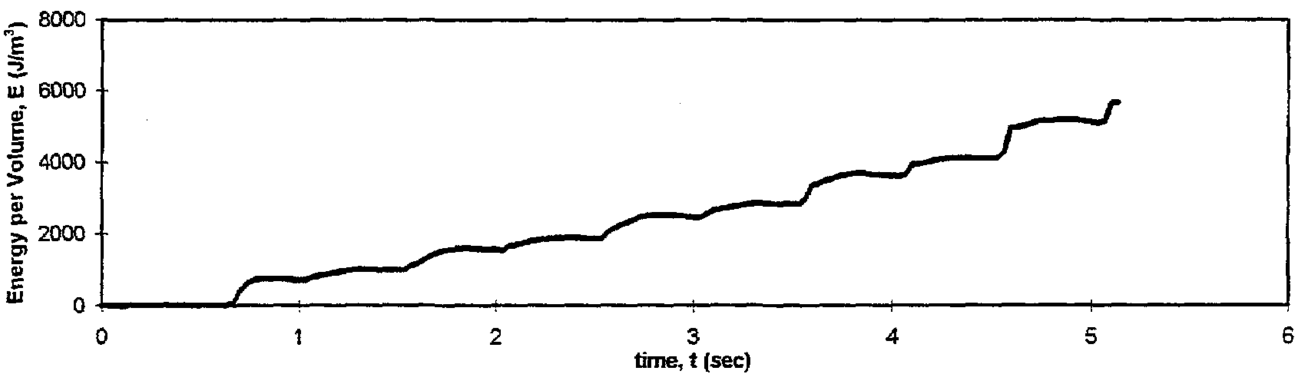

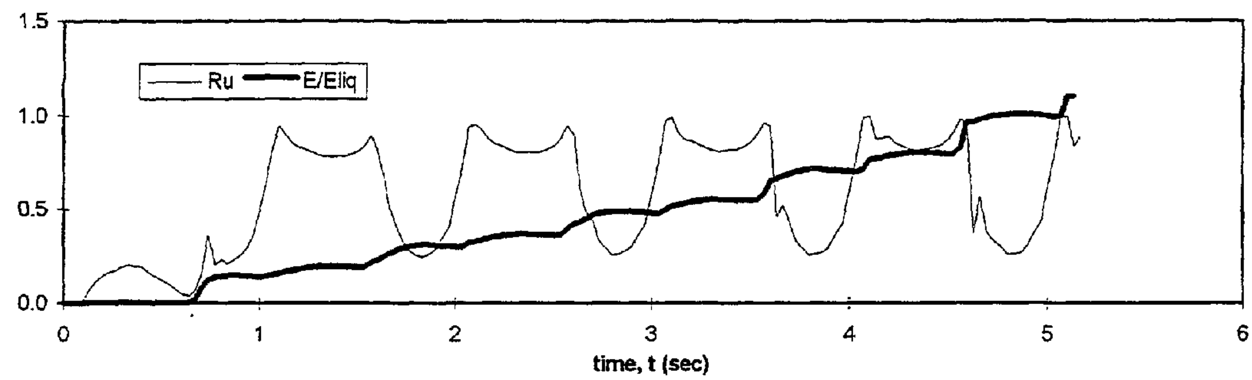

Test I.D.:	BTC3CY1	**Controlled Parameter:**	Stress
Fines Content (%):	5	**Initial Effective Stress (kPa):**	100
Dry Density (kN/m^3)	15.7		

Shear Stress vs. Shear Strain

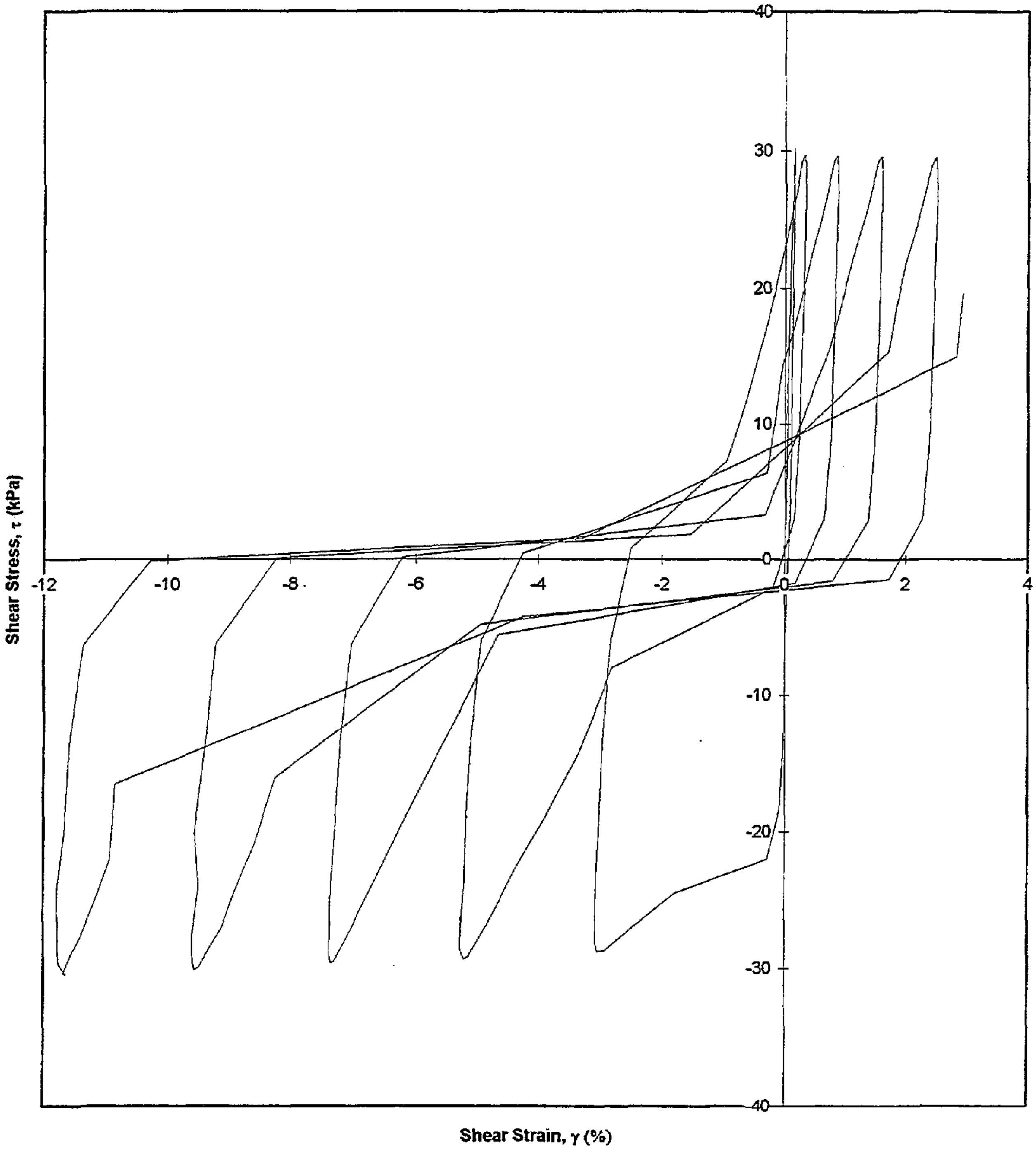

Test I.D.:	BTC3CY2	**Controlled Parameter:**	Stress
Fines Content (%):	5	**Initial Effective Stress (kPa):**	100
Dry Density (kN/m^3)	16.12		

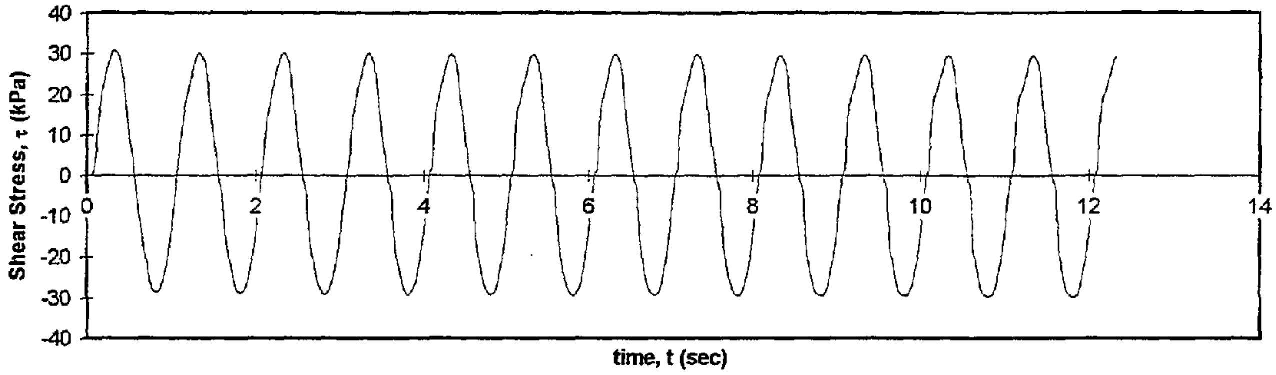

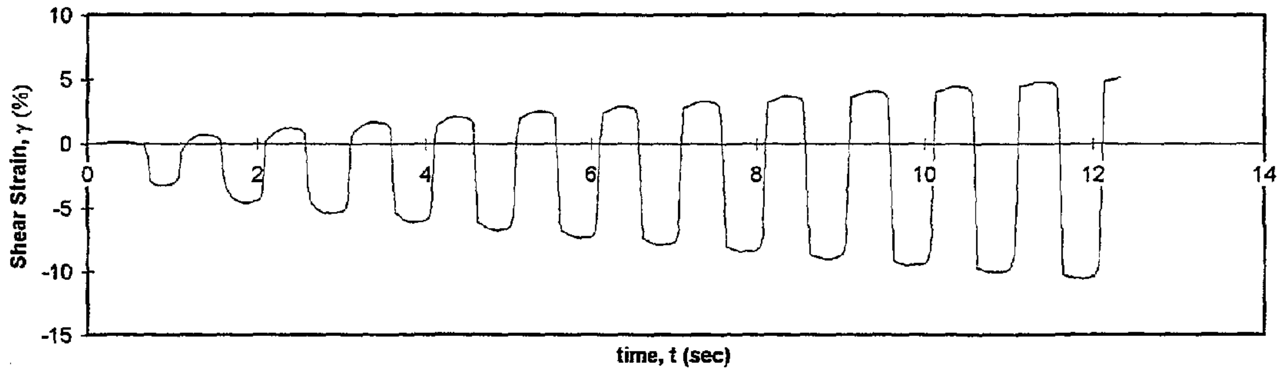

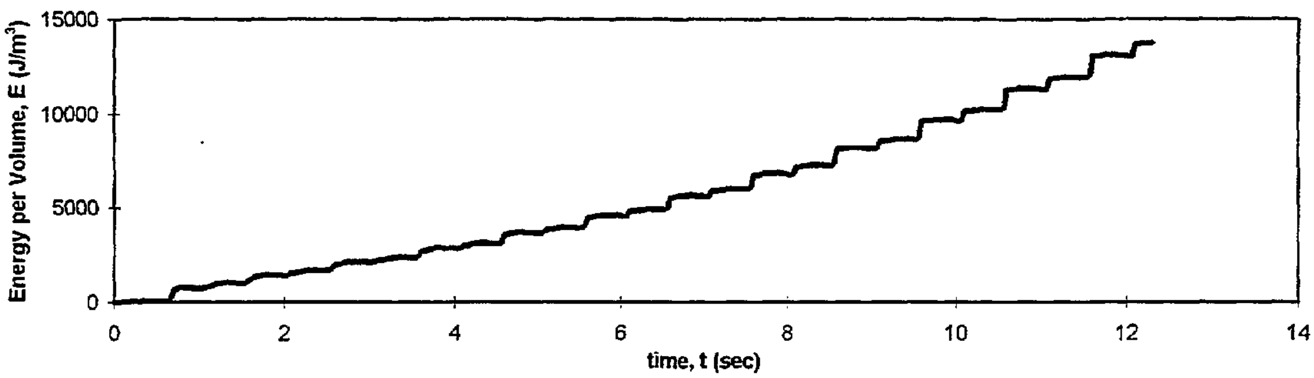

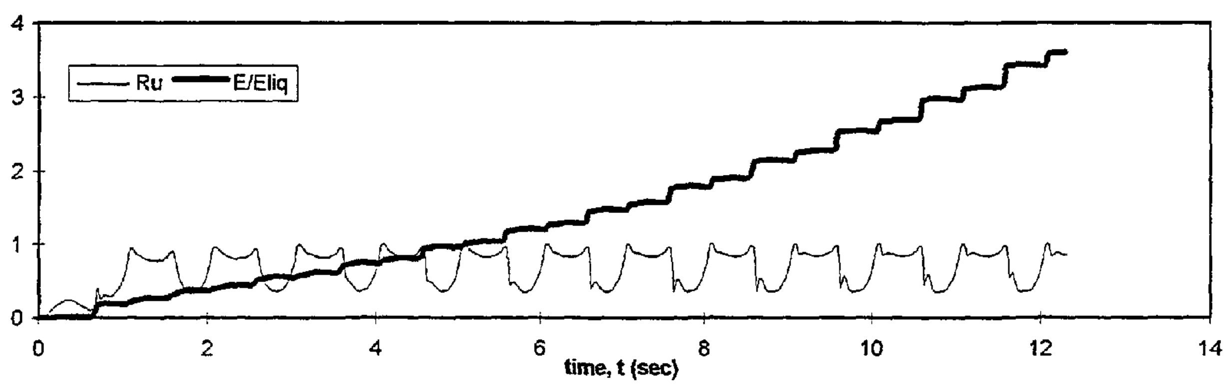

Test I.D.:	BTC3CY2	**Controlled Parameter:**	Stress
Fines Content (%):	5	**Initial Effective Stress (kPa):**	100
Dry Density (kN/m³)	16.12		

Shear Stress vs. Shear Strain

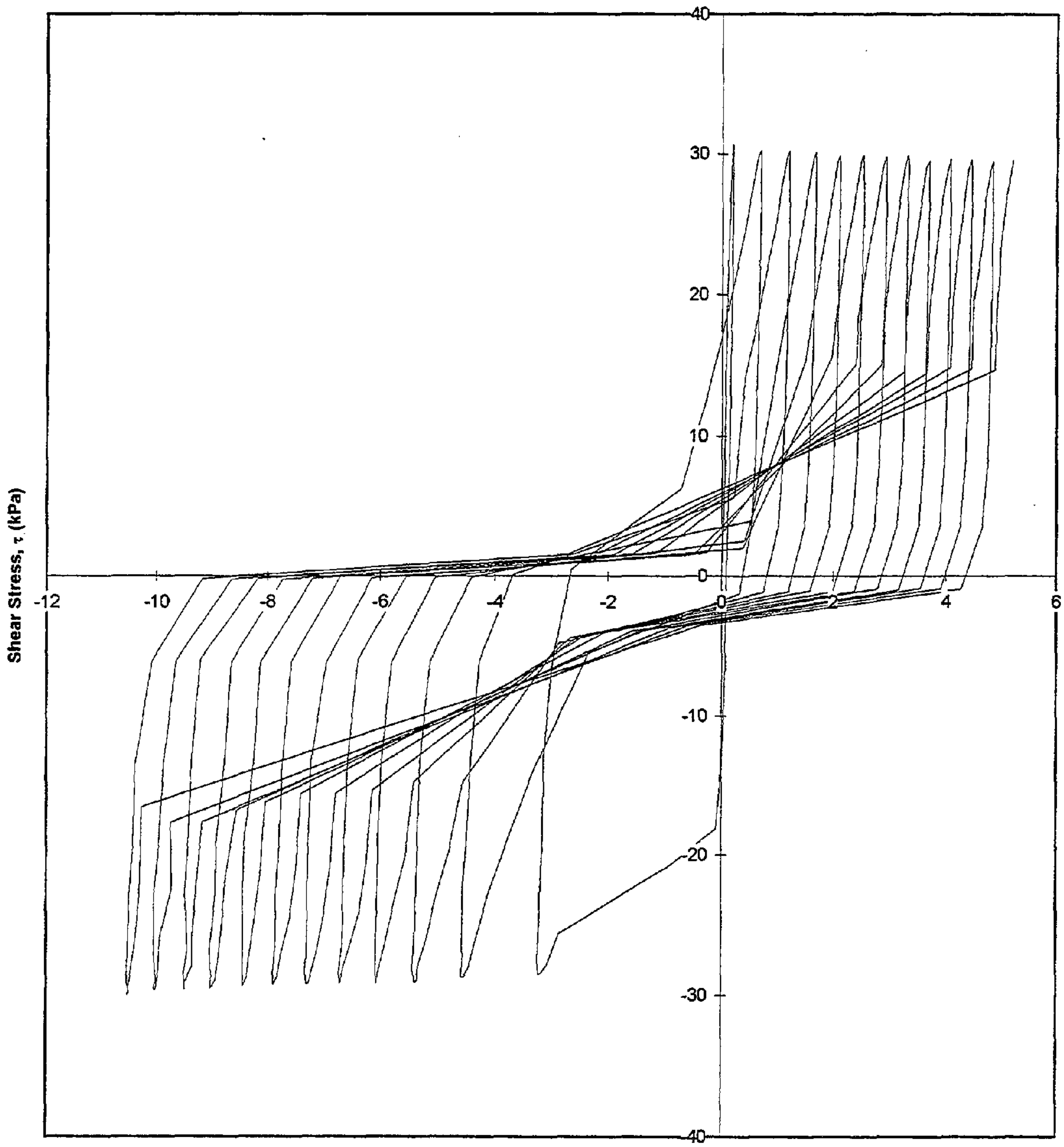

d:\nit\itp\cy_files\BTC3CY2.XLS

8/15/96 10:45 AM

Test I.D.:	BTC3CY3	**Controlled Parameter:**	Stress
Fines Content (%):	5	**Initial Effective Stress (kPa):**	100
Dry Density (kN/m^3)	16.55		

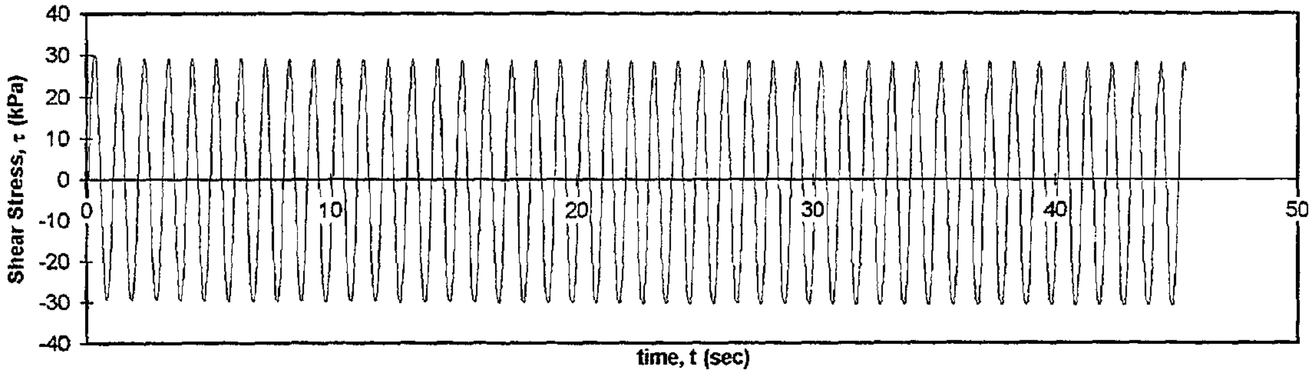

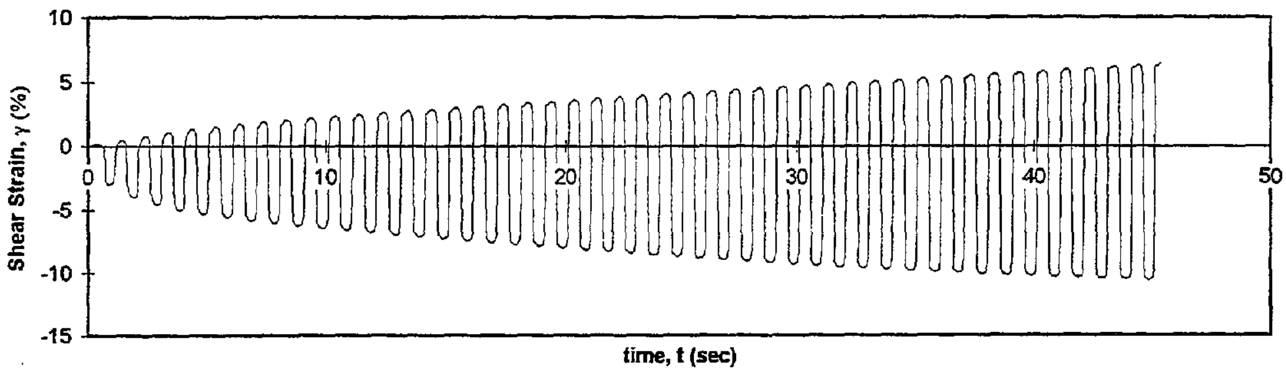

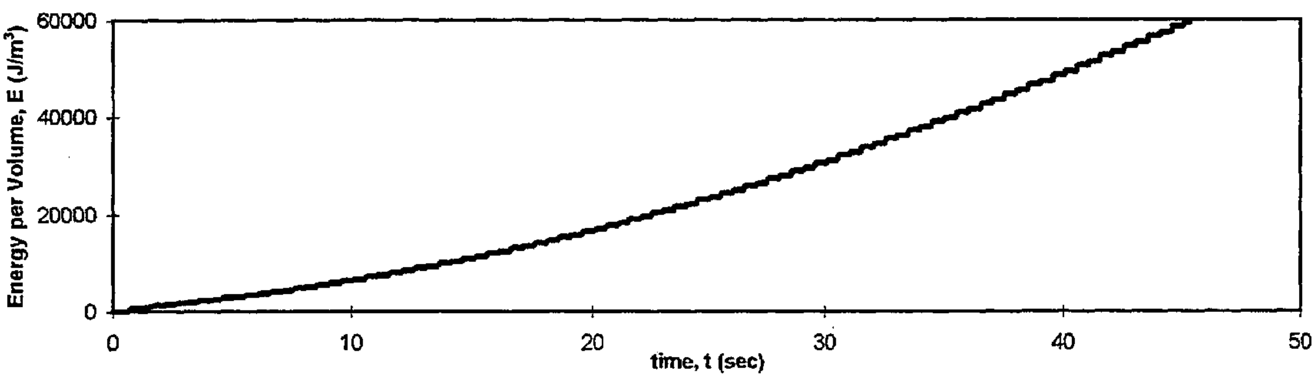

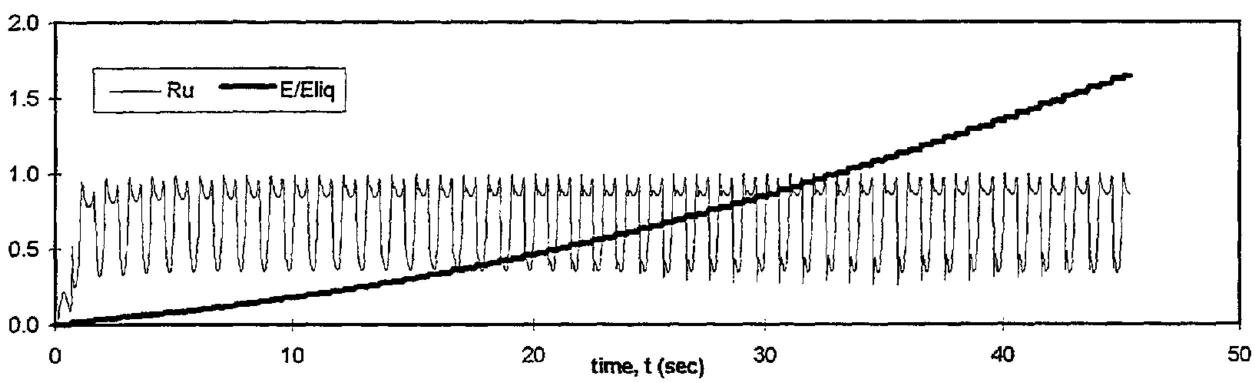

Test I.D.:	BTC3CY3	**Controlled Parameter:**	Stress
Fines Content (%):	5	**Initial Effective Stress (kPa):**	100
Dry Density (kN/m³)	16.55		

Shear Stress vs. Shear Strain

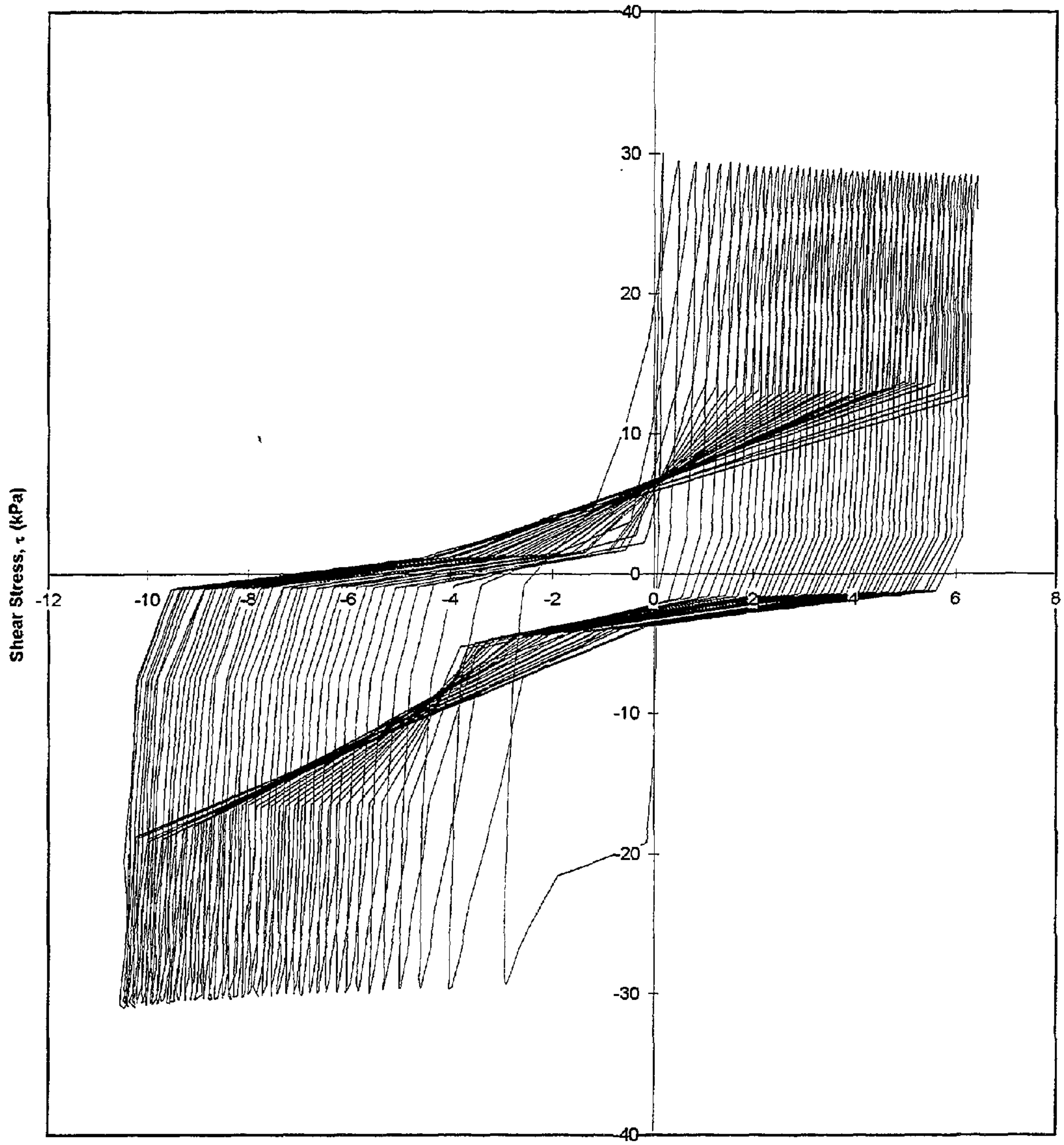

d:\nit\itp\cy_files\BTC3CY3.XLS

8/15/96 10:48 AM

Test I.D.:	BTC4CY1	**Controlled Parameter:**	Stress
Fines Content (%):	5	**Initial Effective Stress (kPa):**	100
Dry Density (kN/m³)	16.35		

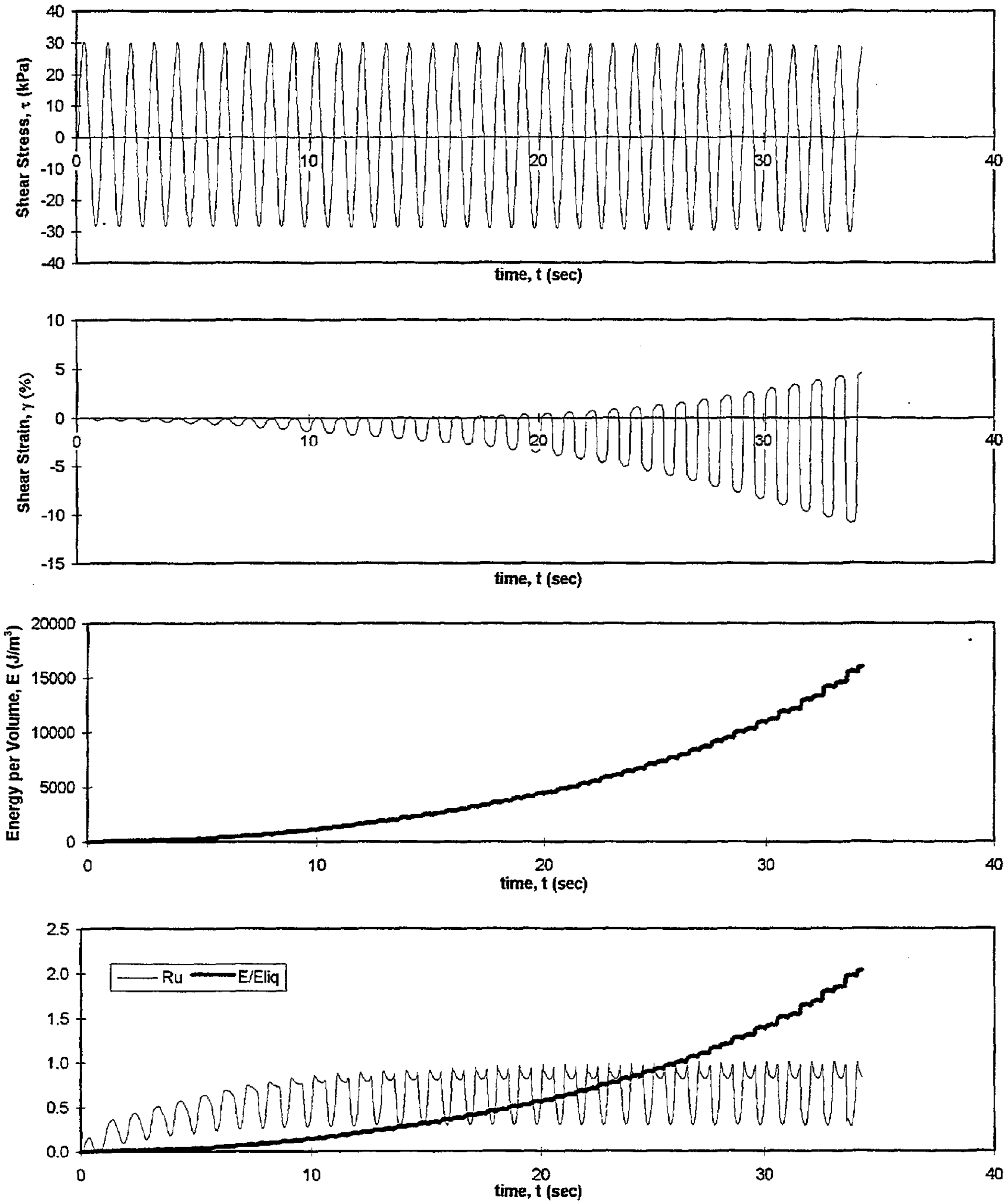

d:\nit\itp\cy_files\BTC4CY1.XLS 8/15/96 10:53 AM

Test I.D.:	BTC4CY1	**Controlled Parameter:**	Stress
Fines Content (%):	5	**Initial Effective Stress (kPa):**	100
Dry Density (kN/m³)	16.35		

Shear Stress vs. Shear Strain

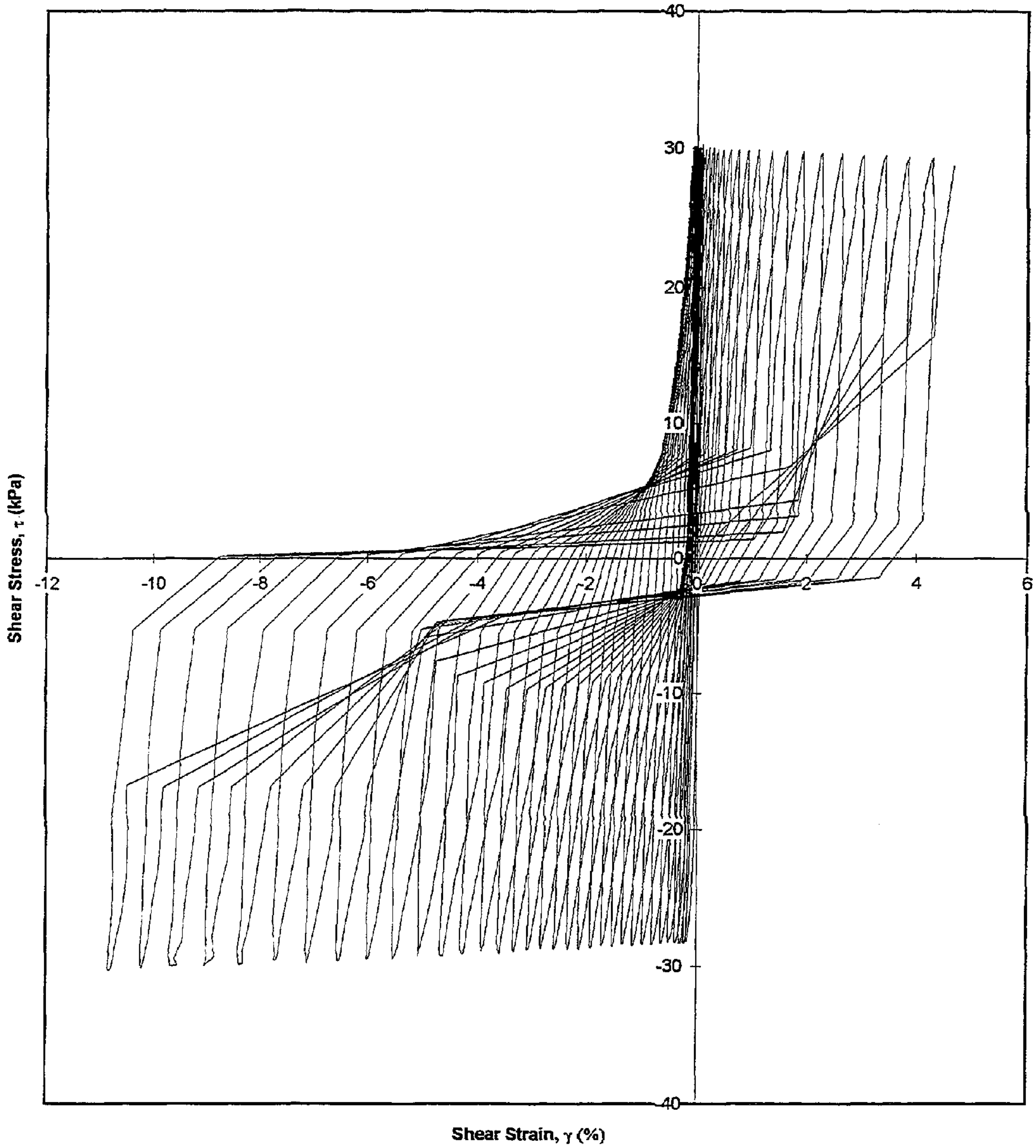

d:\nit\itp\cy_files\BTC4CY1.XLS   8/15/96 10:53 AM

Test I.D.:	BTC4CY2	**Controlled Parameter:**	Stress
Fines Content (%):	5	**Initial Effective Stress (kPa):**	100
Dry Density (kN/m³)	16.72		

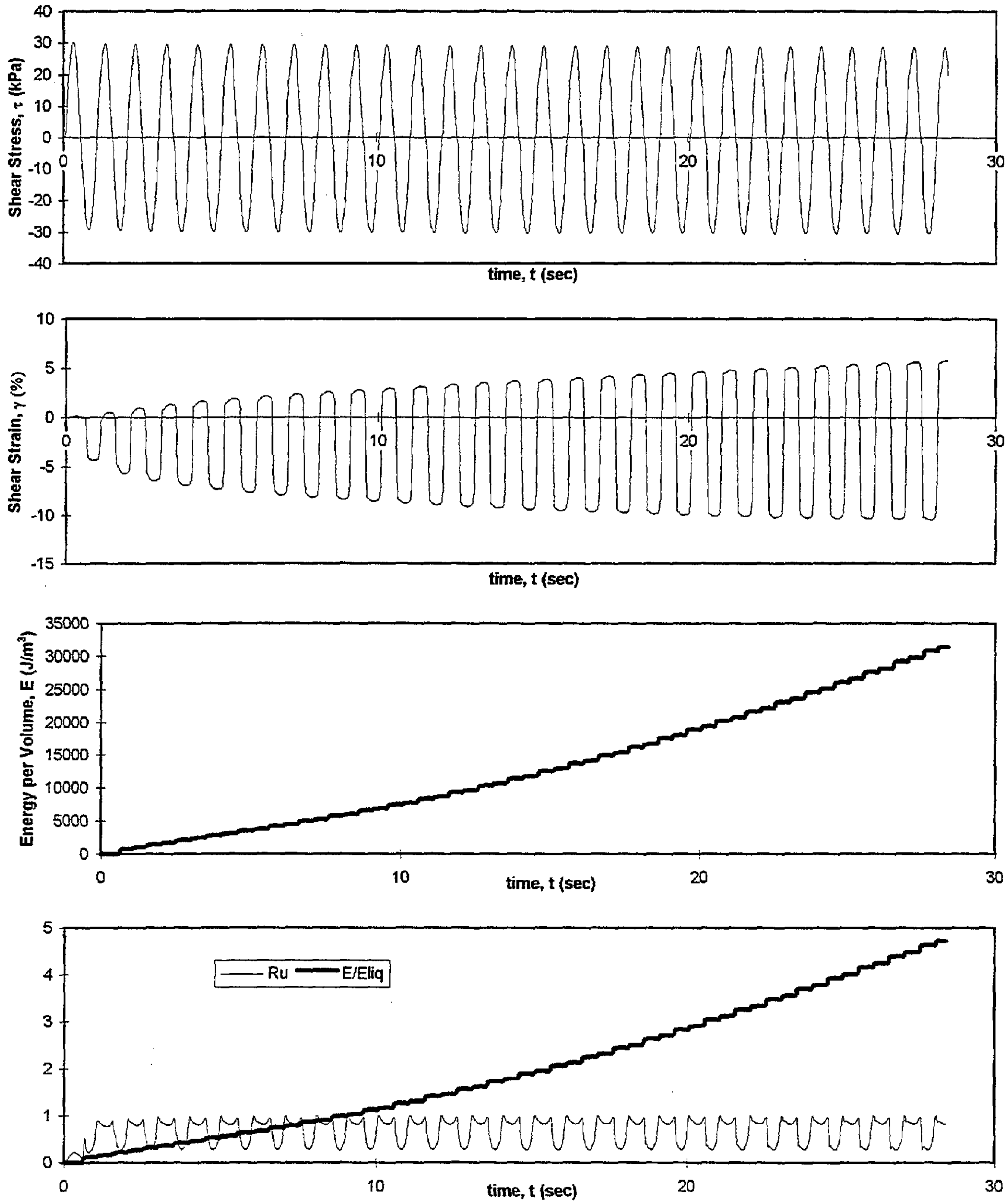

Test I.D.:	BTC4CY2	**Controlled Parameter:**	Stress
Fines Content (%):	5	**Initial Effective Stress (kPa):**	100
Dry Density (kN/m³)	16.72		

Shear Stress vs. Shear Strain

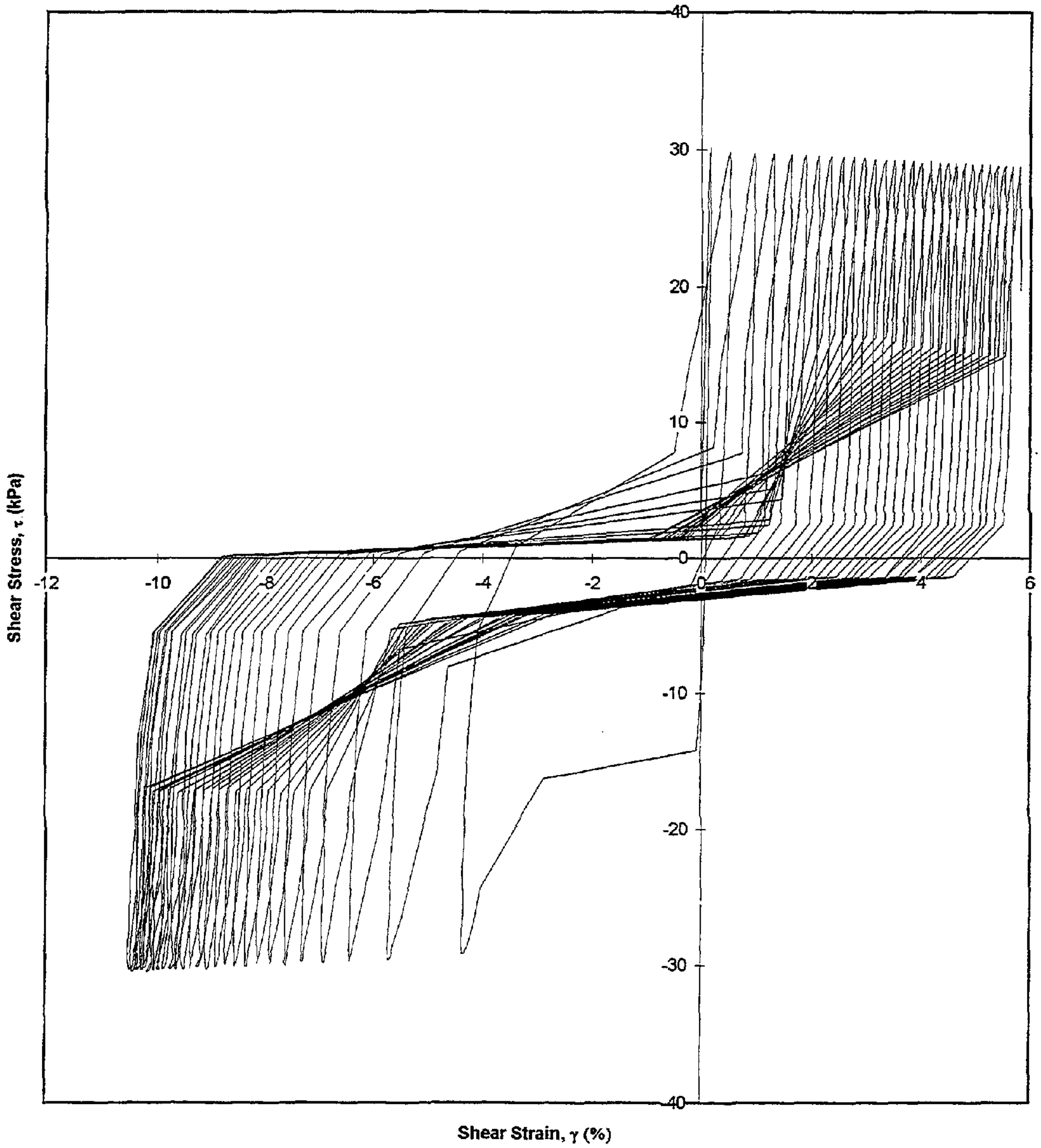

d:\nit\itp\cy_files\BTC4CY2.XLS 8/15/96 10:55 AM

Test I.D.:	BTC6CY1	**Controlled Parameter:**	Stress
Fines Content (%):	5	**Initial Effective Stress (kPa):**	100
Dry Density (kN/m^3)	13.51		

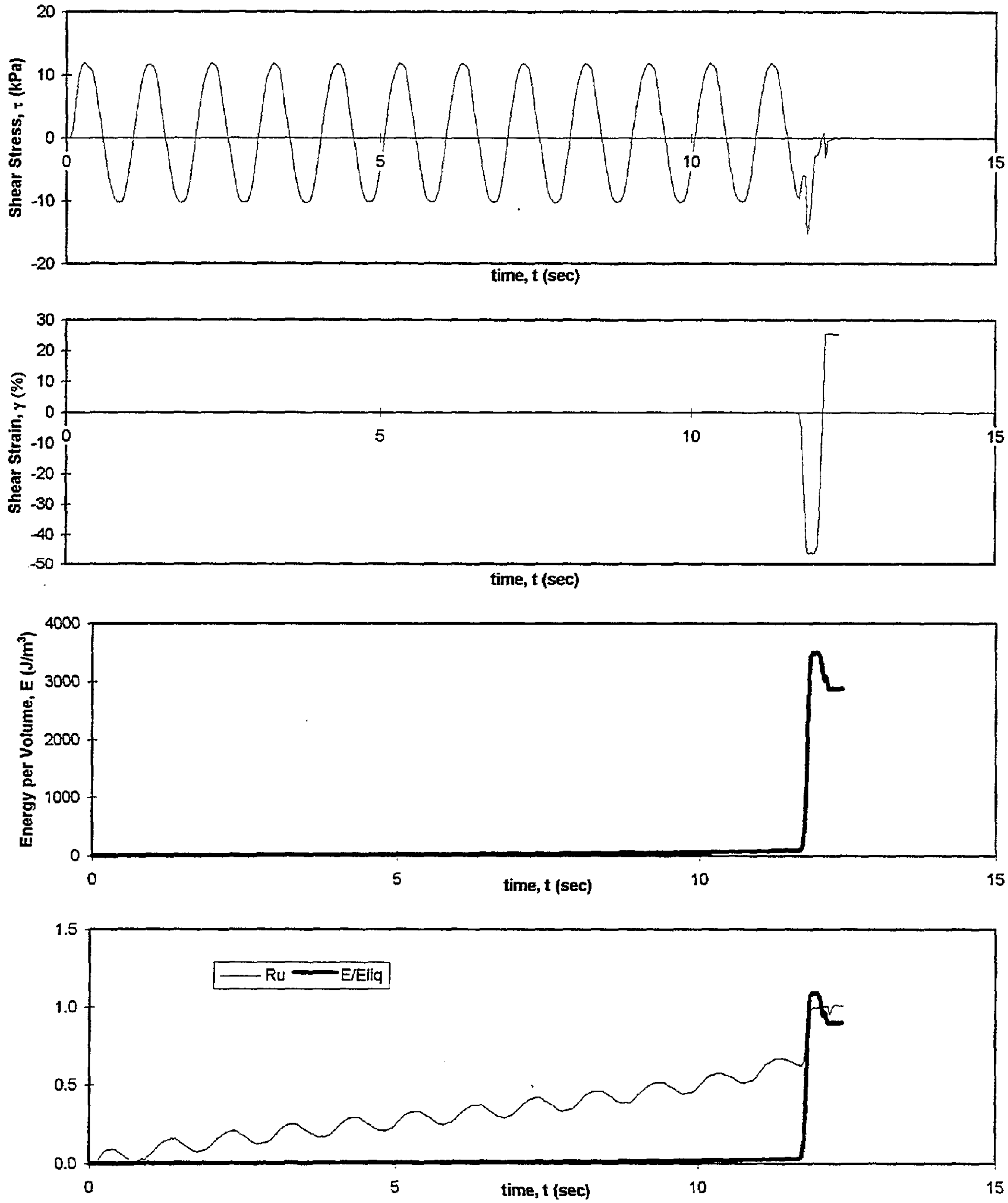

d:\nit\itp\cy_files\BTC6CY1.XLS 8/15/96 10:59 AM

Test I.D.:	BTC6CY1	**Controlled Parameter:**	Stress
Fines Content (%):	5	**Initial Effective Stress (kPa):**	100
Dry Density (kN/m^3)	13.51		

Shear Stress vs. Shear Strain